CONTRIBUTING EDITOR

ABDULLAH A. AL-BADR

GUNAWAN INDRAYANTO

YURI GOLDBERG

FOUNDING EDITOR

KLAUS FLOREY

Academic Press is an imprint of Elsevier
525 B Street, Suite 1900, San Diego, CA 92101-4495, USA
225 Wyman Street, Waltham, MA 02451, USA
32 Jamestown Road, London NW1 7BY, UK

First edition 2012

Copyright © 2012 Elsevier Inc. All rights reserved.

No part of this publication may be reproduced, stored in a retrieval system or transmitted in any form or by any means electronic, mechanical, photocopying, recording or otherwise without the prior written permission of the publisher

Permissions may be sought directly from Elsevier's Science & Technology Rights Department in Oxford, UK: phone (+44) (0) 1865 843830; fax (+44) (0) 1865 853333; email: permissions@elsevier.com. Alternatively you can submit your request online by visiting the Elsevier web site at http://www.elsevier.com/locate/permissions, and selecting, *Obtaining permission to use Elsevier material*

Notice
No responsibility is assumed by the publisher for any injury and/or damage to persons or property as a matter of products liability, negligence or otherwise, or from any use or operation of any methods, products, instructions or ideas contained in the material herein. Because of rapid advances in the medical sciences, in particular, independent verification of diagnoses and drug dosages should be made

ISBN: 978-0-12-397220-0
ISSN: 1871-5125 (Series)

For information on all Academic Press publications
visit our website at elsevierdirect.com

Printed and Bound in United States of America
12 13 14 10 9 8 7 6 5 4 3 2 1

Working together to grow
libraries in developing countries

www.elsevier.com | www.bookaid.org | www.sabre.org

ELSEVIER BOOK AID International Sabre Foundation

PREFACE TO VOLUME 37

The comprehensive profiling of drug substances and pharmaceutical excipients as to their physical and analytical characteristics remains essential to all phases of pharmaceutical development, and such profiles are of immeasurable importance to workers in the field. Consequently, the compilation and publication of comprehensive summaries of physical and chemical data, analytical methods, routes of compound preparation, degradation pathways, uses and applications, etc., have always been and will continue to be a vital function to both academia and industry.

As the science of pharmaceutics grows and matures, the need for information similarly expands along new fronts, and this growth causes an equivalent growth in the repository sources where investigators find the information they need. The content of the *Profiles* series continues to respond and expand to meet this need, and so chapters are published that fall into one or more of the following main categories:

1. Comprehensive profiles of a drug substance or excipient
2. Physical characterization of a drug substance or excipient
3. Analytical methods for a drug substance or excipient
4. Detailed discussions of the clinical uses, pharmacology, pharmacokinetics, safety, or toxicity of a drug substance or excipient
5. Reviews of methodology useful for the characterization of drug substances or excipients
6. Annual reviews of areas of importance to pharmaceutical scientists

This volume contains comprehensive profiles of amlodipine besylate, candesartan, flurbiprofen, gatifloxacin, lamotrigine, pimozide, risperidone, sunitinib maleate, varenicline, and zolpidem. The volume also contains a chapter setting out the polymorphic and solvatomorphic landscape of aripiprazole, and an update on the current state of validation of analytical methodology.

As always, I welcome communications from anyone in the pharmaceutical community who might want to provide an opinion or a contribution.

Harry G. Brittain

Editor, Profiles of Drug Substances,
Excipients, and Related Methodology

hbrittain@centerpharmphysics.com

CHAPTER 1

Aripiprazole: Polymorphs and Solvatomorphs

Harry G. Brittain

Contents

Center for Pharmaceutical Physics, Milford, New Jersey, USA

Profiles of Drug Substances, Excipients, and Related Methodology, Volume 37
ISSN 1871-5125, DOI: 10.1016/B978-0-12-397220-0.00001-5

© 2012 Elsevier Inc.
All rights reserved.

1. GENERAL INFORMATION

1.1. Nomenclature

1.1.1. Systematic chemical name

7-[4-[4-(2,3-Dichlorophenyl)-1-piperazinyl]butoxy]-3,4-dihydro-2(1*H*)-quinolinone

1.1.2. Chemical abstracts registry number

129722-12-9

1.1.3. Nonproprietary names

Aripiprazole

1.1.4. Proprietary names

Abilify, Abilitat

1.2. Formulae

1.2.1. Empirical formula and molecular weight

Molecular formula: $C_{23}H_{27}Cl_2N_3O_2$

Molecular weight: 448.385

1.2.2. Structural formula

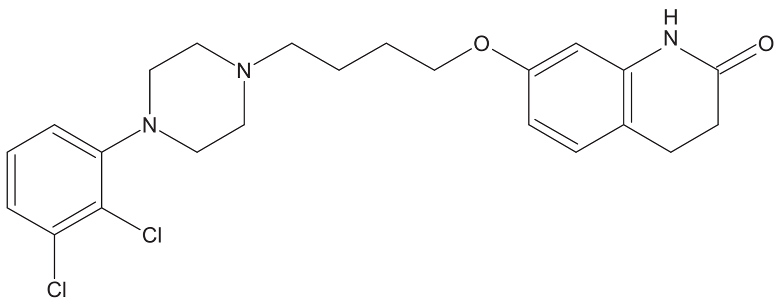

1.3. Elemental analysis

Carbon	61.61%	Chlorine	15.81%
Hydrogen	6.07%	Nitrogen	9.37%
Oxygen	7.14%		

2. OVERVIEW OF THE POLYMORPHIC AND SOLVATOMORPHIC LANDSCAPE

The chemical synthesis of the aripiprazole molecule was disclosed as part of the scope of a US patent issued in 1991 [1], and the existence of multiple crystal forms was disclosed in the published proceedings of a symposium [2].

Hetero Drugs Limited obtained the earliest patents relating to various crystal forms of aripiprazole. One of these disclosed a non-solvated form and two solvatomorphs of the drug substance [3], while the other disclosed six crystalline forms of unspecified solvation state [4]. Teva Pharmaceuticals followed with patents disclosing 10 crystal forms [5], and a process for specifically making Form-II of its earlier patent [6]. Around this time, Synthon obtained three patents that disclosed processes for making various known crystal forms of aripiprazole [7–9].

Otsuka Pharmaceuticals further complicated matters when it obtained a patent disclosing six polymorphs, two hydrates, and the amorphous form of aripiprazole [10], as well as another patent for the preparation of its Form-B [10]. Sandoz extended the proprietary literature with a patent disclosing two solvatomorphs and a process for making Form-X [11],

while Helm disclosed the stabilization of amorphous aripiprazole (or its salts) through the formation of coprecipitates with stabilizing agents [12,13].

Since these patents did not generally attempt to correlate the identities of the various crystal forms, it is entirely possible that the same polymorph or solvatomorph might have been disclosed in the various documents. In other words, if all the crystal forms disclosed in the patent documentation were unique, aripiprazole would have been shown to be able to exist in at least thirty different structural possibilities.

The ability of aripiprazole to form solvatomorphs has been studied when the compound was crystallized from different solvent systems [14]. In this work, the single-crystal structure of a non-solvated form was reported, as well as the methanol, hemi-ethanol, and hydrate forms. In the structures of these forms, the existence of hydrogen-bonded dimers of aripiprazole was identified that involved the cyclic diamide interactions in the solvates, or hydrogen-bonded polymeric aggregates consisting of extended multiple bonding through water bridges in the hydrate. It was also reported that the various modes of supramolecular association involved two different conformers of the drug substance.

Five phase-pure polymorphic forms of aripiprazole have been crystallized and studied by a full range of analytical methodology. The various forms could all be obtained from solvents as well as by thermal transformation (Form-X° to Form-I) or crystallization from the melt (yielding Form-III). Thermodynamic relationships between the polymorphs were evaluated, with Form-X° being the thermodynamically stable polymorph at 20 °C. Form-II was stable over the range of 62–77 °C, and Form-I was stable at temperatures higher than 80 °C. It was noted in this work that the three metastable polymorphs exhibited a high degree of kinetic stability, which would explain why they might have been disclosed in differing patent documents.

In a subsequent report, an extensive characterization of the 1:1 methanol, 2:1 ethanol, 2:1 dichloroethane, and monohydrate solvatomorphs of aripiprazole has been conducted [15]. Here, the crystal structures of five non-solvated polymorphs and the four solvatomorphs were critically analyzed to gain insight into packing similarities and differences. It was found that aside from the monohydrate, the structures of all forms were based on either a common dimeric or a catemeric motif of hydrogen-bonded drug molecules. It was also learned that the three organic solvates were isostructural, and that their desolvation yielded Form-III.

In the following sections, the relationship of the various polymorphic and solvatomorphic crystal forms will be critically examined with the aim of deducing exactly how many genuine crystal forms exist for aripiprazole.

Cross-comparisons of diffraction patterns from the various sources have revealed a number of redundancies, and therefore, a systematic polymorphic and solvatomorphic naming system will be developed. Since the literature studies of Griesser *et al*. are the most definitive [15,16], the numbering system developed in those papers will be used as the nomenclature initiation point.

3. POLYMORPHIC CRYSTAL FORMS

3.1. Form-I

Form-I is the high temperature stable form, which can be obtained by heating other crystal forms at temperatures of approximately 145 °C [15]. This crystal form can also be obtained through a solution-mediated phase transformation when the slurry is maintained above 80 °C and exhibits a melting point of 148.5 °C. According to the single-crystal structural study, the unit cell parameters obtained at ambient temperature of aripiprazole Form-I are as follows:

Space group	$P2_1$	System	Monoclinic
a	8.679 Å	α	90°
b	7.568 Å	β	94.50°
c	17.381 Å	γ	90°

The details of the crystal structure have been coded as MELFIT01 in the Cambridge Structural Database, and the X-ray powder diffraction pattern calculated using the CSD program Mercury is shown in Fig. 1.1. Also shown are the indexed 11 most intense scattering peaks in the powder pattern.

A cross-comparison of the diffraction patterns disclosed in the patent documentation [3–11] revealed that polymorphic Form-C of the Otsuka 7,910,589 patent [10] is the same crystal form as the Form-I polymorph of the Griesser publication [15].

3.2. Form-II

According to Griesser *et al*. [15], aripiprazole Form-II tends to crystallize concomitantly with other polymorphic forms but can be obtained in phase-pure form by suspending the substance in either *n*-butanol or acetonitrile for at least 1 h at 65–75 °C. Form-II exhibited a melting point of 143 °C and was defined by the following ambient temperature unit cell parameters:

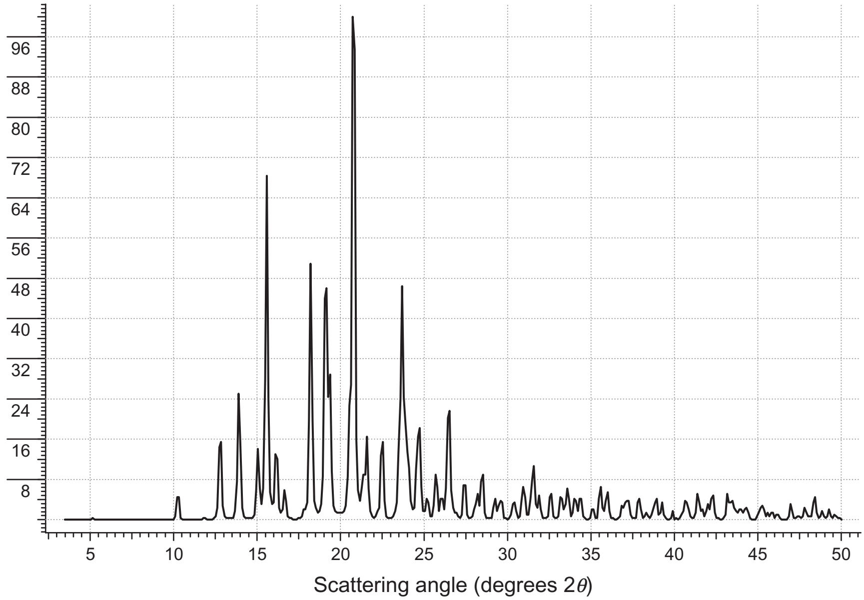

Miller index of peak	*d*-Spacing (Å)	Scattering angle (degrees 2*θ*)	Relative intensity (%)
(0 1 1)	6.936	12.75	15.5
(1 0 –2)	6.377	13.87	25.1
(1 1 0)	5.696	15.54	68.4
(1 1 –2)	4.877	18.18	50.9
(1 0 3)	4.639	19.12	46.0
(2 0 –1)	4.277	20.75	100.0
(2 0 1)	4.122	21.54	16.5
(1 1 3)	3.955	22.46	15.5
(1 0 4)	3.757	23.66	46.4
(2 0 –3)	3.601	24.70	18.2
(1 2 0)	3.467	25.67	21.6

FIGURE 1.1 X-ray powder diffraction of aripiprazole Form-I [15], calculated using the CSD program Mercury from the structural information contained in datafile MELFIT01.

Space group	$P2_1$	System	Orthorhombic
a	23.519 Å	α	90°
b	12.657 Å	β	90°
c	7.756 Å	γ	90°

The details of the crystal structure have been coded as MELFIT02 in the Cambridge Structural Database, and the X-ray powder diffraction pattern calculated using the CSD program Mercury is shown in Fig. 1.2.

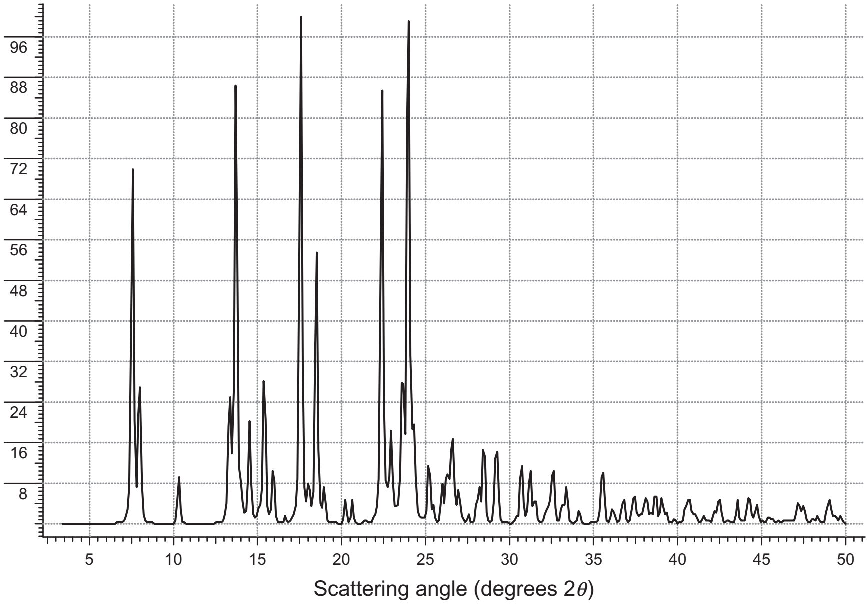

Miller index of peak	*d*-Spacing (Å)	Scattering angle (degrees 2θ)	Relative intensity (%)
(2 0 0)	11.760	7.51	69.9
(1 1 0)	11.146	7.93	26.9
(0 1 1)	6.613	13.38	25.0
(2 0 1)	6.475	13.67	86.4
(1 2 0)	6.111	14.48	20.3
(2 1 1)	5.764	15.36	28.2
(3 1 1)	5.055	17.53	100.0
(1 2 1)	4.800	18.47	53.5
(2 3 0)	3.971	22.37	85.4
(0 3 1)	3.706	23.99	99.1

FIGURE 1.2 X-ray powder diffraction of aripiprazole Form-II [15], calculated using the CSD program Mercury from the structural information contained in datafile MELFIT02. Also shown are the indexed 10 most intense scattering peaks in the powder pattern.

A cross-comparison of the diffraction patterns disclosed in the patent documentation [3–11] revealed that polymorphic Form-E of the Otsuka 7,910,589 [10] patent is the same crystal form as is the Form-II polymorph of the Griesser publication [15].

3.3. Form-III

Aripiprazole Form-III can be obtained by crystallization of a supercooled melt of the substance or by desolvation of the known solvatomorphs [15]. This polymorphic form can also be obtained by crystallization from ethyl

acetate, *n*-butanol, xylene, or *n*-hexane and exhibited a melting point of 139 °C. Form-III was defined by the following ambient temperature unit cell parameters:

Space group	P–1	System	Triclinic
a	10.220 Å	α	82.28°
b	12.208 Å	β	82.52°
c	18.837 Å	γ	82.88°

The details of the crystal structure have been coded as MELFIT03 in the Cambridge Structural Database, and the X-ray powder diffraction pattern calculated using the CSD program Mercury is shown in Fig. 1.3. Also shown are the indexed 10 most intense scattering peaks in the powder pattern.

A cross-comparison of the diffraction patterns disclosed in the patent documentation [3–11] revealed that polymorphic Form-B of the Otsuka 7,910,589 patent [10] and polymorphic Form-B of the Synthon 7,642,353 [7] patent are of the same crystal form as the Form-III polymorph of the Griesser publication [15]. In addition, if one shifts the entire diffraction pattern of Form-I of the Teva 7,504,504 patent [5] to lower angles by an amount equal to 0.3° 2θ, that shifted diffraction pattern turns out to be the same as that of the Form-III polymorph of the Griesser publication [15].

The crystal structure of a non-solvated form of aripiprazole has been reported in the paper published by Tessler and Goldberg [14], the details of which may be found in the Cambridge Structural Database under the filename of MELFIT. A comparison of the powder diffraction pattern calculated for this structure with that of Form-III of the Griesser publication [15] reveals that these are the same polymorphic form.

3.4. Form-IV

Aripiprazole Form-IV can be obtained by crystallization from toluene or dioxane, or hot saturated solutions of isopropanol or acetonitrile if those solutions are cooled very rapidly [15]. Form-III exhibited a melting point of 135 °C was defined by the following ambient temperature unit cell parameters:

Space group	$P-1$	System	Triclinic
a	8.818 Å	α	88.07°
b	9.035 Å	β	86.55°
c	30.417 Å	γ	73.87°

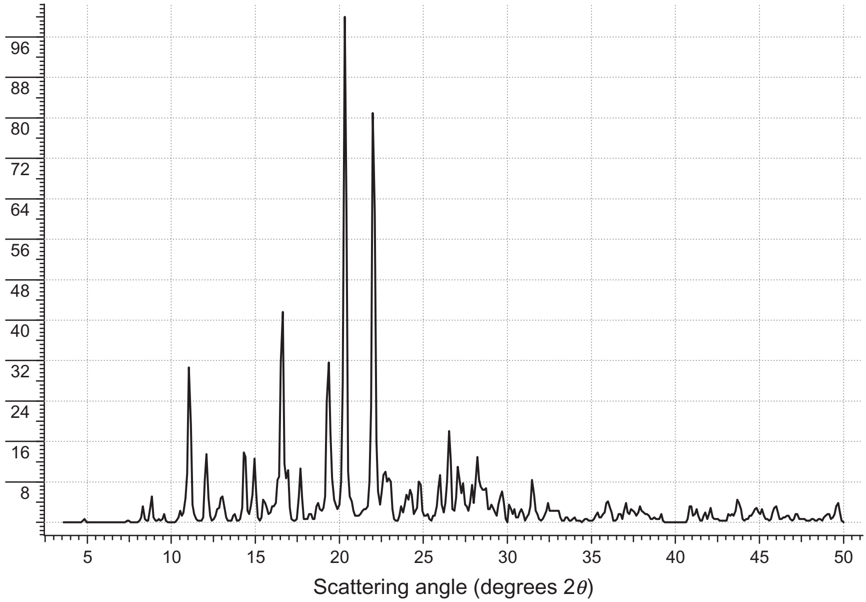

Miller index of peak	*d*-Spacing (Å)	Scattering angle (degrees 2*θ*)	Relative intensity (%)
(1 1 1)	8.013	11.03	30.6
(1 0 2)	7.251	12.20	13.5
(0 0 3)	6.180	14.32	13.9
(0 2 1)	5.933	14.92	12.6
(1 1 3) (0 2 2)	5.406	16.38	41.6
(2 0 1)	5.009	17.69	10.6
(2 1 2)	4.598	19.29	31.6
(0 1 4)	4.511	19.66	100.0
(0 3 1)	4.019	22.10	81.0
(3 0 0)	3.358	26.52	18.1

FIGURE 1.3 X-ray powder diffraction of aripiprazole Form-III [15], calculated using the CSD program Mercury from the structural information contained in datafile MELFIT03.

The details of the crystal structure have been coded as MELFIT04 in the Cambridge Structural Database, and the X-ray powder diffraction pattern calculated using the CSD program Mercury is shown in Fig. 1.4. Also shown are the indexed 10 most intense scattering peaks in the powder pattern.

A cross-comparison of the diffraction patterns disclosed in the patent documentation [3–11] revealed that polymorphic Form-D of the Otsuka 7,910,589 patent [10] and polymorphic Form-III of the Hetero 7,456,181 patent [3] are of the same crystal form as the Form-IV polymorph of the Griesser publication [15].

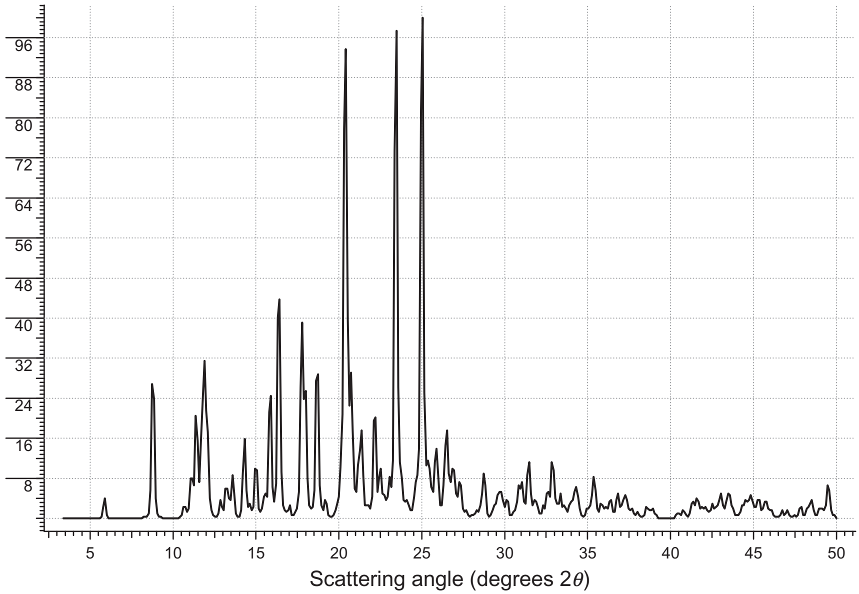

Miller index of peak	*d*-Spacing (Å)	Scattering angle (degrees 2*θ*)	Relative intensity (%)
(0 0 3)	10.119	8.73	26.8
(–1 0 1)	8.039	11.00	20.5
(0 1 2)	7.592	11.65	31.5
(–1 –1 3) (0 –1 4)	5.668	15.62	24.5
(–1 1 0)	5.362	16.52	43.7
(–1 –1 4)	5.046	17.56	39.1
(1 –1 3)	4.783	18.54	28.8
(0 2 0)	4.339	20.45	93.7
(0 2 4)	3.796	23.42	97.4
(2 2 1)	3.560	24.99	100.0

FIGURE 1.4 X-ray powder diffraction of aripiprazole Form-IV [15], calculated using the CSD program Mercury from the structural information contained in datafile MELFIT04.

3.5. Form-V

Aripiprazole Form-V was identified as Form-X° in the Griesser publication [15], but since this authentic polymorphic form was obtained in phase-pure form, it will be renamed as Form-V to maintain the flow in nomenclature. Form-V can be obtained by slurrying aripiprazole in a non-coordinating solvent (such as acetone, *n*-propanol, isopropanol, acetonitrile, or *n*-butanol) at temperatures less than 65 °C. The melting point of Form-V could not be determined as this form converted into Form-I during the determination. Various experiments demonstrated that Form-V is the thermodynamically stable form at temperatures less than

about 60 °C. This polymorph was defined by the following ambient temperature unit cell parameters:

Space group	$P2_1$	System	Monoclinic
a	8.867 Å	α	90°
b	7.762 Å	β	93.25°
c	16.485 Å	γ	90°

The details of the crystal structure have been coded as MELFIT05 in the Cambridge Structural Database, and the X-ray powder diffraction pattern calculated using the CSD program Mercury is shown in Fig. 1.5. Also shown are the indexed 10 most intense scattering peaks in the powder pattern.

A cross-comparison of the diffraction patterns disclosed in the patent documentation [3–11] revealed that polymorphic Form-II of the Teva 7,504,504 patent [5], polymorphic Form-II of the Synthon 7,655,798 patent [8], and polymorphic Form-X of the Sandoz 8,008,490 patent [11] are of the same crystal form as the Form-V (i.e., Form-X°) polymorph of the Griesser publication [15].

3.6. Form-VI

US patent 7,504,504 describes a polymorphic form of aripiprazole that was designated by Teva as Form-VI [5], and that identification will be preserved to maintain the flow in nomenclature. According to the patent, Form-VI was obtained by crystallization of aripiprazole out of propylene glycol.

An X-ray powder diffraction pattern of Form-VI was provided in the Teva patent, which has been reproduced in Fig. 1.6. Since no single-crystal structural information was available, the diffraction pattern was indexed using the ITO program [17], yielding the following unit cell parameters:

System	Monoclinic		
a	13.597 Å	α	90°
b	16.297 Å	β	96.12°
c	9.189 Å	γ	90°

These unit cell parameters correctly predicted the d-spacings and scattering angles of the 10 most intense scattering peaks in the powder pattern of Form-VI, and therefore, the crystal form characterized by the diffraction pattern of Fig. 1.6 has been identified as a genuine polymorph of aripiprazole.

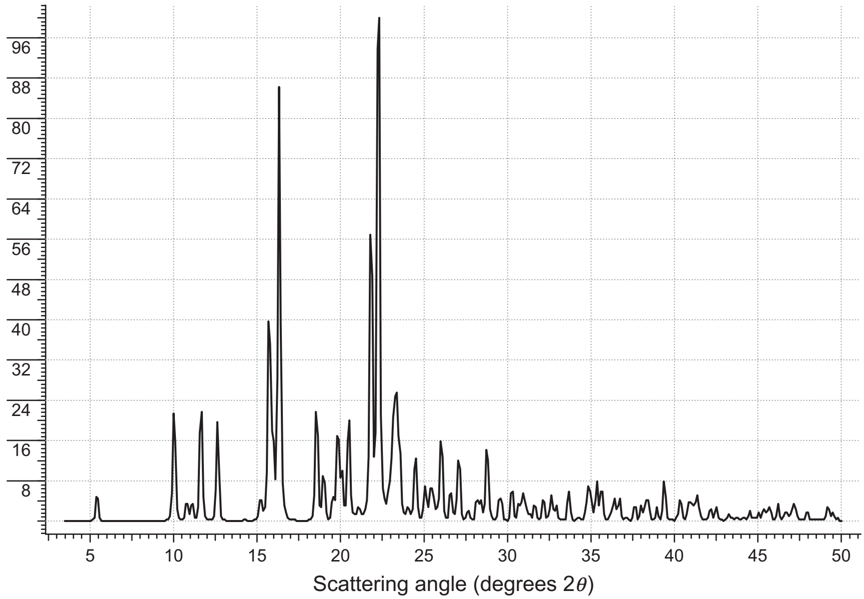

Miller index of peak	*d*-Spacing (Å)	Scattering angle (degrees 2*θ*)	Relative intensity (%)
(1 0 0)	8.860	9.98	21.4
(1 0 1)	7.678	11.52	21.7
(0 1 1)	7.022	12.60	19.7
(0 1 2)	5.649	15.67	39.7
(0 0 3)	5.491	16.13	86.2
(1 0 –3)	4.751	18.66	21.7
(2 0 –1)	4.321	20.54	20.0
(1 1 –3)	4.053	21.91	56.9
(2 0 –2)	3.967	22.39	100.0
(2 0 2)	3.839	23.15	25.5

FIGURE 1.5 X-ray powder diffraction of aripiprazole Form-V, which was identified as Form-X° in the original reference [15]. The pattern was calculated using the CSD program Mercury from the structural information contained in datafile MELFIT05.

3.7. Form-VII

US patent 7,504,504 also describes a polymorphic form of aripiprazole that was designated by Teva as Form-XX [5], but this crystal form will now be renamed as Form-VII to preserve the flow in nomenclature. According to the patent, Form-VII can be obtained by thermally desolvating the hemi-ethanolate solvatomorph of aripiprazole.

An X-ray powder diffraction pattern of Form-VII was provided in the Teva patent, which has been reproduced in Fig. 1.7. Since no single-crystal

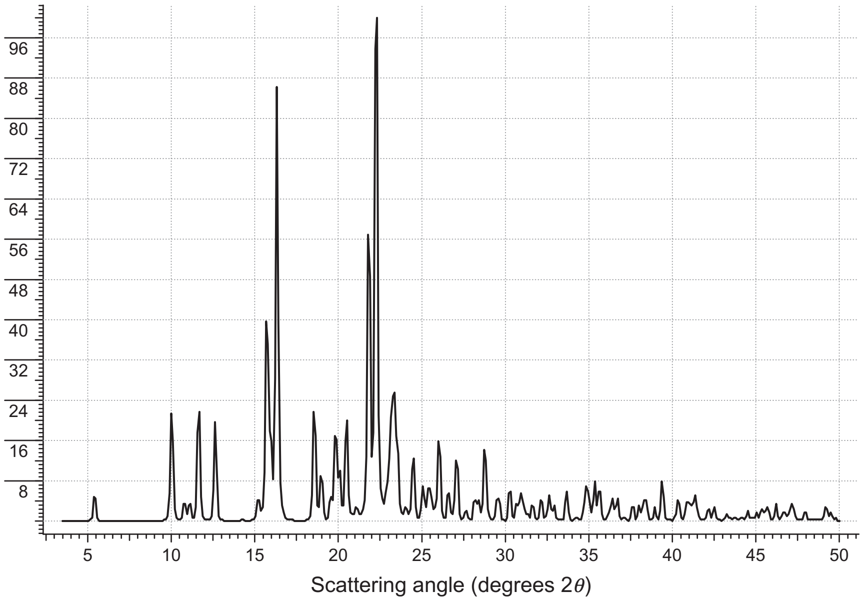

Miller index of peak	*d*-Spacing (Å)	Scattering angle (degrees 2*θ*)	Relative intensity (%)
(0 2 0)	8.149	10.85	4.5
(0 1 1)	7.970	11.09	3.8
(1 2 0)	6.979	12.67	5.0
(1 2 1)	5.404	16.39	5.3
(1 3 0)	5.041	17.58	40.0
(3 1 0) (1 3 1)	4.343	20.43	60.0
(2 3 1)	3.748	23.72	21.1
(2 2 –2)	3.582	24.84	100.0
(1 3 2)	3.320	26.83	12.7
(3 3 –2)	2.879	31.04	8.3

FIGURE 1.6 X-ray powder diffraction of aripiprazole Form-VI, which had been identified as Form-VI in the Teva patent [5].

structural information was given for this crystal form, the diffraction pattern was indexed using the ITO program [17], yielding the following unit cell parameters:

System	Triclinic		
a	15.117 Å	α	98.40°
b	20.687 Å	β	108.02°
c	11.581 Å	γ	85.40°

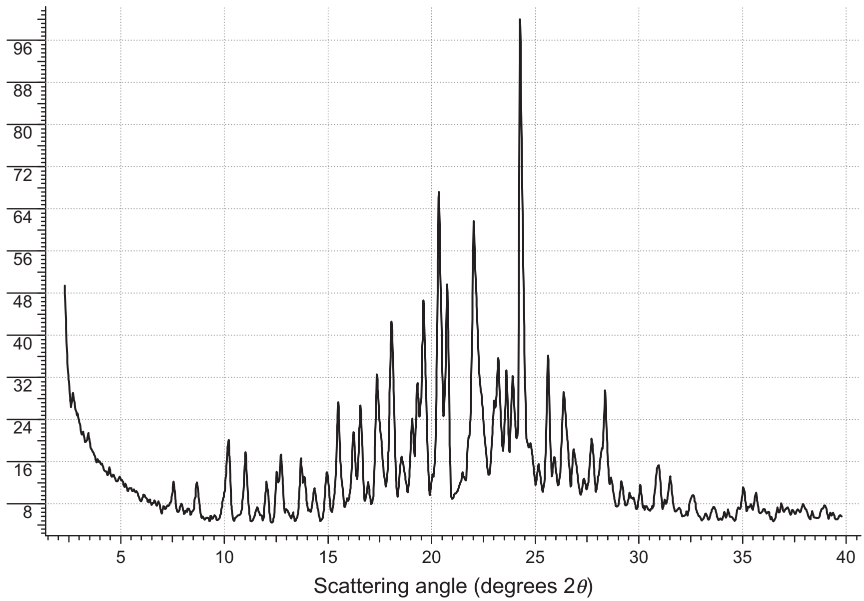

Miller index of peak	*d*-Spacing (Å)	Scattering angle (degrees 2*θ*)	Relative intensity (%)
(1 2 0)	8.481	10.42	20.1
(0 –2 1)	7.992	11.06	17.8
(–1 0 2)	5.709	15.51	27.3
(–1 –2 2)	5.333	16.61	26.7
(0 1 2) (0 4 0)	5.116	17.32	32.6
(–2 –2 2)	4.909	18.05	42.6
(–3 1 0)	4.624	19.18	46.6
(–2 2 2)	4.357	20.37	67.2
(–3 0 2) (–3 2 0)	4.301	20.63	49.7
(1 –3 2)	4.033	22.02	61.7
(–4 –2 1) (–4 1 1)	3.633	24.48	100.0
(–4 –2 2)	3.466	25.68	36.1

FIGURE 1.7 X-ray powder diffraction of aripiprazole Form-VII, which had been identified as Form-XX in the Teva patent [5].

These unit cell parameters correctly predicted the *d*-spacings and scattering angles of the 12 most intense scattering peaks in the powder pattern of Form-VII, and therefore, the crystal form characterized by the diffraction pattern of Fig 1.8 has been identified as a genuine polymorph of aripiprazole.

3.8. Form-VIII

US patent 7,910,589 describes a polymorphic form of aripiprazole that was designated by Otsuka as Form-F [10], but this crystal form will now be renamed as Form-VIII to continue the flow in nomenclature.

According to the patent, Form-VIII can be obtained by suspending an excess of aripiprazole in acetone, and heating at reflux temperature for 7.5h. The crystals must be filtered while hot to preserve the polymorphic identity.

An X-ray powder diffraction pattern of Form-VIII was provided in the Otsuka patent, which has been reproduced in Fig. 1.8. Since no single-crystal structural information was given for this crystal form, the diffraction pattern was indexed using the ITO program [17], yielding the following unit cell parameters:

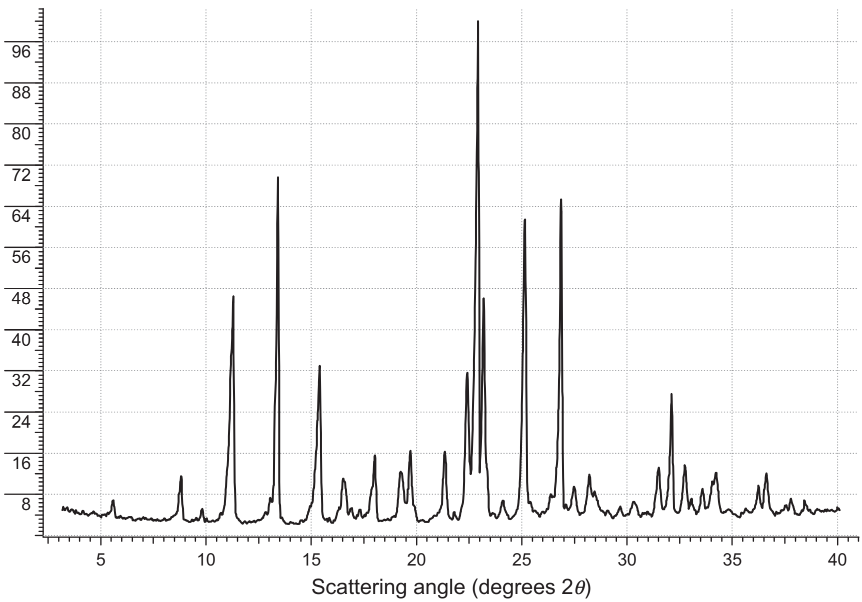

Miller index of peak	d-Spacing (Å)	Scattering angle (degrees 2θ)	Relative intensity (%)
(0 0 2) (1 1 1)	7.859	11.25	46.5
(1 1 –2)	6.597	13.41	69.7
(1 1 2)	5.739	15.43	33.0
(3 2 1)	3.968	22.39	31.6
(2 2 –3)	3.856	23.05	100.0
(1 1 –4)	3.839	23.15	46.1
(1 3 1)	3.516	25.31	61.4
(2 3 –2)	3.314	26.88	65.3
(0 4 0)	2.783	32.13	27.5

FIGURE 1.8 X-ray powder diffraction of aripiprazole Form-VIII, which had been identified as Form-F in the Otsuka patent [10].

System	Monoclinic		
a	21.332 Å	α	90°
b	11.133 Å	β	107.18°
c	16.452 Å	γ	90°

These unit cell parameters correctly predicted the *d*-spacings and scattering angles of the nine most intense scattering peaks in the powder pattern of Form-VIII, and therefore, the crystal form characterized by the diffraction pattern of Fig. 1.8 has been identified as a genuine polymorph of aripiprazole.

3.9. Form-IX

US patent 7,910,589 describes a polymorphic form of aripiprazole that was designated by Otsuka as Form-G [10], but this crystal form will now be renamed as Form-IX to maintain the flow in nomenclature. According to the patent, Form-IX can be obtained by first preparing amorphous aripiprazole by quench cooling the melt and then storing this product in a sealed container at room temperature for approximately 6 months.

An X-ray powder diffraction pattern of Form-IX was provided in the Otsuka patent, which has been reproduced in Fig. 1.9. Since no single-crystal structural information was given for this crystal form, the diffraction pattern was indexed using the ITO program [17], yielding the following unit cell parameters:

System	Monoclinic		
a	21.059 Å	α	90°
b	10.651 Å	β	102.54°
c	16.271 Å	γ	90°

These unit cell parameters correctly predicted the *d*-spacings and scattering angles of the 11 most intense scattering peaks in the powder pattern of Form-IX, and therefore, the crystal form characterized by the diffraction pattern of Fig. 1.9 has been identified as a genuine polymorph of aripiprazole.

3.10. Non-authentic polymorphs

In the Hetero 7,491,726 patent [4], X-ray powder diffraction patterns were disclosed and ascribed to "Form-I" and "Form-II," and were set forth as being polymorphic forms of aripiprazole. However, neither diffraction pattern could be indexed to a single set of unit cell parameters, and consequently, these diffraction patterns cannot be used to suggest the

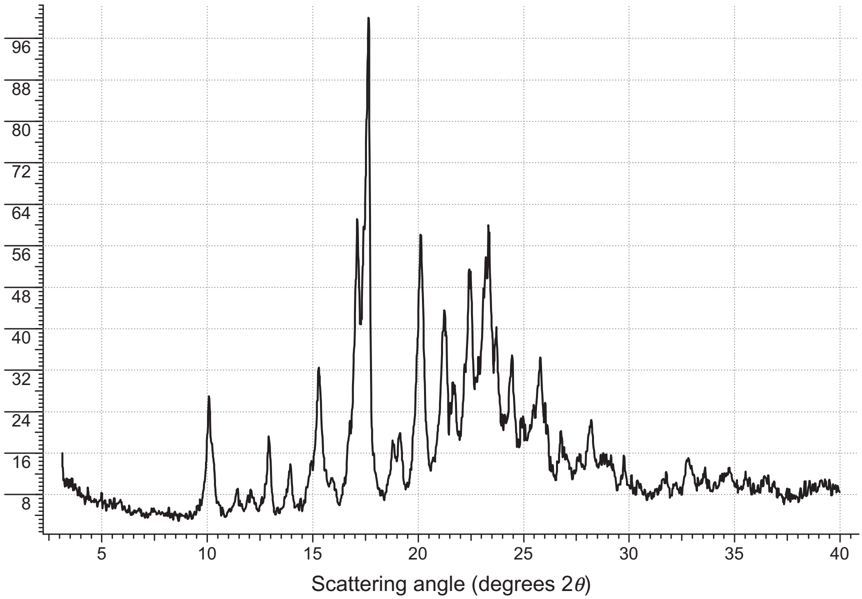

Miller index of peak	*d*-Spacing (Å)	Scattering angle (degrees 2*θ*)	Relative intensity (%)
(0 1 1)	8.846	9.99	27.0
(3 0 0)	6.852	12.91	19.2
(1 1 2)	5.803	15.26	32.5
(1 2 0)	5.155	17.19	61.1
(2 1 2)	5.034	17.60	100.0
(2 2 1)	4.413	20.10	58.1
(3 2 0)	4.205	21.11	43.6
(0 0 4)	3.971	22.37	51.5
(3 0 3)	3.808	23.34	59.9
(1 2 3)	3.597	24.73	34.9
(2 0 4)	3.460	25.73	34.5

FIGURE 1.9 X-ray powder diffraction of aripiprazole Form-IX, which had been identified as Form-G in the Otsuka patent [10].

existence of authentic polymorphic forms other than the ones described above. These patterns must be derived from samples containing mixtures of crystal forms and represent instances of concomitant crystallization.

4. SOLVATOMORPHIC CRYSTAL FORMS

4.1. Methanol as the solvent of crystallization

The structure of the crystalline methanolate solvatomorph of aripiprazole has been determined at 110K [14] and ambient conditions [16]. Since most powder diffraction work is performed at room temperature, this

solvatomorph will defined on the basis of the following unit cell parameters derived from the ambient study:

Space group	P−1	System	Triclinic
a	8.392 Å	α	83.18°
b	10.200 Å	β	82.29°
c	15.524 Å	γ	67.31°

The details of the low-temperature crystal structure [14] have been coded as MELFOZ in the Cambridge Structural Database, while the details of the room temperature crystal structure [16] have been coded as MELFOZ01. The X-ray powder diffraction pattern of the ambient determination (as calculated using the CSD program Mercury) is shown in Fig. 1.10 together with the indexed 10 most intense scattering peaks of the powder pattern.

A cross-comparison of the diffraction patterns disclosed in the patent documentation [3–11] revealed that the methanolate solvatomorphs of the Hetero 7,456,181 patent [3], the Synthon 7,902,198 patent [9], and the Sandoz 8,008,490 patent [11] are of the same crystal form as the methanolate solvatomorph of the Griesser publication [16].

4.2. Ethanol as the solvent of crystallization

The structure of the crystalline hemi-ethanolate solvatomorph of aripiprazole has also been determined at 110 K [14] and ambient conditions [16]. This solvatomorph will defined on the basis of the following unit cell parameters derived from the ambient study:

Space group	P–1	System	Triclinic
a	7.756 Å	α	84.73°
b	10.668 Å	β	80.53°
c	15.499 Å	γ	73.74°

The hemi-ethanolate solvatomorph of aripiprazole is nearly isostructural with the methanolate solvatomorph, with the main differences being in the magnitude of the a-axis and γ-angle unit cell parameters. The details of the low-temperature crystal structure [14] have been coded as MELFEP in the Cambridge Structural Database, while the details of the room temperature crystal structure [16] have been coded as MELFEP01. The X-ray powder diffraction pattern of the ambient determination (as calculated using the CSD program Mercury) is

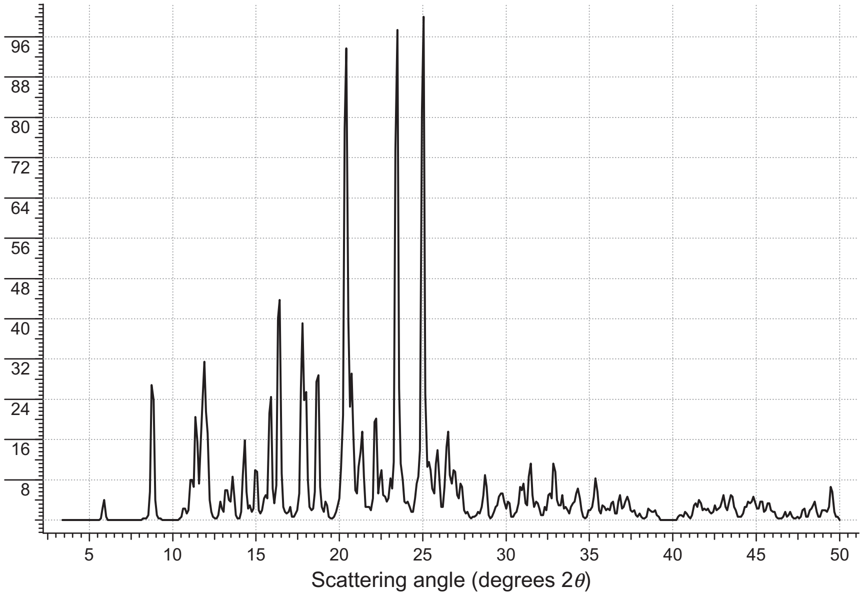

Miller index of peak	*d*-Spacing (Å)	Scattering angle (degrees 2θ)	Relative intensity (%)
(0 1 0)	9.385	9.42	10.9
(0 1 1)	8.281	10.67	21.0
(1 0 0)	7.706	11.47	9.2
(1 1 0)	7.496	11.80	14.0
(1 1 1) (1 0 1)	7.180	12.32	12.0
(–1 0 1)	6.635	13.33	6.5
(–1 1 1)	4.798	18.48	39.3
(1 0 3)	4.464	19.87	41.4
(1 1 4) (0 1 4)	3.647	24.38	100.0
(–2 0 2)	3.317	26.85	8.9

FIGURE 1.10 X-ray powder diffraction of the methanol solvatomorph of aripiprazole [16], calculated using the CSD program Mercury from the structural information contained in datafile MELFOZ01.

shown in Fig. 1.11 together with the indexed 10 most intense scattering peaks of the powder pattern.

A cross-comparison of the diffraction patterns disclosed in the patent documentation [3–11] revealed that the Form-XII of the Teva 7,504,504 patent [5], the ethanolate solvatomorph of the Synthon 7,902,198 patent [9], and the ethanolate solvatomorph of the Sandoz 8,008,490 patent [11] are of the same crystal form as the hemi-ethanolate solvatomorph of the Griesser publication [16].

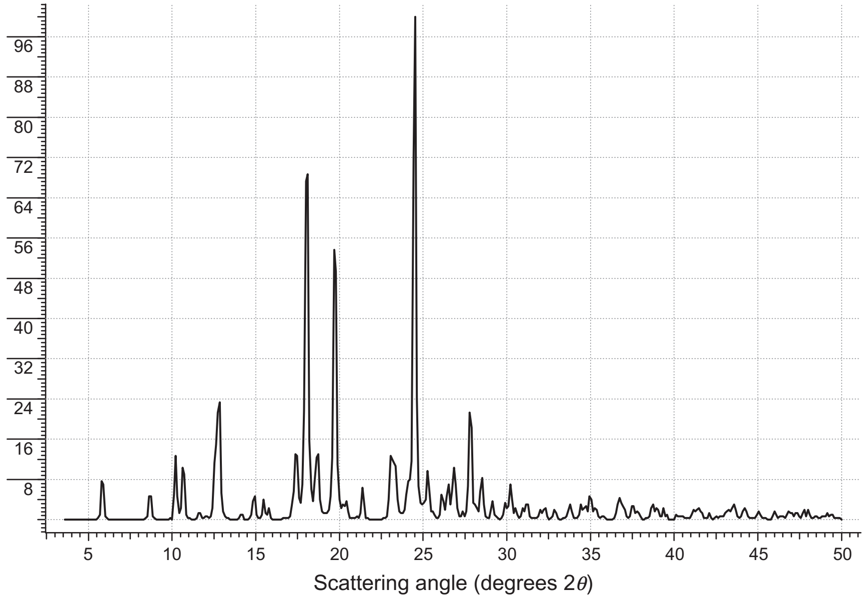

Miller index of peak	*d*-Spacing (Å)	Scattering angle (degrees 2*θ*)	Relative intensity (%)
(0 0 1)	15.270	5.78	7.7
(0 1 1)	8.695	10.16	12.7
(0 –1 1)	8.315	10.63	10.3
(1 1 0)	6.930	12.76	23.3
(0 2 0)	5.115	17.32	13.0
(–1 1 1) (0 2 1)	4.915	18.03	68.7
(–1 –1 2)	4.747	18.68	13.0
(1 0 3)	4.505	19.69	53.7
(0 1 4)	3.635	24.47	100.0
(2 0 3)	3.214	27.73	21.3

FIGURE 1.11 X-ray powder diffraction of the hemi-ethanol solvatomorph of aripiprazole [16], calculated using the CSD program Mercury from the structural information contained in datafile MELFOZ01.

4.3. Dichloroethane as the solvent of crystallization

The structure of the crystalline 1,2-dichloroethane solvatomorph of aripiprazole has been determined at 173K and at ambient conditions [16]. As before, this solvatomorph will defined on the basis of the following unit cell parameters derived from the ambient study:

Space group	*P*–1	System	Triclinic
a	8.311 Å	α	84.05°
b	10.254 Å	β	86.94°
c	15.283 Å	γ	70.79°

The dichloroethane solvatomorph of aripiprazole is nearly isostructural with the ethanolate solvatomorph, with the main difference being in the magnitude of the β-angle unit cell parameter. The details of the low-temperature crystal structure have been coded as MOXDAF01 in the Cambridge Structural Database, while the details of the room temperature crystal structure have been coded as MOXDAF [16]. The X-ray powder diffraction pattern of the ambient determination (as calculated using the CSD program Mercury) is shown in Fig. 1.12 together with the indexed six most intense scattering peaks of the powder pattern.

A cross-comparison of the diffraction patterns disclosed in the patent documentation [3–11] revealed that the methanolate solvatomorph of the Hetero Synthon 7,456,181 patent [9] is of the same crystal form as the methanolate solvatomorph of the Griesser publication [16].

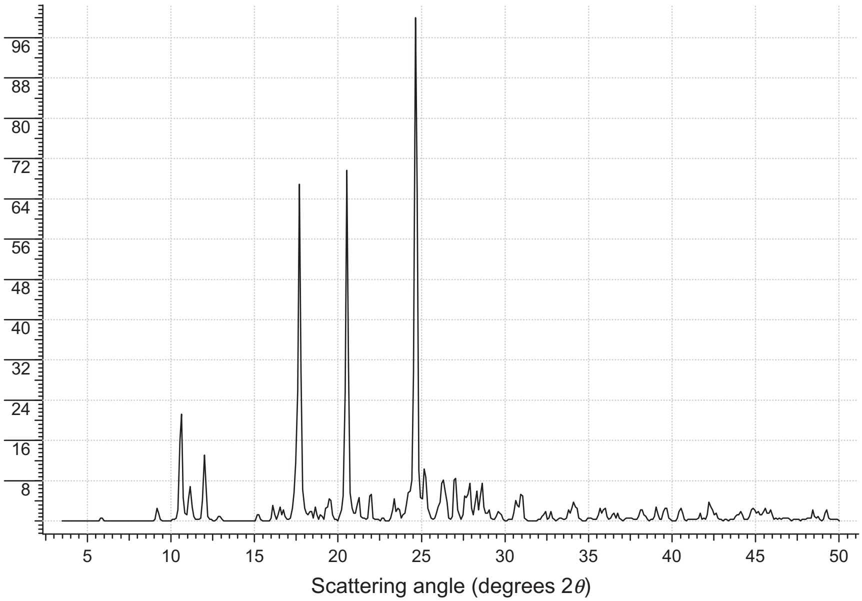

Miller index of peak	*d*-Spacing (Å)	Scattering angle (degrees 2θ)	Relative intensity (%)
(0 1 1)	8.373	10.56	21.3
(1 0 0)	7.844	11.27	6.9
(1 1 0)	7.385	11.97	13.1
(–1 –1 2) (–1 1 1)	5.121	17.30	66.9
(1 0 3)	4.329	20.50	69.7
(–1 2 0) (0 1 4)	3.621	24.56	100.0

FIGURE 1.12 X-ray powder diffraction of the 1,2-dichloroethane solvatomorph of aripiprazole [16], calculated using the CSD program Mercury from the structural information contained in datafile MOXDAF.

4.4. Pyridine as the solvent of crystallization

US patent 7,504,504 also describes a crystal form of aripiprazole that was designated by Teva as Form-XIV [5] and which was reported to be obtained out of pyridine at a temperature of 115–116 °C. The patent discloses that the total volatile content of this crystal form was 9%, which corresponds well with the solvent content of 8.1% that would be anticipated for a hemi-pyridine solvatomorph.

The Teva patent provided an X-ray powder diffraction pattern of the hemi-pyridine solvatomorph, which has been reproduced in Fig. 1.13.

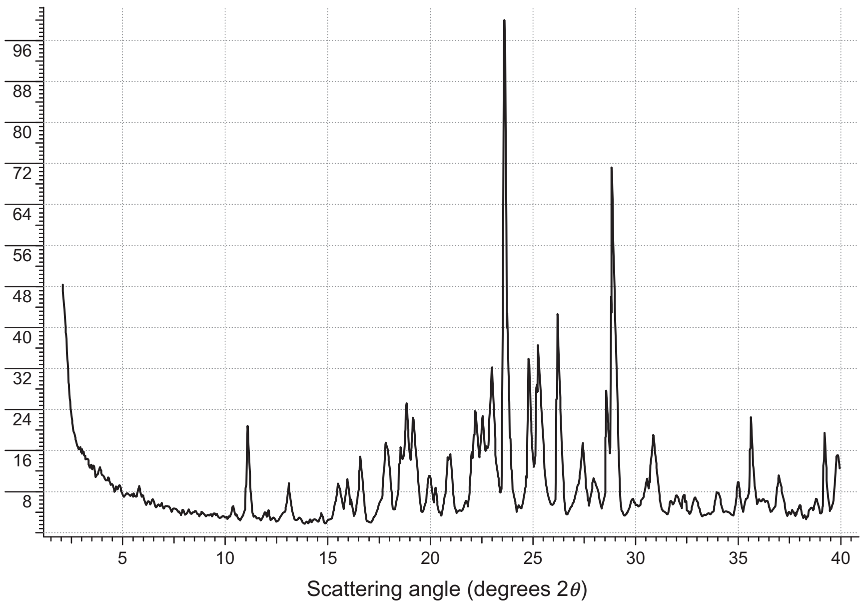

Miller index of peak	*d*-Spacing (Å)	Scattering angle (degrees 2*θ*)	Relative intensity (%)
(0 0 1)	7.947	11.12	20.8
(–2 –2 1)	3.970	22.38	25.2
(2 1 1)	4.234	20.97	22.4
(0 0 2)	3.973	22.36	23.7
(–2 –2 1) (–1 0 2)	3.970	22.38	22.7
(–3 0 1) (0 –1 2)	3.828	23.22	32.3
(–3 1 1) (–3 2 0)	3.799	23.40	100.0
(–3 –1 1)	3.590	24.78	34.0
(3 0 1)	3.507	25.37	36.6
(–1 2 2)	3.401	26.18	42.7
(–2 –2 2)	3.088	28.89	71.2

FIGURE 1.13 X-ray powder diffraction of the hemi-pyridine solvatomorph of aripiprazole, which had been identified as Form-XIV in the Teva patent [5].

Since no single-crystal structural information was given for this crystal form, the diffraction pattern was indexed using the ITO program [17], yielding the following unit cell parameters:

System	Triclinic		
a	12.552 Å	α	91.89°
b	14.018 Å	β	95.80°
c	7.997 Å	γ	98.02°

These unit cell parameters correctly predicted the d-spacings and scattering angles of the 11 most intense scattering peaks in the powder pattern of the hemi-pyridine solvate, and therefore, the crystal form characterized by the diffraction pattern of Fig. 1.13 has been identified as a genuine solvatomorph of aripiprazole.

4.5. Water as the solvent of crystallization

4.5.1. Monohydrate

The structure of aripiprazole monohydrate has been determined at 110 K [14] and ambient conditions [16]. The monohydrate will defined on the basis of the following unit cell parameters derived from the ambient study:

Space group	$P2_1/n$	System	Monoclinic
a	7.931 Å	α	90°
b	28.371 Å	β	106.07°
c	10.747 Å	γ	90°

The details of the low-temperature crystal structure [14] have been coded as MELFUF in the Cambridge Structural Database, while the details of the room temperature crystal structure [16] have been coded as MELFUF01. The X-ray powder diffraction pattern of the ambient determination (as calculated using the CSD program Mercury) is shown in Fig. 1.14 together with the indexed 10 most intense scattering peaks of the powder pattern.

A cross-comparison of the diffraction patterns disclosed in the patent documentation [3–11] revealed that the hydrate form of the Otsuka 7,910,589 patent [10] is of the same crystal form as the monohydrate solvatomorph of the Griesser publication [16].

4.5.2. Sesquihydrate

The Teva 7,504,504 patent discloses aripiprazole Form-XIX, a crystal form that is described as containing 6% of water and which was obtained from 1:1 ethyl acetate/ethanol, 7:3 tetrahydrofuran/methanol, or 5:3

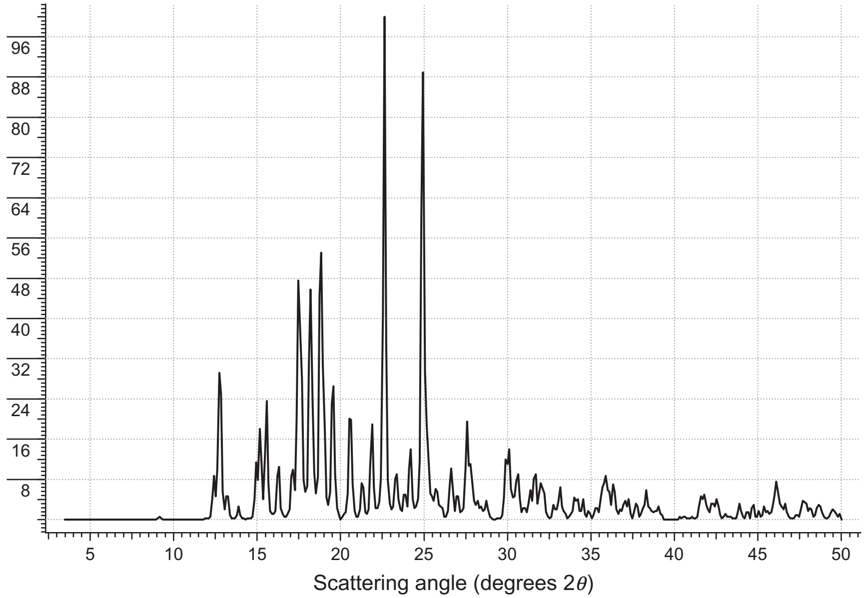

Miller index of peak	*d*-Spacing (Å)	Scattering angle (degrees 2*θ*)	Relative intensity (%)
(0 3 1)	6.974	12.68	29.2
(1 3 –1)	5.703	15.52	23.6
(0 1 2)	5.080	17.44	47.5
(0 2 2)	4.852	18.27	45.8
(1 3 1)	4.724	18.77	53.1
(0 3 2)	4.532	19.57	26.5
(1 4 1)	4.323	20.53	20.1
(1 4 –2)	4.064	21.85	19.0
(2 1 –1)	3.910	22.73	100.0
(2 0 –2)	3.575	24.88	88.9

FIGURE 1.14 X-ray powder diffraction of aripiprazole monohydrate [16], calculated using the CSD program Mercury from the structural information contained in datafile MELFUF01.

chloroform/methanol [5]. The theoretical water content for a 1.5-hydrate would be 5.7%, so Teva Form-XIX is identified as aripiprazole sesquihydrate.

The patent provided an X-ray powder diffraction pattern for this solvatomorph (shown in Fig. 1.15), which is not equivalent to that of the monohydrate. Since no single-crystal structural information was given for this crystal form, the diffraction pattern was indexed using the ITO program [17], yielding the following unit cell parameters:

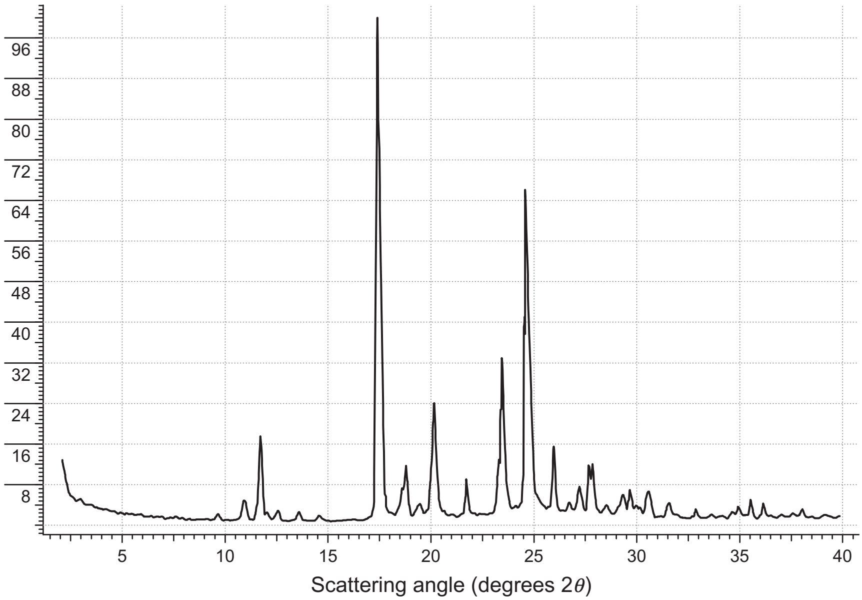

Miller index of peak	*d*-Spacing (Å)	Scattering angle (degrees 2*θ*)	Relative intensity (%)
(1 1 0)	8.036	11.00	4.9
(–1 –1 1)	7.404	11.94	17.6
(0 2 0)	5.077	17.45	100.0
(2 0 0)	4.710	18.82	11.8
(0 –2 1)	4.415	20.09	24.1
(–2 1 1)	4.114	21.58	9.0
(–2 –2 2)	3.702	24.02	32.9
(–3 –1 1)	3.597	24.73	66.1
(–3 0 1)	3.443	25.85	15.5

FIGURE 1.15 X-ray powder diffraction of aripiprazole sesquihydrate, which had been identified as Form-XIX in the Teva patent [5].

System	Triclinic		
a	10.828 Å	α	98.07°
b	10.627 Å	β	115.64°
c	9.666 Å	γ	72.86°

These unit cell parameters correctly predicted the *d*-spacings and scattering angles of the nine most intense scattering peaks in the powder pattern of the sesquihydrate, and therefore, the crystal form characterized by the diffraction pattern of Fig. 1.15 has been identified as a genuine solvatomorph of aripiprazole.

4.5.3. Tetrahydrate

The Teva 7,504,504 patent discloses aripiprazole Form-XI, a crystal form that is described as containing 14% of water and which was obtained from wet dibromomethane [5]. The theoretical water content for a tetrahydrate is calculated to be 13.9%, so Teva Form-XI is identified as aripiprazole tetrahydrate.

The patent provided the X-ray powder diffraction pattern for this solvatomorph (which is shown in Fig. 1.16) and which is not equivalent to that of the monohydrate or the sesquihydrate. Since no single-crystal structural information was given for this crystal form, the diffraction

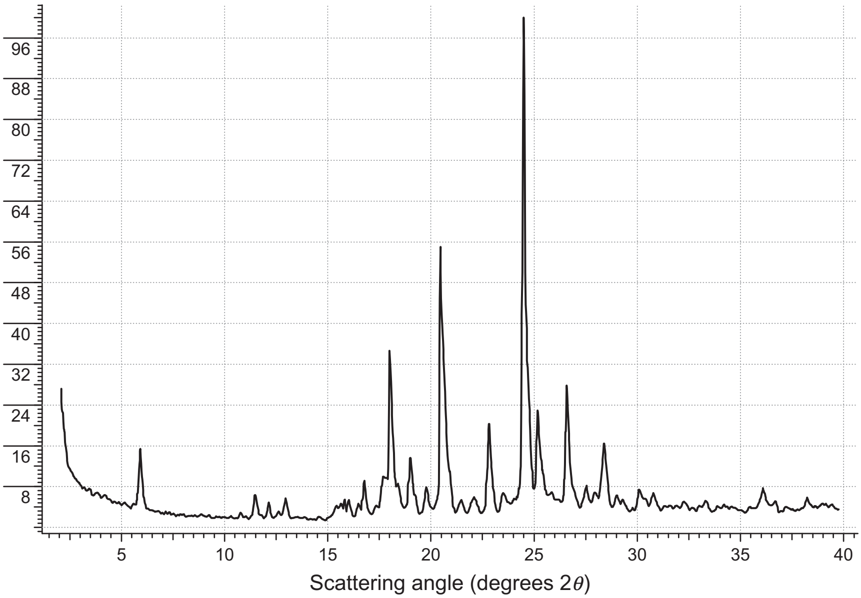

Miller index of peak	*d*-Spacing (Å)	Scattering angle (degrees 2θ)	Relative intensity (%)
(0 1 0)	15.009	5.88	15.4
(1 0 1)	7.755	11.40	6.4
(–1 2 0)	6.837	12.94	5.7
(2 2 0)	4.930	17.98	34.7
(–1 –3 1)	4.654	19.05	13.6
(3 1 0)	4.359	20.36	55.0
(–1 –3 2)	3.887	22.86	20.3
(–1 2 2)	3.628	24.51	100.0
(1 4 0)	3.556	25.02	22.9
(3 –1 2)	3.351	26.58	27.8
(2 2 2)	3.139	28.41	16.5

FIGURE 1.16 X-ray powder diffraction of aripiprazole tetrahydrate, which had been identified as Form-XI in the Teva patent [5].

pattern was indexed using the ITO program [17], yielding the following unit cell parameters:

System	Triclinic		
a	14.048 Å	α	104.88°
b	15.576 Å	β	92.70°
c	10.092 Å	γ	93.59°

These unit cell parameters correctly predicted the *d*-spacings and scattering angles of the 11 most intense scattering peaks in the powder pattern of the sesquihydrate, and therefore, the crystal form characterized by the diffraction pattern of Fig. 1.16 has been identified as a genuine solvatomorph of aripiprazole.

4.5.4. Pentahydrate

The Teva 7,504,504 patent further discloses aripiprazole Form-X, a crystal form that is described as containing 16% of water, and which was obtained from wet dichloromethane [5]. The theoretical water content for a pentahydrate would be 16.7%, so Teva Form-X is identified as aripiprazole pentahydrate.

The patent provided an X-ray powder diffraction pattern for this solvatomorph, shown in Fig. 1.17, and which is not equivalent to that of the monohydrate, the sesquihydrate, or the tetrahydrate. Since no single-crystal structural information was given for this crystal form, the diffraction pattern was indexed using the ITO program [17], yielding the following unit cell parameters:

System	Monoclinic		
a	16.283 Å	α	90°
b	15.647 Å	β	108.50°
c	15.093 Å	γ	90°

These unit cell parameters correctly predicted the *d*-spacings and scattering angles of the 10 most intense scattering peaks in the powder pattern of the pentahydrate, and therefore, the crystal form characterized by the diffraction pattern of Fig. 1.15 has been identified as a genuine solvatomorph of aripiprazole.

4.6. Non-authentic solvatomorphs

In the Teva 7,504,504 patent [5], an X-ray powder diffraction pattern was disclosed and ascribed to aripiprazole ''Form-VIII.'' This diffraction pattern was obtained on material isolated out of dimethyl sulfoxide, and

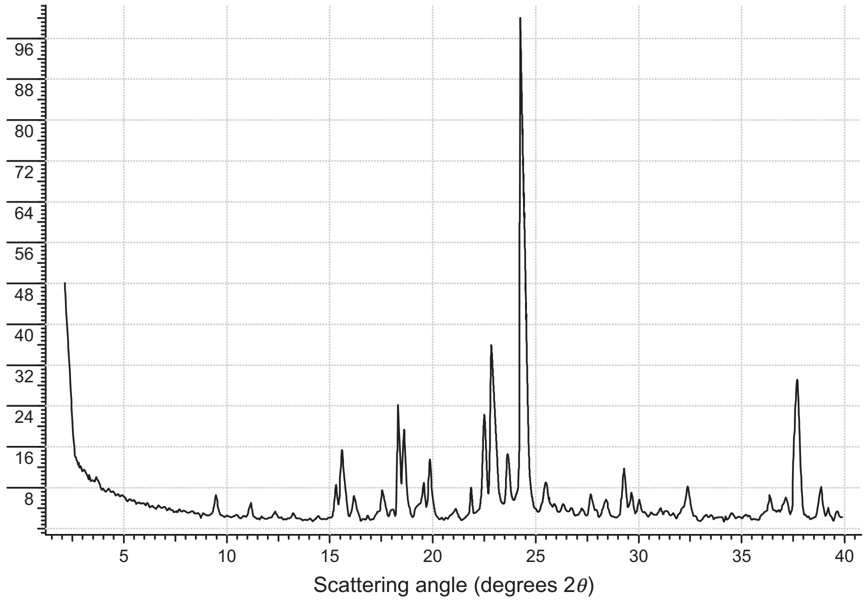

Miller index of peak	*d*-Spacing (Å)	Scattering angle (degrees 2*θ*)	Relative intensity (%)
(1 0 1)	9.194	9.61	6.6
(1 1 1)	7.927	11.15	5.0
(2 1 1)	5.658	15.65	15.4
(1 3 –1)	4.823	18.38	24.2
(3 1 –2)	4.751	18.66	19.4
(3 2 –1)	4.456	19.91	13.5
(2 2 2) (2 3 1)	3.963	22.41	22.2
(1 3 2)	3.894	22.82	35.9
(3 3 0)	3.668	24.25	100.0
(4 4 2)	2.398	37.48	29.2

FIGURE 1.17 X-ray powder diffraction of aripiprazole pentahydrate, which had been identified as Form-X in the Teva patent [5].

whose total volatile content was given as 28%. However, this diffraction pattern could not be indexed to a single set of unit cell parameters, and consequently, the diffraction pattern cannot be used to suggest the existence of another solvatomorphic form of aripiprazole. The pattern must be derived from a sample containing a mixture of crystal forms and represents another instance of concomitant crystallization.

ACKNOWLEDGMENT

Special thanks are due to the Cambridge Crystallographic Centre for providing access to the Cambridge Structural Database.

REFERENCES

[1] Y. Oshiro, S. Sato, N. Kurahashi, Carbostyril Derivatives, (1991) United States Patent 5,006,528, issued April 9.

[2] S. Aoki, T. Bando, N. Kobayashi, Study on Crystal Transformation of Aripiprazole, in: Proceedings of the 4th Japan-Korea Symposium on Separation Technology, October 6–8, 1996, pp. 937–940.

[3] R.B. Parthasaradhi, R.K. Rathnakar, R.R. Raji, R.D. Muralidhara, R.K. Subash-Chander, Aripiprazole Crystalline Forms, (2008) United States Patent 7,456,181, issued November 25.

[4] R.B. Parthasaradhi, R.K. Rathnakar, R.R. Raji, R.D. Muralidhara, R.K. Subash-Chander, Crystalline Forms of Aripiprazole, (2009) United States Patent 7,491,726, issued February 17.

[5] J. Aronhime, B.-Z. Dolitzky, E. Luvchick, J. Hildesheim, H. Eisen-Nevo, R. Izsak, Methods of Preparing Aripiprazole Crystalline Forms, (2009) United States Patent 7,504,504, issued March 17.

[6] H. Eisen-Nevo, Z. Pavlov, Methods of Preparing Anhydrous Aripiprazole Form II, (2010) United States Patent 7,714,129, issued May 11.

[7] G.J. Ettema, R. Westheim, F. Kalmoua, Process of Making Crystalline Aripiprazole, (2010) United States Patent 7,642,353, issued January 5.

[8] G.J. Ettema, R. Westheim, F. Kalmoua, Process of Making Crystalline Type II Aripiprazole, (2010) United States Patent 7,655,798, issued February 2.

[9] G.J. Ettema, R. Westheim, F. Kalmoua, Crystalline Aripiprazole Solvates, (2011) United States Patent 7,902,198, issued March 8.

[10] T. Bando, S. Aoki, J. Kawasaki, M. Ishigami, Y. Taniguchi, T. Yabuuchi, K. Fujimoto, Y. Nishioka, N. Kobayashi, T. Fujimura, M. Takahashi, K.K. Abe, T. Nakagawa, K. Shinhama, N. Utsumi, M. Tominaga, Y. Ooi, S. Yamada, T. Kenji, Low Hygroscopic Aripiprazole Drug Substance and Processes for the Preparation Thereof, (2011) United States Patent 7,910,589, issued March 22.

[11] J. Wieser, H. Lengauer, D. Braun, U. Griesser, R. Tessadri, Polymorphic Forms of Aripiprazole and Method, (2011) United States Patent 8,008,490, issued August 30.

[12] K. Dreyer, U. Löffler, K. Glänzer, Amorphous Aripiprazole and Process for the Preparation Thereof, (2010) United States Patent 7,799,790, issued September 21.

[13] K. Stritzke, U. Löffler, K. Glänzer, Amorphous Aripiprazole and Process for the Preparation Thereof, (2010) United States Patent 7,825,125, issued November 2.

[14] L. Tessler, I. Goldberg, Crystal structures of aripiprazole, a new anti-psychotic drug, and of its inclusion compounds with methanol, ethanol and water, J. Incl. Phenom. Macrocycl. Chem. 55 (2006) 255–261.

[15] D.E. Braun, T. Gelbrich, V. Kahlenberg, R. Tessadri, J. Wieser, U.J. Griesser, Conformational polymorphism in aripiprazole: preparation, stability and structure of five modifications, J. Pharm. Sci. 98 (2009) 2010–2026.

[16] D.E. Braun, T. Gelbrich, V. Kahlenberg, R. Tessadri, J. Wieser, U.J. Griesser, Stability of solvates and packing systematics of nine crystal forms of the antipsychotic drug aripiprazole, Cryst. Growth Des. 9 (2009) 1054–1065.

[17] J.W. Visser, A fully automatic program for finding the unit cell from powder data, J. Appl. Cryst. 2 (1969) 89–95.

CHAPTER 2

Amlodipine Besylate

Gennady Ananchenko, Jasmina Novakovic, and **Johnathan Lewis**

Contents

Apotex Inc., Toronto, Ontario, Canada

Profiles of Drug Substances, Excipients, and Related Methodology, Volume 37
ISSN 1871-5125, DOI: 10.1016/B978-0-12-397220-0.00002-7

© 2012 Elsevier Inc.
All rights reserved.

1. GENERAL INFORMATION

Amlodipine besylate is a drug which belongs to calcium channel blockers (CCBs) [1] and is used to treat hypertension. The molecule contains one chiral carbon atom and exists as a racemic mixture. As only the (−)-(*S*)-enantiomer of amlodipine shows the CCB effect [2,3], some properties of the individual enantiomers are included in this profile for comparison. Also, relevant information concerning amlodipine free base is presented.

1.1. Nomenclature

1.1.1. Systematic chemical name

3-Ethyl 5-methyl (4*RS*)-2-[(2-aminoethoxy)methyl]-4-(2-chlorophenyl)-6-methyl-1,4-dihydropyridine-3,5-dicarboxylate benzenesulfonate

2-[(2-Aminoethoxy)methyl]-4-(2-chlorophenyl)-1,4-dihydro-6-methyl-3,5-pyridinedicarboxylic acid 3-ethyl 5-methyl ester benzenesulfonate [1]

1.1.2. Nonproprietary names

Amlodipine besylate, amlodipine benzenesulfonate

1.1.3. Proprietary names

Amlor, Antacal, Istin, Monopina, Norvasc, UK-48340-26

1.2. Formulae

Tables 2.1 and 2.2

TABLE 2.1 Empirical formula, molecular weight, CAS number

Name	Molecular formula	Formula weight	CAS number
Amlodipine	$C_{20}H_{25}ClN_2O_5$	408.88	88150-42-9
(+)-(*R*)-Amlodipine			103129-81-3
(−)-(*S*)-Amlodipine			103129-82-4
Amlodipine besylate	$C_{20}H_{25}ClN_2O_5 \cdot C_6H_6O_3S$	567.05	111470-99-6
(+)-(*R*)-Amlodipine besylate			828247-64-9
(−)-(*S*)-Amlodipine besylate			150566-71-5

1.3. Elemental analysis

Free base: C 58.75%, H 6.16%, Cl 8.67%, N 6.85%, O 19.57%
Besylate salt: C 55.07%, H 5.51%, Cl 6.25%, N 4.94%, O 22.57%, S 5.65%

1.4. Appearance

White or almost white solid.

2. PHYSICAL PROFILE

2.1. Dissociation constant

Amlodipine free base: pK_a, 8.6 [4]; 9.1 (average value used in Ref. [5]).

2.2. Solubility characteristics

Amlodipine besylate: Slightly soluble in water (2.93±0.03 mg/mL at 37 °C [6] and 1.91 g/L at 32 °C [7]) and sparingly soluble in ethanol [1].

2.3. Partition and distribution coefficients

Amlodipine free base
log *P* (octanol/water): 3.00, 2.96 [5]; 3.17 [8]; 1.5 (32 °C) [7]
log *D* (octanol/water) at pH 7.4: 1.41 [8] and 1.11 [9]
Amlodipine besylate
log *P* (octanol/water): 0.65 (32 °C) [7]

TABLE 2.2 Structural formulae and abbreviations used in this profile

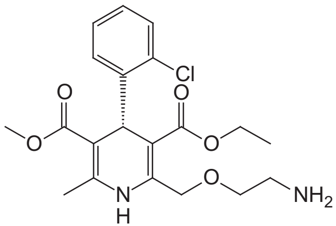	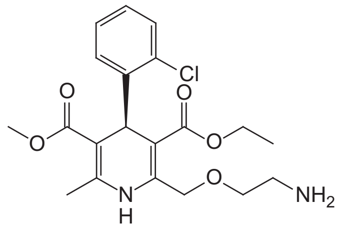	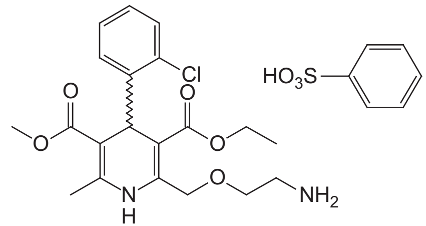
(*S*)-Amlodipine	(*R*)-Amlodipine	Amlodipine besylate
AM		AMB

2.4. Optical activity

(−)-(*S*)-Amlodipine	$[\alpha]_D^{20}$=−19.4 (*c*=0.45 in methanol) [2] $[\alpha]_D^{25}$=−31.9 (*c*=1.0 in methanol) [10] $[\alpha]_D^{25}$=−31.2; −26.4 (*c*=1 in methanol) [11]
(+)-(*R*)-Amlodipine besylate	$[\alpha]_D$=+25.6 (in ethanol) [12]
(−)-(*S*)-Amlodipine besylate	$[\alpha]_D$=−21.0 (in ethanol) [12]
(−)-(*S*)-Amlodipine besylate	$[\alpha]_D$=−21.5 (*c*=1 in methanol), for 98.15% enantiomeric purity [13]
(−)-(*S*)-Amlodipine besylate hemipentahydrate	$[\alpha]_D^{25}$=−26.54 (1% in methanol) [14]

2.5. Crystallographic properties and polymorphism

2.5.1. Single crystal structure

For racemic amlodipine besylate, there is one crystalline form of the anhydrous material characterized by single crystal X-ray diffraction [6,15] (Fig. 2.1). In addition to the anhydrous form, monohydrate and dihydrate forms have been characterized by single crystal and powder X-ray diffraction, as well as by FT-IR and thermal analysis methods [6,16–18]. Both hydrated forms [6] and the anhydrous form (for structures of anhydrous and dihydrate forms, see Figs. 2.1 and 2.2, respectively) reveal a bilayered motif in their crystal structures, where charged (hydrophilic) regions are segregated from hydrophobic regions. This bilayered structure allows one to keep the crystalline forms of hydrated forms intact upon gentle removal of water at about 60 °C or less from the monohydrate [17] or even dihydrate forms [15]. However, heating above this temperature leads to the collapse of these crystalline forms and to formation of the anhydrous form [6,17].

The single crystal structure of enantiomerically pure (−)-(*S*)-amlodipine besylate hemipentahydrate form has also been reported [14].

2.5.2. Powder X-ray diffraction

Powder X-ray diffraction patterns simulated from the single crystal data for the anhydrous and both hydrate forms of amlodipine besylate are shown in Fig. 2.3. The experimental powder X-ray diffraction patterns of the anhydrous and dihydrate forms [6] are in a good agreement with the simulated powder patterns. It should be noted that for the monohydrate form, a disagreement between appearance and positions of some minor peaks was reported [6].

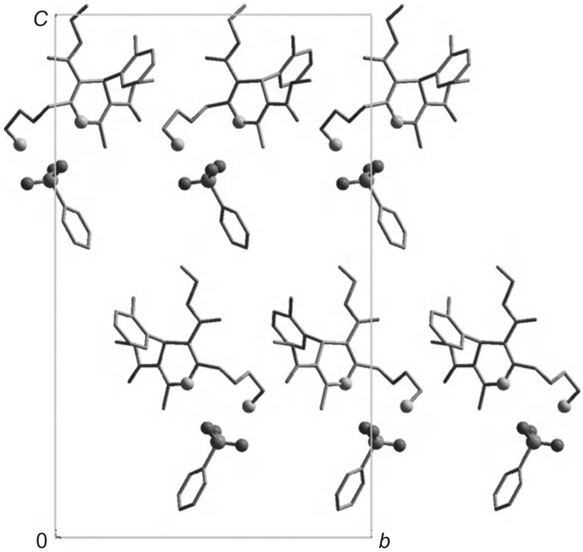

FIGURE 2.1 Slice of the crystal structure of the anhydrous form of amlodipine besylate showing bilayers parallel to the (001) planes (horizontal). Nitrogen atoms of amlodipine as well as oxygen and sulfur atoms of the sulfonate group are shown as ball-and-stick. Hydrogen atoms are omitted for clarity.

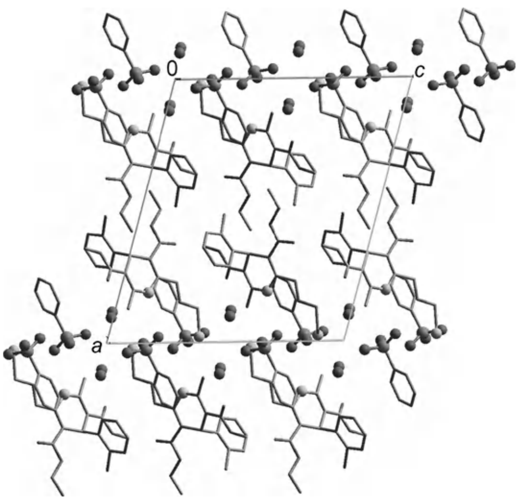

FIGURE 2.2 Slice of the crystal structure of the dihydrate form of amlodipine besylate showing bilayers parallel to the (100) planes (horizontal). Nitrogen atoms of amlodipine, oxygen and sulfur atoms of sulfonate group, and oxygen atom of water are shown as ball-and-stick. Hydrogen atoms are omitted for clarity.

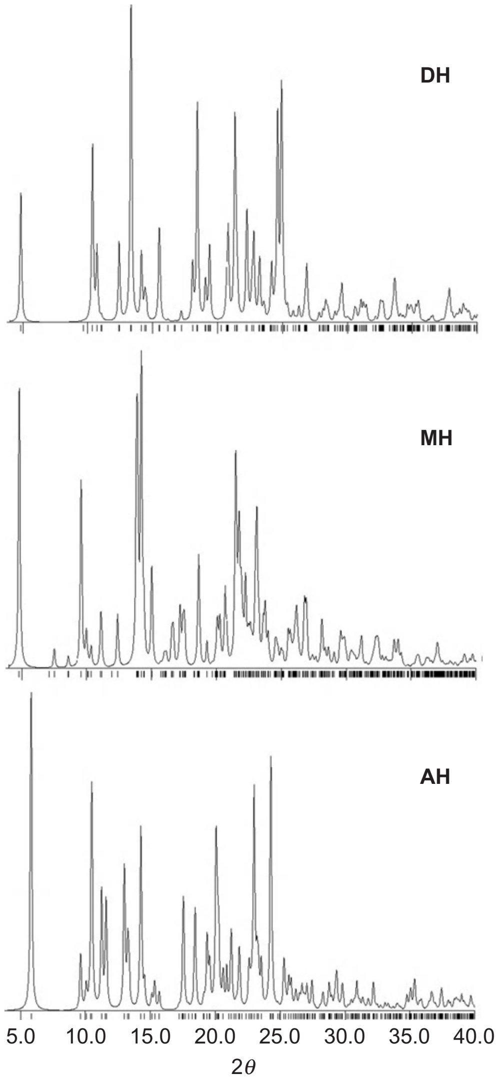

FIGURE 2.3 X-ray powder diffraction patterns of amlodipine besylate solid forms calculated from the single crystal data [6,15]. DH, dihydrate form; MH, monohydrate form; and AH, anhydrous form.

2.6. Hygroscopicity

Amlodipine free base is not hygroscopic. The ability of amlodipine besylate to uptake water strongly depends on the crystalline form of the material. The stable anhydrous form of amlodipine besylate was stored for almost 2 months at 92% relative humidity and 25°C without a significant water uptake [17]. Slow transformation of the anhydrous amlodipine

besylate or its monohydrate form to the dihydrate occurs if the material is placed directly in water [18]. However, if water has been gently removed from the monohydrate form leaving the crystal structure intact, the rehydration takes only a few minutes if stored at 92% relative humidity [17].

2.7. Thermal methods of analysis

The melting point of Amlodipine free base determined by differential scanning calorimetry (DSC) is 141 °C. The thermal behavior of racemic amlodipine besylate strongly depends on the presence of solvent (water). The melting of hydrate forms is observed between 80 and 100 °C in the hot-stage microscopy [6] and in the DSC thermograms of MH and DH forms [6,17] and corresponds to the loss of water. The formed melt crystallizes at 135 °C to the anhydrous form of amlodipine besylate. The melting of the anhydrous form is observed in the DSC thermograms as an endothermic peak at about 201 °C [6,17]. Amorphous form exhibits a glass transition around 75 °C followed by crystallization at 135 °C to the anhydrous form [6].

Two hydrate forms of (−)-(*S*)-amlodipine besylate, dihydrate [19] and hemipentahydrate [14], have been isolated. The reported melting points determined in an open capillary are 68–70 and 60–63 °C, respectively. It was pointed out [14] that (−)-(*S*)-amlodipine besylate hemipentahydrate is unstable under elevated temperature and becomes a dark yellow to greenish solid. One can expect that the two forms are equivalent; however, there is no enough support for this conclusion from the literature [14,19].

2.8. Spectroscopy

2.8.1. UV spectroscopy

Amlodipine free base
UV max (methanol): 210 nm (ε=1.9×10^4), 237 nm (ε=2.0×10^4), 360 nm (ε=6.8×10^3)
Amlodipine besylate
UV max (1.1N HCl): 213 nm (ε=2.4×10^4), 238 nm (ε=1.9×10^4), 360 nm (ε=6.6×10^3)

2.8.2. Vibrational spectroscopy

The infrared spectra of amlodipine free base and anhydrous amlodipine besylate (Figs. 2.4 and 2.5) were obtained from potassium bromide pellets using a Perkin-Elmer Paragon 16PC and Perkin-Elmer Paragon 1000 PC FT-IR spectrometers, respectively (Table 2.3).

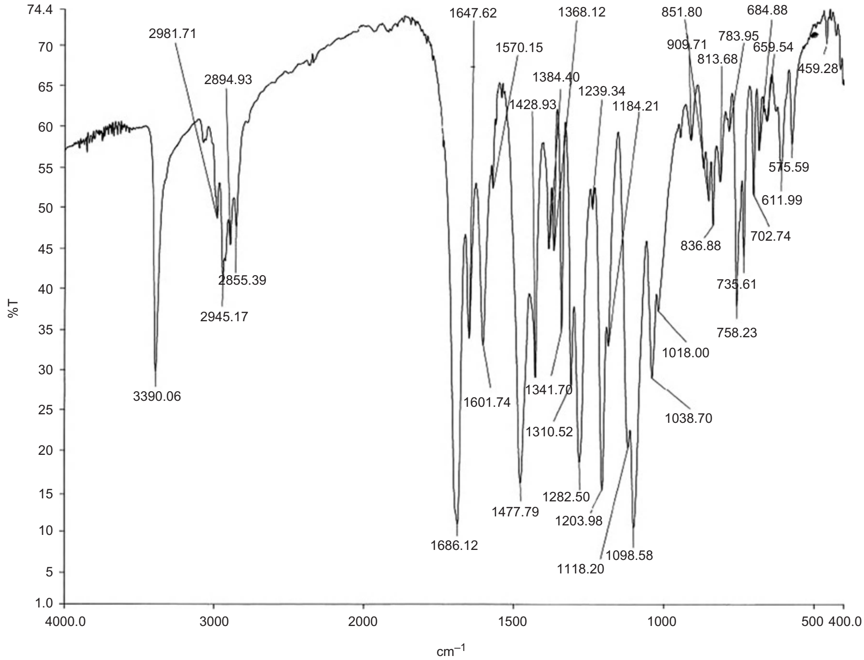

FIGURE 2.4 FT-IR spectrum of amlodipine free base.

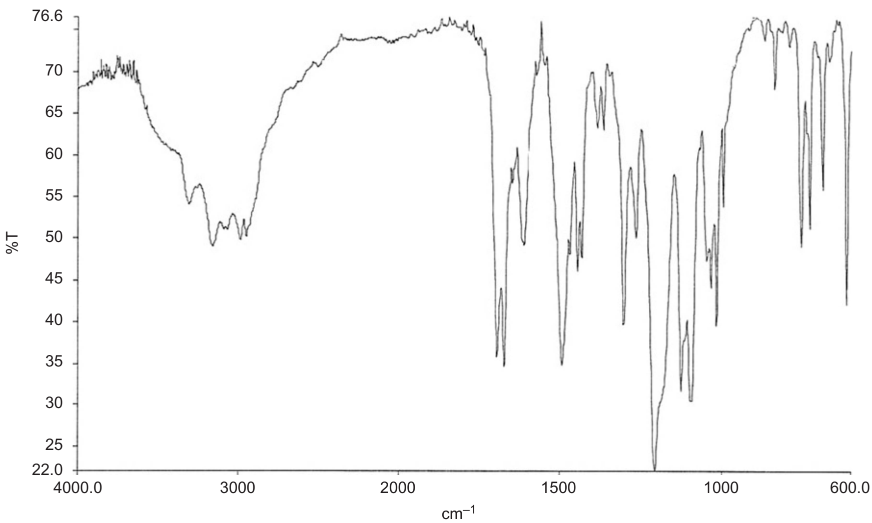

FIGURE 2.5 FT-IR spectrum of anhydrous amlodipine besylate.

TABLE 2.3 Assignments of amlodipine and amlodipine besylate's absorption bands

Assignments[a]	Wavenumber (cm^{-1}) Amlodipine base	Amlodipine besylate[b]
Amine, dihydropyridine, and ammonium (N—H) stretches	3390	3297
Aromatic (C—H) stretch	~3075, ~3065	3158
Aliphatic (C—H) stretch	2982, 2945, 2895, 2855	2982
Ester carbonyl (C=O) stretches	1686	1698, 1676
Enamine (C=C) stretch	1648	
Aromatic skeletal stretches	1602, *1478*	1614, 1493
CH_3, CH_2 bending	*1478*	1445, 1432
Ester (C—O) asymmetric and symmetric stretches, ether (C—O—C) asymmetric stretch	1283, 1204, 1118, *1099*	*1207*, 1126, *1095*
Sulfonate (S=O) asymmetric stretch	–	*1207*
Sulfonate (S=O) symmetric stretch	–	*1095*
Aromatic (C—Cl) stretch	*1099*	*1095*
Ether (C—O—C) symmetric stretch	1039, 1018	1034, 1018
Aromatic (C—H) bending	758, 736, 612	755, 730, 615

[a] Bands with ambiguous assignment are italicized.
[b] Alternative assignments of some bands are made in Ref. [6], Supporting Information. Also, Ref. [20] contains assignments based on the density functional theory (DFT) calculations.

2.8.3. Nuclear magnetic resonance spectroscopy

^{1}H and ^{13}C NMR data for amlodipine besylate (including separated enantiomers) have been reported in various solvents, such as deuterated chloroform [14,21], methanol [22], dimethyl sulfoxide (DMSO-d_6) [19,20], as well as in the solid state [21]. Also, ^{15}N NMR chemical shifts of amlodipine free base (N1, 121.1 ppm; N10, 14.1 ppm with the reference to liquid NH_3) and of amlodipine besylate (N1, 121.1 ppm; N10, 24.8 ppm) have been reported [22]. Refer to Fig. 2.6 for the atom numbering in amlodipine besylate. Figures 2.7 and 2.8 and Tables 2.4 and 2.5 provide comparison of ^{1}H and ^{13}C chemical shifts of amlodipine free base and amlodipine besylate in DMSO-d_6. For this Profile, the ^{1}H and ^{13}C NMR spectra were obtained on a Bruker Avance 400 instrument using DMSO-d_6 as the solvent. Chemical shifts are reported in parts per million relative to TMS as internal standard.

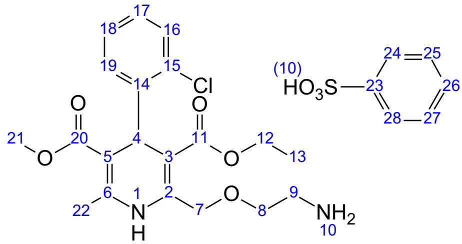

FIGURE 2.6 Atom numbering in amlodipine besylate.

2.8.3.1. ^{1}H NMR spectrum Figure 2.7

2.8.3.2. ^{13}C NMR spectrum Figure 2.8

2.8.4. Mass spectrometry

The electrospray ionization mass spectroscopic study of amlodipine free base was carried out on a Perkin-Elmer/Sciex API-300 triple quadrupole mass spectrometer. The sample was dissolved in methanol and injected into a 5-mL sample loop of the mass spectrometer and carried into ionization source by the mobile phase (1:1 mixture of methanol and 0.1% aqueous acetic acid) at a flow rate of 200 μL/min (Figs. 2.9 and 2.10).

The fragmentation pathway via retro-Diels–Alder cleavage of the parent protonated molecular ion (m/z=409) shown in Scheme 2.1 generally agrees with that discussed in Refs. [23,24], although some variations in the assignments of ions with m/z=248 and 238 are possible [23].

3. STABILITY

Reactivity of amlodipine and its salts is determined mainly by the presence of the dihydropyridine ring and amino group in the molecule. Oxidative aromatization of dihydropyridine fragment (Scheme 2.2) to the pyridine moiety is one of the main degradation pathways of amlodipine [25,26] and related molecules of 1,4-dihydropyridine family (such as nifedipine [27], etc.) and occurs both in solution and in solid state and is promoted by light.

The amino group in amlodipine molecule is another reactive moiety, which is responsible for degradation of amlodipine in the presence of reducing sugars via Maillard reaction [28]. Therefore, a special attention should be paid to pharmaceutical formulations of amlodipine besylate with reducing sugars especially in the presence of basic excipients and

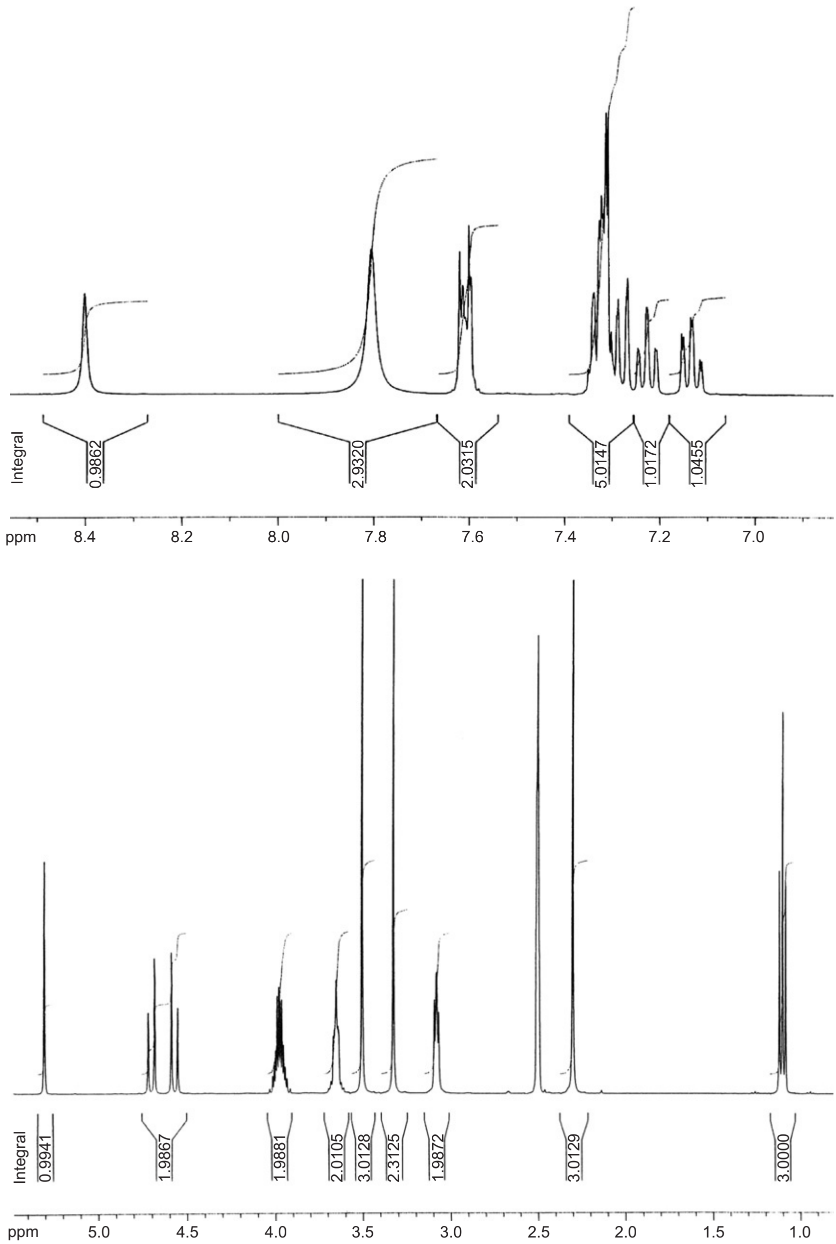

FIGURE 2.7 ^{1}H NMR spectrum (DMSO-d_6, 400 MHz) of anhydrous amlodipine besylate (top, 8.6–6.8 ppm; bottom, 5.5–0.9 ppm).

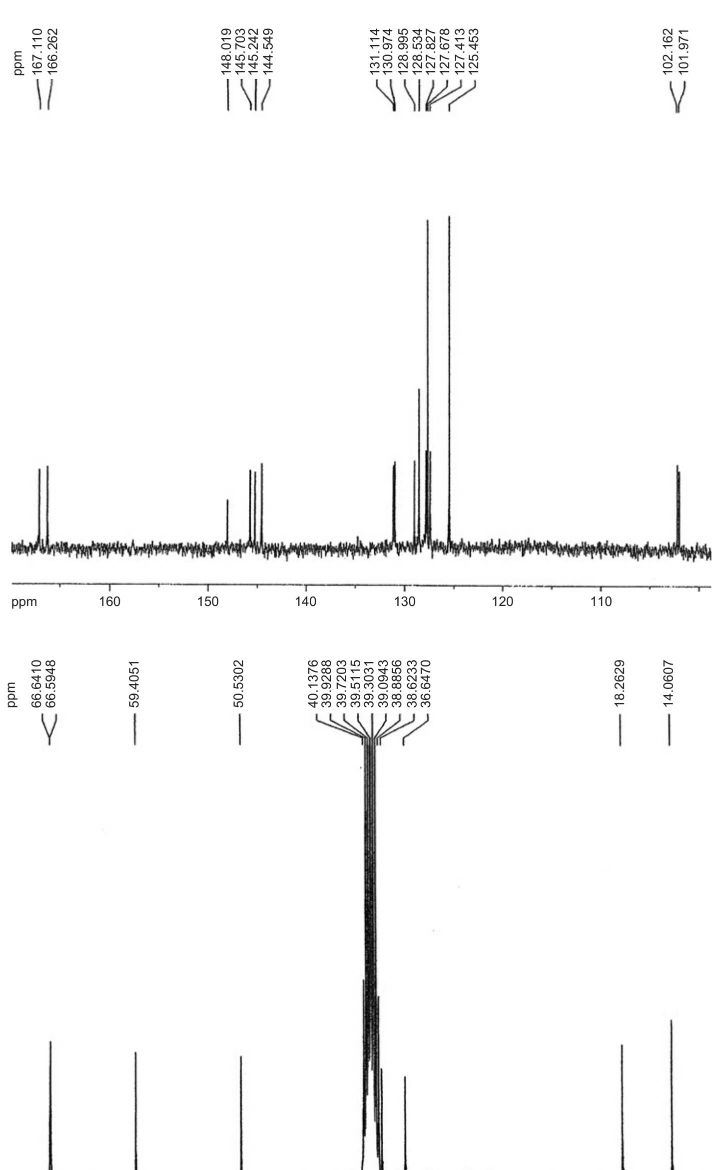

FIGURE 2.8 ^{13}C NMR spectrum (DMSO-d_6, 101 MHz) of anhydrous amlodipine besylate (top, 170–99 ppm; bottom, 70–11 ppm).

TABLE 2.4 Assignment of the resonances in ^{1}H NMR (400 MHz, DMSO-d_6) spectrum of amlodipine free base and amlodipine besylate

	AM		AMB	
Proton at carbon or heteroatom	ppm	Multiplicity, spin–spin coupling (Hz), integration	ppm	Multiplicity, spin–spin coupling (Hz), integration
H1	3.6–3.0	br[a]	8.40	br s, 1H
H10			7.80	br s, 3H
H24/H28	–	–	7.62–7.60	m, 2H
H25–H27	–	–	7.35–7.30	m, 5H
H19	7.35	d, J=7.5, 1H		
H16	7.26	d, J=7.9, 1H	7.28	d, J=7.7, 1H
H18	7.22	t, J=7.4, 2H	7.23	t, J=7.3, 1H
H17	7.11	t, J=7.2	7.13	dt, J=7.6, J=1.3
H4	5.30	s, 1H	5.30	s, 1H
H7	4.65	d, J=15.3 2H total	4.69	d, J=14.3 2H total
	4.57	d, J=15.3	4.57	d, J=14.3
H12	4.02–3.91	sym. m, 2H	4.03–3.92	sym. m, 2H
H21	3.50	s, 3H	3.50	s, 3H
H8	3.44	t, J=5.1, 2H	3.69–3.61	m, 2H
H9	2.73	t, J=5.1, 2H	3.08	t, J=5.1, 2H
H22	2.30	s, 3H	2.30	s, 3H
H13	1.10	t, J=7.0, 3H	1.10	t, J=7.1, 3H

br, broad; s, singlet; d, doublet; t, triplet; m, multiplet; sym, symmetric.
[a] Accurate integration is not possible due very broad nature of the signal and overlap with H8 and H21.

water. The adduct of amlodipine besylate with lactose (Scheme 2.3) has been identified by LC/MS [28].

Intramolecular cyclization (Scheme 2.4) is another possible degradation pathway of amlodipine [29] driven by the ''appropriate'' length of the side substituent and again by the presence of amino group, although the reaction requires significant heating (110–140 °C) and is expected to occur to a minor extent in the formulated product.

Even though a different salt of amlodipine, namely maleate [30], seems to be stable enough for use in the pharmaceutical formulations, it was recently pointed out [31] that amlodipine can react with maleic acid giving a product of the Michael addition (Scheme 2.5).

Besides these reactions, the stability of amlodipine besylate in solutions is strongly pH-dependent giving rise to a number of various degradation products not always detectable by HPLC-UV when using the same

TABLE 2.5 Assignment of the resonances in ^{13}C NMR (101 MHz, DMSO-d_6) spectrum of Amlodipine free base and amlodipine besylate

	ppm			ppm	
Assignment	AM	AMB	Assignment	AM	AMB
C20	167.20	167.11	C18	127.36	127.41
C11	166.35	166.26	C24/C28	–	125.45
C2	146.31	144.55	C5	101.86	102.16, 101.97
C14	146.00	145.70	C3	101.41	
C6	145.57	145.24	C8	73.13	66.64, 66.59
C23	–	148.02	C7	66.65	
C26	–	128.53	C12	59.21	59.41
C25/C27	–	127.68	C21	50.44	50.53
C15	131.09	131.11	C9	40.90	38.62
C19	131.03	130.97	C4	36.74	36.64
C16	128.92	129.00	C22	18.01	18.26
C17	127.68	127.83	C13	14.07	14.06

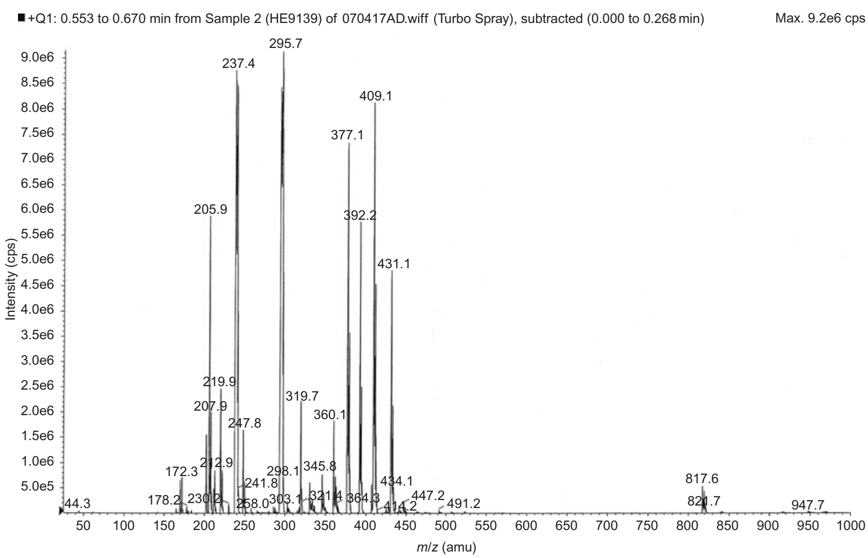

FIGURE 2.9 Electrospray ionization mass spectrum of amlodipine base.

detection wavelength as that utilized for amlodipine [28]. It is also worth mentioning that in solution amlodipine besylate is most stable in the vicinity of pH 5 based on the stability studies performed in phosphate buffer solutions [28].

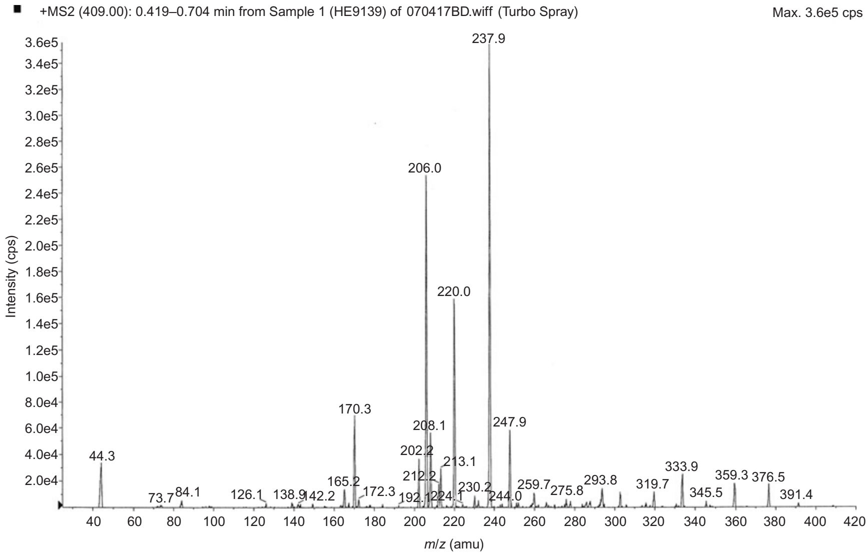

FIGURE 2.10 Tandem mass spectrum of the protonated molecular ion (m/z 409) of amlodipine.

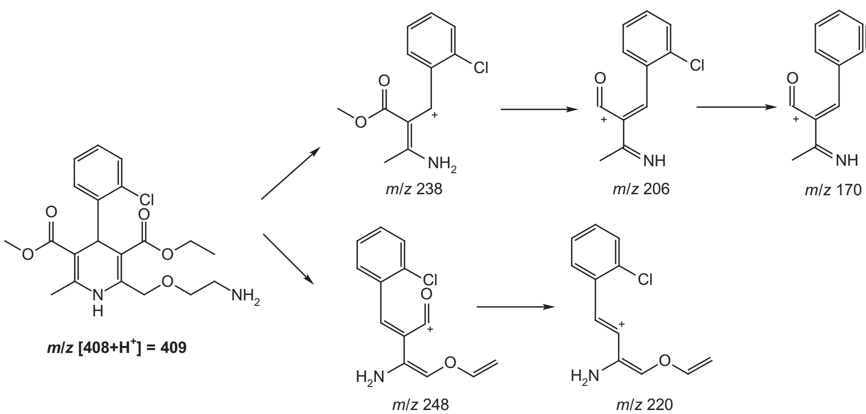

SCHEME 2.1 Fragmentation pathways of the protonated molecular ion of amlodipine.

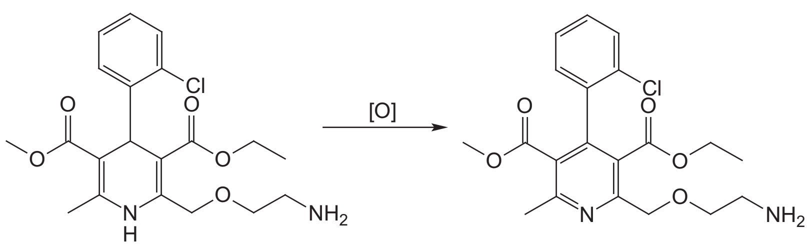

SCHEME 2.2 Oxidation of amlodipine.

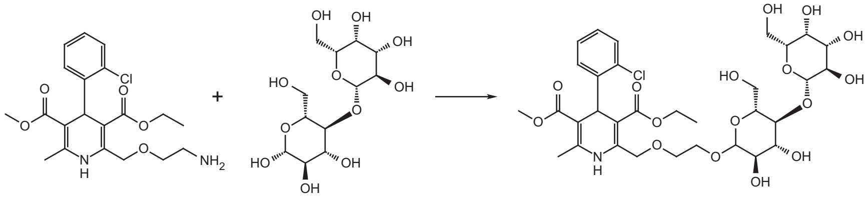

SCHEME 2.3 Condensation of amlodipine with lactose [28].

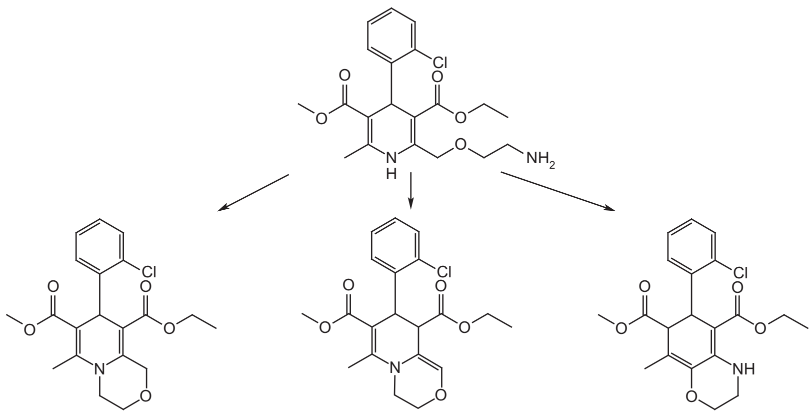

SCHEME 2.4 Intramolecular cyclization of amlodipine.

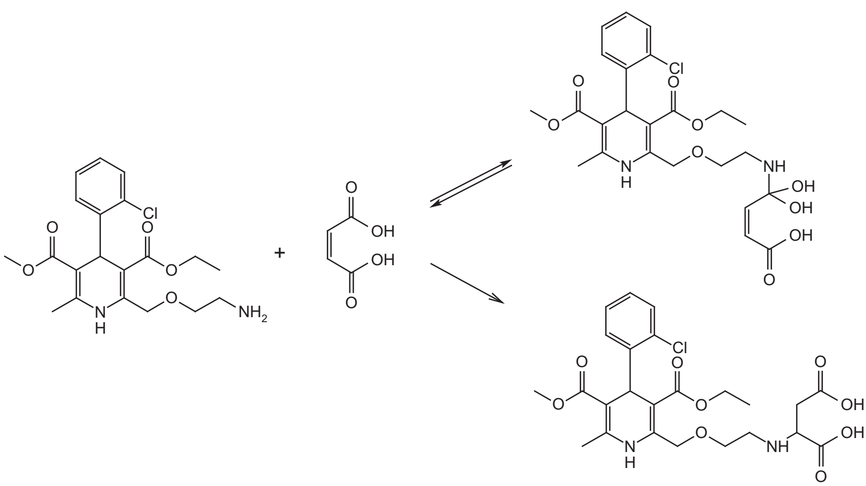

SCHEME 2.5 Reaction of amlodipine with maleic acid.

4. METHODS OF CHEMICAL SYNTHESIS

One of the first methods of amlodipine synthesis (Scheme 2.6) is based on the Hantzsch condensation of the azido-substituted derivative of acetoacetic ester (**1**) with methyl (2-chlorobenzylidene)acetoacetate (**2**) followed by reduction of the azido group to give amlodipine (**4**), which was isolated as a maleate salt [30]. Reduction of the azido group was also performed using Zn and hydrochloric acid [32]. The besylate salt of amlodipine was first mentioned in Ref. [33].

Some variations of this synthetic scheme were performed, such as three-component synthesis of the azido intermediate **3**, as shown in Scheme 2.7 [32].

Alternatively (Scheme 2.8), phthalimido derivative **5** can be used instead of azido derivative **1** in the three-component condensation followed by removal of the phthalimido-protecting group using hydrazine hydrate or ethanolic methylamine or KOH followed by acidification with HCl to give amlodipine **4** [32].

In order to simplify the deprotection step, trityl protection of amino functionality was proposed [22] as alternative to azido or phthalimido groups. After Hantzsch condensation of the corresponding precursors, the trityl intermediate was converted into amlodipine besylate by reaction with benzenesulfonic acid in methanol (Scheme 2.9).

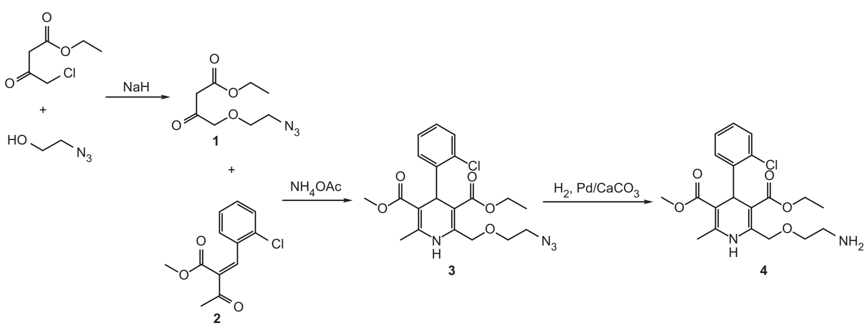

SCHEME 2.6 Hantzsch condensation followed by reduction of the azido group in the synthesis of Amlodipine.

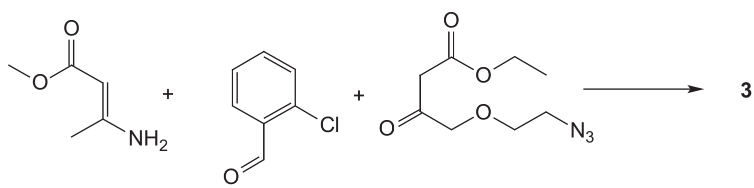

SCHEME 2.7 Three-component synthesis of the azido intermediate 3.

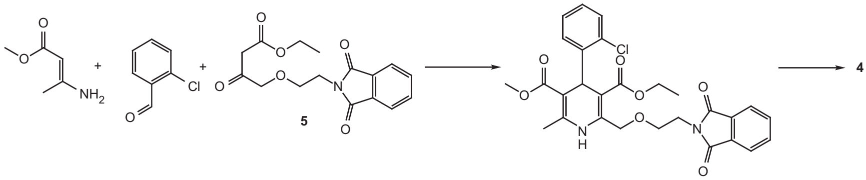

SCHEME 2.8 Three-component condensation using the phthalimido precursor.

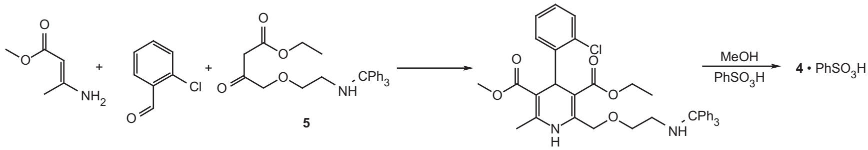

SCHEME 2.9 Three-component condensation using the trityl protected amino precursor.

As an alternative to Hantzsch condensation, aza-Diels–Alder cycloaddition under conventional [34] or microwave [35] heating was proposed for the synthesis of dihydropyridine moiety (Scheme 2.10). The reaction is highly regioselective (**8**:**9**>50:1) in case of conventional heating [34] and less regioselective (**8**:**9**=7:3) with microwave-assisted Diels–Alder reaction. Separation of regioisomer **8** from **9**, followed by removal of benzyl group using formic acid and Pd/C, yields intermediate **10** which after side-chain transformation furnishes amlodipine **4**:

5. ANALYTICAL PROFILE

5.1. Impurities of amlodipine besylate

Table 2.6 summarizes the impurities currently listed in the United States and the European Pharmacopeias (USP [36] and EP [37]). The origin of impurities potentially present in amlodipine besylate drug substance and amlodipine besylate tablets can be derived from the main amlodipine synthetic route and degradation pathways (Sections 4 and 3, respectively). Amlodipine pyridine analog is listed in both pharmacopoeias. It is the main degradation product of amlodipine and also the main metabolite of amlodipine (see Section 6.3). EP impurities A, B, H, E, F, and G are synthetic impurities; however, a very minor transformation of amlodipine into impurities E and F under some storage conditions cannot be completely ruled out. Formulation-specific impurities—products of Maillard reaction of amlodipine with sugars mentioned in

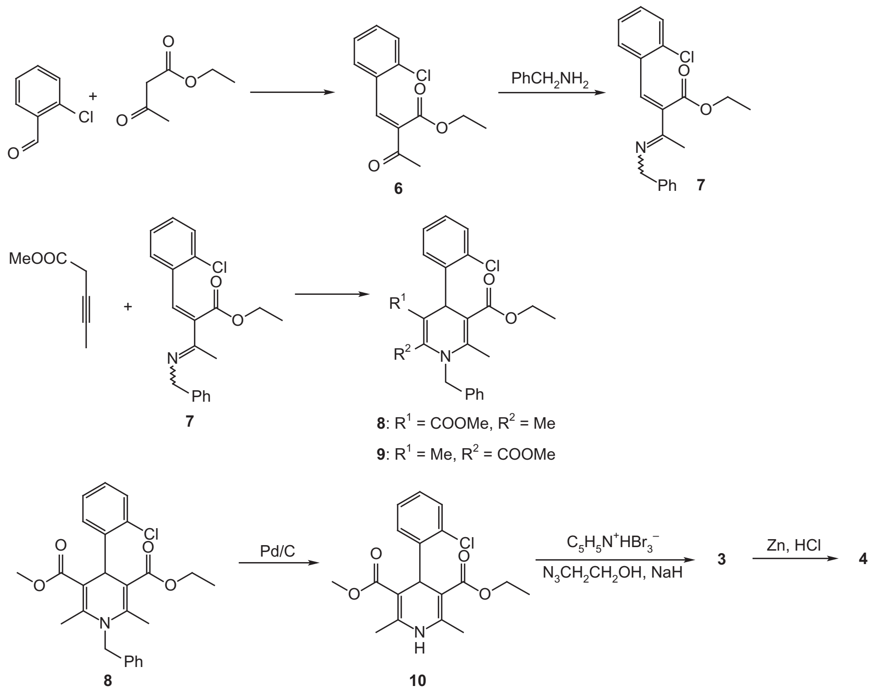

SCHEME 2.10 Synthesis of Amlodipine via azo-Diels-Alder cycloaddition.

Section 3—are listed in the recently updated USP monograph for amlodipine besylate tablets [38]. Their structures are not shown in Table 2.6, since the corresponding monograph does not specify structural details of adducts.

5.2. Compendial tests

Tests and limits listed in the USP and EP monographs for amlodipine besylate drug substance and for amlodipine besylate tablets are listed in Tables 2.7 and 2.8, respectively. Table 2.9 provides details on the pharmacopeial chromatographic methods used for assay and impurities testing.

5.3. Other methods

Many analytical methods have been developed for determination of amlodipine in bulk drug, formulations (single or in combination with other cardiovascular drugs), and biological matrices, such as blood, urine, and tissues. The overview of the analytical methods, grouped based on the techniques and listed chronologically, is presented in Tables 2.10–2.16.

TABLE 2.6 Related compounds of amlodipine besylate listed in USP and EP

Structure (R=2-chlorophenyl)	Amlodipine besylate drug substance USP 34 [36]	EP 7.0 [37]	Amlodipine besylate tablets USP 34 S2 [38]
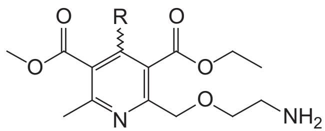	Amlodipine Impurity A	Impurity D	Amlodipine-related compound A
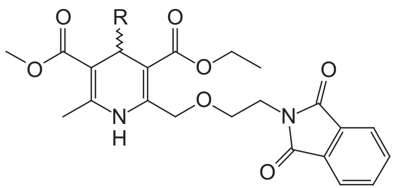	–	Impurity A	–
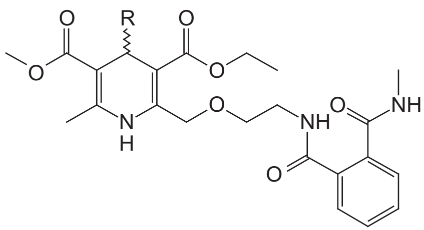	–	Impurity B	–

(*continued*)

TABLE 2.6 (*continued*)

Structure (R=2-chlorophenyl)	Amlodipine besylate drug substance USP 34 [36]	Amlodipine besylate drug substance EP 7.0 [37]	Amlodipine besylate tablets USP 34 S2 [38]
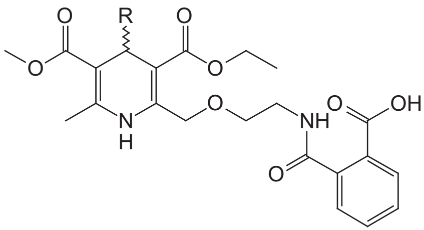	–	Impurity H	–
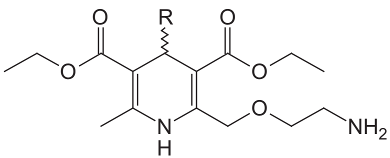	–	Impurity E	–

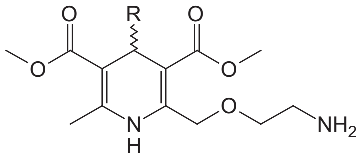	–	Impurity F	–
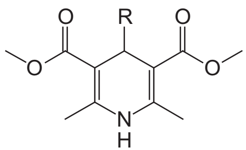	–	Impurity G	–
Amlodipine lactose adduct	–	–	Formulation-specific impurities
Amlodipine glucose/galactose adduct	–	–	

TABLE 2.7 Compendial tests and limits for amlodipine besylate drug substance

Test	USP 34 [36]	EP 7.0 [37]
Identification by IR (compared with amlodipine besylate reference standard spectrum)	⟨197M⟩ (sample prepared in mineral oil)	(2.2.24) (sample prepared in suitable liquid)
Identification by HPLC	The retention time of the major peak in the chromatogram of the assay preparation corresponds to that in the chromatogram of the standard preparation, as obtained in the assay	No requirement
Optical rotation (to confirm the racemic nature of the drug substance)	⟨781A⟩ −0.10 to +0.10 Measured at 20°C for 10 mg/mL solution of amlodipine besylate in methanol	(2.2.7) −0.10 to +0.10 Measured for 10 mg/mL solution of amlodipine besylate in methanol
Water content	⟨921⟩ Method I Anhydrous form: no more than 0.5% Hydrated form: 3.1–5.0%	(2.5.12) Maximum 0.5%
Residue on ignition	⟨281⟩ No more than 0.2%	Sulfated Ash (2.4.14) No more than 0.2% determined on 1.0 g
Heavy metals	⟨231⟩ Method II no more than 0.002%	No requirement
Assay (by HPLC)	97.0–102.0% (anhydrous basis)	97.0–102.0% (anhydrous substance)
Related compounds (refer to Table 2.6 for names)	Amlodipine Impurity A: no more than 0.3% Total of other impurities: no more than 0.3%	Impurity A: no more than 0.15% Impurity D: no more than 0.3% Impurity E: no more than 0.15% Impurity F: no more than 0.15% Unspecified impurity: no more than 0.10% each Total impurities: no more than 0.8%

TABLE 2.8 Compendial tests and limits for amlodipine besylate tablets

Test	USP 34 S2 [38]
Identification by UV	⟨197U⟩ Standard solutions (referred to dissolution test): 0.00695 mg/mL for tablets labeled to contain 2.5 mg; 0.0139 mg/mL for tablets labeled to contain 5 mg; 0.0278 mg/mL for tablets labeled to contain 10 mg
Identification by HPLC	The retention time of the major peak of the sample solution corresponds to that of the standard solution, as obtained in the assay
Dissolution	⟨711⟩ Medium: 0.01 N hydrochloric acid; 500 mL Apparatus 2, 75 rpm (use paddles covered with Teflon or made of any inert material except stainless steel) Quantitation by UV absorbance at about 239 nm (1 cm quartz cell) Time, 30 min; tolerance, no less than 75% (*Q*)
Uniformity of dosage units	⟨905⟩: meet the requirements
Assay (by HPLC)	90.0–110.0% of the labeled amount of amlodipine
Organic impurities (refer to Table 2.6 for names)	Amlodipine related compound A: no more than 1.0% Amlodipine lactose adduct: no more than 0.5% Amlodipine glucose/galactose adduct: no more than 0.5% Any other individual unspecified degradation product: no more than 0.20%

6. ADME

Amlodipine besylate is a dihydropyridine CCB with distinctive pharmacokinetic characteristics which appear to be attributed to a high degree of ionization of this drug [75]. Amlodipine is used as mono or combination therapy as first-line treatment of angina pectoris and hypertension. Amlodipine is available as racemate and, in some countries, also as (−)-(*S*)-enantiomer [3]. The pharmacological activity resides primarily in the (−)-(*S*)-enantiomer [2,3,30]. A single-dose pharmacokinetics of the racemic amlodipine in healthy volunteers has been described by several groups of authors [76–79].

TABLE 2.9 Compendial chromatographic methods for assay and impurity analysis

Method	Mobile phase	UV detection (nm)	Test and sample	References
USP ⟨621⟩, TLC, Absorbent: 0.25-mm layer of silica gel	Developing solvent: methyl isobutyl ketone–water–AcOH (50:25:25 v/v/v)	254	Impurities in drug substance	[36] Test 1
HPLC, Column: 3.9 mm × 15 cm with Waters symmetry or Nova-Pak C18	Buffer (7.0 mL TEA in water, adjusted to pH 3.0 using phosphoric acid, diluted to 1 L)–MeOH–acetonitrile (50:35:15 v/v/v)	237	Assay and Impurities in drug substance and tablets	[36] Test 2; [38]
HPLC, Column: 4.0 mm × 0.25 m, C18	2.3 g/L ammonium acetate and MeOH (30:70 v/v)	237	Assay and impurities in drug substance	[37]

6.1. Absorption

In healthy volunteers, Amlodipine is well absorbed following oral administration of 10 mg single dose resulting in moderately high absolute bioavailability of 64% without excessive inter-subject variability (range 52–88%). Following administration of a single 10 mg oral dose, the mean time to peak concentration (T_{max}) of 7.6 and 6.4 h is reported [76,78]. Mean T_{max} values, ranged from 5.6 to 6.4 h, were observed after oral administration of 2.5, 5, and 10 mg of amlodipine single dose [78]. The dose-related difference in the T_{max} is not significant.

6.2. Distribution

The apparent volume of distribution, observed in healthy volunteers following administration of 10 mg intravenous (i.v.) dose, was reported to be 21.4 ± 4.4 L/kg [76,77]. The large volume of distribution indicates that the drug distributes extensively into tissue compartments. After i.v. dosing, the initial decrease in plasma concentration is rapid and movement of

TABLE 2.10 GC and GC-MS methods

Method	Detection	Matrix/selectivity	Linearity; LOD/LOQ	Ref.
GC following trimethylacetyl derivatization	ECD	Human plasma	0.2–2 mg/mL; LOQ<0.1 ng/mL (lower range); 2–20 ng/mL; LOQ<1 ng/mL (upper range)	[39]
GC	MS using ^{14}C-labeled drug	Human/rat/dog urine; amlodipine metabolites	–	[40]
Enantioselective GC following conversion into acyl derivatives with chiral Mosher's reagent	ECD	Human/rat/dog/plasma/rat organs	LOD for each enantiomer: 0.02 ng/mL	[41]
GC	ECD	Human plasma and gingival crevicular fluid	LOD: 0.5 μg/L	[42]
GC after extractive methylation	MS	Urine/amlodipine/other CCB drugs	–	[43]

TABLE 2.11 HPLC and LC-MS methods

Stationary phase	Mobile phase	Detection	Matrix/selectivity	Linearity; LOD/LOQ	Ref.
C18	0.05 M phosphate buffer (pH 3.1)–acetonitrile (65:35 v/v)+sodium octane sulfonate (0.005 M)+EDTA (5 mg/L)	Amperometric, glassy carbon as working electrode and Ag/AgCl as reference electrode	Rat/human serum	0.2–2 ng/mL	[44]
C18	Methanol–0.04 M ammonium acetate–acetonitrile (38:38:24 v/v/v)+0.02% TEA (final pH 7.1)	UV at 240 nm	Rabbit plasma	2.5–100 ng/mL	[26]
Phenyl (Zorbax SB-phenyl)	Methanol–0.1 M acetate buffer (pH 4.0) (65:35 v/v)+2 mM SDS+1 mg/L EDTA	Amperometric	Human plasma	0.5–10 ng/mL	[45]
α_1-Scid glycoprotein (Chiral–AGP) followed by achiral HPLC (Zorbax SB-Ph)	Chiral: 50 mM acetate buffer (pH 3.9)+0.3% *n*-propanol+5 mM TBAHS Achiral: Methanol–0.1 M acetate buffer (pH 4.0) (55:45 v/v)+EDTA 10 mg/L and 5 mM TBAHS	Amperometric	Human plasma	0.5–10 ng/mL; LOD: 0.2 ng/mL	[46]
C18	10 mM ammonium acetate (pH 4)–methanol (33:67 v/v)	Tandem MS–APCI, selective reactive monitoring mode	Rat serum	0.014–7.2 ng/mL; LOQ: 0.014 ng/mL	[24]

C18	Acetonitrile–water (60:40 v/v)+10mM formic acid	Tandem MS with positive ESI using multiple reaction monitoring	Human plasma	LOQ: 0.1ng/mL	[47]
Chiral AGP column containing α1-acid glycoprotein	10mM acetate buffer (pH 4.5)–1-propranol (99:1 v/v)	Tandem MS with APCI, selected reaction monitoring mode	Human plasma/ stereoselective	LOQ: 0.1ng/mL	[48]
C18	Acetonitrile–methanol–pH 3.0, triethylamine solution (15:35:50 v/v/v)	UV at 237nm	Manufacturing equipment—Swabs	0.39–1.56μg/mL; LOD: 0.02μg/mL LOQ: 0.08μg/mL	[49]
C18	(A) 0.04M ammonium acetate–methanol–acetonitrile (30:30:40 v/v/v); (B) 1% acetic acid–methanol (1:1 v/v)	(A) UV at 240nm; (B) MS at 2kV soft ionization with positive mode	Compatibility study with excipients	–	[28]
C18	1% triethylamine (pH 3.0)–acetonitrile (65:35 v/v)	UV at 220nm	Alkyl benzenesulfonates in AMB	75–180ppm; LOQ: 21–35ppm	[50]
UPLC: C8 (100mm×2.1mm, 1.7μm)	Phosphate buffer, pH 3.0–mixture 1:1 methanol+acetonitrile (45:55 v/v)	UV at 237nm	AMB and benazepril hydrochloride capsules	AMB: 5.21–15.63μg/mL LOQ: 0.01μg/mL	[51]

TABLE 2.12 Planar chromatography methods

Technique	Detection	Matrix/selectivity	Linearity; LOD/LOQ	Reference
HPTLC on Silica-gel 60 F254 stationary phase and chloroform–methanol–acetic acid (15:2:0.4 v/v/v) mobile phase	Densitometric, UV at 365nm	Human plasma	2–100ng (per spot)	[52]
HPTLC on Silica-gel 60 F254 stationary phase and methylene chloride–methanol–25% ammonia solution (8.8:1.3:0.1 v/v/v) mobile phase	Densitometric, UV at 230nm	Dosage form: atenolol+amlodipine tablets	10–500 μg/mL (10 μL sampling volume)	[53]
(a) HPTLC on Silica-gel 60 F254 stationary phase and *n*-butanol–acetic acid–water (5:1:0.1 v/v/v) mobile phase	(a) Densitometric, UV at 254nm	Bulk drug and formulation: AMB and Olmesartan Medoxomil	(a) AMB: 100–1000 ng/spot	[54]

(b) HPLC on C18 column and acetonitrile–ammonium acetate buffer, pH 3 (55:45 v/v)	(b) UV at 254 nm		(b) –	
(a) TLC on Silica-gel 60 F254 stationary phase and ethyl acetate–methanol–ammonium hydroxide (55:45:5 v/v/v) mobile phase	(a) Densitometric, UV at 237 nm	Bulk powder and formulation: AMB and valsartan	(a) AMB: 0.5–4.0 μg/spot	[55]
(b) HPLC on C18 column and methanol–acetonitrile–water–0.05% triethylamine (40:20:30:10 v/v/v/v, pH 3.0)	(b) UV at 237 nm		(b) AMB: 0.2–2 μg/mL	

TABLE 2.13 Capillary electrophoresis (CE) and related techniques

Technique	UV detection	Matrix/selectivity	Linearity; LOD/LOQ	References
CE in acetate running buffer, pH 3.6, positive pressure injection (30 mbar), 20 kV potential applied to the electrodes, electrophoresis time 15 min	254 nm	Rat serum	–	[56]
Stereoselective CE with cyclodextrin as chiral selector in running buffer (100 mM phosphate buffer, pH 3.0) performed on uncoated fused silica capillary (49 cm effective length)	237 nm	AMB enantiomers/tablets	5–150 µg/mL LOD: 0.5 µg/mL	[57]
Stereoselective CE with 5 mM hydroxypropyl-α-cyclodextrin as chiral selector in the running buffer (100 mM phosphate, pH 2.0)	214 nm	Enantiomers/human plasma and urine	15–500 ng/mL (urine); 20–500 ng/mL (plasma) LOD: 3 ng/mL LOQ: 10 ng/mL	[58]
CE in phosphate running buffer, pH 8.0, performed on fused silica capillary (47 cm × 50 µm inner diameter, 40 cm effective length)	214 nm	AMB and valsartan/tablets/human plasma	AML:1.0–35 mg/L LOD: 0.03 mg/L LOQ: 0.09 mg/L	[59]

TABLE 2.14 Spectroscopic techniques

Technique	Detection	Matrix/selectivity	Linearity; LOD/LOQ	Ref.
Two spectrophotometric methods based on (1) complexation with bromothymol blue and (2) formation of oxidative coupling product with 3-methyl-2-benzothiazolinone hydrazone	405 nm (1) and 630 nm (2)	Drug substance/AMB tablets	5–40 μg/mL for both (1) and (2)	[60]
Spectrophotometry after complex formation with *p*-chloranilic acid	540 nm	AMB in the presence of excipients	100–600 μg/mL LOD: 2.46 μg/mL	[61]
Spectrophotometry after derivatization with ninhydrin	595 nm	Pharmaceutical preparations/ tablets	10–60 μg/mL	[62]
Derivative spectrophotometry, third order	200–400 nm	AM and its pyridine photodegradation product (AMLOX)	AMLOX in 40 μg/mL AM solution: LOD: 0.15 μg/mL LOQ: 0.45 μg/mL	[25]
Spectrophotometry after reaction with iron(III) and its reduction to iron (II) and subsequent derivatization with ferricyanide resulting in Prussian blue formation	760 nm	AMB and felodipine tablets	AMB:LOD: 0.13 μg/mL LOQ: 0.43 μg/mL	[63]

(*continued*)

TABLE 2.14 (*continued*)

Technique	Detection	Matrix/selectivity	Linearity; LOD/LOQ	Ref.
Two spectrophotometric methods after reaction with (1) 2,3-dichloro 5,6-dicyano 1,4-benzoquinone (DDQ) and (2) ascorbic acid (AA)	(1) 580 nm (with DDQ) (2) 530 nm (with AA)	AMB tablets	1–125 μg/mL (1); 10–140 μg/mL (2)	[64]
Two spectrofluorimetric methods based on reaction of amlodipine with (1) ninhydrin and phenylacetaldehyde and (2) 7-chloro-4-nitro-2,1,3-benzoxadiazole (NBD-Cl)	(1) λ_{ex}=375 nm, λ_{emiss}=480 nm; (2) λ_{ex}=480 nm, λ_{emiss}=535 nm	AMB tablets	0.35–1.8 μg/mL (1); 0.55–3.0 μg/mL (2) LOD: 0.09 μg/mL (1); 0.16 μg/mL (2)	[65]
Quantitative UV spectroscopy in 0.05% bromo phenol blue/pH 2.4 buffer solution	413 nm	Drug substance/tablets	4–20 μg/mL	[66]
UV spectroscopy in sodium acetate solution	365 nm	Drug substance/tablets	50–250 μg/mL	[67]
Teraherz (THz) absorption spectroscopy to evaluate aging of drug product	3–100 cm^{-1}	AMB tablets	–	[68]

TABLE 2.15 Electrochemical determination

Technique	Experimental conditions	Matrix/selectivity	Linearity; LOD/LOQ	Ref.
Differential pulse voltammetry with a glassy carbon electrode based on the oxidation of dihydropyridine group on the surface of the electrode under stationary and rotating conditions	Supporting electrolyte: 0.2M KCl in 0.1M phosphate buffer and 10% methanol; 0mV most suitable initial potential; pH~5.5 is optimal	N/A	LOD: 0.004mg/mL (rotating technique) 0.0072mg/mL (stationary technique) LOQ: 0.012mg/mL (rotating technique) 0.022mg/mL (stationary technique)	[69]
Adsorptive square-wave anodic stripping voltammetry on glassy carbon electrode	Working electrode: glassy carbon rotating disc; Reference electrode: Ag/AgCl/saturated KCl; Auxiliary electrode: Platinum wire; Supportive electrolyte: Briton-Robinson buffer pH 11	Tablets/human urine and serum	4.0×10^{-8}–2.0×10^{-6}M; LOD: 1.4×10^{-8}M	[70]

(*continued*)

TABLE 2.15 (*continued*)

Technique	Experimental conditions	Matrix/selectivity	Linearity; LOD/LOQ	Ref.
Ratio-voltammetric methods, based on first derivative ratio of differential pulse (DP) and square-wave (SW) voltammetry	Working electrode: glassy carbon; reference electrode: Ag/AgCl/3M KCl; counter electrode: platinum wire	AMB and atorvastatin calcium binary mixture/tablets	Amlodipine: 4×10^{-6}–1×10^{-4}M; LOD: $\sim8\times10^{-7}$M LOQ: $\sim3\times10^{-6}$M	[71]
Cyclic and square-wave voltammetry using single and multi-walled carbon nanotubes modified edge plane pyrolytic graphite electrodes (SWNT/EPPGE and MWNT/EPPGE)	Working electrode: SWNT or MWNT modified EPPGE; reference electrode: Ag/AgCl/3M NaCl; auxiliary electrode: platinum wire; phosphate buffer, pH 7.2	AMB in tablets and human urine	5.0×10^{-9}–1.0×10^{-6}M; LOD: SWNT/EPPGE 1.0×10^{-9}M MWNT/EPPGE 5.0×10^{-9}M	[72]

TABLE 2.16 Enzyme-immunoassay methods

Technique	Experimental conditions	Matrix/selectivity	Linearity; LOD/LOQ	Ref.
Enzyme-linked immunosorbent assay (ELISA)	Anti-amlodipine antibodies (Ab) raised in rabbits against BSA–amlodipine conjugate were used. Amlodipine standard (diluted in buffer or heparinized plasma) is added (50 μL/well), followed by 50 μL/well anti-amlodipine antibodies, incubated for 1 h at 22°C, the absorbance was read at 405 and 600 nm	Human plasma/free amlodipine, bioequivalence study	0.5–40 ng/mL; LOD: 0.1 ng/mL	[73,74]

drug from the blood to tissue seems to be complete or nearly complete, depending on the individual, at 0.75–2h post dose [76]. Amlodipine is 97% bound to plasma proteins [77]. Enantioselective disposition of oral amlodipine in healthy volunteers following administration of single 20mg dose of racemic drug was studied by Laufen and Leitold [80]. Mean plasma concentrations of the pharmacologically active (−)-(*S*)-enantiomer were significantly higher than that of the inactive (+)-(*R*)-enantiomer. Stereoselective plasma protein binding of amlodipine was studied *in vitro* by equilibrium dialysis and upon application of racemic amlodipine besylate [81]. (−)-(*S*)-Amlodipine was bound to higher extend by human serum albumin and human plasma comparing with (+)-(*R*)-enantiomer.

6.3. Metabolism

Metabolism of amlodipine is extensive but relatively slow, and unlike other dihydropiridines, amlodipine is subject to scant first-pass or presystemic metabolism. The initial metabolic aromatization of the dihydropyridine ring is followed by further metabolism involving side-chain oxidation and hydrolysis of the side-chain esters groups (Table 2.17) [40,75,82]. Metabolic transformations of the side chains without aromatization of the dihydropyridine ring were observed in dogs and rats [83,84] and can be expected in humans [75]. None of the metabolites have significant calcium antagonist activity [75]. Only small amounts of unchanged drug are excreted in the urine.

Table 2.17 contains structures of amlodipine metabolites. The structures are grouped based on the possible precursors in the metabolism (from left to right and from top to bottom). Metabolic transformations can affect each site of the dihydropyridine ring independently (columns 2 and 3) or simultaneously (column 4).

6.4. Elimination

Following i.v. administration of radioactively labeled amlodipine, 62% of the dose was recovered in the human urine and the reminder in the feces. Only about 5% of the dose was excreted unchanged in the human urine [85]. A similar excretion pattern was observed after oral dosing. Amlodipine is slowly cleared from the body with the elimination half-life of 40−50h [75].

6.5. Effect of food

Absolute bioavailability of amlodipine upon oral administration is unaffected by food [86]. Grapefruit juice can alter oral drug pharmacokinetics due to irreversible inactivation of intestinal CYP3A4 as well as by inhibiting

TABLE 2.17 Structures of Amlodipine metabolites identified by GC/MS and LC/MS in human [40,82] (R=2-chlorophenyl)

Aromatization	Methyl/methyl ester site transformations	Aminoethyl/ethyl ester site transformations	Both sites transformations
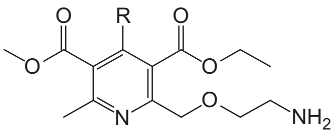	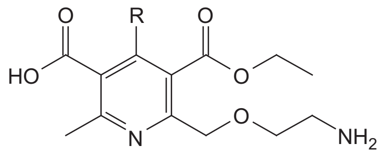	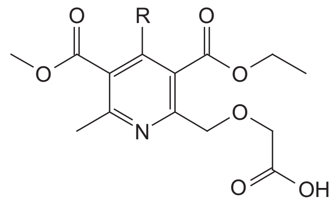	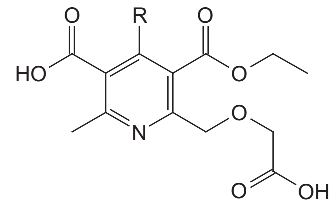
			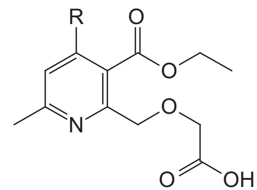
			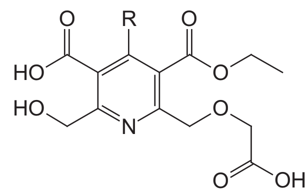

(*continued*)

TABLE 2.17 (*continued*)

Aromatization	Methyl/methyl ester site transformations	Aminoethyl/ethyl ester site transformations	Both sites transformations
		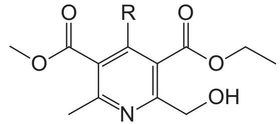	
		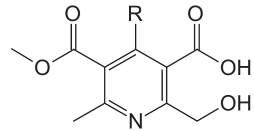	
		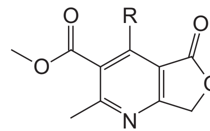 [a]	
		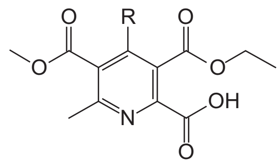	

[a] Product of thermal lactonization under GC/MS conditions rather than a metabolite [40].

P-glycoprotein and subsequently reducing intestinal and/or hepatic efflux transport. Effect of ingestion of grapefruit juice on pharmacokinetics and pharmacodynamics of amlodipine was studied by different groups of authors [87–90]. The clinical significance of once daily intake of grapefruit juice on amlodipine pharmacokinetics and pharmacodynamics was found to be negligible, and a more extensive intake might result in a more pronounced effect. Bioavailability of amlodipine besylate following oral administration as a tablet dispersed in applesauce is unchanged in comparison with drug administered with water [91].

6.6. Pharmacokinetics in special population

Study in elderly normotensive population showed that upon administration of a single 5mg oral dose, the terminal elimination half-life was greater (48h) in comparison with younger subjects (~30–40h), indicating reduced clearance which may lead to higher plasma concentrations at steady state [79].

Amlodipine pharmacokinetics, studied in hypertensive patients following administration of oral 10mg dose, revealed a terminal elimination $t_{1/2}$, $T_{\max}$, and $C_{\max}$ of about 37h, 7.4h, and 6ng/mL, respectively [92], indicating no changes in the pharmacokinetics parameters in comparison to healthy volunteers. In hypertensive patients undergoing hemodialysis, only minor differences were observed in comparison to healthy volunteers and no need for dose adjustment was indicated [93]. Study in hypertensive children and adolescents demonstrated that in young children (1 to <6 years) amlodipine weight-adjusted clearance and the volume of distribution are significantly different than in adolescents and adults, and therefore, higher doses may be suggested when treating young children [94].

6.7. Concurrent administration with other drugs

Concomitant treatment with amlodipine and other antihypertensive or lipid-lowering drugs is a common strategy to manage hypertension and reduce factors contributing to cardiovascular risk. Evaluation of pharmacokinetic interactions between amlodipine, valsartan, and hydrochlorothiazide revealed no clinically relevant interactions [95]. Combination of amlodipine besylate and Olmesartan Medoximil is also shown not to have impact on the pharmacokinetic profiles of individual drugs [96]. Concomitant amlodipine and atorvastatin treatment in patients with hypertension and dyslipidemia was shown to be well tolerated and without adverse pharamacodynamic interaction [97]. Triple combination Olmesartan Medoxomil/amlodipine/hydrochlorothiazide is demonstrated to be safe as well [98].

6.8. Pharmacological effects and daily dosage

Amlodipine is an intrinsically long-acting, vasoselective dihydropyridine calcium antagonist that inhibits calcium ion influx across cell membranes selectively, with a greater effect on vascular smooth muscle cells than on cardiac muscle cells. Amlodipine possesses unique pharmacological properties that distinguish it from other agents of this class, such as more prolonged half-life, high volume of distribution, and gradual elimination. These properties are attributed to the high degree of ionization (>90% at physiologic pH) due to presence of a basic side chain at the dihydropyridine ring.

Amlodipine is indicated for treatment of hypertension and stable angina. The recommended initial dose of amlodipine besylate is 5 mg once daily. If necessary, dose can be increased after 1–2 weeks to a maximum dose of 10 mg once daily.

ACKNOWLEDGMENTS

The authors are indebted to Dr. Pradeep Sanghvi for encouragement and management support. We also wish to express our sincere appreciation to Dr. Yuri Goldberg for his guidance, to Ms. Janet Mensah for her assistance in retrieving literature cited, to Dr. Konstantin Udachin for fruitful discussion on X-ray data, and lastly to many colleagues in our laboratories who contributed material needed for the preparation of this chapter.

REFERENCES

[1] The Merck Index, an Encyclopedia of Chemicals, Drugs, and Biologicals, 14th ed., Merck & Co., Inc, Whitehouse Station, NJ, 2006 monograph 491, p. 83.
[2] S. Goldmann, J. Stoltefuss, L. Born, Determination of the absolute configuration of the active amlodipine enantiomer as (−)-(S): a correction, J. Med. Chem. 35 (1992) 3341–3344.
[3] H.P. Thacker, S-amlodipine—the 2007 clinical review, J. Indian Med. Assoc. 105 (2007) 180–190.
[4] A.C. Moffat, M.D. Osselton, B. Widdop, J. Watts. Clarke's analysis of drugs and poisons, Fourth ed. , vol. 2, Pharmaceutical Press, London, Chicago, 2011, pp. 889–890.
[5] G. Caron, G. Ermondi, A. Damiano, L. Novaroli, O. Tsinman, J.A. Ruell, A. Avdeef, Ionization, lipophilicity, and molecular modeling to investigate permeability and other biological properties of amlodipine, Bioorg. Med. Chem. 12 (2004) 6107–6118.
[6] V. Koradia, H. Lopez de Diego, K. Frydenvang, M. Ringkjøbing-Elema, A. Müllertz, A.D. Bond, J. Rantanen, Solid forms of amlodipine besylate: physicochemical, structural, and thermodynamic characterization, Cryst. Growth Des. 10 (2010) 5279–5290.
[7] Y. Jiang, L. Fang, X. Niu, R. Ma, Z. He, The effect of ion pairing on the skin permeation of amlodipine, Pharmazie 63 (2008) 356–360.
[8] U. Franke, A. Munk, M. Wiese, Ionization constants and distribution coefficients of phenothiazines and calcium channel antagonists determined by a pH-Metric method and correlation with calculated partition coefficients, J. Pharm. Sci. 88 (1999) 89–95.
[9] R.P. Austin, A.M. Davis, C.N. Manners, Partitioning of ionizing molecules between aqueous buffers and phospholipid vesicles, J. Pharm. Sci. 84 (1995) 1180–1183.

[10] S.Y. Jang, S. Kim, S. Yun, H.J. Bang, H.K. Kim, K.H. Suh, US2010/0099884.
[11] Y.-S. Chung, M.-C. Ha, WO2004/024689.
[12] J. Lukša, D.j. Josić, B. Podobnik, B. Furlan, M. Kremser, Semi-preparative chromatographic purification of the enantiomers S-(−)-amlodipine and R-(+)-amlodipine, J. Chromatogr. B 693 (1997) 367–375.
[13] R.J.M. Rohini, A.J.M. Ramesh, K.G.M. Mukund, US6608206, 2003.
[14] D.M. Gotrane, R.D. Deshmukh, P.V. Ranade, S.P. Sonawane, B. Bhaval, M.M. Gharpure, M.K. Gurjar, A novel method for resolution of amlodipine, Org. Proc. Res. Dev. 14 (2010) 640–643.
[15] G.J.B. Ettema, H. Hoorn, J.M. Lemmens, US2003139455.
[16] Z. Ham, B. Furlan, A. Copar, U. Urleb, WO03/101965.
[17] J.M. Rollinger, A. Burger, Physico-chemical characterization of hydrated and anhydrous crystal forms of amlodipine besylate, J. Therm. Anal. Calorim. 68 (2002) 361–372.
[18] V. Koradia, A.F.F. de Lemos, M. Allesø, H.L. de Diego, M. Ringljøbing-Elema, A. Müllertz, J. Rantanen, Phase transformations of amlodipine besylate solid forms, J. Pharm. Sci. 100 (2011) 2896–2910.
[19] H.W. Lee, S.J. Shin, H. Yu, S.K. Kang, C.L. Yoo, A novel chiral resolving reagent, bis((*S*)-mandelic acid)-3-nitrophthalate, for amlodipine racemate resolution: scalable synthesis and resolution process, Org. Proc. Res. Dev. 13 (2009) 1382–1386.
[20] L. Szabó, V. Chiş, A. Pîrnă, N. Leopold, O. Cozar, Sz. Orosz, Spectroscopic and theoretical study of amlodipine besylate, J. Mol. Struct. 924–926 (2009) 385–392.
[21] J.N. Latosińska, ^{13}C CP MAS NMR and DFT study of vascular-selective drugs felodipine and amlodipine, Chem. Phys. Lett. 463 (2008) 195–200.
[22] B. Furlan, S.G. Grdadolnik, S. Hočevar, D. Kocjan, J. Levec, H. Maskill, H. Navrátilová, J. Pospíšil, M. Potáček, U. Urleb, J. Žmitek, Amlodipine benzenesulfonate: a mechanistic investigation of its industrial preparation via detritylation of N-tritylamlodipine and related NMR studies, Croat. Chem. Acta 82 (2009) 299–309.
[23] J. Gibbons, J. Pugh, G. Dimopoulos-Italiano, R. Pike, A qualitative study of amlodipine and its related compounds by electrospray ionization tandem mass spectrometry, Rapid Commun. Mass Spectrom. 20 (2006) 1715–1723.
[24] T. Yasuda, M. Tanaka, K. Iba, Quantitative determination of amlodipine in serum by liquid chromatography with atmospheric pressure chemical ionization tandem mass spectrometry, J. Mass Spectrom. 31 (1996) 879–884.
[25] G. Ragno, A. Garofalo, C. Vetuschi, Photodegradation monitoring of amlodipine by derivative spectrophotometry, J. Pharm. Biomed. Anal. 27 (2002) 19–24.
[26] P.K.F. Yeung, S.J. Mosher, P.T. Pollak, Liquid chromatography assay for amlodipine: chemical stability and pharmacokinetics in rabbits, J. Pharm. Biomed. Anal. 9 (1991) 565–571.
[27] G.S. Sadana, A.B. Ghogare, Quantitative proton magnetic resonance spectroscopic determination of nifedipine and its photodecomposition products from pharmaceutical preparation, J. Pharm. Sci. 80 (1991) 895–898.
[28] A. Abdoh, M.M. Al-Omari, A.A. Badwan, A.M.Y. Jaber, Amlodipine besylate–excipients interaction in solid dosage form, Pharm. Dev. Technol. 9 (2004) 15–24.
[29] A. Siva Lakshmi Devi, Y. Srinivasa Rao, M. Satish, G. Jyothi, K. Babu Rao, T. Omdutt, Structure elucidation of thermal degradation products of amlodipine, Magn. Reson. Chem. 45 (2007) 688–691.
[30] J.E. Arrowsmith, S.F. Campbell, P.E. Cross, J.K. Stubbs, R.A. Burges, D.G. Gardiner, K.J. Blackburn, Long-acting dihydropyridine calcium antagonists. 1,2-Alkoxymethyl derivatives incorporating basic substituents, J. Med. Chem. 29 (1986) 1696–1702.
[31] C. Pan, F. Liu, M. Motto, Identification of pharmaceutical impurities in formulated dosage forms, J. Pharm. Sci. 100 (2011) 1228–1259.
[32] S.F. Campbell, P.E. Cross, J.K. Stubbs, EP 0089167, 1983.

[33] M.E. Davison, J.I. Wells, US 4879303, 1989.
[34] S.-C. Kim, K.-M. Choi, C.-S. Cheong, Synthesis of amlodipine using Aza Diels-Alder reaction, Bull. Kor. Chem. Soc. 23 (2002) 143–144.
[35] Y.A. Lee, S.-C. Kim, Synthesis of 1,4-dihydropyridine using microwave-assisted aza-Diels–Alder reaction and its application to Amlodipine, J. Ind. Eng. Chem. 17 (2011) 401–403.
[36] Amlodipine Besylate, U.S. Pharmacopeia—National Formularly, USP34/NF29, The United States Pharmacopoeial Convention, 2010, pp. 1872–1873.
[37] Amlodypine Besilate, European Pharmacopoeia 7.0, Council of Europe, 2010, pp. 1379–1380.
[38] Amlodipine Besylate Tablets, Second Supplement to the U.S. Pharmacopeia—National Formulary, USP34/NF29, The United States Pharmacopoeial Convention, 2011, pp. 5379–5380.
[39] A.P. Beresford, P.V. Macrae, D.A. Stopher, B.A. Wood, Analysis of amlodipine in human plasma by gas chromatography, J. Chromatogr. 420 (1987) 178–183.
[40] A.P. Beresford, P.V. Macrae, D. Alker, R.J. Kobylecki, Biotransformation of amlodipine. Identification and synthesis of metabolites found in rat, dog and human urine/confirmation of structures by gas chromatography-mass spectrometry and liquid chromatography-mass spectrometry, Arzneimittelforschung 39 (1989) 201–209.
[41] F. Scharpf, K.D. Riedel, H. Laufen, M. Leitold, Enantioselective gas chromatographic assay with electron-capture detection for amlodipine in biological samples, J. Chromatogr. B 655 (1994) 225–233.
[42] S.C. Monkman, J.C. Ellis, S. Cholerton, J.M. Thomason, R.A. Seymour, J.R. Idle, Automated gas chromatographic assay for amlodipine in plasma and gingival crevicular fluid, J. Chromatogr. B 678 (1996) 360–364.
[43] H.H. Mauer, J.W. Arlt, Screening procedure for detection of dihydropyridine calcium channel blocker metabolites in urine as part of a systematic toxicological analysis procedure for acidic compounds by gas chromatography-mass spectrometry after extractive methylation, J. Anal. Toxicol. 23 (1999) 73–80.
[44] K. Shimooka, Y. Sawada, H. Tatematsu, Analysis of amlodipine in serum by a sensitive high-performance liquid chromatographic method with amperometric detection, J. Pharm. Biomed. Anal. 7 (1989) 1267–1272.
[45] M. Josefsson, A.L. Zackrisson, B. Norlander, Sensitive high-performance liquid chromatographic analysis of amlodipine in human plasma with amperometric detection and a single-step solid-phase sample preparation, J. Chromatogr. B 672 (1995) 310–313.
[46] M. Josefsson, B. Norlander, Coupled-column chromatography on a chiral-AGP phase for determination of amlodipine enantiomers in human plasma: an HPLC assay with electrochemical detection, J. Pharm. Biomed. Anal. 15 (1996) 267–277.
[47] M. Carvalho, C.H. Oliviera, G.D. Mendes, M. Sucupira, M.E. Moraes, G. De Nucci, Amlodipine bioequivalence study: quantification by liquid chromatography coupled to tandem mass spectrometry, Biopharm. Drug Dispos. 22 (2001) 383–390.
[48] B. Streel, C. Lainé, C. Zimmer, R. Sibenaler, A. Ceccato, Enantiomeric determination of amlodipine in human plasma by liquid chromatography coupled to tandem mass spectrometry, J. Biochem. Biophys. Methods 54 (2002) 357–368.
[49] R. Klinkenberg, B. Streel, A. Ceccato, Development and validation of a liquid chromatographic method for the determination of amlodipine residues on manufacturing equipment surfaces, J. Pharm. Biomed. Anal. 2 (2003) 345–352.
[50] N.V.V.S.S. Raman, K. Ratnakar Reddy, A.V.S.S. Prasad, K. Ramakrishna, Development and validation of RP-HPLC method for the determination of genotoxic alkyl benzenesulfonates in amlodipine besylate, J. Pharm. Biomed. Anal. 48 (2008) 227–230.
[51] G.B. Kasawar, M.N. Farooqui, Simultaneous determination of amlodipine besylate and benazepril hydrochloride in pharmaceutical dosage form by LC, Anal. Sci. 25 (2009) 1495–1498.

[52] K.L. Pandya, M. Satia, T.P. Gandhi, I.A. Modi, R.I. Modi, B.K. Chakravarthy, Detection and determination of total amlodipine by high-performance thin-layer chromatography: a useful technique for pharmacokinetic studies, J. Chromatogr. B 667 (1995) 315–320.
[53] A.P. Argekar, S.G. Powar, Simultaneous determination of atenolol and amlodipine in tablets by high-performance thin-layer chromatography, J. Pharm. Biomed. Anal. 21 (2000) 1137–1142.
[54] A.Y. Kamble, M.V. Mahadik, L.D. Khatal, S.R. Dhaneshwar, Validated HPLC and HPTLC method for simultaneous quantitation of amlodipine besylate and olmesartan medoxomil in bulk drug and formulation, Anal. Lett. 43 (2010) 251–258.
[55] N.S. Ramadan, H.M. Mohamed, A.A. Moustafa, Rapid and highly sensitive HPLC and TLC methods for quantitation of amlodipine besilate and valsartan in bulk powder and in pharmaceutical dosage forms and in human plasma, Anal. Lett. 43 (2010) 570–581.
[56] S.A. Rozhnova, M.V. Gavrilin, S.P. Senchenko, A.B. Krikova, Use of capillary electrophoresis in studies of the pharmacokinetics of amlodipine besylate, Pharm. Chem. J. 41 (2007) 444–446.
[57] A.R. Fakhari, S. Nojavan, S. Haghgoo, A. Mohammadi, Development of a stability-indicating CE assay for the determination of amlodipine enantiomers in commercial tablets, Electrophoresis 29 (2008) 4583–4592.
[58] S. Nojavan, A.R. Fakhari, Electro membrane extraction combined with capillary electrophoresis for the determination of amlodipine enantiomers in biological samples, J. Sep. Sci. 33 (2010) 3231–3238.
[59] A.O. Alnaijar, Validation of a capillary electrophoresis method for the simultaneous determination of amlodipine besylate and valsartan in pharmaceuticals and human plasma, J. AOAC Int. 94 (2011) 498–502.
[60] K. Sridhar, C.S.P. Sastry, M.N. Reddy, D.G. Sankar, K.R. Srinivas, Spectrophotometric determination of amlodipine besylate in pure forms and tablets, Anal. Lett. 30 (1997) 121–133.
[61] N. Rahman, S.N.H. Azmi, Spectrophotometric determination of amlodipine besylate by charge transfer complex formation with p-chloranilic acid, Anal. Sci. 16 (2000) 1353–1356.
[62] N. Rahman, S.N.H. Azmi, Spectrophotometric method for the determination of amlodipine besylate with ninhydrin in drug formulations, Farmaco 56 (2001) 731–735.
[63] K. Basavaiah, U. Chandrashekar, H.C. Prameela, Sensitive spectrophotometric determination of amlodipine and felodipine using iron(III) and ferricyanide, Farmaco 58 (2003) 141–148.
[64] N. Rahman, M. Nasrul Hoda, Validated spectrophotometric methods for the determination of amlodipine besylate in drug formulations using 2,3-dichloro 5,6-dicyano 1,4-benzoquinone and ascorbic acid, J. Pharm. Biomed. Anal. 31 (2003) 381–392.
[65] H.M. Abdel-Wasood, N.A. Mohamed, A.M. Mahmoud, Validated spectrofluorometric methods for determination of amlodipine besylate in tablets, Spectrochim. Acta A 70 (2008) 564–570.
[66] A. Ali, K. Pasha, S.A. Raju, A. Ahmed, Visible spectrophotometric determination of amlodipine in pharmaceutical formulation and bulk drug by using bromophenol blue, Int. J. Pharmacol. Pharm. Sci. 2 (2010) 128–129.
[67] N. Jain, R. Jain, A. Jain, S.P. Pandey, D.K. Jain, Spectrophotometric method development and validation for quantitative estimation of amlodipine besylate in bulk drug and their dosage forms by using hydrotropic agent, Eurasian J. Anal. Chem. 5 (2010) 212–217.
[68] M. Kawase, T. Saito, M. Ogawa, H. Uejima, Y. Hatsuda, S. Kawanishi, Y. Hirotani, M. Myotoku, K. Ikeda, H. Konishi, I. Iga, J. Yamakawa, S. Nishizawa, K. Yamamoto, M. Tani, Application of terahertz absorption spectroscopy to evaluation of aging variation of medicine, Anal. Sci. 27 (2011) 209–212.

[69] G. Altiokka, D. Ak-Dougrukol, M. Tuncel, H.Y. Aboul-Enein, Determination of amlodipine in pharmaceutical formulations by differential-pulse voltammetry with a glassy carbon electrode, Arch. Pharm. 335 (2002) 104–108.
[70] A.A.A. Gazy, Determination of amlodipine besylate by adsorptive square-wave anodic stripping voltammetry on glassy carbon electrode in tablets and biological fluids, Talanta 62 (2004) 575–582.
[71] B. Dogan-Topal, B. Bozal, B.T. Demircigil, B. Uslu, S.A. Ozkan, Electroanalytical studies and simultaneous determination of amlodipine besylate and atorvastatine calcium in binary mixtures using first derivative of the ratio-voltammetric methods, Electroanalysis 21 (2009) 2427–2439.
[72] R.N. Goyal, S. Bishnoi, Voltammetric determination of amlodipine besylate in human urine and pharmaceuticals, Bioelectrochemistry 79 (2010) 234–240.
[73] K. Matalka, T. Arafat, T. El-Thaher, K. Qawasmeh, S. Shebli, M. Hamd, A. Badwan, Pharmacokinetic and pharmacodynamic profiles of two brands of amlodipine determined by enzyme linked immunosorbent assay, Pharm. Pharmacol. Commun 6 (2000) 539–544.
[74] K. Matalka, T. El-Tharer, M. Saleem, T. Arafat, A. Jehanli, A. Baldwan, Enzyme linked immunosorbent assay for determination of amlodipine in plasma, J. Clin. Labor. Anal. 15 (2001) 47–53.
[75] P.A. Meredith, H.L. Elliott, Clinical pharmacokinetics of amlodipine, Clin. Pharmacokin. 22 (1992) 22–31.
[76] J.K. Faulkner, D. McGibney, L.F. Chasseaud, J.L. Perry, I.W. Taulor, The pharmacokinetics of amlodipine in healthy volunteers after single intravenous and oral doses and after 14 repeated oral doses given once daily, Br. J. Clin. Pharmacol. 22 (1986) 21–25.
[77] D.R. Abernthy, The pharmacokinetic profile of amlodipine, Am. Heart J. 118 (5, Pt. 2) (1989) 1100–1103.
[78] D.M. Williams, L.X. Cubeddu, Amlodipine pharmacokinetics in healthy volunteers, J. Clin. Pharmacol. 28 (1988) 990–994.
[79] H.L. Elliott, S.T. Green, J. Vincent, P.A. Meredith, An assessment of the pharmacokinetics and pharmacodynamics of single doses of amlodipine in elderly normotensives, Pharmacol. Res. 26 (1992) 33–39.
[80] H. Laufen, M.A. Leitold, Enantioselective disposition of oral amlodipine in healthy volunteers, Chirality 6 (1994) 531–536.
[81] S. Maddi, M.R. Yamsani, A. Seeling, G.K.E. Scriba, Stereoselective plasma protein binding of amlodipine, Chirality 22 (2010) 262–266.
[82] A.P. Beresford, D. McGibney, M.J. Humphrey, P.V. Macrae, D.A. Stopfer, Metabolism and kinetics of amlodipine in man, Xenobiotica 18 (1988) 245–254.
[83] A.P. Beresford, P.V. Macrae, D.A. Stopher, Metabolism of amlodipine in the rat and the dog: a species difference, Xenobiotica 18 (1988) 169–182.
[84] B. Suchanova, L. Sispera, V. Wsol, Liquid chromatography–tandem mass spectrometry in chiral study of amlodipine biotransformation in rat hepatocytes, Anal. Chim. Acta 573–574 (2006) 273–283.
[85] D.A. Stopher, A.P. Beresford, P.V. Macrae, M.J. Humphrey, The metabolism and pharmacokinetics of amlodipine in humans and animals, J. Cadiovasc. Pharmacol. 12 (Suppl. 7) (1988) S55–S59.
[86] R.A. Burges, Amlodipine: a once daily calcium antagonist, J. Hum. Hyperten. 5 (Suppl. 1) (1991) 49–54.
[87] D.K. Walker, M.J. Humphrey, D.A. Smith, Importance of metabolic stability and hepatic distribution to the pharmacokinetic profile of amlodipine, Xenobiotica 24 (1994) 243–250.
[88] M. Josefsson, A.L. Zackrisson, J. Ahlner, Effect of grapefruit juice on the pharmacokinetics of amlodipine in healthy volunteers, Eur. J. Clin. Pharmacol. 51 (1996) 189–193.

[89] D.G. Bailey, G.K. Dresser, Interactions between grapefruit juice and cardiovascular drugs, Am. J. Cardiovasc. Drugs 4 (2004) 281–297.
[90] K. Nakagawa, T. Goto, Effects of ingestion of grapefruit juice or grapefruit on the hypotensive effect and plasma concentrations of dihydropyridine calcium antagonists (amlodipine and nifedipine): a case study, Clin. Exp. Hypertens. 32 (2010) 71–75.
[91] M. Chung, D. Garza, M. Gaffney, P. Glue, Bioavailability of amlodipine besylate following oral administration as a tablet dispersed in applesauce, J. Clin. Pharmacol. 45 (2005) 695–698.
[92] S. Bompadre, P. Capone, M.L. Cingolani, L. Ferrante, L. Leone, S. Ripa, Amlodipine pharmacokinetics in hypertensive patients, Pharmacol. Res. 22 (Suppl. 2) (1990) 59.
[93] G. Kungys, H. Naujoks, C. Wanner, Pharmacokinetics of amlodipine in hypertensive patients undergoing haemodialysis, Eur. J. Clin. Pharmacol. 59 (2003) 291–295.
[94] J.T. Flynn, M.C. Nahata, J.D. Mahan Jr., R.J. Portman, Population pharmacokinetics of amlodipine in hypertensive children and adolescents, J. Clin. Pharmacol. 46 (2006) 905–916.
[95] P. Bhad, S. Ayalasomayajula, R. Karan, S. Leon, G.J. Riviere, G. Sunkara, V. Jarugula, Evaluation of pharmacokinetic interactions between amlodipine, valsartan, and hydrochlorothiazide in patients with hypertension, J. Clin. Pharmacol. 51 (2011) 933–942.
[96] S. Rohatagi, J. Lee, M. Shenouda, S. Haworth, M.S. Bathala, M. Allison, I. Rubets, R. Heyrman, R. Noveck, D.E. Salazar, Pharmacokinetics of amlodipine and olmesartan after administration of amlodipine besylate and olmesartan medoxomil in separate dosage forms and as a fixed-dose combination, J. Clin. Pharmacol. 48 (2008) 1309–1322.
[97] R.A. Preston, P. Harvey, O. Herfert, G. Dykstra, J.W. Jukema, F. Sun, D. Gillen, A randomized, placebo-controlled trial to evaluate the efficacy, safety, and pharmacodynamic interaction of coadministered amlodipine and atorvastatin in 1660 patients with concomitant hypertension and dyslipidemia: the respond trial, J. Clin. Pharmacol. 47 (2007) 1555–1569.
[98] E.D. Deeks, Olmesartan medoxomil/amlodipine/hydrochlorothiazide: fixed-dose combination in hypertension, Drugs 71 (2011) 209–220.

CHAPTER 3

Candesartan Cilexetil

Febry Ardiana,* **Maria L.A.D. Lestari,**† and
Gunawan Indrayanto†

Contents

* Research & Development, Bernofarm Pharmaceutical Company, Buduran-Sidoarjo, Indonesia
† Faculty of Pharmacy, Airlangga University, Dharmawangsa Dalam, Surabaya, Indonesia

Profiles of Drug Substances, Excipients, and Related Methodology, Volume 37
ISSN 1871-5125, DOI: 10.1016/B978-0-12-397220-0.00003-9

© 2012 Elsevier Inc.
All rights reserved.

1. INTRODUCTION

Candesartan cilexetil is a white to off-white powder that is an ester prodrug of candesartan, which belongs to the angiotesin-II receptor antagonists (ARA II). Candesartan cilexetil is hydrolyzed to the candesartan active form in the gastrointestinal tract during absorption. Candesartan cilexetil is given per oral once daily (8, 16, and 32 mg), alone or in combination with hydrochlorothiazide. Clinically, candesartan cilexetil can be used for the treatment of hypertension [1]. At the present time, many Pharmacopoeias (such as USP, Europe Pharmacopoeia, British Pharmacopoeia, Japanese Pharmacopoeia, and Indonesian Pharmacopoeia) have not yet included candesartan cilexetil as a compendial item.

1.1. Chemical names

Candesartan cilexetil is known by the following systematic chemical names:

Cyclohexyl carbonate ester of (±)-1-hydroxyethyl 2-ethoxy-1-[*p*-(*o*-1*H*--tetrazol-5-ylphenyl)benzyl]-7-benzimidazolecarboxylate [1]

(±)-1-Cyclohexyloxycarbonyloxy ethyl-2-ethoxy-1-[[2′-(1*H*-tetrazol-5-yl) biphenyl-4-yl]-methyl] benzimidazole-7-carboxylate [2,3]

((±)-1-Hydroxyethyl 2-ethoxy-1-[*p*-(*o*-1*H*-tetrazol-5–ylphenyl)benzyl]-7-benzimidazolecarboxylate, cyclohexyl carbonate) [4,5]

2-Ethoxy-3-[21-(1H-tetrazol-5-yl)biphenyl-4-ylmethyl]-3*H*-benzoimidazole-4-carboxylic acid 1-cyclohexyloxycarbonyloxy ethyl ester [6]

1.2. CAS number

145040-37-5 (candesartan cilexetil)
139481-59-7 (candesartan)

1.3. Molecular formula, molecular weight, and molecular structure

The molecular formula of candesartan cilexetil is $C_{33}H_{34}N_6O_6$, and its molecular weight is 610.7 [1]. The molecular structures are as follows:

Candesartan cilexetil

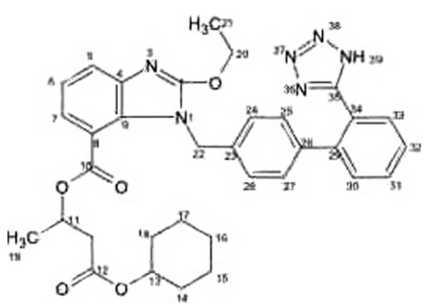

Candesartan

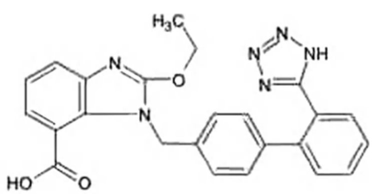

(Numbers on the structure of candesartan cilexetil are related to the Table 3.4)

1.4. Solubility characteristics, partition coefficient, and ionization constant

The solubility of candesartan cilexetil in benzyl alcohol is 205 mg/mL, and its solubility in water is less than 5×10^{-5} mg/mL [7]. The partition coefficient of candesartan cilexetil at pH 1.1, 6.9, and 8.9 exceeds 1000 [7,8].

The pK_a of candesartan cilexetil is 6.0 [8]. In addition, Cagigal *et al.* [9] determined the pK_a value with graphical method (consisting of the inflexion point, first derivative, second derivative, and curve-fitting methods) and a numerical method (using the LETAGROP SPEFO software package). The pK_a values were found to be 6.3 (inflexion point, first derivative, second derivative), 5.9 (curve-fitting method), and 6.0 (LETAGROP SPEFO).

1.5. Melting point

Candesartan cilexetil was reported to have a melting point 163 °C but does so with decomposition [7,10].

1.6. Polymorphism

Initially, it was thought that candesartan cilexetil had only two polymorphic forms (identified as Form-I and Form-II) and the amorphous form. Form-I was obtained by recrystallization from a 3:1 mixture of acetone and water, Form-II was isolated by acetone, and the amorphous form was obtained by milling either crystalline form with a mixer mill. Form-I has a melting point of 163 °C with decomposition, while Form-II has a melting point near 120 °C [11].

Over time, many patents have been issued that disclose additional polymorphic forms of candesartan cilexetil, and these are described in Table 3.1. There are 30 reported polymorphic forms of candesartan cilexetil, and most of these have been characterized using X-ray powder diffraction. In addition, infrared absorption spectroscopy (FTIR method) has been used to analyze the polymorphs of candesartan cilexetil (see Table 3.2).

2. KNOWN IMPURITIES

The impurities of candesartan cilexetil have been the subject of a number of publications, and a summary of these is presented in Table 3.3. It should be noted that most of the impurities found in one publication are also found in other publications. Chemical structures of the known impurities of candesartan cilexetil are shown in Fig. 3.1.

TABLE 3.1 X-ray powder diffraction properties of the reported polymorphic forms of candesartan cilexetil

Polymorph	Scattering angle (degrees 2θ)	Loss on drying by thermogravimetric analysis	Melting point	References
Form-I	9.82, 17.18, 18.58, 19.12, 20.26, 23.22 Radiation source: Cu Kα	n/a	163°C with decomposition	[11]
Form-II	7.28, 12.04, 13.20, 17.36, 19.96, 24.34 Radiation source: Cu Kα	n/a	Shallow endotherm peak at 120°C	[11]
Form-III	12.6, 22.7, 24.6, 25.3, 25.9 Radiation source: n/a	(6–8)%	n/a	[12]
	6.3, 7.3, 8.1, 8.9, 10.1, 14.6, 15.0, 15.8, 18.8 Radiation source: Cu Kα	n/a		[14]
Form-IV	7.3, 12.7, 22.5, 23.4, 25.8 Radiation source: n/a	±6%	n/a	[12]
	6.1, 7.1, 11.6, 11.9, 17.9, 19.8, 21.2 Radiation source: Cu Kα	n/a		[14]
Form-V	9.2, 13.2, 17.4, 20.0, 22.8 Radiation source: n/a	6%	n/a	[12]
Form-VI	12.6, 14.8, 15.5, 24.0, 25.7 Radiation source: n/a	17%	n/a	[12]
Form-VII	8.3, 14.4, 18.8, 19.4, 25.3 Radiation source: n/a	(3–7)%	n/a	[12]
Form-VIII	11.9, 18.9, 19.4, 22.5, 25.3 Radiation source: n/a	(3–4)%	n/a	[12]
Form-IX	9.2, 10.2, 14.8, 19.1, 20.8 Radiation source: n/a	n/a	n/a	[12]

Form-X	10.8, 20.7, 22.4, 24.9, 27.9 Radiation source: n/a	(15–17)%	n/a	[12]
Form-XI	7.4, 13.4, 15.8, 18.6, 22.2 Radiation source: n/a	±6%	n/a	[12]
Form-XIII	10.1, 18.1, 21.3, 23.4, 24.6 Radiation source: n/a	±8%	n/a	[12]
Form-XIV	8.1, 10.4, 15.3, 20.5, 25.3 Radiation source: n/a	±16%	n/a	[12]
Form-XIV-1	6.4, 9.3, 16.7, 25.3, 28.0 Radiation source: n/a	n/a	n/a	[12]
Form-XV	9.3, 12.0, 13.3, 18.3, 23.3 Radiation source: n/a	±8%	n/a	[12]
Form-XVI	8.3, 11.3, 15.1, 20.5, 23.7 Radiation source: n/a	n/a	n/a	[12]
Form-XVII	Broad X-ray powder diffraction peak, maximum ±20 Radiation source: n/a	n/a	n/a	[12]
Form-XVIII	12.8, 16.3, 18.0, 23.3, 25.7 Radiation source: n/a	±35%	n/a	[12]
Form-XIX	9.1, 12.0, 15.1, 20.6, 25.0 Radiation source: n/a	±16%	n/a	[12]
Form-XX	7.4, 11.8, 21.5, 25.0, 31.4 Radiation source: n/a	±16%	n/a	[12]
Form-XXI	10.8, 18.3, 22.4, 23.3, 25.6 Radiation source: n/a	±6%	n/a	[12]

(*continued*)

TABLE 3.1 (*continued*)

Polymorph	Scattering angle (degrees 2θ)	Loss on drying by thermogravimetric analysis	Melting point	References
Form-XXII	7.1, 8.9, 16.3, 20.5, 24.0 Radiation source: n/a	(4–20)%	n/a	[12]
Form-XXIII	10.3, 16.3, 19.8, 21.6, 23.1 Radiation source: n/a	(5–45)%	n/a	[12]
Form-A	7.3, 7.5, 8.2, 14.7, 15.1 Radiation source: Cu target anode	n/a	Exothermic peak at 135.5°C	[15]
Form-B	7.2, 8.1, 14.2, 14.6, 15.8, 25.20 Radiation source: Cu target anode	n/a	Exothermic peak at 109.5 and 138.25°C	[15]
Form-5	6.1, 11.6, 20.0, 21.2, 25.6 Radiation source: Cu Kα	n/a	(112.9–117.0)°C	[16]
Form-6	6.9, 8.9, 16.6, 17.4, 19.4 Radiation source: Cu Kα	n/a	(121.3–127.5)°C	[16]
Form-7	6.0, 9.0, 12.0, 21.3, 22.4 Radiation source: Cu Kα	n/a	n/a	[16]
Form-8	7.1, 16.3, 17.8, 19.5, 20.2, 24.0 Radiation source: Cu Kα	n/a	n/a	[16]
Candesartan cilexetil dioxane solvate	6.0, 10.7, 16.2, 18.0, 19.7, 20.6, 21.3, 21.7, 22.3 Radiation source: Cu Kα	n/a	n/a	[14]

n/a, not available.

TABLE 3.2 Infrared absorption spectral absorption bands of certain polymorphic forms of candesartan cilexetil polymorphs

Polymorph	Absorption band energy (cm^{-1})	References
Form-I	1717	[11]
Form-II	1736	[11]
Amorphous	1754, 1728, 1322, 991, 751	[11,16]
Form-XIV-1	1733, 1479, 1359, 1288, 1253, 1085	[12,13]
Form-XXII	1759, 1723, 1429, 1351, 1279, 1082	[12,13]
Form-XXIII	1759, 1727, 1464, 1438, 1071	[12,13]
Form-A	3430, 2940, 2860, 1750, 1730, 1550, 1430, 1355, 1280, 1245, 1080, 1040, 750	[15]
Form-B	3430, 2940, 2860, 1755, 1730, 1550, 1430, 1355, 1280, 1245, 1080, 1040, 745	[15]
Form-5	1756, 1574, 1465, 1003, 988, 912, 751	[16]
Form-6	1751, 1322, 994, 744	[16]

In the hydrolysis and transesterification study of candesartan cilexetil, Ferreirós *et al.* [17] found two derivates of candesartan cilexetil, namely methyl candesartan and hydroxyethyl candesartan. In this work, it was also found that the hydrolysis and transesterification process was mediated by the glass wall and by methanol. Subsequently, Subha Rao *et al.* [2] successfully separated six different impurities of candesartan cilexetil using isocratic RP-LC methodology during the course of a forced degradation study. Two of the impurities were methyl candesartan and hydroxyethyl candesartan. In this study, it was observed that basic hydrolysis resulted in a major degradation product which is different from the degradation products obtained from acid hydrolysis and aqueous hydrolysis.

During a tablet stability study, Mohan *et al.* [3] found increases in the levels of five impurities up to 0.05–0.4% and noted the same behavior during thermal degradation studies. These impurities were identified as Impurity I to Impurity V, in which two of these impurities were similar in structure to impurities 5 and 6 found previously (see Table 3.3 for details). For Impurity I, FTIR analysis showed absorption bands at 1726 cm^{-1} (C=O stretching) and 1460 cm^{-1} (—NH stretching). In addition, the presence of a —C=O stretching mode, a —NH stretching vibration, and the absence of an —OH stretching vibration were correlated with the hydrolysis of an ethyl group attached to an oxygen atom in the benzimidazole group of candesartan cilexetil, which undergoes ketoenol tautomerism and finally stabilizes as a stable keto form. In the case of Impurity II, FTIR analysis showed the —C=O stretching mode at 1750 cm^{-1} and the —N—C stretching vibration at 1193 cm^{-1}. The FTIR spectrum for impurity IV exhibited the —C=O stretching band at 1742 cm^{-1}. NMR data of

TABLE 3.3 Impurities of candesartan cilexetil

Impurities					
Chemical name	Other name	Molecular formula	Degradation process	Additional note	References
n/a	Methylcandesartan Hydroxyethylcandesartan	$C_{26}H_{24}N_6O_3$ $C_{24}H_{20}N_6O_3$	Hydrolysis and transesterification in basic condition		[17]
2-Ethoxy-3-[2′-(1*H*-tetrazol-5-yl)-biphenyl-4-ylmethyl]-3*H*-benzoimidazole-4-carboxylic acid	Impurity 1	$C_{24}H_{20}N_6O_3$	Basic hydrolysis in 0.1M NaOH for 48h	Having similar structure to hydroxyethylcandesartan	[2]
2-Ethoxy-3-[2′-(1*H*-tetrazol-5-yl)-biphenyl-4-ylmethyl]-3*H*-benzoimidazole-4-carboxylic acid methyl ester	Impurity 2	$C_{25}H_{22}N_6O_3$	n/a		[2]
2-Ethoxy-3-[2′-(1*H*-tetrazol-5-yl)-biphenyl-4ylmethyl]-3*H*-benzoimidazole-4-carboxylic acid ethyl ester	Impurity 3	$C_{26}H_{24}N_6O_3$	Stressed condition with UV and at 60°C for 10 days	Having similar structure to methylcandesartan	[2]
2-Hydroxy-3-[2′-(1*H*-tetrazol-5-yl)-biphenyl-4-ylmethyl]-3*H*-benzoimidazole-4-carboxylic acid 1-cyclohexyloxycarbonyloxyethyl ester	Impurity 4	$C_{31}H_{30}N_6O_6$	Acidic hydrolysis in 0.1M HCl, oxidation in 0.1% H_2O_2, aqueous hydrolysis. All was done for 48h	Major degradation product	[2]
2-Ethoxy-3-[2′-(1-ethyl-1*H*-tetrazol-5yl)-biphenyl-4-ylmethyl]-3*H*-benzoimidazole-4-carboxylic acid 1-cyclohexyloxycarbonyloxyethyl ester	Impurity 5	$C_{35}H_{38}N_6O_6$	Acidic hydrolysis in 0.1M HCl, oxidation in 0.1% H_2O_2, aqueous hydrolysis. All was done for 48h		[2]
2-Ethoxy-3-[2′-(1-ethyl-1*H*-tetrazol-5-yl)-biphenyl-4-ylmethyl]-3*H*-benzoimidazole-4-carboxylic acid 1-cyclohexyloxycarbonyloxyethyl ester	Impurity 6	$C_{35}H_{38}N_6O_6$	Acidic hydrolysis in 0.1M HCl, oxidation in 0.1% H_2O_2, aqueous hydrolysis. All was done for 48h		[2]
1-{[(Cyclohexyloxy)carbonyl]oxy}ethyl-2-oxo-1-{[2′-(1*H*-tetrazol-5-yl)biphenyl-4-yl]methyl}-1*H*-benzimidazole-7-carboxylate	Impurity I; CNS desethyl; desethyl candesartan cilexetil	$C_{31}H_{30}N_6O_6$	Hydrolysis of candesartan cilexetil		[3]

1-{(Cyclohexyloxy)carbonyl]oxy]} ethyl-2-oxo-1-{[2′-(1-ethyl-1H-tetrazol-5-yl)biphenyl-4-yl] methyl}-1H-benzimidazole-7-carboxylate	Impurity II; 1N-ethyl oxocandesartancilexetil	$C_{33}H_{34}N_6O_6$	Ethyl cation formed from hydrolysis of candesartan cilexetil (parent drug) then reacts with impurity I		[3]
1-{[Cyclohexyloxy)carbonyl]oxy} ethyl-2-oxo-1-{[2′-(2-ethyl-1*H*-tetrazol-5yl)biphenyl-4-yl] methyl}-1*H*-benzimidazole-7-carboxylate	Impurity III; 2*N*-ethyl oxocandesartancilexetil	$C_{33}H_{34}N_6O_6$	Ethyl cation formed from hydrolysis of candesartan cilexetil (parent drug) then reacts with Impurity I		[3]
1-{[(cyclohexyloxy)carbonyl]oxy}-ethyl-2-ethoxy-1-{[2′-(1-ethyl-1*H*-tetrazol-5-yl)biphenyl-4-yl] methyl}-1*H*-benzimidazole-7-carboxylate	Impurity IV; 1*N*-ethyl CNS (1*N*-ethyl candesartancilexetil)	$C_{35}H_{38}N_6O_6$	Ethyl cation reacts with the parent drug	Similar structure with Impurity 6 determined by Subha Rao *et al.* [2]	[3]
1-{[(Cyclohexyloxy) carbonyl]oxy} ethyl-2-ethoxy-1-{[2′-(2-ethyl-1*H*-tetrazol-5-yl)biphenyl-4yl] methyl}-1*H*-benzimidazole-7-carboxylate	Impurity V; 2*N*-ethyl CNS (2*N*-ethyl candesartancilexetil)	$C_{35}H_{38}N_6O_6$	Ethyl cation reacts with the parent drug	Similar structure with Impurity 5 determined by Subha Rao *et al.* [2]	[3]
n/a	DP I	$C_{24}H_{21}N_6O_3^+$	Basic hydrolysis at 80°C with 0.1 N NaOH	Proposed as drug devoid of cilexetil	[18]
n/a	DP II	$C_{24}H_{19}N_6O_3^+$	Photolytic study (as described in ICH) under basic condition	Detected as major degradation product	[18]
n/a	DP III	$C_{31}H_{31}N_6O_6^+$	Acidic hydrolysis at 80°C with 0.1 N HCl and also hydrolysis in water		[18]
n/a	DP IV	$C_{33}H_{35}N_6O_6^+$	Hydrolysis in water at 80°C	Both are having same fragmentation pattern suggesting that those are isomeric each other with higher amount of DP V formed	[18]
n/a	DP V	$C_{33}H_{35}N_6O_6^+$			

(*continued*)

TABLE 3.3 *(continued)*

Impurities					
Chemical name	Other name	Molecular formula	Degradation process	Additional note	References
n/a	DP VI	$C_{35}H_{39}N_6O_6^+$	Hydrolysis in water at 80°C	Having similar fragmentation as DP VIII, proposed to be *N*2-ethyl derivative of the drug	[18]
n/a	DP VII	$C_{33}H_{33}N_6O_6^+$	Photolytic study under all condition	Under photolytic basic condition, DP II was formed in addition to DP VII	[18]
n/a	DP VIII	$C_{35}H_{39}N_6O_6^+$	Hydrolysis in water at 80°C	Having similar fragmentation as DP VI, proposed to be *N*1-ethyl derivative of the drug	[18]
2-Ethoxy-3-[2^1-(1*H*-tetrazol-5-yl)-biphenyl-4ylmethyl]-3*H*-benzoimidazole-4-carboxylic acid ethyl ester	CDC I	$C_{26}H_{24}N_6O_3$	Obtained from the process-related impurity of candesartan cilexetil	Similar to Impurity 3 from Rao [2] or methylcandesartan	[19]
2-Ethoxy-1-[[2′-(1-ethyl-1H-tetrazol-5-yl)biphenyl-4-yl]methyl]-1H-benzimidazole-7-carboxylic acid ethyl ester	CDC II	$C_{28}H_{28}N_6O_3$	Obtained from the process-related impurity of candesartan cilexetil	Mass spectral data did not match with known impurity already found	[19]
1-[[(Cyclohexyl-1 oxy)carbonyl]oxy] ethyl 2-ethoxy-1-[[2′-(1-ethyl-1H-tetrazol-5-yl)[1,1′-biphenyl]-4-yl] methyl]-1H-benzimidazole-7-carboxylate	CDC III	$C_{31}H_{30}N_6O_6$	Obtained from the process-related impurity of candesartan cilexetil	Similar to Impurity 4 from Subha Rao *et al.* [2]	[19]
1-[[(Cyclohexyloxy)carbonyl]oxy] ethyl 2-ethoxy-1-[[2′-(2-ethyl-tetrazol-5-yl)[1,1′-biphenyl]-4-yl] methyl]-1H-benzimidazole-7-carboxylate	CDC IV	$C_{35}H_{38}N_6O_6$	Obtained from the process-related impurity of candesartan cilexetil	Similar to Impurity 5 and impurity V from Subha Rao *et al.* [2] and Mohan *et al.* [3], respectively	[19]

n/a, not available.

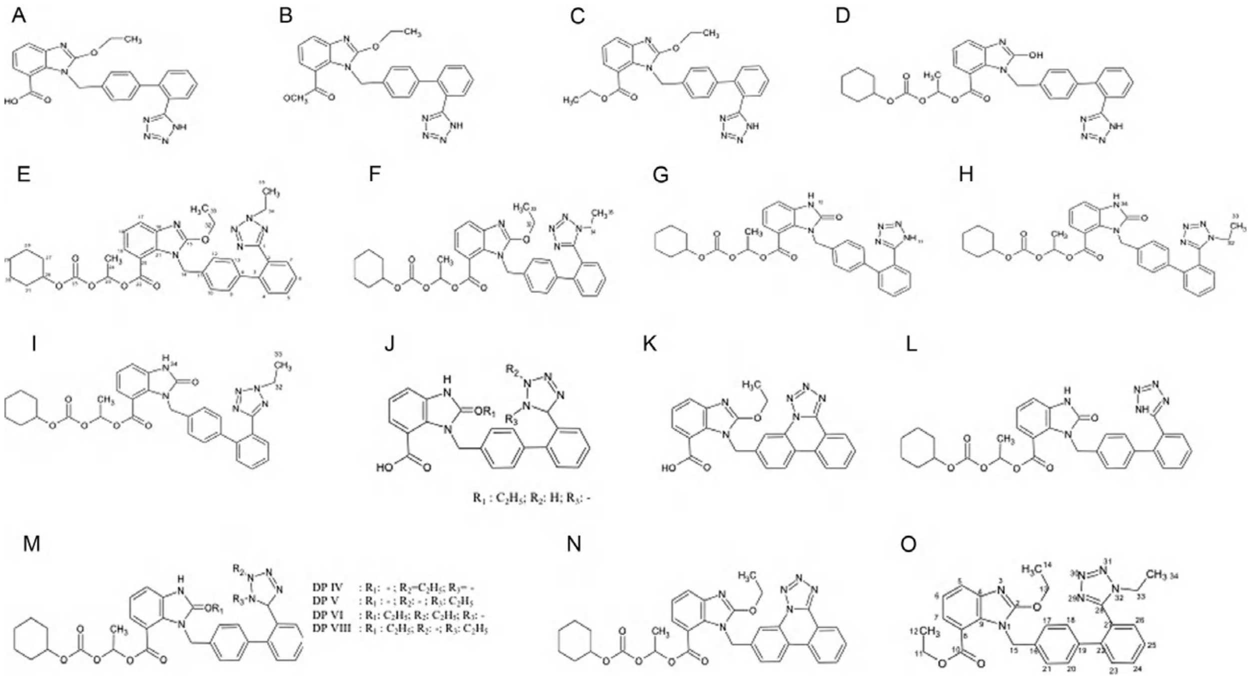

FIGURE 3.1 Chemical structures of the impurities of candesartan cilexetil: (A) impurity 1 or hydroxyethyl candesartan; (B) impurity 2; (C) impurity 3 or methyl candesartan; (D) impurity 4 or CDC III; (E) impurity 5 or impurity V or CDC IV*; (F) impurity 6 or impurity IV*; (G) impurity I or CNS desethyl or desethyl candesartan cilexetil*; (H) impurity II or 1*N*-ethyl oxo candesartan cilexetil*; (I) impurity III or 2*N*-ethyl oxo candesartan cilexetil*; (J) DPI; (K) DP II; (L) DP III; (M) DP IV-DP VI, DP VIII; (N) DP VII; (O) CDC II**.

* Numbers on the structure are related to Table 3.5 of NMR analysis.

** Numbers on the structure are related to Table 3.4 of NMR analysis.

some these impurities are detailed in Tables 3.4 and 3.5, while the mass spectral data are presented in Table 3.6.

3. SPECTROPHOTOMETRIC METHOD OF ANALYSIS

3.1. UV spectrophotometry

A first derivative and ratio derivative spectrophotometric method for the determination of candesartan cilexetil in pharmaceutical dosage forms was reported by Erk [20]. Using the first derivative method, the limit of detection (LOD) for candesartan cilexetil was found to be 0.73 μg/mL, with a recovery of 99.1–100.9%. Using the ratio derivative method, the LOD for candesartan cilexetil was 0.88 μg/mL, with a recovery of 99.4–100.3%.

Stolarczyk *et al.* [21] and Charoo *et al.* [22] reported derivative spectrophotometric methods which were used to determine candesartan cilexetil in combination with hydrochlorothiazide. Stolarczyk *et al.* [21] described that this method enabled the direct analysis of candesartan cilexetil despite interference on the zero-order absorption spectra. The LOD and limit of quantification (LOQ) for candesartan cilexetil were 0.56 and 1.71 μg/mL, and the recovery was 92.30–94.80%. Charoo *et al.* [22] recommended using a 10:90 v/v solvent mixture of methanol and 0.35% polysorbate 20 in phosphate buffer (pH 4.5) to dissolve candesartan cilexetil, and used this method for analysis of pharmaceutical preparations as well as for dissolution studies.

Jignesh *et al.* [6] reported the *Q*-analysis spectrophotometric analysis of candesartan cilexetil in combination with hydrochlorothiazide. The method was based on an absorbance ratio at two selected wavelengths, one at the isoabsorptive point and the other at the wavelength maximum of the two components. Candesartan cilexetil and hydrochlorothiazide have isoabsorptive points at 258.14 nm, and wavelength maxima at 258.14 and 271 nm, respectively. Calculation of candesartan cilexetil was based on an equation which involved absorbance and absorptivity of both candesartan cilexetil and hydrochlorothiazide at the two wavelengths. This method showed good linearity at 2–24 μg/mL for both candesartan cilexetil and hydrochlorothiazide, with a recovery of 101.2–102.1% for candesartan cilexetil.

3.2. Spectrofluorimetry

Sakur and Fael [5] reported the spectrofluorimetric determination of candesartan cilexetil in bulk drug substance and in formulated tablets. Using respective excitation and emission wavelengths of 260 and 381 nm, the linear range was found to be 3.0–288.6 ng/mL (r=0.9999). The LOD and LOQ were found to be 0.25 and 0.77 ng/mL, respectively, and the

TABLE 3.4 NMR data of candesartan cilexetil and its impurities (modified from Refs. [3] and [19])

	Candesartan cilexetil				CDC II				Impurity I		
Position	Integration	δ (ppm)	Multiplicity J (Hz)	^{13}C (δ in ppm)	Integration	δ (ppm)	Multiplicity J (Hz)	^{13}C (δ in ppm)	^{1}H (ppm) (multiplicity)	^{13}C (ppm)	DEPT
1	–	–	–		–	–	–	–		154.89	C
2	–	–	–	158.0	–	–	–	158.3		138.51	C
3	–	–	–	–	–	–	–			138.01	C
4	–	–	–	140.1	–	–	–	141.6	7.45–7.47(d)	130.52	CH
5	1H	6.79	m	121.1	1H	7.66	dd/7.92, 0.91	121.6	7.62–7.67(m)	128.99	CH
6	1H	6.88	t/7.92	121.2	1H	7.16	t/7.92	120.8	7.53–7.57(m[a])	127.72	CH
7	1H	7.45	dd/7.92, 0.91	124.2	1H	7.45	dd/7.92, 0.91	123.1	7.62–7.67(m)	130.62	CH
8	–	–	–	115.2	–	–	–	115.7		136.29	C
9	–	–	–	130.7	–	–	–	130.9	6.98–7.0(d)	128.99	CH
10	–	–	–	163.3	–	–	–	165.6	6.92–6.94(d)	126.51	CH
11	1H	6.63	q/5.48	91.8	2H	4.14	q/7.31	61.0		130.03	C
12	–	–	–	152.4	2H	1.17	t/7.31	13.9	6.92–6.94(d)	126.51	CH
13	1H	4.48		77.7	2H	4.55	q/7.01	66.6	6.98–7.0(d)	128.99	CH
14	4H	1.65	m	31.2	3H	1.35	t/7.01	14.3	5.21–5.34(d)	44.52	CH_2
15	4H	1.16	m	23.5	2H	5.49	s	46.2		140.93	C
16	2H	1.65	m	25.0	–	–	–	136.9		124.24	C
17	4H	1.16	m	23.5	2H	6.85	d/8.22	126.6	7.24–7.27(dt)	122.3	CH
18	4H	1.65	m	31.2	2H	6.97	d/8.22	128.7	7.08–7.12(t)	120.73	CH
19	3H	1.27	d/5.48	14.5	–	–	–	–	7.28–7.30(dt)	113.23	CH

(*continued*)

TABLE 3.4 (*continued*)

	Candesartan cilexetil				CDC II				Impurity I		
Position	Integration	δ (ppm)	Multiplicity *J* (Hz)	^{13}C (δ in ppm)	Integration	δ (ppm)	Multiplicity *J* (Hz)	^{13}C (δ in ppm)	^{1}H (ppm) (multiplicity)	^{13}C (ppm)	DEPT
20	2H	4.07, 4.36	m	67.6	2H	6.97	d/8.22	128.7		113.03	C
21	3H	1.40	t/7.01	14.5	2H	6.85	d/8.22	126.6		128.29	C
22	2H	5.61	s	46.9	–	–	–	140.8		163.44	C
23	–	–	–	136.6	1H	7.69	m	130.3	6.69–6.73(q)	91.86	CH
24	2H	6.69	d/8.22	125.3	1H	7.55	m	131.7	1.34–1.35(m)	19.03	CH_3
25	2H	6.81	d/8.22	129.4	1H	7.55	m	128.0		151.9	C
26	–	–	–	138.1	1H	7.55	m	131.2	4.54–4.60(m)	76.78	CH
27	2H	6.81	d/8.22	129.4	–	–	–	122.4	1.83(m)	30.74	CH_2
28	2H	6.69	d/8.22	125.3	–	–	–	153.8	1.17–1.31(m)	22.92	CH_2
29	–	–	–	140.9	–	–	–	–	1.38–1.48(m)	24.54	CH_2
30	1H	7.28	m	130.5	–	–	–	–	1.17–1.31(m)	22.95	CH_2
31	1H	7.56	m	131.2	–	–	–	–	1.64(m)	30.78	CH_2
32	1H	7.56	m	128.2	–	–	–	–	11.56(s)		NH
33	1H	7.98	m	131.1	–	–	–	–	16.23(bs)		NH
34	–	–	–	123.3	–	–	–	–			
35	–	–	–	154.6	2H	3.58	q/7.31	42.1			
36	–	–	–	–	3H	0.76	t/7.31	13.3			
37	–	–	–	–							
38	–	–	–	–							
39	1H	15.94	brs	–							

s, singlet; d, doublet; m, multiplet; dd, doublet of doublet; t, triplet; q, quartet; m, multiplet; b, broad. Unresolved: dt, doublet of triplet; brs, broad singlet.

[a] ^{1}H–^{1}H coupling constants.

TABLE 3.5 NMR data of impurities II to V (modified from Ref. [3])

	Impurity II			Impurity III			Impurity IV			Impurity V		
Position	^{1}H (ppm) (multiplicity)	^{13}C (ppm)	DEPT	^{1}H (ppm) (multiplicity)	^{13}C (ppm)	DEPT	^{1}H (ppm) (multiplicity)	^{13}C (ppm)	DEPT	^{1}H (ppm) (multiplicity)	^{13}C (ppm)	DEPT
1		154.31	C		165.01	C		158.82	C		164.03	C
2		141.17	C		141.56	C		142.01	C		142.07	C
3		137.91	C		139.92	C		141.51	C		141.19	C
4	7.43–7.55(m)	131.57	CH	7.39–7.50(m)	130.33	CH	7.47–7.55(m)	130.64	CH	7.35–7.37(dt)	131.56	CH
5	7.43–7.55(m)	130.23	CH	7.39–7.50(m)	130.64	CH	7.47–7.55(m)	129.94	CH	7.42–7.51(dt)	127.94	CH
6	7.43–7.55(m)	128.82	CH	7.39–7.50(m)	130.33	CH	7.60–7.64(m)	127.54	CH	7.42–7.51(dt)	128.82	CH
7	7.60–7.64(m)	127.92	CH	7.81–7.83(dt)	129.91	CH	7.60–7.64(m)	130.31	CH	7.81–7.83(dt)	131.53	CH
8		137.14	C		126.31	C		139.98	C		137.91	C
9	7.06–7.10(d)	128.85	CH	7.01–7.08(dt)	129.41	CH	6.95–7.01(d)	129.37	CH	7.02–7.04(d)	130.22	CH
10	7.00–7.02(d)	127.92	CH	7.01–7.08(dt)	126.72	CH	6.95–7.01(d)	126.63	CH	6.92–6.94(d)	127.67	CH
11		122.75	C		135.55	C		129.37	C		137.42	C
12	7.00–7.02(d)	127.92	CH	7.01–7.08(dt)	126.72	CH	6.95–7.01(d)	48.62	CH	6.92–6.94(d)	127.67	CH
13	7.06–7.10(d)	128.85	CH	7.01–7.08(dt)	129.41	CH	6.95–7.01(d)	164.03	CH	7.02–7.04(d)	130.22	CH
14	5.45–5.54(d)	42.44	CH_2	5.42–5.62(d)	45.67	CH_2	5.54–5.66(d)	126.29	CH2	5.59–5.68(d)	46.92	CH_2
15		156.62	C		156.65	C		123.93	C		158.8	C
16		122.75	C		128.68	C		124.24	C		122.77	C
17	7.28–7.30(d)	114.08	CH	7.26–7.29(dt)	127.49	CH	7.60–7.64(m)	122.3	CH	7.55–7.57(dt)	124.29	CH
18	7.06–7.10(t)	121.18	CH	7.01–7.08(t)	120.94	CH	7.14–7.18(t)	120.72	CH	7.13–7.17(t)	120.92	CH
19	7.43–7.55(m)	123.85	CH	7.35–7.37(dt)	113.74	CH	7.72–7.74(dt)	122.55	CH	7.72–7.74(dt)	122.89	CH
20		114.28	C		114.61	C		114.66	C		114.3	C
21		122.75	C		129.53	C		131.89	C		132.16	C
22		163.63	C		163.7	C		165.02	C		164	C

(*continued*)

TABLE 3.5 (*continued*)

	Impurity II			Impurity III			Impurity IV			Impurity V		
Position	^{1}H (ppm) (multiplicity)	^{13}C (ppm)	DEPT	^{1}H (ppm) (multiplicity)	^{13}C (ppm)	DEPT	^{1}H (ppm) (multiplicity)	^{13}C (ppm)	DEPT	^{1}H (ppm) (multiplicity)	^{13}C (ppm)	DEPT
23	6.82–6.86(q)	91.92	CH	6.83–6.87(q)	91.89	CH	6.88–6.93(q[b])	91.75	CH	6.92(q[a])	91.79	CH
24	1.49–1.50(t)	19.57	CH_3	1.42–1.44(d)	19.51	CH_3	1.54–1.56(m)	19.61	CH_3	1.48–1.53(m)	19.64	CH_3
25		152.52	C		152.53	C		152.57	C		152.57	C
26	4.61–4.68(m)	77.68	CH	4.60–4.72(m)	77.65	CH	3.43–3.49(m)	77.59	CH	4.59–4.69(m)	77.57	CH
27	1.71–1.95(m)	31.44	CH_2	1.70–1.93(m)	31.04	CH_2	1.73–1.95(m)	31.4	CH_2	1.75 and 1.91(m)	31.4	CH_2
28	1.22–1.41(m)	23.6	CH_2	1.23–1.31(m)	23.58	CH_2	1.21–1.43(m)	23.59	CH_2	1.33 and 1.53(m)	23.62	CH_2
29	1.44–1.56(m)	25.11	CH_2	1.50–1.54(m)	25.1	CH_2	1.56 and 1.51 (m)	25.12	CH_2	1.44(m)	25.12	CH_2
30	1.22–1.41(m)	23.63	CH_2	1.23–1.31(m)	23.6	CH_2	1.21–1.43(m)	23.59	CH_2	1.26(m)	23.62	CH_2
31	1.71–1.95(m)	31.4	CH_2	1.70–1.93(m)	31.38	CH_2	1.73 and 1.95(m)	31.4	CH_2	1.91(m)	31.4	CH_2
32	3.40–3.47(q)	45.68	CH_2	4.39–4.45(m)	48.08	CH_2	4.60–4.67(m)	66.75	CH_2	4.59–4.69(q)	66.83	CH_2
33	0.84(d)	13.66	CH_3	1.35(t)	14.4	CH_3	1.47(m)	14.68	CH_3	1.43(d)	14.67	CH_3
34	10.75(bs)		NH	9.75(bs)		NH	3.43–3.49(q)	46.92	CH_2	4.37–4.42(q)	42.4	CH_2
35							0.83(t)	14.39	CH_3	1.3(t)	13.61	CH_3

s, singlet; d, doublet; m, multiplet; t, triplet; q, quartet; m, multiplet; b, broad.
[a] Unresolved: dt, doublet of triplet.

TABLE 3.6 ESI/TOF-MS data of some impurities of candesartan cilexetil [3,17,18]

Impurity	Experimental mass	Best possible molecular formula	Theoretical mass	Major fragment ions
DP I	441.1715	$C_{24}H_{21}N_6O_3^+$	441.167	423.1601, 395.1499, 380.1398, 367.1240, 263.1340, 235.1206, 207.0967,192.0853
DP II	439.1534	$C_{24}H_{19}N_6O_3^+$	439.1513	411.1448, 393.1456, 233.0889, 205.0811
DP III	583.2307	$C_{31}H_{31}N_6O_6^+$	583.23	439.1524, 413.1398, 395.1288, 367.1205, 349.1114, 235.1015
DP IV	611.2678	$C_{33}H_{35}N_6O_6^+$	611.2613	567.2391, 441.1705, 423.1634,413.1565, 395.1535, 380.1420, 235.1274, 207.0977, 192.0881
DP V	611.269	$C_{33}H_{35}N_6O_6^+$	611.2613	567.2423, 441.1713, 423.1642, 413.1565, 395.1543, 380.1376, 367.1441, 235.1280
DP VI	639.2994	$C_{35}H_{39}N_6O_6^+$	639.2926	595.2705, 469.2062, 451.1957, 423.1731, 395.1541, 380.1425, 207.1001
DP VII	609.2446	$C_{33}H_{33}N_6O_6^+$	609.2456	439.1510, 411.1436, 393.1330, 365.1033, 233.0872, 205.0793
DP VIII	639.2988	$C_{33}H_{39}N_6O_6^+$	639.2926	595.2723, 469.2043, 451.1942, 423.1696, 395.1543, 235.1288, 192.0889
CDC II	497 $[M+Na]^+$ at 519	n/a	496	469, 451, 426, 423, 395, 370, 352, 263, 235, 192
Methylcandesartan	455	n/a	n/a	n/a
Hydroxyethylcandesartan	485	n/a	n/a	n/a
Impurity I	581 (negative ion, ESI) 605 (Na^+ adduct)	$C_{31}H_{30}N_6O_6$	582	n/a
Impurity II	609 (negative ion, ESI) 633 (Na^+ adduct)	$C_{33}H_{34}N_6O_6$	610	n/a
Impurity IV	637 (negative ion, ESI) 661 (Na^+ adduct)	$C_{35}H_{38}N_6O_6$	638	n/a

n/a, not available.

method accuracy was reported to be 95.66–100.60%. No significant difference (p=0.05) was observed between this spectrofluorimetric method and the HPLC method (see Table 3.7).

Another spectrofluorimetric method was reported by Cagigal *et al.* [9] for the determination of the pK_a values of candesartan cilexetil and its metabolite candesartan M1 (2-ethoxy-1-[[2′-(1*H*-tetrazol-5-yl) biphenyl-4-yl]methyl]-1*H*-benzimidazol-carboxylic acid), as well as of losartan, irbesartan, valsartan, and telmisartan. The method took advantage of the existence of different fluorophores in the respective molecular structures, namely biphenyl, imidazole, and benzimidazole. In this method, the pK_a value was obtained using a graphical procedure (inflexion point, derivative, and curve fitting) and a numerical method using LETAGROP SPEFO software. All of the pK_a values were calculated at 0.5M ionic strength, and these findings were discussed above in Section 1.4.

4. CHROMATOGRAPHIC METHODS OF ANALYSIS

4.1. Thin-layer chromatography

Stolarczyk *et al.* [27] reported a thin-layer chromatography (TLC) method for the determination of candesartan cilexetil in combination with hydrochlorothiazide. The method used a F_{254} plate as the stationary phase, and 12:3:5 v/v/v/v ethyl acetate/tetrahydrofuran/acetic acid as the mobile phase. Quantitation of eluted spots was made by densitometry at a wavelength of 252nm. The Rf value for candesartan cilexetil is 0.89, the LOD was reported as 0.245 μg/band, the LOQ was 0.750 μg/band, and the recovery was 92.1–95.1%.

Mehta and Morge [28] reported a high-performance thin-layer chromatography (HP-TLC) method for analyzing combinations of candesartan cilexetil and hydrochlorothiazide. In this method, the HP-TLC plate was coated with 0.2mm layers of silica gel 60 GF 254 as the stationary phase, and 3:3:3:0.5 v/v/v/v ethyl acetate/chloroform/acetone/methanol was used as the mobile phase. The detection wavelength was 280 nm, and methanol was used as the solvent. The Rf value for candesartan cilexetil was 0.27, the LOD was 9.04 μg, the LOQ was 30.13 μg, and the recovery was 99.36–99.90%.

Gumieniczek *et al.* [29] reported a classical densitometry and video scanning method for the analysis of candesartan cilexetil in combination with losartan. In this method, silica gel 60 F_{254} was used as the stationary phase, 5:5:0.1 v/v/v 1,4-dioxane/hexane/99% formic acid was used as the mobile phase, and methanol was used as the solvent. The detection wavelengths used for candesartan were 258nm (densitometry) and 254 nm (video scanning). The recovery using densitometry was reported to be 99.81%, while the recovery with video scanning was 99.44%.

TABLE 3.7 HPLC methods for candesartan cilexetil

Analyte(s)	Sample	Column	Internal Standard	Mobile Phase	Column Temperature(°C)	Detection (nm)	Solvent	Limit of detection (LOD), limit of quantification (LOQ), and recovery (Rec.)	References
Candesartan cilexetil	Bulk drug, tablets	Zorbax CN (250×4.6mm; 5µm)	n/a	0.02M NaH_2PO_4 pH 3.0: ACN=50:50	27	210	ACN	LOD: n/a LOQ: n/a Rec.: – Bulk drug: (99.0–101.0)% – Tablets: (99.2–101.4)%	[2]
Candesartan cilexetil	Tablets	Purosphere Star RP 18e (150×4.6 mm; 5µm)	n/a	A: ACN:20mm NH_4AC, pH 5.0=10:90 B: ACN:20mm NH_4AC, pH 5.0=90:10 Mobile phase was operated in gradient mode for isolation of impurities	n/a	254	n/a	n/a	[3]
Candesartan cilexetil and hydrochlorothiazide	Tablets	Hypersil (Phenyl)-2 column	n/a	0.02M KH_2PO_4:MeOH: triethylamine=25:75:0.2 pH 6.0±0.1	Room temperature	271	MeOH	LOD: 0.13µg/mL LOQ: 0.22µg/mL Rec.: (99.44–101.02)%	[4]
Candesartan cilexetil and hydrochlorothiazide	Tablets	CN column (250mm×4.6 mm; 5µm)	n/a	Phosphate buffer, pH 3.0: ACN=50:50	25	210	Mobile phase	LOD: n/a LOQ: n/a Rec.: (99.44–102.96)%	[5]
Candesartan cilexetil	Candesartan cilexetil complex with cyclodextrin	Hypersil ODS (250mm×4.6 mm; 5µm)	n/a	0.02M KH_2PO_4 buffer, pH 4.0:ACN=2:8	Ambient	254	ACN	LOD: n/a LOQ: n/a Rec.: n/a	[8]
Candesartan cilexetil and hydrochlorothiazide	Tablets	Supelcocil C18 (150×4.6mm; 5µm)	n/a	10mMKH_2PO_4:MeOH, pH 2.5: ACN=2:80:18	Ambient	260	MeOH	LOD: 2.0ng/mL LOQ: 11.0ng/mL Rec.: (96.9–101.0)%	[23]

(*continued*)

TABLE 3.7 (*continued*)

Analyte(s)	Sample	Column	Internal Standard	Mobile Phase	Column Temperature(°C)	Detection (nm)	Solvent	Limit of detection (LOD), limit of quantification (LOQ), and recovery (Rec.)	References
Candesartan cilexetil and hydrochlorothiazide	Tablets	Kromasil 100 C18 (250×4.6 mm; 5 μm)	n/a	ACN:0.02 M sodium acetate (isocratic and gradient elution)	25±2°C	265	ACN	LOD: 5±0.06 ng/ injection (injection volume 10 μL) LOQ: n/a Rec.: (98.3–101.6)%	[24]
Candesartan cilexetil	Self-microemulsifying drug delivery system (SMEDDS) of candesartan cilexetil	Inertsil ODS-3 (250×4.6 mm; 5 μm)	n/a	0.02 M monobasic potassium phosphate: ACN: triethylamine= 40:60:0.2, pH 6.0	25	254	n/a	n/a	[25]
Candesartan cilexetil	Tablets	Hypersil ODS C-18 (250 mm×4.6 mm; 5 μm)	Bromhexine	ACN:0.05 M KH_2PO_4 buffer= 65:35	n/a	256	ACN	LOD: 0.358 μg/ml LOQ: 1.196 μg/ml Rec.: (98.97–100.41)%	[26]

n/a, not available; MeOH, methanol; ACN, acetonitrile.

4.2. Liquid chromatography

Most of the publications that report the analysis of candesartan in pharmaceutical preparations by high-performance liquid chromatography (HPLC) used C18 columns (six publications). Other columns used were based on cyano derivatization (two publications) and on phenyl derivatization (one publication). These publications also reported the simultaneous separation and determination of candesartan cilexetil and hydrochlorothiazide. Details of the HPLC methods are presented in Table 3.7.

4.3. Micellar electrokinetic capillary chromatography

Hillaert and Van den Bossche [30] reported the optimization for the separation of six angiotensin-II-receptor antagonists (candesartan, eprosartan, irbesartan, losartan potassium, telmisartan, and valsartan) using a capillary zone electrophoretic method. The separation was best carried out using 60 mM sodium phosphate buffer (pH 2.5). The quantitative determination could only be applied to eprosartan, irbesartan, losartan potassium, and telmisartan owing to the poor solubility of candesartan and valsartan in this system.

Hillaert *et al.* [31] described the separation of those six angiotensin-II receptor antagonists using a micellar electrokinetic capillary chromatogram method. The best result was achieved by using 55 mM sodium phosphate buffer solution (pH 6.5) that contained 15 mM sodium dodecyl sulfate. Quantitative determinations can also be performed using this system, except for telmisartan and irbersartan.

Hillaert and Van den Bossche [32] described the simultaneous determination of hydrochlorothiazide with six angiotensin-II-receptor antagonists (candesartan, eprosartan, irbesartan, losartan potassium, telmisartan, and valsartan) using validated capillary zone electrophoretic and micellar electrokinetic capillary chromatography methods.

5. VOLTAMMETRY

Dogan *et al.* [33] reported the analysis of candesartan cilexetil in pharmaceutical preparations using anodic adsorptive stripping voltammetry by adsorptive stripping differential pulse and adsorptive stripping square wave voltammetric techniques. The method used a working electrode consisting of a glassy carbon disc electrode, and the supporting electrolyte contained aqueous 30% acetonitrile (pH 1.5–11). This method was based on the oxidation of candesartan cilexetil at the carbon electrode and can be used for analyzing candesartan cilexetil in tablet dosage forms.

Süslü *et al.* [34] described the adsorptive stripping voltammetric determination of candesartan cilexetil in pharmaceutical formulations. This

method is based on the reduction of candesartan cilexetil at a hanging mercury drop electrode in phosphate buffer (at pH 5.0). Compared to the previous method [33], this method can be considered as being simpler and faster.

6. METABOLITE STUDIES AND BIOANALYSIS

Kondo *et al.* [35] reported the LC-ESI MS/MS separation and characterization of the glucuronide derivatives of candesartan cilexetil in bile and rat plasma after oral administration. Candesartan cilexetil was first hydrolyzed to candesartan and then metabolized to candesartan-acyl glucoronide (CG-1) and candesartan-*N*-glucoronide (CG-2) by glucoronidation at the carboxylic acid and tetrazole ring, respectively. The structures of these two compounds are as follows.

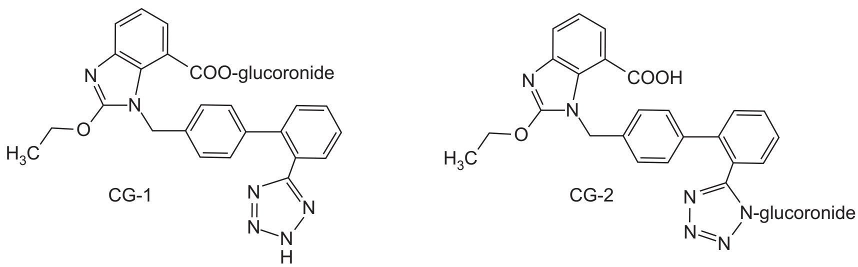

By using liver microsomes from cow, moose, rat, pig, and recombinant UDP-glucoronyltransferase as biocatalysts, Alonen *et al*. [36] synthesized the same two metabolites of candesartan (CG-1 and CG-2) as well as metabolites of losartan and zolarsartan. The metabolites were analyzed by using a LC-ESI-MS/MS system equipped with a Hypersil BDS C18 column (5 μm, 150×4.6 mm). A mixture of 5 mM ammonium acetate (pH 4.5) and acetonitrile (gradient elution) was used as the mobile phase. NMR data of the CG-1 and CG-2 were also reported. Large differences were observed in the production rate of the glucoronides of the three sartans when using these biocatalysts. CG-1 and CG-2 were also determined by means of an HPLC method that used a Hypersil BDS column (5 μm, 250×4.6 mm), and a mobile phase mixture of 1% acetic acid and acetonitrile (gradient elution) [37]. The detection was performed using a fluorescence detector (excitation wavelength of 260 nm, and emission wavelength of 395 nm).

Most of the publications on the bioanalysis of candesartan cilexetil described the analysis of candesartan cilexetil in human plasma and urine. Details of additional reports for the analysis of candesartan cilexetil in human plasma and urine are presented in Table 3.8.

TABLE 3.8 Summary of HPLC analysis for the separation and determination of candesartan cilexetil, and its metabolites in biological matrixes

Analyte(s)	HPLC conditions	Sample	Internal standard	Preparation of standard, sample extraction, and cleanup	Limit of detection (LOD), limit of quantification (LOQ), and recovery (Rec.)	References
Candesartan cilexetil	Column: Supelcocil C18 (150 mm × 4.6 mm; 5 μm) Mobile phase: 10 mM KH_2PO_4:MeOH: ACN = 2:80:18 (pH 2.5) Flow rate: 1.0 mL/min Detector: PDA 260 nm	Human plasma	n/a	Standard: stock solution prepared in MeOH and diluted with mobile phase Plasma samples – Centrifuged at 4000 × *g* for 10 min – 1.0 mL sample + 2.0 mL ACN – The mixture was vortex and standing at room temperature for 5 min – The mixture was centrifuged at 4000 × *g* for 20 min – The supernatant injected into HPLC system	LOD: 2.0 ng/mL LOQ: 11.0 ng/mL Rec.: (97.0–100.3)%	[23]
Candesartan cilexetil; Metabolites: CG1, CG2	Column: YMC AM-312 (150 mm × 6.0 mm; 5 μm) Mobile phase: Water:ACN: trifluoroacetic acid = 70:30:0.1 Flow rate: 1 mL/min Column temperature: ambient Detector: LC-MS positive ion mode	Rat plasma; bile sample	n/a	Standard: n/a Sample – Plasma and bile sample adjusted to pH 3 and 4 with 1 M HCl, stored at −20 °C and thawed – (3 mL) Plasma and (2 mL) bile were extracted with 5 volumes of ethyl acetate – Plasma and bile separately dried under nitrogen at ambient temperature	n/a	[35]

(*continued*)

Analyte(s)	HPLC conditions	Sample	Internal standard	Preparation of standard, sample extraction, and cleanup	Limit of detection (LOD), limit of quantification (LOQ), and recovery (Rec.)	References
				– The residue was dissolved in MeOH (plasma 100 μL; bile 200 μL) – 10 μL solution injected to the HPLC column Methylation of the candesartan glucuronide – 50 μL MeOH solution of the plasma or bile rats extracts (as detailed above) was injected to the HPLC system – The eluate containing M-I glucoronides were collected and lyophilized – The residue was dissolved in 2 mL diethyl ether–MeOH (2:1) and treated with the diazomethane generated from *N*-methylnitrosurea in diethyl ether by addition of 20% aqueous KOH solution at ambient temperature – The solution was concentrated under a stream of nitrogen		

				– The residue was dissolved in MeOH (100 µL) and injected directly into the LC/ESI-MS/MS system		
Candesartan, candesartan cilexetil, and inactive metabolite (CV-15959)	Column: Spherisorb S3P (Phenyl) 100×4.6 mm; 3 µm Mobile phase candesartan in plasma: 100 mL citrate buffer (pH 3.1, I=0.5 containing 50 mM TBA), 185 mL ACN, 180 mL MeOH and diluting to 1000 mL with water Flow rate: 0.9 mL/min Mobile phase candesartan cilexetil in plasma and urine: 200 mL phosphate buffer (pH 2.8, I=0.1 containing 12.5 mM TBA), 420 mL ACN and diluting to 1000 mL with water Flow rate: 1.0 mL/min Mobile phase candesartan and CV-15959 in plasma and urine A: 200 mL phosphate buffer (pH 2.8, I=0.1 containing 12.5 mM TBA), 200 mL	Human plasma and urine	T-57536	Standard for urine sample 50 µL drug free urine+450 µL drug free plasma + 50 µL solution of candesartan and MII in phosphate buffer (pH 7.0, I=0.1 containing 10% MeOH). Blood plasma – Venous blood sample separated by centrifugation for 5 min at 1500×g and frozen at −18°C – Thaw at room temperature, vortex mixed and centrifuged – 500 µL plasma + 450 µL drug free plasma mixed with 50 µL internal standard solution (2.2 µM in phosphate buffer, pH 7.0, I=0.1 containing 10% MeOH) and 500 µL of HCl (0.2 M for candesartan and CV-15959, 0.15 M for candesartan cilexetil) Urine – Collected and frozen	LOD: n/a LOQ: Candesartan: 1 nM Candesartan cilexetil: 5 nM Inactive metabolite (CV-15959): 3 nM Rec.: Candesartan cilexetil: (65.6–72.0)% Candesartan: (81.7–82.4)% Inactive metabolite (CV 15959): (73.8–78.4)% T-57536: 83.6%	[38]

(*continued*)

TABLE 3.8 *(continued)*

Analyte(s)	HPLC conditions	Sample	Internal standard	Preparation of standard, sample extraction, and cleanup	Limit of detection (LOD), limit of quantification (LOQ), and recovery (Rec.)	References
	ACN and diluting to 1000 mL with water B: 200 mL phosphate buffer (pH 2.8, I=0.1 containing 12.5 mM TBA), 600 mL ACN, and diluting to 1000 mL with water			– Thaw at room temperature, vortex mixed and centrifuged – 50 μL urine + 450 μL drug free plasma mixed with 50 μL internal standard solution (2.2 μM in phosphate buffer, pH 7.0, I=0.1 containing 10% MeOH) and 500 μL of HCl (0.2 M for candesartan and CV-15959, 0.15 M for candesartan cilexetil) Sample extraction – 5.0 mL (dichlormethane–diethyl ether, 1:4) was added to the sample above and shaked (300/min) for 20 min Centrifuge for 5 min, the aquoeus phase was frozen in a dry ice-ethanol bath. The organic phase evaporated to dryness under a gentle stream of Nitrogen. The residue was reconstitued in 400 μL		

			redissolution liquid (20 mL ACN, 10 mL citrate buffer (pH 3.1, I=0.5, 50 mM TBA) diluted to 100 mL water), for candesartan and CV-15959 – For candersartan cilexetil, the residue was reconstitued in 300 µL redissolution liquid (60 mL MeOH, 20 mL phosphate buffer (pH 2.8, I=0.1, 12.5 mM TBA)) dilutes to 100 mL water – 80 µL was injected onto the LC-column		
	0–9 min: 20% B 9–14 min: linear increase to 32% 14–25 min: back to 20% 25–29 min: 20% Flow rate: 1.0 mL/min Detector: fluorosence Excitacion: 265 nm Emission: 395 nm				
Candesartan cilexetil; Candesartan metabolite	Column: µBondapak C_{18} (300 mm×3.9 mm; 10 µm) Mobile phase: A: sodium acetate buffer (5 mM, pH 4);	Human urine	Standard: Stock solution prepared in both ACN and MeOH Cleanup of urine samples	LOD: n/a LOQ: Candesartan cilexetil: 0.41 µg/mL	[39]

(*continued*)

TABLE 3.8 (*continued*)

Analyte(s)	HPLC conditions	Sample	Internal standard	Preparation of standard, sample extraction, and cleanup	Limit of detection (LOD), limit of quantification (LOQ), and recovery (Rec.)	References
	B: ACN Gradient setting: 0 min: 70% A, 30% B (1.0 mL/min) 15 min: 25% A, 75% B (1.2 mL/min) 21 min: 5% A, 95% B (1.2 mL/min) 24–25 min: 70% A, 30% B (1.0 mL/min) Column temperature: room temperature Detector: photometric 254 nm			– 1 mL urine vortex and was acidified with phosphate buffer (0.1 M, pH 2; 0.5 mL) – The mixture was shaken and centrifuged at 3500 rpm for 5 min – BondElut C8 cartridges were conditioned with MeOH (2 mL) and phosphate buffer (0.1 M, pH 2; 1 mL) – The column washed with MeOH: phosphate buffer 0.1 M pH 2 and dried at full vacuum (p>200 mmHg) for 20 min – Sample were eluted with 1 mL MeOH – The eluate was evaporated to dryness at 40 °C with nitrogen – The remaining residue was dissolved in initial mobile phase (0.5 mL) and analyzed by HPLC	Candesartan metabolite: 0.45 µg/mL Rec.: Candesartan cilexetil: 70.5% Candesartan metabolite: 99.1%	

Candesartan cilexetil, candesartan metabolite	Column: μBondapak C_{18} (300×3.9, 10μm) Mobile phase: A: 5mM sodium acetate buffer, pH 4 B: ACN 0min: 70% A, 30% B (1.0mL/min) 15min: 40% A, 60% B (1.2 mL/min) 21min: 5% A, 95% B (1.2mL/min) 24–25min: 70% A, 30% B (1.0 mL/min) Detector: Fluorescence, Candesartan cilexetil: exitation 272 nm; emission 384 nm, candesartan metabolite: exitation 259 nm, emission 392 nm Column temperature: room temperature	Human plasma	Bumeta-nide	Plasma sample collection – Blood samples + tripotassium EDTA → gently mixed – Centrifuged at 3500rpm for 10min under controlled room temperature (4°C) Plasma supernatant separated from blood cells and frozen at −20°C SPE extraction – Bond Elut C8 conditioned with 2mL MeOH then 1mL 0.1M phosphate buffer pH 2 and kept from dryness – 0.5mL treated plasma passed through SPE under low vacuum – Column washed with 0.5mL meOH-0.1M phosphate buffer (50:50) and dried under vacuum – Eluated with 0.5 MeOH. Eluate was then added with 0.1mL 10% ethyleneglycol in MeOH and dried under nitrogen at 40°C	LOD: n/a LOQ: Candesartan cilexetil: 3.3ng/mL Candesartan metabolite: 3.2 ng/mL Absolute rec. Candesartan cilexetil 68.3% (low), 70.3% (medium), 71.5% (high). Absolute rec. Candesartan metabolite 86.5% (low), 90.7% (medium), 90.5% (high)	[40]

(*continued*)

TABLE 3.8 (*continued*)

Analyte(s)	HPLC conditions	Sample	Internal standard	Preparation of standard, sample extraction, and cleanup	Limit of detection (LOD), limit of quantification (LOQ), and recovery (Rec.)	References
				– Dried sample was then reconstituted in starting mobile phase and injected		
Candesartan cilexetil	Column: online SPE coupled to electrospray tandem mass spectrometry SPE column obtained from Waters (20 mm × 2.1 mm) packed with OASIS MAX 30 µm	Human plasma, urine	Valsartan	Standard: stock solution in MeOH with 0.5% NH_4OH. Working solution diluted in MeOH Samples – Centrifuged at 2400 × *g* for 5 min – 50 µl deposited in 96-well polypropilene plate – Addition of 50 µL of aqueous acetic acid (15% v/v) and 10 µL of valsartan – Addition 50 µL aqueous acetic acid (15% v/v) and 10 µL of valsartan – The plate was sealed with polypropilene cap – Vortexed at 1000 rpm for 10 s Samples were kept at 4 °C in the autosampler until injection	LOD: n/a LOQ: n/a Human plasma: Rec.: intra-assay: 89.2% at LOQ—99.2%; inter-assay: 100% at LOQ—101% Urine: intra-assay at LOQ—108–103%; inter-assay: at LOQ—111–96.4%	[41]

	Mobile phase: water : acetic acid = 85:15 0.01 min: 100% water 0.5 min : 100% THF 2min : THF: water: formic acid = 95 : 5 : 5 Detector: LC-MS/MS positive electrospray ionization mode SPE column maintained at 45°C					
Candesartan cilexetil	Column: Phenomenex Luna C8 (250×4.6mm, 5µm) Column temperature: 25°C Mobile phase: MeOH–10mM potassium dihydrogen phosphate (pH 3.0)=85:15 Flow rate: 1mL/min Detector: UV 260nm	Human plasma	Irbesartan	Standard Candesartan (50–5000ng/mL) were prepared by spiking stock solutions with 500µL drug free plasma Sample preparation – 500µL of drug free plasma was spiked with candesartan and irbesartan – 1000µL of ACN was added to the drug spiked plasma – The solutions were vortex mixed for 1min and centrifuged at 5000rpm for 15min	LOD: 20ng/mL LOQ: 50ng/mL Rec.: (96.92–101.07)%	[42]

(*continued*)

TABLE 3.8 (*continued*)

Analyte(s)	HPLC conditions	Sample	Internal standard	Preparation of standard, sample extraction, and cleanup	Limit of detection (LOD), limit of quantification (LOQ), and recovery (Rec.)	References
				– The extracted candesartan was reconstituted in mobile phase (50:50 v:v). 20 µL of ultra filtrate was then injected into a HPLC column		
Candesartan cilexetil, valsartan, irbesartan, losartan, telmisartan, eprosartan	Column: Luna phenyl-hexyl 3.5 µm, 50×2 mm, Guard column: same packing material 4×2 mm Mobile phase: Solvent A: 0.1% formic acid + 1 mmol/L ammonium format; solvent B: ACN:0.1% formic acid (95:5 v/v) 0–0.2 min: 5% B 0.2–1 min: 5–35% B linear 1–8 min: 35–45% B linear 8–9 min: 45–70% B linear 9–9.5 min: 70% B 9.5–10.5 min: 70–5% B linear 10.5–12 min: 5% B for equilibrium MRM (ESI MS positive): *m/z* 441–263	Human plasma	Methaqualone	Standard: Candesartan was dissolved in methanol 25, 20, and 0.8 µg/mL Methaqualone 50 µg/mL Sample preparation: Precipitation solvent: $ZnSO_4$: MeOH (1:4 v/v): 0.1 ml QC sample/control blank/calibrator was transferred to 1.5ml Eppendorf cup + 10 ml methaqualone + 0.2 mL protein precipitation reagent. Vortexed 1 min and centrifuge 13200 rpm for 10 min. 20 micoliter supernatant injected to HPLC	Absolute rec. candersartan: 97.7% (low), 89.4% (medium), 94% (high) Precision: Intraday: RSD 2.6–5.53% Interday: RSD 6.54–7.72% LOQ : 8 ng/mL	[43]

n/a, not available; MeOH, methanol; ACN, acetonitrile; TBA, tetrabutylammonium; THF, tetrahydrofuran.

REFERENCES

[1] S.C. Sweetman (Ed.), Martindale: The Complete Drug Reference, 36th ed., The Pharmaceutical Press, London, 2009.
[2] D.V. Subha Rao, P. Radhakrishnanand, M.V. Suryanarayana, V. Himabindu, Chromatographia 66 (2007) 496–507.
[3] A. Mohan, S. Shanmugavel, A. Goyal, B.R. Venkataraman, D. Saravanan, Chromatographia 69 (2009) 1–10.
[4] S.S. Qutab, S.N. Razzaq, M. Ashfaq, Z.A. Shuja, I.U. Khan, Acta Chromatogr. 19 (2007) 119–129.
[5] A.A. Sakur, H. Fael, Int. J. Pharm. Sci. Rev. Res. 4 (2010) 60–63.
[6] P. Jignesh, J.B. Dave, C.N. Patel, P. Dhrumill, J. Chem. Pharm. Res. 2 (2010) 10–14.
[7] Takeda Pharmaceutical Company, Product Monograph Atacand®. http://www.astrazeneca.ca/documents/ProductPortfolio/ATACAND_PM_en.pdf (22 June 2011).
[8] A.A. Al Omari, M.M. Al Omari, A.A. Badwan, K.A. Al-Sou'od, J. Pharm. Biomed. Anal. 54 (2011) 503–509.
[9] E. Cagigal, L. González, R.M. Alonso, R.M. Jimenez, J. Pharm. Biomed. Anal. 26 (2001) 477–486.
[10] S. Budavari (Ed.), The Merck Index, 13th ed., Merck and Co, New Jersey, 2001.
[11] H. Matsunaga, T. Eguchi, K. Nishijima, T. Enomoto, K. Sasaoki, N. Nakamura, Chem. Pharm. Bull. 47 (2) (1999) 182–186.
[12] M.Y. Etinger, B. Fedotev, T. Koltai, Z. Kurgan, O. Malachi, (2005) US Patent Application 2005/0250828 A1.
[13] M.Y. Etinger, B. Fedotev, T. Koltai, Z. Kurgan, O. Malachi, (2010) US Patent Application 2010/0121072 A1.
[14] R.B. Parthasaradhi, R.K. Rathnakar, R.R.R. Raji, R.D. Murlidhara, R.K.S. Chander, (2009) US Patent Application 7,504,516 B2.
[15] Y. Kumar, S. De, S. Swargam, World Intellectual Property, Organization WO/2005/123721, 2005.
[16] L. Antoncic, A. Copar, A. Jeriha, European Patent Application 1 655 298 A1, 2006.
[17] N. Ferreirós, S. Dresen, R.M. Alonso, W. Weinmann, J. Chromatogr. B 855 (2007) 134–138.
[18] S. Mehta, R.P. Shah, R. Priyadarshi, S. Singh, J. Pharm. Biomed. Anal. 52 (2010) 345–354.
[19] B. Raman, B.A. Sharma, G. Mahale, D. Singh, A. Kumar, J. Pharm. Biomed. Anal. 56 (2) (2011) 256–263, doi:10.1016/j.jpba.2011.05.024.
[20] N. Erk, Pharmazie 58 (2003) 796–800.
[21] M. Stolarczyk, A. A. Maślanka, J. Krzek, J. Milczarek, Acta Polon. Pharm. Drug Res. 65 (2008) 275–281.
[22] N.A. Charoo, M. Bashir, E. Abdalla, K.I.H. Ali, Anal. Lett. 42 (2009) 2232–2243.
[23] N. Erk, J. Liq. Chromatogr. Relat. Technol. 26 (2003) 2581–2591.
[24] A.E.M. Khedr, JKAU: Med. Sci. 15 (2) (2008) 3–13.
[25] V. Nekkanti, P. Karatgi, R. Prabhu, R. Pillai, AAPS PharmSciTech 11 (2010) 9–17.
[26] G. Akula, K. Saikrishna, S. Bhuphati, R.R. Kumar, S. Kumar, Int. J. Pharm. Sci. Res. 1 (2010) 191–196.
[27] M. Stolarczyk, M. Anna, J. Krzek, J. Liq. Chromatogr. Relat. Technol. 31 (2008) 1892–1902.
[28] B.H. Mehta, S.B. Morge, J. Planar Chromatogr. 21 (2008) 173–176.
[29] A. Gumieniczek, T. Inglot, A. Kończak, J. Planar Chromatogr. 24 (2011) 99–104.
[30] S. Hillaert, W. Van den Bossche, J. Chromatogr. A 979 (2002) 323–333.
[31] S. Hillaert, T.R.M. De Beer, J.O. De Beer, W. Van den Bossche, J. Chromatogr. A 984 (2003) 135–146.
[32] S. Hillaert, W. Van den Bossche, J. Pharm. Biomed. Anal. 31 (2003) 329–339.

[33] B. Dogan, B. Uslu, S.A. Őskan, Pharmazie 59 (2004) 840–844.
[34] I. Süslü, N. Őzaltin, S. Altinöz, J. Appl. Electrochem. 39 (2009) 1535–1543.
[35] T. Kondo, K. Yoshida, Y. Yoshimura, M. Motohashi, S. Tanayama, J. Mass Spectrom. 31 (1996) 873–878.
[36] A. Alonen, J. Jansson, S. Kallonen, et al., Bioorg. Chem. 36 (2008) 148–155.
[37] A. Alonen, M. Finel, R. Kostiainen, Biochem. Pharmacol. 76 (2008) 763–772.
[38] H. Stenhoff, P. Lagerström, C. Andersen, J. Chromatogr., B 731 (1999) 411–417.
[39] L. González, R.M. Alonso, R.M. Jiménez, Chromatographia 52 (2000) 735–740.
[40] L. González, J.A. López, R.M. Alonso, R.M. Jiménez, J. Chromatogr. A 949 (2002) 49–60.
[41] M. Levi, G. Wuerzner, E. Ezan, A. Pruvost, J. Chromatogr. B 877 (2009) 919–926.
[42] A.K. Peepliwal, C.G. Bonde, K. Mohanraj, Acta Pharm. Sci. 52 (2010) 247–253.
[43] N. Ferreirós, S. Dresen, R.M. Alfonso, W. Weinmann, Ther. Drug. Mot. 29 (2007) 824–834.

CHAPTER 4

Flurbiprofen

Alaa A.-M. Abdel-Aziz, Abdullah A. Al-Badr, and **Gamal Abdel Hafez**

Contents

Department of Pharmaceutical Chemistry, College of Pharmacy, King Saud University, P.O. Box 2457, Riyadh, Kingdom of Saudi Arabia

Profiles of Drug Substances, Excipients, and Related Methodology, Volume 37
ISSN 1871-5125, DOI: 10.1016/B978-0-12-397220-0.00004-0

© 2012 Elsevier Inc.
All rights reserved.

1. DESCRIPTION

1.1. Nomenclature

1.1.1. Systemic chemical names

α-Methyl-α-(2-fluoro-4-biphenylyl) acetic acid

2-Fluoro-α-methyl-[1,1′-biphenyl]-4-acetic acid
2-Fluoro-α-methyl-4-biphenyl-acetic acid
2-(2-Fluoro-4-biphenylyl) propionic acid
(1,1-Biphenyl)-4-acetic acid, 2-fluoro-α-methyl
3-Fluoro-4-phenylhydratropic acid [1–3]

1.1.2. Proprietary names
Flurbiprofen

1.1.3. Nonproprietary names
Ansaid, Antadys, Benactiv, Cebutid, Edolfene, Evril, Fenomel, Flurofen, Froben, Ocufen, Ocuflur, Reupax, Strefen, Strepfen, Transact [1–3]

1.2. Formulae

1.2.1. Empirical formula, molecular weight, and CAS registry number
$C_{15}H_{13}FO_2$, MW=244.26, CAS=5104-49-4

1.2.2. Structural formula

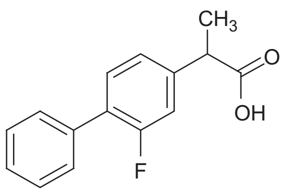

1.3. Elemental composition

C=73.76% H=5.36% O=13.1% F=7.78%

1.4. Optical rotation

Optical rotations were measured on a JASCO DIP-1000 [4–7].

(*S*)-(+)-Flurbiprofen, $[\alpha]_D^{22}=+45.6$ (ethanol, $c=1.0$) [4]
(*S*)-(+)-Flurbiprofen, $[\alpha]_D^{20}=+44.6$ (isopropanol, $c=1.0$) [5]
(*S*)-(+)-Flurbiprofen, $[\alpha]_D^{22}=+41.4$ ($CHCl_3$, $c=1.0$) [6]
(*S*)-(+)-Flurbiprofen, $[\alpha]_D^{20}=-1.46$ (CH_2Cl_2, $c=2.5$) [7]

2. USES AND APPLICATIONS

rac-Flurbiprofen is a nonsteroidal anti-inflammatory drug (NSAID) used in the treatment of pain or inflammation, in humans [8–10]. Flurbiprofen is indicated for the management of vernal keratoconjunctivitis [11],

postoperative ocular inflammation [12], herpetic stromal keratitis [13], excimer laser photorefractive keratectomy [14], and ocular gingivitis [15]. Recent reports suggest potential topical and systemic use of flurbiprofen in radio-protection [16], inhibition of colon tumor [17], protection of postirradiation myelosuppression [18], pain management after foot surgery [19], and peridontal surgery [20]. In 1993, its potent antiplatelet activity was evaluated in a double-blind, placebo-controlled, multicenter study for efficacy on preventing reinfarction and reocclusion after successful thrombolysis or angioplasty in acute myocardial infarction [21]. Although it possesses a chiral center, with the *S*(+)-enantiomer having most of the beneficial activity, both enantiomers may possess analgesic activity and all flurbiprofen preparations to date are marketed as the racemate [8,22,23]. Flurbiprofen has been utilized since 1986 in the North American market and demonstrates stereoselectivity in its pharmacokinetics [24]. Inversion of (*R*)-(−)-flurbiprofen to its optical antipode occurred to a variable extent in the dog (0.39) and the guinea pig (1.00) and to a much lower extent in the rat (0.02) and the gerbil (0.05), and it does not appear to undergo enantiomeric inversion in humans [25,26].

The mechanism of action is known to be the inhibition of prostanoid biosynthesis via blocking of cyclooxygenase enzyme [10,27–29]. Cyclooxygenase (COX), also known as prostaglandin H synthase, is an enzyme implicated in the mediation of pain, fever, and inflammation. It catalyzes the oxidative conversion of arachidonic acid into prostaglandin H2, a key intermediate in the biosynthetic pathway of prostaglandins, prostacyclins, and thromboxanes, which in turn mediate a variety of physiological effects both beneficial and pathological [30]. Recently, it was discovered that two COX isoforms exist: COX-l, expressed constitutively in many tissues, and COX-2, an induced isoform having elevated expression in inflamed tissues. COX-1 is thought to be involved in ongoing ''housekeeping'' functions, for example, gastric cytoprotection, while COX-2 is the isoform implicated in the pathological effects mentioned above [31]. Current COX inhibitors such as ibuprofen and flurbiprofen, used as NSAIDs, inhibit both COX-1 and COX-2 [32]. The *S*(+)-enantiomer of flurbiprofen inhibits prostanoid synthesis about 500 times more potent than the *R*(−)-enantiomer [33].

3. METHOD OF PREPARATION

Racemic flurbiprofen is one of the well-known forms of the NSAID substance. The enantiopure (*S*)-enantiomer exhibits a stronger anti-inflammatory activity (as high as 30-fold higher compared to *rac*-flurbiprofen); however, flurbiprofen is still currently produced in large quantities as a racemic mixture.

3.1. Synthesis of *rac*-flurbiprofen

rac-Flurbiprofen **5** was prepared from 3-fluoro-4-phenyl propiophenone **2** which was prepared from (3-flouro-4-phenyl)phenyl bromide **1** by successive treatments with magnesium, propionaldehyde, and chromic acid. Thus, the ketone **2** was allowed to react with pyrrolidine to give the pyrrolidine enamine **3**, which on treatment with diphenyl phosphorazidate (DPPA) furnished the *N*-phosphorylated amidine **4**. Hydrolysis of **4** with potassium hydroxide afforded *rac*-flurbiprofen (*rac*-**5**) [34] according to the following scheme.

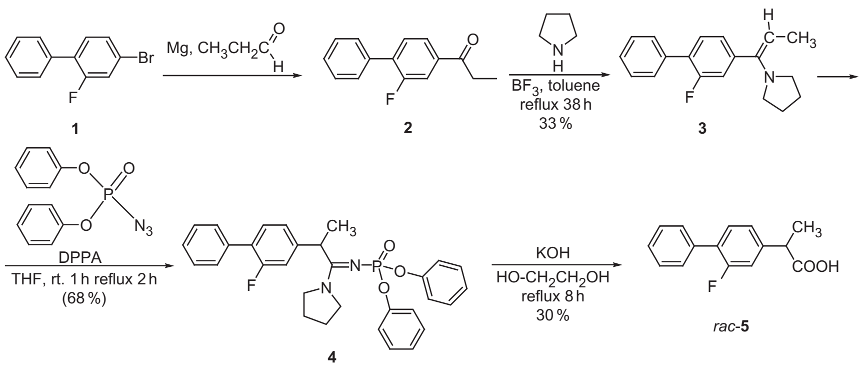

3.2. Synthesis of (*R*)- and (*S*)-flurbiprofen

It is recognized that enantiomers of biologically active compounds usually display different physiological activities. There has also been very rapid progress in asymmetric synthetic methods in recent years. As a result, increasing attention is being paid to the synthesis of nonracemic chiral drugs. One of the major groups of anti-inflammatory agents is the arylpropanoic acid such as flurbiprofen where the activity resides in the (*S*) isomers. The (*R*)-flurbiprofen was considered previously to be the inactive isomer because it does not inhibit COX activity. However, recent studies have revealed that it has antitumor effects [35,36] and can also reduce the level of amyloid β-42 related to Alzheimer's disease [37–39]. Hence, it is highly desirable to supply the market with the enantiopure of (*S*)- and (*R*)-flurbiprofen.

3.2.1. Chemical method for synthesis of (*R*)- and (*S*)-flurbiprofen

3.2.1.1. Enantioselective synthesis of chiral flurbiprofen using chiral auxiliary (R)- and (S)-3-hydroxy-4,4-dimethyl-l-phenyl-2-pyrrolidinone The outlined synthetic strategy whereby asymmetry is introduced into the molecules by the reaction of *rac*-2-(2-fluoro-4-biphenylyl)propanoyl chloride (*rac* **6**) with (*R*)- and (*S*)-3-hydroxy-4,4-dimethyl-l-phenyl-2-pyrrolidinone

(*R*)- and (*S*)-**5**, in the presence of triethylamine, under standard esterification conditions, gave (*R*,*R*)-**7** and (*S*,*S*)-**7**, respectively, with high diastereoselectivity. Controlled acidic hydrolysis afforded the corresponding (*R*)- or (*S*)-2-(2-fluoro-4-biphenylyl) propionic acid (flurbiprofen) with high enantioselectivity [5] according to the following scheme.

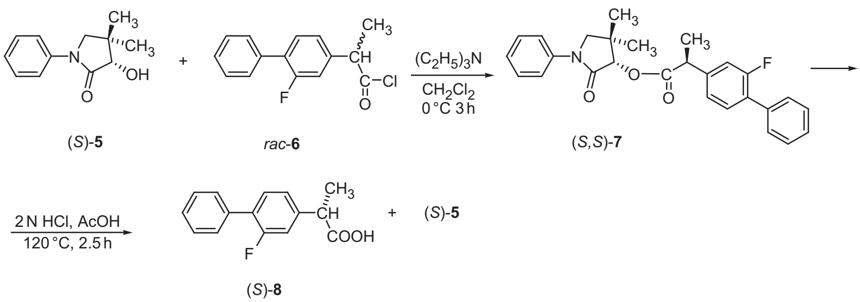

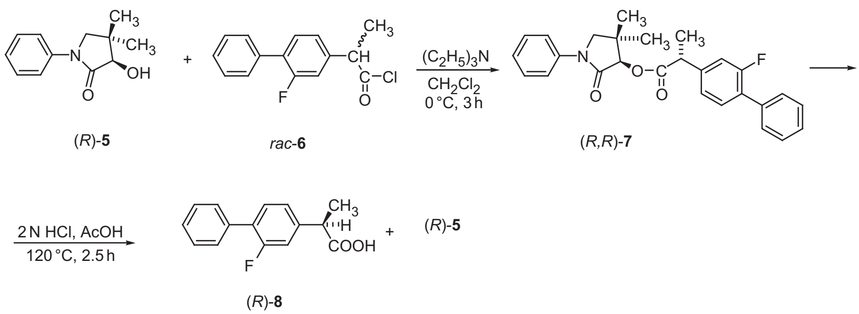

Industrially, (*R*)-flurbiprofen is obtained via the following steps: (i) synthesis of a suitable activated derivative of flurbiprofen, (ii) preparation of the corresponding amide of (*R*,*R*)-thiomicamine to obtain a diastereomeric mixture, (iii) second-order asymmetric resolution, and (iv) hydrolysis of the optically pure amide. This process leads to a 73% yield [7].

3.2.1.2. Enantioselective synthesis of (S)-flurbiprofen via asymmetric dihydroxylation The aryl bromide was converted to the Grignard reagent **9**, and this reacted with acetone to give the alcohol **10** (75%) [40,41]. Dehydration of this alcohol with $MeSO_2CI/Et_3N$ gave the alkene **11** (83%) [42]. Asymmetric dihydroxylation of this alkene was achieved by the use of AD (α mix) to give the diol **12** (93%, 98% ee). The racemic diol was obtained by OsO_4/NMMNO oxidation of the alkene, and the enantiomeric excess of the diol **12** was then determined by the use of chiral shift NMR experiments on the derived mono primary acetates. Conversion of the diol **12** to the monotosylate **13** and then treatment of the tosylate with sodium hydride gave the epoxide **14** (76%) [43]. Catalytic hydrogenolysis (10%Pd/C/EtOH/trace OH^-) at −40°C gave the alcohol

15 (90%). Jones oxidation of the primary alcohol **15** gave (*S*)-(+)-fiurbiprofen **8**, mp 108–110°C (lit. [44] *rac*. 110–111°C), (56%, 98% ee). The enantiomeric excess of flurbiprofen **8** could not be determined from its cinchonidine salt. Instead, it was converted to the methyl ester, and chiral shift NMR experiments [6,45] on this derivative allowed the determination to be made, as in the following scheme.

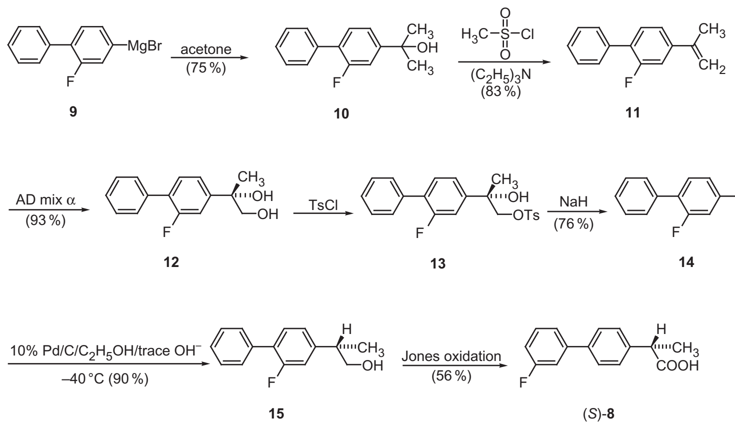

3.2.2. Biocatalyzed enantioselective synthesis of (*R*)- and (*S*)-flurbiprofen

The kinetic resolution of (*S*)- or (*R*)-flurbiprofen has mainly been conducted by chemical methods, such as the asymmetric synthesis of an (*S*)-enantiomer or the use of chiral chromatography and stereoselective crystallization [46–48]; however, these methods entail expensive manufacturing processes and are complex for industrial application.

Therefore, the use of biochemical processes for the kinetic resolution of an optically active (*S*)- and (*R*)-enantiomers from its corresponding racemic molecule using biocatalysts from a microbial origin has recently drawn much attention [49–52]. Lipases (triacylglycerol acylhydrolase, E.C. 3.1.1.3) are most commonly used as the biocatalyst for the enzymatic resolution of an (*S*)-enantiomer [53,54]. For example, a lipase from *Candida rugosa* was found to have a relatively high enantioselective activity toward the (*S*)-flurbiprofen ester compared to other known lipases or esterases; however, the level of the enantiomeric excess was unsatisfactory [52,55]. Plus, the esterase PF1-K from the newly screened *Pseudomonas* sp. KCTC 10122BP was found to effectively hydrolyze (*S*)-flurbiprofen ethyl ester into optically pure (*S*)-flurbiprofen [52].

Immobilized lipase B from *Candida antarctica* (Novozym® 435) has been reported to exhibit a relatively high enantiopreference toward the (*R*)-flurbiprofen, and it has been applied to the flurbiprofen resolution via either esterification or transesterification in organic media [56,57]. It was found that the enzymatic hydrolysis of *rac*-flurbiprofen methyl ester in

aqueous-organic medium gave poor results. Transesterification of the same ester mediated by immobilized lipase from Novozym® 435 in organic solvent proceeded with good enantiomeric excess, but the isolation of the product required chromatographic separation and therefore was unsuitable for large-scale preparation. Direct esterification of **4** with methanol in acetonitrile promoted by Novozym® 435 proved to be the best method since it gave, via a twofold kinetic resolution, *S*-flurbiprofen with excellent enantiomeric excess. The *R*-flurbiprofen methyl ester formed in the reaction can be converted into the starting *rac*-flurbiprofen by alkaline hydrolysis or, alternatively, into *R*-flurbiprofen by hydrolysis with acid [56–58] as in the following scheme:

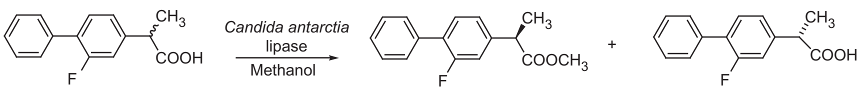

rac-**4** (*R*)-**16** (*S*)-**8**

In the past few years, the synthesis of ester bound has been reported by different microorganisms used as dry mycelia [59,60]. Dry mycelia can show high enantioselectivity and stability to temperature and organic solvent. Dry mycelia of molds are a precious source of enantioselective enzymes with interesting economic and technological benefits, such as improved stability while avoiding costly and time-consuming purifications [59–61]. However, mycelia of *Aspergillus oryzae* display high enantioselectivity toward (*R*)-flurbiprofen and can be efficiently used in pure organic solvent for the resolution of (*R,S*)-flurbiprofen through esterification. The use of the lyophilized mycelia facilitates the separation process so that in one step the two enantiomers of flurbiprofen, which are both valuable for pharmaceutical applications, can be easily separated. The biotransformation can be carried out in different apolar solvents (i.e., *n*-heptane or toluene) using different primary alcohols (i.e., ethanol or 1-octanol) as nucleophiles under very mild conditions [7] according to the following scheme.

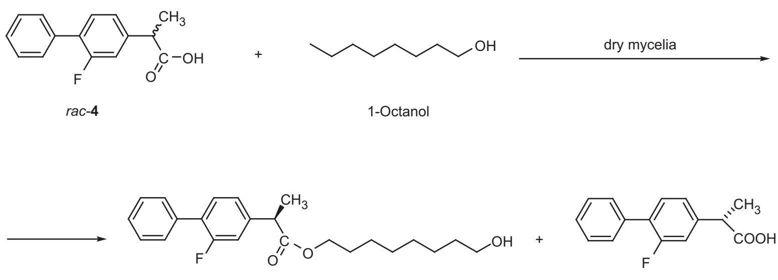

rac-**4** 1-Octanol

(*R*)-**17** (*S*)-**8**

Thorpe and Caster [62] reported the following method for the preparation of flurbiprofen.

The Ullman condensation of 4-bromo-3-nitroacetophenone **1** with benzene in the presence of cupper gives 2-nitro-4-acetylbiphenyl

2 which was reduced to the corresponding amino compound **3**. This was converted by the Schieman reaction into 2-fluoro-4-acetylbiphenyl **4** which by heating with sulfur and morpholine gives 2-fluoro-4-biphenylacetic acid **5**. Compound **5** was converted to the ester **6** by reluxing with ethanol and sulfuric acid.

The reaction of ethyl 2-fluoro-4-biphenylyl acetate **6** with diethyl carbonate and sodium ethoxide and then with dimethyl sulfate in ethanol gives diethyl 2-fluoro-4-biphenylyl-α-methyl malonate **7** which was hydrolyzed with sodium hydroxide in ethanol and finally decarboxylated at 180–200°C to give flurbiprofen **8** [62] as in the following scheme:

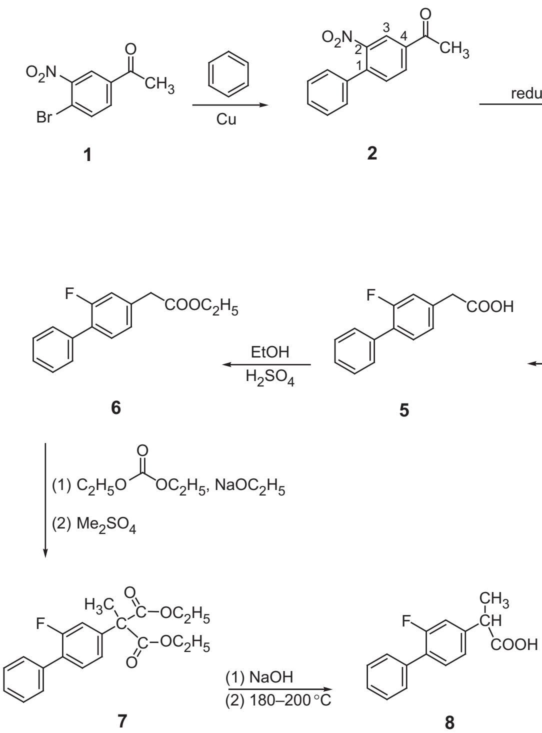

Schlosser and Geneste [63] synthesized flurbiprofen by conversion of 3-fluorotoluene into 2-fluoro-4-methylbiphenyl **4** with consecutive deprotonation and carboxylation of the benzylic methyl group and α-deprotonation followed by methylation to give flurbiprofen **6**.

3-Fluorotoluene **1** was treated with *tert*-butyl lithium and potassium *tert*-butoxide in tetrahydrofuran and pentane, and after acidifying with hydrochloric acid, 2-fluoro-4-methylbenzoic acid was produced **2**. Treatment of **2** with fluorodimethoxyborane diethyl etherate and hydrochloric acid gives 2-fluoro-4-methylphenylboronic acid **3**. A solution of compound **3** with ethanol and aqueous solution of sodium carbonate were added to bromobenzene, and tetrakis (triphenylphosphine) palladium

gives 2-fluoro-4-methyl biphenyl **4**. When compound **4** was treated with lithium diisopropylamine and potassium *tert*-butoxide and after acidification with hydrochloric acid and extraction, 2-fluoro-4-biphenylyl acetic acid **5** was produced. At −75°C, lithium diisopropylamine, *tert*-butoxide, and 2-fluoro-4-biphenylyl acetic acid **5** were added to a solution of butyl lithium in tetrahydrofuran and hexane, and treatment with methyl iodide gives flurbiprofen **6** as in the following scheme:

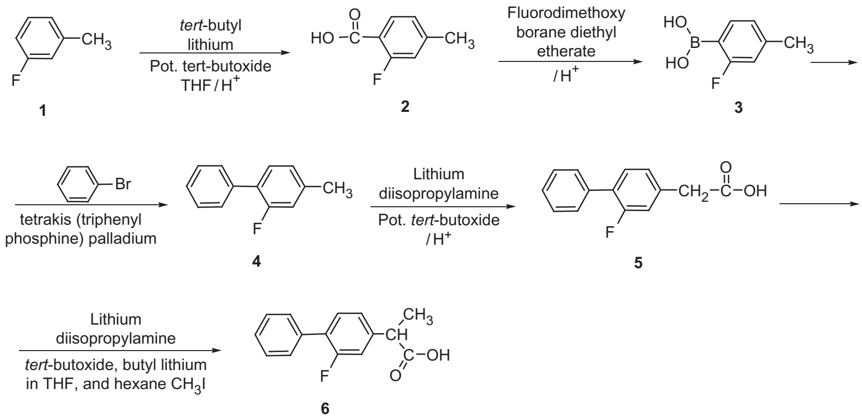

Lu *et al.* [64] reported a procedure for synthesis of flurbiprofen via Suzuki reaction catalyzed by palladium charcoal. 2,4-Difluoro nitrobenzene **1** was reacted with diethyl methylmalonate **2** to give diethyl-2-(3-fluoro-4-nitrophenyl)methylmalonate **3**. Compound **3** was hydrolyzed and decarboxylated to give 3-fluoro-4-nitro-α-methylphenyl acetic acid **4**. Compound **4** was reduced to give 4-amino-3-fluoro-α-methylphenyl acetic acid **5**. Compound **5** was converted to 4-bromo-3-fluoro-α-methylphenyl acetic acid **6,** and finally, compound **6** was coupled with sodium tetraphenhylborate to give flurbiprofen **7** according to the following scheme:

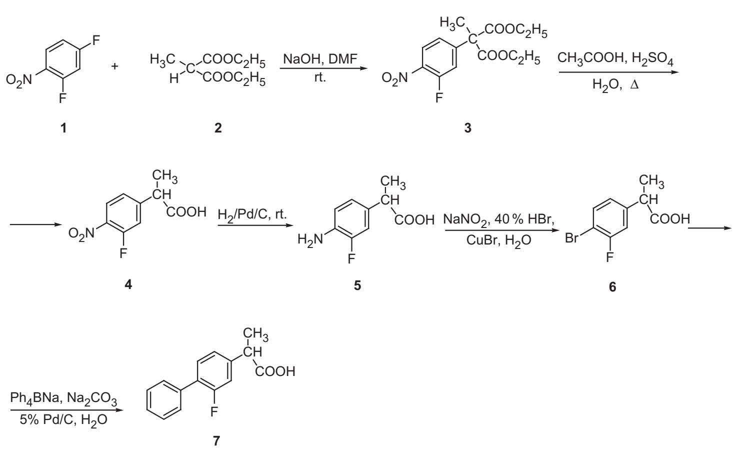

Terao *et al.* [65] described an enzymatic method for the synthesis of (*R*)-flurbiprofen. The drug was prepared from the corresponding malonic acid derivative **3** via asymmetric decarboxylation catalyzed by aryl malonate decarboxylase (EC 4.1.1.76) in high chemical and optical yield.

Esterification of racemic flurbiprofen **1** gives the racemic flurbiprofen methyl ester **2**. Treatment of the ester **2** with lithium diisopropylamide and methyl chloroformate gives dimethyl 3-fluoro-4-biphenylyl-methyl malonate **3**. Compound **3** on hydrolysis gives the corresponding acid **4**. Compound **4** on enzymatic decarboxylation gives (*R*)-flurbiprofen as in the following scheme.

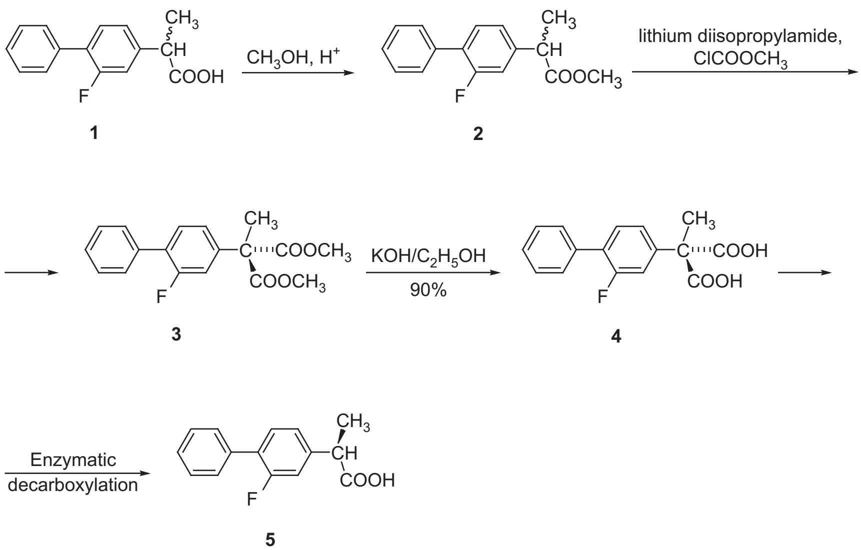

4. PHYSICAL CHARACTERISTICS

4.1. Melting point

Between 114 and 117°C [3].

4.2. Solubility

Practically insoluble in water, freely soluble in most organic solvents. It dissolves in aqueous solutions of alkali hydroxides and carbonates [3].

4.3. Appearance

A white (or almost white) crystalline powder [3].

4.4. Partition coefficient

log *P* (octanol/water) 4.2 [3].

4.5. Half-life

Plasma half-life, 2–6h (mean 3.5) [3].

4.6. Volume of distribution

About 0.1L/kg [3].

4.7. Clearance

Plasma clearance, about 0.3mL/min/kg [3].

4.8. Protein binding

In plasma, about 99% [3].

4.9. Disposition in the body

Readily absorbed after oral administration, about 95% of a dose is excreted in the urine in 24h, mainly as the 4′-hydroxy, 3′,4′-dihydroxy, and 4′-methoxy metabolites, which are excreted partly as conjugates, about 25% of a dose is excreted as unchanged drug [3].

5. SPECTRAL PROPERTIES

5.1. Ultraviolet spectroscopy

UV spectra of flurbiprofen in aqueous acid (Fig. 4.1) were scanned from 200 to 400nm, using UV/VIS spectrophotometer. Flurbiprofen exhibited the maximum absorption at 247nm (Fig. 4.1) [3].

5.2. Infrared spectroscopy

The IR spectrum of *rac*-flurbiprofen as KBr disc is presented in Fig. 4.2 [66].

Principal peaks at wave numbers 1710, 1505, 1596, 1220, 743, 1230 cm^{-1} (KBr disc). FTIR spectrum of (*S*)-flurbiprofen as (Nujol) was recorded on a JASCO FTIR-200 as follows: 3000 (br), 1698, 1580, 1514, 1216, 765, 724, 698 cm^{-1} [7].

5.3. Nuclear magnetic resonance spectrometry

The ^{1}H and ^{13}C NMR spectra of (*S*)-flurbiprofen were registered with a Varian Gemini 200 spectrometer (200MHz), and the ^{19}F NMR spectra were recorded with a Bruker AC 200F (188MHz). Chemical shifts were

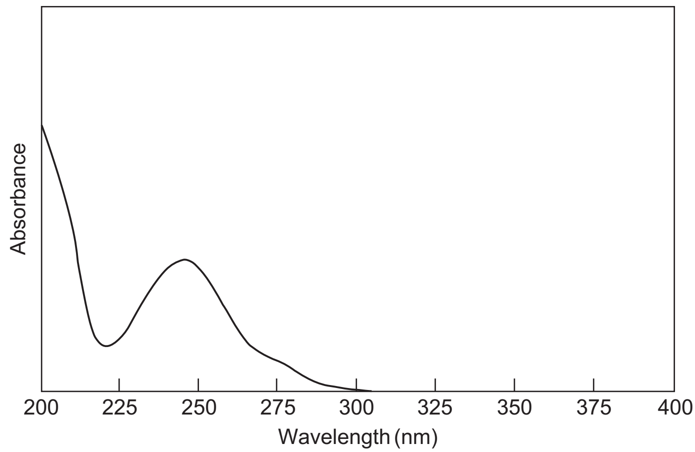

FIGURE 4.1 UV spectrum of flurbiprofen in ethanol [3].

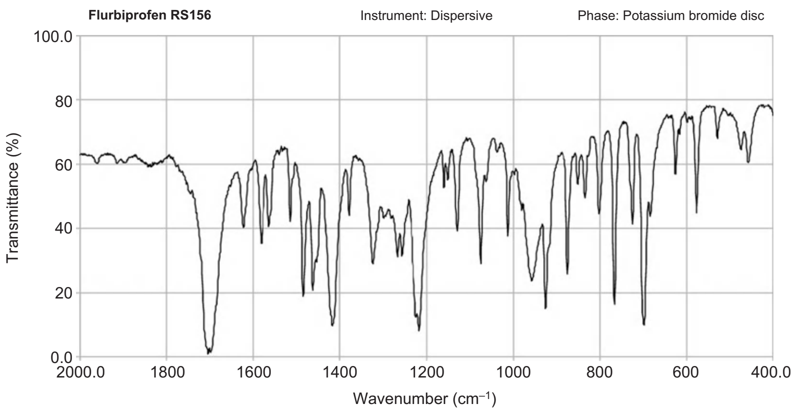

FIGURE 4.2 Infrared spectrum of flurbiprofen (KBr disc) [66].

expressed in parts per million with respect to the tetramethylsilane signal for the ^{1}H and ^{13}C NMR and Ar-CF_3 for ^{19}F [7]. The ^{1}H and ^{13}C NMR spectra of *rac*-flurbiprofen were recorded on a Varian XL 500MHz FT spectrometer (Figs. 4.3–4.6).

5.3.1. ^{1}H NMR spectra

***rac*-Flurbiprofen**, ^{1}H NMR ($CDCl_3$): δ 1.67–1.69 (d, 3H, J=6.5Hz, CH_3), 3.90–3.93 (t, 1H, J=7.0Hz, CH), 7.29–7.31 (d, 2H, J=9.0Hz, H-Ph), 7.48–7.57 (m, 4H, H-Ph), 7.66–7.67 (d, 2H, J= 7.0Hz, H-Ph), 12.19 (s, 1H, COO-H, exchange with D_2O) (Figs. 4.3 and 4.4).

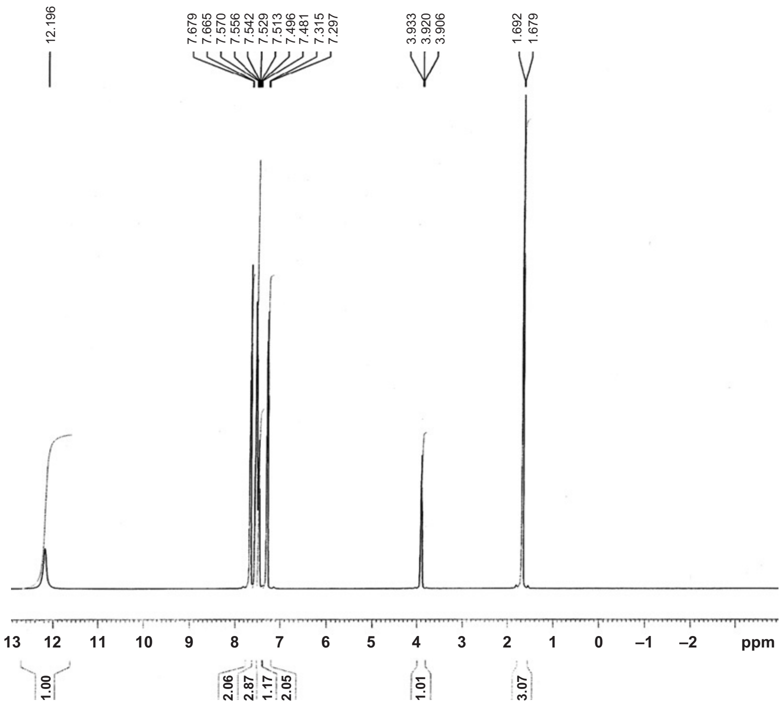

FIGURE 4.3 ^1H NMR spectrum of *rac*-flurbiprofen in $CDCl_3$.

(*S*)-Flurbiprofen, ^1H NMR ($CDCl_3$): δ 1.59 (d, 3H, J=7.3Hz, CH_3), 3.85 (q, 1H, J=7.1Hz, CH), 7.14–7.24 (m, 2H, H-Ph), 7.38–7.60 (m, 6H, H-Ph) [7,67].

5.3.2. ^{13}C NMR spectra

***rac*-Flurbiprofen**, ^{13}C NMR ($CDCl_3$): δ 18.03, 45.04, 115.43, 115.62, 123.58, 123.80, 127.83, 128.25, 128.6, 128.69, 129.06, 129.08, 130.99, 131.02, 135.54, 141.05, 141.11, 158.87, 160.85, 180.77 (Figs. 4.5 and 4.6).

(*S*)-Flurbiprofen, ^{13}C NMR ($CDCl_3$): δ 18.2, 45.0, 115.3, 115.8, 123.8, 123.9, 127.9, 128.2, 128.5, 128.6, 129.1, 129.2, 131.0, 131.1, 135.6, 141.0, 141.1, 157.4, 162.4, 179.6. ^{19}F NMR ($CDCl_3$): δ −117.67 (dd, J_1=8.4Hz, J_2=11.3Hz) [7].

5.3.3. Solid-state nuclear magnetic resonance

All the high-resolution NMR experiments were performed on a Varian Infinity Plus 400 double channel spectrometer operating at the ^1H Larmor frequency of 399.89MHz and the ^{13}C frequency of 100.56MHz, equipped with two CP-MAS probes for rotors with an outer diameter of 3.2 and 7.5 mm. Both the ^{13}C and ^1H 90° pulses were 4.2 and 1.9μs for the 7.5 and 3.2 probes, respectively [68].

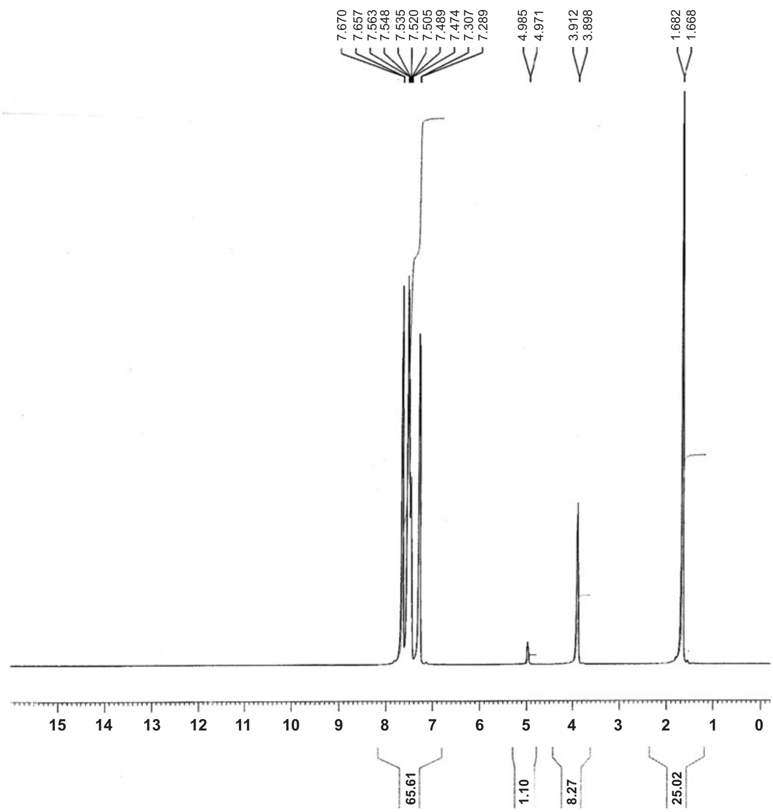

FIGURE 4.4 ^1H NMR spectrum of *rac*-flurbiprofen (D_2O exchange).

The CP-MAS spectra have been recorded using constant radio frequency power for both channels or a linear ramp for the ^{13}C channel power during the contact time [69]. Continuous wave decoupling was used for all samples except for flurbiprofen (FLU-A) and flurbiprofen sodium salt (FLU-S), for which a SPINAL-64 decoupling scheme was employed [70]. The CP-MAS spectra were recorded with a contact time of 1–2ms and spinning frequencies of 5–7.5kHz. The HETCOR experiments on FLU-A and FLU-S were both performed with 240 scans, 146 rows, and a contact time of 0.2ms, while the spinning rate was 6.5kHz for FLU-A and 7.5kHz for FLU-S. ^1H T_1 relaxation time measurements were performed through the ^{13}C-detected inversion recovery cross-polarization technique [71]. ^1H MAS experiments were recorded at a spinning frequency of 25kHz [68].

Both the resonance FID analysis and the ^1H T_1 measurements in low-resolution conditions were performed on a single-channel Varian XL 100 spectrometer interfaced with a Stelar DS-NMR acquisition system: in this

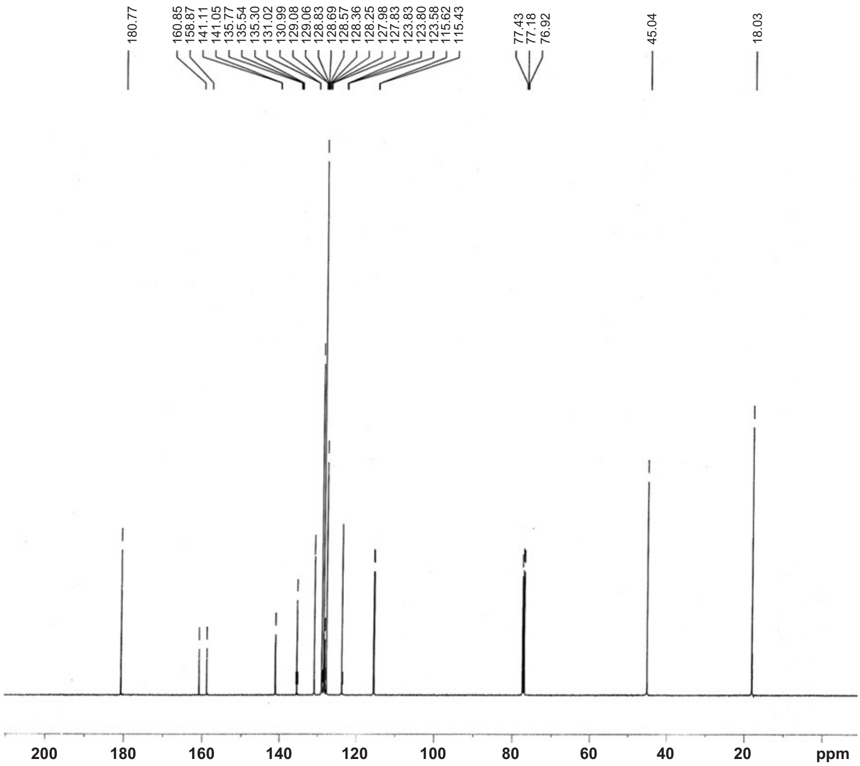

FIGURE 4.5 ^{13}C NMR spectrum of *rac*-flurbiprofen in $CDCl_3$.

case, the ^1H 90° pulse length was 2.8 μs. ^1H FIDs were recorded by means of the Solid Echo technique [72], using an echo delay of 12 μs and a dwell time of 1 μs. The pulse sequence Inversion Recovery with attached solid echo was used for measuring ^1H T_1. All the measurements have been performed at 25.0±0.2 °C [68] (Fig. 4.7).

5.3.4. ^1H MAS spectra

Expansions of the ^1H MAS spectra of FLU-A and FLU-S, recorded at a spinning frequency of 25 kHz, are shown in Fig. 4.8, together with the corresponding spectrum of RL.

The assignment of the peaks is quite straightforward: for FLU-A (Fig. 4.8B) four different signals are clearly distinguishable, corresponding to methyl (≈1 ppm), methine (≈3 ppm), aromatic (≈7 ppm), and acidic (≈14 ppm) protons. Unfortunately, the residual linewidth does not allow a better spectral resolution, and therefore, the different aromatic signals cannot be distinguished [68].

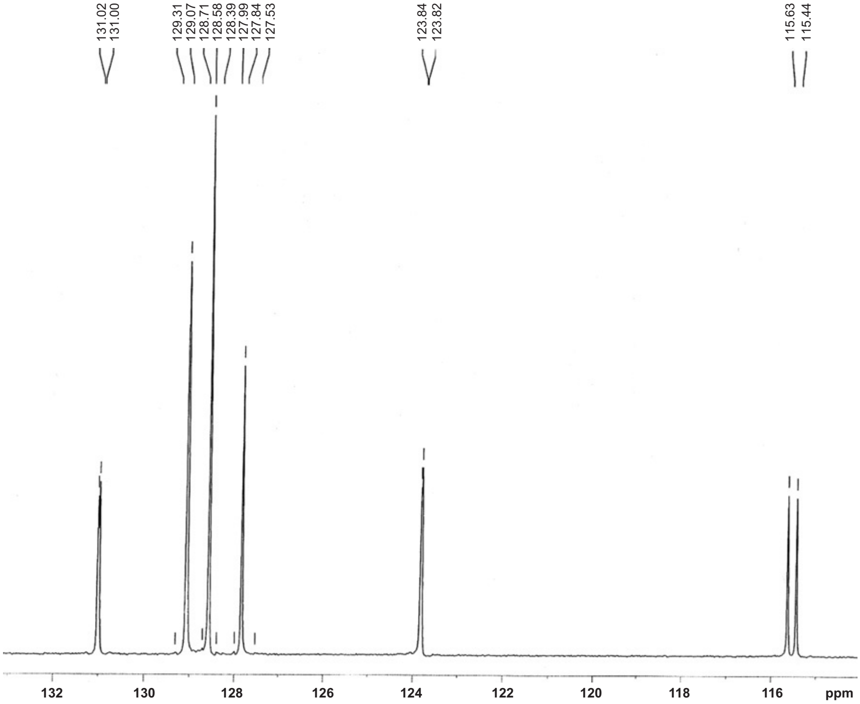

FIGURE 4.6 An expansion of ^{13}C NMR spectrum of *rac*-flurbiprofen in $CDCl_3$.

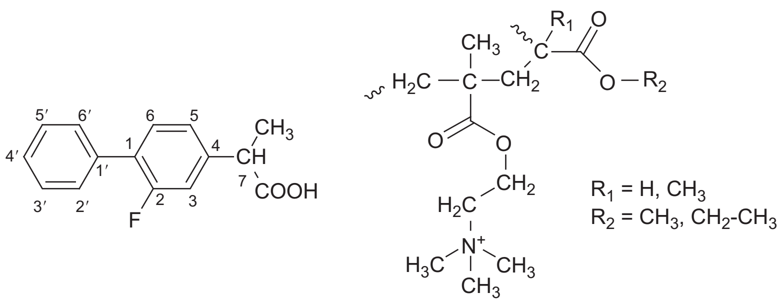

FIGURE 4.7 Chemical structures of FLU-A and Eudragit RL100 matrix (RL).

In the spectrum of FLU-S (Fig. 4.8A), the same group of resonances has been observed, with the obvious exception of that due to the acidic protons. However, some noticeable differences are present in the chemical shift values between FLU-A and FLU-S, mainly concerning the peak of the methyl protons. This difference (about 0.7 ppm) is too large to be explained with the sole different chemical structures between the two forms of FLU

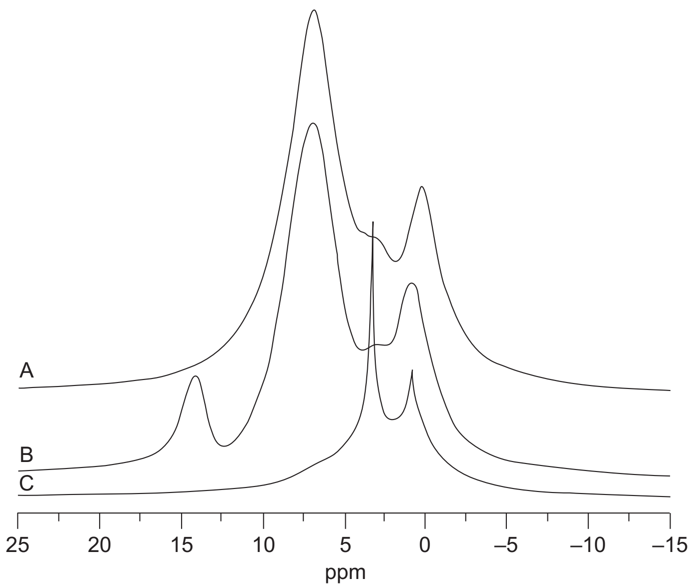

FIGURE 4.8 ^{1}H-MAS spectra of (A) FLU-S, (B) FLU-A, and (C) RL. All the spectra were acquired at a spinning speed of 25kHz [68].

and therefore suggests the presence of significant differences in either conformational properties or molecular packing. The ^{1}H MAS spectrum of RL (Fig. 4.8C) shows three heavily superimposed peaks, and its interpretation has been discussed in Ref. [73]: the signal at 1ppm is due to all the aliphatic protons, with the exception of those close to the ester groups, that give rise to the large resonance centered at about 3.5ppm, the narrow peak at the same chemical shift arises instead from the protons of the trimethylammonium groups, the minor linewidth being in agreement with the fast dynamic processes experienced by these groups [68].

5.3.5. ^{13}C CP-MAS spectra and ^{1}H–^{13}C HETCOR maps

The ^{13}C CP-MAS spectra of the acidic and sodium salt forms of FLU, together with the corresponding spectrum of RL, are shown in Fig. 4.9, while in Fig. 4.10, the ^{1}H–^{13}C FSLG-HETCOR maps of FLU-A and FLU-S are reported. The relatively small linewidths (about 100–150Hz) observed in the ^{13}C spectra of FLU-A indicate that it is crystalline, confirming the reported X-ray diffraction (PXRD) data [74], while slightly larger linewidths (150–250Hz) are present in the spectra of FLU-S. This difference could be in principle ascribable to a higher static disorder present in FLU-S. However, other effects, as for instance differences in anisotropic bulk magnetic susceptibility, possibly due to different degrees of aromatic

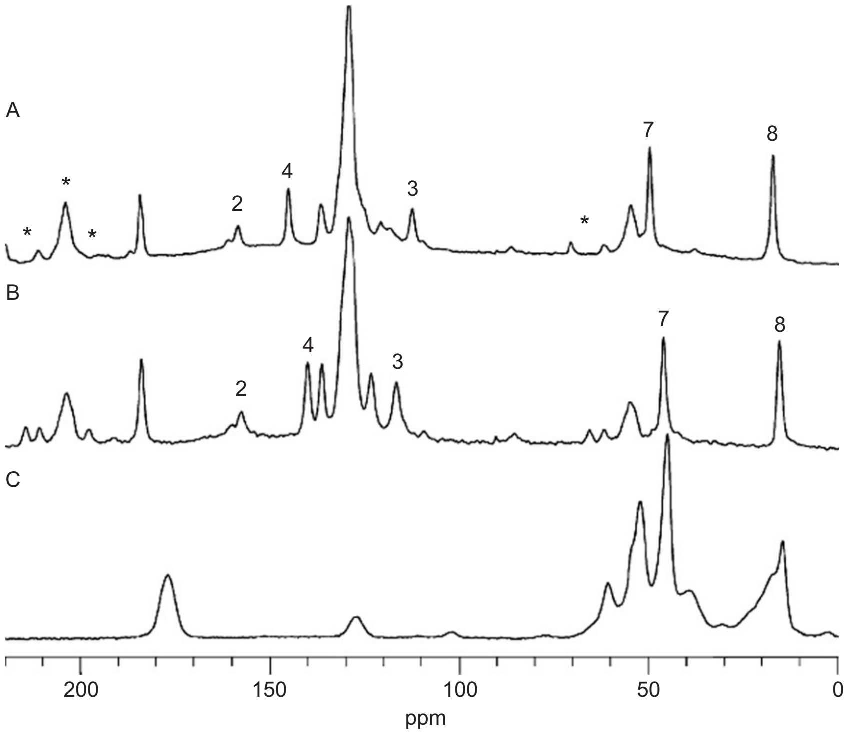

FIGURE 4.9 ^{13}C CP-MAS spectra of (A) FLU-S, (B) FLU-A, and (C) RL. The spinning speed was 7.5 kHz for FLU-A and FLU-S and 5 kHz for RL. The labeling of the peaks refers to Fig. 4.8. Asterisks denote spinning sidebands [68].

stacking, cannot be ruled out and might themselves provide an explanation of the experimental behavior [75,76].

The assignment of the ^{13}C spectrum of FLU-A (Fig. 4.9B) has been previously reported [74], while for FLU-S (Fig. 4.9A), the interpretation of the spectrum has been carried out on the basis of the comparison between the ^{13}C CP-MAS spectra and the ^{1}H–^{13}C HETCOR maps of the two drug forms (Fig. 4.10). The resulting assignments are shown in Table 4.1. In particular, the peaks resonating at 145.2 and 112.9 ppm, exhibiting the largest shifts with respect to the spectrum of FLU-A, have been assigned to carbons 4 and 3, respectively, thanks to the FLU-S HETCOR map (Fig. 4.10B). This has been possible by observing the strong correlation between the carbons resonating at 145.2 ppm and methane protons, and a similar HETCOR correlation profile between the peak at 112.9 ppm and that ascribable to carbon 2 (158.6 and 161.3 ppm), easily recognizable because of the $^{1}J_{C-F}$ doublet [68].

As already pointed out in the description of ^{1}H MAS spectra, also the differences observed in the ^{13}C spectra and HETCOR maps of FLU-A and

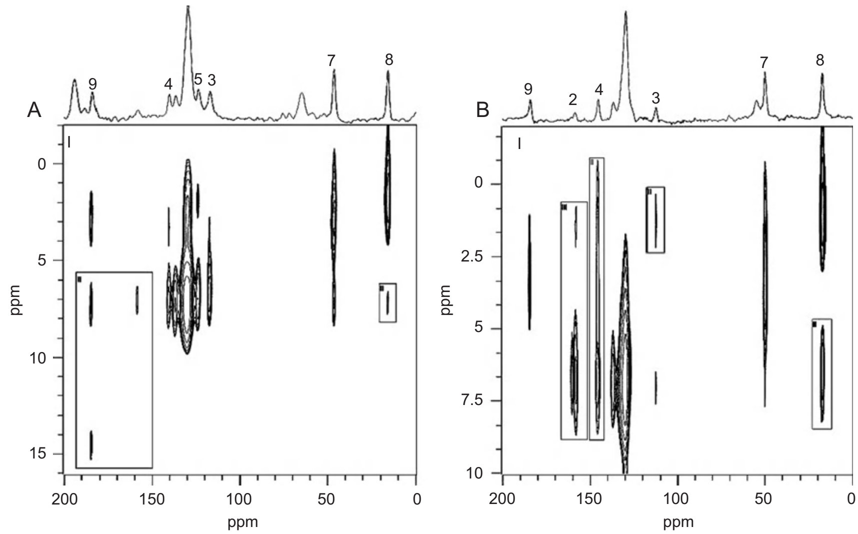

FIGURE 4.10 ^{1}H–^{13}C HETCOR maps of (A) FLU-A and (B) FLU-S. The correlation peaks shown in the different regions, labeled by roman numbers in the map, were sampled at different threshold levels for the sake of clarity, and the maximum peak intensities (in a. u.) are 100 in I and 8 in II for FLU-A; 100 in I, 8 in II, and 5 in III for FLU-S. The correlation peaks relative to ^{13}C spinning sidebands have been removed for simplifying the interpretation of the maps. Both the experiments were performed using 146 rows and a contact time of 0.2 ms, while the spinning speed was 6.5 kHz for FLU-A and 7.5 kHz for FLU-S. The labeling of the ^{13}C peaks refers to Fig. 4.8 [68].

TABLE 4.1 Assignment of ^{13}C solid-state spectra for FLU-A and FLU-S [68]

	^{13}C Chemical Shifts (ppm)	
Nucleus	FLU-A	FLU-S
1′	136.4	136.2
2[a]	157.7	158.6
	160.2	161.3
3	116.9	112.9
4	140.2	145.2
5	123.5	–
7	46.4	50.2
8	16.0	17.8
9	183.9	184.4
1, 6, 2′, 3′, 4′, 5′, 6′	128.5	129.1

The labeling of the nuclei refers to Fig. 4.7.
[a] The doublet observed for this carbon is due to the $^1J_{C\text{–}F}$ scalar coupling [77].

FLU-S must be discussed not only in terms of their different chemical structures, expected to mainly affect the chemical shifts of the signals of the carbonyl and nearest aliphatic carbons, but also taking into account possible different crystalline packing and conformational and dynamic behavior, that can be particularly important in solid-state spectra [68].

By comparing the ^{13}C chemical shifts of FLU-A and FLU-S, several differences can be outlined. Passing from FLU-A to FLU-S, some shifts toward higher frequencies for aliphatic CH and CH_3 signals have been recorded, qualitatively expected by replacing the carboxyl moiety with the carboxylate one. However, these shifts are larger than those predicted by semiempirical calculations for solution-state spectra, based on the mere chemical structural changes (3.8 vs. 2.7 and 1.8 vs. 1.5ppm for methine and methyl carbons, respectively). Nonetheless, the most significant differences are visible in the aromatic spectral region that should be substantially unaffected by the different chemical structures. In particular, carbons 2 and 4 give rise to high-frequency shifts by about 1.0 and 5.0ppm, respectively, while carbon 3 shifts toward lower frequencies by 4.0ppm. These changes clearly indicate that FLU-A and FLU-S experience quite different conformational and/or crystal packing situations, as already hypothesized on the basis of ^{1}H spectra. This point could be further clarified by analyzing the 2D-HETCOR maps, showing dipolarly coupled proton–carbon pairs, mostly determined by their spatial proximity. In addition to the correlation expected on the basis of the chemical structure of FLU (for instance, the methyl protons are obviously correlated to methyl, methane and carboxylic carbons), there are other correlations that shed light on the molecular conformational behavior. In particular, by looking at methyl protons, in FLU-S, they are correlated with aromatic carbons 3 and 2, indicating that the methyl group is closest to the side of the phenyl ring where the fluorine atom is present. A very different situation has been observed in FLU-A, where the same protons are correlated to the aromatic carbon 5, therefore revealing that here the methyl group lies on the opposite part of the phenyl ring, in agreement with the observed aromatic ring shifts [68].

5.4. Mass spectrometry

Mass spectra of (*S*)-flurbiprofen, carried out with electron impact method, were registered at 70eV using a Ion Trap GCQ Finnigan mass spectrometer (Fig. 4.11). EI ($CHCl_3$): m/z 244 [7]. Principal ions and their relative intensities are presented in (Table 4.2).

6. X-RAY POWDER DIFFRACTOMETRY

The X-ray powder diffraction pattern of flurbiprofen was performed using Simmons XRD-5000 diffractometer. Figure 4.12 shows the X-ray powder diffraction pattern of flurbiprofen which was obtained on a

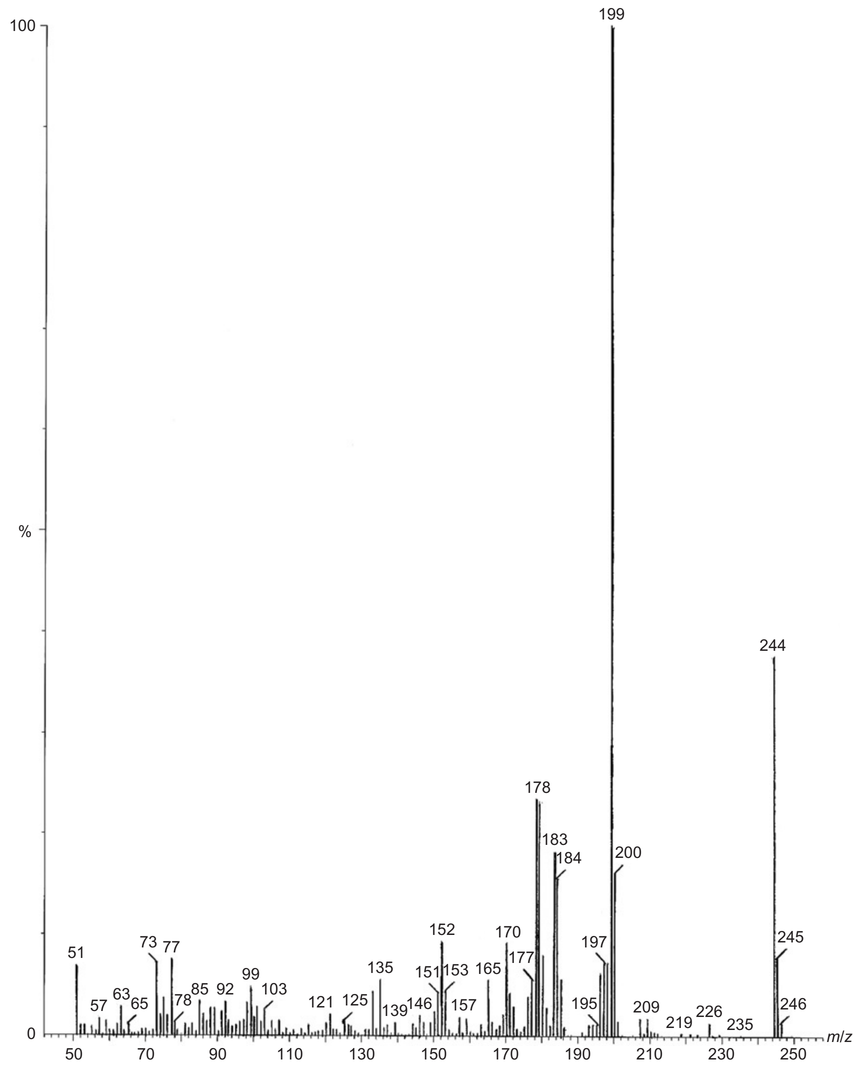

FIGURE 4.11 Mass spectrum of flurbiprofen.

pure sample of the drug substance. Table 4.3 shows the values for the scattering angles (deg, 2θ), the interplanar d-spacing (Å), and the relative intensities (%) observed for the major diffraction peaks of flurbiprofen.

Diffraction patterns were recorded with a Philips diffractometer PW 1050/25 for powders. A voltage of 40 kV and a current of 30 mA for the generator were used, with Cu as the tube anode material. The solids were exposed to Cu Kα radiation (α_1=1.54060 Å and α_2=1.54439 Å, with an α_1/α_2 ratio of 0.5), over a range of 2θ angles from 3° to 30°, at an angular speed of

TABLE 4.2 Mass spectrum fragmentation pattern of flurbiprofen

		Fragment	
m/z	Relative intensity (%)	Formula	Ions
245	7.9	$C_5H_{14}FO_2$	M+1
244	37.8	$C_{15}H_{13}FO_2$	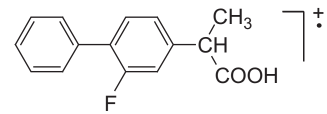
229	0.2	$C_{14}H_{10}FO_2$	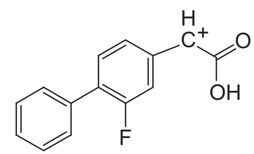
199	100	$C_{14}H_{13}F$	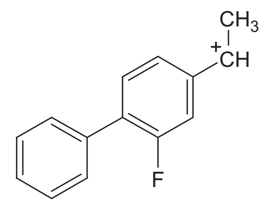

(*continued*)

TABLE 4.2 (*continued*)

		Fragment	
m/z	Relative intensity (%)	Formula	Ions
184	15.7	$C_{13}H_9F$	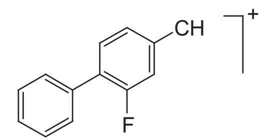
171	4.4	$C_{12}H_8F$	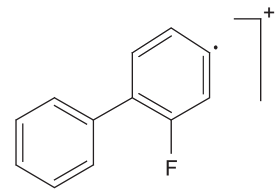
153	9.4	$C_{12}H_9$	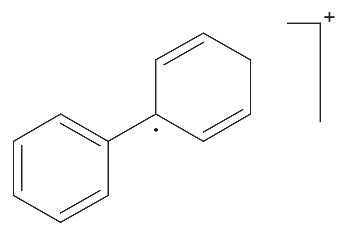
73	7	$C_3H_5O_2$	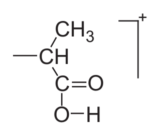

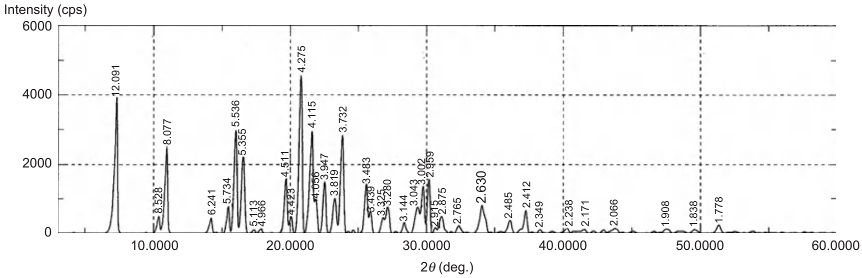

FIGURE 4.12 X-ray powder diffraction pattern of flurbiprofen.

TABLE 4.3 The X-ray powder diffraction pattern for flurbiprofen

Scattering angle (°) (2θ)	*d*-Spacing (Å)	Relative intensity (%)	Scattering angle (°) (2θ)	*d*-Spacing (Å)	Relative intensity (%)
7.305	12.0914	3827	23.270	3.8194	1008
10.365	8.5276	480	23.820	3.7324	2832
10.945	8.0769	2427	25.555	3.4828	1422
14.180	6.2407	428	25.885	3.4392	649
15.440	5.7342	765	26.790	3.3250	440
15.995	5.5364	2964	27.165	3.2800	756
16.540	5.3552	2304	28.365	3.1439	308
17.330	5.1128	109	29.325	3.0431	741
17.845	4.9664	126	29.740	3.0016	1361
19.665	4.5107	1578	30.175	2.9593	1563
20.060	4.4227	475	30.640	2.9154	162
20.760	4.2752	4553	31.085	2.8747	484
21.575	4.1155	2934	32.350	2.7651	215
21.895	4.0560	979	34.060	2.6301	802
22.510	3.9466	1481	36.420	2.4847	368

1° (2θ) per minute, using divergence and receiving slits of 0.5° or 1° and 0.2°, respectively. As Fig. 4.13 shows, PXRD analysis of pure flurbiprofen showed the diffractographic profile of a crystalline product [74].

7. X-RAY CRYSTALLOGRAPHY

7.1. Crystal structure of (±)-2-(2-fluoro-4-biphenyl) propionic acid (flurbiprofen)

Data were collected on an automatic diffractometer with the θ–2θ scanning technique (1.7° scan in 2θ at a scanning speed of 2° min^{-1}) using Cu Kα radiation (λ=1–54,178 Å, Ni filter). Unit-cell parameters were

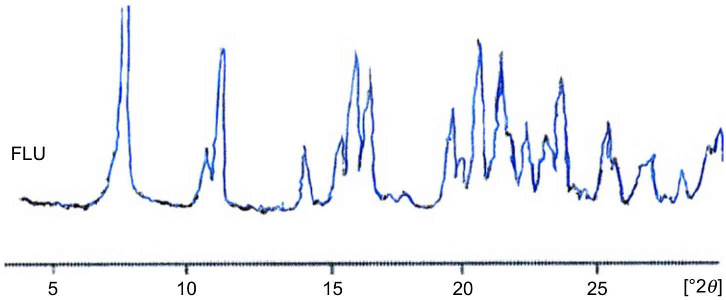

FIGURE 4.13 X-ray diffraction patterns of pure flurbiprofen [74].

determined from a least-squares fit of the coordinates of 12 reflections which were individually centered on the diffractometer. During data collection, three standard reflections were monitored after each 50 new reflections had been measured. The monitored data gave no indication of crystal deterioration [78].

The structure was solved by using a fragment of the molecule obtained in an E map derived from the symbolic addition procedure as a partial structure for the tangent formula in space group $P1$ (Figs. 4.1 and 4.2). The crystal data for $C_{15}H_{13}O_2F$ were, $P\bar{1}$, a=9.315 (4), b=12.738 (9), and c=5.823 (2) Å, α=83.0 (1), β=107.2 (1), γ=107.0 (1)°, Z=2, d_{calc}=1.29 g cm^{-3} (Figs. 4.14 and 4.15).

7.2. Crystal structures and physical properties of flurbiprofen salts

Flurbiprofen is bearing a carboxyl group. As the free acid its aqueous solubility is only 0.03 mg/mL. Hydrophobicity of the counter ion does not fully determine the solubility of its amine salts, being 0.37, 2.80, 0.64, and 0.17 mg/mL for the cyclohexyl (CH)-, hexyl-, octyl-, and adamantyl

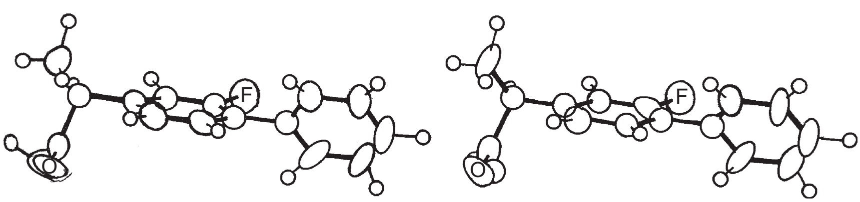

FIGURE 4.14 Stereo configuration of the molecule drawn by program *ORTEP*. The heavy atoms are shown at their final refined coordinates with anisotropic thermal parameters. The hydrogens are drawn at their difference map coordinates with arbitrary isotropic parameters [78].

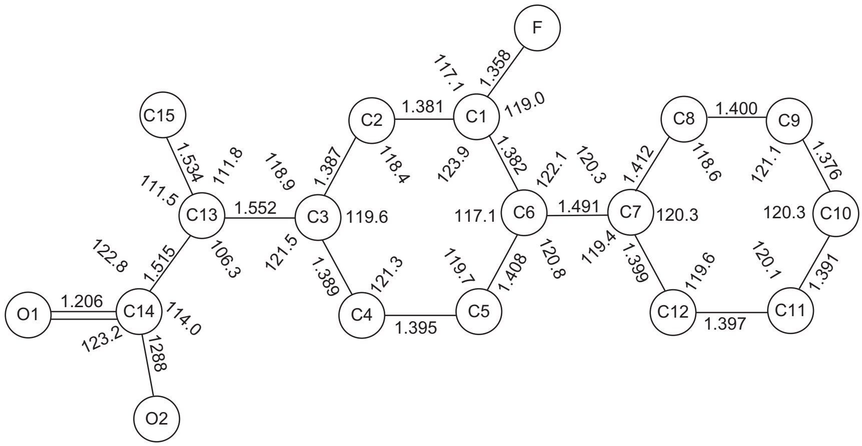

FIGURE 4.15 Bond distances and angles. The numbering scheme does not correspond to the chemical numbering used to name the compound. Standard deviations are of the order of 0.009 Å for the bond lengths and 0.6° for the bond angles [78].

(AD)-ammonium salts, respectively. Δ*H* of fusion is 159.0 J/g for the CH but only 81.0 J/g for the hexylammonium salt. It was reported that the structures of the stable CH and AD salts, acquired with synchrotron radiation because they exist as fine needles [79].

In both cases, the cycloalkyl group covers the twofold disordered fluorophenyl ring, forming a clear hydrophobic domain. Hydrogen bonds join three ammonium H atoms to two carboxylate O atoms and create infinite ladders along the short *b*-axis, which in CH shows no thermal expansion, while the *a*-axis expands by 1.9% over 141 K (Table 4.4) [80,81].

7.3. X-ray crystallographic determination of the absolute configuration of (+)-flurbiprofen utilizing β-cyclodextrin complexation

The crystal structure of the β-cyclodextrin complex with an optically active (+)-flurbiprofen was determined by the X-ray method to establish the absolute configuration of the chiral guest molecules **4**. The single

TABLE 4.4 Crystal data of flurbiprofen salts [80,81]

Crystal, *T* (K)	*a* (Å)	*b* (Å)	*c* (Å)	*β* (°)	*ρ* (mg/m^3)
CH, 150	14.7991	6.3014	19.7845	91.273	1.237
CH, 291	15.0841	6.2988	19.8939	91.146	1.207
AD, 150	39.350	6.3973	16.9976	90	1.228
AD, 291	39.514	6.4257	17.1454	90	1.213

crystal of (+)-FP–β-CyD complex was prepared by slowly cooling a hot β-CyD solution saturated with (+)-FP. Lattice parameters and reflection intensities were measured on a Nicolet P3/F diffractometer with graphite-monochromated Cu Kα radiation. By using the θ–2θ scan mode, 9639 independent reflections with $[F_o] \geq 3\sigma$ (F) were obtained up to 117° in 2θ. The crystal structure was deduced on the basis of the isomorphous structure of n-propanol–β-CyD complex and refined by the block-diagonal least-squares method to the R-value of 0.095. Crystal data were as follows: $(C_{42}H_{70}O_{35}\cdot C_{15}H_{13}O_2F)_2\cdot 21H_2O$, F.W.=3136.8, triclinic, space group $P1$, z=1, a=15.446 (2), b=15.513 (2), and c=18.107 (2)Å, α=113.52 (1)°, β=99.32 (1)°, γ=102.89 (1)°, V=3721.9 (7)$Å^3$, D_x=1.40 g cm^{-3}, D_m= 1.41 g cm^{-3} (Fig. 4.16) [4].

8. METHODS OF ANALYSIS

8.1. Compendial methods of analysis

8.1.1. United States Pharmacopoeia [82]

Flurbiprofen contains not less than 99% and not more than 100.5% of $C_{15}H_{13}FO_2$, calculated on the dried basis.

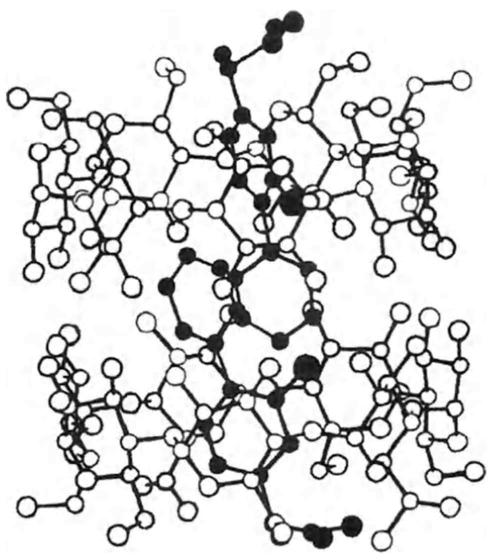

FIGURE 4.16 Projection of the 2:2 (+)FP–β-CyD complex. The atoms of the flurbiprofen are drawn with shading, and the circles represent fluorine, oxygen, and carbon atoms in the order of decreasing size [4].

Packaging and storage: Preserve in a tight container.

Identification

Test A: *Infrared absorption*: The test should be carried out as directed in the general procedure ⟨197K⟩, the infrared absorption spectrum of a potassium bromide dispersion of flurbiprofen previously dried, exhibits maxima only at the same wavelength as that of a similar preparation of *USP Flurbiprofen RS*.

Test B: *Ultraviolet absorption*: The test should be carried out as directed in the general procedure ⟨197U⟩, the ultraviolet absorption spectrum of a 10 μg/mL of flurbiprofen in 0.1 N sodium hydroxide, absorption maximum at 247 nm is about 0.8.

Melting range: The test should be carried out as directed in the general procedure ⟨741⟩, between 114 and 117 °C.

Loss on drying: The test should be carried out as directed in the general procedure ⟨731⟩. Dry flurbiprofen in a vacuum at 60 °C to constant weight: it loses not more than 0.5% of its weight.

Residue on ignition: The test should be carried out as directed in the general procedure ⟨281⟩, residue not more than 0.1%.

Heavy metal: The test when carried out as directed in the general procedure "Method II" ⟨231⟩, 0.001%.

Related Compounds

Diluent—Prepare a mixture of water and acetonitrile (11:9).

Mobile phase—Prepare a filtered and degassed mixture of water, acetonitrile, and glacial acetic acid (12:7:1). Make adjustments if necessary (see *System Suitability* under *Chromatography* in the general procedure ⟨621⟩).

Standard stock solution—Dissolve an accurately weighed quantity of USP Flurbiprofen-Related Compound A RS in *Diluent* to obtain a solution having a concentration of about 50 μg/mL.

System suitability solution—Pipet 2 mL of *Standard stock solution* into a 10-mL volumetric flask, add about 20 mg of USP Flurbiprofen RS, dilute with *Diluent* to volume and mix.

Standard solution—Transfer 2 mL of *Standard stock solution* to a 10-mL volumetric flask, dilute with Diluent to volume and mix.

Test solution—Prepare a solution of Flurbiprofen in *Diluent* containing 2 mg/mL.

Chromatographic system (see *Chromatography* in the general procedure ⟨621⟩—The liquid chromatograph is equipped with a 254-nm detector and a 3.9-nm × 15-cm column that contains 4-μm packing L1. The flow rate is about 1 mL/min. Chromatograph the *System suitability solution* and record the peak responses as directed for *Procedure*: the relative retention times are about 0.9 for flurbiprofen-related compound A and 1 for flurbiprofen, and the relative standard deviation for replicate injections is not more than 1%.

Procedure—Separately inject equal volumes (about 20 µL) of the *Standard solution* and the *Test solution* into the chromatograph, record the chromatograms, and measure the areas for the major peaks. Calculate the percentage of flurbiprofen-related compound A in the portion of flurbiprofen taken by the formula:

$$100(C_s/C_U)(r_U/r_s)$$

in which C_s is the concentration, in µg/mL, of USP Flurbiprofen-Related Compound A RS in the *Standard solution*, C_U is the concentration, in µg/mL of flurbiprofen in the *Test solution*, and r_U and r_s are the peak responses for Flurbiprofen-Related Compound A obtained from the *Test solution* and the *Standard solution*, respectively: not more than 0.5% of flurbiprofen-related compound A is found. Calculate the percentage of each impurity in the portion of flurbiprofen taken by the formula:

$$100(r_i/r_s)$$

in which r_i is the peak response for each impurity obtained from the *Test solution*, and r_s is the sum of the responses of all the peaks obtained from *Test solution*: the sum of all impurities is not more than 1%.

Assay—Dissolve about 0.5 g of flurbiprofen, accurately weighed, in 100 mL of alcohol, previously neutralized with 0.1 N sodium hydroxide VS to the phenolphthalein end-point, add phenolphthalein TS, and titrate with 0.1 N sodium hydroxide VS to the first appearance of a faint pink color that persists for not less than 30 s. Each milliliter of 0.1 N sodium hydroxide is equivalent to 24.43 mg of $C_{15}H_{13}FO_2$.

Flurbiprofen Tablets

Flurbiprofen tablets contain not less than 90% and not more than 110% of the labeled amount of flurbiprofen ($C_{15}H_{13}FO_2$).

Packaging and storage—Preserve in a well-closed container.

Identification

Test A: Place a number of tablets, equivalent to 100 mg of flurbiprofen, in a flask, add 10 mL of 0.1 N hydrochloric acid, and sonicate until the tablets disintegrate. Extract with two 15-mL portions of ether, combining the ether extracts in a flask containing about 1 g of anhydrous sodium sulfate. Decant the ether and evaporate to dryness: The IR absorption spectrum of a mineral oil dispersion of the residue so obtained exhibits maxima only at the same wavelengths as that of a similar preparation of USP flurbiprofen RS.

Test B: The retention time of the flurbiprofen peak in the chromatogram of the *Assay preparation* corresponds to that in the chromatogram of the *Standard preparation*, as obtained in the *Assay*.

Dissolution—Carry out the experiment as directed in the general procedure ⟨711⟩.

pH 7.2 Phosphate buffer—Dissolve 245 g of monobasic potassium phosphate and 50 g of sodium hydroxide in water to make 2000 mL of solution. Dilute 333 mL of this stock solution to 6000 mL of water. If necessary, adjust with 5N sodium hydroxide or with phosphoric acid to a pH of 7.20 ± 0.05.

Medium: pH 7.2 phosphate buffer, 900 mL.

Apparatus 2: 50 rpm.

Time: 45 min.

Procedure—Determine the amount of $C_{15}H_{13}FO_2$ dissolved from UV absorbance at the wavelength of maximum absorbance at about 247 nm on filtered portions of the solution under test, suitably diluted with *Dissolution Medium*, in comparison with a Standard solution having a known concentration of USP Flurbiprofen RS in the same *Medium*.

Tolerances—Not less than 75% (*Ω*) of the labeled amount of $C_{15}H_{13}FO_2$ is dissolved in 45 min.

Uniformity of dosage units

To be carried out as described in the general procedure ⟨9057⟩: meet the requirements, the following procedure being used where the test for *Content Uniformity* is required.

Procedure for content uniformity—Proceed as directed in the *Assay*, except in preparing the *Assay preparation* to use 1 tablet and to use 10 mL of *Internal standard solution* for each 25 mg of flurbiprofen in the tablet, based on the labeled amount.

Assay

Mobile phase—Dissolve 1.4 g of monobasic sodium phosphate in 570 mL of water, add 430 mL of acetonitrile, and adjust with phosphoric acid to a pH of 3. Filter and degas. Make adjustments if necessary (see *System suitability* under *Chromatography* in the general procedure ⟨621⟩).

Internal standard solution—Dissolve acetophenone in *Mobile phase* to obtain a solution having a concentration of about 0.8 μL/mL.

Standard preparation—Accurately weigh about 30 mg of USP Flurbiprofen RS. Add 10 mL of *Internal standard solution* and swill to dissolve. This stock solution contains about 3 mg of USP Flurbiprofen RS per milliliter. Dilute a portion of this stock solution with 20 volumes of *Mobile phase* and mix.

Assay preparation—Place 3 tablets in a stoppered container. Based on the labeled amount, in milligrams, of flurbiprofen in each tablet, add 25 mL of *Internal standard solution* for each 75 mg of flurbiprofen in the three tablets. Shake by mechanical means for about 15 min and centrifuge. Dilute a portion of this solution with 20 volumes of *Mobile phase* and mix.

Chromatographic system (see *Chromatography* in the general procedure ⟨621⟩)—The liquid chromatograph is equipped with a 254-nm

detector and a 4-mm X 25-cm column containing packing L7. The flow rate is about 2mL/min. Chromatograph the *Standard preparation* and record the responses as directed for *Procedure*: the relative retention times are about 0.4 for acetophenone and 1 for flurbiprofen, the resolution, ***R***, between the acetophenone and flurbiprofen is not less than 8, and the relative standard deviation for replicate injections is not more than 2%.

Procedure—Separately inject equal volumes (about 20 µL) of the *Standard preparation* and the *Assay preparation* into the chromatograph, record the chromatograms, and measure the responses for the major peaks. Calculate the quantity, in milligrams, of flurbiprofen ($C_{15}H_{13}FO_2$) in the portion of tablets taken by the formula:

$$(WV/10)(R_U/R_s)$$

in which W is the quantity, in milligrams, of USP Flurbiprofen RS used to prepare the *Standard preparation*, V is the volume, in milliliters, of *Internal Standard solution* used to prepare the *Assay preparation*, and R_U and R_s are the ratios of the flurbiprofen peak response to the acetophenone peak response obtained from the *Assay preparation* and the *Standard preparation*, respectively.

Flurbiprofen sodium

Flurbiprofen sodium contains not less than 97% and not more than 103% of $C_{15}H_{12}FNaO_2 \cdot 2H_2O$.

Packaging and storage—Preserve in well-closed containers.

USP Reference Standard: When carried out as directed in the general procedure ⟨11⟩—USP Flurbiprofen RS. *USP Flurbiprofen sodium RS. USP Flurbiprofen-Related Compound A RS.*

Identification

Test A: *Infrared absorption*: The test should be carried out as directed in the general procedure ⟨197M⟩. The infrared absorption spectrum of a potassium bromide dispersion of flurbiprofen previously dried exhibits maxima only at the same wavelength as that of a similar preparation of *USP Flurbiprofen RS*.

Test B: *Ultraviolet absorption*: The test should be carried out as directed in the general procedure ⟨197U⟩. The ultraviolet absorption spectrum of a 10 µg/mL of flurbiprofen in pH 6 buffer consisting of 2.42 g of monobasic sodium phosphate and 0.66 g of dibasic sodium phosphate dissolved in water to make 1000 mL. Absorptivities at 246 nm, calculated on the dried basis, do not differ by more than 3%.

Test C: The residue obtained by igniting it meets the requirements of the tests for *Sodium* as directed in the general procedure ⟨191⟩.

Specific rotation, when the test is carried out as directed in the general procedure ⟨781S⟩: between $-0.45°$ and $+0.45°$.

Test solution: 50 mg/mL, in methanol.

Loss on drying: Carry the test as directed in the general procedure ⟨731⟩—Dry about 0.3 g of it in vacuum at a pressure not exceeding 1 mm of mercury over phosphorous pentoxide in a suitable drying tube at 60 °C for 18 h: it loses not less than 11.3% and not more than 12.5% of its weight.

Heavy metals: The method should be carried out as directed in the general procedure ⟨231⟩ Method II: 0.001%.

Limit of flurbiprofen-related compound A

Diluent, *Mobile phase*, and *System suitability preparation*—Proceed as directed in the *Assay*.

Standard solution—Use *Standard flurbiprofen-related compound A preparation*, prepared as directed in the *Assay*.

Test solution—Use the *Assay preparation*.

Chromatographic system—Proceed as directed in the *Assay*, except to chromatograph the *Standard solution* instead of the *Standard preparation*.

Procedure—Separately inject equal volumes (about 20 μL) of the *Standard solution* and the *test solution* into the chromatograph, record the chromatogram, and measure the areas for the major peaks. Calculate the percentage of flurbiprofen-related compound A in the portion of flurbiprofen sodium taken by the formula:

$$200(C/W)(r_U/r_s)$$

in which C is the concentration, in microgram per milliliter of USP Flurbiprofen-Related Compound A RS in the *Standard solution*, W is the weight, in milligrams, of the portion of flurbiprofen sodium taken to prepare the *Test solution*, and r_U and r_s are the peak areas for flurbiprofen-related compound A obtained from the *Test solution* and the *standard solution*, respectively: not more than 1.5% is found.

Organic volatile impurities—Carry out this test as directed in the general procedure ⟨467⟩ Method I: Meets the requirements.

Assay

Diluents—Mix 500 mL of methanol and 250 mL of water.

Mobile phase—Prepare a filtered and degassed mixture of acetonitrile, water, and glacial acetic acid (50:49:1). Make adjustment if necessary (see *System Suitability* under *Chromatography* as directed in the general procedure ⟨621⟩).

Standard flurbiprofen-related compound A preparation—Dissolve an accurately weighed quantity of USP Flurbiprofen-Related Compound A RS in methanol to obtain a stock solution having a known concentration of about 150 μg/mL. Transfer 1 mL of this solution to a 200-mL volumetric flask, dilute with *Diluent* to volume, and mix.

Standard preparation—Dissolve an accurately weighed quantity of USP Flurbiprofen RS in methanol to obtain a stock solution having a known

concentration of about 1mg/mL. Transfer 5mL of this solution to a 100-mL volumetric flask, dilute with *Diluent* to volume, and mix.

System suitability preparation—Transfer 5mL of the stock solution used to prepare the *Standard preparation* and 2mL of the stock solution used to prepare the *Standard flurbiprofen-related compound A preparation* to a 100-mL volumetric flask, dilute with *Diluent* to volume, and mix.

Assay preparation—Transfer about 100mg of flurbiprofen sodium, accurately weighed, to a 100-mL volumetric flask, dissolve in and dilute with methanol to volume, and mix. Transfer 5mL of this solution to a second 100-mL volumetric flask, dilute with *Diluent* to volume, and mix.

Chromatographic system—See *Chromatography* in the general procedure ⟨621⟩: The liquid chromatograph is equipped with a 254-nm detector and a 4-mm × 25-cm column that contains 10-μm packing L7. The flow rate is about 2mL/min. Chromatograph the *System suitability preparation* and record the peak responses as directed for *Procedure*: the resolution *R*, between flurbiprofen-related compound A and flurbiprofen is not less than 1. Chromatograph the *Standard preparation* and record the peak responses as directed for *Procedure*: The tailing factor is not more than 2.5, and the relative standard deviation for replicate injections is not more than 1%.

Procedure—Separately inject equal volumes (about 20μL) of the *Standard preparation* and the *Assay preparation* into the chromatograph, record the chromatograms, and measure the areas for the major peaks. Calculate the percentage of $C_{15}H_{12}FNaO_2 \cdot 2H_2O$ in the portion of flurbiprofen sodium taken by the formula:

$$200(302.27/244.27)(C/W)(r_U/r_s)$$

in which 302.27 and 244.27 are the molecular weights of flurbiprofen sodium dihydrate and anhydrous flurbiprofen, respectively, C is the concentration, in microgram per milliliter, of USP Flurbiprofen RS in the *Standard preparation*, W is the weight, in milligrams, of the portion of flurbiprofen sodium taken to prepare the *Assay preparation*, and r_U and r_s are the flurbiprofen peak responses obtained from the *Assay preparation* and the *Standard preparation*, respectively.

Flurbiprofen Sodium Ophthalmic Solution

Flurbiprofen sodium ophthalmic solution contains not less than 90% and not more than 110% of the labeled amount of flurbiprofen sodium ($C_{15}H_{12}FNaO_2 \cdot 2H_2O$).

Packaging and storage—Preserve in a tight container.

USP Reference Standards: ⟨11⟩—**USP Flurbiprofen RS**. USP Flurbiprofen-Related Compound A RS.

Identification—The retention time for the major peak in the chromatogram of the *Assay preparation* corresponds to that in the chromatogram of the *Standard preparation*, as obtained in the *Assay*.

pH—The test should be carried out as directed in the general procedure ⟨791⟩: between 6 and 7.

Antimicrobial effectiveness—The test should be carried out as directed in the general procedure ⟨51⟩: Meets the requirements.

Sterility—The test should be carried out as directed in the general procedure ⟨71⟩—It meets the requirements when tested as directed for *Membrane Filtration* under *Test for Sterility of the Product to be Examined*.

Assay—*Diluent*, *Mobile phase*, *Standard flurbiprofen-related compound A preparation*, *Standard preparation*, and *System suitability preparation*—Proceed as directed in the *Assay* under *Flurbiprofen sodium*.

Assay preparation—Use the undiluted ophthalmic solution.

Chromatographic system—Proceed as directed in the *Assay* under *Flurbiprofen sodium* using a 4-mm × 5-cm guard column that contains 5-μm packing L1.

Procedure—Separately inject equal volumes (about 15 μL) of the *Standard preparation* and the *Assay preparation* into the chromatograph, record the chromatograms, and measure the areas for the major peaks. Calculate the quantity of flurbiprofen sodium ($C_{15}H_{12}FNaO_2 \cdot 2H_2O$) in each milliliter of the ophthalmic solution taken by the formula:

$$(302.27/244.27)C(r_U/r_s)$$

in which 302.27 and 244.27 are the molecular weights of flurbiprofen sodium dihydrate and anhydrous flurbiprofen, respectively, C is the concentration, in milligram per milliliter, of USP Flurbiprofen RS in the *Standard preparation*, and r_U and r_s are the peak responses obtained from the *Assay preparation* and the *Standard preparation*, respectively.

8.1.2. British Pharmacopoeia [66]

Flurbiprofen contains not less than 99% and not more than the equivalent of 101% of (2*RS*)-2-(2-fluorobiphenyl-4-yl)propanoic acid, calculated with reference to the dried substance.

Identification

Test A. Melting point: The test should be carried out as directed in the general procedure (2.2.14): 114–117°C.

Test B. Dissolve 0.1 g of flurbiprofen in 0.1 M *sodium hydroxide* and dilute to 100 mL with the same alkaline solution. Dilute 1 mL of the solution to 100 mL with 0.1 M *sodium hydroxide*. Examined between 230 and 350 nm, as directed in the general procedure (2.2.25), the solution shows an absorption maximum at 247 nm. The specific absorbance at the maximum is 780–820 nm.

Test C. Examine by infrared absorption spectrophotometry, as directed in the general procedure (2.2.24), comparing with the spectrum obtained with *flurbiprofen CRS*.

Test D. Mix about 5mg with 45mg of *heavy magnesium oxide R* and ignite in a crucible until an almost white residue is obtained (usually less than 5min). Allow to cool, add 1mL of *water R*, 0.05mL of *phenolphthalein solution R1*, and about 1mL of *dilute hydrochloric acid* R to render the solution colorless. Filter. To a freshly prepared mixture of 0.1mL of *alizarin S solution R* and 0.1mL of *zirconyl nitrate solution R* and 1 mL of the filtrate. Mix, allow to stand for 5min, and compare the color of the solution with that of a blank prepared in the same manner. The test solution is yellow, and the blank is red.

Tests

Appearance of Solution

Dissolve 1g of flurbiprofen in *methanol R* and dilute to 10mL with the same solvent. The solution is clear when the test is carried out as directed in the general procedure (2.2.1) and colorless when the test is carried out as directed in the general procedure (*2.2.2 or Method 1*).

Optical rotation, general procedure (2.2.7).

Dissolve 0.5g of flurbiprofen in *methanol R* and dilute to 20mL with the same solvent. The angle of optical rotation is $-0.1°$ to $+0.1°$.

Related substances

Examine by liquid chromatography, as directed in the general procedure (2.2.29).

Test solution: Dissolve 0.2g of flurbiprofen in a mixture of 45 volumes of *acetonitrile R* and 55 volumes of *water R* and dilute to 100mL with the same mixture of solvents.

Reference solution: (a) Dilute 1mL of the test solution to 50mL with a mixture of 45 volumes of *acetonitrile R* and 55 volumes of *water R*. Dilute 1mL of the solution to 10mL with a mixture of 45 volumes of *acetonitrile R* and 55 volumes of *water R*.

Reference solution: (b) Dissolve 10mg of *flurbiprofen impurity A CRS* in a mixture of 45 volumes of *acetonitrile R* and 55 volumes of *water R* and dilute to 100mL with the same mixture of solvents. Dilute 10mL of this solution to 100mL with a mixture of 45 volumes of *acetonitrile R* and 55 volumes of *water R*.

Reference solution: (c) Dissolve 10mg of flurbiprofen in a mixture of 45 volumes of *acetonitrile R* and 55 volumes of *water R* and dilute to 100mL with the same mixture of solvents. Dilute 1mL of the solution to 10mL with reference solution (b).

The chromatographic procedure may be carried out using:

(a) A stainless steel column 0.15m long and 3.9mm in internal diameter packed *with octadecylsilyl silica gel for chromatography R* (5μm)
(b) As mobile phase at a flow rate of 1mL/min a mixture of 5 volumes of *glacial acetic acid R*, 35 volumes of *acetonitrile R*, and 60 volumes of *water R*
(c) As detector a spectrophotometer set at 254nm

Inject 10μL of reference solution (c). Adjust the sensitivity of the system so that the heights of the two principal peaks in the chromatogram obtained are at least 40% of the full scale of the recorder.

The test is not valid unless the resolution between the peak corresponding to impurity A and the peak corresponding to flurbiprofen is at least 1.5.

Inject 10μL of the test solution and of reference solutions (a) and (b). Continue the chromatography for twice the retention time of flurbiprofen. In the chromatogram obtained with the test solution, the area of any peak corresponding to impurity A is not greater than the area of the peak in the chromatogram obtained with reference solution (b) (5%), the area of any peak, apart from the principal peak and the peak due to impurity A, is not greater than the area of the principal peak in the chromatogram obtained with reference solution (a) (0.2%), and the sum of the areas of any such peaks is not greater than five times the area of the principal peak in the chromatogram obtained with reference solution (a) (1%). Disregard any peak with area less than 0.1 times that of the principal peak in the chromatogram obtained with reference solution (a) (0.02%).

Heavy metals, general procedure (2.4.8).

Dissolve 2g of flurbiprofen in a mixture of 10 volumes of *water R* and 90 volumes of *methanol R* and dilute to 20mL with the same mixture of solvents. Twelve milliliters of the solution complies with the limit test B for heavy (10ppm). Prepare the standard using *lead standard solution* (*1ppm Pb*) obtained by diluting *lead standard solution* (*100ppm Pb*) *R* with a mixture of 10 volumes of *water R* and 90 volumes of *methanol R.*

Loss on drying: general procedure (2.2.32).

Not more than 0.5%, determined on 1g of flurbiprofen by drying at 60°C at a pressure not exceeding 0.7kPa for 3h.

Sulfated ash: general procedure (2.4.14).

Not more than 0.1%, determined on 1g of flurbiprofen in a platinum crucible.

Assay

Dissolve 0.2g of flurbiprofen in 50mL of *alcohol R*. Titrate with *0.1M sodium hydroxide*, determining the end-point potentiometrically as directed in the general procedure (2.2.20). One milliliter of *0.1M sodium hydroxide* is equivalent to 24.43mg of $C_{15}H_{13}FO_2$.

IMPURITIES

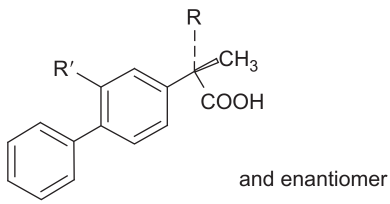

A. R=R′=H: (2*RS*)-2-(biphenyl-4-yl)propanoic acid,
B. R=CH(CH_3)—COOH: 2-(2-fluorobiphenyl-4-yl)-2,3-dimethylbutane-dioic acid,
C. R=OH, R′=F: (2*RS*)-2-(2-flurobiphenyl-4-yl)-2-hydroxypropanoic acid,

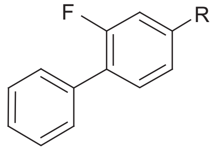

D. R=CO—CH_3: 1-(2-fluorobiphenyl-4-yl)ethanone,
E. R=COOH: 2-fluoro-biphenyl-4-carboxylic acid.

Flurbiprofen Sodium

Flurbiprofen Sodium is sodium (*RS*)-2-(2-fluorobiphenyl-4-yl)propionate dihydrate. It contains not less than 98.5% and not more than 101.5% of $C_{15}H_{12}FNaO_2$, calculated with reference to the dried substance.

Identification

Test A. The *infrared absorption spectrum* according to the general test in Appendix IIA is in concordance with the *reference spectrum* of flurbiprofen sodium (*RS* 157).

Test B. Heat 0.2g over a flame until charred and then heat at 600°C for 2h. The residue yields the reactions characteristic of *sodium* salts. Appendix VI.

TESTS

Related substances

Carry out the method for *liquid chromatography*, according to the general procedure in Appendix IIID, using solutions in a mixture of 25 volumes of *water* and 50 volumes of *methanol* containing (1) 0.1% (w/v) of flurbiprofen, (2) 0.0002% (w/v) of flurbiprofen, (3) 0.0005% (w/v) of *2-(biphenyl-4-yl) propionic acid BPCRS*, and (4) 0.0005% (w/v) of flurbiprofen and 0.0005% (w/v) of *2-(biphenyl-4-yl) propionic acid BPCRS*.

The chromatographic procedure may be carried out using:

(a) A stainless steel column (15cm×3.9mm) packed with *stationary phase C* (5μm) (resolve 5*μ* is suitable), (b) a mixture of 5 volumes of *glacial acetic acid*, 35 volumes of *acetonitrile*, and 60 volumes of *water* as the mobile phase with a flow rate of 1mL/min, and (c) a detection wavelength of 254 nm. Adjust the sensitivity so that the height of the principal peaks in the chromatogram obtained with solution (4) is about 40% of full-scale deflection on the chart paper.

The test is not valid unless, in the chromatogram obtained with solution (4), the *resolution factor* between two principal peaks is at least 1.5.

In the chromatogram obtained with solution (1), the area of any peak corresponding to 2-(biphenyl-4-yl) propionic acid is not greater than the

area of the peak in the chromatogram obtained with solution (3) (0.5%), the area of any other *secondary peak* is not greater than the area of the peak in the chromatogram obtained with solution (2) (0.2%), and the sum of the areas of any *secondary peak*s is not greater than five times the area of the peak in the chromatogram obtained with solution (2) (1%).

Heavy metals

Twelve milliliters of a 20% (w/v) solution in *methanol* complies with *limit test A for heavy metals*, Appendix VII (10ppm). Use 10mL of the solution obtained by diluting 10mL of *lead standard solution* (*20ppm Pb*) to 100mL with *methanol* to prepare the standard and 10mL of *methanol* and 2mL of the solution of flurbiprofen sodium to prepare the reagent blank.

Loss on drying

11.3–12.5% when determined by drying over *phosphorous pentoxide* at 60°C at a pressure of 2kPa for 18h. Use 1g.

ASSAY

Carry out the method for *liquid chromatography*, Appendix IIID, using solutions in a mixture of 25 volumes of *water* and 50 volumes of *methanol* containing

(1) 0.015% (w/v) of flurbiprofen sodium,
(2) 0.015% (w/v) of *flurbiprofen sodium* BPCRS, and
(3) 0.00075% (w/v) of flurbiprofen sodium and 0.00075% (w/v) of *2-(biphenyl-4-yl) propionic acid PBCRS*.

The chromatographic procedure described under related substance may be used.

The assay is not valid unless, in the chromatogram obtained with solution (3), the *resolution factor* between the two principal peaks is at least 1.5. Calculate the content of $C_{15}H_{12}FNaO_2$ in flurbiprofen sodium using declared content of $C_{15}H_{12}FNaO_2$ in *flurbiprofen sodium BPCRS*.

IMPURITIES

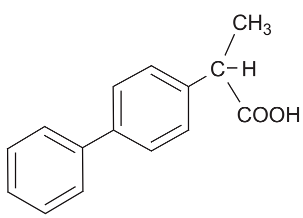

A. 2-(Biphenyl-4-yl) propionic acid

Flurbiprofen Eye Drops

Flurbiprofen Eye Drops are a sterile solution of flurbiprofen sodium in purified water.

IDENTIFICATION

Test A. Carry out the method for *thin-layer chromatography*, Appendix IIIA, using *silica gel* GF_{254} as the coating substance and a mixture of 5 volumes of *propan-2-ol* and 95 volumes of *dichloromethane* as the mobile phase. Apply separately to the plate 5 μL of each of the following solutions. For solution (1) dilute the eye drops, if necessary, with a mixture of 25 volumes of *water* and 50 volumes of *methanol* to produce a solution containing 0.01% (w/v) of flurbiprofen sodium. Solution (2) contains 0.01% (w/v) of *flurbiprofen sodium BPCRS* in a mixture of 25 volumes of *water* and 50 volumes of *methanol*. After removal of the plate, allow it to dry in air and examine under *ultraviolet light* (*254 nm*). The principal spot in the chromatogram obtained with solution (1) corresponds to that in the chromatogram obtained with solution (2).

Test B. In the Assay, the principal peak in the chromatogram obtained with solution (1) has the same retention time as the principal peak in the chromatogram obtained with solution (2).

TESTS

Acidity or Alkalinity

pH 6 and 7, Appendix VL.

2-(Biphenyl-4-yl) propionic acid

Carry out the method for *liquid chromatography*, Appendix IIID, using the following solutions. For solution (1), dilute the eye drop, if necessary, with a mixture of 25 volumes of *water* and 50 volumes of *methanol* to produce a solution containing 0.03% (w/v) of flurbiprofen sodium. Solution (2) contains 0.00015% (w/v) of *2-(biphenyl-4-yl) propionic acid BPCRS* in a mixture of 25 volumes of *water* and 50 volumes of *methanol*. Solution (3) contains 0.0005% of *flurbiprofen sodium BPCRS* and 0.0005% (w/v) of *2-(biphenyl-4-yl) propionic acid BPCRS* in a mixture of 25 volumes of *water* and 50 volumes of *methanol*.

The chromatographic procedure may be carried out using (a) a stainless steel column (15 cm × 3.9 mm) packed with *stationary phase C* (5 μm) (resolve 5μ is suitable); (b) a mixture of 5 volumes of *glacial acetic acid*, 35 volumes of *acetonitrile*, and 60 volumes of *water* as the mobile phase with a flow rate of 1 mL/min; and (c) a detection wavelength of 254 nm. Adjust the sensitivity so that the height of the principal peaks in the chromatogram obtained with solution (3) is at about 40% of full-scale deflection on the chart paper.

The test is not valid unless the *resolution factor* between the two principal peaks in the chromatogram obtained with solution (3) is at least 1.5.

In the chromatogram obtained with solution (1), the area of any peak corresponding to 2-(biphenyl-4-yl) propionic acid is not greater than the area of the peak in the chromatogram obtained with solution (2) (0.5%).

ASSAY

Carry out the method for *liquid chromatography*, Appendix IIID, using the following solutions. For solution (1), dilute the eye drop, if necessary,

with a mixture of 25 volumes of *water* and 50 volumes of *methanol* to produce a solution containing 0.015 (w/v) of flurbiprofen sodium. Solution (2) contains 0.015% (w/v) of *flurbiprofen sodium BPCRS* in a mixture of 25 volumes of *water* and 50 volumes of *methanol*. Solution (3) contains 0.0005% (w/v) of *flurbiprofen sodium BPCRS* and 0.0005% (w/v) of *2-(biphenyl-4-yl) propionic acid BPCRS* in a mixture of 25 volumes of *water* and 50 volumes of *methanol*.

The chromatographic procedure described under the test for 2-(biphenyl-4-propionic acid may be used. The assay is not valid unless the *resolution factor* between the two principal peaks in the chromatogram obtained with solution (3) is at least 1.5. Calculate the content of $C_{15}H_{12}FNaO_2 \cdot 2H_2O$ in the eye drops using the declared content of $C_{15}H_{12}FNaO_2 \cdot 2H_2O$ in *flurbiprofen sodium BPCRS*.

Flurbiprofen suppositories

Flurbiprofen suppositories contain flurbiprofen in a suitable suppository basis.

The suppository complies with the requirements stated under rectal preparations and with the following requirements.

Content of flurbiprofen $C_{15}H_{13}FO_2$, 95–105% of the stated amount.

IDENTIFICATION

Test A. Carry out the method for *thin-layer chromatography*, Appendix IIIA, using a silica gel F_{254} precoated plate (Merck plates are suitable) and a mixture of 10 volumes of *glacial acetic acid*, 10 volumes of *methyl acetate*, and 80 volumes of *trichloroethylene* as the mobile phase but allowing the solvent front to ascend 10 cm above the line of application.

Apply separately to the plate 2 μL of each of the following solutions. For solution (1), cut a suitable number of the suppositories into small pieces, add 50 mL of *methanol* to a quantity containing 0.1 g of flurbiprofen, heat gently until melted, shake mechanically for 10 min, allow to cool at 2–8°, filter (Whatman No. 1 paper is suitable) and evaporate to dryness. Dissolve the residue in 5 mL of a mixture of equal volumes of *methanol* and *water*. Solution (2) contains 0.2% (w/v) of *flurbiprofen sodium BPCRS* in a mixture of equal volumes of *methanol* and *water*. After removal of the plate, allow to dry in air and examine under *ultraviolet light* (*254 nm*). The principal spot in the chromatogram obtained with solution (1) corresponds to that in the chromatogram obtained with solution (2).

Test B. In the assay, the principal peak in the chromatogram obtained with solution (1) has the same retention time as that in the chromatogram obtained with solution (2).

Related substances

Carry out the method for *liquid chromatography*, Appendix IIID, using the following solutions. For solution (1), cut a suitable number of the suppositories into small pieces, add 50 mL of *methanol* to a quantity containing 0.1 g of flurbiprofen, heat gently until melted, shake mechanically for 10 min, and

filter (Whatman No. 1 paper is suitable). Dilute the filtrate with sufficient of a mixture containing 35 volumes of *acetonitrile* and 65 volumes of *water* to produce 100 mL and filter. For solution (2), dilute 1 volume of solution (1) to 100 volumes with a mixture of 45 volumes of *acetonitrile* and 55 volumes of *water* and further dilute 1 volume to 5 volumes with the same solvent mixture. Solution (3) contains 0.0005% (w/v) of *2-(biphenyl-4-yl) propionic acid BPCRS* in a mixture of 45 volumes of *acetonitrile* and 55 volumes of *water*. Solution (4) contains 0.0005% of *4-acetyl-2-fluorobiphenyl BPCRS* in a mixture of 45 volumes of *acetonitrile* and 55 volumes of *water*. For solution (5), dilute 1 volume of solution (1) to 200 volumes with solution (3).

The chromatographic procedure may be carried out using (a) a stainless steel column (15 cm × 3.9 mm) packed with *stationary phase C* (5 μm) (resolve 5μ is suitable) fitted with a stainless steel guard column (2 cm × 4.6 mm) packed with the same material; (b) a mixture of 5 volumes of *glacial acetic acid*, 35 volumes of *acetonitrile*, and 60 volumes of *water* as the mobile phase with a flow rate of 1 mL/min; and (c) a detection wavelength of 254 nm.

Adjust the sensitivity so that the heights of the principal peaks in the chromatogram obtained with solution (5) are about 40% of full-scale deflection on the chart paper.

The test is not valid unless, in the chromatogram obtained with solution (5), the *resolution factor* between the two principal peaks is at least 1.5. In the chromatogram obtained with solution (1), the area of any peak corresponding to 2-(biphenyl-4-yl) propionic acid is not greater than the area of the peak in the chromatogram obtained with solution (3) (0.5%), the area of any peak corresponding to 4-acetyl-2-fluorobiphenyl is not greater than the area of the peak in the chromatogram obtained with solution (4) (0.5%), the area of any other *secondary peak* is not greater than the area of the peak in the chromatogram obtained with solution (2) (0.2%), and the sum of the areas any such peaks is not greater than 2.5 times the area of the peak in the chromatogram obtained with solution (2) (0.5%).

Assay

Carry out the method for liquid chromatography, Appendix IIID, using the following solutions. For solution (1), cut a suitable number of the suppositories into small pieces, add 50 mL of *methanol* to a quantity containing 0.1 g of flurbiprofen, heat gently until melted, shake mechanically for 10 min, and filter (Whatman No. 1 is suitable). Dilute the filtrate with sufficient of a mixture containing 35 volumes of *acetonitrile* and 65 volumes of *water* to produce 100 mL, filter, and dilute 1 volume of the filtrate to 25 volumes with the same solvent mixture.

Solution (2) contains 0.005% (w/v) of *flurbiprofen sodium BPCRS* in a mixture of 35 volumes of *acetonitrile* and 65 volumes of *water*. Solution (3) contains 0.0005% (w/v) of each of *flurbiprofen sodium BPCRS* and *2-(biphenyl-4-yl) propionic acid BPCRS* in a mixture of 35 volumes of *acetonitrile* and 65 volumes of *water*.

The chromatographic procedure described under related substances may be used.

The assay not valid unless, in the chromatogram obtained with solution (3), the *resolution factor* between the two principal peaks is at least 1.5.

Calculate the content of $C_{15}H_{13}NO_2$ in the suppositories using the declared content of $C_{15}H_{13}FO_2$ in *flurbiprofen sodium BPCRS*.

Flurbiprofen tablets

Flurbiprofen tablets contain flurbiprofen. They are coated.

The tablets comply with requirements stated under tablets and with the following requirements.

Contents of flurbiprofen $C_{15}H_{13}FO_2$, 92.5–107.5% of the stated amount.

IDENTIFICATION

Extract a quantity of the powdered tablets containing 0.5g of flurbiprofen with 25mL of *acetone*, filter, evaporate the filtrate to dryness with the aid of a current of air without heating, and dry at 60°C at a pressure of 2kPa. The residue complies with the following tests.

Test A. The *infrared absorption spectrum*, Appendix IIA, is concordant with the *reference spectrum* of flurbiprofen (*RS* 156).

Test B. Heat 0.5mL of *chromic–sulfuric acid mixture* in a small test tube, in a water bath for 5min; the solution wets the side of the tube readily and there is no greasiness. Add 2 or 3mg of the residue and heat in a water bath for 5min, the solution does not wet the side of the tube and does not pour easily from the tube.

Test C. *Melting point*, about 114°C, Appendix VA.

Related substances

Carry out the method for *liquid chromatography*, Appendix IIID, using the following solutions. For solution (1), disperse a quantity of the powdered tablets containing 0.5g of flurbiprofen in 50mL *water*, add 200mL of *acetonitrile*, mix, centrifuge, and use for the supernatant liquid. For solution (2) dilute 1 volume of solution (1) to 100 volumes with a mixture of 45 volumes of acetonitrile and 55 volumes of *water* and further dilute 1 volume to 5 volumes with the same solvent mixture. Solution (3) contains 0.001% (w/v) of *2-(biphenyl-4-yl) propionic acid BPCRS* in a mixture of 45 volumes of *acetonitrile* and 55 volumes of *water*. For solution (4), dilute 1 volume of solution (1) to 200 volumes with solution (3).

The chromatographic procedure may be carried out using (a) a stainless steel column (15cm × 3.9mm) packed with *stationary phase C* (5μm) (resolve 5μ is suitable); (b) a mixture of 5 volumes of *glacial acetic acid*, 35 volumes of *acetonitrile*, and 60 volumes of *water* as the mobile phase with a flow rate of 1mL/min; and (c) a detection wavelength of 254nm.

Adjust the sensitivity so that the heights of the principal peaks in the chromatogram obtained with solution (4) are about 40% of full-scale deflection on the chart paper.

The test is not valid unless the *resolution factor* between the two principal peaks in the chromatogram obtained with solution (4) is at least 1.5.

In the chromatogram obtained with solution (1), the area of any peak corresponding to 2-(biphenyl-4-yl) propionic acid is not greater than the area of the peak in the chromatogram obtained with solution (3) (0.5%), the area of any other *secondary peak* is not greater than the area of the peak in the chromatogram obtained with solution (2) (0.2%), and the sum of the areas of any *secondary peak* is not greater than five times the area of the peak in the chromatogram obtained with solution (2) (1%).

Assay

Weigh and powder 20 tablets. Shake a quantity of the powder containing 0.1 g of flurbiprofen with 60 mL of 0.1 M *sodium hydroxide* for 5 min, dilute to 100 mL with 0.1 M *sodium hydroxide*, filter if necessary, and dilute 10 mL of the filtrate to 100 mL with the same solvent. Further dilute 10–100 mL with the same solvent and measure the *absorbances* of the resulting solution at the maximum at 247 nm, Appendix IIB. Calculate the content of $C_{15}H_{13}FO_2$ taking 802 as the value of A (1%, 1 cm) at the maximum at 247 nm.

8.2. Reported methods of analysis

8.2.1. Spectrophotometric methods

El-Bagary [83] proposed an accurate and sensitive first derivative spectrophotometric method for the determination of flurbiprofen in bulk powder and pharmaceutical dosage forms. The method is based on the determination of fluoride content, after flurbiprofen had been treated by the oxygen combustion flash method, using the first derivative spectrophotometric technique of samples treated with zirconium (IV) chloride and eriochrome cyanine R reagent against a blank with zero fluoride concentration treated similarly.

Sajeev *et al*. [84] developed a new and rapid UV spectrophotometric method and a reversed-phase high-performance liquid chromatographic (HPLC) method for the quantitative estimation of flurbiprofen in pure and in pharmaceutical dosage form. The column used in the liquid chromatography was a reversed-phase 4.6 mm × 12.5 cm (5 μm) of LiChroCART Purospher end-capped C_{18} LC column. The mobile phase was methanol–acetonitrile–phosphate buffer (pH 5.6, 40:20:40) at a flow rate of 0.75 mL/min. The eluate was analyzed at a wavelength of 248 nm.

Chauthan *et al*. [85] developed a simple and sensitive ultraviolet spectrophotometric method for the estimation of flurbiprofen sodium in urine. The method is based on extraction of the drug from urine sample using chloroform after proper treatment. The chloroform extract shows absorbance maximum at 256 nm and obeys Beer's law in the concentration range of 2–12 μg/mL of the drug. No interference was observed from the common metabolites present in the urine after proper extraction.

Baraka *et al*. [86] determined flurbiprofen and tiaprofenic acid by a spectroscopic method. Both drugs reacted easily and quantitatively with copper acetate forming bluish green precipitates. The drugs were determined calorimetrically by extracting the precipitates obtained in chloroform and measuring the absorbance at 686 nm for flurbiprofen and 696 nm for tiaprofenic acid. To improve the sensitivity of the method, the precipitates of the drugs with copper were dissolved in the least amount of dilute ammonia and the copper content was determined via reaction with sodium diethyldithiocarbamate. The yellow solution was measured at 477 nm. The method was applied for the determination of the drugs in pharmaceuticals, and the results obtained were in good agreement those of the official methods.

Wang *et al*. [87] determined flurbiprofen by a micellar-sensitized fluorescence spectrometric method. The experiments indicated that sodium dodecyl sulfate can enhance greatly the fluorescence signal. Based on these results, a new method of sensitized fluorescence using the micellar system for the trace analysis of flurbiprofen was developed. The linear range was 2×10^{-8} to 2.5×10^{-6} mol/L. The recovery of sample was within the range of 99.2–100%, and relative standard deviation was 1.8%.

8.2.2. Atomic absorption spectrometric method

Baraka *et al*. [86] determined flurbiprofen by an atomic absorption spectrometry procedure through the determination of the copper content of the precipitate. The optimum conditions for precipitation were carefully studied. The molar ratio of the reactants was ascertained. Statistical analysis of the results obtained was compared with the official methods. The results were of equal accuracy and reproducibility.

8.2.3. Potentiometric methods

Bunaciu *et al*. [88] constructed an ion-selective electrode (ISE) response characteristic (slope, intercept, linear range, and detection limit) for flurbiprofen using a computer program, written in TurboPascal 5.5. The sensor response characteristics were evaluated for selectivity coefficients and quantitative determinations.

Bunaciu *et al*. [89] prepared another ion-selective membrane electrode for flurbiprofen using a PVC membrane impregnated with the ion pair complex formed between the tricaprylmethylammonium chloride cation and the flurbiprofen anion. The electrode was used for the determination of flurbiprofen in Froben 50 and Froben 100 by a standard addition method at pH 6.8. The calibration graph for flurbiprofen was linear for 70 μM to 10 mM, and the detection limit was 41 μM. The RSD ($n=4$) for the determination of flurbiprofen in tablets was ⟨2%).

8.2.4. Chromatographic methods

8.2.4.1. Thin-layer chromatography Dhaves *et al*. [90] added plasma (1mL) to flurbiprofen, 1mL 3M HCl was added and extracted with 5mL hexane/diethyl ether (4:1) twice. The pooled extract was dried, and the residue was dissolved in 500μL methanol. A portion (20μL) was spotted on to an Al silica gel 60F 254 plate for development with *n*-hexane/ethyl acetate/glacial acetic acid (6:3:1) as mobile phase, a 10-min run time and UV detection at 247nm. The calibration graph was linear from 40 to 800ng flurbiprofen, with a detection limit of 20ng and RSD of <4% (n=6). Recoveries were 87.2–87.9%.

Clarcke [3] recommended the following seven systems:

(1) Plates: Silica gel G, 250-μm thick.
Mobile phase, ethyl acetate.
Reference compounds: hydrochlorothiazide R_F=11, sulfafurazole R_F=33, salicylamide R_F=52, prazepam R_F=72.
R_F=45.

(2) Plates: Silica gel G, 250-μm thick.
Mobile phase, chloroform:cyclohexane:acetic acid (4:4:2).
R_F=69.

(3) Plates: Silica gel G, 250-μg thick.
Mobile phase, chloroform:methanol:propionic acid (72:18:10).
R_F=91.

(4) Plates: Silica gel G, 250-μm thick.
Mobile phase, chloroform:acetone (80:20).
Reference compounds: paracetamol R_F=15, clonazepam R_F=35.
Secobarbital R_F=55, methylphenobarbital R_F=70.
R_F=30.

(5) Plates: Silica gel G, 250-μm thick.
Mobile phase, ethyl acetate:methanol:strong ammonia solution (85:10:5).
Reference compounds: sulfamidine R_F=13, hydrochlorothiazide R_F=34, temazepam R_F=63, prazepam R_F=81.
R_F=6.

(6) Plates: Silica gel G, 250-μm thick.
Mobile phase, ethyl acetate.
Reference compounds: Sulfathiazole R_F=20, phenacetin R_F=38, salicylamide R_F=55, secobarbital R_F=68.
R_F=30.

(7) Plates: Silica gel G, 250-μm thick.
Mobile phase, ethyl acetate:methanol:strong ammonia solution (80:10:10).
R_F=16.

8.2.4.2. Liquid chromatography Santoro *et al.* [91] developed and validated a chiral liquid chromatographic method for the rapid quantitative determination of flurbiprofen enantiomers in pharmaceutical preparations. Baseline resolution of *R*- and *S*-flurbiprofen was achieved on a [(3*S*,4S)-4-(3,4-dinitrobenzamido)-1,2,3,4-tetrahydro-phenanthrene] coated on 5 μm silica gel column with mobile phase of hexane–ethanol–acetic acid (950:50:2). The standard curve of *S*-flurbiprofen showed good linearity over the concentration range from 2 to 8 μg/mL with correlation coefficient of 0.9993. The intraday precision of the sample, determined at two concentration levels (8 and 20 μg/mL of racemic flurbiprofen), was 0.16 and 0.23 for *R*-flurbiprofen and 0.14 and 0.46 for *S*-flurbiprofen. The intraday accuracy of the sample expressed as percentage recovery was 100.1% and 100.4% for *R*- and *S*-flurbiprofen, respectively. The results showed precision, accuracy, and specificity of the method for the analysis of *S*-flurbiprofen in pharmaceutical formulation.

8.2.4.3. Miceller electrokinetic capillary chromatography Zhang *et al.* [92] used a micellar electrokinetic capillary chromatography method for the determination of flurbiprofen in rabbit plasma. Rabbit plasma (0.2 mL) was deproteined by methanol which was then evaporated under nitrogen flow. The residue was resolved by methanol for injection. The electrophoretic conditions were as follows: -75-μm $\times$ 100-cm capillary tube, buffer: 20 mmol/L of borate solution containing 20 mmol/L of sodium dodecyl sulfate. The method using ketoprofen as an internal standard was linear in the range of 1–24 μg/mL of flurbiprofen with good precision. The added recovery of 2.4, 7.2, and 12 μg was 95.36%, 93.55%, and 95.22%, respectively, and the detection limit was 0.2 μg/mL. The method is accurate, simple and can be used for the pharmacokinetic study of flurbiprofen.

8.2.4.4. Gas chromatography Clarcke [3] recommended the following three systems:

(1) Packed column: 3% SE-30 or OV-1 on 80–100 mesh Chromosorb G HP (acid-washed and dimethyldichlorosilane-treated), 2 m $\times$ 2 mm i.d. glass column, it is essential that the support be fully deactivated.

Column temperature: Normally between 100 and 300 °C, for isothermal conditions, an approximate guide to temperature is to use RI $\div$ 10.

Carrier gas: Nitrogen at 45 mL/min.

Capillary column: 10–15 m $\times$ 0.32 or 0.53 mm i.d., 100% dimethyl-PSX (X-1) with a 1.5- to 3-μm film thickness.

Carrier gas: Helium.

Temperature program, 4min at 135°C, 13°C/min to 200°C, 6°C/min to 312°C, 6min final hold.

Retention index: 1900.

(2) Column: SE-30 on 80–100 mesh Chromosorb G (acid-washed and dimethyldichlorosilane-treated), 2m × 3mm i.d. glass column.

Column temperature: 120°C for 2min and then programmed at 10°C/min to 260°C and held for 5min.

Carrier gas: Nitrogen at 40mL/min.

Reference compound: Hexadecane (n-$C_{16}H_{34}$).

Retention index=1.3.

(3) Column: HP1 (methyl-PSX) 12m × 0.2mm i.d. fused-silica capillary, 0.33μm film thickness.

Injector: 280°C splitless mode.

Column temperature: 100°C for 2min and then programmed at 30°C/min to 310°C and held for 8min.

Carrier gas: Helium, constant flow 1mL/min.

Retention index: 1880.

8.2.4.5. High-performance liquid chromatography Snider *et al*. [93] developed an HPLC method with an automated sample extraction for the determination of flurbiprofen and ibuprofen in dog serum. Sample extraction was automated by use of cartridges packed with a styrene–divinylbenzene macroreticular resin in a microprocessor-controlled centrifugal system. The average recoveries were 98.9% for flurbiprofen. The limits of detection were approximately 0.04μg/mL for flurbiprofen at 254nm. The relative standard deviation for the determination of a laboratory standard between days was 2.4% (20μg/mL) for flurbiprofen. Peak height ratios were linear with concentrations of 0.04–100μg/mL for flurbiprofen. The method is simple, rapid sensitive, and specific. The use of an automated sample preparation procedure improved the between-day precision by a factor of 2 when compared to a manual extraction procedure. The method was applied to bioavailability studies in dogs.

Adams *et al*. [94] used an HPLC method for the determination of flurbiprofen and 4′-hydroxyflurbiprofen in serum and urine. The sample was treated with sodium chloride and sodium hydroxide. (±)-2-(2-Methoxybiphenyl-4-yl) propionic acid was used as internal standard. The samples were injected on a column (30cm × 3.9mm) of micro Bondapak C_{18} fitted with an RP-8 guard column (3cm × 4.6mm), with 0.05M potassium phosphate–tetrahydrofuran (11:9) as mobile phase (1.9mL/min) and fluorimetric detection at 320nm (excitation at 260nm). Response was rectilinear for ≤50μg/mL of flurbiprofen or 4′-hydroxyflurbiprofen and 3′-hydroxy-4′-methoxyflurbiprofen.

Babhair [95] described an HPLC method with fluorometric detection at 337 nm (excitation at 254 nm) for the determination of flurbiprofen in dosage form urine and plasma. The method was applied on a stainless steel column (30 cm × 3.9 mm) of micro-Bondapak Phenyl with aq. 35% acetonitrile as mobile phase. Calibration graphs were rectilinear up to 20 μg/mL of flurbiprofen in the final test solution. Recovery from plasma and urine was 95–98%.

Kandler and Hall [96] used an HPLC analysis of the enantiomers of flurbiprofen and the 4′-hydroxy, 3′-hydroxy-4′-methoxy, and 3′,4′-dihydroxy metabolites in plasma and urine containing racemic isoprofen as internal standard, and derivatized with *S*-α-methylbenzylamine. The derivatives were determined by HPLC on a column (25 cm × 4.6 mm) of Ultrasphere ODS (5 μm) and Brownlee RP18 guard column. Mobile phases (1 mL/min) were aqueous 62% acetonitrile for flurbiprofen in plasma; acetonitrile–0.05 M acetic acid (11:9) for flurbiprofen and 4′-hydroxyflurbiprofen in urine; and acetonitrile:tetrahydroxyfuran:acetic acid (43:2:55) for 4′-hydroxyflurbiprofen, 3′-hydroxyflurbiprofen, and 4′-methoxyflurbiprofen in plasma and urine. Flurbiprofen in plasma was detected at 254 nm; flurbiprofen in urine and 4′-hydroxy, 3′-hydroxy, 4-methoxy, and 3′,4′-dihydroxy metabolites in plasma and urine were detected fluorimetrically. Calibration graphs were rectilinear from 25 to 500 ng/mL for the drug and the three metabolites in plasma; 25 to 750 ng/mL for the drug and its 4′-hydroxy- and 3′-hydroxy-4-methoxy metabolites; and 125 to 750 ng/mL for 3,4-dihydroxy metabolite in urine. Detection limits in plasma were 10 ng/mL, and the coefficient of variation was 10%.

Sane *et al*. [97] determined flurbiprofen in tablets, using HPLC on a column (30 cm × 3.9 mm) of micro Bondapak C_{18} with acetonitrile:water:phosphoric acid (500:500:1) as mobile phase (1.5 mL/min) and detection at 254 nm. Ketoprofen was used as internal standard. The calibration graph was rectilinear from 0.02 to 0.08 mg/mL, and recoveries were quantitative and the coefficient of variation was 2.5%. No interference was observed.

Kumbhat and Mathur [98] determined flurbiprofen in aqueous humor of human by HPLC on a column (25 cm × 4.6 mm) of Partisil 5 ODS 3 C_{18} (5 μm) with a guard column, acetonitrile–0.05 M acetic acid (2:3) as mobile phase (2 mL/min) and detection at 254 nm. The retention time for flurbiprofen was 8.3 min. Calibration graphs based on peak height were rectilinear for 50–600 ng/mL of the drug, and the detection limit was 20 ng/mL.

Aboul-Enein and Bakr [99] separated flurbiprofen enantiomers in biological fluids were derivatized by reaction with diazomethane to form the methyl esters by HPLC in a column (25 cm × 4.6 mm) of Daicel Chiralcel OJ (cellulose tris-(4-methylbenzoate) ester) coated on to silica gel (10 μm) with a mobile phase (1.0 mL/min) of hexane:propan-2-ol (9:1)

and detection at 254 nm. A separation factor of 1.32 was achieved. For urine analysis, the flurbiprofen was extracted into ethyl ether, and the solvent was evaporated before derivatization.

Kim and Chi [100] developed an HPLC procedure with UV detection for the quantitation of flurbiprofen released into isopropyl myristate used as the receptor phase in an *in vitro* membraneless drug diffusion cell. The drug and the internal standard, oxaprozin, were extracted from isopropyl myristate with a mixture of dimethyl sulfoxide:methanol:water (2:1:1) and quantitated using a reversed-phase C_{18} column. The chromatograms were completely free from interfering peak, and the relative retention times of flurbiprofen and the internal standard were 4.9 and 6.8 min, respectively. Calibration plots were linear over the concentration range of 1–200 μg/mL of flurbiprofen with correlation coefficient of >0.99.

Mathew *et al*. [101] developed a stability-indicating HPLC method for the determination of flurbiprofen in tablets. The method is accurate, precise, and the relative standard deviation was 0.7%. The inactive ingredients present in the tablet did not interfere with Assay procedure. The extraction procedure from the tablets was very simple. The recovery from the synthetic mixtures was quantitative. The drug appears to be very sensitive to strong acid and bases since a 5-min boiling caused the degradation of the drug (100%) in both the solutions. Samples were mixed with methanol for 5 min and filtered. The filtrate was treated with methanolic ibuprofen solution (internal standard, 4 mg/mL) and diluted with 40% methanol in 0.02 M potassium dihydrogen phosphate aqueous buffer before analysis by HPLC on a column (30 cm × 3.9 mm) of C_{18} with a mobile phase (2.2 mL/min) of 48% acetonitrile in 0.01 M potassium dihydrogen phosphate aqueous buffer and detection at 234 nm. The method was used to study the degradation of flurbiprofen.

Spraul *et al*. [102] identified the two major human urinary metabolites of flurbiprofen, namely the glucuronides of flurbiprofen and 4′-hydroxyflurbiprofen using ^{1}H and ^{19}F NMR spectroscopy. *In vivo* conjugation of the racemic drug and its metabolites with D-glucuronic acid results in diastereomeric molecules which give NMR spectra, thereby permitting the diastereomeric proportions to be evaluated. The cause of the observed deviation from equal proportions is discussed. This study represents the first use of both ^{19}F NMR and 600 MHz ^{1}H NMR spectroscopy coupled to HPLC. Urine was freeze dried and reconstituted at a 10-fold increase in concentrated $2H_2O$ containing 2% acetonitrile. Portions (50 μl) of the solution were analyzed on a Spherisorb ODS-2 column (25 cm × 4.6 mm) with gradient elution with $2H_2O$/acetonitrile/phosphate (detail given) and detection at 254 nm. On-flow ^{19}F NMR and stopped-flow ^{1}H NMR were used to detect any metabolites; the two major urinary metabolites, the glucuronides of flurbiprofen and of 4′-hydroxyflurbiprofen, were identified.

Chi *et al*. [103] determined flurbiprofen by an HPLC analysis of flurbiprofen in rat plasma. Plasma was vortex mixed with a methanolic solution of oxaprozin (internal standard, 10 μg/mL) and 0.1 M HCl. Flurbiprofen was extracted into cyclohexane, and the extract was evaporated to dryness under N_2. The residue was reconstituted in the mobile phase, and the solution was analyzed by HPLC on a column (15 cm × 4.6 mm i.d.) of Cosmosil C_{18} (5 μm) with a guard column packed with pellicular C_{18} (30 μm), 0.02 M phosphate buffer of pH 7:acetonitrile (19:6) as mobile phase (1.2 mL/min) and detection at 254 nm. The calibration graph was linear from 0.1 to 30 μg/mL of flurbiprofen. Mean intraday and interday RSD were 4.74% and 5.08%, respectively. The mean recovery was 93.1%. The method was validated by analyses of flurbiprofen injected into rats and sampled in blood at intervals up to 36 h.

Foda and Al-Gohary [104] described that an HPLC method was used for determination of flurbiprofen in pharmaceutical dosage forms using a Bonda Pack C_{18} column (10 cm × 8 mm i.d.), 0.05 M ammonium acetate/acetonitrile (2:3, pH 5.2) as mobile phase (0.8 mL/min), methyl-*p*-hydroxybenzoate (1 mg/mL as internal standard) and detection at 247 nm. The calibration graph was linear for 0.5–9 μg/mL, and the recovery and RSD were 100.1% and 0.4%, respectively.

Deshpande *et al*. [105] determined flurbiprofen by an HPLC method using fluorescence detector at 315 nm (excitation at 250 nm) in plasma on 5 μm C_{18} column (15 cm × 4.6 mm i.d.) and acetonitrile:phosphate buffer of pH 5.9 (68:32) as mobile phase (1.2 mL/min). The internal standard used was biphenyl benzoic acid. The calibration graph was linear from 1 to 24 μg/mL of flurbiprofen. At the 4 μg/mL level, intraday and interday RSD were 2.36% and 2.03%, and the corresponding values at the 8 μg/mL were 2.13% and 3.61%. The recovery was 85.88 ± 2.75%.

Park *et al.* [106] determined flurbiprofen in rat plasma using HPLC with fluorescence detection. Plasma (50 μl) was deproteinized by vortexing and centrifuging with 125 μl acetonitrile. A 10 micro l portion of the supernatant was analyzed by HPLC on a 5 micro m C_{18} column (25 cm × 4.6 mm i.d.) with a guard column of similar material with acetonitrile:water:phosphoric acid (1200:800:1) as mobile phase (1.5 mL/min) and fluorescence detection at 285 nm (excitation at 250 nm). The calibration graph ranged from 0.05 to 5 μg/mL with a mean recovery of 95.14%. The mean interday RSD was 1.37%. There was no interference from endogenous substances observed in any of the biological samples analyzed.

Giagoudakis and Markantonis [107] presented and validated an HPLC method employing ultraviolet detection for the analysis of flurbiprofen and diclofenac in a 225 μL plasma sample. Chromatographic separations were performed using a C_{18} Sperisorb 5 μm column (25 cm × 4.6 mm). The mobile phase was pumped isocratically at a flow rate of 1 mL/min. The degassed mobile phase consisted of acetonitrile–0.1 M sodium acetate

(35:65) adjusted to pH 6.3 with glacial acetic acid. The method is simple with short retention time and excellent limits of detection.

Hutzler *et al*. [108] developed a sensitive and specific HPLC assay for 4′-hydroxyflurbiprofen and flurbiprofen in human urine and plasma. No extraction procedure was necessary for analysis of these compounds, which reduced the time involved in sample preparation. The analytes were separated on a Brownlee Spheri-5 C_{18} column with a mobile phase of acetonitrile: 20 mM dibasic potassium phosphate buffer of pH 3 (2:3). Fluorescence detection at 320 nm (excitation at 260 nm) was utilized, providing excellent sensitivity. The limit of quantitation for 4′-hydroxyflurbiprofen and flurbiprofen was 0.25 μg/mL in urine and 0.05 and 0.25 μg/mL, respectively, in plasma. Intraday, interday, freeze–thaw, and in-process stability were tested for both compounds, and the coefficient of variation was <14% in all cases.

Tu *et al*. [109] determined the content of flurbiprofen and 2-(4-biphenyl) propionic acid in flurbiprofen sustained release tablets by HPLC method. The contents were determined at 247 nm for flurbiprofen and 245 nm for 2-(4-biphenyl) propionic acid (a Shimpack CLS-ODS column with methanol-aqueous phase) (60:40) as mobile phase. The average recovery was 100.61% with relative standard deviation of 0.45% for flurbiprofen and 100.18% with relative standard deviation of 1.75 for 2-(4-biphenyl) propionic acid. The detection limit for 2-(4-biphenyl) propionic acid was 12.5 ng/mL. The method was simple, accurate, and reproducible.

Péhourcq *et al*. [110] developed a rapid and stereospecific HPLC micro-method to quantify flurbiprofen enantiomers. Both flurbiprofen enantiomers and indomethacin, used as internal standard, were extracted with methylene chloride from 100 μL of acidified plasma. The resolution of the *R*- and *S*-forms was performed on a bonded vancomycin chiral stationary phase (Chirobiotic V) with 20% of tetrahydrofuran in ammonium nitrate (100 mM, pH 5) as mobile phase. Calibration curves were linear in the range 0.5–10 μg/mL for both enantiomers. A good accuracy was obtained for all quality controls, with intraday and interday variation coefficients equal or less than 7.7%. Recovery of both enantiomers was found in the range of 77.4–86.3%. The lower limit of quantitation was 0.25 μg/mL for both enantiomers, without interference of endogenous components. This validated micro-method has been successfully applied for quantifying *R*- and *S*-flurbiprofen in rat plasma.

Ding *et al*. [111] determined flurbiprofen in human plasma by reversed-phase HPLC method. The plasma concentration of flurbiprofen was determined by HPLC at 247 nm on Irregular-HC_{18} column with methanol–7.42 mM phosphoric acid solution (75:25) as a mobile phase and flow rate of 1 mL/min. Samples were pretreated by solvent extraction. The linear range was 0.05–20 μg/mL with detection limit of 0.2 ng.

The average recovery was 98.3%. The results showed that the method was convenient and practicable.

Aboul-Enein and Ali [112] investigated the thermodynamic study of the enantiomeric resolution of flurbiprofen by HPLC using Chiralpak AD-RH column. The chiral resolution of (±)-flurbiprofen was achieved using water–acetonitrile (60:40, v/v) containing 0.1% acetic acid on a Chiralpak AD-RH column at 20°C. The enantioresolution was studied with different percentages of acetonitrile. Thermodynamic parameters (enthalpy, entropy, and free energy) were calculated by carrying out the enantioresolution experiments at 0–60°C. The enantioresolution was found to be exothermic in nature. Attempts have been made to explain the mechanism of chiral resolution of flurbiprofen on the Chiralpak AD-RH column.

Sajeev *et al*. [84] described a rapid UV spectrophotometric method and a reversed-phase HPLC method for the determination of flurbiprofen in bulk and in pharmaceuticals. The solvent system wavelength of detection and chromatographic conditions were obtained in order to maximize the sensitivity of both methods. The detection limit was 0.34 μg/mL for the UV method and 15 mg/mL for the HPLC method. The methods were employed with a high degree of precision and accuracy for the determination of total drug in two ophthalmic drop formulations of flurbiprofen. The results of analysis were treated statistically, as USP 2000 and International Conference of Harmonization Guidelines for validation of analytical procedure, and by recovery studies. The results obtained in the ultraviolet method were comparable with those obtained by using HPLC. The column used in the liquid chromatography was a reversed-phase 4.6 mm × 12.5 cm (5 μm) of LiChroCART Purospher end-capped C_{18} LC column. The mobile phase was methanol–acetonitrile–phosphate buffer (pH 5.6, 40:20:40) at a flow rate of 0.75 mL/min. The eluate was analyzed at a wavelength of 248 nm.

Teng *et al*. [113] assessed a method of analysis of flurbiprofen in biological fluids. A simple HPLC method was developed for simultaneous determination of flurbiprofen enantiomers in rat serum. Serum (0.1 mL) was extracted with 2,2,4-trimethylpentane–isopropanol (95:5, v/v) after addition of the internal standard, *S*-naproxen and acidification with sulfuric acid. Separation was achieved on a Chiralpak AD-RH column with UV detection at 247 nm. The calibration curve was linear ranging from 0.05 to 50 μg/mL for each enantiomer. The assay was applied to the *in vivo* kinetic study of flurbiprofen in rats.

Paik *et al*. [114] performed the enantiomeric composition tests on flurbiprofen present in patch products and in urine excretions following patch applications as diastereomeric (*R*)-(+)-1-phenylethylamides by achiral gas chromatography and by gas chromatography-mass spectrometry (GC-MS) in selected ion-monitoring mode. The method for

determination of (*R*)- and (*S*)-enantiomers in the range from 0.1 to 5.0 μg was linear (r=0.9996) with acceptable precision and accuracy. The enantiomeric compositions of flurbiprofen in one patch product were identified to be racemic with relatively good precision. The urinary excretion level of (*R*)-flurbiprofen was two times higher than its antipode.

Péhourcq *et al*. [115] studied the chiral resolution of flurbiprofen enantiomers by HPLC on a glycopeptide-type column chiral stationary phase. Bonded vancomycin chiral stationary phase (chirobiotic V) was investigated for the chiral liquid chromatography analysis of flurbiprofen. The selectivity factor (α) and the chiral resolution (R_s) of chirobiotic V were evaluated first as a function of the buffer pH and molarity, and second as a function of organic modifier type and composition of the mobile phase. Four organic modifiers, tetrahydrofuration, isopropanol, dioxane, and methanol, have been tested for their selectivity. Optimized conditions using 20% of tetrahydrofuran in ammonium nitrate (100 mM, pH 5) were selected for the enantioseparation of flurbiprofen from their racemic forms.

Radwan and Abnoul-Enein [116] determined the stereoselective HPLC of flurbiprofen in rat plasma. The influence of sustained release formulation on the pharmacokinetics of flurbiprofen enantiomers *R*- and *S*-flurbiprofen was investigated. Therefore, a stereoselective HPLC method was developed and validated for the rapid, quantitative determination of *R*- and *S*-flurbiprofen in rat plasma. Flurbiprofen-loaded poly(D,L-lactide-*co*-glycolide) nanoparticles (*rac*-flurbiprofen-PLGA) were prepared by in emulsion-solvent evaporation technique. Optimum conditions for *rac*-flurbiprofen-PLGA nanoparticle preparation were considered, and the *in vitro* release of *rac*-flurbiprofen, *R*-, and *S*-flurbiprofen were followed up to 48 h in phosphate buffer (pH 7.4).

Charoo *et al*. [117] developed a simple reversed-phase HPLC method for the determination of flurbiprofen in rat plasma, excised skin extract, and transdermal path formulations. The mobile phase was methanol–1% phosphoric acid in water (80:20), at a flow rate of 0.5 mL/min. Ibuprofen was used as the internal standard. Flurbiprofen and ibuprofen were detected by UV absorption at 250 and 220 nm, respectively. The limit of quantification was 0.1 μg/mL. The response was linearly dependent on concentration in the range of 0.1–10 μg/mL, and accuracy and reproducibility were good. At these concentrations, intraday and interday assay variability was below 8%. Recovery of flurbiprofen was greater than 94% over the linear range of calibration plot.

Lo *et al*. [118] developed and validated a sensitive and accurate stability-indicating HPLC method for determining the photodegradation of flurbiprofen with linear regression of calibration curve, intraday test, and interday test. The relative standard deviations of intraday and interday tests were lower than 1.1% and 1.7%, respectively. The percentage recovery was between 98.2% and 102%.

Albert *et al.* [119] determined flurbiprofen in human serum by reversed-phase HPLC with fluorescence detection. Flurbiprofen was extracted from hydrochloric acid-acidified serum with pentane–ether (80:20). An octadecyl silane column was used with a mobile phase of acetonitrile–water–phosphoric acid (650:350:0.5). A fluorescence detector with excitation at 250nm and emission at 315nm proved a quantifiable peak for 0.1 μg/mL of flurbiprofen in 0.5mL of plasma. A comparison between UV and fluorescence detection systems is presented. The method is applicable to human bioavailability and pharmacokinetic studies with flurbiprofen.

Han *et al.* [120] developed a method based on cloud-point extraction for the determination of flurbiprofen in rat plasma after oral and transdermal administration by HPLC coupled with ultraviolet detection. The nonionic surfactant Genapol X-080 was chosen as the extract solvent. Variable parameters affecting the cloud-paint extraction efficiency were evaluated and optimized. Chromatography separation was performed on a Diamond C_{18} column (4.6mm × 25cm, 10 μm) by isocratic elution with UV detection at 254nm. The assay was linear over the range of 0.2–50 and 0.1–10 μg/mL for oral and transdermal administration, respectively, and the lower limit of quantification was 0.1 μg/mL. The extraction recoveries were more than 84.5%, the accuracies were within ±3.8%, and the intraday and interday precisions were less than 10.1% in all cases. The method indicated good performance in terms of reproducibility, specificity, linearity, precision, and accuracy and was applied to pharmacokinetic study of the drug in rats after oral and transdermal administration.

Yang *et al.* [121] determined the flurbiprofen content in flurbiprofen dry suspension by an HPLC method. The Hypersil C_{18} column (25cm × 4.6mm, 5 μm) was used with the mobile phase of acetronitrile–0.02mol/L potassium dihydrogen phosphate (54:46, adjusting pH 6 with triethylamine), and the detection wavelength was 254nm. The method had a good linear relationship in the range of 2–64 μg/mL (r=0.9999). The precision of the intraday and interday relative standard deviation was about 0.79% and 1.04%, respectively. The average recovery rates of low, medium, and high concentration of flurbiprofen were 99.38%, 100.05% and 99.78%, respectively. The method is selective and accurate for the content determination of the drug in flurbiprofen dry suspension.

Liu *et al.* [122] established a reversed-phase HPLC method for determining the contents of flurbiprofen and preservative in flurbiprofen ophthalmic solution and to forecast its expiration date at room temperature. The expiration date of the eye drops was delivered classical constant temperature. The results showed that the assay was linear for flurbiprofen within a range of 6–72mg/L and for ethyl hydroxybenzoate within a range of 7.5–90mg/L. The mean recovery of flurbiprofen was 100%, and relative standard deviation was 0.62%. The mean recovery of ethyl hydroxybenzoate was 99.9%, and relative standard deviation was 0.70%. The

expiration date (t0.9) for flurbiprofen at 25°C was 3.7 years, and that for ethyl hydroxybenzoate at 25°C was 1.9 years. The method is simple, rapid, and accurate and can be used for the quality control of flurbiprofen ophthalmic solution.

Unal *et al*. [123] developed and validated a bioanalytical method for the determination of flurbiprofen from human plasma by liquid chromatography with UV detection. This method is reliable and robust. The validation results were included specificity, accuracy, extraction recovery, linearity, and range. The assay can be applied to the pharmacokinetic and bioequivalence studies. The method was carried out at room temperature using a reversed-phase Nucleosil C_{18} (15cm × 4.6mm, 5μm) column. The mobile phase consists of a mixture of 0.1M sodium acetate–acetonitrate (65:35), and the pH of the mobile phase was adjusted to 6.30 by 85% orthophosphoric acid. Flow rate of the mobile phase was 1mL/min. The detection wavelength, 248nm, was determined by scanning the maximum absorbance wavelength of flurbiprofen and losartan (internal standard) in the mobile phase.

Clarcke [3] recommended the following six systems:

(1) Column: C_8 symmetry (250 × 4.6 mm i.d., 5μm) with symmetry C_{18} precolumn (20mm).

Column temperature: 30°C.

Mobile phase: (A:B) phosphate buffer (pH 3.8):acetonitrile.

Elution program: (85:15) for 6.5min to (65:35) until 25min to (20:80) for 30min and back to initial condition for equilibration for 7 min.

Flow rate: 1mL/min for 6.5min, then linear increase to 1.5mL/min for 6.5–25min and hold for 3min (re-equilibration is made at 1.5 mL/min).

Detection: UV diode array.

Retention time: 21.3min.

(2) Column: LiChrospher 60 RP-Select B (125 × 4mm i.d., 5μm) with precolumn LiChrospher 60 RP-Select B (4 × 4mm i.d., 5μm).

Mobile phase: (A:B) triethylammonium phosphate buffer (25mM, pH 3):acetobnitrile.

Elution program: (A:B) (100:0) to (30:70) in 30min, hold for 10min and back to initial conditions in 3min with equilibration for 10min before next injection.

Flow rate: 1mL/min.

Detection: UV diode array.

Standards: Nitro-*n*-alkanes (C_1 to C_{11}) 10μL in 10mL acetonitrile.

Retention index: 585 [124].

(3) Column: C_{18} end-capped LiChrospher 100 RP-18e, (125 × 4m i.d., 5μm) with precolumn LiChrospher 124.4.

Mobile phase: Add 146μL triethylamine and about 750μL phosphoric acid to 530mL water. Adjust pH to 3.3 using a

10% potassium hydroxide solution and finally add 470mL acetonitrile.

Flow rate: 0.6mL/min.

Detection: UV diode array.

Retention time: 11.8min.

(4) Column: ODS Sphirisorb (200×4.6mm, i.d., 5μm).

Mobile phase: Acetonitrile:acetic acid (45:55) for 2min, to (75:25) at 3%/min, hold for 6min.

Flow rate: 1.7 mL/min.

Retention time: 0.89 (relative to meclofenamic acid) [125].

(5) Column: Supelcosil LC-DP (250×4.6mm, i.d., 5μm).

Eluent: (A:B:C) Acetonitrile:phosphoric acid (0.025%, v/v):triethylamine buffer.

Isocratic elution: (25:10:5).

Flow rate: 0.6mL/min.

Detection: UV diode array (λ=229nm).

Note: The triethylamine buffer is prepared by adding 9mL concentrated phosphoric acid and 10mL triethylamine to 900mL water, adjusted to pH 3.4 with dilute phosphoric acid and made up to 1L with water.

Retention time: 8min.

(6) Column: LiChrospher 100 RP-8 (250×4mm i.d., 5μm).

Eluent: (A:B:C) Acetonitrile:phosphoric acid (0.025%):triethylamine buffer.

Isocratic elution: (60:25:15).

Flow rate: 0.6mL/min.

Detection: UV diode array (λ=229nm).

8.2.4.6. Gas chromatography–mass spectrometry Paik *et al.* [114] performed the enantiomeric composition tests on flurbiprofen present in patch products and in urine excretions following patch applications as diastereomeric (*R*)-(+)-1-phenylethylamides by achiral gas chromatography and GC-MS in selected ion-monitoring mode. The method for determination of (*R*)- and (*S*)-enantiomers in the range from 0.1 to 5.0μg was linear (r= 0.9996) with acceptable precision and accuracy. The enantiomeric compositions of flurbiprofen in one patch product were identified to be racemic with relatively good precision. The urinary excretion level of (*R*)-flurbiprofen was two times higher than its antipode.

Chao *et al.* [126] identified flurbiprofen and its photo-products in methanol by GC-MS. A sample of 10mM flurbiprofen in methanol (or ethanol) was photoirradiated with sixteen 8W low-pressure quartz mercury lamps, irradiated at 306nm in a Panchum PR-2000 photochemical reactor. In total, four major photo-products derived from each sample

were observed from the HPLC chromatogram. The photo-products were separated and their structures elucidated by various spectroscopic methods. Alternatively, using GC-MS, 11 major photo-products were observed. A reaction scheme of flurbiprofen in methanol was proposed: the photochemical reaction routes occur mainly via esterification and decarboxylation, followed by oxidation with singlet oxygen to produce a ketone, alcohols, and other derivatives.

Satomoto *et al* [127] developed a GC-MS assay method for the quantitation of flurbiprofen in human plasma. Extraction or condensing procedure was not required and the method reduced time involved in sample preparation. The analytes were separated on the fused-silica capillary column. The operating conditions were injector, 250°C; detector, 300°C; and column, 50–280°C. The total gas flow rate of helium (carrier) was 50mL/min, and the pressure of column inlet was 100–200kPa. The retention time was 18.1min, and the limit of quantitation was 0.5μg/mL. This method provides an easy and simple method for the detection of flurbiprofen.

Liu *et al*. [128] used liquid chromatography tandem/mass spectrometric method for the determination of flurbiprofen in human serum. The serum samples were precipitated with methanol. The drug was determined by the method, using electrospray ionization. Flurbiprofen and its internal standard, indomethacin, were detected on multiple reaction monitoring by the transitions from the precursor to the product ion (m/z 243.3/198.8 and m/z 356.3/312.0). The retention times of these two analytes were 0.9 and 1.6min, respectively. An API3000 tandem mass spectrometer and a Shimadzu liquid chromatograph were used for all analytes. The analytical column was a Gemini C_{18} column (5cm × 2.1mm, 5μm). The mobile phase, acetonitrile–water (18:82), was used at a flow rate of 0.3mL/min. The injection volume was 3μL, and the total run time was 3min. The calibration curve had good linearity in the range of 0.05–50μg/mL (r=0.9995). The method was sensitive, accurate, and simple for the determination of flurbiprofen in human serum. It is suitable for the pharmacokinetics and bioavailability study of the drug.

8.2.4.7. Capillary zone electrophoresis Zhu and Lin [129] studied the chiral separation of flurbiprofen by capillary electrophoresis. The acidic chiral drugs flurbiprofen were successfully separated into two enantiomers when β-cyclodextrins (β-CyDs) were used as chiral selectors by capillary zone electrophoresis, under the conditions of 0.1mol/L phosphate buffer with pH 4.92. The comparison of four CyDs, namely β-CyD, DM-β-CyD, HP-β-CyD, and TM-β-CyD for chiral separation was made. Flurbiprofen can only be separated by TM-β-CyD among the CyDs. The method of chiral separation for weak acidic compounds was also developed. The optimum pH value for their chiral separation was about 5, close to its pK_a value.

Hamoudova and Pospisilova [130] determined flurbiprofen in pharmaceuticals by capillary zone electrophoresis with spectrophotometric detection. The separation was carried out in a fused-silica capillary (60 cm × 100 μm i.d. effective length 45 cm) at 30 kV with UV detection at 232 nm. The optimized background electrolyte was 20 mM *N*-(2-acetamido)-2-aminoethane sulfonic acid with 20 mM imidazole and 10 mM α-cyclodextrin of pH 7.3. 2-Naphthoxyacetic acid was used as internal standard. A single analysis took less than 5 min. Rectilinear calibration ranges were 1–60 mg/L for flurbiprofen. The relative standard deviations values (n=6) was 1.29% for flurbiprofen (at 10 mg/L). This validated method has been successfully applied for the routine analysis of 10 commercially available pharmaceutical preparations (syrup, tablets, cream, and gel).

Rousseau *et al*. [131] reported the determination of flurbiprofen enantiomers in plasma samples using a single-isomer amino cyclodextrin derivative in nonaqueous capillary electrophoresis using 6-monodeoxy-6-mono (3-hydroxy) propylamino-β-cyclodextrin as the chiral sector. The nonaqueous background electrolyte was made up of 40 mM ammonium acetate in methanol, and flufenamic acid was used as internal standard. Solid-phase extraction was used for sample cleanup prior to the nonaqueous capillary electrophoresis separation. The nonaqueous capillary electrophoresis method reducibility was optimized by evaluating different capillary washing sequences between runs. After having tested various conditions, trifluoroacetic acid (1 M) in methanol was finally selected. The solid phase extraction procedure was good, reproducible analyte recoveries were obtained using methanol for protein denaturation, and a polymeric phase combining hydrophobic interactions with anion exchange properties (Oasis MAX) was selected as extraction sorbent. The method was validated with respect to response function, trueness, precision, accuracy, linearity, and limit of quantification.

Sadecka *et al*. [132] described an isotachophoretic method for the determination of flurbiprofen in serum. The method involved deprotonization of the biological samples with ethanol. No interference from metabolites or other drugs was observed.

9. PHARMACODYNAMICS

The major pharmacological properties have already been reviewed in 1975 [9]. Several discriminating techniques were applied to determine the lowest effective oral dose (mg/kg) as anti-inflammatory, analgesic, and antipyretic drug. In the anti-inflammatory tests, three animal species were used: guinea pig, rat, and mouse [21,22,133]. In the guinea pig, the UV-erythema test was employed in which the reference compound (aspirin, 80 mg/kg) was found to correspond to 0.25 mg/kg of flurbiprofen. In the mouse model, the

capillary permeability of the peritoneum was evaluated by use of a dye (Pontamine sky blue). Aspirin at 120mg/kg was equivalent to 0.47mg/kg of flurbiprofen. In the rat, three methods were employed: the carrageenan edema test, and two adjuvant arthritis models for the developing state and the established state. Reference compounds were, respectively, aspirin (81 mg/kg) in the first and indomethacin (1mg/kg) and phenylbutazone (10 mg/kg) in the two latter models. The corresponding lowest effective dose for flurbiprofen was 0.11 and 0.33mg/kg in the two latter models. With the carrageenan edema test, a subgroup of rats was also tested that were bilaterally adrenalectomized to rule out any adrenocortical interference. Several conclusions were drawn from this study. Flurbiprofen was devoid of adrenocortical stimulating properties and was one of the most potent agents of this type reported yet, at least 10 times more potent than ibuprofen. It was postulated that the mode of action in the mouse and rat was not identical to that of aspirin. In US patent 3,755,427 (August 28, 1973) [134], it was stated that flurbiprofen was between 75 and over 100 times as potent as aspirin. It was reported that the relative potency of various hydratropic acids were tested for their relaxing ability on guinea pig tracheal ring contraction after sensitization by rat SRS-A [22]. Furthermore, the paper provided information not only for flurbiprofen but also for the levorotary (−)- and dextrorotary (+)-enantiomers. It became apparent that the relaxing potency of the racemic mixture (±) was unexpectedly too low as compared to the dextrorotary component, suggesting that the dextrorotary component was hindered by the simultaneous presence of the levorotary component. The putative interaction between the two enantiomers was tested by the simultaneous addition of the two separate enantiomers to the muscle bath. Reversal by the dextrorotary component was diminished by the simultaneous presence of the (−) flurbiprofen. Taking this into consideration (+), flurbiprofen was approximately 80-fold more potent than (−) flurbiprofen.

10. PHARMACOKINETICS

Pharmacokinetic properties have been assessed in different species [135]. In human, when assessed by HPLC of the racemic molecule, a two-compartment open model appeared the most appropriate for flurbiprofen [136]. Drug absorption efficiency was found independent of the oral dose. The intact drug resides mainly in the peripheral and central compartments, disappearing with a terminal half-life of approximately 5.5h. More than 99% of flurbiprofen is bound to serum proteins. The serum flurbiprofen concentrations in clinical use, however, show occupancy of less than 10% of the primary binding sites. Drug interactions will therefore not automatically occur with simultaneous use.

10.1. Metabolic pathway in human

Oxidation and conjugation are the main pathways of metabolism in human. More than 95% of an oral dose is excreted via the kidney within 24h. In all, 40–47% of a daily oral dose is excreted as 2-[2-fluoro-4′-hydroxy-4-biphenylyl]propionic acid, 5% as 2-[2-fluoro-3′,4′-hydroxy-4-biphenylyl]propionic acid, 20–30% as 2-[2-fluoro-3′-hydroxy-4′-methoxy-4-biphenylyl]propionic acid, and 20–25% as the parent molecule flurbiprofen. Between 65% and 85% of flurbiprofen and its metabolites are present as glucuronide and sulfate conjugates. Stereoselective HPLC of human plasma has also been performed [137]. After oral administration of 25mg of the *R*(−)-enantiomer of flurbiprofen, no indication was found that inversion to the *S*(+)-enantiomer occurred. This was confirmed in healthy volunteers taking either 50mg *R*-(−) flurbiprofen or *S*(+) flurbiprofen [138].

Stereoselective studies have been performed following the disposition of flurbiprofen in normal volunteers after a single 50mg racemic dose [139], in healthy female subjects following oral administration of the single enantiomers of flurbiprofen, 50mg *S*(+)- or *R*(−) flurbiprofen or 100mg *R*(−) flurbiprofen or placebo, in a four-way crossover design with placebo [140], in patients with end-stage renal disease undergoing continuous ambulatory peritoneal dialysis (CAPD) after administration of a single 100mg racemic dose [141], and stereoselective disposition of racemic flurbiprofen in single and multiple dosing in uraemic patients [142]. In patients with liver disease with ascites and in renal failure patients with a creatinine clearance of less than 10mL/min, significant higher free fractions of *R*(−)- and *S*(+)-flurbiprofen were detected in conjunction with lower albumin concentrations [143].

An overview of the clinical pharmacokinetics of flurbiprofen and its enantiomers is presented in Ref. [144]. In a review [145] on the binding of flurbiprofen to albumin in human plasma, it was reported that at low therapeutic concentrations, the *S*(+)-enantiomer has a higher protein binding than its *R*(−) antipode. At high drug concentrations, there is no measurable difference, however. In an ultrafiltration study done with normal volunteers, the free fraction of *R*(−) flurbiprofen was higher than its *S*(+) antipode at lower drug levels but similar for both enantiomers at higher drug levels. Patients with renal impairment and patients exhibiting hypoalbuminemia have higher free fractions of flurbiprofen enantiomers than normal volunteers. Plasma protein binding of an enantiomer is not influenced by its own concentration or the presence of its antipode under clinical therapeutic conditions [146]. As mentioned above, the main routes of biotransformation of flurbiprofen are through oxidation and conjugation. Oxidation has been investigated more specifically [147] for the enantiomers of flurbiprofen utilizing human liver

microsomes. The most prominent oxidative metabolism route is by cytochrome P450. It was established that cytochrome P450 2C9 and its allelic variant R144C catalyzed the oxidative reaction. Interestingly, there was no stereoselective preference of one enantiomer over the other. Safety for intestinal permeability changes when using the racemate or the separate enantiomers of flurbiprofen was studied in rats, for which species, it was established that only a minimal inversion of the *R*(−)-enantiomer takes place. Intestinal permeability was measured by urinary excretion of ^{51}Cr–EDTA [148].

It was established that at both dosages used (1 and 3 mg/kg for the racemic drug and half for the enantiomers), permeability was significantly different from control. *R*(−) flurbiprofen was safest in both dosage ranges. *S*(+) flurbiprofen inflicted similar damage as the racemic form. It was shown [149] that in rats *R*(−) flurbiprofen gave the same increase of intestinal permeability, but the difference was that the impact on mucosal prostanoid production was smaller and not accompanied by ulcerative changes in the small intestine. Although it would seem attractive to develop therapeutic *R*(−)-enantiomers of 2-arylproionic acids due to its supposedly lower toxicological profile, it must be borne in mind that the presumed pharmacological action required for reducing inflammation is inhibition of prostaglandin synthesis. This property resides primarily, in the case of flurbiprofen, in the *S*(+)-enantiomer for which a difference of 30–100 times compared to the *R*(−)-enantiomer was established depending on the model used. Only with full metabolic inversion of a *R*(−)- to a *S*(+)-enantiomer would such a therapeutic drug be a possibility. For flurbiprofen, this is not the case in humans [150–152].

10.2. Elimination profile in equine urine

Flurbiprofen and its main acidic metabolites were detected in equine urine after a single-dose administration of 500 mg flurbiprofen to two 2.5- to 3.5-years-old mares, in order to be used in equine doping control routine analysis. The urine levels of the parent drug were determined using GC/MS. Five acidic metabolites were found in the urine (Fig. 4.17). The structure of the proposed metabolites was confirmed by HRMS accurate mass measurements (Fig. 4.18 and Table 4.5). The highest flurbiprofen concentration was 204 μg/mL at 1- to 3-h post administration. Flurbiprofen could be detected for 24–37 h in urine using the standard screening procedure. All metabolites were present 25-h post administration, while 4′-hydroxyflurbiprofen could be traced for more than 48 h, and it is regarded as the long-term metabolite of flurbiprofen in horse [153].

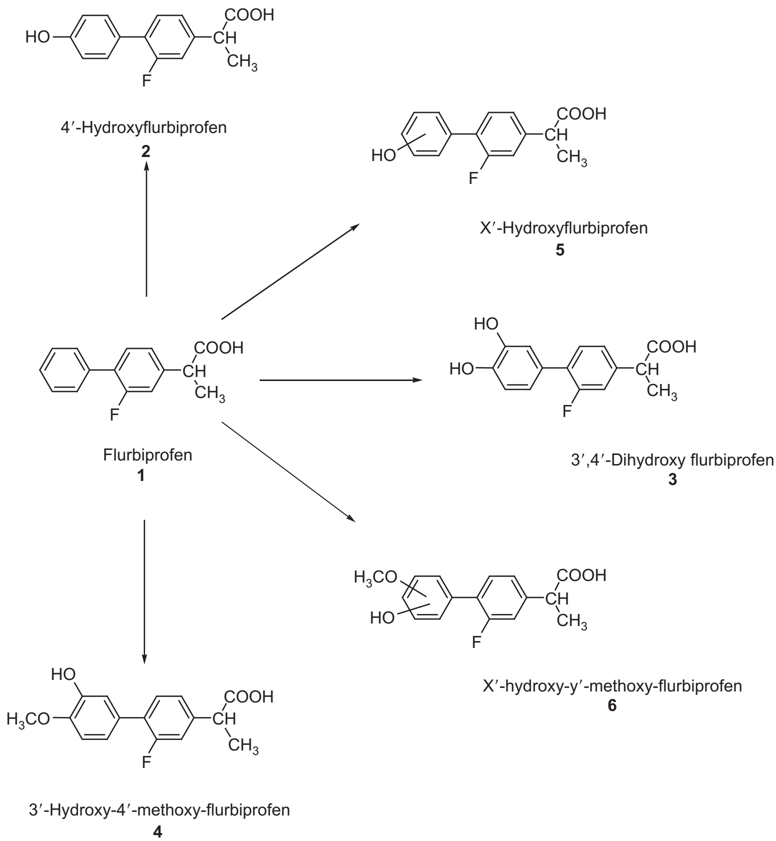

FIGURE 4.17 The chemical structures of flurbiprofen and its five metabolites [135].

TABLE 4.5 Calculated data of the exact mass measurements of the flurbiprofen and its metabolites (**I–V**) [153]

Compound	Calculated mass	Real mass	$\Delta m/m$ (ppm)[a]
Flurbiprofen (I)	316.1271	316.1296	7.9
	301.1039	301.1061	7.3
4′-OH-flurbiprofen (II)	404.1633	404.1640	1.7
	389.1426	389.1405	−5.4
3′-4′-diOH-flurbiprofen (III)	492.2090	492.1985	−21.3
	477.1755	477.1750	−1.0
3′OH-4′-MeO-flurbiprofen (IV)	434.1769	434.1746	−5.3
	419.1459	419.1511	12.4
x'-OH-flurbiprofen (V)	404.1635	404.1640	1.2
	389.1382	389.1405	5.9

[a] $\Delta m/m$ = (real mass − calculated mass/real mass) × 10^6 [153].

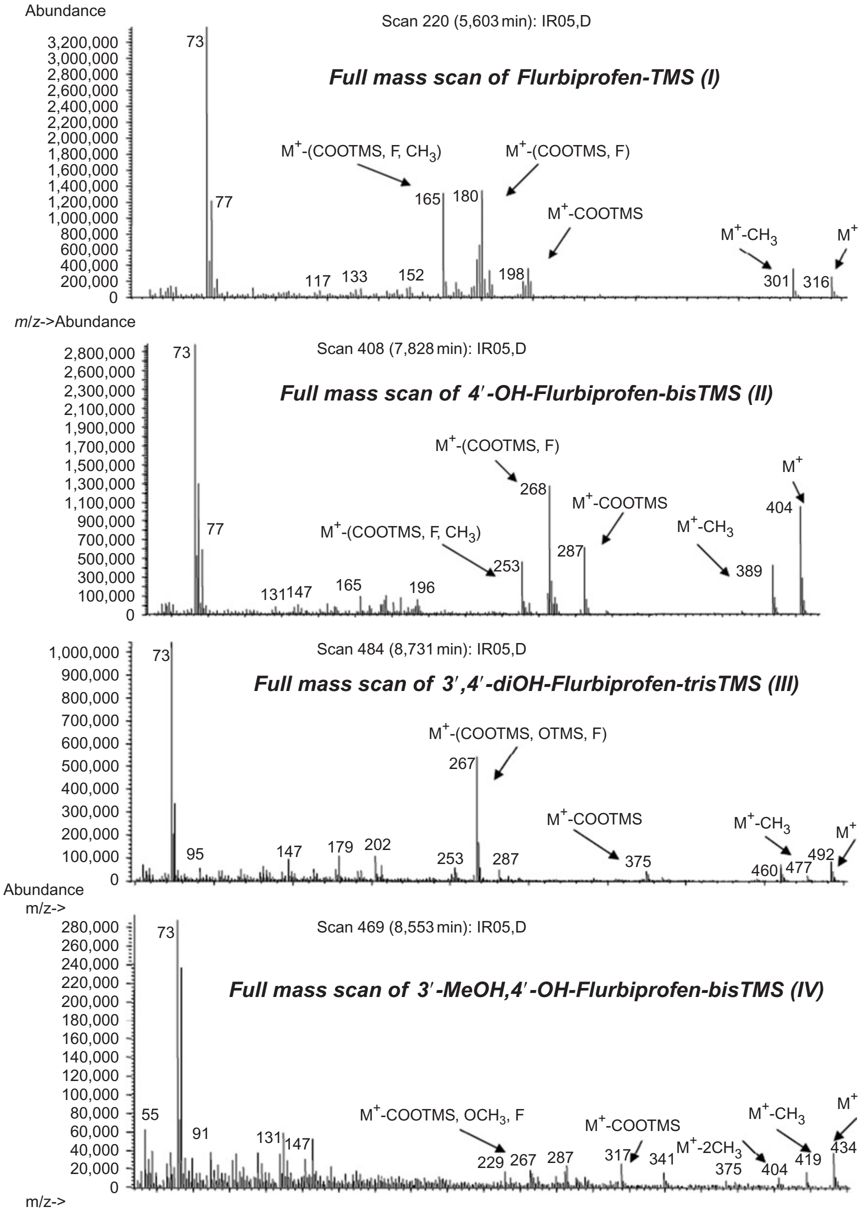

FIGURE 4.18 Mass spectrum and fragmentation pattern of TMS derivatives of flurbiprofen (**I**) and flurbiprofen metabolites (**II**–**VI**) in urine samples taken from a Skyrian mare 5h after oral administration of 500mg flurbiprofen. The sample had been prepared according to the screening procedure for NSAIDs [153].

ACKNOWLEDGMENTS

The authors wish to thank Mr. Tanvir A. Butt, Pharmaceutical Chemistry Department, College of Pharmacy, King Saud University for his secretarial assistance in preparing this chapter.

REFERENCES

[1] 14th ed., Maryadele J. O'Neil (Ed.), The Merck Index, an Encyclopedia of Chemicals, Drugs and Biologicals, Merck Research Laboratories Division of Merck Co., Inc., Whitehouse Station, NJ, 2006.
[2] 13th ed., S. Budavari (Ed.), The Merck Index, Merck & Co., Inc, Rahway, NJ, 2001.
[3] Anthony C. Moffat, M. David Osselton, Brian Widdop, third ed., Clarcke's Analysis of Drugs and Poisons in Pharmaceuticals, Body Fluids and Postmortem Materials, vol. 2, Pharmaceutical Press, London, UK, 2004 1056.
[4] K. Uekama, T. Imai, F. Hirayama, M. Otagiri, K. Harata, Chem. Pharm. Bull. 32 (1984) 1662–1664.
[5] P. Camps, S. Giménez, Tetrahedron Asymm. 6 (1995) 991–1000.
[6] R. Morrone, G. Nicolosi, A. Patti, M. Piattelli, Tetrahedron Asymm. 6 (1995) 1773–1778.
[7] P. Spizzo, A. Basso, C. Ebert, L. Gardossi, V. Ferrario, D. Romano, F. Molinari, Tetrahedron 63 (2007) 11005–11010.
[8] S. Grösch, K. Schilling, A. Janssen, T.J. Maier, E. Niederberger, G. Geisslinger, Biochem. Pharmacol. 69 (2005) 831–839.
[9] S.S. Adams, K.F. McCullough, J.S. Nicholson, Arzneim. Forsch. 25 (1975) 1786–1791.
[10] Analgesic and anti-inflammatory agents, 29th ed., J.E.F. Reynolds (Ed.), Martindale: The Extra Pharmacopeia, The Pharmaceutical Press, London, UK, 1989, pp. 1–46.
[11] R.N. Sud, R.S. Greval, R.S. Bajwa, Indian J. Med. Sci. 49 (1995) 205–209.
[12] M. Diestelhorst, B. Schmidt, W. Konen, U. Mester, P.S. Raj, J. Cataract Refract. Surg. 22 (Suppl. 1) (1996) 788–793.
[13] R.B. Vajpayee, B.P. Dhakal, S.K. Gupta, M.S. Sachdev, G. Satpathy, S.G. Honavar, A. Panda, Aust. N. Z. J. Ophthalmol. 24 (1996) 131–135.
[14] A. Appiotti, L. Gualdi, M. Alberti, M. Gualdi, Clin. Ther. 20 (1998) 913–920.
[15] D.S. Jones, C.R. Irwin, A.D. Woolfson, J. Djokic, V. Adams, Pharm. Sci. 88 (1999) 592–598.
[16] M. Hofer, M. Pospisil, I. Pipalova, Folia Biol. 42 (1996) 267–269.
[17] J.D. McCracken, W.J. Wechter, Y. Liu, R.L. Chase, D. Kantoci, E.D. Murray Jr., D. D. Quiggle, Y. Mineyama, J. Clin. Pharmacol. 36 (1996) 540–545.
[18] L. Juchelkova, M. Hofer, M. Pospisil, I. Pipalova, Physiol. Res. 47 (1998) 73–80.
[19] S.M. Soulier, J.C. Page, L.C. Larsen, B.C. Grose, J. Foot Ankle Surg. 36 (1997) 414–417 discussion 446.
[20] U. Bragger, T. Muhle, I. Fourmousis, N.P. Lang, A. Mombelli, J. Periodontal Res. 32 (1997) 575–582.
[21] M.L. Brochier, Eur. Heart J. 14 (1993) 951–957.
[22] M.E. Greig, R.L. Griffin, J. Med. Chem. 18 (1975) 112–116.
[23] J. Lotsch, G. Geisslinger, P. Mohammadian, K. Brune, G. Kobal, Br. J. Clin. Pharmacol. 40 (1995) 339–346.
[24] N.M. Davies, Clin. Pharmacokinet. 28 (1995) 100–114.
[25] G. Geisslinger, S.H. Ferreira, S. Menzel, D. Schlott, K. Brune, Life Sci. 54 (1994) PL173–PL177.
[26] W.J. Wechter, J. Clin. Pharmacol. 34 (1994) 1036–1042.
[27] D. Picot, P.J. Loll, R.M. Garavito, Nature 367 (1994) 243–249.
[28] R. Garg, A. Kurup, S.B. Mekapati, C. Hansch, Chem. Rev. 103 (2003) 703–732.

[29] A.S. Michaelidou, D. Hadjipavlou-Litina, Chem. Rev. 105 (2005) 3235–3271.
[30] J.R. Vane, R.M. Botting, Inflamm. Res. 44 (1995) 1–10.
[31] W.L. Smith, R.M. Garavito, D.L. DeWitt, J. Biol. Chem. 271 (1996) 33157–33160.
[32] B. Cryer, M. Feldman, Am. J. Med. 104 (1998) 413–421.
[33] B.M. Peskar, S. Kluge, B.A. Peskar, S.M. Soglowek, K. Brune, Prostaglandins 42 (1991) 515–531.
[34] N. Kawai, N. Kato, Y. Hamada, T. Shioiri, Chem. Pharm. Bull. 31 (1983) 3139–3148.
[35] D.D. Leipold, D. Kantoci, E.D. Murray Jr., D.D. Quiggle, W.J. Wechter, Chirality 16 (2004) 379–387.
[36] W.J. Wechter, D.D. Leipold, E.D. Murray Jr., D.D. Quiggle, J.D. McCracken, R. S. Barrios, N.M. Greenberg, Cancer Res. 60 (2000) 2203–2208.
[37] J.L. Eriksen, S.A. Sagi, T.E. Smith, S. Weggen, P. Das, D.C. McLendon, V.V. Ozols, K.W. Jessing, K.H. Zavitz, E.H. Koo, T.E. Golde, J. Clin. Invest. 112 (2003) 440–449.
[38] G.K. Wilcock, Alzheimers Dement. 2 (2006) 150–152.
[39] L. Gasparini, E. Ongini, D. Wilcock, D. Morgan, Brain Res. Rev. 48 (2005) 400–408.
[40] R.C. Griesbach, D.P.G. Hamon, R.J. Kennedy, Tetrahedron Asymm. 8 (1997) 507–510.
[41] D.P.G. Hamon, R.A. Massy-Westropp, J.L. Newton, Tetrahedron 51 (1995) 12645–12660.
[42] B.J. Armitage, J. S. Nicholson, US Patent 4,036,989..
[43] W. Engel, E. Seeger, H. Teufel, G. Engelhardt, US Patent 3,859,338..
[44] S.S. Adams, B.J. Armitage, J.S. Nicholson, A. Ribera Blancafort, US Patent 4,053,639..
[45] S.C. Stinson, Chem. Eng. News 9 (1995) 44–72.
[46] T.Z. Wang, E. Pinard, L.A. Paquette, J. Am. Chem. Soc. 118 (1996) 1309–1318.
[47] N.M. Davies, J. Chromatogr. B Biomed. Sci. Appl. 691 (1997) 229–261.
[48] S. Beilles, P. Cardinael, E. Ndzie, S. Petit, G. Coquerel, Chem. Eng. Sci. 56 (2001) 2281–2294.
[49] Q.M. Gu, C.S. Chen, C.J. Sih, Tetrahedron Lett. 27 (1986) 1763–1766.
[50] W. Rhys-Williams, F. McCarthy, J. Baker, Y.F. Hung, M.J. Thomason, A.W. Lloyd, G. W. Hanlon, Enzyme Microb. Technol. 22 (1998) 281–287.
[51] H.-A. Bae, K.-W. Lee, Y.-H. Lee, J. Mol. Catal. B Enzym. 40 (2006) 24–29.
[52] E.G. Lee, H.S. Won, H.-S. Ro, Y.-W. Ryu, B.H. Chung, J. Mol. Catal. B Enzym. 26 (2003) 149–156.
[53] J.Y. Wu, S.W. Liu, Enzyme Microb. Technol. 26 (2000) 124–130.
[54] J.D. Stewart, Curr. Opin. Chem. Biol. 5 (2001) 120–129.
[55] S.H. Wu, Z.W. Guo, C.J. Sih, J. Am. Chem. Soc. 112 (1990) 1990–1995.
[56] G. Duan, C.B. Ching, Biochem. Eng. J. 2 (1998) 237–245.
[57] H.Y. Zhang, X. Wang, C.B. Ching, J.C. Wu, Biotechnol. Appl. Biochem. 42 (2005) 67–71.
[58] R. Gandolfi, R. Gualandris, C. Zanchi, F. Molinari, Tetrahedron Asymm. 12 (2001) 501–504.
[59] A. Romano, R. Gandolfi, F. Molinari, A. Converti, M. Zilli, M.D. Borghi, Enzyme Microb. Technol. 36 (2005) 432–438.
[60] F. Molinari, R. Gandolfi, A. Converti, M. Zilli, Enzyme Microb. Technol. 27 (2000) 626–630.
[61] R. Gandolfi, A. Converti, D. Pirozzi, F. Molinari, J. Biotechnol. 92 (2001) 21–26.
[62] P. Thorpe, J. Castar, Drugs Fut. 1 (1976) 323 US Patent 3755427.
[63] M. Schlosser, H. Geneste, Chem. Eur. J. 4 (1989) 1969–1973.
[64] G. Lu, R. Franzen, X.J. Yu, Y.J. Xu, Chin. Chem. Lett. 17 (2006) 461–464.
[65] Y. Terao, Y. Ijima, H. Kakidani, H. Ohta, Bull. Chem. Soc. Jpn. 76 (2003) 2395–2397.
[66] 16th ed., British Pharmacopoeia, vol. 1, Her Majesty Stationary Office Publication, Ltd., London, 2000 Online, CD.
[67] I. Kumar, K. Manju, R.S. Jolly, Tetrahedron Asymm. 12 (2001) 1431–1434.
[68] G. Mollica, M. Geppi, R. Pignatello, C.A. Veracini, Pharm. Res. 23 (2006) 2129–2140.

[69] G. Metz, X.L. Wu, S.O. Smith, J. Magn. Reson. 110 (1994) 219–227.
[70] B.M. Fung, A.K. Khitrin, K. Ermolaev, J. Magn. Reson. 142 (2000) 97–101.
[71] R. Kitamaru, F. Horii, K. Murayama, Macromolecules 19 (1986) 636–643.
[72] J.G. Powles, J.H. Strange, Proc. Phys. Soc. 82 (1963) 6–15.
[73] M. Geppi, S. Guccione, G. Mollica, R. Pignatello, C.A. Veracini, Pharm. Res. 22 (2005) 1544–1555.
[74] R. Pignatello, M. Ferro, G. Puglisi, AAPS PharmSciTech 3 (2002) 35–45.
[75] D.L. VanderHart, W.L. Earl, A.N. Garroway, J. Magn. Reson. 44 (1981) 361–401.
[76] P. Hodgkinson, Prog. Nucl. Magn. Reson. Spectrosc. 46 (2005) 197–222.
[77] G. Antonioli, P. Hodgkinson, J. Magn. Reson. 168 (2004) 124–131.
[78] J.L. Flippen, R.D. Gilardi, Acta Cryst. B31 (1975) 926–928.
[79] J.R. Yates, S.E. Dobbins, C.J. Pickard, F. Mauri, P.Y. Ghi, R.K. Harris, Phys. Chem. Chem. Phys. 7 (2005) 1402–1407.
[80] C.H. Schwalbe, S.J. Teat, S.E. David, W.J. Irwin, B.R. Conway, P. Timmins, Acta Cryst. A61 (2005) C350.
[81] B.D. Anderson, R.A. Conradi, J. Pharm. Sci. 74 (1985) 815.
[82] United States Pharmacopoeia, USP 24-NF 19 through supplement 3, 24th ed., United States Pharmaceutical Convention, Inc, Rockville, MD, 2001 pp. 2214–2216.
[83] R.I. El-Bagary, Bull. Facul. Pharm. Cairo University, 38 (2000) 67–73 .
[84] C. Sajeev, P.R. Jadhav, D. Ravishankar, R.N. Saha, Anal. Chim. Acta 463 (2002) 207–217.
[85] C.S. Chauthan, I. Singhvi, P.K. Choudhury, Asian J. Chem. 19 (2007) 3286–3288.
[86] M.M. Baraka, M.M. El-Henawee, H.M. Khalil, Zagazig J. Pharm. Sci. 5 (1996) 138–142.
[87] X.X. Wang, G. Aodeng, A. Juan, Neimenggu Daxue Xuebao, Ziran Kexueban 40 (2009) 431–434.
[88] A.A. Bunaciu, C. Petrisor, H.Y. Aboul-Enein, Instrum. Sci. Technol. 26 (1998) 353–362.
[89] A.A. Bunaciu, A. Grasu, H.Y. Aboul-Enein, Anal. Chim. Acta 311 (1995) 193–197.
[90] V.V. Dhavse, D.V. Parmar, P.V. Devarajan, J. Chromatogr. B 694 (1997) 449–453.
[91] M.I.R.M. Santoro, A.K. Singh, E.R.M. Kedor-Hackmann, J. Liq. Chromatogr. Relat. Technol. 26 (2003) 517–527.
[92] G. Zhang, Y. Chai, S. Ji, Y. Zhong, X. Ying, J. Li, Y. Wu, Acad. J. Sec. Mil. Med. Univ. Shanghai 20 (10) (1999).
[93] B.G. Snider, L.J. Beaubien, D.J. Sears, P.D. Rahn, J. Pharm. Sci. 70 (1981) 1347–1349.
[94] W.J. Adams, B.E. Bothwell, W.M. Bothwell, G.J. VanGiessen, D.G. Kaiser, Anal. Chem. 59 (1987) 1504–1509.
[95] S.A. Babhair, J. Liq. Chromatogr. Relat. Technol. 11 (1988) 463–473.
[96] M.P. Knadler, S.D. Hall, J. Chromatogr. Biomed. Appl. 494 (1989) 173–182.
[97] R.T. Sane, S.M. Purandare, V.G. Nayak, M.D. Joshi, S.N. Dhumal, P.S. Mainkar, V.R. Nerukar, V.R. Bhate, Indian Drugs 26 (1989) 503–505.
[98] S. Kumbhat, N.K. Mathur, Anal. Lett. 23 (1990) 627–634.
[99] H.Y. Aboul-Enein, S.A. Bakr, J. Liq. Chromatogr. 15 (1992) 1983–1992.
[100] H. Kim, S.C. Chi, Yakche Hakhoechi 22 (1992) 63–68.
[101] M. Mathew, V. Das Gupta, C. Bethea, Drug Dev. Ind. Pharm. 19 (1993) 493–498.
[102] M. Spraul, M. Hofmann, I.D. Wilson, E. Lenz, J.K. Nicholson, J.C. Lindon, J. Pharm. Biomed. Anal. 11 (1993) 1009–1015.
[103] S.C. Chi, H. Kim, S.C. Lee, Anal. Lett. 27 (1994) 377–389.
[104] N.H. Foda, O.M. Al-Gohary, Anal. Lett. 27 (1994) 2523–2534.
[105] S.G. Deshpande, K.K. Singh, M.R. Baichwal, Indian Drugs 32 (1995) 227–229.
[106] K.M. Park, Z.G. Gao, C.K. Kim, J. Liq. Chromatogr. Relat. Technol. 20 (1997) 1849–1855.
[107] G. Giagoudakis, S.L. Markantonis, J. Pharm. Biomed. Anal. 17 (1998) 897–901.
[108] J.M. Hutzler, R.F. Frye, T.S. Tracy, J. Chromatogr. B 749 (2000) 119–125.
[109] L. Tu, W. Weng, H. Xu, Fudan Xuebao, Yixue Kexueban 28 (2001) 78–79.

[110] F. Péhourcq, M. Matoga, C. Jarry, B. Bannwarth, Biomed. Chromatogr. 18 (2004) 330–334.
[111] X. Ding, S. Wang, Y. Zhang, S. Gao, Zhongguo Yiyuan Yaoxue Zazhi 21 (2001) 472–473.
[112] H.Y. Aboul-Enein, I. Ali, Pharmazie 57 (2002) 682–685.
[113] X.W. Teng, S.W.J. Wang, N.M. Davies, J. Pharm. Biomed. Anal. 33 (2003) 95–100.
[114] M.J. Paik, D.T. Nguyen, K.R. Kim, Arch. Pharm. Res. 27 (2004) 1295–1301.
[115] F. Péhourcq, C. Jarry, B. Bannwarth, Biomed. Chromatogr. 15 (2001) 217–222.
[116] M.A. Radwan, H.Y. Aboul-Enein, Chirality 16 (2004) 119–125.
[117] N.A. Charoo, A.A.A. Shamsher, K. Kohli, K.K. Pillai, Z. Rahman, Chromatographia 62 (2005) 493–497.
[118] C. Lo, Y. Liou, Y. You, A. Wu, Fenxi Huaxue 34 (2006) 1327–1330.
[119] K.S. Albert, W.R. Gillespie, A. Raabe, M. Garry, J. Pharm. Sci. 73 (1984) 1823–1825.
[120] F. Han, R. Yin, X.L. Shi, Q.A. Jia, H.Z. Liu, H.M. Yao, L. Xu, S.M. Li, J. Chromatogr. B 868 (2008) 64–69.
[121] M. Yang, J. Huang, X. Lei, X. Zhong, Zhongguo Yaoye 17 (2008) 15–16.
[122] A.W. Liu, J. Li, Y. Sang, S. Xu, S. Xu, Z. He, Shenyang yaoke Daxue Xuebao 25 (2008) 800–805.
[123] B.O. Unal, S. Guler, D.D. Erol, Hacettep Univ. J. Facul. Pharm. 29 (2009) 25–35.
[124] J. Hartstra, J.P. Franke, R.A. de Zeeuw, through ref. 3, vol. 1, p. 517.
[125] E.M. Koves, J. Chromatogr. 692 (1995) 103–119.
[126] S.H. Chao, H.T. Ho, F.A. Chen, P.Y. Lin, Y.C. Yu, A.B. Wu, Biomed. Chromatogr. 21 (2007) 527–533.
[127] M. Satomoto, Y. Adachi, H. Higuchi, K. Watanabe, T. Satoh, Masui 51 (2002) 431–434.
[128] Y. Liu, G. Liu, Y. Liu, S. Li, J. Jia, C. Yu, Yaowu Fenxi Zazhi 28 (2008) 1248–1251.
[129] X.F. Zhu, B.C. Lin, SePu 18 (2000) 70–72.
[130] R. Hamoudova, M. Pospisilova, J. Pharm. Biomed. Anal. 41 (2006) 1463–1467.
[131] A. Rousseau, M. Pedrini, P. Chiap, R. Ivanyi, J. Crommen, M.F. Jacques, A.C. Servais, Electrophoresis 29 (2008) 3641–3648.
[132] J. Sadecka, A. Hercegova, J. Polonsky, Pharmazie 55 (2000) 859–860.
[133] E.E. Nishizawa, D.J. Wynalda, D.E. Suydam, B.A. Molony, Thromb. Res. 3 (1973) 577–588.
[134] S.S. Adams, J.B. Armitage, J.S. Nicolson, US Patent 3,755,427, 1973..
[135] P.C. Risdall, S.S. Adams, E.L. Crampton, B. Marchant, Xenobiotica 8 (1978) 691–703.
[136] D.G. Kaiser, C.D. Brooks, P.L. Lomen, Am. J. Med. 80 (1986) 10–15.
[137] F. Jamali, B.W. Berry, M.R. Tehrani, A.S. Russell, J. Pharm. Sci. 77 (1988) 666–669.
[138] G. Geisslinger, S. Menzel-Soglowek, J. Chromatogr. Biomed. Appl. 573 (1992) 163–167.
[139] M.P. Knadler, D.C. Brater, S.D.S. Hall, Br. J. Clin. Pharmacol. 33 (1992) 369–375.
[140] G. Geisslinger, J. Lotsch, S. Menzel, G. Kobal, K. Brune, Br. J. Clin. Pharmacol. 37 (1994) 392–394.
[141] E.A. Cefali, W.J. Poynor, D. Sica, S. Cox, J. Clin. Pharmacol. 31 (1991) 808–814.
[142] M.P. Knadler, D.C. Brater, S.D. Hall, Br. J. Clin. Pharmacol. 33 (1992) 377–383.
[143] R. Blouin, I. Chaudhary, K. Nishihara, S. Cox, Br. J. Clin. Pharmacol. 35 (1993) 62–64.
[144] N.M. Davies, Clin. Pharmacokinet. 28 (1995) 100–114.
[145] F. Lapicque, N. Muller, E. Payan, N. Dubois, P. Netter, Clin. Pharmacokinet. 25 (1993) 115–123.
[146] M.P. Knadler, D.C. Brater, S.D. Hall, J. Pharmacol. Exp. Ther. 249 (1989) 378–385.
[147] T.S. Tracy, B.W. Rosenbluth, S.A. Wrighton, F.J. Gonzalez, K.R. Korzekwa, Biochem. Pharmacol. 49 (1995) 1269–1275.
[148] N.M. Davies, M.R. Wright, A.S. Russell, F. Jamali, J. Pharm. Sci. 85 (1996) 1170–1173.
[149] T. Mahmud, S. Somasundaram, G. Sigthorsson, R.J. Simpson, S. Rafi, R. Foster, I. A. Tavares, A. Roseth, A.J. Hutt, M. Jacob, J. Pacy, D.L. Scott, J.M. Wrigglesworth, I. Bjarnason, Gut 43 (1998) 775–782.

[150] M.R. Wright, N.M. Davies, F. Jamali, J. Pharm. Sci. 83 (1994) 911–912.
[151] S. Menzel-Soglowek, G. Geisslinger, W.S. Beck, K. Brune, J. Pharm. Sci. 81 (1992) 888–891.
[152] G. Geisslinger, S. Menzel-Soglowek, W.S. Beck, K. Brune, Agents Actions Suppl. 44 (1993) 31–36.
[153] C. Tsitsimpikou, M.-H.E. Spyridaki, I. Georgoulakis, D. Kouretas, M. Konstantinidou, C.G. Georgakopoulos, Talanta 55 (2001) 1173–1180.

CHAPTER 5

Gatifloxacin

Ebtehal S. Al-Abdullah

Contents

Department of Pharmaceutical Chemistry, College of Pharmacy, King Saud University, Riyadh, Saudi Arabia

Profiles of Drug Substances, Excipients, and Related Methodology, Volume 37
ISSN 1871-5125, DOI: 10.1016/B978-0-12-397220-0.00005-2

© 2012 Elsevier Inc.
All rights reserved.

1. HISTORY THERAPEUTIC CATEGORY

The quinolone class of drugs were discovered in the 1960s when Lesher *et al*. isolated nalidixic acid as a by-product of chloroquine synthesis [1]. More than 1000 quinolones and analogs have since been synthesized and evaluated in an attempt to reduce toxicity and increase antimicrobial potency. Fluoroquinolones (i.e., 7-fluoro-4-oxo-1,4-dihydroquinoline-3-carboxylic acid) (see Fig. 5.1) are an important class that possesses potent antibacterial activity with a broad spectrum of activity against Gram-positive, Gram-negative, and mycobacterial organisms as well as anaerobes with great therapeutic potential, particularly against those organism resist to other classes of antibacterial drugs [2].

Quinolone antibacterial agents have emerged as one of the dominant classes of chemotherapeutic drugs for the treatment of various bacterial infections because of their broad spectrum, high potency, and low toxicity. Some of these, such as ciprofloxacin, ofloxacin, and sparfloxacin, were recommended as second-line agents by the World Health Organization (WHO) to treat multidrug-resistant tuberculosis (MDR-TB) and tuberculosis (TB) in patients who have intolerance to first-line anti-TB drugs. However, the emergence and spread of quinolone resistance became inevitable with wide use (and some abuse). Furthermore, these drugs

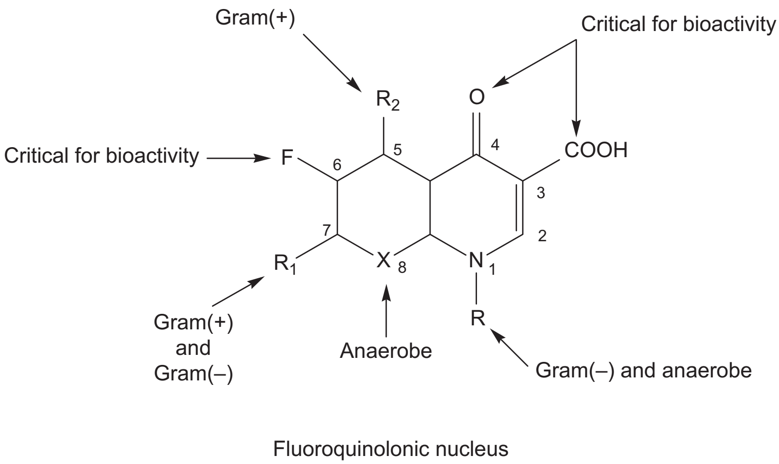

FIGURE 5.1 Structure activity relationships in the fluoroquinolone nucleus.

have relatively low activity against anaerobic bacteria, *Mycoplasma*, *Chlamydia*, mycobacteria, and Gram-(+) bacteria.

Even worse, these compounds even have the potential to cause joint cartilage damage in juvenile animals. Therefore, finding novel quinolones with more potential activity and lower toxicity by changing and modifying their structures is still a hot spot at present and will be in the future. Newly marketed 8-methoxy quinolones, gatifloxacin, not only provide greatly improved Gram-(+) antibacterial activity, while retaining the excellent Gram-(−) activity of earlier fluoroquinolones, but also show good activity against MDR-TB and may be able to reduce the length of therapy owing to activity against non-replicating bacilli [3].

Gatifloxacin is classified as a third-generation fluoroquinolone and was marketed in the United States in 1999 by Bristol-Myers Squibb as Tequin [2]. It has a broad spectrum of activity, with potent activity against Gram-(+) bacteria, including penicillin-resistant *Streptococcus pneumoniae*, as well as excellent activity against Gram-(−) and atypical organisms [4].

2. DESCRIPTION

2.1. Nomenclature

2.1.1. Chemical name

(a) (±)-1-Cyclopropyl-6-fluoro-8-methoxy-7-(3-methyl-1-piperazinyl)-4-oxo-1,4-dihydroquinoline-3-carboxylic acid

(b) 1-Cyclopropyl-6-fluoro-8-methoxy-7-(3-methylpiperazin-1-yl)-4-oxo-1,4-dihydroquinoline-3-carboxylic acid
(c) 11,12,13,13*a*-Tetrahydro-7-methoxy-9-oxo-9H-imidazo[1.5-*a*]pyrrolo [2.1-*c*][1.4]benzodiazepine-1-carboxylic acid ethyl ester
(d) 1-Cyclopropyl-6-fluoro-1,4-dihydro-8-methoxy-7-(3-methyl-1-piperazinyl)-4-oxo-3-quinoline carboxylic acid
(e) 3-Quinolinecarboxylic acid,1-cyclopropyl-6-fluoro-1,4-dihydro-8-methoxy-7-(3-methyl-1-piperazinyl)-4-one-(-+)

2.1.2. Nonpropriety name
Gatifloxacin

2.1.3. Propriety names
Gatifloxacin, Gatifloxacine HCl, Gatifloxacin sesquihydrate, Tequin, Gatifloxacin lactate

2.1.4. Brand names
Tequin (Bristol-Myers Squibb), Zymar (Allergan)

2.2. Formulae

2.2.1. Empirical formulae, molecular weight, and CAS number

Gatifloxacin	$C_{19}H_{22}FN_3O_4$	375.3	112811-59-3
Gatifloxacine HCl	$C_{19}H_{22}FN_3O_4 \cdot HCl$	411.8	160738-57-8
Gatifloxacin sesquihydrate	$C_{19}H_{22}FN_3O_4 \cdot 1.5\ H_2O$	402.42	180200-66-2
Tequin	$C_{19}H_{22}FN_3O_4 \cdot 1.5\ H_2O$	402.42	130477-52-0
Gatifloxacin lactate	$C_{19}H_{22}FN_3O_4 \cdot C_3H_6O_3$	465.48	112811-72-0

2.2.2. Structural formulae

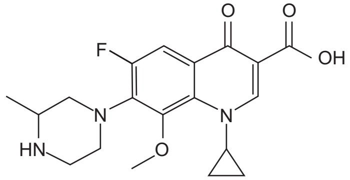

2.3. Appearance

White to off-white crystalline powder [5–9]

3. METHODS OF PREPARATION

3.1. U.S. Patent 4,890,470 (cf. European Patent 230,295)

This patent disclosed the synthesis of gatifloxacin via the substitution of 2-methyl piperazine on the 9,10-difluoro carboxylic derivative. The reaction is described to occur in the absence of solvent or in the presence of organic polar solvents such as DMSO, pyridine, dimethylformamide, alcohol, water, or hexamethylphosphoric amide. This reaction can reportedly be carried out in the presence of an acid acceptor such as triethylamine, diazabicyclo bases, or potassium carbonate. The yield of this reaction in DMSO is 20% [10].

3.2. U.S. Patent Application 2007/0072868

Gatifloxacin was synthesized in bulky form according to Valerie *et al*. by charging a 100-L reactor with 120L of dimethyl sulfoxide and 8.6kg of 2-methylpiprazine at 55°C. Under a nitrogen atmosphere, 1-cyclopropyl-6,7-difluoro-1,4-dihydro-8-methoxy-4-oxo-3-quinoline carboxylic acid (12kg, divided in four portions of 3kg) was added every 2h. After completion of the reaction (about 24h, monitoring by HPLC), the reaction mixture was cooled to about 47–50°C, and 24L of water were added at this temperature. The resulting reaction mixture was cooled to 5°C over 2h and maintained at this holding temperature for a time of 18h. The resulting precipitated residue was collected by filtration to obtain 15.9kg of wet gatifloxacin (11.6kg dry, 76% yield) [11].

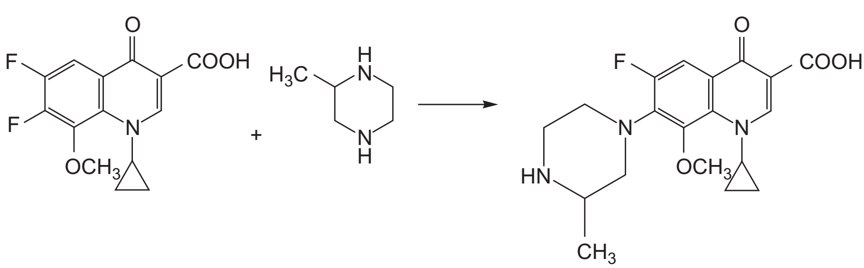

3.3. WO Patent Application 2006/004561

Ruzic improved the synthetic process of gatifloxacin by comprising a process for regeneration of a side product of gatifloxacin and an analysis method for process control in the synthesis of gatifloxacin [12].

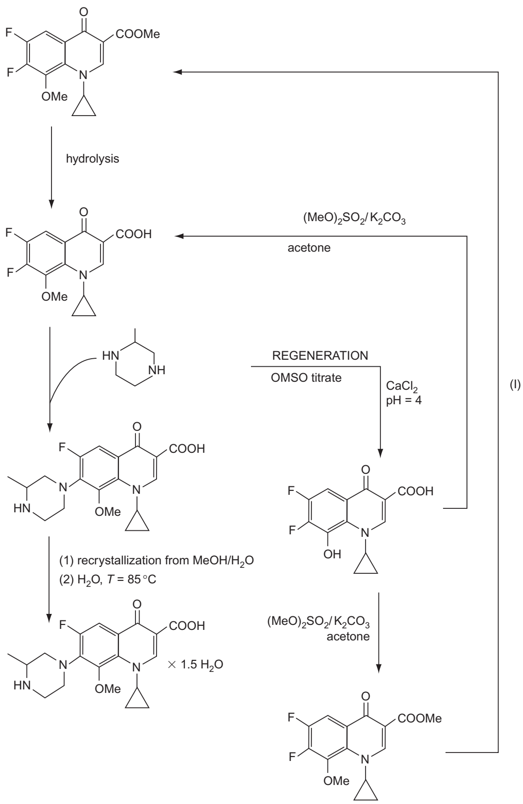

3.4. Method of Shiming *et al.*

Shiming *et al*. prepared gatifloxacin starting from 3,4,5,6-tetrafluorophthalic acid via hydrolysis, decarboxylation, methylation, acylation, condensation, decarboxylation, propylamine esters, cyclization, boron esterification, and condensation with piperazine in an overall yield of 18.3%. The reaction conditions were optimized to adapt industrial scale-up concerns [13].

3.5. Method of Villasante *et al.*

An improved process has been developed by Villasante to prepare gatifloxacin (**1**) through use of boron chelate intermediates. The methodology involves an initial activation step, which accelerates the formation of the first chelate under low-temperature conditions and prevents demethylation of the starting material. To increase the overall yield and to avoid the

isolation and manipulation of the resulting intermediates, the process has been designed to be carried out in one pot. As a result, the authors present in this study an easy, scaleable, and substantially impurity-free process to obtain gatifloxacin (**1**) in high yield [14].

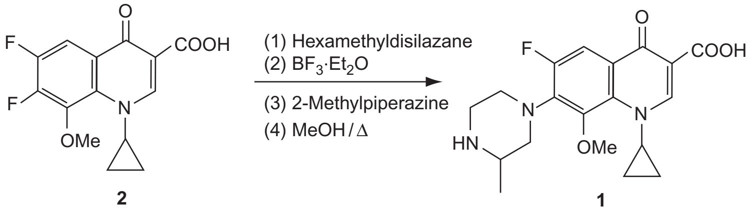

2 **1**

85 %

4. PHYSICAL PROPERTIES

Gatifloxacin exists as a racemate and therefore exhibits no net optical rotation. The solubility of the drug is pH dependent. The maximum aqueous solubility (40–60 mg/mL) occurs at a pH range of 2–5.

4.1. X-ray powder diffraction

The X-ray powder diffraction pattern of gatifloxacin was performed using a SimonXRD-5000 diffractometer. Figure 5.2 shows the X-ray powder diffraction pattern of the drug, and Table 5.1 shows the values of scattering angles (2θ), the interplaner d-spacings (d-value), and the relative intensities (I/I_o), which were automatically obtained on a digital printer.

4.2. Spectroscopy

4.2.1. UV–Visible spectroscopy

The ultraviolet spectrum of gatifloxacin in methanol shown in Fig. 5.3 was recorded using Ultrospec 2100 pr UV/Visible Spectrophotometer (Amersham Biosciences, manufactured by Biochrom Ltd., Cambridge CB4 OFJ, England). The drug exhibited two maxima at 205 and 240 nm [15].

4.2.2. Vibrational spectroscopy

The infrared (IR) absorption spectrum of gatifloxacin was obtained in a KBr pellet using a Perkin-Elmer Spectrum BX FTIR spectrometer. The IR spectrum is shown in Fig. 5.4, and assignments of the absorption bands are found in Table 5.2.

The IR spectrum of gatifloxacin is multifaceted due to the presence of numerous functional groups in the molecules. The energy of the

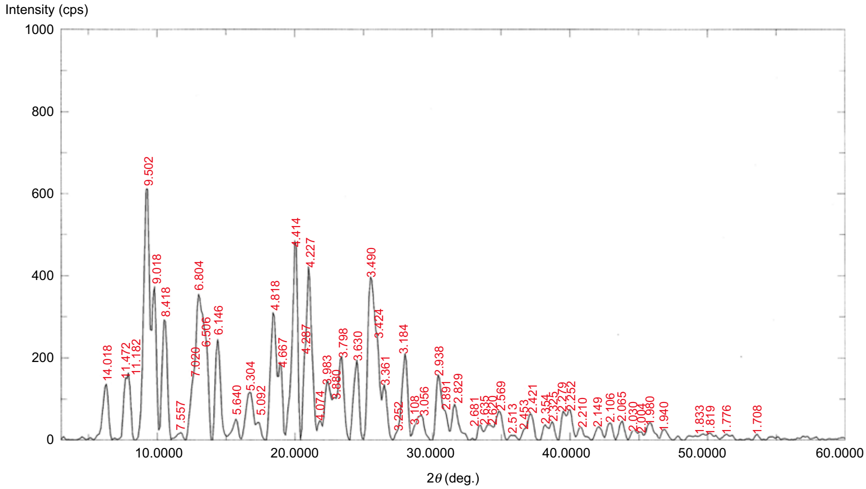

FIGURE 5.2 The X-ray powder diffraction pattern of gatifloxacin.

carboxylate stretching mode (C═O) was found at 1726 cm^{-1}, and the pyridone stretch (C═O) was at 1618 cm^{-1} [16]. It was found that the IR spectrum of gatifloxacin sesquihydrate does not show a well-defined carboxylic acid stretching mode because in this form, the drug substance exists as its zwitterionic form [17,18]. The ionic carboxylates [19] show no carbonyl stretching at about 1700 cm^{-1} but have two attributed bands in the range of 1650–1510 and 1460–1400 cm^{-1} that could be assigned as carboxylate anion (O—C—O) asymmetric and symmetric stretching vibrations.[20]

4.2.3. Nuclear magnetic resonance

4.2.3.1. ^{1}H NMR spectrum The proton nuclear magnetic resonance (NMR) spectrum of gatifloxacin was obtained using a Bruker AC 500 Ultra Shield NMR spectrometer (Fallanden, Switzerland) at 500.13 MHz for ^{1}H and 125.76 MHz for ^{13}C. The sample was dissolved in deuterated acetic acid, and all resonance bands were referenced to the internal standard tetramethylsilane (TMS). The ^{1}H NMR spectra of gatifloxacin are shown in Figs. 5.5 and 5.6, and the ^{1}H NMR assignments of gatifloxacin are shown in Table 5.3.

4.2.3.2. ^{13}C NMR spectrum ^{13}C NMR spectra of gatifloxacin were obtained using a Bruker instrument operating at 125 MHz. The sample was dissolved in deuterated acetic acid, and TMS was added to function as the internal

TABLE 5.1 Crystallographic data from the x-ray powder diffraction pattern of gatifloxacin

Peak no.	2θ	Flex width	*d*-Value	Intensity	I/I_o	Peak no.	2θ	Flex width	*d*-Value	Intensity	I/I_o
1	6.300	0.471	14.0178	137	23	30	28.700	0.235	3.1079	36	6
2	7.700	0.353	11.4720	152	25	31	29.200	0.588	3.0558	61	10
3	7.900	0.235	11.1820	164	27	32	30.400	0.353	2.9379	160	27
4	9.300	0.588	9.5016	610	100	33	30.900	0.353	2.8915	71	12
5	9.800	0.353	9.0179	372	61	34	31.600	0.353	2.8290	88	15
6	10.500	0.471	8.4182	293	48	35	33.400	0.353	2.6805	37	7
7	11.700	0.235	7.5574	18	3	36	34.000	0.235	2.6346	39	7
8	12.600	0.235	7.0195	155	26	37	34.200	0.235	2.6196	37	7
9	13.1000	0.353	6.8044	356	59	38	34.900	0.588	2.5687	69	12
10	13.600	0.353	6.5055	231	38	39	35.700	0.235	2.5129	12	2
11	14.400	0.588	6.1459	246	41	40	36.600	0.235	2.4532	25	5
12	15.700	0.353	5.6398	51	9	41	37.100	0.588	2.4213	65	11
13	16.700	0.706	5.3042	116	20	42	38.200	0.353	2.3540	38	7
14	17.400	0.353	5.0924	41	7	43	38.700	0.353	2.3248	45	8
15	18.400	0.588	4.8178	311	51	44	39.500	0.353	2.2795	71	12
16	19.000	0.353	4.6670	179	30	45	40.000	0.353	2.2522	74	13
17	20.100	0.353	4.4140	471	78	46	40.800	0.471	2.2098	32	6
18	20.700	0.235	4.2874	209	35	47	42.000	0.471	2.1494	31	6
19	21.000	0.235	4.2268	423	70	48	42.900	0.471	2.1064	42	7

(*continued*)

TABLE 5.1 (*continued*)

Peak no.	2θ	Flex width	*d*-Value	Intensity	I/I_o	Peak no.	2θ	Flex width	*d*-Value	Intensity	I/I_o
20	21.800	0.353	4.0735	48	8	49	43.800	0.353	2.0652	47	8
21	22.300	0.471	3.9833	137	23	50	44.600	0.471	2.0300	25	5
22	22.900	0.235	3.8803	104	18	51	45.200	0.353	2.0044	20	4
23	23.400	0.353	3.7985	204	34	52	45.800	0.471	1.9795	43	8
24	34.500	0.588	3.6304	196	33	53	46.800	0.471	1.9395	26	5
25	25.500	0.588	3.4902	398	66	54	49.700	0.353	1.8329	15	3
26	26.000	0.235	3.4242	252	42	55	50.100	0.353	1.8192	17	3
27	26.500	0.471	3.3607	136	23	56	51.400	0.353	1.7762	15	3
28	27.400	0.235	3.2524	21	4	57	53.600	0.353	1.7084	14	3
29	28.000	0.588	3.1840	211	35						

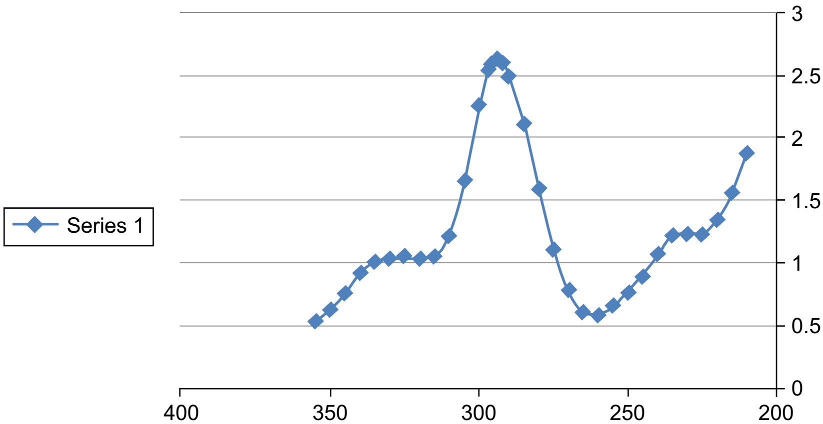

FIGURE 5.3 Ultraviolet absorption spectrum of gatifloxacin.

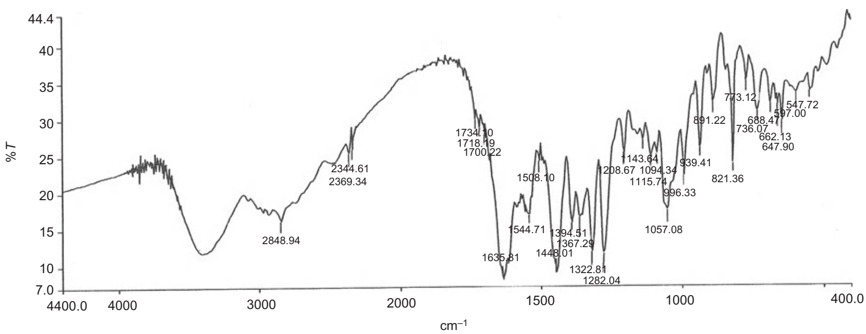

FIGURE 5.4 The infrared absorption spectrum of gatifloxacin.

standard. The ^{13}C NMR spectra of gatifloxacin are shown in Figs. 5.7–5.10. The ^{13}C NMR assignments for the observed resonance signals associated with the various carbons of gatifloxacin are provided in Table 5.4.

4.3. Mass spectrometry

The mass spectrum of gatifloxacin was obtained using LC/MS/MS, the 3200 QTRAP, AB Applied Biosystems, MDS SCIEX. Figure 5.11 shows the detailed E.I. mass spectrum of gatifloxacin, whereas Table 5.5 shows the proposed mass fragmentation pattern.

TABLE 5.2 Vibrational assignments for gatifloxacin infrared absorption bands

Energies (cm^{-1})	Assignment
~3600	NH and OH stretch
3407	(OH) intermolecular
3400–2400	OH bonded
~3040	Olefenic and aromatic CH stretch
2848	(CH) aliphatic stretch
1734	Carboxylic C=O stretch
1635	Pyridine C=O stretch
1600	COO^{-} asym. stretch
1480	Quinoline ring C—C and C—N stretch
1448	(C=C and C—N) stretch
1394	(COO−) sym. stretch
1367	(C—N)
1280	C—F and C—O stretch
1094	C—F and C—O bending

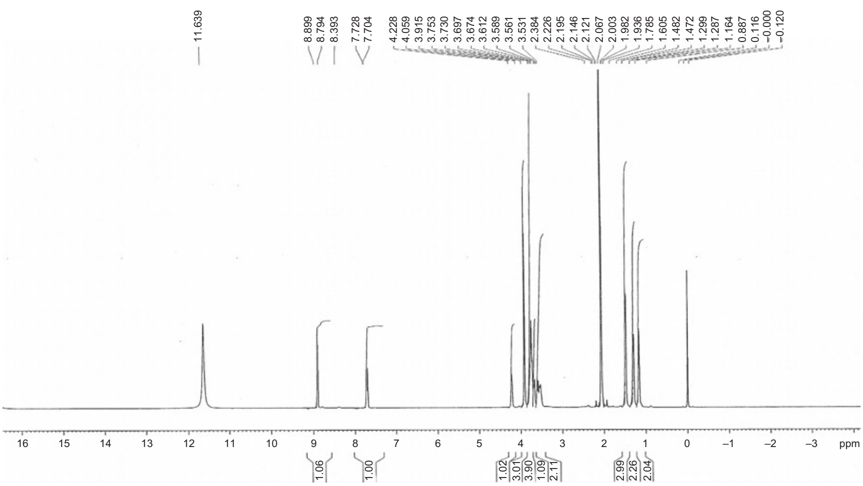

FIGURE 5.5 The [1]H NMR spectrum of gatifloxacin in deuterated acetic acid.

5. METHODS OF ANALYSIS

5.1. Compendial methods of analysis

5.1.1. United States Pharmacopeia compendial methods [9]

Gatifloxacin contains not less than 98.0% and not more than 102.0% of $C_{19}H_{22}FN_3O_4$, calculated on the anhydrous basis.

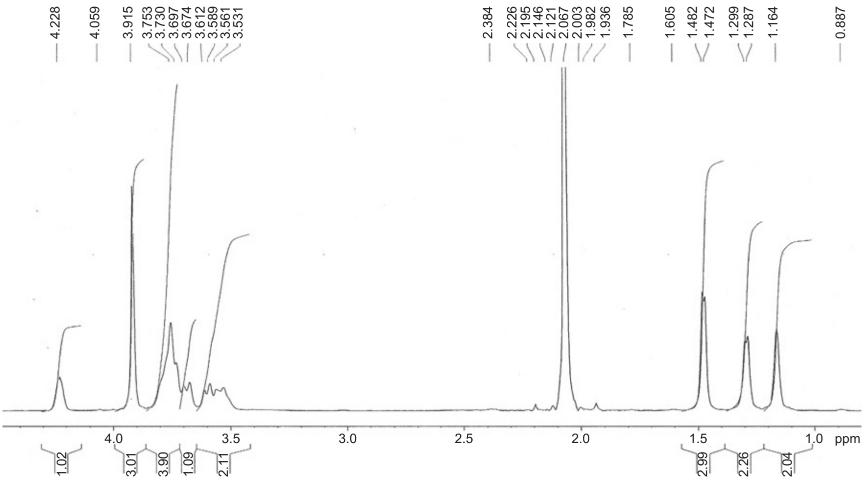

FIGURE 5.6 Expanded ^{1}H NMR spectrum of gatifloxacin in deuterated acetic acid.

TABLE 5.3 Assignment of the resonance bands in the ^{1}H NMR spectrum of gatifloxacin

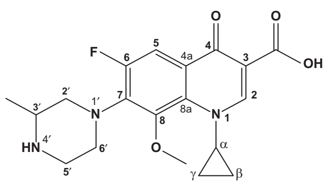

Chemical shift (ppm, relative to TMS)	Number of protons	Multiplicity	Assignment (proton at carbon number)
1.16–1.30	4	m	CH_2 of cyclopropane protons
1.47–1.48	3	d	CH_3
3.53–3.6	2	m	H-5′
3.61–3.67	1	m	CH of cyclopropane
3.70–3.75	4	m	H-2′ and H-6′
3.92	3	s	OCH_3
4.23	1	brs	H-3′
7.70–7.73	1	d	H-5
8.80	1	s	H-2
11.64	1	brs	COOH

s, singlet; brs, broad singlet; d, doublet; m, multiplet.
Signals at 1.98–2.07 ppm derived from the NMR-solvent CD_3COOD.

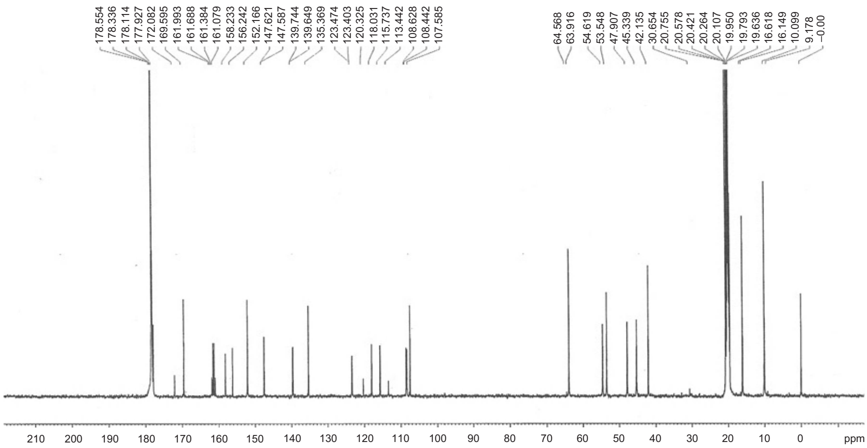

FIGURE 5.7 The ^{13}C NMR spectrum of gatifloxacin in deuterated acetic acid.

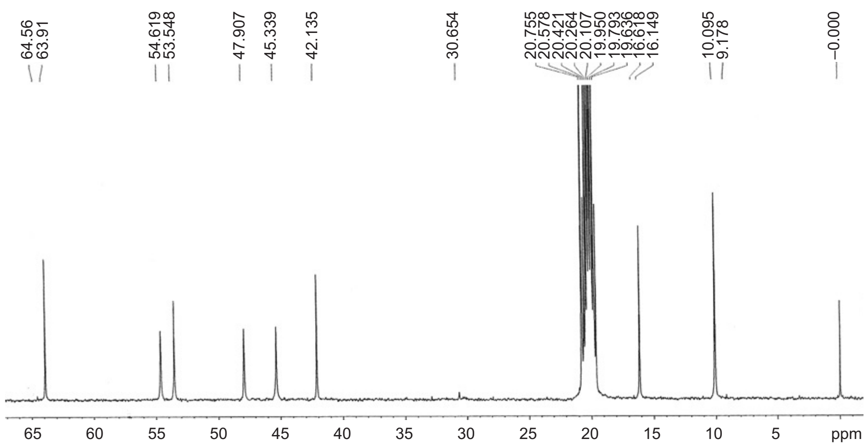

FIGURE 5.8 Expanded ^{13}C NMR spectrum of gatifloxacin in deuterated acetic acid.

Identification

Test 1: IR absorption. This test must be carried out according to the general procedure ⟨197K⟩. The spectrum obtained from the sample of gatifloxacin should be identical with that spectrum obtained from *USP* gatifloxacin R.S.

Test 2: The retention time of the major peak for gatifloxacin in the chromatogram of the *Assay preparation* corresponds to that in the chromatogram of the *Standard preparation,* as obtained in the *Assay*.

Water, *Method I* ⟨921⟩**:** between 7.5% and 10.0% if labeled as dihydrate.
Residue on ignition ⟨281⟩: not more than 0.1%.

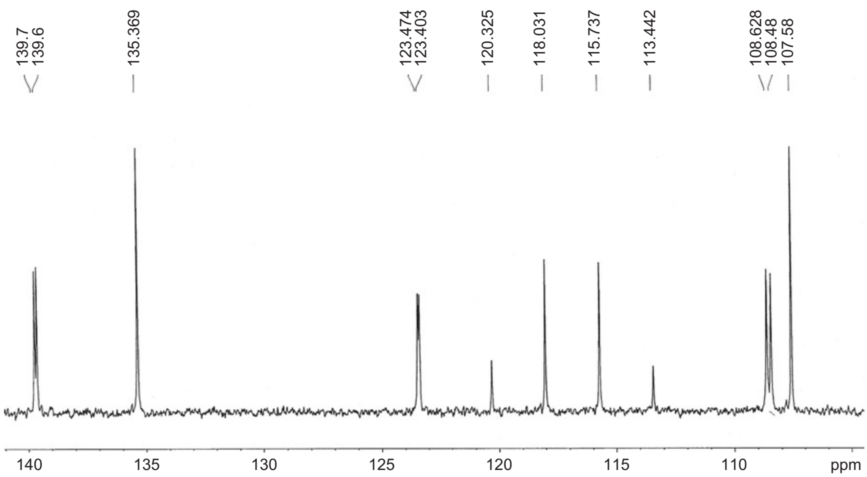

FIGURE 5.9 Expanded ^{13}C NMR spectrum of gatifloxacin in deuterated acetic acid.

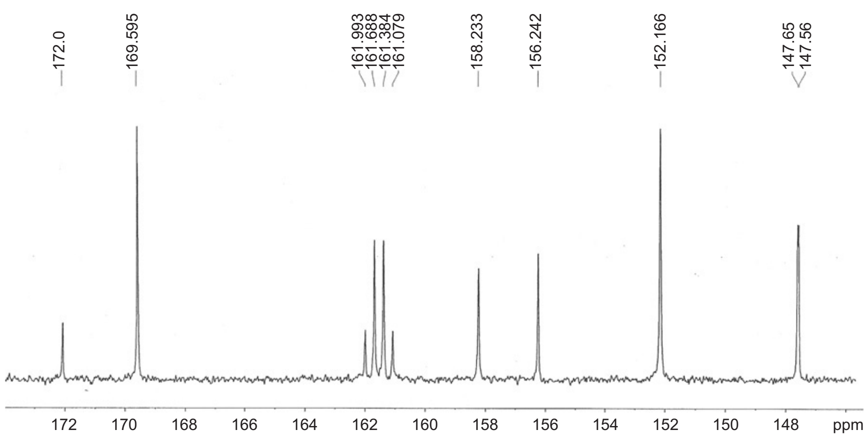

FIGURE 5.10 Expanded ^{13}C NMR spectrum of gatifloxacin in deuterated acetic acid.

Heavy metals, *Method II* ⟨231⟩**:** 0.002%.

Related compounds—(*Note*: Protect solutions of gatifloxacin from light).

Buffer solution, Solution A, Solution B, and *Diluent*—Prepare as directed in the *Assay*.

Mobile phase—Use variable mixtures of *Solution A* and *Solution B* as directed for *Chromatographic system. Standard stock solution 1*—Dissolve an accurately weighed quantity of USP Gatifloxacin RS in acetonitrile (about 10% final volume) using a sonicator, and dilute with water to obtain a

TABLE 5.4 ^{13}C NMR Assignments of gatifloxacin in CD_3COOD

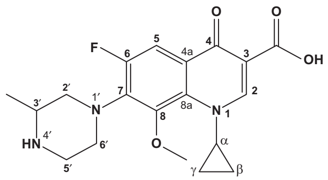

No.	Assignment	Chemical shift (δ ppm)
1	C-γ	9.18[a]
2	C-β	10.10[a]
3	C3′-CH_3	16.15
4	C-α	42.14
5	C-2′	54.62
6	C-3′	53.55
7	C-5′	45.34
8	C-6′	47.91
9	C8-OCH_3	64.56
10	C-2	152.17
11	C-3	107.51
12	C-4	177.93
13	C-5	108.68, 44
14	C-6	158.23, 161.08, 161.38, 161.69, 161.99
15	C-7	135.37, 139.65, 139.74
16	C-8	147.51, 147.61
17	C-4a	123.40[b], 123.47
18	C-8a	113.44, 115.74, 118.03, 120.33[b]
19	COOH	169.60

a, interchangeable signals; b, interchangeable signals.
Unassigned signals at — are attributed to C—F couplings.
Multiplets at 19.64–20.76 and 178.11, 178.55 ppm are derived from the NMR-solvent CD_3COOD.

solution containing about 0.2 mg/mL. Dilute an aliquot of this solution with water to obtain a solution containing a known concentration of about 0.004 mg/mL. *Standard stock solution 2*—Dissolve an accurately weighed quantity of USP Gatifloxacin-Related Compound A RS in acetonitrile (about 10% final volume) using a sonicator, and dilute with water to obtain a solution containing a known concentration of about 0.2 mg/mL. Dilute an aliquot of this solution with water to obtain a solution containing a known concentration of about 0.004 mg/mL.

Standard solution—Transfer 5 mL each of *Standard stock solution 1* and *Standard stock solution 2* to a 20-mL volumetric flask, and dilute with *Diluent* to volume. This solution contains about 0.001 mg/mL each of

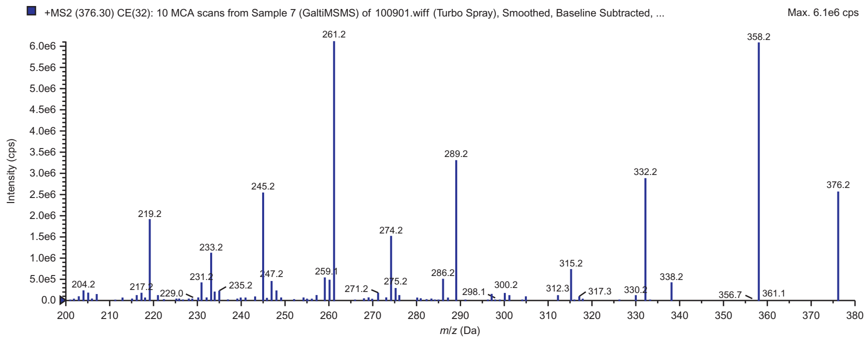

FIGURE 5.11 E.I. mass spectrum of gatifloxacin.

gatifloxacin and gatifloxacin-related compound A. *Test solution*—Dissolve an accurately weighed quantity of gatifloxacin in acetonitrile (about 10% final volume) using a sonicator, and dilute quantitatively with water to obtain a solution containing a known concentration of about 1mg/mL. *Chromatographic system* (see *Chromatography* ⟨621⟩)—Proceed as directed in the *Assay*, except that a liquid chromatograph with either a programmable variable wavelength detector or dual detectors capable of monitoring at 240 and 285nm is used. The chromatograph is programmed as follows.

Time (min)	Solution A (%)	Solution B (%)	Elution
0–8	100	0	Isocratic
8–30	100→0	0→100	Linear gradient
30–30.1	0→100	100→0	Step gradient
30.1–35	100	0	Re-equilibration

Chromatograph the *Standard solution*, and record the peak responses for gatifloxacin and gatifloxacin-related compound A at 285 and 240nm, respectively. The resolution, *R*, between gatifloxacin and gatifloxacin-related compound A at 285nm is not less than 4.5; and the relative standard deviation for replicate injections for gatifloxacin-related compound A peak is not more than 10.0%.

Procedure—Separately inject equal volumes (about 20mL) of the *Standard solution* and the *Test solution* into the chromatograph, record the chromatograms, and measure the responses for all the major peaks. Identify the peaks using the relative retention times as shown in Table 5.1. Calculate the percentage of all the related compounds, except gatifloxacin-related compound A, gatifloxacin-related compound B, and gatifloxacin-related compound C, in the portion of gatifloxacin taken by the formula:

TABLE 5.5 Mass spectral fragmentation pattern of gatifloxacin

m/z	Relative intensity (%)	Fragment	
		Formula	Structure
376.2	46	$C_{19}H_{23}FN_3O_4$	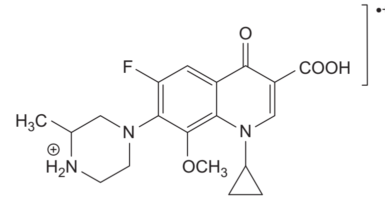
358.2	100	$C_{19}H_{21}FN_3O_3$	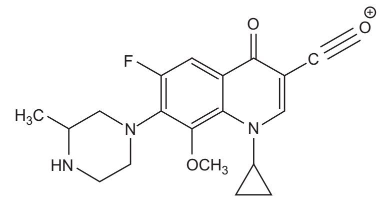
332.2	46	$C_{17}H_{19}FN_3O_3$	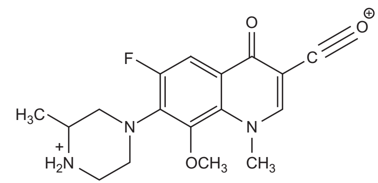

330.2	3	$C_{18}H_{21}FN_3O_2$	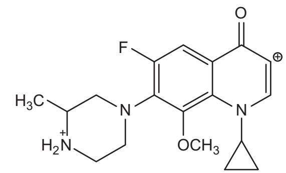
315.2	19	$C_{17}H_{18}FN_3O_2$	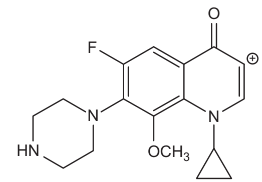
312.2	3	$C_{18}H_{22}N_3O_2$	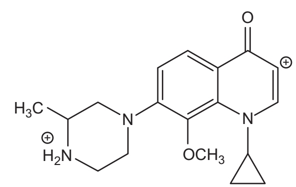

(*continued*)

TABLE 5.5 (*continued*)

m/z	Relative intensity (%)	Fragment	
		Formula	Structure
289.2	56	$C_{15}H_{16}FN_3O_2$	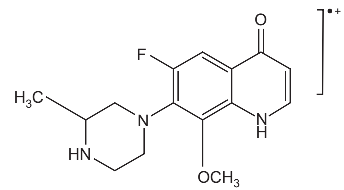
286.2	8	$C_{15}H_{14}FN_3O_2$	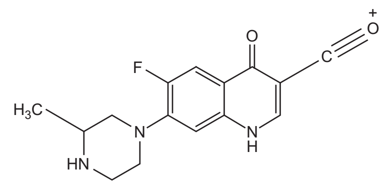
274.2	25	$C_{14}H_{13}FN_3O_2$	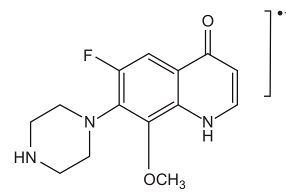

271.2	3	$C_{14}H_9FN_3O_2$	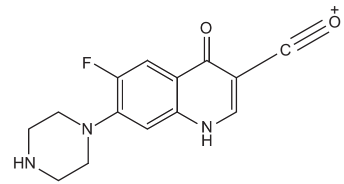
261.2	100	$C_{13}H_{10}FN_2O_3$	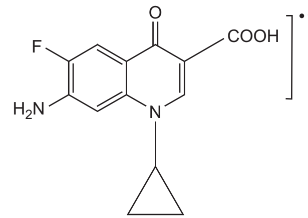
259.2	9	$C_{14}H_{14}FN_3O$	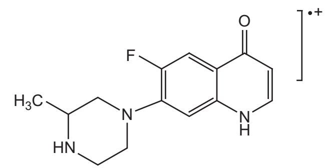

(*continued*)

TABLE 5.5 *(continued)*

m/z	Relative intensity (%)	Fragment	
		Formula	Structure
247.2	8	$C_{13}H_{12}FN_2O_2$	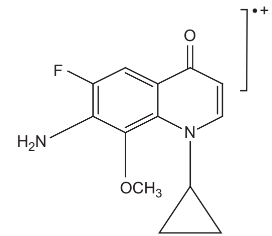
245.2	46	$C_{13}H_8FNO_3$	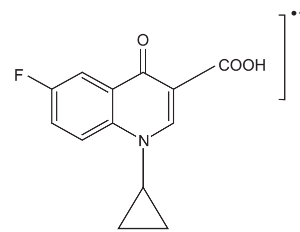
233.2	24	$C_{11}H_9N_2O_4$	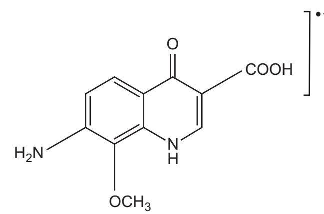

231.2	4	$C_{13}H_{10}FNO_2$	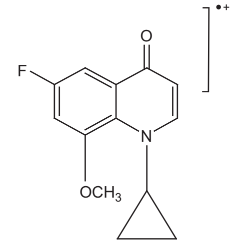
219.2	32	$C_{11}H_6FNO_3$	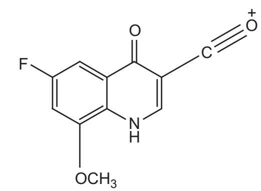
204.2	3	$C_{10}H_5FN_2O_2$	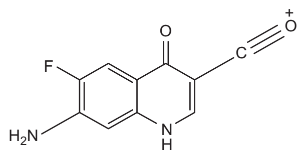

$$100(CS/CT)(rU/rS)$$

in which CS is the concentration, in mg/mL, of USP Gatifloxacin RS in the *Standard solution*; CT is the concentration, in mg/mL, of gatifloxacin in the *Test solution*; rU is the peak response for each related compound; and rS is the peak response for gatifloxacin obtained from the *Standard solution*, all monitored at 285nm. Calculate the percentage of gatifloxacin-related compound A, gatifloxacin-related compound B, and gatifloxacin-related compound C in the portion of gatifloxacin taken by the formula:

$$100(1/F)(CS/CT)(rU/rS)$$

in which F is the relative response factor provided in Table 5.1; CS is the concentration, in mg/mL, of USP Gatifloxacin-Related Compound A RS in the *Standard solution*; CT is the concentration, in mg/mL, of gatifloxacin in the *Test solution*; rU is the peak response for each related compound obtained from the *Test solution*; and rS is the peak response of gatifloxacin-related compound A obtained from the *Standard solution*, all monitored at 240nm. The limits of impurities meet the requirements specified in the pharmacopeia.

Assay

Buffer solution—Dissolve 6.6mL of a 40% tetrabutylammonium hydroxide solution in water and 6.6g of dibasic ammonium phosphate in about 500mL of water and dilute with water to 1000mL. Adjust with ammonium hydroxide to a pH of 9.5, mix, and filter.

Solution A—Prepare a mixture of *Buffer solution* and acetonitrile (86:14).

Solution B—Prepare a mixture of *Buffer solution*, acetonitrile, and methanol (70:20:10). Mobile phase—Use variable mixture of *Solution A* and *Solution B* as directed for *Chromatographic system*. Make adjustments if necessary (see *System Suitability* under *Chromatography* (621)).

Diluent—Prepare a mixture of water and acetonitrile (90:10).

Resolution solution—Dissolve an accurately weighed quantity of USP Gatifloxacin RS and USP Gatifloxacin-Related Compound A RS in *Diluent* to obtain a solution containing about 1mg/mL of each component. Dilute an aliquot of this solution with water to obtain a solution containing about 0.1mg/mL of each component.

Standard preparation—Dissolve an accurately weighed quantity of USP Gatifloxacin RS in acetonitrile (about 10% final volume) using a sonicator and dilute quantitatively with water to obtain a solution containing a known concentration of about 0.2mg/mL.

Assay preparation—Dissolve an accurately weighed quantity of gatifloxacin in acetonitrile (about 10% final volume) using a sonicator and dilute quantitatively with water to obtain a solution containing about 0.2 mg/mL. Dilute an aliquot of this solution with *Diluent* to obtain a solution containing about 0.02mg/mL.

Chromatographic system (see *Chromatography* (621))—The liquid chromatograph is equipped with a 285-nm detector and a 4.6-mm×6×25-cm column that contains 5-mm packing L1. The flow rate is about 1.5mL/min. The column temperature is maintained at 388. The chromatograph is programmed as follows.

Time (min)	Solution A (%)	Solution B (%)	Elution
0–8	100	0	Isocratic
8–15	100→70	0→30	Linear gradient
15–15.1	70→100	30→0	Step gradient
15.1–20	100	0	Re-equilibration

Chromatograph the *Resolution solution* and record the peak responses as directed for *Procedure:* The resolution, *R*, between gatifloxacin and gatifloxacin-related compound A is not less than 4.5. Chromatograph the *Standard preparation* and record the peak responses as directed for *Procedure:* the relative standard deviation for replicate injections is not more than 2.0%. *Procedure*—Separately inject equal volumes (about 20mL) of the *Standard preparation* and the *Assay preparation* into the chromatograph, record the chromatograms, and measure the responses for the major peaks. Calculate the quantity, in percentage, of $C_{19}H_{22}FN_3O_4$ in the portion of gatifloxacin taken by the formula:

$$100(CS/CU)(rU/rS)$$

in which CS and CU are the concentrations, in mg/mL, of gatifloxacin in the *Standard preparation* and the *Assay preparation,* respectively; and rU and rS are the peak responses obtained from the *Assay preparation* and the *Standard preparation,* respectively.

Packaging and storage—Preserve in tight containers, protect from light, and store in a refrigerator.

Labeling—Label it to indicate the specific hydrated form.

USP Reference standards (11)—*USP Gatifloxacin RS. USP Gatifloxacin-Related Compound A RS.*

5.2. Reported methods of analysis

5.2.1. Nonaqueous titration

Marona *et al*. described an inexpensive, simple, precise, and rapid method for the determination of fluoroquinolone gatifloxacin in tablets. The procedure is based on the use of volumetric titration with 0.1M perchloric acid in a nonaqueous medium (glacial acetic acid). The method validation yielded good results and included precision, recovery, and accuracy. It was also found that the excipients in the commercial tablet preparation did not interfere with the assay [21].

5.2.2. Atomic absorption spectroscopy

Al-Ghannam used an aliquot containing 0.5–15.0 mg of the investigated drug and then successively added 4.0 mL of 0.005 M of ammonium reineckate solution and 1.0 mL of 0.01 M HCl. The mixture was left to stand for 10 min, and then the precipitate was filtered. The precipitate is separated and dissolved in least amount of acetone and diluted to volume with water in a 100-mL calibrated flask. This solution is then aspirated directly in the atomic absorption spectrometer and the chromium ion concentration measured. The concentration of the tested drug is calculated from the relevant calibration graph [22].

5.2.3. Conductometric methods

Al-Ghannam used a volume containing 2.0–21 mg of drug, transferred this to a 50-mL calibrated flask, and diluted to volume with 50% (v/v) acetone/water. The contents of the calibrated flask were transferred to a beaker, and the conductivity cell was inserted. 0.005 M ammonium reineckate solution was then added from a microburette, and the conductance was measured subsequent to each addition of reagent solution and after thorough stirring. The conductance reading, taken 2.0 min after each addition, was corrected for dilution assuming that conductivity is a linear function of dilution. A plot of corrected conductivity against the volume of added titrant was constructed, and the end-point determined. 0.1 mL of 0.005 M ammonium reineckate solution is theoretically equivalent to 0.116, 0.114, and 0.12 mg of GTF, MXF, and SPF, respectively.

The optimum conditions for performing the titration in a quantitative manner were evaluated using three different titration protocols: (i) aqueous drug solution with aqueous reagent solution, (ii) acetone drug solution with acetone reagent solution, and (iii) drug solution with reagent solution, both in 50% (v/v) acetone–water. Preliminary experiments showed that procedure (iii) was the most suitable for successful results because in procedures (i) and (ii), precipitates were formed which caused some errors. The reagent concentration in each titration must be not less than 10 times that of the drug solution in order to minimize the dilution effect on the conductivity throughout the titration. The optimum concentration of ammonium reineckate was 0.005 M to achieve a constant and highly stable conductance reading after 2.0 min of mixing. Concentrations less than these led to unstable readings, and more time was needed to obtain constant conductance values. On raising the temperature to 40 °C, no change in the conductance reading was observed. Above 40 °C, the conductance value changed as well as the shape of the titration curve [22].

5.2.4. Colorimetry

Ilango *et al*. described two simple and sensitive spectroscopic methods (i.e., operating in the ultraviolet and visible regions) for the estimation of gatifloxacin in pharmaceutical dosage forms. Method-A is based on a

measurement of the absorbance at 295 nm of gatifloxacin dissolved in methanol. Method-B is based on the reaction of gatifloxacin with 0.2% (w/v) 3-methyl-2-benzthiazolinone hydrazone reagent in the presence of 1% (w/v) ferric chloride solution, to yield a yellow orange color. This reaction product has a characteristic absorption at 433 nm that is suitable for quantitative purposes. Beer's law is obeyed over the concentration ranges of 2–10 μg/mL (Method-A) and 50–150 μg/mL (Method-B). The proposed method is precise, accurate, and reproducible and can be extended to the analysis of gatifloxacin in tablet formulations [23].

Al-Ghannam used the reaction of ammonium reineckate with the studied drugs to form stable precipitates of ion-pair complexes, which were then dissolved in acetone. The resulting pink-colored complexes were determined colorimetrically at a wavelength of 525 nm against a reagent blank solution prepared in the same way but without drug. The calibration graph was obtained by applying the procedure to a series of standard drug solutions [22].

5.2.5. UV–visible spectrophotometry

Patel *et al*. proposed two simple, rapid, accurate, and economical methods for the estimation of gatifloxacin and ornidazole in mixtures. The method is based on the fact that when dissolved in distilled water, gatifloxacin has an absorbance maximum at 286.2 nm, and ornidazole has an absorbance maximum at 319 nm. Linearity was observed over the concentration range of 2–14 μg/mL for gatifloxacin and 2–20 μg/mL for ornidazole. The first method is based on the solution of simultaneous equations, and the second method is based on a *Q*-absorbance ratio. Absorbance values were obtained at the isoabsorptive point of 299.2 nm and at the wavelength maximum of ornidazole. These methods were validated statistically, and recovery studies confirmed the accuracy of the proposed methods [24].

Venugopal and Saha described a simple and cost-effective UV-spectrophotometric method for the estimation of gatifloxacin in bulk drug substance and in pharmaceutical formulations. Gatifloxacin was estimated at 286 nm when dissolved in 100 mM phosphate buffer (pH 7.4) and at 292 nm when dissolved in 100 mM hydrochloric acid (pH 1.2). The linearity range was found to be 1–18 μg/mL (regression equation: absorbance=0.0684×concentration in μg/mL+0.0050; r^2=0.9998) in the phosphate buffer (pH 7.4) and 1–14 μg/mL (regression equation: absorbance=0.0864×concentration in μg/mL+0.0027; r^2=0.9999) in hydrochloric acid medium (pH 1.2). The apparent molar absorptivity was found to be 2.62×104 L/(mol cm) in phosphate buffer, and 3.25×104 L/(mol cm) in hydrochloric acid. In both the proposed methods, Sandell's sensitivity was found to be about 0.01 μg/cm^2/(0.001 A). These methods were tested and validated for various parameters according to ICH and USP guidelines. The quantitation limits were found to be 0.312 and 0.3 μg/mL in phosphate buffer and hydrochloric acid, respectively. The proposed

methods were successfully applied for the determination of gatifloxacin in pharmaceutical formulations (tablets, injection, and ophthalmic solution). The results demonstrated that the simple procedure is accurate, precise, and reproducible (relative standard deviation less than 2%) and can be suitably applied for the estimation of gatifloxacin in different dosage forms and dissolution studies [25].

Mali *et al*. described a simple, sensitive, rapid, accurate, and precise spectrophotometric method for estimation of gatifloxacin in pharmaceutical dosage forms. The method is based on formation of an orange-colored chromogen due to reaction of gatifloxacin with ferric nitrate reagent solution, which exhibits maximum absorption at 470nm against blank. The stability of the chromogen was found up to 1h, and the chromogen exhibited a linearity range of 20–200μg/mL [26].

Paramane *et al*. disclosed three simple, accurate, and economic methods (multicomponent, two wavelength, and simultaneous equations using area under curve) for the simultaneous determination of gatifloxacin and ornidazole in tablet dosage forms. Gatifloxacin shows an absorption maximum at 287.5nm, and ornidazole shows an absorption maximum at 319.5nm in distilled water. Beer's law was obeyed over the concentration range of 2–20μg/mL for gatifloxacin and 10–60μg/mL for ornidazole. The methods allow rapid analysis of binary pharmaceutical formulations with accuracy, with the three methods being validated and found satisfactory by recovery studies [27].

Sivasubramanian and Muthukumaran used three simple and sensitive spectrophotometric methods in ultraviolet region for the determination of gatifloxacin in bulk drug substance, pharmaceutical preparations, and biological samples. Gatifloxacin exhibited a maximum absorbance at 289nm (Method-A) with an apparent molar absorptivity of 1.23×10 4L/(molcm) when dissolved in sodium hydroxide. When dissolved in hydrochloric acid, the compound exhibited an absorbance maximum at 292nm (Method-B) with an apparent molar absorptivity of 1.71×10 4L/(molcm). The third developed method (Method-C) was based on the formation of a yellow-colored chromogen with ferric chloride and potassium dichromate, which showed a maximum absorbance at 352nm with an apparent molar absorptivity of 1.23×10 4L/(molcm). Beer's law was obeyed in the concentration range of 5–30μg/mL. All three analysis methods were validated statistically and by recovery studies [28].

Amin *et al*. described simple, rapid, and extractive spectrophotometric methods for the determination of gatifloxacin in bulk drug substance and in pharmaceutical dosage forms. These methods are based on the formation of yellow ion-pair complexes between the basic nitrogen of the drug and three sulfonphthalein acid dyes, bromocresol green (BCG), bromocresol purple (BCP), bromophenol blue (BPB), and bromothymol blue (BTB) in phthalate buffer pH 3.0, 3.4, and 3.2, using BCG, BCP, and BPB

or BTB, respectively. The formed complexes were extracted with chloroform and measured at 415, 417, 412, and 414 nm for BCG, BPB, BCP, and BTB, respectively. The analytical parameters and their effects on the reported systems were investigated. The reactions were extremely rapid at room temperature, and the absorbance values remained unchanged at 48 h for all reactions. Beer's law was obeyed in the concentration ranges of 2.0–20, 2.0–14 and 2.0–16 μg/mL for BCG, BCP and (BPB or BTB), respectively. The composition of the ion pairs was found to be 1:1 by Job's method. Beer's law studies enabled method validation as to accuracy, precision, limits of detection, and limits of quantification. The proposed methods have been applied successfully for the analysis of the drug bulk and its dosage forms. The results were in good agreement with those obtained by the official and reported methods [29].

A new method for the determination of gatifloxacin has been developed by Zhang *et al*. that is based on the interaction between alizarin red (ARS) and gatifloxacin, resulting in an absorbance enhancement of ARS at 261 nm. At the same time, the linear relationship between the absorbance intensity and concentration of gatifloxacin was over the range of 0.20–110.00 μg/mL. The method has been applied to the determination of gatifloxacin in tablets, injections, and urine, and the results are very close to those obtained by the fluorimetry method [30].

A novel and sensitive method for the quantitative determination of gatifloxacin by spectrophotometric estimation in UV region was developed by Jain *et al*. using 7.5 M *N,N*-dimethylurea solution as a hydrotropic reagent. Gatifloxacin shows a maximum absorbance at 333 nm, while *N,N*-dimethylurea does not absorb above 260 nm. Beer's law was obeyed in the concentration range of 10–60 μg/mL. Commonly used tablet excipients and *N,N*-dimethylurea did not interfere with the spectrophotometric estimation. The analysis method was statistically validated and by recovery studies. Using 7.5 M *N,N*-dimethylurea solution for analysis of two different tablet formulations of gatifloxacin, the percent label claims and percent recoveries estimated were close to 100%, with low values of standard deviation and relative standard deviation [31].

Madhuri *et al*. described a simple, quick, and sensitive UV-spectrophotometric method for the quantitative estimation of gatifloxacin in bulk drug and in pharmaceutical formulation. The method was based on complexation with a neutral surfactant (Tween 20) in aqueous phosphate buffer at pH 7.4. The product exhibited an absorption maximum at 295 nm and obeyed Beer's law over the concentration range of 2–4 μg/mL. The limits of detection and quantification were calculated, and the relative standard deviation was less than 1.242. The analysis method has been statistically validated and by recovery studies, the results obtained with the proposed method were in agreement with the labeled amounts [32].

5.2.6. Spectrofluorometry

Gandhimathi *et al*. described two simple methods (a spectrofluorimetric method and a spectrophotometric method) for the determination of gatifloxacin in pharmaceutical formulations. For the spectrofluorimetric method, the excitation and emission wavelengths used were 365 and 492nm, respectively. In the case of spectrophotometric method, gatifloxacin in alkaline medium gave a green-colored chromogen (wavelength maximum of 452nm) on treatment with ceric ammonium sulfate and 3-methyl-2-benzothiazolinone hydrazone. For the spectrofluorimetric and spectrophotometric methods, linearity in analyte response was found over the range of 0.2–1 and 10–30μg/mL, respectively [33].

Ocaña *et al*. reported a spectrofluorimetric method to determine gatifloxacin and applied this method to its quantification in spiked human urine and serum samples. The native fluorescence of gatifloxacin in aqueous acetic acid–sodium acetate buffer (pH 3.5) allows its determination over the concentration range of 0.040–0.700μg/mL, using an excitation wavelength (EX) of 292nm and an emission wavelength (EM) of 484nm. Micelle-enhanced (12mM sodium dodecyl sulfate (SDS)) fluorescence led to enhancement in fluorescence intensity, allowing the determination of 0.020–0.450μg/mL of the fluoroquinolone (with EX=292nm and EM=470 nm). Both methods were successfully applied to the determination of gatifloxacin in spiked human urine and serum [34].

Zhu *et al*. determined gatifloxacin by developing the strong fluorescence of gatifloxacin after adding the yttrium in pH 7.0 buffer solutions. In the final method, the linear range was 4.00×10^{-8}–1.00×10^{-6}g/mL, and the detection limit was 3.36×10^{-9}g/mL (correlation coefficient r=0.9997). The relative standard deviation was 1.1% for 11 measurements of 5.6×10^{-7} g/mL gatifloxacin standard solution. The mechanism of the sensitizing effect of Y^{3+} was discussed, and the method was used to determine gatifloxacin in real samples. Good agreement was obtained between results obtained using the fluorimetric method and those obtained using an HPLC method [35].

Guo *et al*. developed a europium-sensitized fluorescence spectrophotometric method using an anionic surfactant (sodium dodecyl benzene sulfonate, SDBS) for the determination of gatifloxacin. The gatifloxacin–Eu^{3+}–SDBS system was found to significantly enhance the fluorescence intensity of the gatifloxacin–Eu^{3+} complex (about 25-fold). The optimal experimental conditions were determined to be excitation and emission wavelengths of 338 and 617nm, pH 7.5, 3.0×10^{-6}mol/L Eu^{3+}, and 5.0×10^{-5}mol/L SDBS. The enhanced fluorescence intensity of the system showed a good linear relationship with the concentration of gatifloxacin over the range 1.0×10^{-8}–8.0×10^{-7}mol/L with a correlation coefficient of 0.9990. The detection limit (S/N=3) was determined as 1.0×10^{-9}mol/L. This method has been successfully used for the determination of gatifloxacin in

pharmaceuticals and human urine/serum samples. Compared with most other methods reported, the rapid and simple procedure proposed here offered higher sensitivity, wider linear range, and good stability. The luminescence mechanism of the system was also discussed in detail in Ref. [36].

Fu reported that using λ_{EX}=470nm and λ_{EM}=566nm to obtain fluorescence, together with dodecyl benzene sodium sulfonate and BR buffer solution (pH 5.72), an effective energy transfer between acridine orange (AO) and rhodamine 6G (R6G) would drive a significant increase in R6G fluorescence intensity. Injecting gatifloxacin into the solution resulted in a quenching of the R6G fluorescence. The results exhibited a linear correlation between the quenching by gatifloxacin over the range of 0.6–9.0μ mol/L. The lower limit was approximately 0.52μmol/L, with a relative standard deviation of 0.62%–0.84% from six parallel measurements of gatifloxacin, and the recovery was 90%–105%. Common metal ions and drug dressing showed no interference with the determination. This method can be applied to the determination of gatifloxacin in samples without separation [37].

Wu *et al*. proposed a cloud point extraction process using mixed micelles consisting of the anionic surfactant SDS and the nonionic surfactant polyoxyethylene (7.5) nonylphenylether (PONPE 7.5) to extract two fluoroquinolone antimicrobial agents (ofloxacin and gatifloxacin) from aqueous media. The method is based on the mixed micelle-mediated extraction of fluoroquinolones in the presence of NaCl as an inducing agent in phase separation, followed by spectrofluorimetric determination. The effect of different variables (such as pH, PONPE 7.5 concentration, SDS concentration, NaCl concentration, cloud point temperature, and time) was investigated, and optimum conditions were established. At the optimal conditions, linear calibration plots were obtained in the concentration range of 0.1–150 and 0.1–250ng/mL for ofloxacin and gatifloxacin, respectively. The limits of detection were 0.04 and 0.06ng/mL, respectively. The procedure was applied successfully for the detection of the investigated drugs in their pharmaceutical dosage forms, in spiked plasma, spiked urine, and urine samples, with good precision and accuracy [38].

5.2.7. Kinetic spectrophotometric method

Darwish *et al*. described a selective and simple kinetic spectrophotometric method for the determination of gatifloxacin in its dosage forms. The method was based on the formation of a colored *N*-vinyl chlorobenzoquinone derivative of gatifloxacin by its reaction with 2,3,5,6-tetrachloro-1,4-benzoquinone in presence of acetaldehyde. The formation of the colored product was monitored spectrophotometrically by measuring its absorbance at 655nm. The factors affecting the reaction were studied and optimized, with the stoichiometry of the reaction being determined, and the reaction pathway postulated. Under the optimized conditions, the

initial rate and fixed time (i.e., 5min) methods were utilized for constructing the calibration graphs. The graphs were linear over the concentration ranges of 2–100 and 10–140μg/mL with limits of detection of 0.84 and 3.5μg/mL for the initial rate and fixed time methods, respectively. The analytical performance of both methods was fully validated, and the results were satisfactory. The proposed methods were successfully applied to the determination of gatifloxacin in its commercial dosage forms. The label claim percentages were 99.7–100.5% and 98.2–99.5% for the initial rate and fixed time methods, respectively. Statistical comparison of the results with those of the reference method showed excellent agreement and proved that there was no significant difference in the accuracy and precision between the reference and the proposed methods. The proposed methods are superior to all the previously reported spectrophotometric methods in terms of the procedure simplicity and assay selectivity [39].

5.2.8. Microbiological assay method

Salgado *et al*. used a simple, sensitive, and specific agar diffusion bioassay for gatifloxacin using a strain of *Bacillus subtilis* ATCC 9372 as the test organism. Gatifloxacin could be measured in tablets and raw material at concentrations over the range of 4–16μg/mL. The calibration graph for gatifloxacin was linear over 4.0–16.0μg/mL, and the method validation demonstrated that the method was linear (r^2=0.9993), precise (RSD=1.14%), and accurate. The results confirmed precision and did not differ significantly from those obtained using other methods described in the literature. The validated method yielded good results in terms of the range, linearity, precision, accuracy, specificity, and recovery. It was concluded that the microbiological assay is satisfactory for *in vitro* quantification of the antibacterial activity of gatifloxacin [40].

5.2.9. Voltammetry

Two simple, precise, inexpensive, and sensitive voltammetric methods for the determination of lomefloxacin, sparfloxacin hydrochloride, gatifloxacin, and moxifloxacin were developed by Abdel Ghani *et al*. The methods were first used to explore the adsorption behavior of the four investigated antibacterial agents at a hanging mercury dropping electrode (HMDE), by a direct method and, second, by a modification via their complexation with $PdCl_2$. For the direct method, drugs were accumulated on the HMDE, and a well-defined reduction peak was obtained in Britton–Robinson buffer of pH 7 for lomefloxacin and sparfloxacin hydrochloride, and pH 6 for gatifloxacin and moxifloxacin. The adsorptive stripping response was evaluated as a function of variables such as the scan rate, pH, accumulation time, and potential. For the modified method, the adsorptive behavior of Pd(II)-4-quinolone complexes at the HMDE

yielded a stripping voltammetry peak at a more negative potential than that of the free Pd(II) ions (-1.05 V). The limit of detection was 2×10^{-8}M, while the limit of quantification was 6×10^{-8}M for the investigated drugs. The methods were applied to the determination of the four drug substances in biological samples and pharmaceutical preparations and were also compared with the official reference methods. Complete validation of the proposed methods was performed [41].

El-Desoky described a fully validated, sensitive, and precise stability-indicating square-wave adsorptive cathodic stripping voltammetric method for the determination of gatifloxacin in its bulk drug substance, pharmaceutical formulations, and in spiked human serum and real plasma samples. The detection limits of gatifloxacin in the bulk form and human serum were 1.5×10^{-9} and 2.2×10^{-9}mol/L, respectively. The described method was applied successfully without prior extraction for the determination of gatifloxacin in formulations and in human biological samples. No significant interferences from common excipients, some common metal ions, organic species, coadministrated drugs, and acid-induced degradation products were obtained during the analysis. Pharmacokinetic parameters of gatifloxacin in the plasma of healthy volunteers (following the administration of a 400-mg single oral dose) were also estimated by means of the stripping voltammetric method [42].

5.2.10. Chromatographic methods of analysis

5.2.10.1. High-performance thin-layer chromatography Motwani *et al.* described a simple, sensitive, selective, precise, and stability-indicating high-performance thin-layer chromatographic method for the determination of gatifloxacin both as a bulk drug and from polymeric nanoparticles [43]. The method was developed and validated as per the ICH guidelines and used TLC aluminum plates pre-coated with silica gel 60F-254 as the stationary phase. The mobile phase consisted of *n*-propanol–methanol-concentrated ammonia solution (25%) (5:1:0.9, v/v/v). This solvent system was found to give compact spots for gatifloxacin (R_f value of 0.60 ± 0.02). Densitometric analysis of gatifloxacin was carried out at 292nm in absorbance mode. Good linear calibration plots ($r=0.9953$) with respect to peak area were obtained over the concentration range of 400–1200ng/spot. The mean values of the slope and intercept were 9.66 ± 0.05 and 956.33 ± 27.67, respectively. The method was validated as to precision, accuracy, ruggedness, and recovery. The limits of detection and quantitation were found to be 2.73 and 8.27ng/spot, respectively. Gatifloxacin was subjected to acid and alkali hydrolysis, oxidation, photodegradation, and dry heat treatment. The drug undergoes degradation under acidic and basic conditions, and upon wet and dry heat treatment. The degraded products were well separated from the pure drug in the TLC analysis. The statistical analysis proved that the method for quantification of gatifloxacin as its bulk drug and from

polymeric nanoparticles is reproducible and selective. As the method could effectively separate the drug from its degradation products, it can be employed as stability-indicating assay [43].

5.2.10.2. Liquid chromatography Vishwanathan *et al*. developed a rapid, sensitive, and selective method for the determination of gatifloxacin in human plasma, as this was essential for understanding the pharmacokinetics of the drug when administered orally or intravenously. Solid-phase extraction using Oasis® HLB was used to extract gatifloxacin and the internal standard ciprofloxacin from plasma. A method based on liquid chromatography/electrospray tandem mass spectrometry (LC/ESI-MS/MS) was developed and validated to quantitate gatifloxacin in human plasma. The precursor and major product ions of the analyte were monitored on a triple quadrupole mass spectrometer with positive ion electrospray ionization in the multiple reaction monitoring mode. Mechanisms for the formation of collision-induced dissociation products of gatifloxacin were proposed. Linear calibration curves were generated from 10 to 1000 ng/mL, with correlation coefficients exceeding 0.99. The inter- and intraday precision was less than 6.0%, and the accuracy was less than 5.4% for gatifloxacin. The limit of detection for the method was 500 pg/mL based on a signal-to-noise ratio of 3 [44].

Nguyen *et al*. were used liquid chromatography with a column-switching technique for the simultaneous direct quantification of levofloxacin, gatifloxacin, and moxifloxacin in human serum. Serum samples were injected on a LiChroCART® 4-4 pre-column filled with a LiChrospher® 100 RP-18, 5 μm, where fluoroquinolones were purified and concentrated. The fluoroquinolones were back-flushed from the column and then separated on a Supelcosil ABZ+ Plus (150 mm × 4.6 mm i.d.) analytical column with a mobile phase containing 10 mM phosphate buffer (pH 2.5), acetonitrile (88:12, v/v), and 2 mM tetrabutylammonium bromide. The effects of ion-pair reagents, buffer type, pH, and acetonitrile concentrations in the mobile phase on the separation of the three fluoroquinolones were investigated. Fluorescence detection provided sufficient sensitivity to achieve a quantification limit of 125 ng/mL for levofloxacin and moxifloxacin, and 162.5 ng/mL for gatifloxacin with a 5-μL sample size. The online process of extraction avoids time-consuming treatment of the samples before injection, and the run time is shortened. The recovery, selectivity, linearity, precision, and accuracy of the method are convenient for pharmacokinetic studies or for routine assays [45].

5.2.10.3. High-performance liquid chromatography Liang *et al*. developed, validated, and applied a selective, sensitive, and accurate HPLC method with UV and fluorescence detection for the determination of fluoroquinolones in human plasma. The effects of mobile-phase composition,

ion-pair and competing-base reagents, buffers, pH, and acetonitrile concentrations were investigated on the separation of six quinolones (cinoxacin, levofloxacin, ciprofloxacin, gatifloxacin, moxifloxacin, and trovafloxacin). Sample preparation was carried out by adding internal standard and displacing agent, and processing by ultrafiltration. This method uses ultraviolet and fluorescence detection, and separation was effected using a C18 column. The recovery, selectivity, linearity, precision, and accuracy of the method were evaluated from spiked human plasma samples. The method was successfully applied to patient plasma samples in support of a levofloxacin pharmacokinetic study [46].

Overholser *et al*. developed and validated a simple and sensitive HPLC method for the determination of gatifloxacin concentrations in human serum and urine. Serum proteins were removed by ultrafiltration through a filtering device after adding a displacing agent. Urine samples were diluted with mobile phase prior to injection, separation was achieved with a C18 reverse-phase column, and gatifloxacin concentrations were determined using ultraviolet detection. The quantitation limits of the assay were 100 ng/mL in serum and 1.0 μg/mL in urine. The assay method was successfully used as part of a pharmacokinetic study of gatifloxacin in healthy volunteers [47].

Al-Dgither *et al*. described a simple reversed phase HPLC method for the determination of gatifloxacin stability in human plasma. Using ciprofloxacin as an internal standard, separation was achieved on an X Terra MS C18 (3 mm × 50 mm, 5 μm) column. The mobile phase, 0.025 M disodium hydrogen phosphate (pH 3.0) and acetonitrile (80:20, v/v), was delivered at a flow rate of 1.0 mL/min. The eluent was monitored using spectrophotometric detection at 293 nm. Plasma samples were deproteinized using an Amicon Centrifree system. No interference in blank plasma, or by commonly used drugs, was observed. The relationship between gatifloxacin concentration and the observed peak height ratio (gatifloxacin to internal standard) was linear over the range of 0.10–6.0 μg/mL. The intra- and interday coefficients of variation were less than or equal to 2.77% and 4.59%, respectively. The extraction recovery of gatifloxacin and the internal standard from plasma samples were more than 85%. Gatifloxacin solutions were found to be stable for at least 5 h at room temperature, for 7 weeks at −20 °C, and after three freeze–thaw cycles in plasma. In deproteinized plasma, gatifloxacin was stable for 16 h at room temperature and 48 h at −20 °C. Gatifloxacin in phosphate buffer was stable for 24 h at room temperature and 7 weeks at −20 °C [48].

Santoro *et al*. developed and validated analytical methods for the quantitative determination of third-generation fluoroquinolones. Simple and rapid HPLC methods were developed and validated for quantitative determination of four quinolone antibiotics in tablets and injection preparations. The fluoroquinolones studied in this work were gatifloxacin,

levofloxacin, lomefloxacin, and pefloxacin. The quinolones were analyzed by using a LiChrospher® 100 RP-18 column (125 mm × 4 mm, 5 μm), and a mobile phase consisting of water:acetonitrile (80:20, v/v) with 0.3% of triethylamine and pH adjusted to 3.3 with phosphoric acid. The flow rate was 1.0 mL/min, and the analyses were performed using UV detection with wavelengths varying from 279 to 295 nm. The analyses were performed at room temperature, and all fluoroquinolones were separated within 5 min. The calibration curves were linear (calibration coefficient exceeding 0.9999) over a concentration range from 4.0 to 24.0 μg/mL. The relative standard deviation of the method was less than 1.0%, and the average recovery was above 99.54% [49].

A simple reversed phase HPLC method was developed by Sultana *et al*. for the quantitative determination of gatifloxacin in the bulk material, pharmaceutical formulations, and human serum using a Mediterranean C18 (25 mm × 0.46 mm, 5 μm) column. The mobile phase (40:40:20, v/v/v, acetonitrile, methanol, and water, pH 2.7, adjusted by phosphoric acid) was delivered at a flow rate of 1.0 mL/min. The eluent was monitored using spectrophotometric detection at 286 nm. The method is specific to gatifloxacin and was able to resolve the drug peak from formulation excipients and metal ion impurities. The method is accurate (99.18–101.87%), precise (intraday variation 0.14–1.67% and interday variation 0.32–1.80%), and linear over the concentration range of 0.1–25 μg/mL (R^2=0.999) and was successfully used in monitoring left-over drug in drug–metal complexes. The detection limit of gatifloxacin at a signal-to-noise ratio of 3 was 1.73 ng/mL in human plasma, while the quantification limit in human serum was 5.77 ng/mL. The proposed method is applicable to routine analysis of gatifloxacin in pharmaceutical formulations as well as in human plasma samples [50].

Tasso and Dalla Costa developed and validated an automated system using online solid-phase extraction and HPLC with fluorimetric detection for the quantification of gatifloxacin in rat plasma. The extraction was carried out with a high extraction yield using C18 cartridges (BondElut). After washing, gatifloxacin was eluted from the cartridge with mobile phase onto a C18 HPLC column. The mobile phase consisted of a mixture of phosphoric acid (2.5 mM), methanol, acetonitrile, and triethylamine (64.8:15:20:0.2, v/v/v/v, apparent pH of 2.8). All samples and standard solutions were chromatographed at 28 °C. The method was selective and linear for drug concentrations ranging between 20 and 600 ng/mL. Gatifloxacin recoveries ranged from 95.6% to 99.7%, and the limit of quantification was 20 ng/mL. The intra- and interassay accuracy was as high as 94.3%, and the precision did not exceed 5.8% of the coefficient of variation. High extraction yields as much as 95% were obtained. Gatifloxacin in plasma was stable for 1 month at −20 °C after three freeze–thaw cycles, and for 24 h in the autosampler after processing. The assay has

been successfully applied to measure gatifloxacin plasma concentrations during pharmacokinetic studies in rats [51].

An HPLC method to determine gatifloxacin was presented by Jia *et al*. The stationary phase was an Ultimate XB-C18 column, the flow rate was 1.0 mL/min, and the temperature of the column was 29 °C. The mobile phase consisted of 40:60 methanol–0.08 M KH_2PO_4 adjusted to pH 3.87 with phosphoric acid. The detection wavelength was 285 nm, and 20 μL of sample solution was injected to the sampler. The calibration curve was linear in response over the range of 10.3–51.5 μg/mL (r=0.9995), with a recovery of 98.0% and a relative standard deviation of 1.2% (n=6). The method is simple and accurate and can be used in quality control for gatifloxacin in preparations [52].

Patel *et al*. described a simple, precise, accurate, and precise reversed phase HPLC method for the simultaneous estimation of satranidazole and gatifloxacin in combination dosage forms. A LiChrospher 100 C18 and a mobile phase consisting of water/acetonitrile/triethylamine (75:25:0.35, v/v/v) were used for separation. Final pH was adjusted to 3.2±0.02 with 10% (v/v) phosphoric acid. Measurements were made at the effluent flow rate of 1.0 mL/min with an injection volume of 20 μL and UV detection at 320 nm, as both components show reasonably good response at this wavelength. The retention times of satranidazole and gatifloxacin were 6.0 and 3.44 min, respectively. The method was validated in terms of linearity, accuracy, precision, robustness, and specificity. Linearity of satranidazole and gatifloxacin was in the range of 1–70 and 1–70 μg/mL, respectively. Average percent recoveries obtained for satranidazole and gatifloxacin were 99.80% and 100.20%, respectively. The limits of detection and quantification were found to be 0.3 and 1.0 μg/mL for satranidazole, respectively, and were 0.5 and 1.0 μg/mL for gatifloxacin. The method is useful in the quality control of bulk manufacturing and pharmaceutical dosage forms [53].

Lan *et al*. established an HPLC method for the determination of gatifloxacin in gatifloxacin hydrochloride tablets. The analysis was carried on a Diamonsil C18 column (250 mm×4.6 mm, 5 μm), and the mobile phase was composed of acetonitrile–0.01 M phosphoric acid (20:80) (pH adjusted to 3.0 with triethylamine). The detection wavelength was 293 nm, and the flow rate was 1.0 mL/min. The calibration curve was linear between 10 and 120 μg/mL (r=0.9999), and the average recovery and relative standard deviation for gatifloxacin were 99.7% and 1.29% (n=9), respectively. This method is simple, accurate, sensitive, specific, reproducible, and suitable for the quality control of gatifloxacin hydrochloride tablets [54].

Ramakrishna *et al*. developed a normal phase HPLC method for the separation of enantiomeric gatifloxacin and (±)-1-cyclopropyl-6-fluoro-8-methoxy-7-(3-methylpiperazin-1-yl)-4-oxo-quinoline-3-carboxylic acid. The method involved the use of an amylose-based Chiralpak AD-H (150 mm×4.6 mm, 5 μm) column using a mobile-phase system containing

hexane–ethanol–diethylamine (85:15:0.1%, v/v/v). The conditions affording the best resolution were found by selection and variation of the mobile-phase components, and the differences in separation capability of the method were noted. The relative standard deviation in retention times and peak areas was better than 0.2% and 0.4%, respectively. Gatifloxacin sample solutions and mobile phase were found to be stable for at least 48h [55].

5.2.10.4. Capillary electrophoresis methods Zhu *et al*. established a method for the determination of gatifloxacin by high-performance capillary electrophoresis (HP-CE). The separation was performed on a fused silica capillary of 50μm×56cm (50cm effective length). 100mmol/L sodium dihydrogen phosphate–methanol (85:15, pH was adjusted to 9 with 1mmol/L NaOH) was used as the running buffer. Samples were injected hydrodynamically (15s, 138kPa) into the capillary. The applied voltage was 15kV, and the detection was set at 293nm. The running time was 30min, the linearity range was over 0.05–2mg/L, and the average recovery was 99. 3% (RSD=0.9%). The method was found to be efficient, reproducible, and feasible for the determination of gatifloxacin [56].

Sane *et al*. used capillary zone electrophoresis for the determination of gatifloxacin in its pharmaceutical tablet preparation using fused silica capillary. Separation was achieved by applying 21kV after hydrodynamic injection, with phosphate buffer solution (pH 9.5) used as the separation electrolyte. Under these experimental conditions, the analysis takes 8min. Detection was at 280nm using UV detection. The linearity range for gatifloxacin was between 20.0and 60.0μg/mL. The method was validated; was found to be specific, precise, accurate, reproducible, and robust; and can be applied for the routine analysis of gatifloxacin in formulations and bulk substance [57].

Lü *et al*. used pressurized capillary electrophoresis for the separation and determination of seven fluoroquinolones. The effect of different experimental conditions, such as the concentration and pH of the buffer, the organic modifier concentration, the surfactant, and ion-pairing agents added to the electrolyte, and applied voltage was studied. All seven fluoroquinolones were baseline separated using a mobile phase containing 27% (v/v) acetonitrile, 5mmol/L Na_2HPO_4 buffer (adjusted pH to 4.0 using citric acid), 11mmol/L SDS, and 0.01% triethylamine at a detection wavelength of 287nm and at an applied voltage of -10kV. The calibration curves were linear (r>0.9991) over a concentration range of 1.0–50.0mg/L for norfloxacin; 2.5–50.0mg/L for fleroxacin, ciprofloxacin, and lomefloxacin; and 5.0–50.0mg/L for enoxacin, ofloxacin, and gatifloxacin. The detection limits (S/N=3) for enoxacin, ofloxacin, fleroxacin, ciprofloxacin, lomefloxacin, and gatifloxacin were 0.5, 0.8, 0.4, 0.2, 0.4, 0.5, and 1.0mg/L, respectively. The method is simple, rapid, and reproducible and was

successfully applied to the analysis of fish muscle samples spiked with fluoroquinolones. With mean recoveries ranging from 81.6% to 97.6% [58].

Zhou *et al*. investigated capillary zone electrophoresis for the enantiomeric separation of lomefloxacin, gatifloxacin, pazufloxacin, and ofloxacin. Resolution of the enantiomers was achieved using hydroxypropyl-β-cyclodextrin (HP-β-CD) as the chiral selector. Parameters influencing separation included cyclodextrin concentration, separation potential, pH, and organic additives. A buffer consisting of 70 mM phosphate buffer and 40 mM HP-β-CD at pH 3.96 was found to be highly efficient for the separation of lomefloxacin, at pH 3.90 for gatifloxacin, at pH 5.04 for pazufloxacin, and at pH 2.16 for ofloxacin. This appears to be is the first capillary electrophoresis report on the enantiomeric resolution of lomefloxacin and gatifloxacin [59].

Yao *et al*. used an affinity capillary electrophoresis (ACE) method (mobility shift) to investigate the interaction between bovine serum albumin (BSA) and gatifloxacin. The mobility ratio of the internal standard and the sample was used to calculate the binding constant, K_b, of BSA and gatifloxacin. Initially, using 20 mM sodium phosphate buffer (pH 7.4) mixed with 0–1000 μmol/L gatifloxacin as a running buffer was used, and BSA as the sample. The value of K_b calculated from this experiment was 0.00044 L/mol. Then 0–12.5 μmol/L BSA was used as an additive to run the ACE experiment, and then the value of K_b was 0.00042 L/mol. In order to improve the shape of the peak and restrain the adsorption of BSA to the internal wall of the quartz column, in a second method, 0.25 M glycine and 0.5 mM ethylenediamine tetracetate (EDTA) were added to the running buffer, and 0.5% SDS solution was used to rinse the column. Satisfactory effect was obtained. The value of K_b obtained using a fluorescence method was found to be 0.00027 L/mol. This work demonstrated that the determination of binding constants by ACE methodology is simple with high performance [60].

Sun *et al*. developed a simple, rapid, and accurate method for the effective separation and simultaneous determination of lomefloxacin, gatifloxacin, enoxacin, ciprofloxacin, ofloxacin, enrofloxacin, and pefloxacin residues in porcine tissue by capillary electrophoresis with diode-array detection. The sample was extracted with acetonitrile, and a mixture consisting of 25 mM NaH_2PO_4, 25 mM $Na_2B_4O_7$, and 25 mM H_3BO_3 (pH 9.0) was used as a running buffer. A linear relationship between concentration and peak area for each compound was obtained over the concentration range of 0.5–100 mg/L with a correlation coefficient greater than 0.9994. For analysis of porcine tissue, the detection limits of lomefloxacin, gatifloxacin, enoxacin, ciprofloxacin, ofloxacin, enrofloxacin and pefloxacin were 0.013, 0.012, 0.023, 0.040, 0.037, 0.035 and 0.034 mg/kg, respectively. The recoveries were in the range of 72–93%, the intraday precision was less than 5%, and the interday precision was less than 10%.

The proposed method has high resolution, speed and requires only an extremely small sample volume. It can be used to confirm the presence of the studied seven fluoroquinolones in porcine tissue at the required maximum residue limit level [61].

Faria described an alternative capillary zone electrophoresis method for the determination of ciprofloxacin (CPFLX), gatifloxacin (GTFLX), moxifloxacin (MFLX), and ofloxacin (OFLX) through a simple aqueous electrolyte system consisting of 25 mmol/L of tromethamine hydrochloride and 15 mmol/L of sodium tetraborate buffer (pH 8.87) within 3 min using direct UV detection at 282 nm. The analytical validation parameters were reported as: linearity (r>0.998), selectivity (comparison between slope of the calibration curve of external standard and calibration curve of standard addition), repeatability in area for sample (RSD%: <3.94% for CPFLX, <3.87% for GTFLX, 1.30% for MFLX, and <1.88% for OFLX), intermediate precision in area for sample (RSD%: <3.59% for CPFLX, <3.09% for GTFLX, 2.67% for MFLX, and <2.25% for OFLX), accuracy (mean of recovery range: 101.2% for CPFLX, 101.0% for GTFLX, 101.3% for MFLX, and 99.9% for OFLX), limit of detection (mg/L: 2.72 for CPFLX, 1.92 for GTFLX, 0.795 for MFLX, and 1.05 for OFLX), limit of quantification (mg/L: 9.06 for CPFLX, 6.40 for GTFLX, 2.65 for MFLX, and 3.50 for OFLX), and robustness. Due to its simplicity, selectivity, precision, accuracy, and rapidity, the methodology can be an interesting alternative for these drugs in their quality assurance [62].

6. STABILITY

El-Bary *et al*. studied the photostability of gatifloxacin both in solution forms and in its tablet formulations using the guidelines of the International Conference on Harmonization. In addition, the effect of packaging of this dosage form on the photostability of the drug was determined. The light irradiation was performed using a solar simulator in the form of a Xenon lamp within a selected wavelength range of 250–400 nm. Samples were irradiated with two light doses for a period of 90 min. Dose-I was 3 $W/m^2/h$ visible light, 50 $W/m^2/h$ UV-A, and 2.9 $W/m^2/h$ UV-B; while Dose-II was 6.5 $W/m^2/h$ visible light and 150 $W/m^2/h$ UV-A, and 12.38 $W/m^2/h$ UV-B. The photodegradation process was monitored by UV spectrophotometry and by IR absorption spectroscopy. All of the prepared tablets (unpackaged and in blister packs), together with the commercially available Tequin tablets in blister sheets, and gatifloxacin in solution showed neither discoloration nor change in appearance when exposed to Dose-I. On the contrary, exposing gatifloxacin powder to

Dose-II caused a color change. Negligible degradation of gatifloxacin was observed for the drug as its bulk drug substance when irradiated with Dose-II (97.94% gatifloxacin remaining), while Dose-II had a larger effect on gatifloxacin in solution (92.7% gatifloxacin remaining after 90 min exposure). The remaining percentages of gatifloxacin after 90 min exposure of unpackaged tablets to Dose-I and Dose-II were acceptable (99.1% and 98.34% remaining, respectively). However, there was 2.65% degradation of gatifloxacin in Tequin tablets in blister packaging after 90 min of exposure to Dose-II, while prepared tablets showed no degradation after 90 min exposure to the same dose. It was concluded that the prepared tablets were photostable under stress conditions, but the degree of photostability was dependent on the excipients used in the tablet formulations and on the nature of any packaging [63].

Devi and Chandrasekhar developed a validated, specific, stability-indicating reversed phase HPLC method for the quantitative analysis of gatifloxacin, its degradation products, and its process-related impurities in bulk samples and in pharmaceutical dosage forms. Forced degradation of gatifloxacin bulk sample was conducted in accordance with ICH guidelines. Acidic, basic, neutral, and oxidative hydrolysis, thermal stress, and photolytic degradation were used to assess the stability-indicating power of the method. Substantial degradation was observed during oxidative hydrolysis, but no degradation was observed under the other stress conditions. The method was optimized using samples generated by forced degradation and by the use of sample solutions spiked with impurities. Good resolution of the analyte peak from peaks corresponding to process-related impurities and degradation products was achieved on a C18 column using a simple linear mobile-phase gradient prepared from mixtures of acetonitrile, an aqueous solution of sodium dihydrogen orthophosphate dihydrate (adjusted pH to 6.5 using phosphoric acid), and triethylamine. Detection was performed at a wavelength of 240 nm. Limits of detection and quantification were established for gatifloxacin and its process-related impurities. When the stressed test solutions were assayed by comparison with a gatifloxacin working standard, the mass balance was always close to 99.3%, indicating that the method was stability indicating. The method was found to be suitable for evaluating the quality of bulk samples of gatifloxacin at the time of batch release and also during storage [64].

El-Desoky developed a fully validated, sensitive, and precise stability-indicating square-wave adsorptive cathodic stripping voltammetric method for the determination of gatifloxacin in its bulk form, pharmaceutical formulations, and spiked human serum and real plasma samples. The detection limits achieved for gatifloxacin in the bulk form and human serum were 1.5×10^{-9} and 2.2×10^{-9} mol/L, respectively. The described

method was applied successfully for the determination of gatifloxacin in formulations and human biological samples without extraction prior to the analysis. No significant interferences from common excipients, some common metal ions, organic species, coadministrated drugs, or the acid-induced degradation products were noted during the analysis of gatifloxacin in various analyzed samples. Pharmacokinetic parameters of gatifloxacin in the plasma of healthy volunteers following administration of an oral single dose (400mg gatifloxacin) were also estimated by means of the described stripping voltammetric method [65].

Ge *et al*. investigated kinetics, influencing factors, and mechanisms on the photodegradation of gatifloxacin, as these can be detected as emerging pollutants in aqueous environments. The photodegradation follows the pseudo-first-order kinetics. Gatifloxacin photodegrades with a quantum yield of $(5.94\pm0.95)\times10^{-3}$ in pure water and undergoes direct photolysis as well as self-sensitized photodegradation. Fluoroquinolones photodegrade slower in freshwater and seawater relative to pure water, which is attributed to the synergistic effects of pH and aqueous dissolved matter (such as humic acids and nitrate ions) on the photodegradation. A toxicity test using *Vibrio fischeri* revealed the formation of hazardous photoproducts [66].

The ubiquity of fluoroquinolone antibiotics in surface waters requires study into their fate in the aqueous euphotic zone. Ge *et al*. studied eight fluoroquinolones (ciprofloxacin, danofloxacin, levofloxacin, sarafloxacin, difloxacin, enrofloxacin, gatifloxacin, and balofloxacin) upon exposure to simulated sunlight, and their photodegradation was observed to follow apparent first-order kinetics. Based on the determined photolytic quantum yields, solar photodegradation half-lives for the fluoroquinolones in pure water and at 45° North latitude were calculated to range from 1.25min for enrofloxacin to 58.0min for balofloxacin, suggesting that fluoroquinolones would intrinsically photodegrade rapidly in sunlit surface waters. However, it was found that freshwater and seawater constituents inhibited the photodegradation. The inhibition was further explored by a central composite design using sarafloxacin and gatifloxacin as representatives. Interaction with humic acids, ferric ion, nitrate ion, and humic chloride salts inhibited the photodegradation, as these mainly acted as radiation filters and/or scavengers for reactive oxygen species. The photodegradation product identification and ROS scavenging experiments indicated that the fluoroquinolones underwent both direct photolysis and self-sensitized photooxidation via *OH and (1)O(2) groups. Piperazinyl *N*(4)-dealkylation was primary for *N*(4)-alkylated fluoroquinolones, whereas decarboxylation and defluorination were comparatively important for the other fluoroquinolones. These results are of importance toward the goal of assessing the persistence of fluoroquinolones in surface waters [67].

7. DRUG METABOLISM AND PHARMACOKINETICS

Gatifloxacin is an 8-methoxy fluoroquinolone antibacterial agent and has a broader spectrum of antibacterial activity than do older fluoroquinolones (such as ciprofloxacin). The drug shows good activity against many Gram-positive and Gram-negative pathogens, atypical organisms, and some anaerobes. Notably, gatifloxacin is highly active against both penicillin-susceptible and penicillin-resistant strains of *S. pneumoniae*, a common causative pathogen in community-acquired pneumonia, acute sinusitis, and acute bacterial exacerbations of bronchitis.

Gatifloxacin is absorbed well from the gastrointestinal tract, as its oral bioavailability is almost 100%. Therefore, patients can be switched from intravenous to oral therapy without an adjustment in dosage. High concentrations of gatifloxacin are achieved in plasma and target tissues/fluids. Gatifloxacin has a long plasma elimination half-life, thus allowing once-daily administration. Few clinically significant interactions between gatifloxacin and other drugs have been reported.

Gatifloxacin is generally well tolerated, and its tolerability profile was broadly similar to those of comparator agents in comparative trials. The most common adverse events are gastrointestinal symptoms (oral formulation) and injection site reactions [68].

7.1. Pharmacokinetics

Lober *et al*. studied the pharmacokinetics of gatifloxacin (400 mg taken orally) and the influence of the antacid aluminum magnesium hydroxide (20 mL of Maalox 70) on the bioavailability of gatifloxacin in 24 healthy volunteers. In an open, randomized, six-period crossover study, the volunteers received gatifloxacin alone (treatments A and D); aluminum magnesium hydroxide concomitant with gatifloxacin (treatment C); or aluminum magnesium hydroxide 2 h before (treatment B), 2 h after (treatment E), or 4 h after gatifloxacin administration (treatment F). Gatifloxacin concentrations were measured by a validated bioassay and high-performance liquid chromatography. Pharmacokinetics of a single 400-mg dose of gatifloxacin alone were characterized as follows (mean±SD): peak concentration (C_{max}), 3.8±0.5 (treatment A), and 3.4±0.9 (treatment D) μg/mL; time to C_{max}, 1.4±0.8 (treatment A) and 1.7±0.7 (treatment D) h; area under the curve from time zero to infinity ($AUC_{0-\infty}$), 33.5±5.9 (treatment A) and 31.4±3.4 (treatment D) μg h/mL; urine recovery, (83±6)% (treatment A) and (84±8)% (treatment D). Comparison of the results obtained by bioassay showed a good correlation. Aluminum magnesium hydroxide administration 2 h before (treatment B) or concomitant with (treatment C) gatifloxacin decreased the C_{max} by 45% (2.1±1.2 μg/mL)

or even 68% (1.2±0.4 μg/mL) highly significantly ($P<0.01$). The $AUC_{0-\infty}$ was significantly reduced from 33.5±5.9 to 19.4±6.9 μgh/mL (by 42%) or even to 11.9±3.3 μgh/mL (by 64%) ($P<0.01$). If aluminum magnesium hydroxide was given 2h after gatifloxacin (treatment E), there was no significant reduction of concentration in serum, but the $AUC_{0-\infty}$ was significantly reduced from 31.4±3.4 to 25.9±5.3 μgh/mL (18%) ($P<0.01$). Aluminum magnesium hydroxide given 4h after gatifloxacin (treatment F) showed no influence on the gatifloxacin pharmacokinetics. Therefore, the optimal time between gatifloxacin application and the intake of an aluminum-containing antacid should be 4h [69].

Wise *et al*. measured the concentrations of gatifloxacin in the plasma, the cantharidine-induced inflammatory fluid, and the urine after a single 400-mg oral dose of drug was given to each of nine healthy male volunteers and was measured over the following 24h. The mean peak concentration in plasma of 4.1 mg/L was attained at a mean time of 1.8h post-dose. The mean peak concentration in inflammatory fluid was 3.6 mg/L, which was attained at a mean time of 4.2h post-dose. The mean plasma elimination half-life of gatifloxacin was 6.8h and that in inflammatory fluid was 7.2h. The mean penetration into the inflammatory fluid was 117%. Recovery of drug from urine during the first 24h post-dose was 65% of that administered. The data suggest that gatifloxacin orally dosed at 400 mg should be adequate to treat systemic infections caused by most bacterial species [70].

Niki *et al*. studied the influence of gatifloxacin on the pharmacokinetics of theophylline in five healthy adult male volunteers. After 200 mg of theophylline in a sustained-release preparation was administered twice daily for four consecutive days, the same dose of theophylline and 200 mg of gatifloxacin were administered concurrently to the subjects twice daily for five consecutive days. Comparison of the pharmacokinetic parameters on day 4 of theophylline alone and days 3 and 5 of coadministration revealed no significant differences in the maximum concentrations (C_{max}), areas under the serum concentration–time curve (AUC_{0-12}), total body clearances, and the amounts and proportions of theophylline and its metabolites in urine. One subject, however, showed 55% and 44% increases in C_{max} and AUC_{0-12}, respectively, on day 5 of coadministration relative to values on day 4 of theophylline alone. Thus, coadministration of gatifloxacin seemed to have a little effect on the pharmacokinetics of theophylline. Further studies will be necessary to clarify the pharmacokinetic interaction between quinolones and theophylline, and it was recommended that, when both gatifloxacin and theophylline are administered, the backgrounds of the patients (such as their age, liver and cardiac functions, and other concomitant medications) should be considered [71].

Naber *et al*. investigated gatifloxacin penetration into prostatic and seminal fluid as an interesting candidate for the treatment of chronic bacterial prostatitis (CBP). Besides the antibacterial spectrum, the

concentrations in the target tissues and fluids are crucial for the treatment of CBP. Thus, gatifloxacin concentrations in plasma, urine, ejaculate, prostatic and seminal fluid, and sperm cells were determined by a HPLC method after oral intake of a single 400-mg dose in 10 male Caucasian volunteers in their fasting states. Simultaneous application of the renal contrast agent iohexol was used to estimate the maximal possible contamination of ejaculate and prostatic and seminal fluid by urine. Gatifloxacin was well tolerated by the test subjects. The means and standard deviations for the following parameters were determined to be: time to maximum concentration of drug in serum, 1.66 (SD=0.91)h; maximum concentration of drug in serum, 2.90 (SD=0.39)mg/mL; area under the concentration-time curve from 0 to 24h, 25.65mg z h/mL; and half-life, 7.2 (SD=0.90)h. Within 12h, about 50% of the drug was excreted unchanged into the urine, and the mean renal clearance was 169mL/min. The gatifloxacin concentrations in ejaculate, seminal fluid, and prostatic fluid were in the range of the corresponding plasma concentrations which were 1.92 (SD=0.27) mg/mL at approximately the same time point (4h after drug intake). The concentrations in sperm cells (0.195, 0.076, and 0.011mg/mL) were determined in three subjects. The good penetration into prostatic and seminal fluid, the good tolerance, and the previously reported broad antibacterial spectrum suggest that gatifloxacin may be a good alternative for the treatment of CBP. Clinical studies need to be performed to confirm this assumption [72].

Rodvold and Neuhauser found that the characteristics of gatifloxacin include excellent oral bioavailability (90–99%), extensive penetration into tissues and body fluids, and an elimination half-life (6–12h) that allows for once-daily dosing in patients with normal renal function. Gatifloxacin is excreted primarily unchanged in the urine. The pharmacodynamic values that correlated with successful clinical and microbiologic outcomes, and which prevent the emergence of bacterial resistance, are ratios of maximum or peak unbound drug concentration (C_{max}) to minimum inhibitory concentration (MIC), and 24-h unbound area under the concentration curve ($AUC_{0-24\ h}$) to MIC. For Gram-negative infections, a C_{max}:MIC greater than or equal to 10, and an $AUC_{0-24\ h}$:MIC greater than or equal to 125, are associated with an increased probability of a successful outcome. For infections caused by *S. pneumoniae*, an $AUC_{0-24\ h}$:MIC of 30 or more was suggested for favorable clinical outcomes. Pharmacokinetic and pharmacodynamic values influence rational therapeutic decisions in the selection and dosages of these drugs [73].

Trampuz *et al*. assessed the pharmacokinetics of gatifloxacin in serum and in skin blister fluid (SBF) as well as the pharmacodynamic activity in SBF. Five hours after a single dose of gatifloxacin, gatifloxacin killed 2.5 logs of *S. pneumoniae* and 1.5 logs of *Staphylococcus aureus* during a 2-h incubation *ex vivo*. These findings suggest a potent bactericidal effect of gatifloxacin

against the test strains investigated, and a complete equilibration of the drug between serum and artificial inflammatory exudate. The killing of *S. pneumoniae* by gatifloxacin was significantly better in PMN-containing SBF samples than in centrifuged SBF samples without PMN. In contrast, the additive effect of PMN with gatifloxacin in the killing of *S. aureus* was observed only at the first sampling time point (1h), when the phagocytic bactericidal activity was more important than the antibiotic activity [74].

Boy *et al.* used an open randomized double-crossover to study 12 volunteers who received a single oral dose of gatifloxacin (400mg) or ciprofloxacin (500mg) to assess urinary bactericidal activity (in eight intervals up to 120h) and pharmacokinetic (PK) parameters (up to 36h). Plasma concentrations and urinary excretion were determined by HPLC with fluorescence detection, and urinary bactericidal titers (UBT; the highest twofold dilution (antibiotic-free urine as diluent) of urine still being bactericidal) by a microdilution method, using antibiotic-free urine of each volunteer. The mean maximum plasma concentration of gatifloxacin was 3.35mg/L, and that of ciprofloxacin was 2.12mg/L. The mean cumulative renal excretion of the parent drug was for gatifloxacin 81 (median=83)% of the administered dose within 120h and for ciprofloxacin 43 (median=45)%. The UBTs were determined for an *Escherichia coli* ATCC reference strain and nine clinical uropathogens with the following MICs (mg/L) for gatifloxacin/ciprofloxacin (microdilution, MHB): *E. coli* ATCC 25922 (0.008/0.008), *E. coli* 523 (0.06/0.06), *Klebsiella pneumoniae* 1058 (0.03/0.016), *Proteus mirabilis* 524 (0.125/0.016), *Pseudomonas aeruginosa* 561 (1/0.125); *Enterococcus faecalis* strains 60 and 55 (0.5/1 and 8/32); *S. aureus* strains 248 and 596 (both 0.03 and 0.125), and *Staphylococcus saprophyticus* Ho94 (0.125/0.25). The median UBTs measured within the first 6h for gatifloxacin were between 1:16 and 1:≥1024 for the Gram-negative strains and between 1:8 and 1:≥1024 for the five Gram-positive strains. The median UBTs for ciprofloxacin were between 1:64 and 1:≥1024 for the Gram-negative strains and between 1:1.5 and 1:768 for the five Gram-positive strains. The UBTs up to 12<0.05h showed no difference (P<0.05) for both *E. coli* strains, but ciprofloxacin was superior to gatifloxacin against *Klebsiella*, *Proteus*, and *Pseudomonas* strains, and gatifloxacin was superior to ciprofloxacin against all Gram-positive strains. For the UBTs at 12–24h, gatifloxacin was generally superior to ciprofloxacin but showed no difference in the *Proteus* and *Pseudomonas* strains. The areas under the UBT-time-curve (AUBT) up to 120h showed statistically significant differences between both quinolones in favor of gatifloxacin against 8 of 10 strains tested, no difference for *P. mirabilis* and significantly higher activity of ciprofloxacin against *P. aeruginosa*. It was concluded that gatifloxacin and ciprofloxacin had an overall comparable initial urinary bactericidal activity with some differences for specific pathogens, and this sometimes favored of gatifloxacin (usually

Gram-positives) and sometimes favored of ciprofloxacin (usually Gram-negatives). This suggested that for empiric therapy, a single oral dose of gatifloxacin (400 mg) would be clinically equivalent to ciprofloxacin (500 mg) taken twice daily, which is in agreement with the results of a clinical study in a complicated UTI performed previously [75].

Kikuchi *et al*. used bronchoscopic microsampling (BMS), making it possible to obtain multiple samples from bronchial ELE and bronchoalveolar lavage (BAL). This is an established technique for measuring antibiotic concentrations in the epithelial lining fluid (ELF) of the bronchiolar and alveolar regions, and for the analysis of the pharmacokinetics of gatifloxacin in bronchial ELF from healthy young adult subjects and adult patients with chronic bronchitis. Based on the findings of this study performed in small number of healthy young adult volunteers and patients with chronic bronchitis, BMS appears to be a promising method for measuring drug concentrations and determining the pharmacokinetic profile of gatifloxacin in bronchial ELE. Additional studies are needed to correlate measured concentrations obtained by BMS with clinical and/or microbiologic outcomes in larger populations [76].

Fish *et al*. investigated the steady-state pharmacokinetics of gatifloxacin in 20 adult patients in a medical Intensive Care Unit (ICU) using a prospective, open-label study. Twelve patients had normal or moderately impaired renal function (creatinine clearance ≥40 mL/min) and received gatifloxacin 400 mg intravenously once daily. Eight patients had creatinine clearance levels that were less than 40 mL/min and received 200 mg doses. Gatifloxacin plasma and urine concentrations were determined by a validated HPLC method. Mean gatifloxacin elimination half-lives ($t_{1/2}$), systemic clearance, and volume of distribution in patients with creatinine clearance levels that were less than 40 mL/min were 10.8±1.5 h, 156±29 mL/min, and 1.8±0.2 L/kg, respectively. Maximum and minimum serum concentrations and area under the serum concentration–time curve from 0 to 24 h (AUC_{0-24}) in these patients were 4.77±0.76 mg/L, 1.08±0.28 mg/L, and 44.4±9.2 mg h/L, respectively. Observed $t_{1/2}$, C_{max}, and AUC_{0-24} following 200 mg doses in patients with poor renal function (clearance levels <40 mL/min) were 18.2±3.3 h, 2.85±0.76 mg/L, and 36.6±3.4 mgh/L, respectively. Statistically significant ($P<0.05$) increases in AUC_{0-24} and decreases in $t_{1/2}$ and clearance (total and renal) were observed in ICU patients who were administered intravenous gatifloxacin compared with previous data in healthy volunteers. Pharmacodynamic evaluation by Monte Carlo simulation indicated that approved gatifloxacin dosage regimens appear to be adequate for most pathogens (MIC≤0.5 μg/mL) associated with community-acquired infections in severely ill ICU patients; less susceptible pathogens (MIC≥1 μg/mL) do not appear to be optimally treated with currently approved doses [77].

Rubino *et al*. evaluated the extent of gatifloxacin to examine the relationship between drug exposure and response to therapy in children with recurrent otitis media or early treatment failures of acute otitis media. The patient population included 187 patients from an open-label, multi-center, noncomparative study using gatifloxacin 10mg/kg once daily. Gatifloxacin exposure was estimated using a single steady-state blood sample in conjunction with a pharmacostatistical model developed using a separate pediatric data set. Gatifloxacin exposure was equivalent to that in adults given 400mg daily. Of the 41 patients who had *S. pneumoniae* from a middle ear culture, there were only three bacteriologic failures. Thus, there was no relationship between plasma AUC_{0-24}:MIC ratio and outcome. In conclusion, population pharmacokinetic/pharmacodynamic methods allowed the estimation of drug exposure using one sample per patient [78].

Raipuria *et al*. investigated the pharmacokinetics and urinary excretion of gatifloxacin after a single intravenous injection of 4mg/kg body weight in buffalo calves, where the therapeutic plasma drug concentration was maintained for up to 12h. Gatifloxacin rapidly distributed from blood to tissue compartments, which was evident from the high values of the distribution rate constant, α_1 ($11.1\pm1.06\,h^{-1}$), and the rate constant of transfer of drug from central to peripheral compartment, k_{12} ($6.29\pm0.46\,h^{-1}$). The area under the plasma drug concentration–time curve and apparent volume of distribution were 17.1 ± 0.63(μgh)/mL and 3.56 ± 0.95L/kg, respectively. The elimination half-life ($t_{1/2\beta}$), total body clearance, and the ratio of drug present in tissues and plasma were 10.4 ± 2.47h, 235.1 ± 8.47 mL/(kgh) and 10.1 ± 2.25, respectively. About 19.7% of the administered drug was excreted in urine within 24h. A satisfactory intravenous dosage regimen for gatifloxacin in buffalo calves would be 5.3mg/kg at 24h intervals [79].

Tasso *et al*. investigated gatifloxacin distribution into skeletal muscle and lung interstitial fluid by microdialysis and to correlate free tissue and free plasma levels of the drug. Microdialysis recoveries were determined *in vitro* by extraction efficiency and retrodialysis at 80, 160 and 400ng/mL, resulting in 33.5 ± 1.3%, 33.1 ± 1.2%, 31.8 ± 2.7%, 31.4 ± 2.6%, 33.1 ± 2.2%, 30.6 ± 3.3%, respectively. *In vivo* recovery by retrodialysis in Wistar rats' skeletal muscle and lung were 29.1 ± 1.0% and 30.7 ± 1.4%, respectively. The recovery was constant and independent on the method or media used. Gatifloxacin tissue penetration was investigated after intravenous dosing of 6mg/kg to Wistar rats. Free skeletal muscle, lung and plasma profiles were virtually superimposable, resulting in similar area under the curve (AUC_{0-9}) of 3888 ± 734, 4138 ± 1071, and 3805 ± 577(ngh)/mL, respectively. The tissue distribution factors were 1.02 and 1.08 for muscle and lung relative to plasma. It was concluded that free plasma levels are a good surrogate for gatifloxacin active levels at the infection site [80].

Shang-Rong *et al*. studied the pharmacokinetics of gatifloxacin in ocular cornea of rabbit after ocular instillation, where the eyes of 24 New England rabbits were topically applied with 501 gatifloxacin eye drops. Ocular corneas were sampled at different intervals after drug instillation, and the drug levels were assayed by HPLC. The pharmacokinetic parameters were evaluated by a DAS 1.0 process. The peak concentrations of gatifloxacin in cornea was (3.18±1.39)g/g, the half-lives of elimination was (2.33±0.58)h. The areas under the curve after 6h was (7.40±2.07)g/(hL). Blank cornea fluid did not interfere with the determination of gatifloxacin. It was concluded that gatifloxacin has a good pharmacokinetic character and permeability in rabbit ocular cornea [81].

Seiko *et al*. used pharmacokinetic/pharmacodynamic (PK/PD) principles to propose improved dosing regimens for various antimicrobial agents. In this study, they investigated the relationship between dosing interval and antibacterial efficacy in an *in vitro* PK model mimicking postoperative endophthalmitis. The *in vitro* PK model simulated the aqueous humor concentration following topical application of 0.3% gatifloxacin ophthalmic solution to rabbit eyes. An isolate of *E. faecalis* was exposed to gatifloxacin three times repeatedly at various intervals from 0 to 8h, and the area between the control growth curve and the bacterial killing and regrowth curve for 24h (ABBC) was used to evaluate efficacy. The ABBC showed a bell-shaped dependence on the dosing interval with a peak at 3h. Under limited condition of total exposure amount (i.e., the area under the concentration–time curve), the antimicrobial efficacy appears to be associated with the cumulative time of a 24-h period such that the concentration exceeds the MIC rather than the peak concentration:MIC ratio. The length of the T>MIC period during repeated dosing appears to be proportional to the decrease in efficacy of gatifloxacin against *E. faecalis*. A longer dosing interval, as long as T>MIC is continuous, would probably be more efficient at preventing postoperative enterococcal endophthalmitis. However, further investigation is necessary to explore whether this model is applicable to a variety of pathogens and drugs [82].

7.1.1. Absorption

Oral gatifloxacin is rapidly and extensively absorbed, with mean $T_{\max}$ values among various groups defined by age and gender ranging from 1.0 to 2.28h [83–91]. In subjects with normal renal and hepatic function, the mean concentration maximum ($C_{\max}$) after single oral doses of 400mg was 3.35–4.1mg/L [83–85]. Over an oral dose range of 100–600mg, $C_{\max}$ and AUC are increased in a linear and dose proportional manner [84]. Similar results were seen with an intravenous administration of 200–800 mg. The oral bioavailability of gatifloxacin was estimated to be 96% [89].

Bioequivalence between intravenous and oral formulations allows for comparable plasma concentrations at the same recommended dosage by

either route. The pharmacokinetics did not differ significantly after administration of oral gatifloxacin in a fasting state or after ingestion of a standard high fat meal or green tea [86]. In addition, concurrent administration of food or green tea does not have an effect on the absorption and bioavailability of the drug. The AUC was slightly reduced when gatifloxacin was coadministered with a light morning meal (14.5 vs. 12.7(mgh)/L, 12.4% decrease) or milk (14.2 vs. 12.0(mgh)/L, 15.5% decrease) [84]. These results suggest that the agent may be administered with or without food. Limited information is available regarding the plasma concentrations of gatifloxacin at steady state [84,88,90]. A pharmacokinetic study of gatifloxacin 300mg twice/day for 7 days predicted steady-state C_{max} and C_{min} values of 3.7 and 1.0mg/L, respectively [84]. In comparison, gatifloxacin administered intravenously 400mg once per day for 14 days resulted in steady-state C_{max} of 4.49mg/L [90]. The steady state was reached after 3 days of intravenous administration.

7.1.2. Distribution

The mean V/F of gatifloxacin was 1.98–2.31L/kg after single oral doses of 100–600mg. Serum protein binding is approximately 20% and appears to be independent of drug concentrations (range 0.29–2.0mg/L) [84]. Similar to other fluoroquinolones, gatifloxacin is widely distributed into various body fluids and tissues [70,4]. In nine healthy male volunteers who received a single oral dose of 400mg, the mean percentage of penetration into cantharidine-induced inflammatory fluid was 117% (range 103.7–138.5%) [12]. The mean penetration into prostatic and seminal fluids after a single dose of 400mg was 129% (range 105–172%) and 102% (range 81–121%), respectively. Gatifloxacin achieves higher concentrations in bone and lung tissues than in plasma [4]. Concentrations in saliva were 80% of serum concentrations after single oral doses of 200 and 400mg [91]. After oral doses of 100 and 200mg, concentrations in the mucosa of the middle ear, paranasal sinuses, and parotid gland ranged from undetectable to 1.11, 1.06–4.29, and 0.34–2.52μg/g, respectively. The penetration by gatifloxacin into CSF was evaluated in patients receiving single and multiple oral doses of 200mg [92]. Respective mean concentrations in CSF and serum at 3h after a single dose were 0.21±0.16 and 1.67±0.43mg/L, respectively (mean penetration 11%). After 200mg of gatifloxacin was administered twice per day for 3 days, respective CSF and serum concentrations were 0.82±0.31 and 2.47±0.96mg/L, respectively (mean penetration 35%).

7.2. Metabolism

Gatifloxacin undergoes minimal hepatic metabolism. After single doses of 100, 200, 400, and 600mg, the percentage of unchanged drug excreted in the urine within 72h was 82–88% [83]. Several studies using shorter collection periods (36h) documented high recoveries of unchanged drug in the urine [84–91]. Among four potential metabolites (M-1, M-2, M-3, M-4):

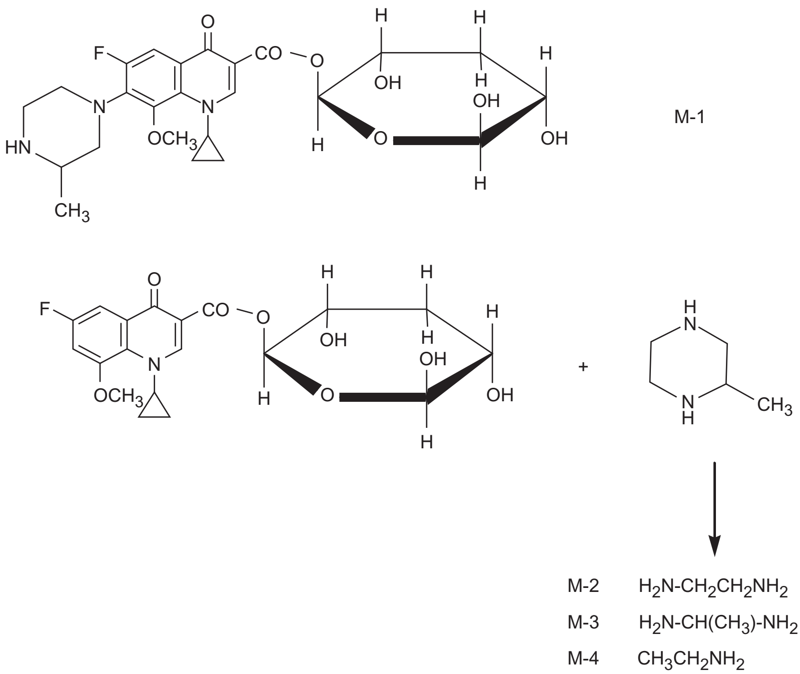

the 72-h cumulative urinary recoveries for M-2 and M-3 were 0.03% and 0.03%, respectively, while M-1 and M-4 were not detected. The 72-h cumulative fecal recovery of unchanged gatifloxacin was 5.7% after a single 400-mg dose. The mean elimination half-life of gatifloxacin in healthy subjects was 6.52–9.62 h after single doses [83]. The mean Cl/F was 183.2–247 mL/min [83,86,90,91]. The range of mean Clr in these studies was 110.5–202 mL/min. A decrease in Clr (and Cl/F) tends to occur at higher doses (400 and 600 mg) and suggests that tubular secretion contributes to the renal excretion of the drug. A single 1.5 g dose of probenecid prolonged the elimination half-life (7.10–10.2 h) and decreased Clr (197–122 mL/min), Cl/F (235–164 mL/min), and urinary recovery (83.4–74.9%) of gatifloxacin [84]. These effects indicate that active secretion contributes to the drug's renal elimination.

Tsuyoshi *et al.* investigated the metabolism of gatifloxacin in rats, rabbits, and dogs and identified unchanged drug, an ester-type glucuronide of gatifloxacin (M-1), and three metabolites possessing cleaved 3-methylpiperazinyl moiety, 3-ethylenediamine (M-2), 2-methylethylenediamine (M-3), and amino (M-4) forms in rat bile and urine collected after oral administration of gatifloxacin. In addition, the radioactivity excreted from the body amounted to 99.9%, 83.6%, and 70.5% of the dose up to 24 h following oral administration of ^{14}C-labeled gatifloxacin in rats, rabbits,

and dogs, respectively. The respective urine-to-feces excretion ratios of radioactivity were 34:66, 40:60, and 69:31. 3. Gatifloxacin accounted for about 90% of the total radioactive excreta in urine of rats, rabbits, and dogs. In addition, 3% of M-1, 1–2% of M-4, and 1% each of M-2 and M-3 were also detected. No marked species differences were found in the metabolic profiles of gatifloxacin in urine. Furthermore, most of the radioactivity in feces of these animals was unchanged gatifloxacin. One to two percent each of the total fecal radioactivity was also excreted as M-2, M-3, and M-4. 4. In bile-duct-cannulated rats, 96.1% of the total radioactivity was excreted from the body up to 24h following oral administration of ^{14}C-gatifloxacin. The excretion ratios of radioactivity in urine, bile, and feces were 41:45:14, respectively. In rat bile, 54% of M-1, 18% of gatifloxacin, and also small amounts of M-2, M-3 and M-4 were quantitated. Gatifloxacin and M-1 accounted for 82%, 91%, and 89% of the total radioactivity in urine and feces 24h following oral administration of ^{14}C-gatifloxacin in rats, rabbits, and dogs, respectively. Radioactivity in serum existed mostly as unchanged gatifloxacin following oral administration of ^{14}C-gatifloxacin in rats. The *in vitro* antibacterial activity of M-2, M-3, and M-4 against a number of reference strains was found to be 4–256 times less active than that of gatifloxacin [93].

8. PHARMACOLOGY

Gatifloxacin entered the United States pharmaceutical market in 2000 and is used to treat a broad array of Gram-positive and Gram-negative bacterial infections. The mechanism of gatifloxacin action involves inhibition of bacterial DNA gyrase, which is essential for DNA replication, and it has been proposed that metal complex intermediates are involved in this process. DNA gyrase is an essential bacterial enzyme that catalyzes the ATP-dependent negative super coiling of double-stranded closed-circular DNA. Gyrase belongs to a class of enzymes known as topoisomerases that are involved in the control of topological transitions of DNA. The mechanism by which gyrase is able to influence the topological state of DNA molecules is of inherent interest from an enzymological standpoint. In addition, much attention has been focused on DNA gyrase as the intracellular target of a number of antibacterial agents as a paradigm for other DNA topoisomerases [94]. It is believed that the methoxy group mediates the binding of the DNA–DNA gyrase complex to the DNA–topoisomerase complex and potentially decreases the likelihood of high-level resistance [95]. Gatifloxacin is a synthetic broad-spectrum antimicrobial fluoroquinolone active against both *Gram-negative* and *Gram-positive* organisms and is used in the treatment of a wide range of infections [96].

Naber *et al*. compared MICs of gatifloxacin with those of gemifloxacin, moxifloxacin, trovafloxacin, ciprofloxacin, and ofloxacin using an agar dilution method for 400 uropathogens cultured from the urine of urological patients with complicated and/or hospital-acquired urinary tract infections. The strain collection consisted of Enterobacteriaceae (34.5%), enterococci (31.5%), staphylococci (21.2%), and non-fermenting bacteria (12.8%). The antibacterial activity of the three newer fluoroquinolones (gatifloxacin, gemifloxacin, and moxifloxacin) was similar but showed some drug-specific differences. Gemifloxacin was most active against *E. coli* but less so against *P. mirabilis*. In this series, all isolates of *E. coli* were inhibited at a MIC of 0.25 mg/L gatifloxacin and moxifloxacin and by 0.125 mg/L gemifloxacin. The MIC distribution of all fluoroquinolones showed a bimodal distribution for staphylococci, enterococci, and *P. aeruginosa*. The two modes for *P. aeruginosa* were 1 and 64 mg/L for gemifloxacin and moxifloxacin, and 0.5 and 64 mg/L for gatifloxacin. For staphylococci, the two modes were 0.125 and 2 mg/L for gatifloxacin, 0.03 and 4 mg/L for gemifloxacin, and 0.03 and 2 mg/L for moxifloxacin. In addition, the two modes for enterococci were 0.25 and 16 mg/L for gatifloxacin, 0.06 and 2 mg/L for gemifloxacin, and 0.25 and 8 mg/L for moxifloxacin. Compared with trovafloxacin, the MIC values were similar, but the newer fluoroquinolones were more active than ciprofloxacin and ofloxacin against Gram-positive bacteria. Of the newer fluoroquinolones, gatifloxacin had the highest rate of renal excretion and could be considered a promising alternative fluoroquinolone agent for the treatment of urinary tract infections [97].

Yamada *et al*. learned that gatifloxacin can cause both hypoglycemia and hyperglycemia in both diabetic and nondiabetic patients. Gatifloxacin has recently been reported to stimulate insulin secretion by inhibition of ATP-sensitive K+ (KATP) channels in pancreatic β-cells. Gatifloxacin-induced hypoglycemia is associated with concomitant use of sulfonylureas and usually occurs immediately after administration of the drug. It was found that gatifloxacin acutely stimulates insulin secretion from mouse pancreatic islets, and that glibenclamide has additive effects on gatifloxacin-induced insulin secretion. However, gatifloxacin-induced hyperglycemia often takes several days to develop. It was also demonstrated that chronic gatifloxacin treatment decreases islet insulin content by inhibiting insulin biosynthesis and may be associated with gatifloxacin-induced hyperglycemia. Moreover, discontinuation of gatifloxacin results in improved insulin secretory response. These data clarify the differing mechanisms of gatifloxacin-induced hyperglycemia and hypoglycemia and suggest that blood glucose levels should be carefully monitored during gatifloxacin administration, especially in elderly patients with renal insufficiency, unrecognized diabetes, or other metabolic disorders. Because the risk of potentially life-threatening dysglycemia is

increased during gatifloxacin therapy, these findings have important implications for clinical practice [98].

Ge *et al*. demonstrated that since gatifloxacin modulates transcription and reduces the expression and function of GLUT1 gene in HepG2 cells, gatifloxacin may induce life-threatening dysglycemia. The facilitated glucose transporter type 1 (GLUT1) protein is ubiquitously expressed in many tissues. Disturbed GLUT1 protein function weakens the systemic glycemic control and may cause dysglycemia. In this study, it was found that treatment with gatifloxacin at concentrations of 3.4 μg/mL (8.4 μM) and 17 μg/mL (42 μM), GLUT1 promoter activity was stimulated by 2.8- and 3.8-fold, respectively. GLUT1 mRNA expression was decreased by 41% and 31%, and glucose uptake was decreased by 41% and 52%, respectively. These findings imply that disturbed GLUT1 gene expression and protein function may underlie the dysglycemic effect of gatifloxacin [99].

Drozak *et al*. described the action of gatifloxacin in isolated rabbit hepatocytes and kidney-cortex tubules by measuring the activity of gluconeogenesis, a process that maintains whole-body glucose homeostasis. The data showed that in kidney-cortex tubules, application of gatifloxacin at up to 100 μM was followed by a marked accumulation of the drug in the intracellular milieu and a decrease in the rate of glucose formation from pyruvate by 20–50%. Gatifloxacin did not affect the rate of gluconeogenesis from either alanine+glycerol+octanoate, or aspartate+glycerol+octanoate. At concentrations between 25 and 200 μM, the drug decreased mitochondrial oxygen consumption by 20–45% with pyruvate+malate and ADP. As in the case of α-cyano-4-hydroxycinnamate (a well-established inhibitor of the mitochondrial pyruvate transporter), gatifloxacin diminished pyruvate uptake by both renal and hepatic mitochondria. The inhibitory action of gatifloxacin was less pronounced in hepatocytes, whereas reduction in pyruvate-dependent glucose formation and mitochondrial respiration was by no more than 25%. The antibiotic did not influence mitochondrial oxygen consumption with glutamate+malate in either kidney-cortex or liver mitochondria. A differential substrate dependence of gatifloxacin action on gluconeogenesis and mitochondrial respiration combined with a decrease in pyruvate uptake by mitochondria suggests that the inhibitory action of this drug on gluconeogenesis might result from its impairment of pyruvate transport into mitochondria [100].

Bharal *et al*. assessed the neurological and neurobehavioral effects of gatifloxacin after its oral administration in two doses (25 and 50 mg/kg for 7 and 14 days) in mice. The neurobehavioral parameters used for the short-term 7-day study were pentylenetetrazole-induced seizure, forced swim test, elevated plus-maze, spontaneous alternation behavior, and rotarod tests. However, only pentylenetetrazole-induced seizure and rotarod tests were performed in long-term 14-day study. The results showed a proconvulsant effect of gatifloxacin (50 mg/kg) in

pentylenetetrazole-induced seizure test after both short- and long-term administration studies, and in both doses showed an anxiogenic effect. However, in both doses, gatifloxacin did not show any effect on memory and mood, and the drug did not show any effect in alternation behavior and forced swim tests. In the long-term study, gatifloxacin in 50 mg/kg, p. o. produced a grip impairing effect only after 14 days of administration. These results reveal that gatifloxacin possesses proconvulsant and anxiogenic effects, but it does not have an effect on mood and memory. The long-term administration of gatifloxacin for 14 days reduced grip strength and impairment of movement in mice [101].

Riahi *et al*. attempted to gain a better understanding of the physicochemical interaction between a novel anticancer drug, gatifloxacin, and DNA. Considering the physicochemical properties of the drug, as well as the mechanism by which it interacts with DNA, one should eventually be able to conduct a rational design of novel anticancer or antiviral drugs. Molecular modeling of the complex formed between gatifloxacin and DNA presented the full ability of the drug to participate in formation of a stable intercalation site. The molecular geometries of gatifloxacin and the DNA bases (adenine, guanine, cytosine, and thymine) were optimized with the aid of the B3LYP/6-31G method. The properties of the isolated intercalator site and its stacking interactions with the adenine/thymine (AT) and guanine/cytosine (GC) base pairs were studied using the DFTB method (an approximate version of the DFT method that was extended to cover the London dispersion energy). The B3LYP/6-31G stabilization energies were found to be -26.99 kcal/mol for the AT-gatifloxacin intercalator and -37.62 kcal/mol for the GC-gatifloxacin intercalator. It was concluded that the dispersion energy and the electrostatic interaction contributed to the stability of the intercalator/DNA base pair complexes [102].

REFERENCES

[1] G.Y. Lesher, E.D. Froelich, M.D. Gruet, J.H. Bailey, R.P. Brundage, 1,8-Naphthyridine derivatives. A new class of chemotherapeutic agents, J. Med. Pharm. Chem. 5 (1962) 1063–1068.

[2] M. Vinicius, N. Souza, Promising current drug candidates in clinical trials and natural products against multidrug-resistant tuberculosis, in: I. Ahmed, F. Aqil (Eds.), New Strategies Combating Bacterial Infection, Wiley-VCH verlag GmbH & Co. KGaA, Weinheim, 2009, pp. 75–76.

[3] L. Mingliang, G. Huiyuan, New developments in the study of structural modification and pharmacological activity of quinolones, Zhongguo Kangshengsu Zazhi 34 (Suppl.) (2009) 51–59.

[4] D.N. Fish, D.S. North, Gatifloxacin, an advanced 8-methoxy fluoroquinolone, Pharmacotherapy 21 (2001) 35–59.

[5] Tuberculosis, Handbook of Anti-Tuberculosis Agents **Gatifloxacin**Vol. 88, 2008, pp. 109–111 Issue 2, (March 2008).
[6] http://www.drugbank.ca/search/search?query=Gatifloxacin Drug bank, 4/10/2010 at 11:30 am.
[7] S. Budavari, M.J. O'Neil, P.E. Heckelman, C.B. Koch, K.J. Roman, C.M. Kenny, M.R. D'Arecca (Eds.), The Merck Index, 14th ed., Merck & Co.,Inc., White House Station,NJ, 2006 p. 753.
[8] Sean C. Sweetman (Ed.), Martindale: The Complete Drug Referance, 33rd ed., Pharmaceutical Press, London, 2002, pp. 209–210.
[9] United State Pharmacopoeia, 32rd ed., United State Pharmaceutical Conversion, Inc., Rockville, MD, 2010.
[10] S. Greta, N. Valerie, D. Ben-Zion, P. Gideon, Synthesis of Gatifloxacin, (2004) U.S. Patent No. 4,890,470 (cf. European Patent 230,295), 2495271 A.
[11] N. Valerie, D. Ben-Zion, P. Gideon, S. Greta, Novel synthesis of Gatifloxacin, (2007) US Patent No. 2007,0072868 A1.
[12] R. Milos, R. Milenka, T. Zdenka, M. Mirjana, Process for the preparation of gatifloxacin and regeneration of degradation products, (2006) PATENTNA PISARNA D.O.O.; Copova 14, POB 1725, 1001 Ljubljana (SI). Pup. No. WO/2006/004561.
[13] L. Shiming, Q.Z. Zhenfu, L.S. Youguang, Process improvement of synthesis of gatifloxacin, Jingxi Huagong Zhongjianti 39 (5) (2009) 37–40.
[14] F.J. Villasante, L. Gude, S.P. Fernndez, O. Alonso, E. Garca, A. Cosme, A high-throughput impurity-free process for gatifloxacin, Org. Process Res. Dev. 12 (5) (2008) 900–903.
[15] K. Ilango, P. Valentina, K.S. Lakshmi, A. Canhea, S.R. Abraham, V.B. Raju, A.K. Kumar, Indian J. Pharm. Sci. 68 (2006) 273–275.
[16] L.I. Ze-Quan, W.U. Feng-Jing, G. Yun, H.U. Chang-Wen, Z. Yun-Huai, G. Meng-Yu, Synthesis, characterization and activity against Staphylococcus of metal(II)-gatifloxacin complexes, Chin. J. Chem. 25 (12) (2007) 1809–1814.
[17] A. Sivalakshmidevi, K. Vyas, G. Om Reddy, Sprafloxacin, an antibacterial drug, Acta Crystallogr. C 56 (2000) e115–e116.
[18] I. Turel, P. Bukovec, M. Quirós, Crystal structure of ciprofloxacin hexahydrate and its characterization, Int. J. Pharm. 152 (1997) 59–65.
[19] M. Parvez, M.S. Arayne, N. Sultana, A.Z. Siddiqi, Pefloxacinium methanesulfonate 0.10-hydrate, Acta Cryst. C56 (2000) 910–912.
[20] N. Sultana, A. Naz, M.S. Arayne, M.A. Mesaik, Synthesis, characterization, antibacterial, antifungal and immunomodulating activities of gatifloxacin–metal complexes, J. Mol. Struct. 969 (1–3) (2010) 17–24.
[21] H.R.N. Marona, C.C.G.O. Lopes, S.G. Cardoso, Non-aqueous titration of gatifloxacin in pharmaceutical formulations using perchloric acid, Lat. Am. J. Pharm. 22 (4) (2003) 339–342.
[22] S.M. Al- Ghannam, Atomic absorption spectroscopic, conductometric and colorimetric methods for determination of some fluoroquinolone antibacterials using ammonium reineckate, Spectrochim. Acta A 69 (2008) 1188–1194.
[23] K. Ilango, P. Valentina, K.S. Lakshmi, C. Arvind, A.S. Rachel, R.V. Bhaskar, K.A. Kiran, UV spectroscopic and colorimetric methods for the estimation of Gatifloxacin in tablet dosage forms, Indian J. Pharm. Sci. 68 (2) (2006) 273–275.
[24] P.U. Patel, B.N. Suhagia, C.N. Patel, M.M. Patel, G.C. Patel, G.M. Patel, Simultaneous spectrophotometric estimation of gatifloxacin and ornidazole in mixture, Indian J. Pharm. Sci. 67 (3) (2005) 356–357.
[25] K. Venugopal, R.N. Saha, New, simple and validated UV-spectrophotometric methods for the estimation of gatifloxacin in bulk and formulations, Il Farmaco 60 (2005) 906–912.
[26] A. Mali, R. Dhavale, V. Mohite, A. Mahindrakar, Y. Pore, B. Kuchekar, Spectrophotometric estimation of Gatifloxacin in tablets, Indian J. Pharm. Sci. 68 (3) (2006) 386–387.

[27] S. Paramane, L. Kothapalli, A. Thomas, A.D. Deshpande, Simultaneous spectrophotometric estimation of gatifloxacin and ornidazole in tablet dosage form, Indian J. Pharm. Sci. 68 (6) (2006) 819–821.
[28] L. Sivasubramanian, A. Muthukumaran, Spectrophotometric determination of gatifloxacin in pharmaceutical formulations and biological samples, Indian J. Pharm. Sci. 68 (5) (2006) 672–675.
[29] A.S. Amin, A.A. Gouda, R. El-Sheikh, F. Zahran, Spectrophotometric determination of gatifloxacin in pure form and in pharmaceutical formulation, Spectrochim. Acta A 67 (5) (2007) 1306–1312.
[30] L. Zhang, X. Dong, W. Hu, X. Wang, M. Jiao, Ultraviolet characteristic of alizarin red-gatifloxacin and determination of gatifloxacin, Huaxue Yanjiu 20 (4) (2009) 91–94.
[31] P.K. Jain, A. Thakur, A. Jain, A. Modi, R.K. Maheshwari, New spectrophotometric method for the estimation of gatifloxacin in tablets using N, N-dimethylurea as hydrotropic agent, J. Global Pharma Technol. 2 (3) (2010) 117–119.
[32] D. Madhuri, K.B. Chandraekhar, G. Somasekhar, K. Harinadhababa, M. Ramkotiah, B. Dhandapani, Spectrophotometric determination of Gatifloxacin through complexation with surfactant, Int. J. Pharma Sci. Res. (IJPSR) 1 (2) (2010) 84–89.
[33] M. Gandhimathi, T.K. Ravi, J.V. Susheel, Analysis of gatifloxacin in tablet dosage form, Indian J. Pharm. Sci. 67 (6) (2005) 759–762.
[34] J.A. Ocaña, F.J. Barragán, M. Callejón, Spectrofluorimetric and micelle-enhanced spectrofluorimetric determination of gatifloxacin in human urine and serum, J. Pharm. Biomed. Anal. 37 (2005) 327–332.
[35] X. Zhu, A. Gong, S. Yu, Fluorescence probe enhanced spectrofluorimetric method for the determination of gatifloxacin in pharmaceutical formulations and biological fluids, Spectrochim. Acta A 69 (2008) 478–482.
[36] C. Guo, P. Dong, Z. Chu, L. Wang, W. Jiang, Rapid determination of gatifloxacin in biological samples and pharmaceutical products using europium-sensitized fluorescence spectrophotometry fluorescence spectrophotometry, Luminescence 23 (1) (2008) 7–13.
[37] L. Fu, Measurements of gatifloxacin with a technique of energy transfer fluorescence quenching, J. Mol. Sci. Int. Ed. 25 (6) (2009) 407–410.
[38] H. Wu, G. Zhao, L. Du, Determination of ofloxacin and gatifloxacin by mixed micelle-mediated cloud point extraction-fluorimetry combined methodology, Spectrochim. Acta A 75 (2010) 1624–1628.
[39] I.A. Darwish, M.A. Sultan, H.A. Al-Arfaj, Selective kinetic spectrophotometric method for determination of Gatifloxacin based on formation of its N-vinyl chlorobenzoquinone derivative, Spectrochim. Acta A 75 (2010) 334–339.
[40] H.R.N. Salgado, C.C.G.O. Lopes, M.B.B. Lucchesi, Microbiological assay for gatifloxacin in pharmaceutical formulations, J. Pharm. Biomed. Anal. 40 (2006) 443–446.
[41] N.T. Abdel Ghani, M.A. El-Ries, M.A. El-Shall, Validated polarographic methods for the determination of certain antibacterial drugs, Anal. Sci. 23 (9) (2007) 1053–1058.
[42] H.S. El-Desoky, Stability indicating square-wave stripping voltammetric method for determination of gatifloxacin in pharmaceutical formulation and human blood. J. Braz. Chem. Soc. 20 (10) (2009). doi:10.1590/S0103-50532009001000004 São Paulo.
[43] S.K. Motwani, R.K. Khar, F.J. Ahmad, S. Chopra, K. Kohli, S. Talegaonkar, Z. Iqbal, Stability indicating high-performance thin-layer chromatographic determination of gatifloxacin as bulk drug and from polymeric nanoparticles, Anal. Chim. Acta 576 (2) (2006) 253–260.
[44] K. Vishwanathan, M.G. Bartlett, J.T. Stewart, Determination of gatifloxacin in human plasma by liquid chromatography/ electrospray tandem mass spectrometry, Rapid Commun. Mass Spectrom. 15 (12) (2001) 915–919.

[45] H.A. Nguyen, J. Grellet, B. BaB, C. Quentin, M.C. Saux, Simultaneous determination of levofloxacin, gatifloxacin and moxifloxacin in serum by liquid chromatography with column switching, J. Chromatogr. B 810 (2004) 77–83.
[46] H. Liang, M.B. Kays, K.M. Sowinski, Separation of evofloxacin, ciprofloxacin, gatifloxacin, moxifloxacin, trovafloxacin and cinoxacin by high-performance liquid chromatography: application to levofloxacin determination in human plasma, J. Chromatogr. B 772 (2002) 53–63.
[47] B.R. Overholser, M.B. Kays, K.M. Sowinski, Determination of gatifloxacin in human serum and urine by high-performance liquid chromatography with ultraviolet detection, J. Chromatogr. B 798 (2003) 167–173.
[48] S. Al-Dgither, S.N. Alvi, M.M. Hammami, Development and validation of an HPLC method for the determination of Gatifloxacin stability in human plasma, J. Pharm. Biomed. Anal. 41 (2006) 251–255.
[49] M.R.M. Santoro, N.M. Kassab, A.K. Singh, E.R.M. Kedor-Hackmam, Quantitative determination of gatifloxacin, levofloxacin, lomefloxacin and pefloxacin fluoroquinolonic antibiotics in pharmaceutical preparations by high-performance liquid chromatography, J. Pharm. Biomed. Anal. 40 (2006) 179–184.
[50] N. Sultana, M.S. Arayne, A. Naza, Development and validation of an HPLC-UV method for the determination of Gatifloxacin in bulk material, pharmaceutical formulations, human plasma and metal complexes, Pak. J. Pharm. Sci. 19 (4) (2006) 269–275.
[51] L. Tasso, T. Dalla Costa, High performance liquid chromatography for quantification of gatifloxacin in rat plasma following automated on-line solid phase extraction, J. Pharm. Biomed. Anal. 44 (1) (2007) 205–210 Epub 2007 February 25.
[52] Z. Jia, T. Bingwen, Z. Hongbing, Y. Zemin, Y. Aiqun, Determine the contents of s-gatifloxacin by hplc, Jiepouxue Yanjiu 31 (6) (2009) 453–454.
[53] A.B. Patel, N.J. Shah, N.M. Patel, Development and validation of HPLC method for the simultaneous estimation of satranidazole and gatifloxacin tablet dosage form International, J. ChemTech Res. 1 (3) (2009) 587–590.
[54] T. Lan, W. Guofang, G. Yi, L. Tiegang, Determination of gatifloxacin in gatifloxacin hydrochloride tablets by HPLC, Hebei Yike Daxue Xuebao 30 (5) (2009) 495–497.
[55] N. Ramakrishna, K. Srinivasulu, V. Saritha, L. Bujjibabu, K. Vishwottam, M. Koteshwara, V. Hima Bindu, High-performance liquid chromatographic method for the separation of enantiomeric, J. Chromatogr. Sci. 48 (2) (2010) 100–103.
[56] B. Zhu, S.j Jiang, C.Q. Hu, Determination of gatifloxacin by high performance capillary electrophoresis, Chin. J. Pharm. Anal. (2002–2005) 1 (Abstract).
[57] R.T. Sane, S. Menon, A.R. Pathak, A.Y. Deshpande, M. Mahale, Capillary electrophoretic determination of gatifloxacin from pharmaceutical preparation, Chromatographia 61 (5/6) (2005) 303–306.
[58] H. Lü, X. Wu, C. Xu, Z.X. Lin, L. Guo, C. Yan, G. Chen, Separation and determination of seven fluoroquinolones by pressurized capillary electro-chromatography, J. Sep. Sci. 28 (16) (2005) 2210–2217.
[59] S. Zhou, J. Ouyang, W.R. Baeyens, H. Zhao, Y. Yang, Chiral separation of four fluoroquinolone compounds using capillary electrophoresis with hydroxypropyl-beta-cyclodextrin as chiral selector, J. Chromatogr. A 1130 (2) (2006) 296–301.
[60] Z. Yao, H. Zhang, Y. Wu, H. Guo, Determination of the binding constant of bovine serum albumin and gatifloxacin using affinity capillary electrophoresis, Se Pu 25 (6) (2007) 930–933.
[61] H.-W. Sun, P. He, Y.-K. Lv, S.-X. Liang, Effective separation and simultaneous determination of seven fluoroquinolones by capillary electrophoresis with diode-array detector, J. Chromatogr. B 852 (1–2) (2007) 145–151.
[62] A.F. Faria, M.V.N. de Souza, M.A.L. de Oliveira, Validation of a capillary zone electrophoresis method for the determination of ciprofloxacin, gatifloxacin, moxifloxacin and

ofloxacin in pharmaceutical formulations. J. Braz. Chem. Soc. [Online] 0103-505319 (3) (2008) 389–396, doi:10.1590/S0103-50532008000300004.

[63] A.A. El-Bary, I.I. Soliman, M.F.M. Ali, T.Y.A. El-Wahed, S.F. El-Menshawee, The photostability study of gatifloxacin under stressed conditions, J. Med. Res. Inst. 26 (2) (2005) 128–136.

[64] M.L. Devi, K.B. Chandrasekhar, A validated, specific, stability-indicating RP-LC method for analysis of gatifloxacin in the presence of degradation products and process-related impurities, Chromatographia 69 (9/10) (2009) 985–992.

[65] H.S. El-Desoky, Stability indicating square-wave stripping voltammetric method for determination of gatifloxacin in pharmaceutical formulation and human blood, J. Braz. Chem. Soc. 20 (10) (2009) 1790–1799.

[66] L.K. Ge, J.W. Chen, S.Y. Zhang, X.Y. Cai, Z. Wang, C.L. Wang, Photodegradation of fluoroquinolone antibiotic gatifloxacin in aqueous solutions. Chin. Sci. Bull. 55 (2010) 1495−1500–1495−1500, doi:10.1007/s11434-010-3139-y.

[67] L. Ge, J. Chen, X. Wei, S. Zhang, X. Qiao, X. Cai, Q. Xie, Aquatic photochemistry of fluoroquinolone antibiotics: kinetics, pathways, and multivariate effects of main water constituents, Environ. Sci. Technol. 44 (7) (2010) 2400–2405.

[68] C.M. Perry, D. Ormrod, M. Hurst, S.V. Onrust, Gatifloxacin: a review of its use in the management of bacterial infections, Drugs 62 (1) (2002) 169–207.

[69] S. Lober, S. Ziege, M. Rau, G. Schreiber, A. Mignot, P. Koeppe, H. Lode, Pharmacokinetics of gatifloxacin and interaction with an antacid containing aluminum and magnesium, Antimicrob. Agents Chemother. 43 (1999) 1067–1071.

[70] R. Wise, J.M. Andrews, J.P. Ashby, J. Marshall, A study to determine the pharmacokinetics and inflammatory fluid penetration of gatifloxacin following a single oral dose, J. Antimicrob. Chemother. 44 (1999) 701–704.

[71] Y. Niki, K. Hashiguchi, N. Miyashita, M. Nakajima, T. Matsushima, Influence of gatifloxacin, a new quinolone antibacterial, on pharmacokinetics of theophylline, J. Infect. Chemother. 5 (3) (1999) 156–162.

[72] C.K. Naber, M.A. Steghafner, M. Kinzig-Schippers, C. Sauber, F. So¨rgel, H.-J. Stahlberg, K.G. Naber, Concentrations of gatifloxacin in plasma and urine and penetration into prostatic and seminal fluid, ejaculate, and sperm cells after single oral administrations of 400 milligrams to volunteers, Antimicrob. Agents Chemother. 45 (1) (2001) 293–297.

[73] K.A. Rodvold, M. Neuhauser, Pharmacokinetics and pharmacodynamics of fluoroquinolones, Pharmacotherapy 21 (10 Pt. 2) (2001) 233S–252S.

[74] A. Trampuz, G. Laifer, M. Wenk, Z. Rajacic, W. Zimmerli, Pharmacokinetics and pharmacodynamics of gatifloxacin against *Streptococcus pneumoniae* and *Staphylococcus aureus* in a granulocyte-rich exudate, Antimicrob. Agents Chemother. 46 (11) (2002) 3630–3633.

[75] D. Boy, M. Well, M. Kinzig-Schippers, F. Sörgel, D. Ankel-Fuchs, K.G. Naber, Urinary bactericidal activity, urinary excretion and plasma concentrations of gatifloxacin (400 mg) versus ciprofloxacin (500 mg) in healthy volunteers after a single oral dose, Int. J. Antimicrob. Agents 23 (Suppl. 1) (2004) S6–16.

[76] Junko Kikuchi, Koichi Yamazaki, Eiki Kikuchi, Akitoshi Ishizaka, Masaharu Nishimura, Pharmacokinetics of gatifloxacin after a single oral dose in healthy young adult subjects and adult patients with chronic bronchitis, with a comparison of drug concentrations obtained by bronchoscopic microsampling and bronchoalveolar lavage, Clin. Ther. 29 (1) (2007) 123–130.

[77] D.N. Fish, Evaluation of gatifloxacin pharmacokinetics and pharmacodynamics in severely ill adults in a medical Intensive Care Unit, Int. J. Antimicrob. Agents 29 (2007) 715–723.

[78] C.M. Rubino, P. Ambrose, B. Cirincione, A. Arguedas, L. Sher, E. Lopez, S.X. Llorens, D.M. Grasela, Pharmacokinetics and pharmacodynamics of gatifloxacin in children

with recurrent otitis media: application of sparse sampling in clinical development, Diagn. Microbiol. Infect. Dis. 59 (2007) 67–74.
[79] M. Raipuria, V.K. Dumka, H.S. Sandhu, Plasma concentrations, pharmacokinetics and urinary excretion of gatifloxacin after single intravenous injection in buffalo calves, Vet. Res. Commun. 31 (8) (2007) 1013–1020.
[80] L. Tasso, C.C. Bettoni, L.K. Oliveira, T.D. Costa, Evaluation of gatifloxacin penetration into skeletal muscle and lung by microdialysis in rats Int, J. Pharm. 358 (2008) 96–101.
[81] Z. Shang-rong, W. Yan-dong, D. Xia-wei, Pharmacokinetics of gatifloxacin in ocular cornea of rabbit, Jinri Yaoxue 19 (8) (2009) 13–15.
[82] K. Seiko, W. Tomoyuki, K. Tetsuo, T. Tetsuya, S. Hideyuki, O. Akira, Effect of dosing interval on the efficacy of topical ophthalmic gatifloxacin against Enterococcus faecalis in an in vitro pharmacokinetic model simulating the local eye compartment, Int. J. Antimicrob. Agents 34 (6) (2009) 561–565.
[83] A. Lubasch, I. Keller, K. Borner, P. Koeppe, H. Lode, Comparative pharmacokinetics of ciprofloxacin, gatifloxacin, grepafloxacin, levofloxacin, trovafloxacin, and moxifloxacin after single oral administration in healthy volunteers, Antimicrob. Agents Chemother. 44 (2000) 2600–2603.
[84] M. Nakashima, T. Uematsu, K. Kosuge, H. Kusajima, T. Ooie, Y. Masuda, R. Ishida, H. Uchida, Single- and multiple-dose pharmacokinetics of AM-155, a new 6-fluoro-8-methoxy quinolone in humans, Antimicrob. Agents Chemother. 39 (12) (1995) 2635–2640.
[85] H.J. Stahlberge, K. Goehler, M. Guillaume, A. Mignot, Single dose pharmacokinetics of the R- and S-enantiomers of gatifloxacin in volunteers, Drugs 58 (suppl 2) (1999) 222–224.
[86] F. LaCreta, G. Kollia, G. Duncan, D. Behr, R. Stoltz, D. Grasela, Effect of a high-fat meal on the bioavailability of gatifloxacin in healthy volunteers [abstr], in: Program and Abstracts of the 38th Interscience Conference on Antimicrobial Agents and Chemotherapy, San Diego, 1998.
[87] D.A. Gajjar, F.P. LaCreta, G.D. Kollia, R.R. Stolz, S. Berger, W.B. Smith, M. Swingle, D.M. Grasela, Effect of multipledose gatifloxacin or ciprofloxacin on glucose homeostasis and insulin production in patients with noninsulin-dependent diabetes mellitus maintained with diet and exercise, Pharmacotherapy 20 (6 Pt. 2) (2000) 76S–86.
[88] F.P. LaCreta, G.D. Kollia, G. Duncan, D. Behr, D. Grasela, Age and gender effects on the pharmacokinetics of gatifloxacin, Pharmacotherapy 20 (6 Pt 2) (2000) 67S–75.
[89] F.P. LaCreta, S. Kaul, G.D. Kollia, G. Duncan, D.M. Randall, D.M. Grasela, Interchangeability of 400-mg intravenous and oral gatifloxacin in healthy adults, Pharmacotherapy 20 (6 Pt. 2) (2000) 59S–66.
[90] D.A. Gajjar, F.P. LaCreta, H.D. Uderman, G.D. Kollia, G. Duncan, M.J. Birkhofer, D.M. Grasela, A dose-escalation study of the safety, tolerability, and pharmacokinetics of intravenous gatifloxacin in healthy adult men, Pharmacotherapy 20 (6 Pt. 2) (2000) 49S–58.
[91] D.M. Grasela, B. Christofalo, G.D. Kollia, G. Duncan, R. Noveck, J.A. Manning Jr., F. P. LaCreta, Safety and pharmacokinetics of a single oral dose of gatifloxacin in patients with moderate to severe hepatic impairment, Pharmacotherapy 20 (6 Pt. 2) (2000) 87S–94.
[92] K. Motoshi, H. Hiroshi, K. Toshihiro, M. Shin'ichi, D. Yamauchi, N. Yasuhiko, M. Shinji, U. Yosuke, O. Yoshitada, Pharmacokinetic study of gatifloxacin: penetration into cerebrospinal fluid [abstr], Jap. J. Chemother. 47 (1340–7007) (1999) 248–252.
[93] O. Tsuyoshi, H. Hideo, T. Yoko, K. Masakatsu, T. Fukutaro, O. Hideo, Structural elucidation and quantification of metabolites of gatifloxacin a new quinolone, in rats, rabbits, and dogs, Jap. J. Chemother. 47 (Suppl. 2) (1999) 147–160.

[94] I.R.J. Reece, A. Maxwell, DNA gyrase structure and function, Crit. Rev. Biochem. Mol. Biol. 26 (1991) 335–375.
[95] D.M. Grasela, Clinical pharmacology of gatifloxacin a new fluoroquinolone, Clin. Infect. Dis. 31 (2000) S51–S58.
[96] J.M. Blondeau, R. Laskowski, J. Bjarnason, C. Stewart, Comparative in vitro activity of gatifloxacin, grepafloxacin, levofloxacin, moxifloxacin and trovafloxacin against 4151 Gram-negative and Gram-positive organisms, Int. J. Antimicrob. Agents 14 (2000) 45–50.
[97] K.G. Naber, K. Hollauer, D. Kirchbauer, W. Witte, In vitro activity of gatifloxacin compared with gemifloxacin, moxifloxacin, trovafloxacin, ciprofloxacin and ofloxacin against uropathogens cultured from patients with complicated urinary tract infections, Int. J. Antimicrob. Agents 16 (2000) 239–243.
[98] C. Yamada, K. Nagashima, A. Takahashi, H. Ueno, Y. Kawasaki, Y. Yamada, Y. Seino, N. Inagaki, Gatifloxacin acutely stimulates insulin secretion and chronically suppresses insulin biosynthesis, Eur. J. Pharmacol. 553 (2006) 67–72.
[99] T.-F. Ge, P.Y.P. Law, H.Y. Wong, Y.-Y. Ho, Gatifloxacin affects GLUT1 gene expression and disturbs glucose homeostasis in vitro, Eur. J. Pharmacol 573 (2007) 70–74.
[100] J. Drozak, A. Miecznik, R. Jarzyna, J. Bryla, The inhibition of gluconeogenesis by gatifloxacin may contribute to its hypoglycaemic action, Eur. J. Pharmacol. 594 (2008) 39–43.
[101] N. Bharal, S. Gupta, S. Khurana, P.K. Mediratta, K.K. Sharma, Anxiogenic and proconvulsant effect of gatifloxacin in mice, Eur. J. Pharmacol. 580 (2008) 130–134.
[102] S. Riahi, M.R. Ganjali, M. Bagheri, Theoretical investigation of interaction between gatifloxacin and DNA: implications for anticancer drug design, Mater. Sci. Eng. C 29 (2009) 1808–1813.

CHAPTER 6

Lamotrigine

Kevin Beattie, Geeta Phadke, and **Jasmina Novakovic**

Contents

Apotex Inc., Toronto, Ontario, Canada

Profiles of Drug Substances, Excipients, and Related Methodology, Volume 37
ISSN 1871-5125, DOI: 10.1016/B978-0-12-397220-0.00006-4

© 2012 Elsevier Inc.
All rights reserved.

1. PHYSICAL PROFILE

1.1. General information

1.1.1. Nomenclature

1.1.1.1. Systematic chemical names 6-(2,3-Dichlorophenyl)-1,2,4-triazine-3,5-diamine

3,5-Diamino-6-(2,3-dichlorophenyl)-1,2,4-triazine

1.1.1.2. Nonproprietary names Lamotrigine

1.1.1.3. Proprietary names Lamictal®, LTG, BW-430C [1]

1.1.2. Formula

1.1.2.1. Empirical formula, molecular weight, CAS number Empirical formula: $C_9H_7Cl_2N_5$, MW: 256.09, CAS# 84057-84-1 [1]

1.1.2.2. Structural formula

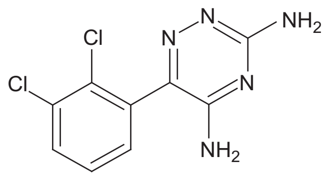

1.1.3. Elemental analysis

C 42.21%, H 2.76%, Cl 27.69%, N 27.35% [1]

1.1.4. Appearance

White to pale cream-colored powder [1]

1.2. Physical characteristics

1.2.1. Ionization constants

p*K*a=5.7 [1–3]

1.2.2. Solubility characteristics

The solubility of Lamotrigine in water is reported to be 0.17 mg/mL at 25 °C and 0.57 mg/mL at 37 °C [1,4]. Under these conditions, Lamotrigine, in terms of United States Pharmacopeia (USP) solubility, can be considered as being very slightly soluble. Lamotrigine is slightly soluble in anhydrous ethanol [5].

An aqueous solubility profile for Lamotrigine at room temperature throughout the physiological pH range is pH dependent (Table 6.1).

In acidic media, Lamotrigine is protonated. Its solubility reaches its maximum (about 5 mg/mL) at pH 2.5 and decreases rapidly with increasing pH. The minimum solubility of Lamotrigine is found to be about 0.1 mg/mL in pH 7.4 phosphate buffer.

The solubility of Lamotrigine in water at 25 °C is increased by 205% when present as a 1:1 inclusion complex with β-cyclodextrin. Solid dispersions of Lamotrigine:polyvinyl pyrrolidone K30 (ranging from 1:1 to 1.5) ratios increase solubility of Lamotrigine from 144% to 635%. Solid dispersions with polyethylene glycol 6000 also increase solubility to a lesser extent, that is, up to 68% [6]. Enhancement of the solubility of

TABLE 6.1 Aqueous solubility of Lamotrigine (pH=1–7.4)

Aqueous medium*	Solubility (mg/mL)
0.1 N HCl	2.217
0.01 N HCl	2.654
SGF	1.881
pH 2.5 buffer	5.473
pH 3.5 buffer	0.7692
pH 4.5 buffer	0.4272
pH 5.5 buffer	0.2724
pH 6.0 buffer	0.1914
pH 6.8 buffer	0.1452
pH 7.2 buffer	0.1474
pH 7.4 buffer	0.1355

* "Buffer" refers to 0.05 M potassium phosphate at the indicated pH value.

Lamotrigine at 298K has also been reported in various binary solvent mixtures, such as *N*-methyl-2-pyrrolidone/water [7], ethanol/water [8], and propylene glycol/water+carboxymethylcellulose [9].

1.2.3. Partition coefficients

The Log *P* of Lamotrigine is calculated (using ACD Labs) to be 1.24±0.63 [10].

1.2.4. Crystallographic properties

1.2.4.1. Single crystal structure Single crystal structure X-ray data of Lamotrigine confirms that the unit-cell dimensions are: a=19.136 Å, b=8.6409 Å, c= Å 13.5549, and; β =109.172. This is consistent with a monoclinic space group *Aa*. The individual rings are almost planar with the dichlorophenyl ring tilted with respect to the 1,2,4-triazine ring. The crystal structure is stabilized by N—H···N and N—H···Cl hydrogen bonds. All the N atoms of the triazine ring participate in intermolecular hydrogen bonding [11].

1.2.4.2. Powder x-ray diffraction Various polymorphic and solvatomorphic forms for Lamotrigine have been described in literature [3,6,12–15]. The power X-ray diffraction pattern of anhydrous Lamotrigine is shown in Fig. 6.1. A monohydrate form has also been reported [14,16].

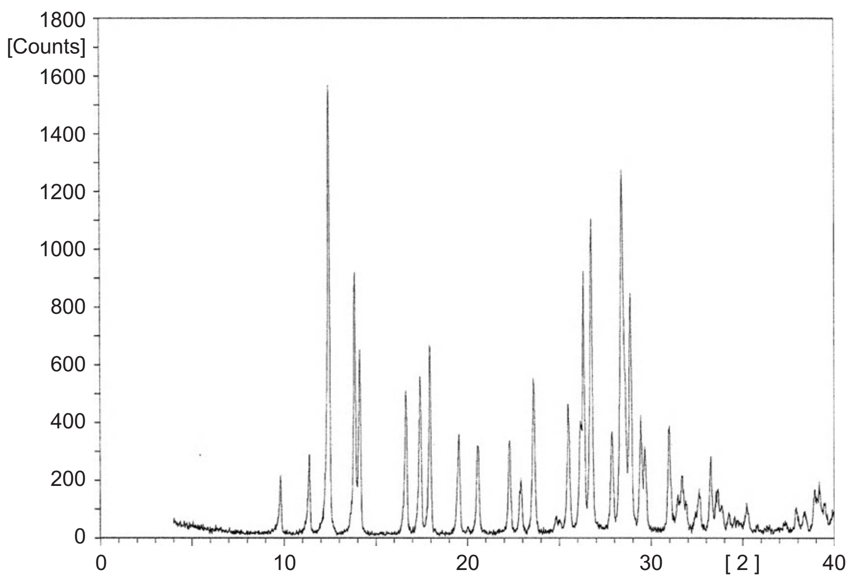

FIGURE 6.1 PXRD of anhydrous Lamotrigine.

Other solvatomorphic forms described in literature [14] that can be prepared from anhydrous Lamotrigine include: Lamotrigine dimethyl formamide solvate (Form B, C, D, P), methanol solvates (Form E, O), ethanol solvate (Form E1, H), isopropyl solvates (Form J, Q), acetone solvates (Form F, L), THF solvate (Form K), dimethyl acetamide solvate (Form M), methyl isobutyl ketone solvate (Form R), and methyl *tert*-butyl ether solvate (Form U).

1.2.5. Hygroscopicity

Analysis of anhydrous Lamotrigine by Dynamic Vapor Sorption confirmed that this substance is nonhygroscopic based on the step-isotherm. From the dry state to 95% RH, Lamotrigine showed less than 0.1% increase (reversible) in weight during the adsorption/desorption process (Fig. 6.2).

1.2.6. Thermal methods of analysis

1.2.6.1. Melting behavior Lamotrigine is known to have a melting range of 216–218 °C (uncorrected) [1].

1.2.6.2. Differential scanning calorimetry Differential Scanning Calorimetry of anhydrous Lamotrigine resulted in one endothermic thermal event (T_{onset}=215.87 °C and T_{max}=217.21 °C), as illustrated in Fig. 6.3. This thermal event corresponds to melting of Lamotrigine, as confirmed by hot-stage microscopy. For this analysis, the sample was weighed directly into an aluminum holder with the lid crimped into place. The sample was

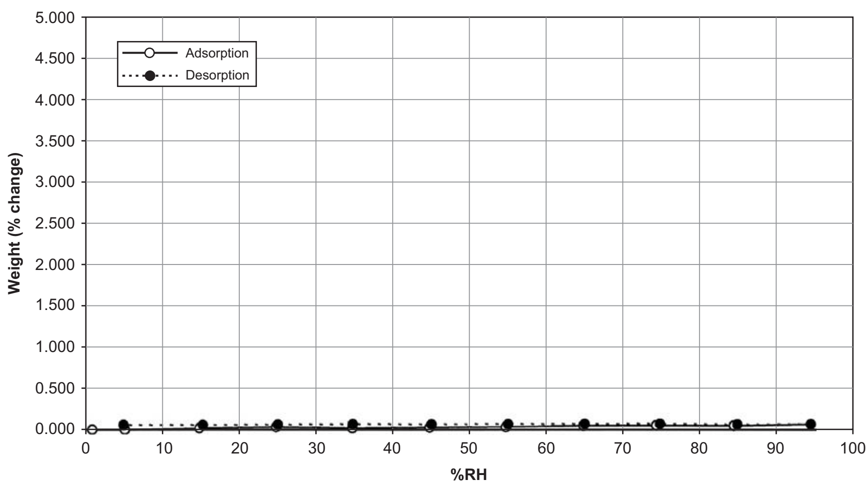

FIGURE 6.2 Adsorption/desorption isotherm of anhydrous Lamotrigine.

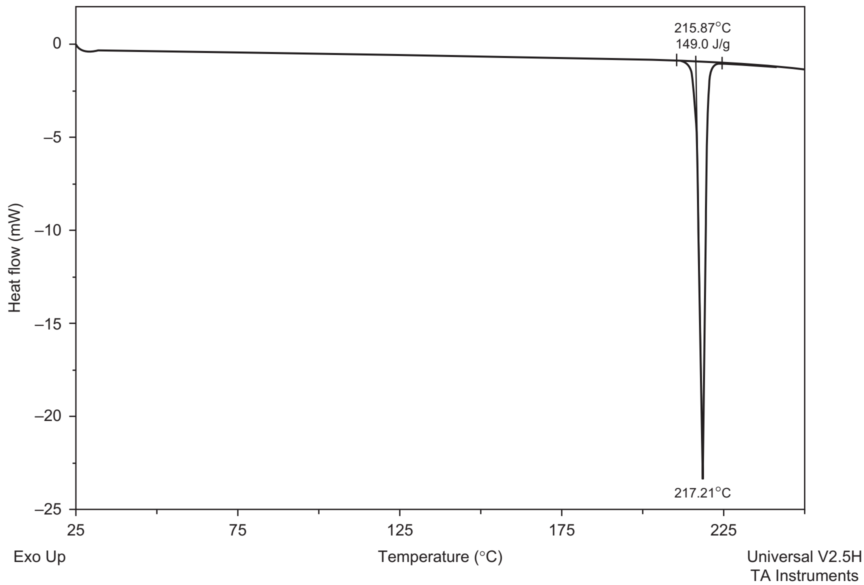

FIGURE 6.3 DSC analysis of anhydrous Lamotrigine.

equilibrated at 25 °C and then heated to 250 °C at a rate of 10 °C/min under a purge of nitrogen (50 cc/min).

1.2.6.3. Thermogravimetric analysis Thermal analysis of anhydrous Lamotrigine by Thermogravimetric Analysis confirmed that when Lamotrigine was heated from ambient temperature to 300 °C at 10 °C/min, <0.1% weight loss was observed up to 150 °C. Subsequent weight loss beyond 250 °C is reflection of thermal decomposition of Lamotrigine (Fig. 6.4).

1.2.7. Spectroscopy

1.2.7.1. UV spectroscopy The UV spectrum of the Lamotrigine was obtained on a Perkin-Elmer Lambda 2 UV/Vis spectrometer. The sample was dissolved in methanol at a concentration of 10 mg/l and scanned from 200 to 400 nm in the absorbance mode. The UV spectrum (Fig. 6.5) shows absorption maxima at λ_{max} 307 nm (ε=7.0×10^3), arising from n→π* and π→π* electronic transitions. This is close to the λ_{max} value of 308 nm reported for Lamotrigine by Zufia *et al.* [2]. In ethanol, the λ_{max} is shifted very slightly to 310 nm [17].

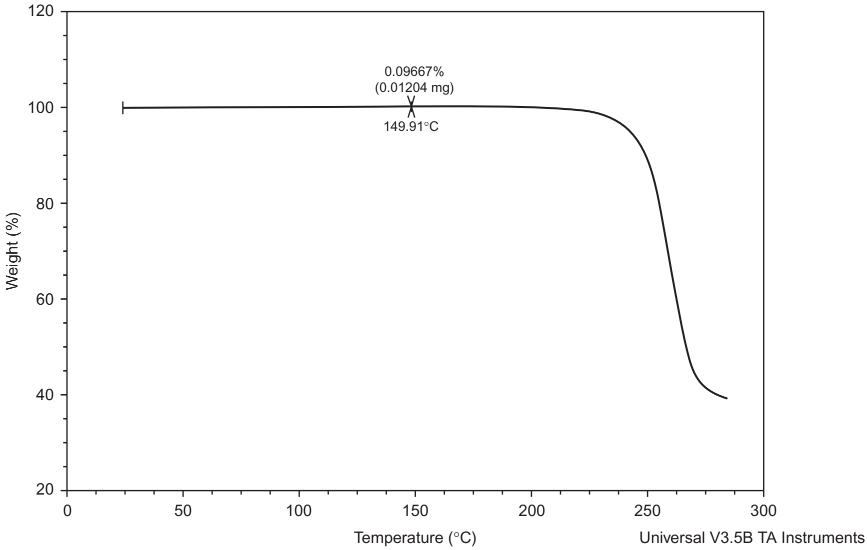

FIGURE 6.4 TGA analysis of anhydrous Lamotrigine.

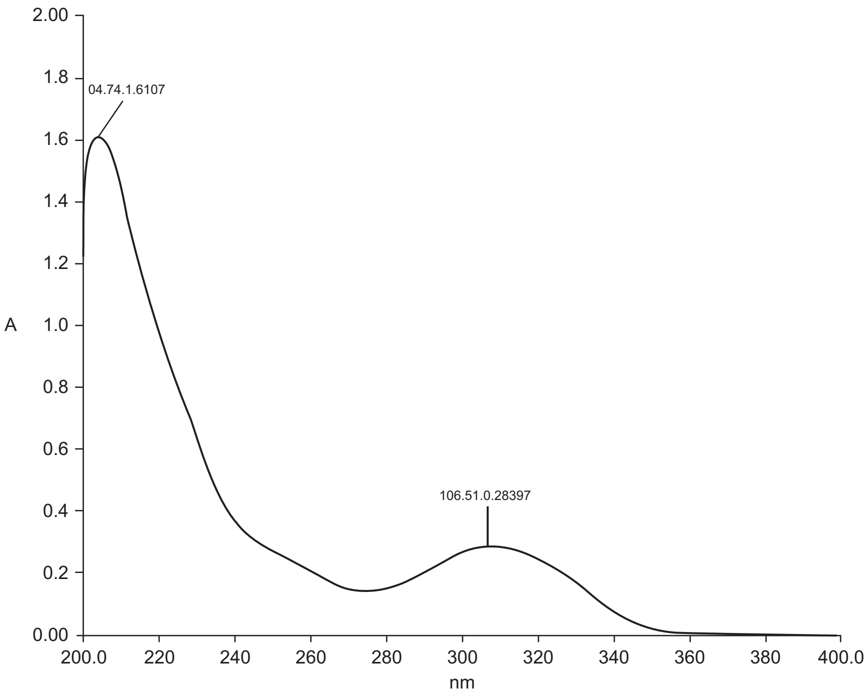

FIGURE 6.5 UV spectrum of Lamotrigine.

1.2.7.2. Vibrational spectroscopy The FTIR spectrum for Lamotrigine (recorded from a KBr pellet) is illustrated in Fig. 6.6. Characteristic infrared (IR) absorption bands due to amine N—H stretching (3450, 3314, 3212 cm^{-1}), aromatic (C═C) stretching (1619 cm^{-1}), and ortho-distributed aryl C—Cl stretching (1052 cm^{-1}) are observed.

1.2.7.3. Nuclear magnetic resonance spectrometry

1.2.7.3.1. ^{1}H-NMR spectrum The ^{1}H-NMR of Lamotrigine illustrated in Fig. 6.7 was obtained on a 400 MHz NMR using a 5-mm QNP probe and DMSO-d_6 as the solvent. Spectra were acquired at 400 MHz using a 5-mm QNP probe. Chemical shifts are reported in ppm relative to TMS using the residual solvent signal in the ^{1}H NMR spectrum as internal reference. Expanded ^{1}H-NMR spectrum and D_2O exchange spectrum are shown in Figs. 6.8 and 6.9, respectively. The proton magnetic resonance signal assignments are given in Table 6.2 (for the numbering of Lamotrigine, see Scheme 6.1).

1.2.7.3.2. ^{13}C-NMR spectrum The ^{13}C NMR spectra of Lamotrigine (Figs. 6.10 and 6.11) were obtained at 100 MHz using a 5-mm dual frequency ^{1}H–^{13}C probe. Chemical shifts are reported in ppm relative to tetramethyl silane using the residual solvent signal in the ^{13}C NMR spectrum as internal reference. The ^{13}C magnetic resonance signal assignments are given in Table 6.3 (for the numbering of Lamotrigine, refer to Scheme 6.1).

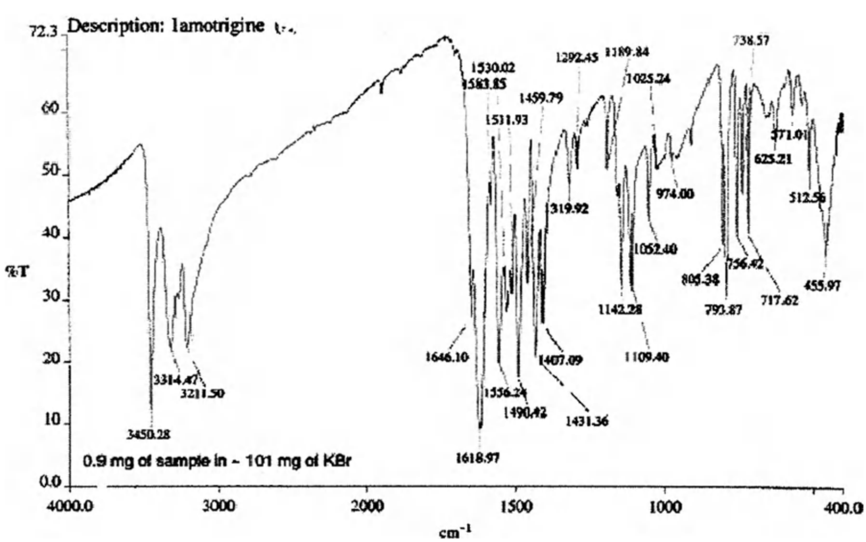

FIGURE 6.6 Infrared absorption spectrum of Lamotrigine (KBr pellet).

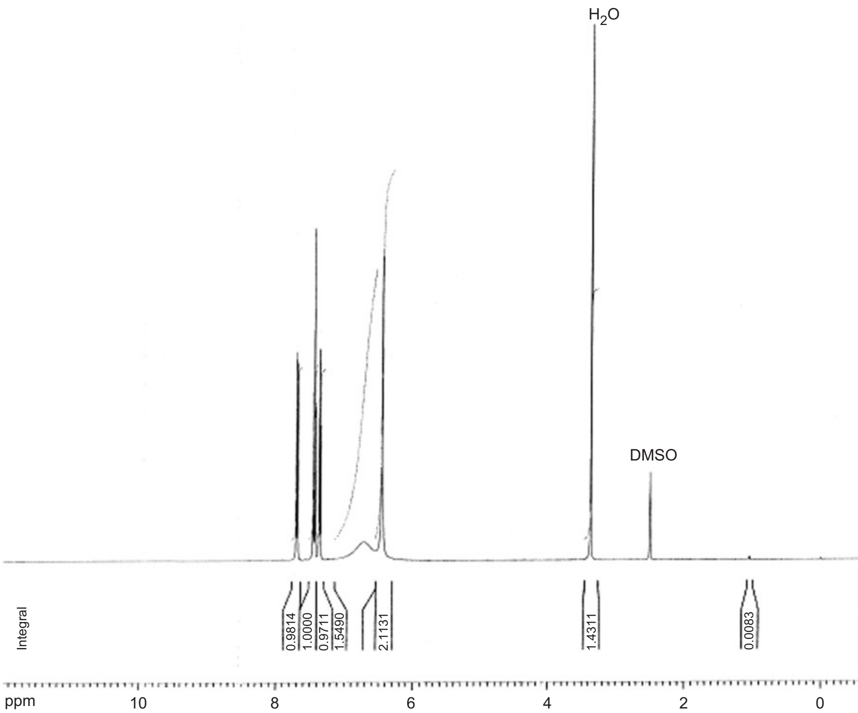

FIGURE 6.7 Full ^{1}H-NMR exchange spectrum of Lamotrigine.

The interpretation of the ^{1}H and ^{13}C NMR results from Sections 1.2.7.3.1 and 1.2.7.3.2 (Tables 6.2 and 6.3, respectively) was confirmed by ^{13}C{DEPT} (Fig. 6.12) spectroscopy study.

1.2.8. Mass spectrometry

The mass spectra (ESI MS and MS/MS) results of the positive mode electrospray ionization mass spectroscopic study of Lamotrigine are summarized below. The ESI MS spectrum (Fig. 6.13) shows the presence of the protonated Lamotrigine molecular ion peaks $[M+H]^+$ at m/z 256, 258, and 260 in the ratio corresponding to two chlorine atoms in the molecule. The fragmentation pattern for the MS/MS spectrum (Fig. 6.14) of $[M+H]^+$ is schematically depicted in Scheme 6.2.

1.3. Stability

1.3.1. Solid-state stability

In the solid state, Lamotrigine drug substance is very stable with respect to heat, heat/high humidity, and light. Prolonged exposure to heat (80 °C, 14 days), irradiation with UV/Vis light (1.9×10^{6} lux-h), and direct

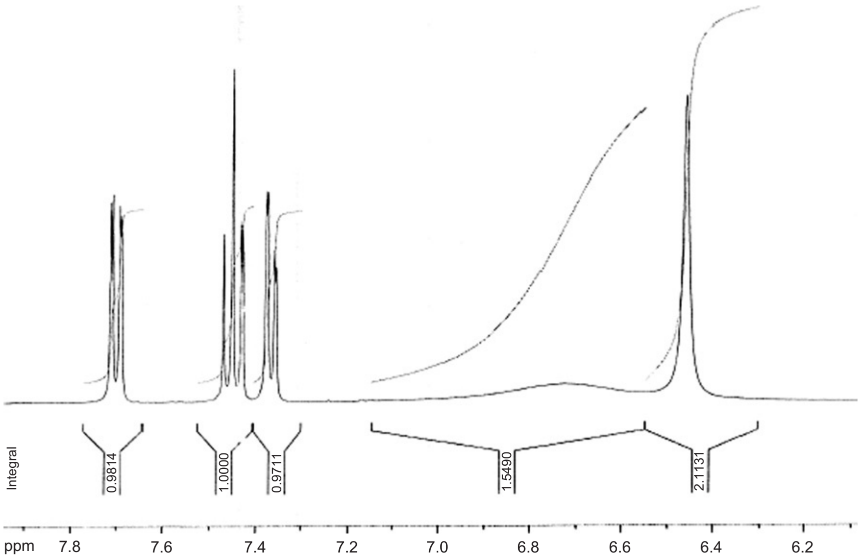

FIGURE 6.8 [1]H-NMR expansion spectrum of Lamotrigine (7.9–6.1ppm).

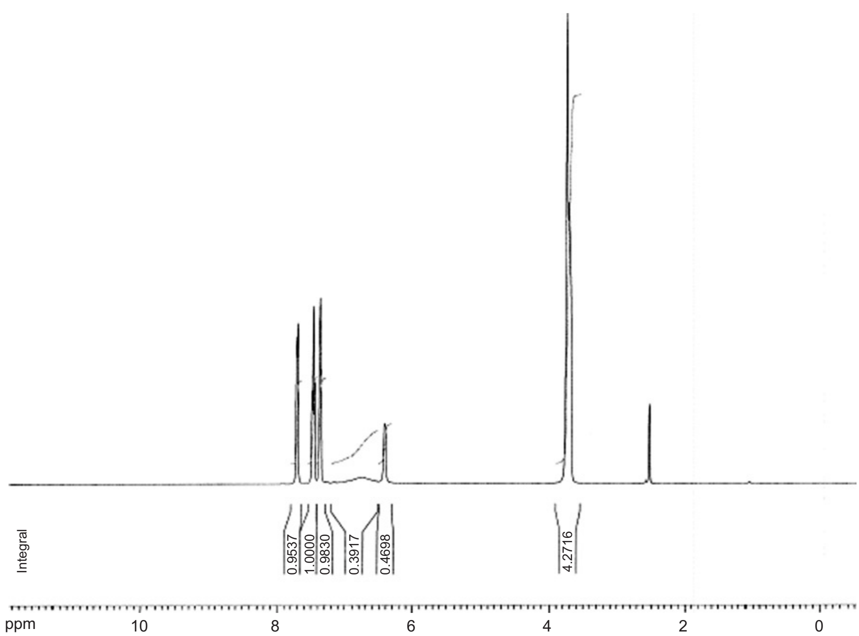

FIGURE 6.9 Full [1]H-NMR D_2O exchange spectrum of Lamotrigine.

TABLE 6.2 ^{1}H NMR spectroscopy data for Lamotrigine in DMSO-d_6

^{1}H Chemical shift (δ, ppm)	Multiplicity, spin–spin coupling constant (J, Hz)	Integration	Assignment
7.70	dd (J=7.8, 6.5)	1H	H10, H12
7.37	dd (J=7.6, 6.3)	1H	
7.45	app t (J=7.8)	1H	H11
6.72	bs	2H*	H13, H14
6.46	s	2H*	

* These protons are partially exchangeable in D_2O.

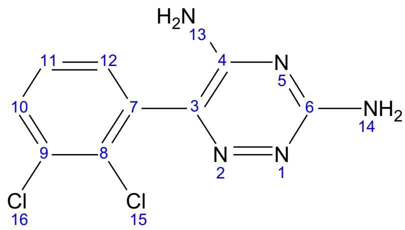

SCHEME 6.1 Numbering of Lamotrigine.

exposure to heat/high humidity (40 °C, 75% RH, 14 days) did not result in the formation of any degradation products above 0.05%. Mass balance of all solid stress samples was about 100%.

1.3.2. Solution-phase stability

Results of a solution stress study of Lamotrigine (Table 6.4) confirm that this drug substance is not susceptible to acidic, basic, thermal, and UV/Vis light stress in solution. No individual degradation product >0.05% was generated under these conditions.

Oxidative stress in the presence of hydrogen peroxide resulted in N-oxidation of Lamotrigine molecule containing four potential sites susceptible to oxidants. Two major oxidants were identified as (A) N-oxide (about 13.1%) and (B) hydroxyamino derivative (about 3.5%). An unknown degradant was also detected at low level (2.4%; Table 6.4). The oxidative degradation pathway is shown in Scheme 6.3. This transformation is a solution specific and does not occur in the solid state even under harsh conditions.

Under harsh basic hydrolysis conditions (i.e., prolonged heating under reflux), 1,2,4-triazine-5-(4H)-one can be generated [18] as depicted in Scheme 6.4 below. This is a USP-specified degradation product.

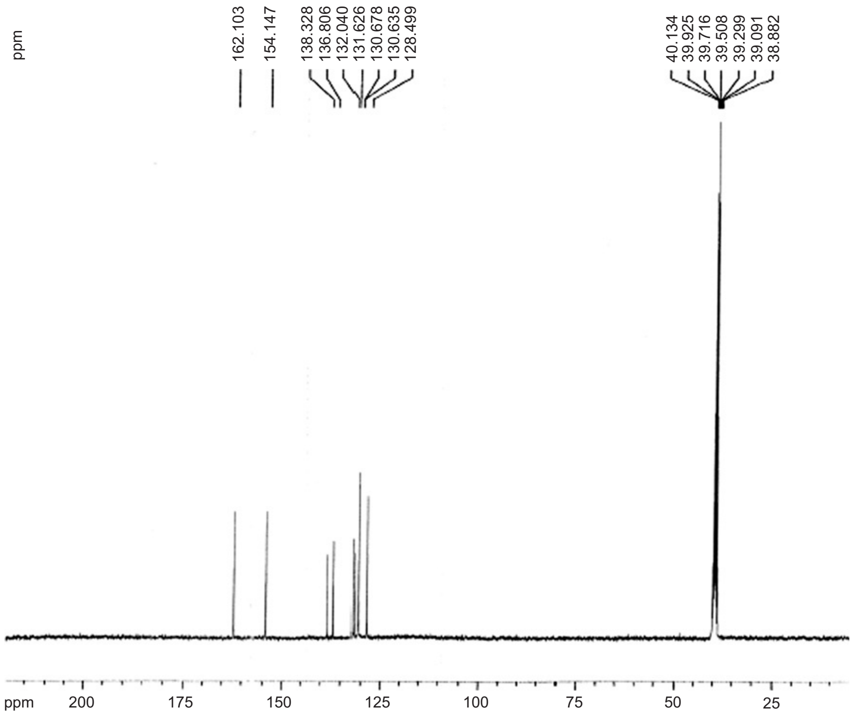

FIGURE 6.10 ^{13}C-NMR of Lamotrigine (225–0 ppm).

2. ANALYTICAL PROFILE

2.1. Compendial methods of analysis

Official monographs for Lamotrigine drug substance are currently available in the USP [16], European Pharmacopoeia (EP) [5], and British Pharmacopoeia (BP) [19]. A monograph for Lamotrigine tablets is also official in the USP.

2.1.1. Identification

2.1.1.1. Bulk drug substance According to the USP, Lamotrigine is identified by IR absorption spectrophotometry (USP ⟨197K⟩), using the USP Lamotrigine as reference standard. In addition to the IR test, the USP includes examination using liquid chromatography, where the retention time of the major peak in the chromatogram of the assay preparation corresponds to that in the chromatogram of the standard preparation, as obtained in the assay.

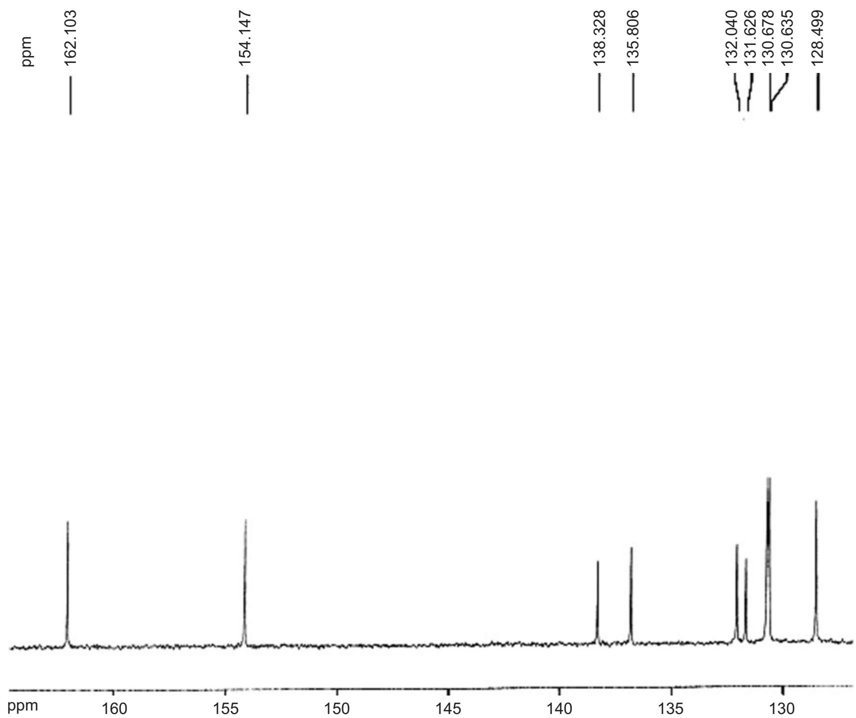

FIGURE 6.11 ^{13}C-NMR expansion spectrum of Lamotrigine (165–125 ppm).

TABLE 6.3 ^{13}C NMR spectroscopy data for Lamotrigine in DMSO-d_6

^{13}C Chemical shift (δ, ppm)	DEPT data	Assignment
162.1, 154.1	Each C	C4, C6
138.3, 136.8, 132.0, 131.6	Each C	C3, C7, C8, C9
130.7, 130.6, 128.5	Each CH	C10, C11, C12

Identification testing according to the EP is performed only by IR absorption spectrophotometry as per the EP general procedure (2.2.24).

2.1.1.2. Drug substance in pharmaceutical preparations Identification tests for Lamotrigine in tablet preparations according to the USP are performed by two tests (Test A and B). Test A is based on ultraviolet absorption, and the acceptance criterion is that the spectra of the standard solution and sample solution exhibit maxima at the same wavelengths. Test B is performed by liquid chromatography, and the criterion is that the retention time of the Lamotrigine peak sample solution corresponds to that of the standard solution, as obtained in the assay.

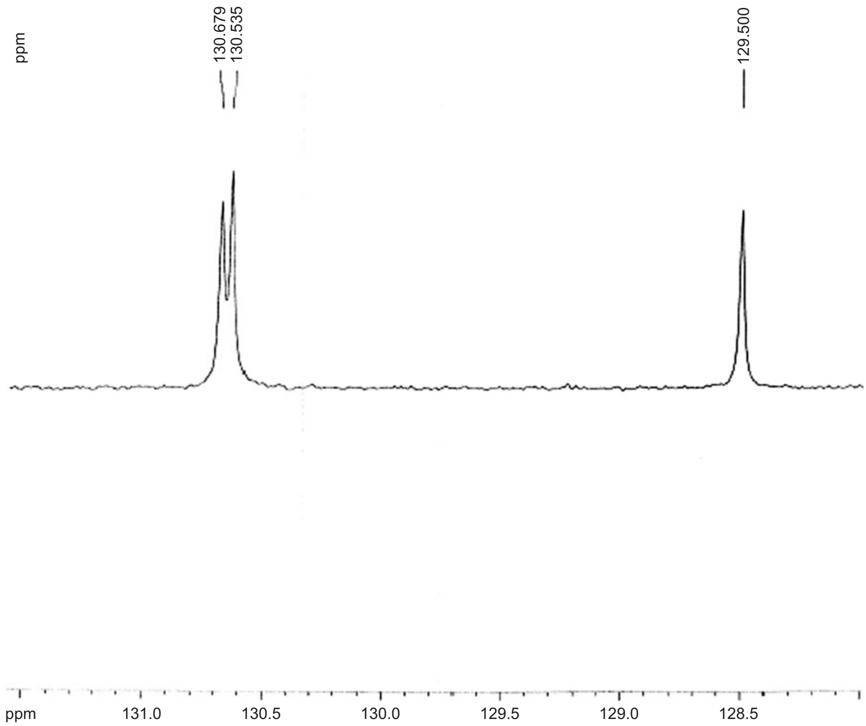

FIGURE 6.12 DEPT-135 NMR expansion spectrum of Lamotrigine (131.5–128.0 ppm).

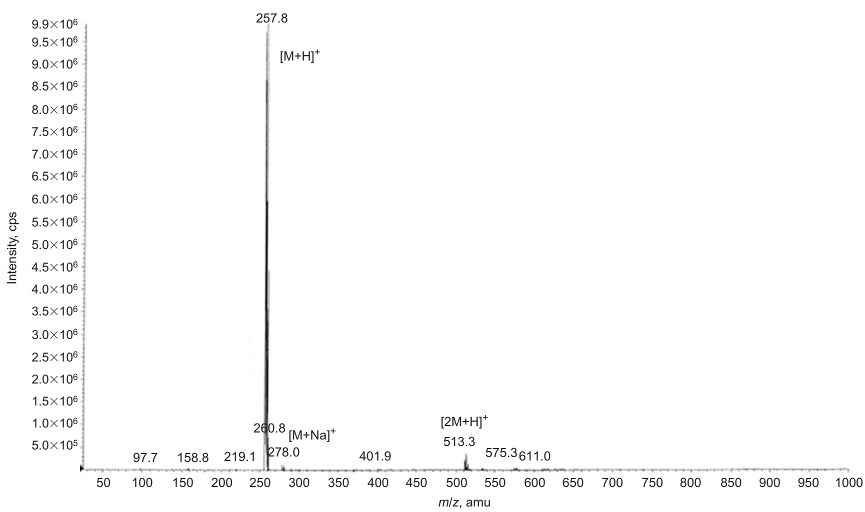

FIGURE 6.13 Electrospray ionization mass spectrum of Lamotrigine (0–1000 amu).

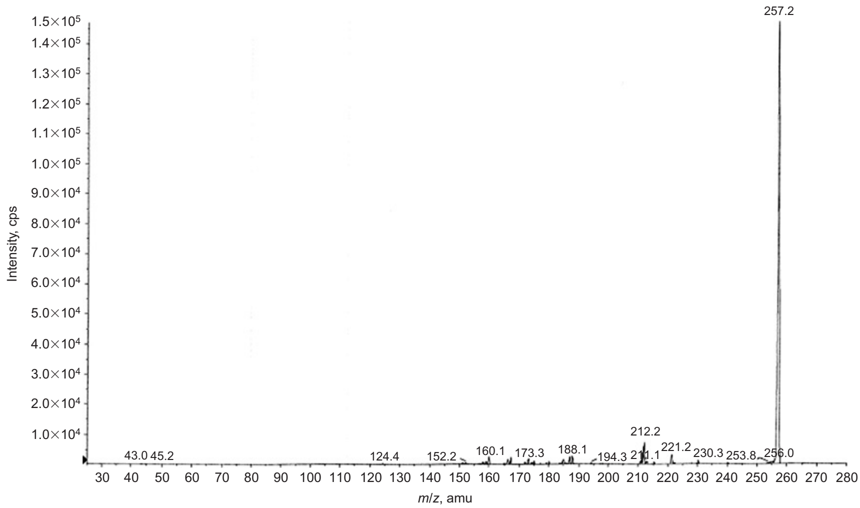

FIGURE 6.14 Tandem mass spectrum of the protonated molecular ion of Lamotrigine (20–340 amu).

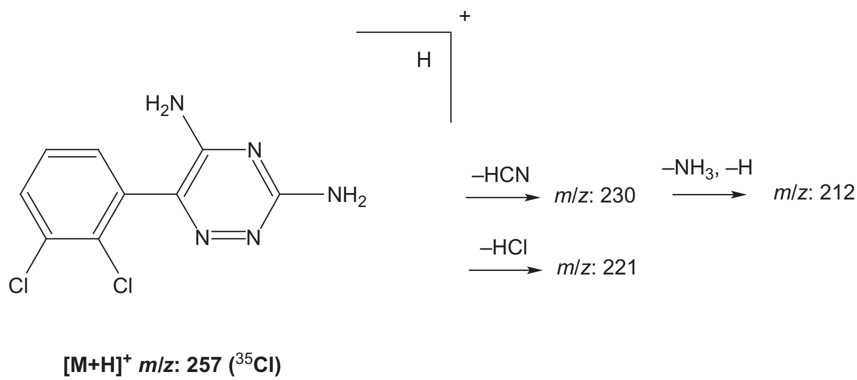

SCHEME 6.2 Fragmentation pattern of the protonated molecular ion of Lamotrigine.

2.1.2. Assays

2.1.2.1. Bulk drug substance

2.1.2.1.1. Potentiometric titration According to the EP, the assay for Lamotrigine is performed by a titration method. About 0.2 g of the substance to be assayed is dissolved in 60 mL of anhydrous acetic acid and is titrated with 0.1 M perchloric acid, determining the end point potentiometrically. An aliquot of 1 mL of 0.1 M perchloric acid is equivalent to 25.61 mg of Lamotrigine.

2.1.2.1.2. High-performance liquid chromatography According to the USP, the assay for Lamotrigine is performed by a liquid chromatography method. The mobile phase consists of variable mixtures (gradient) of

TABLE 6.4 Summary of Lamotrigine solution stress study

	% Impurities found	
Sample	Identified	Unidentified
Nonstressed	ND	0.05
Acidic (0.1N HCl, RT, 3h)	ND	0.05
Basic (0.1N NaOH, RT, 3h)	ND	0.05
Oxidative (3% H_2O_2, RT, 3h)	13.1 (A)*, 3.5 (B)*	2.4
Light (1.1×10^6 lux-h, water)	ND	0.04
Thermal (60°C, water, 3h)	ND	0.05

* See Section 1.3.1.

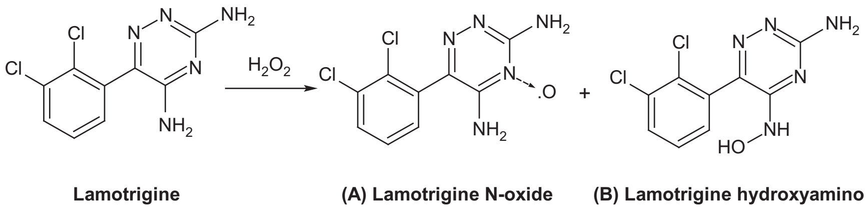

SCHEME 6.3 Oxidative degradation pathway of Lamotrigine in solution.

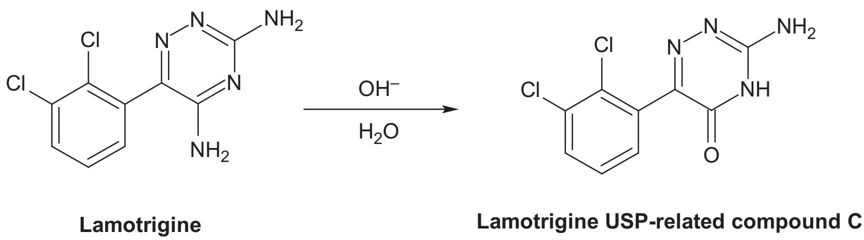

SCHEME 6.4 Hydrolytic degradation pathway of Lamotrigine in solution.

Solution A (potassium phosphate buffer and triethylamine (150:1, v/v), pH adjusted to 2.0) and Solution B (acetonitrile). The liquid chromatograph is equipped with a 270-nm detector and a 4.6mm×15cm column that contains 5-μm packing L1. The flow rate is about 1.0mL/min. The column temperature is maintained at 35°C.

2.1.2.2. Tablets Assay procedure for Lamotrigine determination in tablets, based on isocratic liquid chromatography, is described in the USP. The chromatography is performed using mixture of methanol and ammonium acetate buffer pH 4.5 (3:2, v/v) as the mobile phase delivered at

flow rate of 1mL/min. The liquid chromatograph is equipped with a UV detector operating at 210nm and a 4.6mm×15cm column that contains 5-µm packing L1 (octadecyl silane chemically bound to porous silica or ceramic microparticles). The column temperature is maintained at 35°C.

2.1.3. Impurity analysis

2.1.3.1. Impurities in drug substance and pharmaceutical preparations The USP, EP, and BP describe liquid chromatographic methods for the determination of Lamotrigine-related substances. The structures, chemical names, and classification of the impurities of Lamotrigine are shown in Table 6.5.

The EP/BP method for related substances employs base-deactivated end-capped octadecylsilyl silica gel (0.15m×4.6mm, 5µm) as the stationary phase with column temperature of 35°C and detection at 270nm. The gradient chromatography was performed using the mobile phase consisting of Mobile Phase A (1 volume of triethylamine and 150 volumes of a 2.7g/L solution of potassium dihydrogen phosphate, adjusted to pH 2.0 with phosphoric acid) and Mobile Phase B (acetonitrile) delivered at 1.2mL/min flow rate. Determination of 2,3-dichlorobenzoic acid (EP Impurity E) is performed as per the above BP/EP method for related substances modified as follows: isocratic chromatography with Mobile Phase A and Acetonitrile (35:65, v/v) and UV detection at 210nm, while all other method parameters remain the same.

As per USP, the chromatographic conditions for the drug substance testing for impurities and assay are the same. Similar to the EP/BP, a separate method is used in USP for determination of 2,3-dichlorobenzoic acid (USP Impurity B) using a modified USP procedure for related substances (i.e., isocratic chromatography with Solution A and Acetonitrile (35:65, v/v) and UV detection at 210nm).

For Lamotrigine tablets, the USP method for organic impurities employs a liquid chromatograph equipped with a UV detector operating at 210nm and a 4.6mm×25cm column that contains 5-µm packing L1. The mobile phase is a mixture of acetonitrile, methanol, and ammonium acetate buffer pH 4.5 (1:3:6, v/v/v) delivered at 1mL/min flow rate.

2.1.4. Other tests

2.1.4.1. Loss on drying When the sample is dried at 105°C at a pressure not exceeding 0.7kPa for 3h according to the EP general procedure (2.2.32) or by the USP procedure ⟨731⟩ (drying 105°C for 3h), it loses not more than 0.5% of its weight.

2.1.4.2. Sulfated ash/residue on ignition The sample does not contain more than 0.1% sulfated ash when tested according to the USP procedure ⟨281⟩ or the EP procedure 2.4.14.

TABLE 6.5 Impurities in Lamotrigine

Structure	Chemical name	Classification
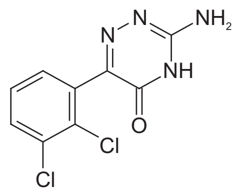	3-Amino-6-(2,3-dichloro phenyl)-1,2,4-triazin-5 (4*H*)-one	EP Impurity A/USP-related compound C Synthetic impurity
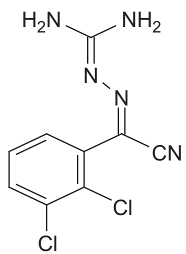	(2E)-[2-(diaminomethylidene)-diazanylidene](2,3-dichlorophenyl)-acetonitrile	EP Impurity B Synthetic impurity
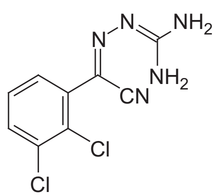	(2Z)-[2-(diaminomethylidene)diazanylidene](2,3-dichlorophenyl)acetonitrile	EP Impurity C Synthetic impurity

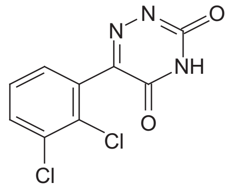	6-(2,3-Dichlorophenyl)-1,2,4-triazine-3,5 (2H,4*H*)-dione	EP Impurity D Synthetic impurity
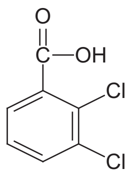	2,3-Dichlorobenzoic acid	EP Impurity E/USP-related compound B Synthetic impurity
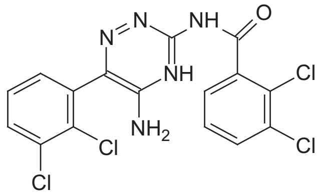	*N*-[5-amino-6-(2,3-dichlorophenyl)-1,2,4-triazin-3-yl]-2,3-dichlorobenzamide	EP Impurity F/USP-related compound D Synthetic impurity
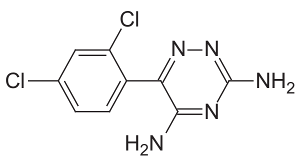	6-(2,4-Dichlorophenyl)-1,2,4-triazine-3,5-diamine	EP Impurity G Synthetic impurity

(*continued*)

TABLE 6.5 (*continued*)

Structure	Chemical name	Classification
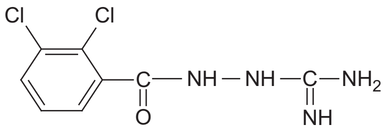	N-Guanidinyl-2,3-dichlorobenzamide	Synthetic impurity
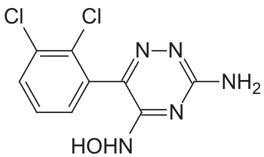	3-Amino-6-(2,3-dichlorophenyl)-5-(hydroxyamino)-1,2,4-triazine	Degradation product
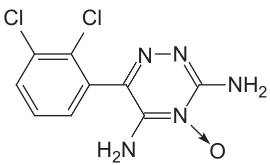	3,5-Diamino-6-(2,3-dichlorophenyl)-1,2,4-triazin-4-N-oxide	Degradation product

2.1.4.3. Heavy metals The heavy metal content of Lamotrigine is determined using the USP general procedure ⟨231⟩, as well as the procedure of EP (2.4.8). The limit on heavy metals in the substance is 0.001%.

2.2. Electrochemical methods

Highly sensitive electrochemical techniques for determination of Lamotrigine in Lamotrigine capsules have been reported in literature [20,21]. Carbon screen-printed electrodes modified with silver nanoparticles were used for the determination of Lamotrigine using differential pulse adsorptive-stripping voltammetry. The detection limit for this analytical procedure is 3.72×10^{-7} M.

2.3. Microemulsion electrokinetic chromatography

Altria [22] has shown that microemulsion electrokinetic chromatography is a highly applicable technique for analysis of wide range of drugs including Lamotrigine.

2.4. Spectoscopic methods

2.4.1. Spectrofluorimetry

A sensitive, simple, and selective spectrofluorimetric method was developed by El-Enany *et al*. [23] for the determination of Lamotrigine in pharmaceutical formulations. The method is based on reaction of Lamotrigine with *o*-phthalaldehyde in presence of 2-mercaptoethanol in borate buffer of pH 9.8 to yield a highly fluorescent derivative that is measured at 448 nm after excitation at 337 nm. The fluorescence concentration plot was linear over the range of 0.1–1.0 μg/mL, with a limit of detection of 0.02 μg/mL and a limit of quantitation of 0.06 μg/mL.

2.4.2. Spectrophotometry

Youssef *et al*. [24] developed and validated a spectrophotometric method for the assay of Lamotrigine in presence of its impurity for drug substance and dosage forms. The UV absorption spectra of Lamotrigine and its impurity 2,3-dichlorbenzoic acid display complete overlap from 200 to 320 nm in methanol and dilute acid with broad absorption at 275 nm. The reaction of Lamotrigine with *p*-chloranilic acid yields a pink color at ambient temperature. This colored product is measured at λ_{max} 519±2 nm. The bathochromic shift is due to the formation of ion-association complex between Lamotrigine and *p*-chloranilic acid. Beer's law was observed over concentration range 10–200 μg/mL.

2.5. Chromatographic methods

2.5.1. Planar chromatography

Youssef *et al.* [24] developed and validated a TLC method for separation of Lamotrigine and its impurity 2,3-dichlorbenzoic acid followed by densitometric measurement of the spots at 275 nm. The separation was carried out on silica gel plates using ethyl acetate:methanol:ammonia 35% (17:2:1 v/v/v) as the developing solvent. A linear calibration curve was obtained in the concentration range 0.5–10 μg per spot. Dreassi et al. [25] developed a planar chromatography method for determination of Lamotrigine in tablets and this was compared with liquid chromatography and UV spectrophotometry methods. The separation was carried out on Si_{60} plates using mobile phase diethyl ether:methanol:glacial acetic acid (80:19:1 v/v/v) as the developing solvent. The plate was scanned at 306 nm. The detection limit was 0.26 μg/mL.

2.5.2. High-performance liquid chromatography

The HPLC methods, reported in the literature for the analysis of Lamotrigine, are summarized in Table 6.6.

2.6. Determination in body fluids and tissues

Antiepileptic drugs, including Lamotrigine, are known for their narrow therapeutic range and complex drug–drug interactions. A concomitant therapy with several antiepileptic drugs is common in clinical practice. For the above reasons, therapeutic drug monitoring is often conducted for this class of drugs. Consequently, numerous analytical techniques have been reported for determination of Lamotrigine and its metabolites in the presence of other antiepileptic drugs in the blood serum/plasma and other biological matrices. The overview of the reported methods and the corresponding major analytical parameters (i.e., selectivity, linearity/range, limit of detection, limit of quantification, etc) is presented in Tables 6.7–6.12 below.

3. ADME PROFILE

3.1. Uses, applications, and pertinent history

Lamotrigine, a phenyltriazine anticonvulsant, is a newer antiepileptic drug, introduced for treatment of seizure disorders in the early 90s. It exerts its antiseizure activity by blocking voltage-activated sodium channels [76], thereby preventing the presynaptic release of the excitatory neurotransmitters [77–79]. Lamotrigine is used clinically as monotherapy

TABLE 6.6 Summary of HPLC methods

Stationary phase	Mobile phase	Detection	Lamotrigine sample	Linearity; LOD/LOQ	Reference
RP C8 (5 µm, 250 mm × 4.6 mm)	MeOH–0.01 M ammonium acetate buffer pH 4.3 (50:50, v/v)	UV 225 nm	Tablets	40–160 µg/mL	[26]
RP, C8 (5 µm, 150 mm × 4.6 mm)	Gradient Mobile phase A: CH_3CN Mobile phase B: water with 0.1% formic acid	Q-TOF-MS	Water samples	10–5000 ng/L LOD: 1 ng/L LOQ: 10 ng/L	[27]
RP, C8 (5 µm, 250 mm × 4.6 mm)	0.05 M Acetate buffer, pH 5.6: CH_3CN (72:28, v/v)	UV 306 nm	Tablets	0.044–7.8 µg/mL LOD (on-column): 0.9 ng LOQ (on-column): 1.7 ng	[28]
RP, C18 (10 µm, 250 mm × 4.6 mm)	CH_3CN: methanol: 0.01 M potassium orthophosphate (pH 6.7) (30:20:50 v/v/v)	UV 275 nm	Drug substance and tablets	1–12 µg/mL	[24]

TABLE 6.7 HPLC-UV methods for Lamotrigine determination in body fluids and tissues

Stationary phase	Mobile phase	Detection, nm	Matrix/selectivity	Linearity; LOD/LOQ	Reference
PR, C18	CH_3CN–50 mM phosphoric acid (pH 2.2)+10 mM SDS (33:67, v/v)	277	Guinea pig whole blood and urine/ 2-N-glucuronide	0.05 µg/mL (LOD) 0.10 µg/mL (LOQ)	[29]
RP, C18	1 mM K_2HPO_4–CH_3CN–MeOH (53:46:1, v/v/v), pH 6	Dual, at 220 and 310	Human serum/ phenobarbitone, phenytoin, carbamazepine	0–13 µg/mL LOD 0.2 mg/L (20.7 ng on-column)	[30]
RP, C18	CH_3CN–10 mM phosphate buffer (pH 3.5)+5 mM Na-octanesulfonate (27:73, v/v)	265	Human serum/ phenobarbital, zonisamide, carbamazepine	0.5–40 µg/mL 0.2 µg/mL (LOQ)	[31]
RP, C18	CH_3CN–30 mM KH_2PO_4, pH 3.7 (25:75, v/v)	270	Human plasma (pediatric)	0–15 µg/mL 0.02 µg/mL (LOD) 0.1 µg/mL (LOQ)	[32]
RP, C18	Potassium dihydrogen phosphate–water–MeOH–TEA (750 mL+550 mL+430 mL+100 µL)	220 and 306	Human serum/barbiturates	0.5–20 µg/mL; 0.5 µg/mL (LOD)	[33]
RP, C18	Potassium phosphate buffer (pH 6.8)–CH_3CN–MeOH (70:16:14, v/v/v)	310	Human plasma and urine	0–10.0 µg/mL; 0.02 µg/mL (LOD, plasma); 0.03 µg/mL (LOD, urine)	[34]
RP, C18	0.01 M KHPO4–CH_3CN–MeOH (70:20:10, v/v/v), pH=6.7	214	Human plasma	LOD 20 ng/mL	[35]

RP, C18	0.01 M Phosphate buffer–CH_3CN–MeOH, pH 7.5 (65:18:17, v/v/v)	220	Human plasma/ ethosuximide, primidone, phenobarbital, phenytoin/ carbamazepine/ carbamazepine-diol, carbamazepine epoxide	0.5–15 mg/L 0.2 mg/L	[36]
RP, C18	Phosphate buffer pH3.8–CH_3CN (55:45, v/v)	210	Human serum/common anticonvulsants	0.2–20 μg/mL	[37]
RP, C18	CH_3CN–40 mM phosphoric acid (20:80, v/v, pH 2.1)	205	Human serum/primidone, ethosuximide, sulthiame, felbamate, phenobarbital, carbamazepine, phenytoin, oxcarbazepine	1–20 μg/mL 0.3 μg/mL (LOD)	[38]
RP, C18	MeOH–KH_2PO_4–TEA (35:64.7:0.3, v/v/v)	306	Human plasma and rat brain	0.1–15 mg/L (plasma) 0.1–5 mg/L (brain) LOD: 0.008 mg/L (plasma) 0.023 mg/L (brain)	[39]
RP, C18	Phosphate buffer (pH 6.5)–CH_3CN–MeOH (65:18:17, v/v/v)	220	Human plasma/ carbamazepine, carbamazepine epoxide	0.05-10.0 μg/mL; 0.05 μg/mL (LOQ)	[40]
RP, C18	50 mM KH_2PO_4 buffer, pH 4.5–CH_3CN/MeOH 3:1 (65:35, v/v)	210	Human plasma/ oxcarbazepine monohydroxy derivative, felbamate	1–20 μg/mL 0.5 μg/mL (LOQ)	[41]
RP, C18	MeOH–CH_3CN–25 mM phosphate buffer+12.5 mM NaCl (14.5:19.5:66, v/v/v, pH 6.7)	215 and 275	Human serum/primidone, phenobarbital, phenytoin, carbamazepine and metabolites, zonisamide	0–21.6 mg/L 0.008 mg/L (LOD) 0.014 mg/L (LOQ)	[42]

(*continued*)

TABLE 6.7 (*continued*)

Stationary phase	Mobile phase	Detection, nm	Matrix/selectivity	Linearity; LOD/LOQ	Reference
RP, C18	Phosphate buffer pH 4.5–CH_3CN (60:40, v/v)	260	Whole blood	0.2–20 μg/mL LOD 0.05 μg/mL LOQ 0.2 μg/mL	[43]
RP, C8	0.05 M Acetate buffer, pH 5.6–CH_3CN (72:28, v/v)	306	Human plasma and urine	0.087–3.49 μg/mL LOD (on-column): 1.1 ng (plasma) 1.2 ng (urine)	[28]
RP, C8	Water–0.5 M phosphate buffer, pH 6.5–CH_3CN (790:10:200, v/v/v)	306	Human serum/ carbamazepine, carbamazepine epoxide, ethosuximide, valproic acid, theophylline, primidone, procainamide, *N*-acetyl procainamide, quinidine	2–32 μM	[44]
RP, C8	0.5 M Phosphate buffer, pH 6.5–water–CH_3CN (10 mL+790 mL+200 mL)	306	Human plasma/commonly monitored antiepileptic drugs	1–20 μg/mL 0.6 μg/mL (LOD) 1 μg/mL (LOQ)	[45]
RP, C8	Methanol–0.45 mM phosphate buffer pH 3.5+0.17% TEA (24:76, v/v)	220	Human plasma/ Lamotrigine 2-N-glucoronide, Lamotrigine 2-N-methylated	0.1–15 μg/mL 0.1 μg/mL (LOQ) 0.05 μg/mL (LOD)	[46]
RP, C18	30 mM KH_2PO_4 buffer, pH 3.7–CH_3CN (65:35, v/v)	270	Human plasma/ zonisamide, carbamazepine	1–30 μg/mL 0.5 μg/mL (LOD)	[47]

RP, C6	20 mM KH_2PO_4 pH 3.0–CH_3CN (70:30, v/v)	215	Human serum/ oxcarbazepine, 10-monohydroxycarbazepine	30–15,00 0 ng/mL 10 ng/mL (LOD) 30 ng/mL (LOQ)	[48]
NP, Silica	*n*-Hexane–absolute EtOH–35% ammonia (80:20:0.25, v/v/v)	313	Human plasma	N/A	[49]
NP, Silica	MeOH–water–ammonium phosphate (94:5.92:0.08, v/v/v, pH 4.0)	280	Human plasma/ carbamazepine, carbamazepine epoxide, ethosuximide, phenobarbital, phenytoin, valproate	0.5–30 mg/L	[50]
NP, Silica	MeOH–*n*-heptane–dichloromethane–ammonium hydroxide (20:40:40:0.3, v/v/v/v)	240	Human plasma/ carbamazepine, vigabatrin, phenobarbital	0.4–16 μg/mL; 0.4 μg/mL (LOQ)	[51]
NP, Silica	CH_3CN–water+0.2% H_3PO_4+0.3% TEA, pH 2.7 (84:16, v/v)	225	Human plasma	0.1–5 μg/mL; 0.1 μg/mL (LOQ)	[52]
RP, Cyano	CH_3CN–0.01 M ammonium acetate, pH 3.5 (55:45, v/v)	280	Human plasma	Up to 15 mg/L LOD 55 μg/L (2 ng on-column)	[53]
RP, Cyano	MeOH–CH_3CN–5 mM Na-acetate (5:20:75, v/v/v, pH 6.3)	205	Human plasma/ carbamazepine, phenytoin, phenobarbital	1–10 μg/mL; 50–100 ng/mL (LOD)	[54]
RP, Cyanopropyl	Water–CH_3CN–MeOH–acetic acid–TEA (725:150:125:1.0:0.6, v/v/v/v/v)	214	Human serum/phenytoin, carbamazepine, carbamazepine epoxide	0.3–80 mg/L; 0.3 mg/L (LOD)	[55]
RP, Cyano	Water–CH_3CN–methanol–acetic acid–TEA (725:150:125:1:0.6, v/v/v/v/v)	214	Human plasma/ oxcarbazepine and the metabolites, carbamazepine and carbamazepine epoxide	0.3–80 μg/mL; 0.2 μg/mL (LOQ)	[56]

(*continued*)

TABLE 6.7 (*continued*)

Stationary phase	Mobile phase	Detection, nm	Matrix/selectivity	Linearity; LOD/LOQ	Reference
RP, Diphenyl	CH_3CN–3% H_3PO_4 (30:70 v/v, pH 3.5)	265	Human plasma	0.5–20 μg/mL 0.2 μg/mL (LOQ)	[57]
Internal surface RP GFFI (glycin-phenylalanine-phenylalanine bonded)	0.01 M Potassium phosphate bibasic, pH 6.0–CH_3CN (82:18, v/v)	330	Human plasma/serum, carbamazepine	0.1–20.0 mg/L 0.05 mg/L (LOD)	[58]
RP, Monolithic column	0.1 M Phosphate buffer pH 6.5–MeOH–CH_3CN (77:20:3, v/v/v)	210	Human serum or plasma/carbamazepine, carbamazepine-10,11-epoxide, felbamate, 10,11-dihydro-10-hydroxycarbamazepine, pentobarbital, phenobarbital, phenytoin, primidone, zonisamide	0.4–38.8 μg/mL 0.4 μg/mL (LOQ)	[59]

TABLE 6.8 LC-MS methods for Lamotrigine determination in body fluids and tissues

Ionization	Detection	Matrix/selectivity	Linearity; LOD/LOQ	Reference
Thermospray (TSP)	MS	Urine/urinary metabolites identification	N/A	[60]
Electrospay (ESI)	MS	Human plasma/Lamotrigine-2-N-glucoronide, Lamotrigine-*N*-methyl, Lamotrigine N-oxide	0.1–100 μmol/L 0.08 μmol/L (LOD) 0.26 μmol/L (LOQ)	[61]
ESI	MS/MS	Human blood/NSAIDs and AEDs of various classes*	69 μg/L (LOD) 220 μg/L (LOQ)	[62]
ESI	MS/MS	Human plasma	0.025–10.0 μg/mL; 0.025 μg/mL (LOQ) 50 pg/mL (LOD)	[63]
ESI	MS/MS	Human serum	0.1–20 μg/mL; 4 ng/L (LOD) 70 ng/L (LOQ)	[64]

* NSAIDs, nonsteroidal anti-inflammatory drugs; AEDs, antiepileptic drugs (Carbamazepine, Oxcarbazepine, Phenytoin, Phenobarbital).

TABLE 6.9 GC and GC-MS methods for Lamotrigine determination in body fluids and tissues

Method	Detection	Matrix/selectivity	Linearity; LOD/LOQ	Reference
GC with solid-phase microextraction (SPME)	Thermionic specific detection (TSD)	Human plasma/AEDs	0.20–10.0 μg/mL; 0.20 μg/mL (LOQ)	[65]
GC	Nitrogen phosphorous detection (NPD)	Human serum or plasma	0.13–10.4 μg/mL; $<$0.15 μg/mL (LOQ)	[66]
GC as t-BuMe$_2$Si-derivative	MS; selective ion monitoring mode using electron ionization	Human plasma/TCAs, common BDZs, common AEDs and barbiturates, salicylate and acetaminophen*	0.5–20 μg/mL; 0.25 μg/mL (LOD)	[67]
GC	MS; specified ions monitoring (SIM) mode	Human serum/carbamazepine, carbamazepine epoxide	0.625–20 μg/mL; 0.25 μg/mL (LOD)	[68]

* AEDs, Carbamazepine, Carbamazepine Epoxide, Phenytoin, Phenobarbital, and Primidone; BDZs, Benzodiazepines (valium and librium).

TABLE 6.10 Planar chromatography methods for determination in body fluids and tissues

Technique	Detection	Matrix/selectivity	Linearity; LOD/LOQ	Reference
TLC, Si_{60} 10×10cm plates	Densitometric at 306nm	Spiked ("fortified") human plasma	LOD 0.27μg/mL	[25]
HPTLC, normal phase	Densitometric at 312nm	Human and rabbit serum/ carbamazepine	20–300 ng/spot; 6ng/spot (LOD); 10ng/spot (LOQ)	[69]

or in combination with other anticonvulsants. The pharmacokinetics of Lamotrigine was studied after single and multiple doses in healthy volunteers and epileptic patients. Clinical pharmacokinetic data of Lamotrigine are summarized in several review articles [77–82].

3.2. Absorption

Following oral administration, Lamotrigine is virtually completely absorbed. The absolute bioavailability of Lamotrigine, assessed by comparing oral and intravenous dose, is 98% [83]. A study in healthy volunteers with radioactively labeled Lamotrigine administered orally as a single 240mg dose supports apparent complete absorption of Lamotrigine [84]. Maximum concentrations (C_{max}) are achieved 2.8±1.3 h post oral dosing [80]. A linear relationship has been observed between the dose administered and the C_{max} of Lamotrigine [85]. No first-pass effect was observed, and the presence of food does not affect the absorption of Lamotrigine [82].

3.3. Distribution

Lamotrigine is uniformly and widely distributed, with a volume of distribution after oral administration ranging from 0.87 to 1.2L/kg and 1.25 to 1.47L/kg in healthy volunteers [83,85] and in patients with epilepsy receiving concurrent antiepileptic agents [86,87], respectively. The degree of plasma protein binding assessed *in vitro* by equilibrium analysis is 56% [80]. Protein binding of Lamotrigine, estimated based on plasma and saliva concentrations, is approximately 55% [85].

TABLE 6.11 Capillary electrophoresis methods for Lamotrigine determination in body fluids and tissues

Technique	Detection	Matrix/selectivity	Linearity; LOD/LOQ	Reference
Capillary zone electrophoresis (CZE)	UV	Human serum	0.5–10 mg/L 0.3 mg/mL	[70]
CZE	UV 220 nm	Human plasma and serum	3.9–39 μM 0.4 μM (LOD)	[71]
CZE	Electrospray ionization–mass spectrometry	Human plasma/Lamotrigine	0.1–5.0 μg/mL; 0.05 μg/mL (LOD)	[72]
Micellar electrokinetic capillary chromatography (MEKC)	UV 214 nm	Human plasma/Lamotrigine and the metabolites	1–20 μg/mL; 0.5 μg/mL (LOD)	[73]

TABLE 6.12 Miscellaneous techniques for Lamotrigine determination in body fluids and tissues

Technique	Detection	Matrix/selectivity	Linearity; LOD/LOQ	Reference
Radioimmunoassay (RIA)	Gamma counter	Human plasma	0.5–12 μg/mL 20 ng/mL (LOD)	[74]
Immunofluorometric assay	Immunofluorescence (Eu^{3+}-labeled antirabbit IgG)	Human plasma	N/A	[75]
Spectrofluorimetric, derivatization with *o*-phthalaldehyde	Fluorescence at 448 nm, excitation at 337 nm	Human plasma	0.1–1.0 g/mL 0.02 μg/mL (LOD) 0.06 μg/mL (LOQ)	[23]
Electrochemical analysis by DPAdSV and square-wave adsorptive-stripping voltammetry (SWAdSV)	Voltammetric	Human plasma (spiked)	4×10^{-9} to 1.2×10^{-7} M LOD 4.68×10^{-9} (DPAdSV) 3×10^{-9} to 1.9×10^{-8} M LOD 5.02×10^{-9} (SWAdSV)	[21]

3.4. Metabolism

Lamotrigine, a weak base, is extensively metabolized primarily by the action of uridine 5′-diphosphate–glucuronosyl transferases at *N*-2 position. The major metabolite (70%) in humans is the 2-N-glucuronide conjugate [82]. Diminished glucuronidation of Lamotrigine is associated with age-related decline in drug clearance [88]. There is no evidence of saturable metabolism and autoinduction [86].

3.5. Elimination

Lamotrigine is eliminated primarily via hepatic glucuronidation. About 70% of oral 120-mg dose was recovered in urine within 144h, 90% in the form of 2-N-glucuronide and 10% as unchanged drug [85]. Apparent oral clearance of Lamotrigine after administration of single oral dose to healthy subjects ranged from 26.6 to 41.7mL/min. The corresponding half-life was from 24.1 to 35 h [83,85,89]. Prolonged half-life by 37% was observed in subjects with unconjugated hyperbilirubinemia (Gilbert's syndrome) [89].

In summary, Lamotrigine exhibits linear pharmacokinetics that can be significantly affected by coadministration of other AEDs. The elimination rate of Lamotrigine is increased by coadministration of enzyme inducing drugs, such as phenytoin, carbamazepine, phenobarbital, and primidone, and prolonged by administration of valproic acid [90].

3.6. Pharmacological effects

Lamotrigine is used clinically as monotherapy or in combination with other anticonvulsants for treatment of partial and generalized seizures. Lamotrigine is available in tablet form as immediate-release and extended-release formulation. Due to common concomitant administration of other anticonvulsants, dosing recommendations for Lamotrigine are variable and, to optimize treatment, therapeutic drug monitoring is often recommended.

4. METHOD OF CHEMICAL SYNTHESIS

Three general routes for the synthetic preparation of Lamotrigine have been documented in literature.

Route 1

This general synthetic route for the synthesis of Lamotrigine (Scheme 6.5), referenced by GlaxoWellcome [18], involves oxidation of the 2,3-dichlorobenzaldehyde starting material **10** with hydrogen

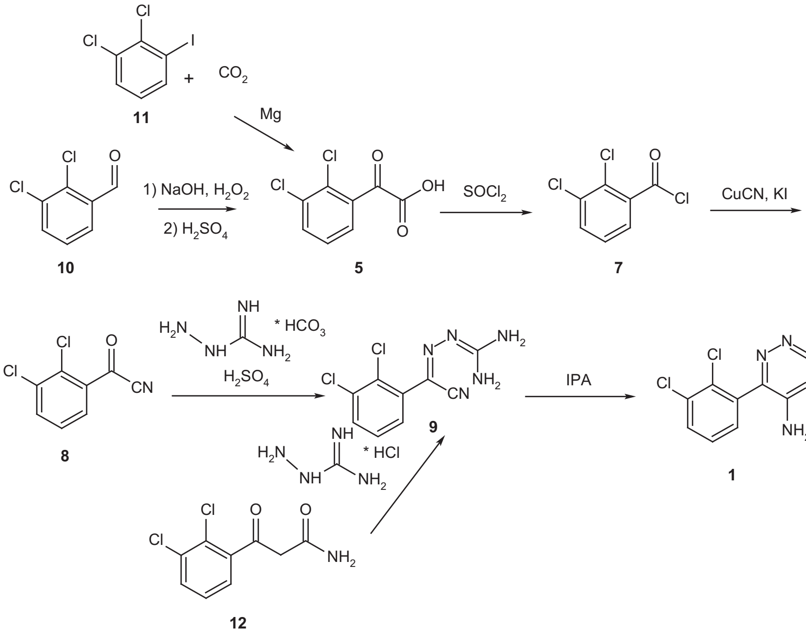

SCHEME 6.5 Synthesis of Lamotrigine (Route 1).

peroxide to the corresponding benzoic acid **5**. The acid chloride **7** is generated from the reaction of **5** with thionyl chloride. Conversion to the corresponding oxo-acetonitrile **8** is achieved via reaction with KI/CuCN under elevated temperature. Preparation of the Schiff base **9** involves reaction of **8** (dissolved in acetonitrile) with aminoguanidine bicarbonate in sulfuric acid. Cyclization of **9** to generate Lamotrigine **1** is performed under reflux conditions with isopropanol. Other variations involve using 2,3-dichlorobenzoic acid **5**, directly, as the starting material [13] or the benzoic acid **5** is generated from Grignard reagent formed from the reaction of 1,2-dichloro-3-iodobenzene **11** and carbon dioxide. Others have reported synthesis of the Schiff base **9** directly from 3-(2,3-dichlorophenyl)-3-oxopropanamide **12** [91]. Other similar and/or variations of this synthetic pathway are also referenced in literature [12,13,91,92].

Route 2

The second route shown in scheme 6.6 [93] begins with oxidation of 2,3-dichloroacetophenone **6** with a suitable oxidizing agent (i.e., chromium trioxide), yielding 2,3-dichlorophenylglyoxylic acid **5**. This acid is subsequently treated with thiosemicarbazide under alkaline conditions to generate the 5-hydroxy-3-thiol-1,2,4-triazine species **4**. Compound **4** (in either amide or imide tautomer) undergoes methylation to yield the related 5-oxo-3-thiomethyl triazine **3**. Chlorination at the 5 position of the

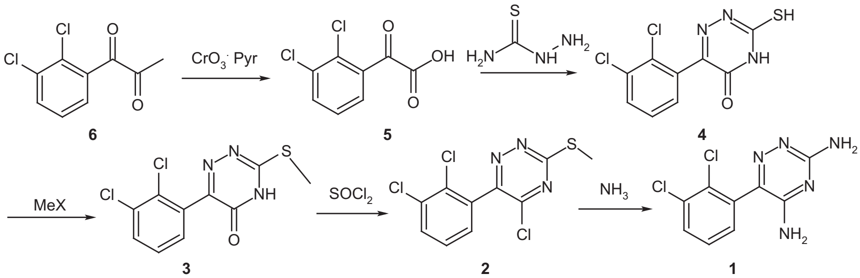

SCHEME 6.6 Synthesis of Lamotrigine (Route 2).

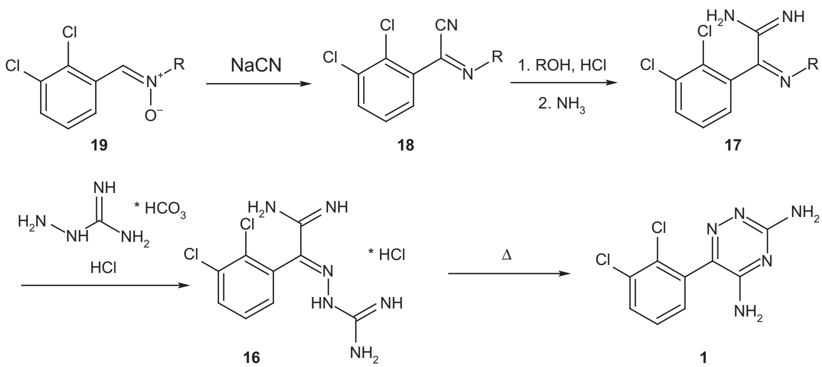

SCHEME 6.7 Synthesis of Lamotrigine (Route 3).

triazine ring with a suitable chlorinating agent (i.e., thionyl chloride) results in the 3-thiomethyl-5-chloro triazine derivative **2** which is then treated with ammonia to afford Lamotrigine **1**.

Route 3

Another approach in the formation of the 1,2,4-triazine ring has been reported [94] and is summarized in Scheme 6.7. In this example, the nitrone **19** is reacted (ambient to 80°C) with sodium cyanide in an aqueous buffer (pH=4–8) with a low-alcohol cosolvent (i.e., methanol). The resulting cyanoimine **18** is reacted with mineral acid (HCl) in alcohol (methanol) and then basified with ammonia. Compound **17** is reacted with an aminoguanidine salt in the presence of a mineral acid. Lamotrigine **1** is achieved via intramolecular cyclization of compound **16** in DMF, followed by extraction, recrystallization from aqueous isopropanol, and drying under vacuum at elevated temperature. The claimed advantages to this synthetic route are the mild conditions of the triazinyl cyclization and the high purity of Lamotrigine obtained.

ACKNOWLEDGMENTS

The authors are indebted to Dr. Pradeep Sanghvi for encouragement and management support. We also wish to express our appreciation to Dr. Yuri Goldberg for his guidance and to Ms. Janet Mensah for her assistance in retrieving the cited literature and finally to many colleagues in our laboratories who contributed materials needed for the preparation of this manuscript.

REFERENCES

[1] *The Merck Index (online)*, 14th ed., Merck & Co. Inc., Whitehouse Station, NJ. http://www.medicinescomplete.com/, Search Term: Lamotrigine, accessed on: Nov. 2, 2011.
[2] L. Zufia, et al., LC method for the therapeutic drug monitoring of lamotrigine: evaluation of the assay performance and validation of its application in the route area, J. Pharm. Biomed. Anal. 49 (2009) 547–553.
[3] M. Hanna et al., WO 2009/061513 A1, 2009.
[4] A.G. Floyd, S. Jain, US 5,942,510, 1999.
[5] European Pharmacopoeia 7.0, vol. 2, Lamotrigine Monograph, 2011.
[6] V.R. Shinde, et al., Enhanced solubility and dissolution rate of lamotrigine by inclusion complexation and solid dispersion technique, J. Pharm. Pharmacol. 60 (2008) 1121–1129.
[7] A. Shayanfar, et al., Solubility of clonazepam, diazepam, lamotrigine, and phenobarbital in n-methyl-2-pyrrolidone + water mixtures at 298.2 K, J. Chem. Eng. Data 54 (2009) 2964–2966.
[8] S. Soltanpour, et al., Effects of different concentrations of poly(vinyl pyrrolidone) on the solubility of lamotrigine and diazepam in ethanol + water mixtures at 298.2 K, J. Chem. Eng. Data 55 (2010) 570–573.
[9] S. Soltanpour, A. Jouyban, Solubility of lamotrigine and diazepam in propylene glycol + water + carboxymethyl cellulose at a temperature of 298.2 K, J. Chem. Eng. Data 55 (2010) 2890–2893.
[10] ACD Labs, Release 11.00, Product Version 11.02, Build 25941, May 21, 2008.
[11] B. Sridhar, K. Ravikumar, Lamotrigine, an antiepileptic drug, and its chloride and nitrate salts, Acta Crystallogr. C C65 (2009) o460–o464.
[12] K. Murthy, MX PA04006216 A, 2005.
[13] C. Kishore, WO 2005/003104 A2, 2005.
[14] N. Garti, et al., US 2008/0139808 A1, 2008.
[15] N. Garti, et al., WO 02/068398 A1, 2002.
[16] United States Pharmacopeia, 34 Revision. National Formulary 29th ed., Lamotrigine Monograph, 2011.
[17] M. Hosseini, et al., Solubility analysis of clozapine and lamotrigine in supercritical carbon dioxide using static system, J. Supercrit. Fluids 52 (2010) 30–35.
[18] L.M. Edmeades, EP 0 963 980 A2, 1999.
[19] British Pharmacopoeia, vol. 2, Lamotrigine Monograph, 2011.
[20] M.E. Burgoa Calvo, et al., Determination of lamotrigine by adsorptive stripping voltammetry using silver nanoparticle-modified carbon screen-printed electrodes, Talanta 74 (2007) 59–64.
[21] M.E. Burgoa Calvo, et al., Optimization of the experimental parameters in the determination of lamotrigine by adsorptive stripping voltammetry, Anal. Chim. Acta 549 (2005) 74–80.
[22] K.D. Altria, Application of microemulsion electrokinetic chromatography to the analysis of a wide range of pharmaceuticals and excipients, J. Chromatogr. A 844 (1999) 371–386.

[23] N.M. El-Enany, et al., Validated spectrofluorimetric method for the determination of lamotrigine in tablets and human plasma through derivatization with o-phthalaldehyde, J. Fluoresc. 20 (2010) 463–472.
[24] N.F. Youssef, E.A. Taha, Development and validation of spectrophotometric, TLC and HPLC methods for the determination of lamotrigine in presence of its impurity, Chem. Pharm. Bull. 55 (2007) 541–545.
[25] E. Dreassi, et al., Quantitative analysis of lamotrigine in plasma and tablets by planar chromatography and comparison with liquid chromatography and UV spectrophotometry, J. AOAC Int. 79 (1996) 1277–1280.
[26] V.R. Ram, et al., Development and validation of a stability indicating HPLC assay method for determination of lamotrigine in tablet formulation, Der Chemica Sinica 2 (2011) 58–65.
[27] I. Ferrer, E.M. Thurman, Identification of a new antidepressant and its glucuronide metabolite in water samples Using liquid chromatography/quadrupole time-of-flight mass spectrometry, Anal. Chem. 82 (2010) 8161–8168.
[28] I.N. Papadoyannis, et al., Solid-phase extraction study and RP-HPLC Analysis of lamotrigine in human biological fluids and in antiepileptic tablet formulations, J. Liq. Chromatogr. 18 (1995) 2593–2609.
[29] M.W. Sinz, R.P. Remmel, Analysis of lamotrigine and lamotrigine 2-N-glucuronide in guinea pig blood and urine by reversed-phase ion-pairing liquid chromatography, J. Chromatogr. 571 (1991) 217–230.
[30] S. Ramachandran, et al., Measurement of lamotrigine under conditions measuring phenobarbitone, phenytoin and carbamazepine using reversed-phase high-performance liquid chromatography at dual wavelengths, Ther. Drug Monit. 16 (1994) 75–82.
[31] S. Yamashita, et al., Simple and rapid analysis of lamotrigine, a novel antiepileptic, in human serum by high-performance liquid chromatography using a solid-phase extraction technique, J. Chromatogr. B 670 (1995) 354–357.
[32] E. Forssblad, et al., Liquid chromatographic determination of plasma lamotrigine in pediatric samples, J. Pharm. Biomed. Anal. 14 (1996) 755–758.
[33] A.P. Hart, et al., A rapid cost-effective high-performance liquid chromatographic (HPLC) assay of serum lamotrigine after liquid-liquid extraction and using HPLC conditions routinely used for analysis of barbiturates, Ther. Drug Monit. 19 (1997) 431–435.
[34] S. Ren, et al., Determination of lamotrigine in biologic materials by a simple and rapid liquid chromatographic method, Ther. Drug Monit. 20 (1998) 209–214.
[35] K.M. Matar, et al., A rapid liquid chromatographic method for the determination of lamotrigine in plasma, J. Pharm. Biomed. Anal. 17 (1998) 525–531.
[36] K.M. Matar, et al., Liquid chromatographic determination of six antiepileptic drugs and two metabolites in microsamples of human plasma, Ther. Drug Monit. 21 (1999) 559–566.
[37] M. Torra, et al., Optimized procedure for lamotrigine analysis in serum by high-performance liquid chromatography without interferences from other frequently coadministered anticonvulsants, Ther. Drug Monit. 22 (2000) 621–625.
[38] G.A. Khoschsorur, et al., Simple and rapid HPLC method for simultaneous determination of multiple antiepileptic drugs in human serum, Chromatographia 54 (2001) 345–349.
[39] M.M. Castel-Branco, et al., Lamotrigine analysis in blood and brain by high-performance liquid chromatography, J. Chromatogr. B 755 (2001) 119–127.
[40] M.E.C. Queiroz, et al., Solid-phase microextraction-liquid chromatography (SPME-LC) determination of lamotrigine simultaneously with carbamazepine and carbamazepine 10,11-epoxide in human plasma, J. Sep. Sci. 25 (2002) 91–95.
[41] M. Contin, et al., Simultaneous liquid chromatographic determination of lamotrigine, oxcarbazepine monohydroxy derivative and felbamate in plasma of patients with epilepsy, J. Chromatogr. B 828 (2005) 113–117.

[42] T.A.C. Vermeij, P.M. Edelbroek, Robust isocratic high performance liquid chromatographic method for simultaneous determination of seven antiepileptic drugs including lamotrigine, oxcarbazepine and zonisamide in serum after solid-phase extraction, J. Chromatogr. B 857 (2007) 40–46.
[43] S. Bompadre, et al., Determination of lamotrigine in whole blood with on line solid phase extraction, J. Chromatogr. B 863 (2008) 177–180.
[44] A.D. Fraser, Lamotrigine analysis in serum by high-performance liquid chromatography, Ther. Drug Monit. 17 (1995) 174–178.
[45] P. Angelis-Stoforidis, et al., Determination of lamotrigine in human plasma by high-performance liquid chromatography, J. Chromatogr. B 727 (1999) 113–118.
[46] M.A. Saracino, et al., Rapid HPLC analysis of the antiepileptic lamotrigine and its metabolites in human plasma, J. Sep. Sci. 30 (2007) 2249–2255.
[47] E. Greiner-Sosanko, et al., Simultaneous determination of lamtrigine, zonisamide, and carbamazepine in human plasma by high-performance liquid chromatography, Biomed. Chromatogr. 21 (2007) 225–228.
[48] C. Greiner, E. Haen, Development of a simple column-switching high-performance liquid chromatograph (HPLC) method for rapid and simultaneous routine serum monitoring of lamotrigine, oxcarbazepine and 10-monohydroxycarbazepine (MHD), J. Chromatogr. B 854 (2007) 338–344.
[49] A. Fazio, et al., A liquid chromatographic assay using a high-speed column for the determination of lamotrigine, a new antiepileptic drug, in human plasma, Ther. Drug Monit. 14 (1992) 509–512.
[50] B.C. Sallustio, R.G. Morris, High-performance liquid chromatography quantitation of plasma lamotrigine concentrations: application measuring trough concentrations in patients with epilepsy, Ther. Drug Monit. 19 (1997) 688–693.
[51] A. Bartoli, et al., A rapid and specific assay for the determination of lamotrigine in human plasma by normal-phase HPLC, Ther. Drug Monit. 19 (1997) 100–107.
[52] C.L. Cheng, et al., Determination of lamotrigine in small volumes of plasma by high-performance liquid chromatography, J. Chromatogr. B 817 (2005) 199–206.
[53] M. Cociglio, et al., Performance analysis of a reversed-phase liquid chromatographic assay of lamotrigine in plasma using solvent-demixing extraction, J. Chromatogr. 572 (1991) 269–276.
[54] M. Meyler, et al., New method for the determination of four antiepileptic drugs in human plasma by high performance liquid chromatography, Chromatographia 36 (1993) 27–32.
[55] G.L. Lensmeyer, et al., Optimized high-performance liquid chromatographic method for determination of lamotrigine in serum with concomitant determination of phenytoin, carbamazepine and carbamazepine epoxide, Ther. Drug Monit. 19 (1997) 292–300.
[56] L. Franceschi, M. Furlanut, A simple method to monitor plasma concentrations of oxcarbazepine, carbamazepine, their main metabolites and lamotrigine in epileptic patients, Pharmacol. Res. 51 (2005) 297–302.
[57] D. Londero, P.L. Greco, New micromethod for the determination of lamotrigine in human plasma by high-performance liquid chromatography, J. Chromatogr. B 691 (1997) 139–144.
[58] D. Croci, et al., New high-performance liquid chromatographic method for plasma/serum analysis of lamotrigine, Ther. Drug Monit. 23 (2001) 665–668.
[59] C. Heideloff, et al., A novel HPLC method for quantification of 10 antiepileptic drugs or metabolites in serum/plasma using a monolithic column, Ther. Drug Monit. 32 (2010) 102–106.
[60] M.V. Doig, R.A. Clare, Use of thermospray liquid chromatography—mass spectrometry to aid in the identification of urinary metabolites of a novel antiepileptic drug, lamotrigine, J. Chromatogr. 554 (1991) 181–189.

[61] O. Beck, et al., Determination of lamotrigine and its metabolites in human plasma by liquid chromatography-mass spectrometry, Ther. Drug Monit. 28 (2006) 603–607.
[62] L.K. Sorensen, Determination of acidic and neutral therapeutic drugs in human blood by liquid chromatography-electrospray tandem mass spectrometry, Forensic Sci. Int. 206 (2011) 119–126.
[63] H.J. Shah, et al., Rapid quantification of lamotrigine in human plasma by two LC systems connected with tandem MS, J. Chromatogr. Sci. 48 (2010) 375–381.
[64] W. Lee, et al., Determination of lamotrigine in human serum by high-performance liquid chromatography-tandem mass spectrometry, Neurol. Sci. 31 (2010) 717–720.
[65] M.E.C. Queiroz, et al., Determination of lamotrigine simultaneously with carbamazepine, carbamazepine epoxide, phenytoin, phenobarbital, and primidone in human plasma by SPME-GC-TSD, J. Chromatogr. Sci. 40 (2002) 219–223.
[66] M. Watelle, et al., Analysis of the antiepileptic phenyltriazine compound lamotrigine using gas chromatograph with nitrogen phosphorus detection, Ther. Drug Monit. 19 (1997) 460–464.
[67] A. Dasgupta, A.P. Hart, Lamotrigine analysis in plasma by gas chromatography-mass spectrometry after conversion to a tert-butyldimethylsilyl derivative, J. Chromatogr. B 693 (1997) 101–107.
[68] J. Hallbach, et al., Determination of lamotrigine, carbamazepine and carbamazepine epoxide in human serum by gas chromatography mass spectrometry, Eur. J. Clin. Chem. Clin. Biochem. 35 (1997) 755–759.
[69] K.M. Patil, S.L. Bodhankar, High-performance thin-layer chromatographic determination of lamotrigine in serum, J. Chromatogr. B 823 (2005) 152–157.
[70] Z.K. Shihabi, K.S. Oles, Serum lamotrigine analysis by capillary electrophoresis, J. Chromatogr. B 683 (1996) 119–123.
[71] R. Theurillat, et al., Therapeutic drug monitoring of lamotrigine using capillary electrophoresis. Evaluation of assay performance and quality assurance over a 4-year period in the routine arena, J. Chromatogr. A 979 (2002) 353–368.
[72] J. Zheng, et al., Development of capillary zone electrophoresis-electrospray ionization-mass spectrometry for the determination of lamotrigine in human plasma, Electrophoresis 25 (2004) 2033–2043.
[73] V. Pucci, et al., Analysis of lamotrigine and its metabolites in human plasma and urine by micellar electrokinetic capillary chromatography, Electrophoresis 26 (2005) 935–942.
[74] R.A. Biddlecombe, et al., Validation of a radioimmunoassay for the determination of human plasma concentrations of lamotrigine, J. Pharm. Biomed. Anal. 8 (1990) 691–694.
[75] J.M. Sailstad, J.W. Findlay, Immunofluorometric assay for lamotrigine (Lamictal) in human plasma, Ther. Drug Monit. 13 (1991) 433–442.
[76] D.A. Coulter, Antiepileptic drug cellular mechanisms of action: where does lamotrigine fit in? J. Child Neurol. 12 (1997) S2–S9.
[77] K.L. Goa, et al., Lamotrigine: a review of its pharmacological properties and clinical efficacy in epilepsy, Drugs 46 (1993) 152–176.
[78] A. Fitton, K.L. Goa, Lamotrigine: an update of its pharmacology and therapeutic use in epilepsy, Drugs 50 (1995) 691–713.
[79] A.H. Burstein, Evaluation of new drugs: lamotrigine, Pharmacotherapy 15 (1995) 129–143.
[80] B. Rambeck, P. Wolf, Lamotrigine clinical pharmacokinetics, Clin. Pharmacokinet. 25 (1993) 433–443.
[81] V. Biton, Pharmacokinetics, toxicology and safety of lamotrigine in epilepsy, Expert Opin. Drug Metab. Toxicol. 2 (2006) 1009–1018.
[82] W.R. Garnett, Lamotrigine: pharmacokinetics, J. Child Neurol. 12 (1997) S10–S15.
[83] W.C. Yuen, W. Peck, Lamotrigine pharmacokinetics: oral and i.v. infusion in man, Br. J. Clin. Pharmacol. 26 (1988) 242P.

[84] A.W. Peck, Clinical pharmacology of lamotrigine, Epilepsia 32 (1991) S9–S12.
[85] A.F. Cohen, et al., Lamotrigine, a new anticonvulsant: pharmacokinetics in normal humans, Clin. Pharmacol. Ther. 42 (1987) 534–541.
[86] R.E. Ramsey, et al., Pharmacokinetics and safety of lamotrigine (Lamictal®) in patients with epilepsy, Epilepsy Res. 10 (1991) 191–200.
[87] S. Jawad, Lamotrigine: single-dose pharmacokinetics and initial 1 week experience in refractory epilepsy, Epilepsy Res. 1 (1987) 194–201.
[88] H. Arif, et al., The effect of age and comedication on lamotrigine clearance tolerability, and efficacy, Epilepsia 52 (2011) 1905–1913.
[89] J. Posner, et al., The pharmacokinetics of lamotrigine (BW430C) in healthy subjects with unconjugated hyperbilirubinaemia (Gilbert's syndrome), Br. J. Clin. Pharmacol. 28 (1989) 117–120.
[90] A.W. Yuen, et al., Sodium valproate acutely inhibits lamotrigine metabolism, Br. J. Pharmacol. 33 (1992) 511–513.
[91] R. G. Winter et al., US 5,912,345, 1999.
[92] Y. Qian, et al., Synthesis, antimicrobial activity of lamotrigine and its ammonium derivatives, J. Chem. Sci. 121 (2009) 463–470.
[93] G. Lee, WO 96/20935.
[94] G. Schneider et al., US 2003/0191310 A1, 2003.

CHAPTER 7

Pimozide

Robert Smyj, Xiao-Ping Wang, and **Feixue Han**

Contents

Apotex Inc., Toronto, Ontario, Canada

Profiles of Drug Substances, Excipients, and Related Methodology, Volume 37
ISSN 1871-5125, DOI: 10.1016/B978-0-12-397220-0.00007-6

© 2012 Elsevier Inc.
All rights reserved.

1. GENERAL INFORMATION

1.1. Nomenclature

1.1.1. Systematic chemical names

1-[1-[4,4-Bis(4-fluorophenyl)butyl]piperidin-4-yl]-1,3-dihydro-2*H*-benzimidazol-2-one [1]
2*H*-Benzimidazol-2-one, 1-[1-[4,4-bis(4-fluorophenyl)butyl]-4-piperidinyl]-1,3-dihydro- [2,3]
1-[1-[4,4-Bis(*p*-fluorophenyl)butyl]-4-piperidyl]-2-benzimidazolinone [2–4]
1-[1-[4,4-Bis(4-fluorophenyl)butyl]-4-piperidinyl]-1,3-dihydro-2*H*-benzimidazol-2-one [4–6]
1-[4,4-Di-(4-fluorophenyl)butyl]-4-(2-oxo-1-benzimidazolinyl)-piperidine [4]

1.1.2. Nonproprietary name

Pimozide (INN, USAN, BAN, JAN) [3]

1.1.3. Proprietary names

Orap [3–6], Opiran [4,6], Antalon [5], Antolan [6], Pizide [6]

1.2. Formulae

1.2.1. Empirical formula, molecular weight, CAS number

Empirical formula: $C_{28}H_{29}F_2N_3O$
Molecular weight: 461.55
CAS number: 2062-78-4

1.2.2. Structural formula

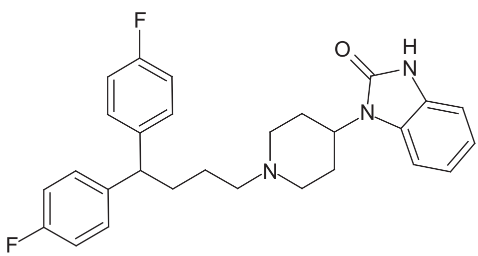

1.3. Elemental analysis

%C: 72.86; %H: 6.33; %F: 8.23; %N: 9.10; %O: 3.47

1.4. Appearance

White or almost white powder [1]
White, crystalline powder [7]

2. PHYSICAL CHARACTERISTICS

2.1. Ionization constant

pK_a: 7.32 [4], 7.3 [6]

2.2. Solubility characteristics

In the USP [7], pimozide is described as being freely soluble in chloroform, slightly soluble in ether and in alcohol, and insoluble in water. It is also noted that 1 g of pimozide is soluble in 100 mL of acetone, in 1000 mL of methanol, and in more than 1000 mL of 0.1 N HCl [8].

The EP monograph for pimozide [1] states that the drug substance is practically insoluble in water, soluble in methylene chloride, sparingly soluble in methanol, and slightly soluble in 96% aqueous ethanol.

The Merck Index [4] describes pimozide as being almost insoluble in water (<0.01 mg/mL) and very slightly soluble in dilute aqueous solutions of organic and mineral acids (<5 mg/mL).

The aqueous solubility of pimozide with respect to pH has been determined in our laboratory and is described in Table 7.1.

2.3. Partition coefficient

log *P*: 5.34 [9]

log *P*: 6.3 (octanol/water) [6,10]

2.4. Melting behavior

Melting range: 214–218 °C [4,6]

Maximum temperature of melting endotherm by DSC: 219 °C [9]

TABLE 7.1 Aqueous solubility of pimozide at different pHs

Solvent	pH	Solubility (mg/mL)
0.1 N HCl	1.2	0.03
SGF (without enzymes)	1.3	0.02
0.01 N HCl	2.0	0.23
0.05 M phosphate buffer	2.5	0.02
0.05 M phosphate buffer	4.0	0.09
0.05 M phosphate buffer	4.5	0.03
Water	5.7	<0.001
0.05 M phosphate buffer	6.0	0.002
0.05 M phosphate buffer	6.8	<0.001
0.05 M phosphate buffer	7.2	<0.001
0.05 M phosphate buffer	7.5	<0.001

SGF, simulated gastric fluid.

2.5. Spectroscopy

2.5.1. UV/Vis spectroscopy

The UV absorption spectrum of pimozide (dissolved in methanol at a concentration of 10.91 mg/L) was obtained over a range of 200–400 nm using a Perkin-Elmer UV/Vis Lambda 2 spectrometer. As illustrated in Fig. 7.1, the compound exhibits an absorption maximum in the 210–400 nm interval at 282 nm (molar absorptivity=6.58×10^3).

2.5.2. Vibrational spectroscopy

The infrared spectrum of pimozide was obtained on a Perkin-Elmer Spectrum 400 spectrometer equipped with a Spotlight 400 Imaging System. The compound was flattened and mounted on a KBr pellet, and the resulting IR absorption spectrum is shown in Fig. 7.2. A summary of functional group assignment for the major observed bands is provided in Table 7.2.

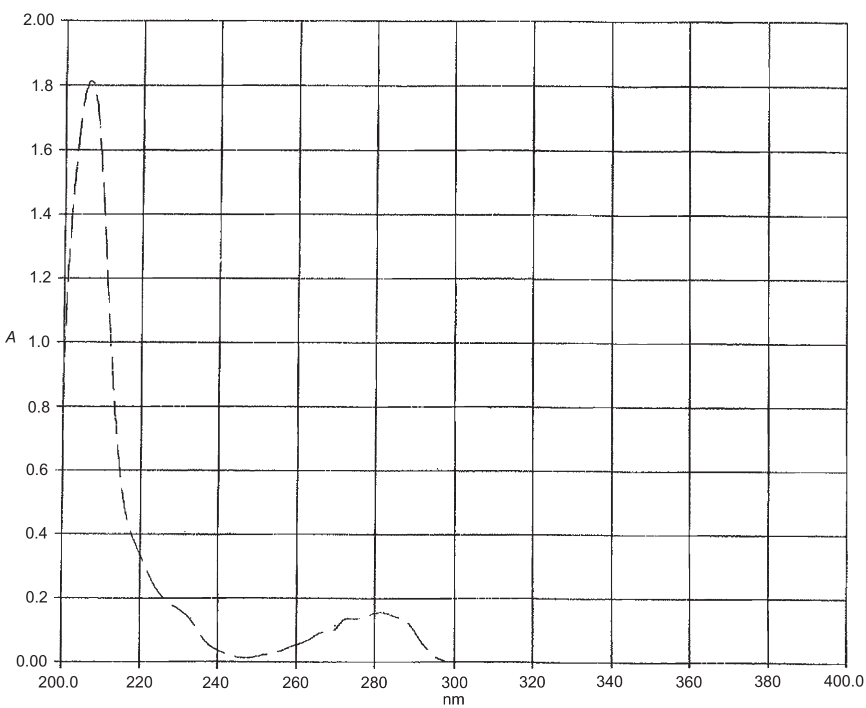

FIGURE 7.1 Ultraviolet absorption spectrum of pimozide.

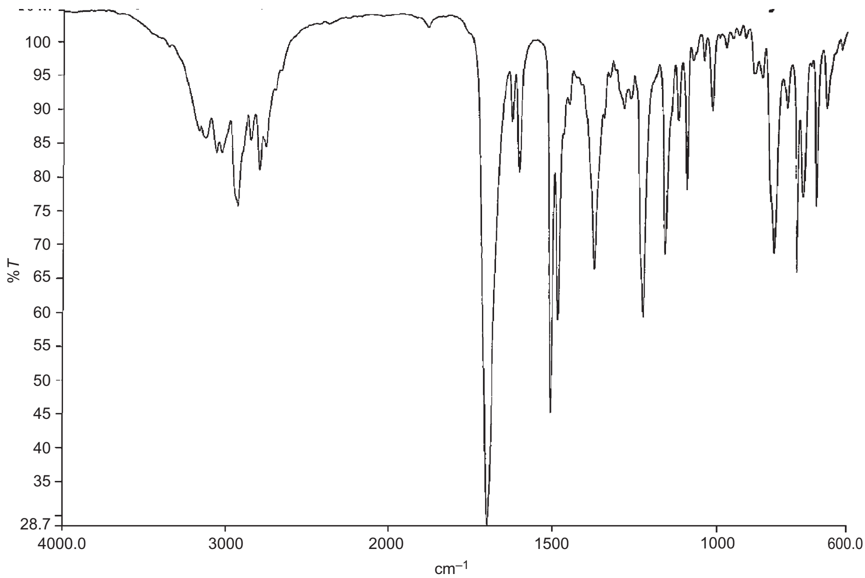

FIGURE 7.2 Infrared absorption spectrum of pimozide.

2.5.3. Nuclear magnetic resonance spectroscopy

Both the ^{1}H NMR and ^{13}C NMR spectra of pimozide were obtained on a Bruker ARX-300 spectrometer, operating at 300.135MHz (^{1}H NMR) or at 75.475MHz (^{13}C NMR). Spectra were recorded for a solution of pimozide in $CDCl_3$. Chemical shifts are reported in parts per million relative to TMS.

2.5.3.1. ^{1}H NMR spectrum The ^{1}H NMR spectrum of pimozide is shown in Fig. 7.3, and the resonance signal assignments are provided in Table 7.3.

TABLE 7.2 Band assignments for the infrared absorption spectrum of pimozide

Band energy (cm^{-1})	Assignment
3035	Aromatic (C—H) stretch
2937, 2808	Aliphatic (C—H) stretch
1698	Imidazolidin-2-one (C═O) stretch
1625, 1604, 1507, 1484	Aromatic ring skeleton stretch
1223, 1157	Fluoroaromatic (C—F) stretch
828, 756, 738, 696	Aromatic (C—H) out of plane bend

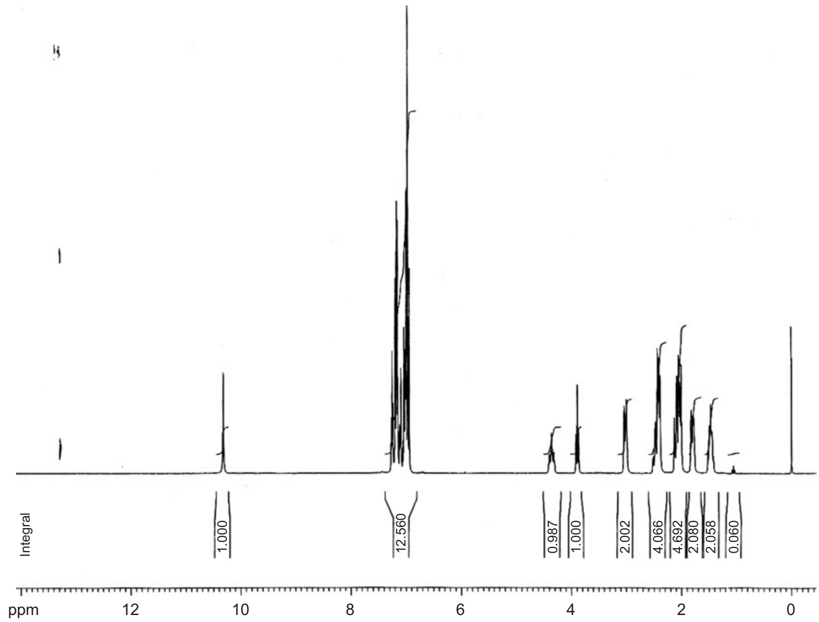

FIGURE 7.3 ^{1}H NMR spectrum of pimozide.

2.5.3.2. ^{13}C NMR spectrum The ^{13}C NMR and DEPT ^{13}C NMR spectra of pimozide are shown in Figs. 7.4 and 7.5, respectively, and the assignments for the observed signals are provided in Table 7.4.

2.5.4. Mass spectrometry

An electrospray ionization mass spectrometry study of pimozide was carried out on a Perkin-Elmer/Sciex API-300 triple quadrupole mass spectrometer. The sample was dissolved in a mobile phase consisting of aqueous acetonitrile (50/50 v/v) and 0.05% of acetic acid. The sample was introduced into the mass spectrometer at a flow rate of 0.3mL/h using a syringe pump. The electrospray ionization mass spectrum (ESI MS) of pimozide is shown in Fig. 7.6. The spectrum displays the protonated pimozide molecular ion peak $[M+H]^+$ at m/z 462. The MS/MS spectrum of this ion is shown in Fig. 7.7. The major fragment ions (i.e., those with m/z of 201 and 328) are proposed to originate from the protonated molecular ion of pimozide as shown in Scheme 7.1.

TABLE 7.3 ^{1}H NMR spectral data for pimozide

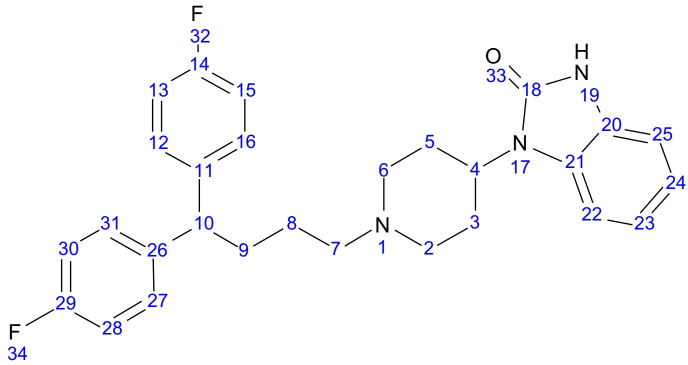

Chemical shift (ppm)	Multiplicity; coupling constant (Hz)	Integration	Assignment[a]
10.32	s	1H	H19[b]
7.27–6.93	m	12H	H12/H16/H27/H31, H13/H15/H28/H30, H22, H23, H24, H25
4.41–4.30	m	1H	H4
3.89	t; J=7.8	1H	H10
3.03–3.00	m	2H	H2e, H6e
2.52–2.39	m	4H	H2a, H6a, H7
2.14–2.00	m	4H	H3e, H5e, H9
1.82–1.78	m	2H	H3a, H5a
1.52–1.42	m	2H	H8

[a] Assignments separated by a slash "/" refer to chemical shift equivalent protons. The letters "a" and "e" denote axial and equatorial protons, respectively.
[b] This proton is exchangeable with D_2O.

3. STABILITY

3.1. Solid-state stability

From studies of material stressed in the solid state, pimozide has been observed to be a stable molecule. Thermal stress (60 and 80°C, 105 days), heat/high humidity stress (40°C/75%RH, 105 days), and light stress (310–800nm, 3.0×10^{6}luxh) did not result in any significant levels of degradation.

3.2. Solution-phase stability

The stability of pimozide has also been investigated under solution-phase stress conditions. Pimozide was stable from acidic (0.1N HCl in 90% methanol, 90°C, 6h), basic (0.1N NaOH in 90% methanol, 90°C, 6h),

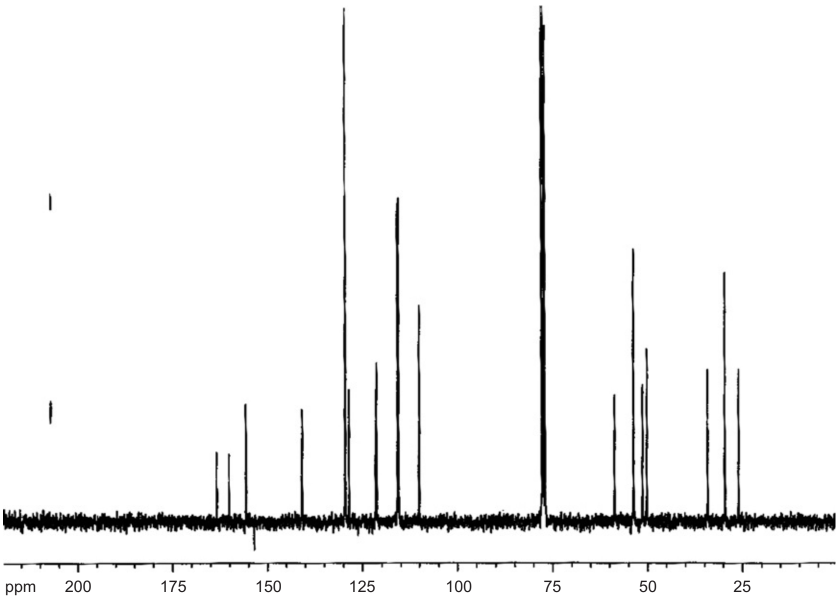

FIGURE 7.4 ^{13}C NMR spectrum of pimozide.

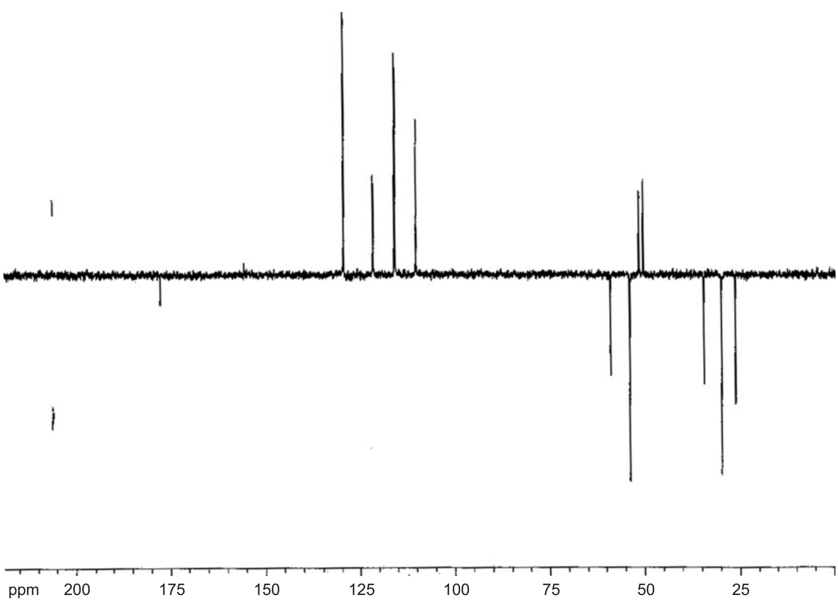

FIGURE 7.5 DEPT ^{13}C NMR spectrum of pimozide.

TABLE 7.4 ^{13}C NMR spectral data for pimozide

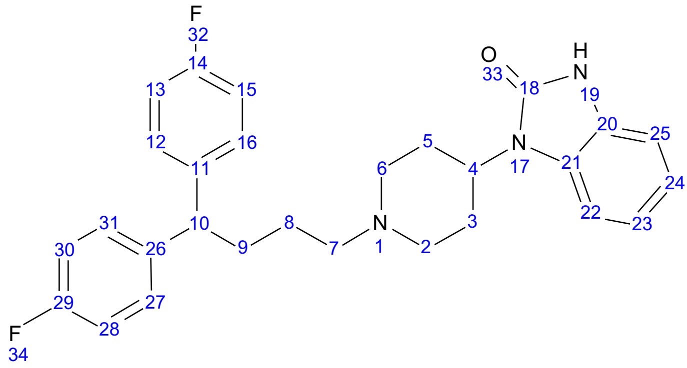

Chemical shift (ppm); multiplicity[a] Coupling constant (Hz)	DEPT	Assignment[b]
161.77; d; $^1J_{C\text{–}F}$=245.1	C	C14/C29
155.66	C	C18
140.95	C	C11/C26
129.50; d; $^3J_{C\text{–}F}$=7.7	CH	C12/C16/C27/C31
128.54	C	C20, C21
121.54, 121.35	CH	C23, C24
115.68; d; $^2J_{C\text{–}F}$=20.9	CH	C13/C15/C28/C30
110.12	CH	C22, C25
58.73	CH_2	C7
53.72	CH_2	C2/C6
51.33, 50.17	CH each	C4, C10
34.28	CH_2	C8
29.66	CH_2	C3/C5
26.02	CH_2	C9

[a] Multiplicities with coupling constants are noted for ^{13}C–^{19}F coupling where observed.
[b] Assignments separated by a slash "/" refer to chemical shift equivalent carbons.

thermal (90% aqueous methanol, 85–90 °C, 6 h), and light (90% aqueous methanol, 310–800 nm, 3.0×10^6 lux h) stress, however, degraded from oxidative stress (3% H_2O_2 in 90% methanol, room temperature, 3 h). The principal degradation product of pimozide from oxidative solution stress conditions is the N-oxide of pimozide.

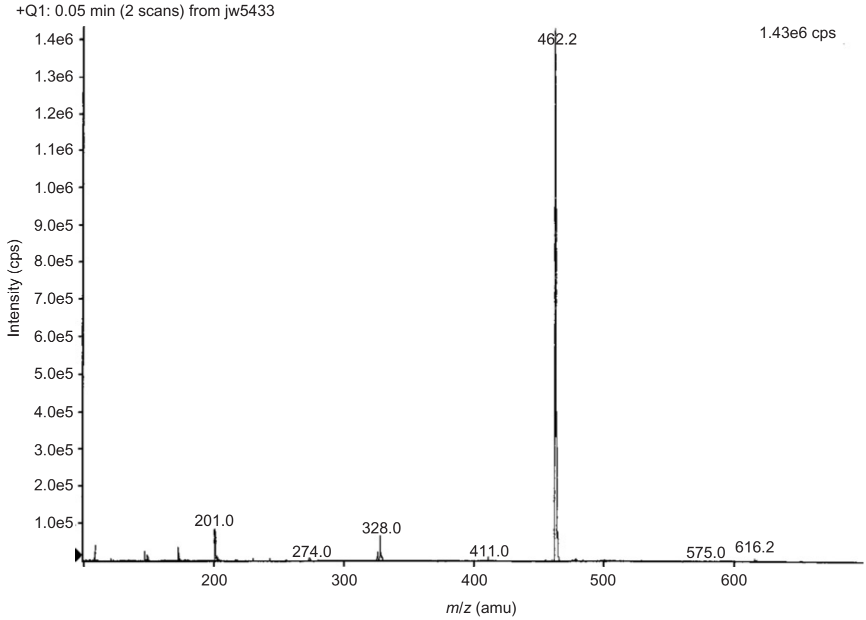

FIGURE 7.6 Electrospray ionization mass spectrum of pimozide.

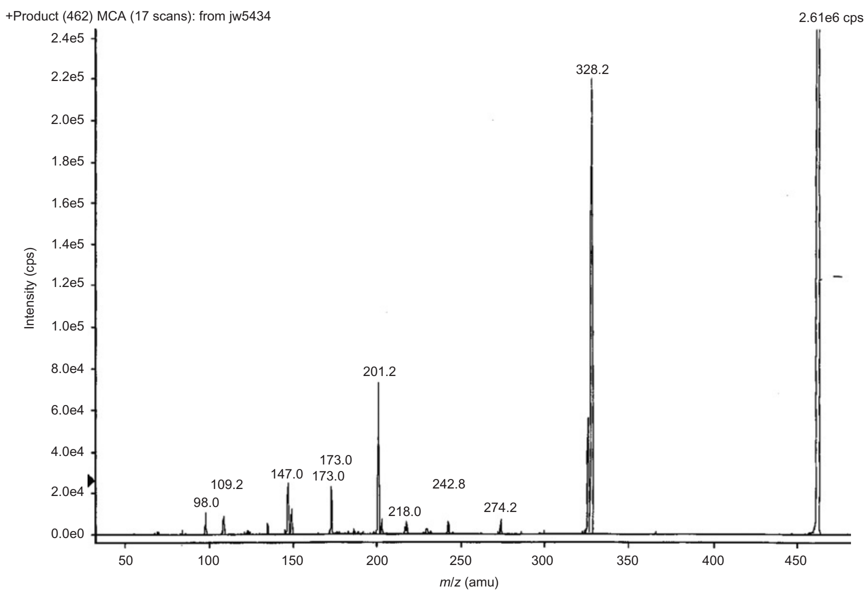

FIGURE 7.7 MS/MS spectrum of the protonated pimozide ion peak $[M+H]^+$ at *m/z* 462.

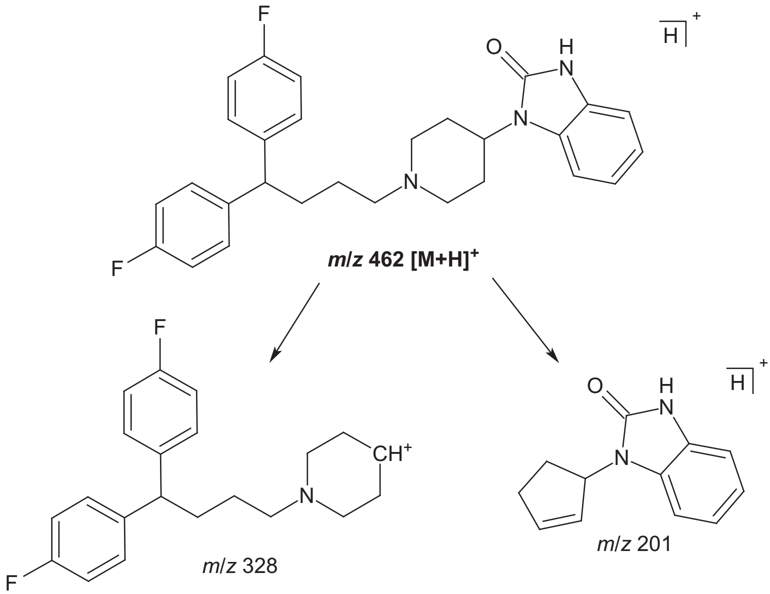

SCHEME 7.1 Proposed fragmentations observed in the MS/MS spectrum of the protonated pimozide ion peak.

4. METHOD OF ANALYSIS

4.1. Known impurities of pimozide

The structures, chemical names, and classification of the known impurities of pimozide are shown in Table 7.5. Impurities A–E are specified impurities listed in the EP/BP monographs of pimozide drug substance [11,12]. All of the compendial listed impurities are potential manufacturing process-related impurities. In addition, impurity A is also the major active metabolite of pimozide [13–15] and impurity E is a degradation product formed under oxidative conditions.

4.2. Compendial methods of analysis

4.2.1. USP methods of analysis

The USP [2] prescribes the following tests for pimozide drug substance:

- Identification A: Infrared absorption ⟨197K⟩
- Identification B: Ultraviolet absorption ⟨197U⟩
- Melting range, Class I ⟨741⟩: between 216 and 220°C
- Loss on drying: ⟨731⟩: In vacuum at 80°C for 4h; loses not more than 0.5%

TABLE 7.5 Impurities of pimozide

Structure	Chemical name	Classification
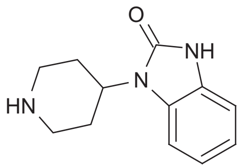 A	1-(Piperidin-4-yl)-1,3-dihydro-2*H*-benzimidazol-2-one	EP/BP Impurity A Synthetic impurity Active metabolite
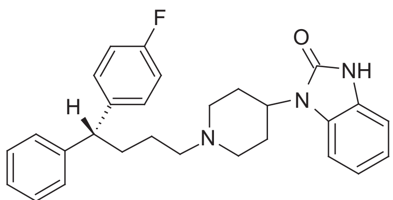 and enantiomer B	1-[1-[(4*RS*)-4-(4-Fluorophenyl)-4-phenylbutyl]piperidin-4-yl]-1,3-dihydro-2*H*-benzimidazol-2-one	EP/BP Impurity B Synthetic impurity
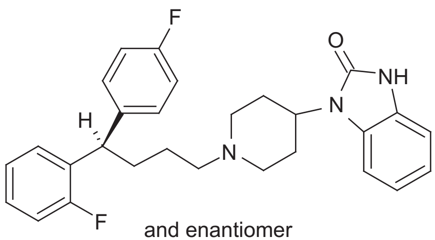 and enantiomer C	1-[1-[(4*RS*)-4-(2-Fluorophenyl)-4-(4-fluorophenyl)butyl] piperidin-4-yl]-1,3-dihydro-2*H*-benzimidazol-2-one	EP/BP Impurity C Synthetic impurity

(*continued*)

TABLE 7.5 (*continued*)

Structure	Chemical name	Classification
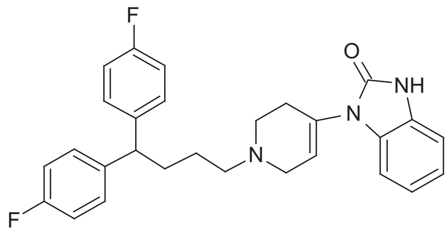 D	1-[1-[4,4-Bis(4-fluorophenyl)-butyl]-1,2,3,6-tetrahydropyridin-4-yl]-1,3-dihydro-2*H*-benzimidazol-2-one	EP/BP Impurity D Synthetic impurity
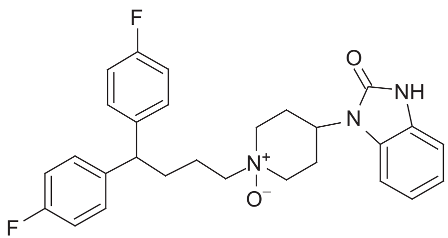 E	1-[1-[4,4-Bis(4-fluorophenyl)-butyl]piperidin-4-yl-1-oxide]-1,3-dihydro-2*H*-benzimidazol-2-one	EP/BP Impurity D Synthetic impurity Degradation product

- Residue on ignition ⟨281⟩: Not more than 0.2% for a 2-g sample
- Heavy metals, method II⟨231⟩: Not more than 0.002%
- Assay–potentiometric titration: 98.0–102.0% calculated on the dried basis
- Ordinary impurities: Thin-layer chromatography (TLC) ⟨466⟩; the total of any ordinary impurities observed does not exceed 1.0%

Also in the USP, a monograph for pimozide tablets is given [16]. The following tests are prescribed for USP pimozide tablets:

- Identification: The retention time of the major peak in the chromatogram of the *Assay preparation* corresponds to that of the *Standard preparation*, both relative to the internal standards, as obtained in the *Assay*.
- Assay—Isocratic HPLC; 90.0–110.0% of the labeled amount of pimozide.
- Dissolution ⟨711⟩
  Medium: 0.01 N HCl; 900 mL
  Apparatus 2: 50 rpm
  Time: 30 min
  Quantitative method: UV at 277 nm; not less than 80% (*Q*) of the labeled amount of pimozide is dissolved in 30 min.
- Uniformity of dosage units ⟨905⟩: Quantitative method by UV at 277 nm; meets the requirements of ⟨905⟩.

4.2.2. EP/BP methods of analysis

The EP/BP harmonized Ph Eur monograph 1254 [11,12] prescribes the following tests for pimozide drug substance:

- Identification: First identification B; second identification A, C, D.
  A: Melting point (2.2.14): 216–220 °C.
  B: Infrared absorption (2.2.24): Comparison with pimozide CRS
  C: TLC (2.2.27): The principal spot in the chromatogram obtained with the test solution is similar in position and size to the principal spot in the chromatogram obtained with reference solution.
  D: Mix about 5 mg with 45 mg of *heavy magnesium oxide R* and ignite in a crucible until an almost white residue is obtained. Allow to cool, then add 1 mL of *water R*, 0.05 mL of *phenolphthalein solution R1*, and about 1 mL of *dilute hydrochloric acid R* to render the solution colorless. The solution is then filtered. To a freshly prepared mixture of 0.1 mL of *alizarin S solution R* and 0.1 mL of *zirconyl nitrate solution R*, add 1.0 mL of the filtrate. Mix, allow to stand for 5 min, and compare the color of the solution with that of a blank prepared in the same manner. The test solution is yellow, and the blank is red.
- Appearance of solution: The solution is clear (2.2.1) and not more intensely colored than reference solution Y_7 (2.2.2, method II).

- Loss on drying: (2.2.32): Drying in an oven at 105°C; determined on 1.000 g; loses not more than 0.5%.
- Sulfated ash (2.4.14): Not more than 0.1% determined on a 1.0-g sample in a platinum crucible.
- Related substances: HPLC gradient; Impurities A, B, C, D, E: Not more than 0.5% each; not more than 0.75% total impurities found; disregard limit 0.05%.
- Assay: Potentiometric titration, 99.0–101.0% calculated on the dried basis.

A monograph for pimozide tablets is also included in the BP [17]. The following tests are prescribed for BP pimozide tablets:

- Identification A: The infrared absorption spectrum of drug product residue is concordant with BP's reference spectrum of pimozide (*RS 389*).
- Identification B: The principal peak in the chromatogram obtained with *Assay* sample solution has the same retention time as the principal peak in the chromatogram obtained with the reference standard solution.
- Related substances: Gradient HPLC; not more than 0.5% for any second peak; not more than 0.75% for total impurities found; disregard limit 0.05%.
- Assay: Gradient HPLC method as described under *Related substances*; 95.0–105.0% of the labeled amount of pimozide tablets.
- Dissolution:
  Medium: 0.01 N HCl; 900 mL
  Apparatus 2: 100 rpm
  Time: 45 min
  Quantitative method: Gradient HPLC method as described under *Related substances*.
- Uniformity of content: Quantitation by gradient HPLC method as described under *Related substances*.

4.3. Thin-layer chromatography

Pluym *et al*. reported a procedure for the two-dimensional TLC detection and differentiation of pimozide in the presence of other butyrophenone–diphenylbutylpiperidine compounds and phenothiazine derivatives [18]. IPre-coated TLC silica gel 60 F 254 plates were used. Eluent A consisted of ethyl acetate–chloroform–methanol–0.1 M sodium acetate (pH 4.7) (54:23:18:5). Eluent B consisted of chloroform–ethanol (90:10). The detection spray reagents were (1) 0.1% ethanolic bromocresol purple solution containing a few drops of 10% ammonia solution or (2) 40 mg of bromocresol green dissolved in 100 mL of ethanol, with 0.1 N NaOH added to

make the solution blue. After spraying, the TLC plate was heated at 100 °C for 30 min. A complete separation was obtained for pimozide, which has an R_f value of 0.75 using eluent A and an R_f value of 0.52 using eluent B.

Ojanpera *et al*. [19] also reported a TLC method with the combined use of normal and reverse phase used for the detection and determination of pimozide.

4.4. High-performance liquid chromatography with electrochemical detection

Özkan *et al*. reported a high-performance liquid chromatographic method with electrochemical detection (HPLC-EC) for the analysis of pimozide, which allowed pimozide to be detected down to a level of 2.7×10^{-10} M (0.25 ppb) [20]. Pimozide was irreversibly oxidized at high positive potentials. The oxidation product undergoes a chemical reaction to a second product, which is more readily oxidized/reduced than the original compound. A highly sensitive HPLC method with glassy carbon EC mode (HPLC-EC) was then developed for trace measurements of pimozide. The results obtained by HPLC-EC method show that the linearity ranges of calibration plots can be expanded to 5000 times lower concentrations than that reported in the literature [21] using HPLC with UV detection. Additionally, the limit of detection for the HPLC-EC method has no significant difference in comparison to the reported HPLC-MS procedure [22].

4.5. High-performance liquid chromatography–mass spectrometry

Several research groups around the world have reported quantitative determination of pimozide in drug dosage forms, plasma, human serum, and blood samples using high-performance liquid chromatography–mass spectrometry (LC-MS) [22–27]. These LC-MS analytical methods have demonstrated to be suitable for the quantitative determination of pimozide at extremely low concentrations. Some of these methods have been validated and demonstrated to be selective, linear, accurate and precise, and robust for routine analysis.

4.6. Spectrophotometric and conductometric analysis

Kurzawa *et al*. reported a spectrophotometric and conductometric determination of pimozide [28]. The spectrophotometric method is based on the reaction of pimozide with $[Cr(NCS)_6]^{3-}$ and picric acid. Calibration plots are consistent with Beer's law in the concentration ranges of 0.18–2.68 μg/mL with $[Cr(NCS)_6]^{3-}$ and 0.06–0.91 μg/mL with picric acid for pimozide. Conductometric titrations were performed with $(NH_4)_6Mo_7O_{24}$, $NaVO_3$,

and $NaAsO_2$ as titrants. Both spectrophotometric and conductometric methods are accurate and precise with the relative standard deviation less than 1%.

Kelani *et al*. also reported a procedure for spectrophotometric determination of pimozide using 2,3-dichloro-5,6-dicyano-*p*-benzoquinone (DDQ) [29]. The method depends on the interaction of pimozide with DDQ as π acceptor to form a highly colored reaction product. The analytical wavelength chosen is 588nm, which gives maximum sensitivity.

4.7. Potentiomeric titration

Hopkala *et al*. reported a potentiometric titration method for the determination of pimozide [30]. Pimozide contains fluorine which allows an assay based on the determination of this element. Potentiometric titration of fluorides with lanthanum nitrate was carried out in ethanolic medium, thus ensuring a slight solubility of nascent lanthanum fluoride. In the course of titration, one sharp change of the potential occurred at the molar ratio of 1:3 of the reacting ions.

4.8. Determination of body fluids and tissues

The biological analytical methods of pimozide (^{3}H labeled or ^{14}C labeled) in animal samples were developed in late 1960s by Janssen Pharmaceutical. Samples of blood, brain, and liver of rat and dogs were collected and assayed for total radioactivity (^{3}H) by liquid scintillation spectrometry [31,32]. The samples of urine and feces were collected and assayed for total radioactivity (^{14}C) by the same technology [14]. The authors described the technology in detail in the early studies [33,34]. The amount of unchanged pimozide and its metabolites was estimated by inverse isotope dilution techniques in aliquots of urine and of feces extract [14,34]. A radioimmunoassay method for pimozide in rabbit serum was developed later by the same group [35].

Methods of analysis for pimozide originating from human blood samples have involved differential pulse voltammetry [20], TLC [36], spectrophotometry with the use of a complexing agent [36], and HPLC employing fluorescence detection [37,38]. Methods have also been developed for the identification and quantitative determination of drugs present simultaneously in human blood samples, including pimozide. In one example, LC-MS has been used to separate, identify, and quantify pimozide in a sample including 14 other neuroleptics and 3 of their metabolites [25]. Similarly, LC-MS/MS has been used to analyze pimozide in human blood samples containing 29 other antipsychotics [23] as well as in a mixture containing a total of 48 antidepressants and antipsychotics [24].

5. PHARMACOKINETICS AND METABOLISM

5.1. Uses, application, and pertinent history

Pimozide is a potent neuroleptic drug belonging to the diphenylpiperidine class. It was extensively investigated as a new antipsychotic drug in 1970s and early 1980s [39–41]. Currently, pimozide is widely used in Europe for the treatment of delusions, schizophrenia, and other psychiatric disorders. The use of pimozide in the United States is restricted to the management of motor and phonic tics associated with Gilles de la Tourette's syndrome [42,43]. It is the first drug approved by FDA under the Orphan Drug Act [43].

5.2. Absorption

More than 50% of a dose of pimozide is absorbed after oral administration [13]. The absorption is slow [44,45]. Peak plasma concentrations generally occur 6–8h after dosing. The t_{max} is not statistically different among patients with chronic schizophrenics or Tourette's syndrome and healthy volunteers. The extent of absorption between children and adults with Tourette's syndrome shows no apparent difference. Wide inter-subject variability is observed in pharmacokinetics of pimozide due to the different metabolic capacity of patients. The relative bioavailability of 2-mg pimozide tablets is equivalent to an oral solution [41]. There is little information regarding the effect of food on pimozide absorption.

5.3. Distribution

The volume of distribution of pimozide at steady state has been determined to be 19.9 (±14.5) and 28.8 (±18.3)L/kg in children and in adults with Tourette's syndrome, respectively [45]. The results were not appreciably different from the volume of distribution (30 (±15)L/kg) found in healthy volunteers [46]. This large volume of distribution indicates extensive distribution to extravascular tissue.

5.4. Metabolism

Pimozide is extensively metabolized in the liver after oral administration. The metabolites are believed to be pharmacologically inactive, since peak pharmacological activity had been found to correlate with maximum brain levels of unchanged pimozide, but not of the total radioactivity [47]. Only a very small fraction of unchanged pimozide is recovered in the urine. Pimozide is metabolized primarily by oxidative N-dealkylation. This metabolism is catalyzed mainly by the cytochrome P450 3A4

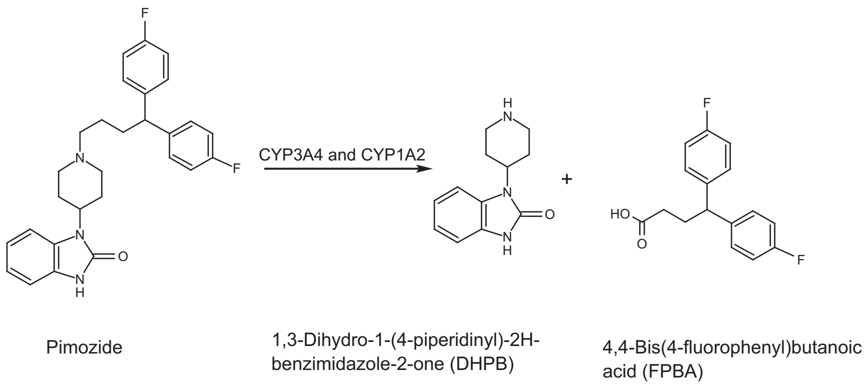

SCHEME 7.2 Metabolic pathway of pimozide in humans.

(CYP3A4) enzymatic system and, to a lesser extent, by cytochrome P450 1A2 (CYP1A2) [48]. Two major metabolites have been identified (Scheme 7.2).

In rats, 32% of the radioactivity of ^{14}C-labeled pimozide was excreted in urine, mainly as DHPB, and 42% in the feces, half as unchanged pimozide, half as DHPB [14].

5.5. Elimination

The major route of elimination of the metabolites is through the kidney. The mean elimination half-life in schizophrenic patients was 55±6.8h for multiple doses and 53.1±3.1h for a single dose [44]. Children with Tourette's syndrome appeared to have shorter $t_{1/2}$ than adult patients [45]. Severely extrapyramidal reactions due to the prolonged half-life (~154h) had been reported [49].

6. PHARMACOLOGICAL EFFECTS

6.1. Mechanism of action

The pharmacological profile of pimozide in laboratory animals resembles that of other antipsychotics. Its pharmacological properties are similar to haloperidol, but it has a slower onset and longer duration of action than the later [42]. Although its exact mode of action has not been established, the ability of pimozide to suppress motor and phonic tics in Tourette's syndrome is thought to be a function of its dopaminergic blocking activity. Pimozide is a potent antagonist to amphetamine- and apomorphine-induced stereotypes in most animal species tested. It also blocks

apomorphine-induced emesis. At the low-dose levels, pimozide is a highly selective blocker of central dopamine receptors and increases the turnover of dopamine in the central nervous system; at higher doses, increased turnover of noradrenaline has also been observed. In addition, pimozide has a reported calcium channel-blocking ability. This property may contribute to pimozide's tendency to prolong the ECG QT interval [50].

6.2. Adverse reactions

Neurologic side effects (e.g., extrapyramidal symptoms) of pimozide appear to be less severe than those observed from haloperidol [51]. The potential of pimozide to prolong the cardiac QT interval associated with fatal ventricular arrhythmia of the torsades de points type has been well documented in patients taking the drug and from *in vitro* animal experiments. It is now generally recommended that a baseline ECG to be performed before beginning treatment with pimozide and periodically thereafter.

6.3. Drug interactions

Pimozide is extensively metabolized mainly via the cytochrome P450 subtype 3A4 (CYP 3A4) enzyme system. Therefore, coadministration with drugs that inhibit cytochrome P450 (e.g., clarithromycin, erythromycin, ketoconazole, and itraconazole) is likely to elevate plasma concentration of pimozide and increase the risk for pimozide-related cardiac and neurologic adverse effects [41].

Coadministration of pimozide with drugs known to prolong QT interval, such as phenothiazines, tricyclic antidepressants, or antiarrhythmic agents, is also contraindicated [41].

7. METHOD OF CHEMICAL SYNTHESIS

The synthesis of pimozide is convergent, involving the preparation of intermediates **1** (1-chloro-4,4-di-(4-fluorophenyl)-butane) and **2** (1-(piperidin-4-yl)-1,3-dihydro-2*H*-benzimidazol-2-one), which are coupled to produce pimozide (Scheme 7.3) [5,52,53]. The preparation of **1** begins with a Grignard reaction between 4-fluorophenylmagnesium bromide (**3**) and cyclopropane-carboxylic acid ethyl ester (**4**). The resulting carbinol **5** undergoes a chlorination reaction with thionyl chloride to give the alkene **6**. Compound **1** is produced from hydrogenation of the double bond of **6** in the presence of palladium on charcoal catalyst. The synthesis of the intermediate **2** begins with the conjugate addition of benzylamine

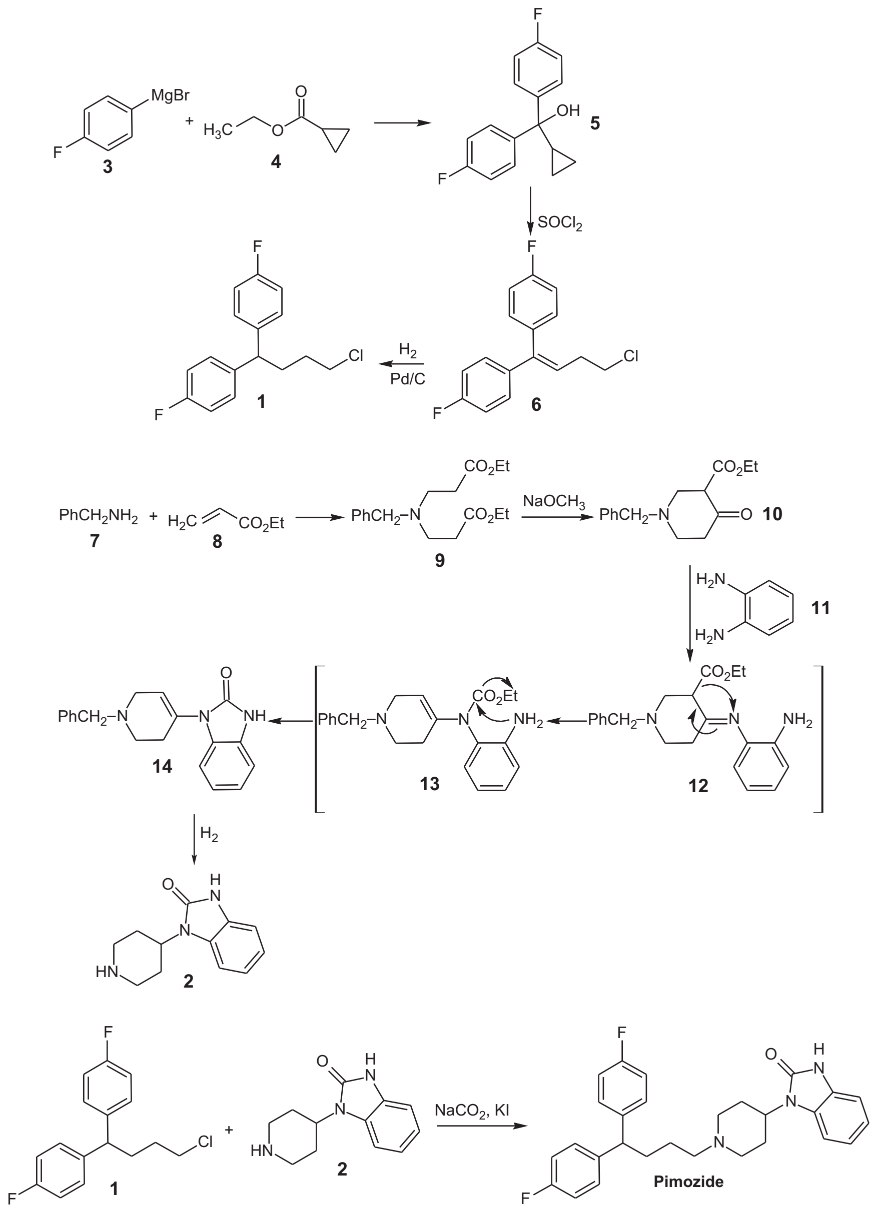

SCHEME 7.3 Synthesis of pimozide.

(**7**) to ethyl acrylate (**8**), resulting in the formation of diethyl ester **9**. Compound **9** then experiences a Dieckmann cyclization to be transformed into the oxopiperidine **10**. Benzene-1,2-diamine (**11**) reacts with **10** to provide the benzimidazolone **14** via a reaction mechanism assumed to initially involve imine **12** formation, followed by its rearrangement to the enamine **13**. Intramolecular ring closure of **13** results in the formation of **14**. The benzyl and alkene groups in **14** are then hydrogenated to yield the *N*-piperidino-bezimidazolone **2**. Finally, the latter compound (**2**) is alkylated with **1** in the presence of sodium carbonate and a catalytic amount of potassium iodide to produce pimozide.

ACKNOWLEDGMENT

The authors are indebted to Dr. Pradeep Sanghvi for encouragement and management support. We also wish to express our appreciation to Dr. Yuri Goldberg for his guidance and to Ms. Janet Mensah for her assistance in retrieving the cited literature, and lastly, many thanks go to our colleagues in the laboratories who contributed material needed for the preparation of this chapter.

REFERENCES

[1] Pimozide, European Pharmacopoeia, seventh ed., Supplement 7.3, Directorate for the Quality of Medicines & Healthcare of the Council of Europe (EDQM), Strasbourg, 2011, pp. 3993–3994.

[2] Pimozide, United States Pharmacopeia 34 National Formulary 29., The United States Pharmacopeial Convention, Rockville, MD, 2010 p. 3930.

[3] Pimozide, USP Dictionary Online of USAN and International Drug Names. (2011) http://www.uspusan.com/usan/pub/toc/go_usan07287_1.xml October 27.

[4] Pimozide, Merck Index., 14th ed., Merck & Co., Inc., Whitehouse Station, NJ, 2006 pp. 1281–1282.

[5] Pimozide, A. Kleemann, J. Engel, B. Kutscher, D. Reichert (Eds.), Pharmaceutical Substances: Syntheses, Patents, Applications, 4th ed., Pimozide, Thieme, Stuttgart, 2001, pp. 1453–1454.

[6] Pimozide, Clarke's Analysis of Drugs and Poisons., in: A.C. Moffat, M.D. Osselton, B. Widdop, L.Y. Galichet (Eds.), Pharmaceutical Press, London, 2004, pp. 1453–1454.

[7] Reference [2], p. 1032.

[8] Reference [2], p. 1055.

[9] J.A. Baird, et al., A classification system to assess the crystallization tendency of organic molecules from undercooled melts, J. Pharm. Sci. 99 (2010) 3787–3806.

[10] S. Riahi, et al., Partition coefficient prediction of a large set of various drugs and poisons by a genetic algorithm and artificial neural network, J. Chin. Chem. Soc. 55 (2008) 345–355.

[11] Pimozide, European Pharmacopoeia, seventh ed., Directorate for the Quality of Medicines & Healthcare of the Council of Europe (EDQM), Strasbourg, 2010, pp. 2734–2736.

[12] Pimozide, British Pharmacopoeia 2012., The Stationery Office, London, 2011 pp. 1737–1739.

[13] Orap® (Pimozide) Tablets, FDA, Reference ID: 2870808 (accessed from FDA website in 2011).

[14] W. Soudijn, I. van Wijngaarden, The metabolism and excretion of the neuroleptic drug pimozide (R6238) by the Wistar rat, Life Sci. 8 (1969) 291–295.

[15] H.H. Van Roolj, et al., Dynamic cation-exchange systems for the separation of drugs derived from butyrophenone and diphenylpiperidine by high-performance liquid chromatography and applied in the determination of halopemide in plasma, J. Chromatogr. 164 (1979) 177–185.
[16] Pimozide Tablets, United States Pharmacopeia 34 National Formulary 29, The United States Pharmacopeial Convention, Rockville, MD, 2010, pp. 3930–3931.
[17] Pimozide Tablets, British Pharmacopoeia 2012., The Stationery Office, London, 2011 pp. 3203-3204.
[18] A. Pluym, et al., TLC differentiation of butyrophenone and diphenylbutylpiperidine compounds from phenothiazine derivatives, J. Pharm. Sci. 68 (1979) 1050.
[19] I. Ojanpera, et al., Combined use of normal and reverse phase thin layer chromatography in the screening for basic and quaternary drugs, J. Liq. Chromatogr. 14 (1991) 1435–1446.
[20] S.A. Özkan, et al., Electrooxidation of pimozide and its differential pulse voltammetric and HPLC-EC determination, Anal. Chim. Acta 453 (2002) 221–229.
[21] G. Misztal, et al., HPLC-methode zur bestimmung von pimozid in tabletten, Pharmazie 47 (1992) 232–233.
[22] A.M.A. Verweij, et al., Liquid chromatographic-thermospray tandem mass spectrometric quantitative analysis of some drugs with hypnotic, sedative and tranquilizing properties in whole blood, J. Chromatogr. B 686 (1996) 27–34.
[23] E. Saar, et al., Identification and quantification of 30 antipsychotics in blood using LC-MS/MS, J. Mass Spectrom. 45 (2010) 915–925.
[24] H. Kirchherr, W.N. Kühn-Velten, Quantitative determination of forty-eight antidepressants and antipsychotics in human serum by HPLC tandem mass spectrometry: a multilevel, single-sample approach, J. Chromatogr. B 843 (2006) 100–113.
[25] C. Kratzsch, et al., Screening, library-assisted identification and validated quantification of fifteen neuroleptics and three of their metabolites in plasma by liquid chromatography/mass spectrometry with atmospheric pressure chemical ionization, J. Mass Spectrom. 38 (2003) 283–295.
[26] H. Seno, et al., Analyses of butyrophenones and their analogues in whole blood by high-performance liquid chromatography-electrospray tandem mass spectrometry, J. Chromatogr. B 746 (2000) 3–9.
[27] Q.A. Xu, T.L. Madden, Analytical methods for therapeutic drug monitoring and toxicology, John Wiley & Sons, Inc., Hoboken, NJ, 2011 pp. 389–390.
[28] M. Kurzawa, et al., Conductometric and spectrophotometric determination of haloperidol, droperidol and pimozide, Chem. Anal. (Warsaw) 49 (2004) 91–99.
[29] K. Kelani, et al., Spectrophotometric determination of some n-donating drugs using DDQ, Anal. Lett. 30 (1997) 1843–1860.
[30] H. Hopkala, L. Przyborowski, Determination of drugs containing fluorine with ion-selective electrode, Pharmazie 44 (1989) 65.
[31] P.A.J. Janssen, F.T. Allewijin, Pimozide, a chemically novel, highly potent and orally long-acting neuroleptic drug. Part II: kinetic study of the distribution of pimozide and metabolites in brain, liver, and blood of the Wistar rat, Arzneimittel Forsch. 18 (1968) 279–282.
[32] P.A.J. Janssen, et al., Pimozide, a chemically novel, highly potent and orally long-acting neuroleptic drug. Part III: regional distribution of pimozide and of haloperidol in the dog brain, Arzneimittel Forsch. 18 (1968) 282–287.
[33] I. van Wijingaarden, W. Soudijn, The metabolism and excretion of the analgesic fentanyl (R 4263) by Wistar rat, Life Sci. 7 (1968) 1239–1244.
[34] I. van Wijingaarden, W. Soudijn, The metabolism and excretion of the analgesic benzetimide hydrochloride (R 4929) by rats, Life Sci. 7 (1968) 225–229.
[35] L.J.M. Michiels, et al., Radioimmunoassay of the neuroleptic drug pimozide, Life Sci. 16 (1975) 937–944.

[36] G. Misztal, et al., Analysis of psychotropic drugs in blood. I. Chromatographic separation and spectrophotometric determination of butyrophenones, Chem. Anal. (Warsaw) 33 (1988) 149–153.
[37] T. Kerbusch, et al., Sensitive assay for pimozide in human plasma using high-performance liquid chromatography with fluorescence detection: application to pharmacokinetic studies, J. Chromatogr. B. 694 (1997) 163–168.
[38] Y. Miyao, et al., A sensitive assay method for pimozide in human plasma by high-performance liquid chromatography with fluorescence detection, J. Chromatogr. 275 (1983) 443–449.
[39] P.A.J. Janssen, A new series of neuroleptic drugs. The 4,4-diphenylbutyl-piperidines and their relationship with other neuroleptics, Clin. Trials J. 8 (Suppl. II) (1971) 7.
[40] J. Riding, A. Munro, Pimozide in the treatment of monosymptomatic hypochondriacal psychosis, Acta Psychiatr. Scand. 52 (1975) 23–30.
[41] R.M. Pinder, et al., Pimozide: a review of its pharmacological properties and therapeutic uses in psychiatry, Drugs 12 (1976) 1–40.
[42] C.L. Colvin, R.M. Tankanow, Pimozide: use in Tourette's Syndrome, Drug Intell. Clin. Pharm. 19 (1985) 421–424.
[43] M.J. Tueth, J.A. Cheong, Clinical uses of pimozide, South. Med. J. 86 (1993) 344–349.
[44] R.G. McCreadie, et al., Plasma pimozide profiles in chronic schizophrenics, Br. J. Clin. Pharmacol. 7 (1979) 533–534.
[45] F.R. Sallee, et al., Pharmacokinetics of pimozide in adults and children with Tourette's syndrome, J. Clin. Pharmacol. 27 (1987) 776–781.
[46] Z. Desta, et al., Effect of clarithromycin on the pharmacokinetics and pharmacodynamics of pimozide in healthy poor and extensive metabolizers of cytochrome P450 2D6 (CYP2D6), Clin. Pharmacol. Ther. 65 (1999) 10–20.
[47] W. Soudijn, I. van Wijingaarden, Localization of [^{3}H] pimozide in the rat brain in relation to its anti-amphetamine potency, J. Pharm. Pharmacol. 24 (1972) 773–780.
[48] Z. Desta, et al., Identification and characterization of human cytochrome P450 isoforms interacting with pimozide, J. Pharmacol. Exp. Ther. 285 (1998) 428–437.
[49] F.A. Logan, et al., Pimozide: adverse reaction and prolonged half-life, Br. J. Psychiatry 140 (1982) 433–434.
[50] R.J. Gould, et al., Antischizophrenic drugs of the diphenylbutylpiperidine type act as calcium channel antagonists, Proc. Natl. Acad. Sci. USA 80 (1983) 5122–5125.
[51] F.R. Sallee, et al., Relative efficacy of haloperidol and pimozide in children and adolescents with Tourette's disorder, Am. J. Psychiatry 158 (1997) 1057–1062.
[52] P.A.J. Janssen, U.S. Patent No. 3,196,157, 1965.
[53] D. Lednicer, Strategies for Organic Drug Synthesis and Design, second ed., John Wiley & Sons, Inc., Hoboken, NJ, 2009 pp. 333–334.

CHAPTER 8

Risperidone

David Germann, Natalie Kurylo, and **Feixue Han**

Contents

Apotex Inc., Toronto, Ontario, Canada

Profiles of Drug Substances, Excipients, and Related Methodology, Volume 37
ISSN 1871-5125, DOI: 10.1016/B978-0-12-397220-0.00008-8

© 2012 Elsevier Inc.
All rights reserved.

1. DESCRIPTION

1.1. Nomenclature

Risperidone is known by the following names:

Systematic chemical name

- 3-[2-[4-(6-Fluoro-1,2-benzisoxazol-3-yl)-1-piperidinyl]ethyl]-6,7,8,9-tetrahydro-2-methyl-4*H*-pyrido[1,2-a]pyrimidin-4-one [1].

Alternate systematic chemical names

- 3-[2-[4-(6-Fluoro-1,2-benzisoxazol-3-yl)-1-piperidinyl]ethyl]-2-methyl-4*H*-pyrido[1,2-a]pyrimidin-4-one [2].

1.2. Formulae

1.2.1. Empirical formula, molecular weight, CAS number

Risperidone [3]	$C_{23}H_{27}FN_4O_2$	410.48	106266-06-2

1.2.2. Structural formula

The structural formula of risperidone is:

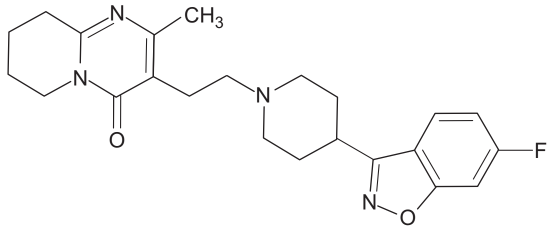

1.3. Appearance

A white or almost white powder [4] or white to almost white to slightly beige crystalline powder [5].

1.4. Elemental analysis

Elemental analysis has been performed on a Costech Elemental Analyzer ECS 4010.

Carbon, hydrogen, and nitrogen content are reported.

	%C	%H	%N
Observed (average of three measurements)	67.02	6.46	13.80
Formula $C_{23}H_{27}FN_4O_2$	67.30	6.63	13.65

1.5. Uses and applications

Risperidone, a derivative of benzisoxazole, is a second-generation antipsychotic (SGA) and a potent inhibitor of the serotonin 5-HT_2 and dopamine D_2 receptors located in the brain [6,7]. It is indicated for the acute treatment and maintenance treatment of schizophrenia and other related psychotic disorders including acute bipolar mania [8–13]. Risperidone was developed by Janssen Pharmaceutica Inc. and won FDA approval on December 29, 1993 [14] where it is marketed under the proprietary name Risperdal® and has subsequently achieved worldwide acceptance. The major metabolite of risperidone, 9-hydroxy-risperidone, exhibits similar receptor binding activity [8,15], and therefore, the clinical activity of a dose of risperidone is manifested in the combined effect of each moiety. Risperidone is an atypical antipsychotic, owing to its apparent suppression, or notably reduced severity and frequency, of extrapyramidal symptoms such as dystonia, akathisia, parkinsonism, and tardive dyskinesia [15–18]. These collateral effects are commonly associated

with the antipsychotic drugs that emerged soon after the introduction of chlorpromazine in 1952. Wang and Pan [19] have reported a crystalline hydrate (2.5 hydrate) form of the hydrogen chloride salt of risperidone; however, it is the free form of the drug that is widely used in pharmaceutical formulations. Risperidone has been formulated in oral solid dosage immediate-release and orally disintegrating tablets, oral solution, and intramuscular injection. The oral solution contains tartaric acid and in this dosage format the active ingredient is claimed as risperidone tartrate. Risperidone is normally administered at doses between 4 and 8 mg/day for schizophrenia and about 1 and 6 mg/day for the treatment of mania; safety above 16-mg total daily dose for the orally administered dosage form has not been established [8,10,20].

Route of administration	Dosage form/ strength	Comment
Oral	Tablet: 0.25, 0.5, 1, 2, 3, and 4 mg	6-mg tablet is available in some countries
	Solution: 1 mg/mL	Each milliliter contains 1 mg of risperidone as risperidone tartrate
	Orally disintegrating tablet: 0.5, 1, 2, 3, and 4 mg	Contains aspartame as a sweetener[a]
Intramuscular	Long-acting injection: 12.5, 25, 37.5, and 50 mg	Provided as a dose pack consisting of a vial containing risperidone microspheres, a prefilled syringe containing 2 mL of diluent, a Smart-site® Needle-Free Vial Access Device, and two Needle-Pro® safety needles for deep intramuscular injection (21 G UTW 1″ for deltoid administration and a 20 G TW 2″ for gluteal administration)[b]

[a] Risperdal M-Tab®.
[b] Risperdal Consta®.

2. METHODS OF PREPARATION

Kennis and Vandenberk [2] give the following method for preparing risperidone set forth in Scheme 8.1.

1-Acetylpiperidine-4-carboxylic acid **1** was halogenated to the acid chloride **2** which was then coupled with 1,3-difluorobenzene yielding compound **3**. Compound **3** was refluxed in concentrated hydrochloric acid to cleave the amide bond and generated (2,4-difluorophenyl)(piperidin-4-yl) methanone hydrochloride **4**. Treatment of **4** with hydroxylamine hydrochloride converted the ketone to the corresponding oxime **5** (mixture of *syn*- and *anti*-oximes). Cyclization of the *syn* oxime **5** by refluxing in a 1:1 solution of potassium hydroxide and water yielded the 6-fluoro-3-(piperidin-4-yl)-1,2-benzisoxazole intermediate **6**. 2-Aminopyridine **7** was condensed with

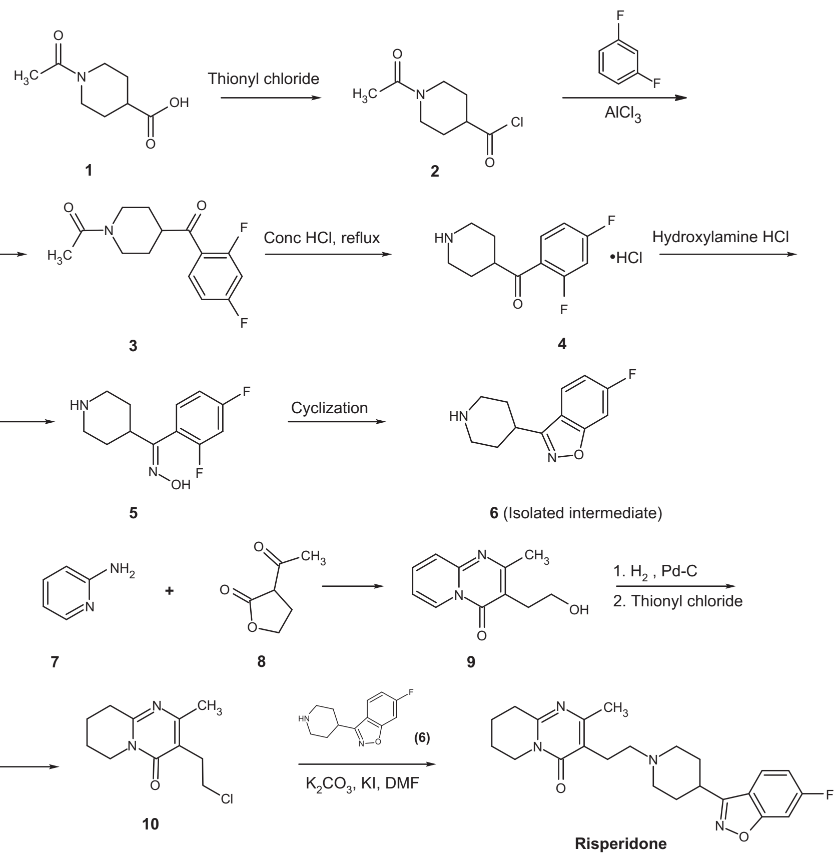

SCHEME 8.1 Preparation of Risperidone [2].

3-acetyldihydrofuran-2(3*H*)-one **8** through a bimolecular cyclo-addition reaction and produced 3-(2-hydroxyethyl)-2-methyl-4*H*-pyrido[1,2-a] pyrimidin-4-one **9.** Compound **9** was then hydrogenated, and substitution of the alcohol using thionyl chloride yielded the chlorinated intermediate 3-(2-chloroethyl)-2-methyl-6,7,8,9-tetrahydro-4*H*-pyrido[1,2-a]pyrimidin-4-one **10**. Risperidone was formed in the final step where compound **10** was coupled with the intermediate compound **6**.

In Spanish patent No. 2,050,069, the inventors Olondriz *et al.* coupled the aforementioned pyrimidinone derivative **10** and the benzoylpiperidine derivative **4** yielding an intermediate which was further subjected to oximation and concluded with the benzisoxazole ring closure to form risperidone as shown in Scheme 8.2 [21].

In another method [22], Barjoan *et al.* devised the process shown in Scheme 8.3.

Compound **1** was subjected to amino de-halogenation by coupling with dibenzylamine **2** to yield compound **3** which was reductively cleaved by hydrogenolysis to liberate intermediate **4,** bearing a primary amino group. The acyl halide **5** was coupled with difluorobenzene **6,** producing the difluorobenzyl ketone derivative **7**. Oximation reaction converted **7** to compound **8** (mixture of *syn-* and *anti*-oximes), followed by cyclization of the *syn* oxime to close the benzisoxazole ring **9**. Pyran ring cleavage generated terminal halogen and hydroxy groups **10**. The hydroxy group was substituted with a good leaving group (e.g., halogen, mesylate, or *p*-tosylate) to yield the intermediate **11**. Reaction of intermediate **4** with intermediate **11** under refluxing conditions with sodium bicarbonate in acetonitrile (ACN) completed the formation of risperidone.

Nadkarni and Shah [23] described a process that simultaneously carried out condensation and cyclization of the hydrochloride salt of the halo-pyrimidinone derivative (compound **1** of Scheme 8.3) with

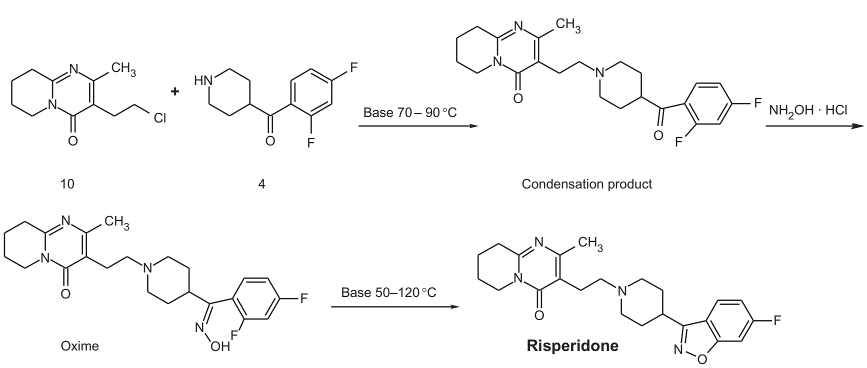

SCHEME 8.2 Preparation of Risperidone [21].

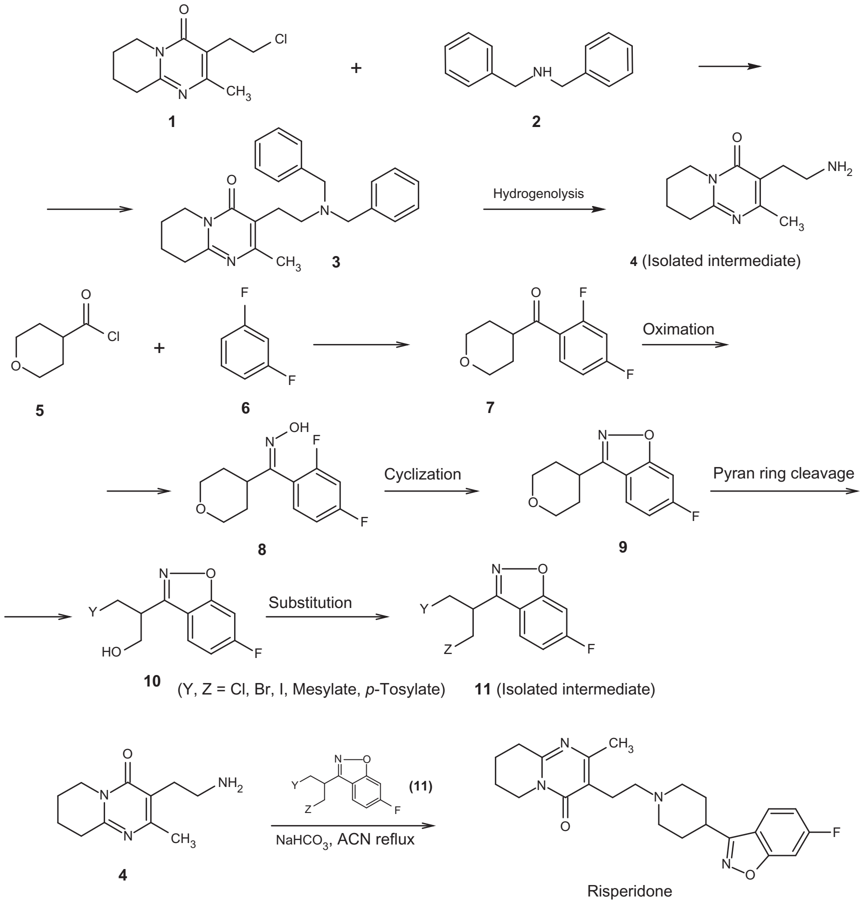

SCHEME 8.3 Preparation of Risperidone [22].

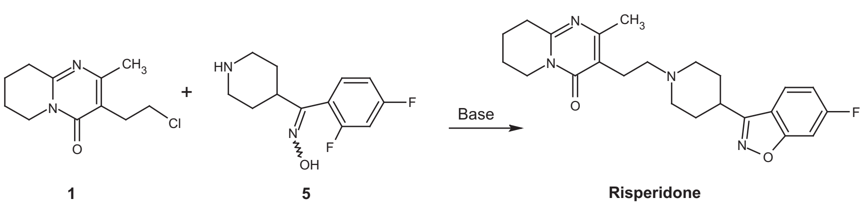

SCHEME 8.4 Preparation of Risperidone [23].

cis/trans oximes (compound **5** of Scheme 8.1). To achieve this, the condensed product reaction mixture was refluxed for 4–10h followed by addition of base to the cooled refluxed mixture maintained at 20–40°C for 10–18h which yielded risperidone shown in Scheme 8.4.

Kim *et al.* [24] utilized a Stille reaction in an effort to improve the efficiency of risperidone synthesis. The process illustrated in Scheme 8.5 avoids the use of dimethylformamide, a frequently employed solvent in risperidone synthesis which is harmful to human health and is very difficult to remove from the end product.

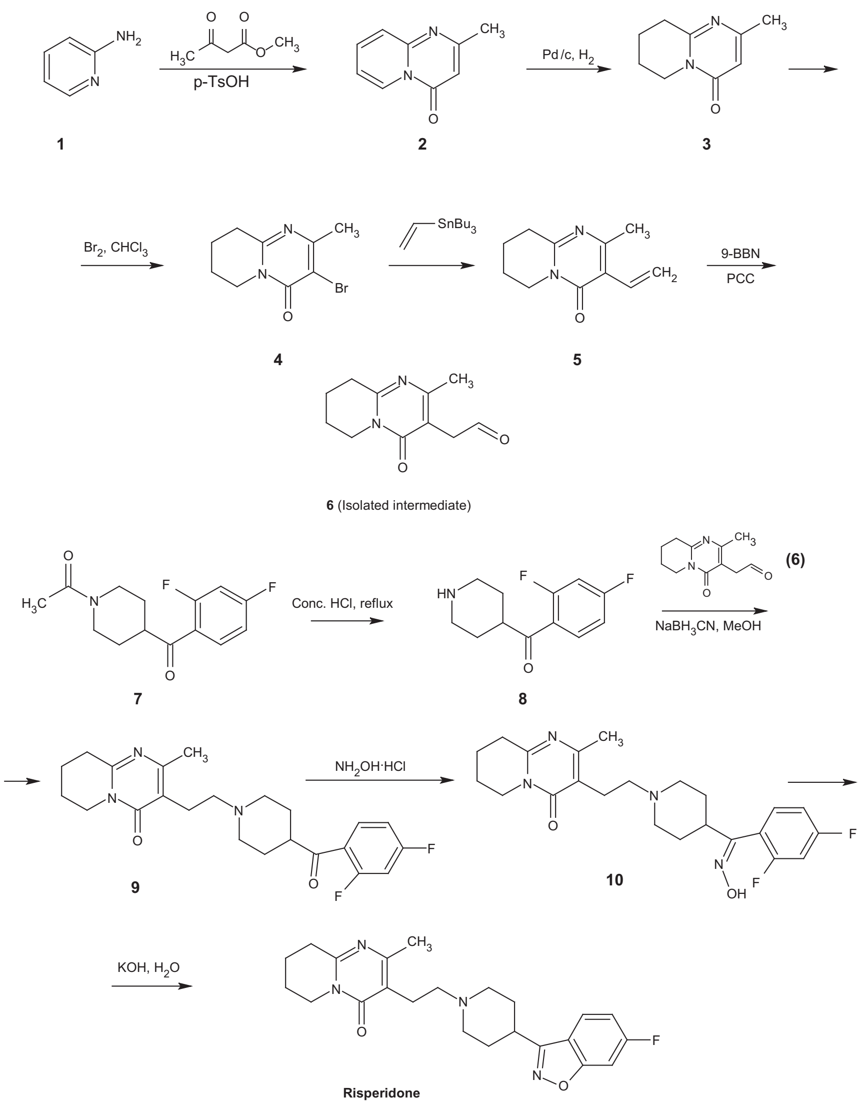

SCHEME 8.5 Preparation of Risperidone [24].

2-Aminopyridine **1** and methyl acetoacetate with *p*-toluene sulfonic acid as a catalyst were reacted to produce the pyridopyrimidinone compound **2**. Reduction of the aromatic ring of **2** was carried out with hydrogen (125 psi) over palladium on carbon catalyst in 6 N hydrochloric acid solution to yield compound **3**. Dropwise addition of bromine to a solution of **3** in chloroform (0 °C) over a 1-h period, with stirring at room temperature for 3 h to produce compound **4**. The Stille reaction was used to displace the bromide substituent of **4** with a vinyl group using tributyl (vinyl)stannane and tetrakis(triphenylphosphine)-palladium catalyst to produce compound **5**. The olefinic arm of **5** was oxidized to acetaldehyde in two steps; first by the addition of 9-borabicyclo[3.3.1]nonane (9-BBN) to a stirred mixture of **5** dissolved in THF, followed by oxidation of the terminal end with pyridinium chlorochromate in dichloromethane. The reaction mixture was heated (90–98 °C) for 3 h to form the intermediate compound **6**. Compound **7** was refluxed in HCl to generate compound **8** which was coupled with intermediate **6** in a methanolic medium containing sodium cyanoborohydride and acetic acid to give compound **9**. The ketone function of **9** was converted to oxime **10** with hydroxylamine hydrochloride in a solution of pyridine and methanol heated to 100–110 °C for 8 h. The process concluded with the elimination of the fluoro substituent from the ortho position to close to the ring by dissolving compound **10** in 30% KOH and heating to 120 °C for 5 h to yield risperidone.

3. PHYSICAL CHARACTERISTICS

3.1. Ionization constant

Two ionization constants are given for risperidone, pK_{a1}=8.24, pK_{a2}=3.11 [25].

3.2. Solubility characteristics and partition coefficient

Risperidone is practically insoluble in water, freely soluble in methylene chloride, and sparingly soluble in ethanol (96%). It dissolves in dilute acid solutions [3]. The partition coefficient Log *P* (octanol/water) is 3.49 [26].

The solubility of risperidone over a wide pH range has been determined.

Medium[a]	pH	Solubility (mg/mL)
0.05 M Potassium phosphate	2.1	>200
0.05 M Potassium phosphate	2.8	177
0.05 M Potassium phosphate	3.1	85.2
0.1 N HCl	4.2	17.5
0.05 M Potassium phosphate	4.9	27.5

(*continued*)

(*continued*)

0.05M Potassium phosphate	6.3	4.99
0.01N HCl	6.6	4.43
0.05M Potassium phosphate	7.0	1.11
0.05M Potassium phosphate	7.6	0.29

[a]The pH of the phosphate buffer solutions was adjusted with phosphoric acid or potassium hydroxide solution to achieve the indicated pH reading.

3.3. Crystallographic properties

Three polymorphic forms described in the literature as A, B, and E have been reported for risperidone [27]. Form A is the crystalline form predominantly used in pharmaceutical products. The powder X-ray diffraction pattern of risperidone Form A was obtained with a Philips PW3710 X-ray diffractometer using CuKα irradiation, generator tension 40kV, generator current 40mA, monochromator proportional counter, divergence slit ½°, receiving slit 0.2mm, spinner on, start angle 4.0° 2θ, end angle 40.0° 2θ, step size 0.02° 2θ, and time per step 1.2 s. The diffraction pattern and table of angles and calculated d-spacings of the most intense scattering peaks are shown in Fig. 8.1. The diffractogram of polymorphic Form B is most readily distinguished from Form A by the presence of strong peaks at 21.7±0.2°, 17.5±0.2°, and 18.4±0.2° 2θ, while Form E displays a strong peak at 16.5±0.2° 2θ [27].

3.4. Thermal properties

3.4.1. Melting range

Polymorphic Form A of risperidone crystallized from DMF and isopropanol has a reported melting point of 170.0°C [3].

3.4.2. Differential scanning calorimetry

The differential scanning calorimetry (DSC) measurements were obtained on risperidone Form A using TA 2920 DSC unit with Universal Thermal Solutions V2.5H Software. The sample was weighed directly into an aluminum holder with the lid placed on top. After an initial equilibration at 25°C, the sample was heated to 230°C at a rate of 10°C/min. The analysis was carried out under a N_2 purge (50cc/min). The thermogram is shown in Fig. 8.2 and displays a sharp endothermic melting peak with onset temperature around 168.6°C and a T_{max} of 171.6°C.

3.4.3. Hygroscopicity by dynamic vapor sorption analysis

Risperidone is nonhygroscopic, based on the step-isotherm. From dry state to 95% RH less than 0.1% increase in weight was observed for the sample during the adsorption processes.

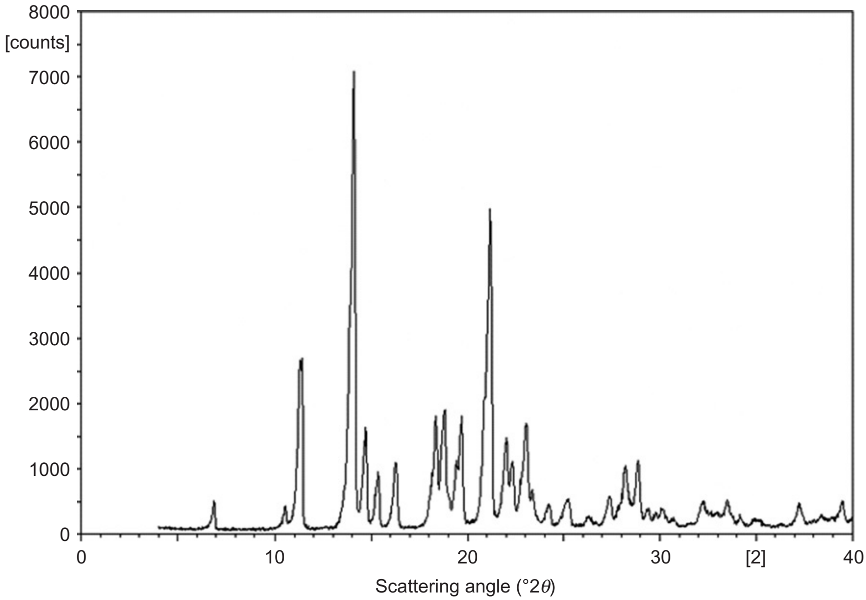

Scattering angles and *d*-spacings of the most intense peaks

Scattering angle (°2θ)	*d*-Spacing (Å)	Scattering angle (°2θ)	*d*-Spacing (Å)
10.53	8.408	22.03	4.037
11.31	7.827	22.33	3.984
11.38	7.779	23.06	3.859
14.09	6.288	23.36	3.810
14.71	6.025	24.23	3.676
15.35	5.775	25.25	3.529
16.28	5.449	26.28	3.393
18.79	4.725	27.41	3.255
19.69	4.511	28.22	3.164
21.19	4.196	28.87	3.094

FIGURE 8.1 X-ray powder diffraction pattern of risperidone, Form A.

3.5. Spectroscopic properties

3.5.1. Ultraviolet absorption spectroscopy

The UV spectrum of the risperidone was obtained on a Perkin-Elmer Lambda 2 UV/Vis spectrometer. The sample was dissolved in methanol at a concentration of 9.65mg/L and scanned from 200 to 400nm in the absorbance mode. The spectrum as shown in Fig. 8.3 displays absorption maxima at λ_{max} 237nm (ε=1.2$\times$10^4) and λ_{max} 279nm (ε=1.1$\times$10^4).

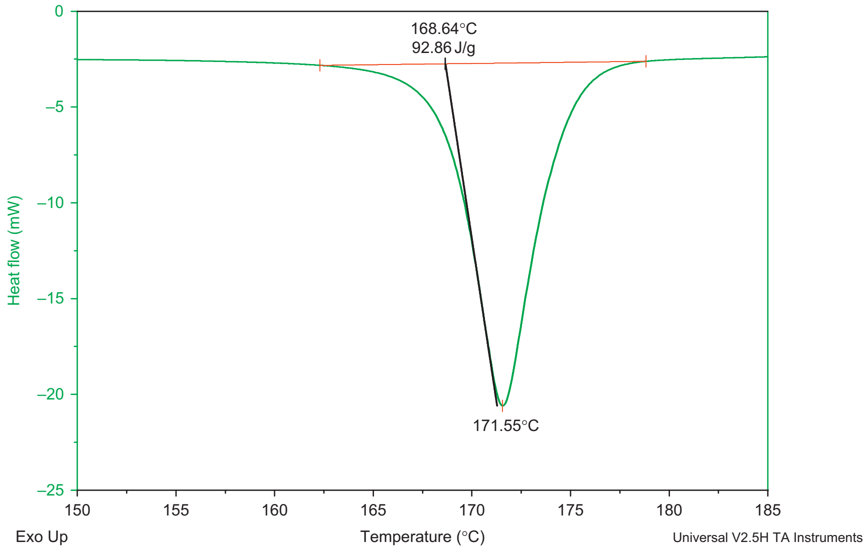

FIGURE 8.2 Differential scanning calorimetry thermogram of risperidone Form A.

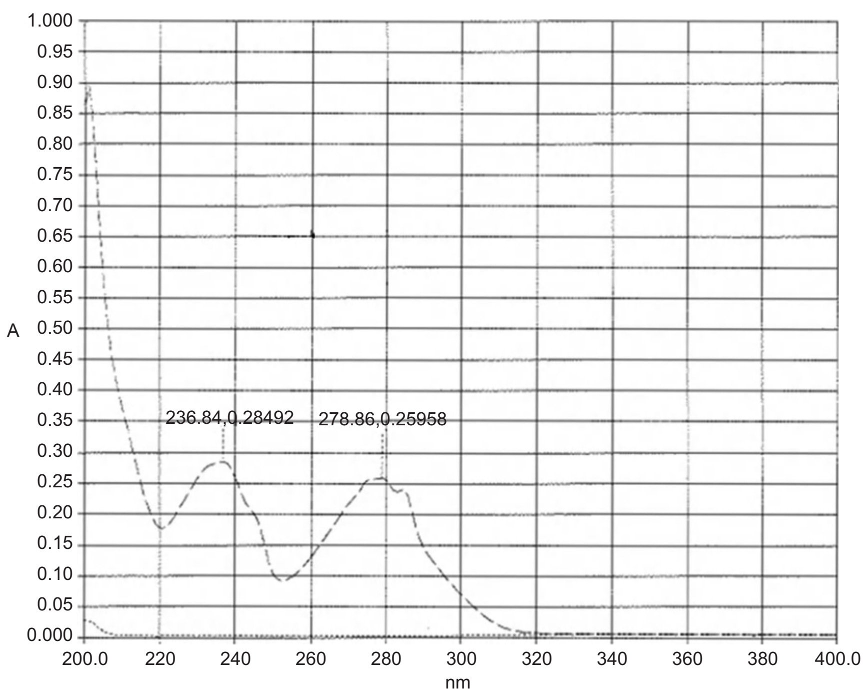

FIGURE 8.3 Ultraviolet spectrum obtained on risperidone, dissolved at a concentration of 9.65 mg/L in methanol.

3.5.2. Infrared absorption spectroscopy

The infrared spectrum of risperidone (polymorphic Form A) was obtained using a Perkin-Elmer Spectrum 1000 Fourier Transform-IR spectrophotometer. The spectral resolution was set at 4.0 cm^{-1}. The sample was prepared in the form of a potassium bromide disc by compressing a powdered mixture of KBr and risperidone ground in an agate mortar. The spectrum of polymorphic Form A has a strong single absorption band at about 1650 cm^{-1} as shown in Fig. 8.4 which distinguishes it from polymorphic Form B which has multiple overlapping peaks at this frequency [28].

3.5.3. Raman spectroscopy

Karrabas *et al.* [28] report numerous differences between Raman spectra obtained from crystalline risperidone Forms A and B. The spectra were recorded using FRA-106/S FT-Raman (Bruker) instrument with laser excitation line of 1064 nm from a Nd:YAG laser, and a secondary filter was used to remove the Rayleigh line. The scattered light was collected at a 180° angle. The instrumentation was equipped with a liquid nitrogen cooled Ge detector (D 418). The power of the incident laser beam was approximately 370 mW on the surface of the risperidone sample, the spectral line width was 0.5 cm^{-1}, and the recorded spectra were taken from the average of 300 scans. Aluminum cylindrical sample cups of 10 mm diameter and 4 mm height with a cavity in the center of 2 mm diameter and 1 mm depth were used to hold the sample powder. Risperidone

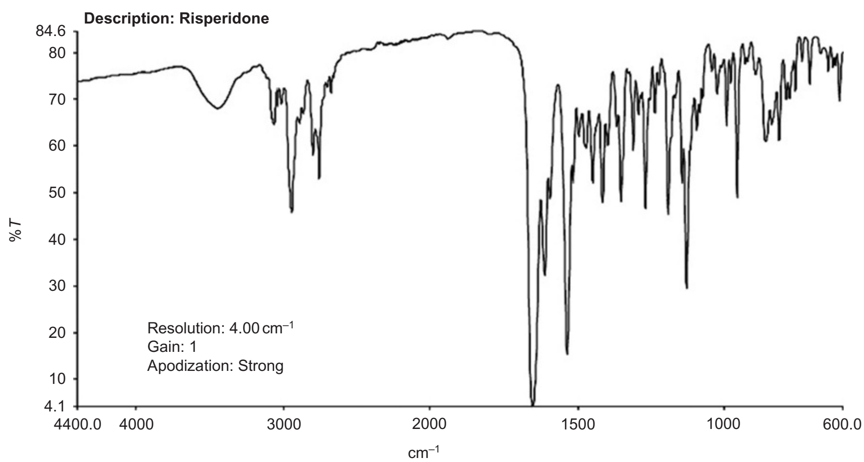

Wave number (cm^{-1})	Characteristic peak assignment
3057, 2943, 2800, 2757	Aromatic and aliphatic (C-H) stretch
1652	Pyridopyrimidinone (C=O) stretch
1131	Aromatic (C-F) stretch

FIGURE 8.4 Infrared absorption spectrum of risperidone (Form A) with table of wavenumber (cm^{-1}), %*T* values, and characteristic peak assignments.

Form A exhibited a double peak at 3051–3069 cm^{-1} with the latter having a stronger vibration than the former. Other characteristic peaks were double peaks at 432–440 cm^{-1}, double peaks at 1260–1271 cm^{-1}, and a single peak at 1397 cm^{-1}. For risperidone polymorphic Form B, the differentiating peaks were exhibited as a single peak at 3055 cm^{-1} having a shoulder at 3069 cm^{-1}, a strong peak at 2963 cm^{-1}, single peaks at 434–1266 cm^{-1}, and a double peak at 1390–1402 cm^{-1}. The authors noted that while it may be possible to utilize Raman spectroscopy for identifying the presence of risperidone in commercial tablets, the technique was not sufficiently sensitive to distinguish the actual polymorphic form of the active ingredient in the presence of formulation excipients due to the low concentration of risperidone in the commercial tablet (4.3% w/w).

3.5.4. Nuclear magnetic resonance spectrometry

The ^{1}H and ^{13}C NMR spectra of risperidone were obtained on a Bruker XWIN-400 instrument using $CDCl_3$ as the solvent. ^{1}H NMR spectra were acquired at 400 MHz and ^{13}C NMR spectra were recorded at 100 MHz. Chemical shifts are reported in ppm relative to TMS using the residual solvent signals as internal references. The proton NMR spectra are shown in Figs. 8.5 and 8.6 and ^{13}C NMR and DEPT 135 spectra are shown in Figs. 8.7 and 8.8. The proton peak assignments are summarized

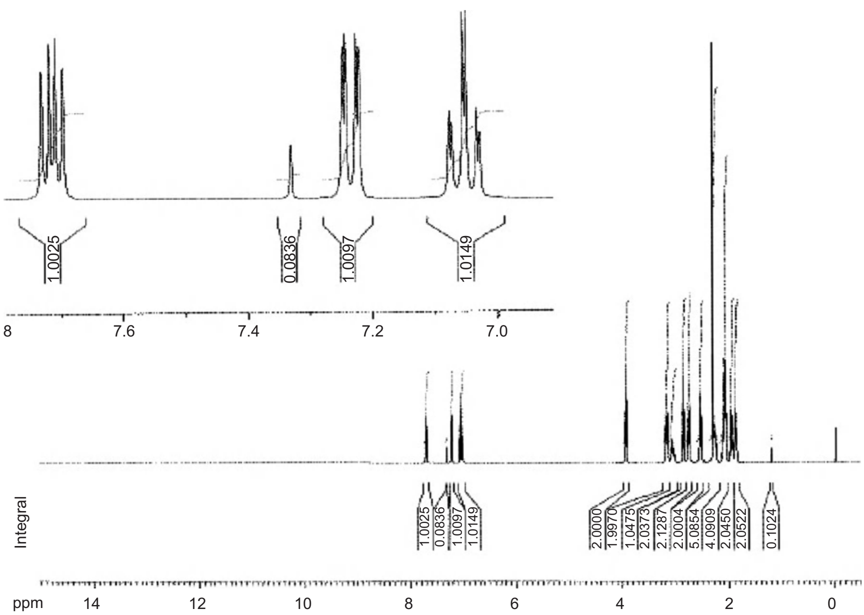

FIGURE 8.5 ^{1}H NMR spectrum of risperidone.

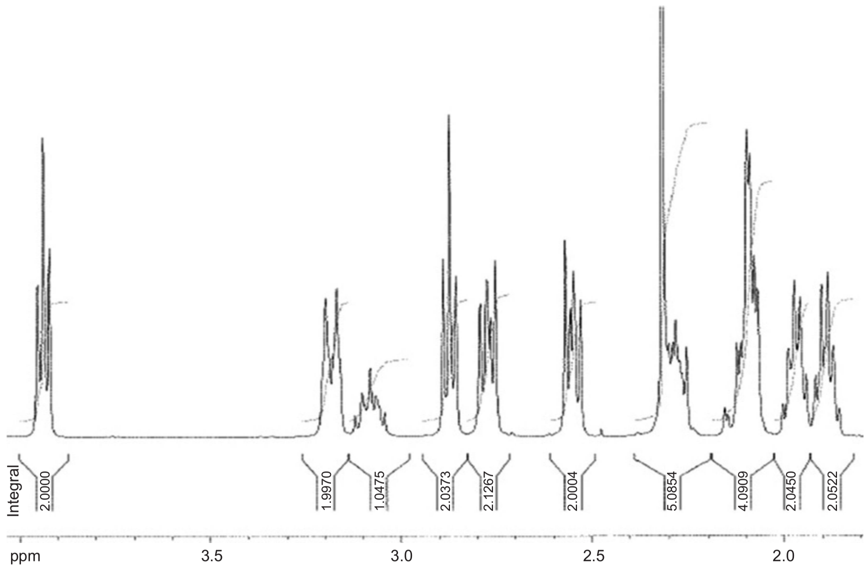

FIGURE 8.6 ^{1}H NMR spectrum of risperidone (expanded view).

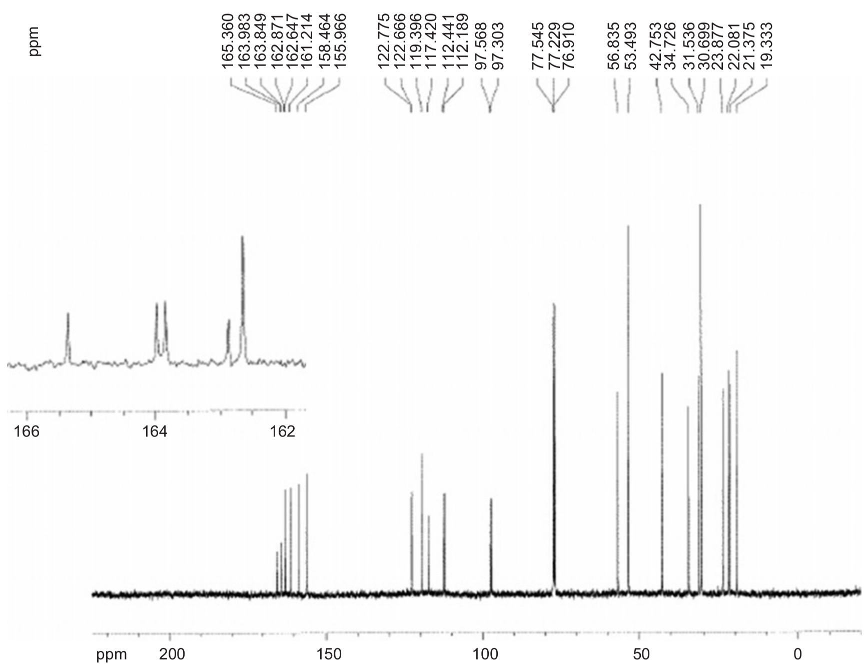

FIGURE 8.7 ^{13}C NMR spectrum of risperidone.

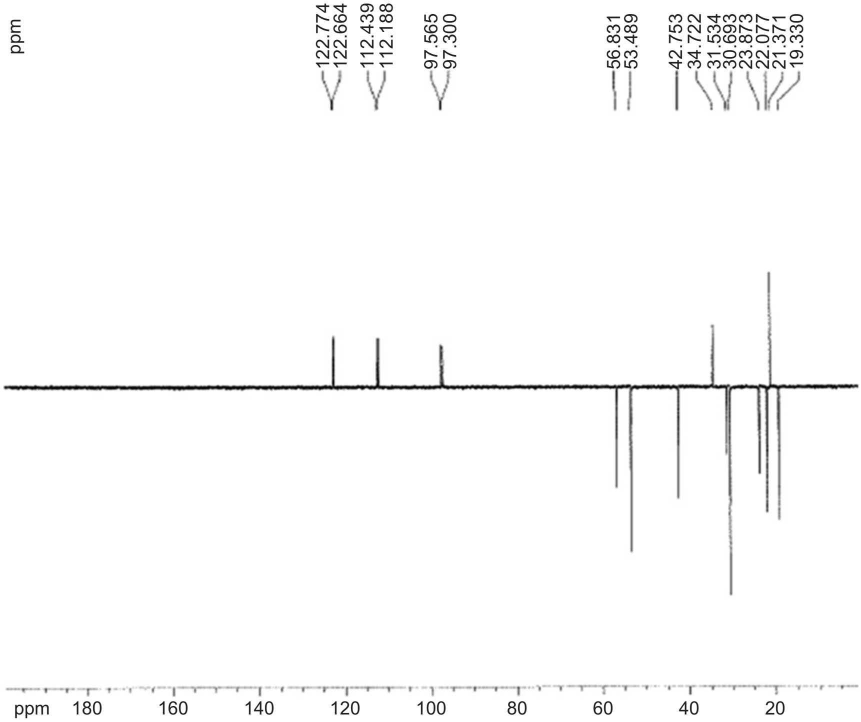

FIGURE 8.8 ^{13}C DEPT135 NMR spectrum of risperidone.

in Table 8.1 and the carbon assignments are shown in Table 8.2. The NMR peak assignments were aided by COSY, HSQC, and HMBC NMR spectra shown in Figs. 8.9–8.11.

3.5.5. Mass spectrometry

The mass spectroscopic study of risperidone was carried out on a QTRAP-LC-MS/MS system. The sample was dissolved in methanol and injected using a 1 μL injection volume and a mobile phase consisting of 30% A (100% water/0.2% formic acid) and 70% B (ACN) at a flow rate of 100 μL/min. The mass spectra (ESI MS and MS/MS) are shown in Figs. 8.12 and 8.13. The ESI MS spectrum shows the presence of the protonated molecular ion peak $[M+H]^+$ at *m/z* 411 and pseudo-molecular ion peaks $[M+Na]^+$ at *m/z* 433 and $[M+K]^+$ at *m/z* 449.

TABLE 8.1 ^{1}H NMR spectroscopy data for risperidone in $CDCl_3$

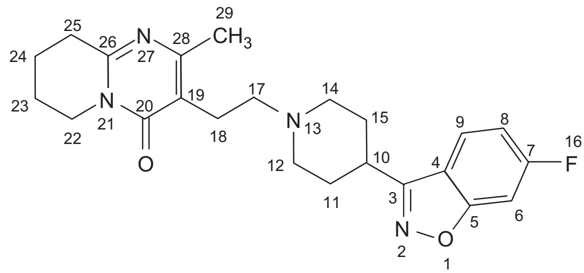

^{1}H Chemical shift (δ, ppm)	Multiplicity, spin–spin coupling constant (J, Hz)	Integration	Assignment
7.72	dd; $^{3}J_{HH}$=8.8, $^{4}J_{HF}$=5.1	1H	H9
7.24	dd; $^{3}J_{HF}$=8.5, $^{4}J_{HH}$=1.9	1H	H6
7.06	Apparent dt; $^{3}J_{HF}\approx J_{HH}\approx$8.6, $^{4}J_{HH}$=1.8	1H	H8
3.94	t; J=6.2	2H	H22
3.19	m	2H	H12e, H14e
3.08	m (Distorted pentet)	1H	H10
2.87	t; J=6.7	2H	H25
2.77, 2.55	Each m	2H each	H17, H18
2.39–2.24	m	5H	H12a, H14a, H29
2.16–2.04	m	4H	H11, H15
2.04–1.85	m	4H	H23, H24

Abbreviations: a, axial proton; d, doublet; dd, doublet of doublets; dt, double triplet; e, equatorial proton; m, multiplet; ppm, parts per million; t, triplet.

4. METHODS OF ANALYSIS

4.1. Known impurities of risperidone

A number of impurities have been identified as related compounds of risperidone [1,4]. The structures, chemical names, and characterization of the impurities are shown in Table 8.3. Impurities A to E are specified impurities listed in the USP and EP monographs of risperidone drug substance. The EP also includes desfluoro-risperidone (Impurity K) as a specified impurity. Impurities F, H, I, J, L, and M are included in the EP monograph as ‘‘other detectable impurities.’’ All of the compendial

TABLE 8.2 ^{13}C NMR spectroscopy data for risperidone in $CDCl_3$

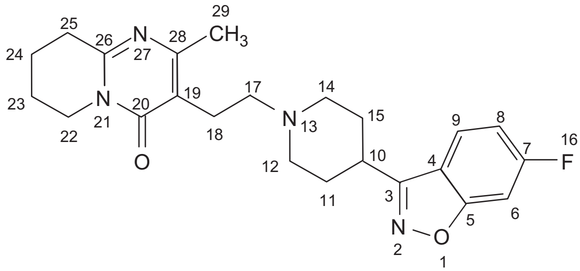

^{13}C Chemical shift (δ, ppm), spin–spin coupling constant (J, Hz)	DEPT data	Assignment
165.4/162.9; d, ^{1}J=250	C	C7
164.0/163.8; d, ^{3}J=13	C	C5
162.6	C	C20
161.2	C	C26
158.5	C	C3
156.0	C	C28
122.8; d, ^{3}J=11	CH	C9
119.4	C	C19
117.4	C	C4
112.3; d, ^{2}J=25	CH	C8
97.5; d, ^{2}J=27	CH	C6
56.9	CH_2	C17
53.5	CH_2	C12, C14
42.8	CH_2	C22
34.7	CH	C10
31.5	CH_2	C25
30.7	CH_2	C11, C15
23.9	CH_2	C18
22.1	CH_2	C23
21.4	CH_3	C29
19.3	CH_2	C24

listed impurities are potential manufacturing process-related impurities. Impurity C is also a degradation product formed under oxidative conditions, and it is the major active metabolite of risperidone which was approved by the FDA in 2006 for the treatment of schizophrenia under the drug name paliperidone [29]. Impurity P (bicyclorisperidone) and Impurity Q are specified impurities of the USP monographs of risperidone tablets and oral solution. Impurity P is prepared from

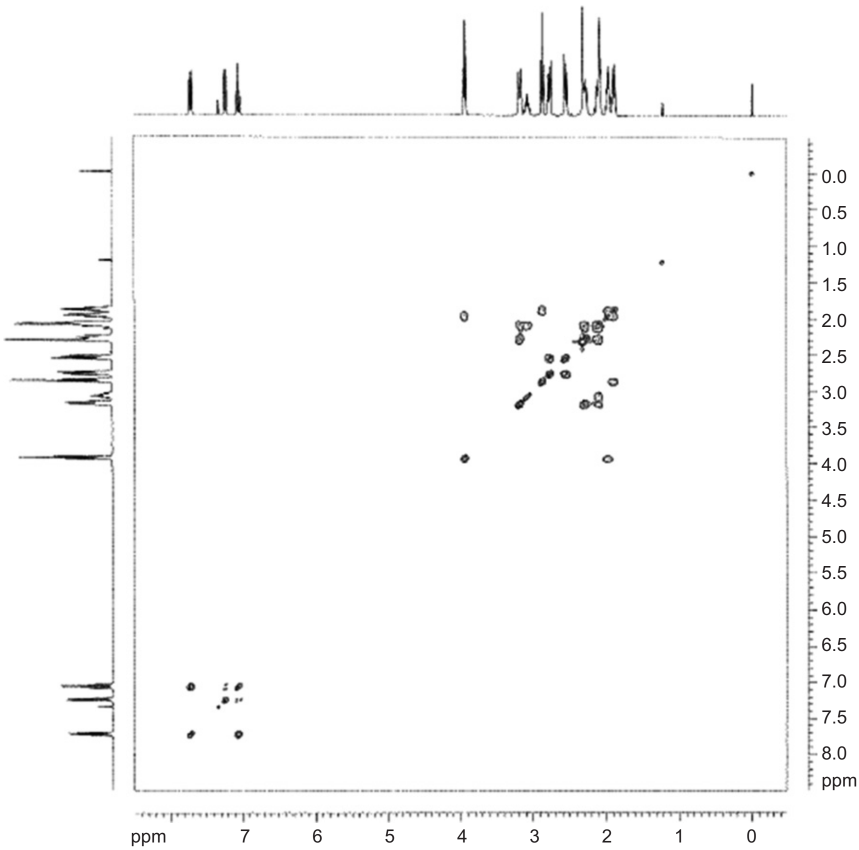

FIGURE 8.9 COSY H[1] NMR spectrum of risperidone.

risperidone under a combination of harshly basic and oxidative stressing conditions as described in the aforementioned USP monographs. Impurity Q, risperidone N-oxide, is a potential degradation product which has *cis* and *trans* isomer configurations; however, only the *cis* isomer is specified by the USP. Impurity R (9-methylene risperidone) is reported by Sattanathan *et al.* as a process-related impurity that was found to occur in the first step of the synthetic route when dichloromethane was used as a solvent [30]. Impurity S is an isomer of risperidone reported by Barathi *et al.* [31] as a potential degradation product which is discussed in further detail in Section 9. Impurity T is presented as a potential degradation product by El-Sherif *et al.* [32], resulting from decomposition of the active ingredient when the drug product has been stored under inappropriate conditions.

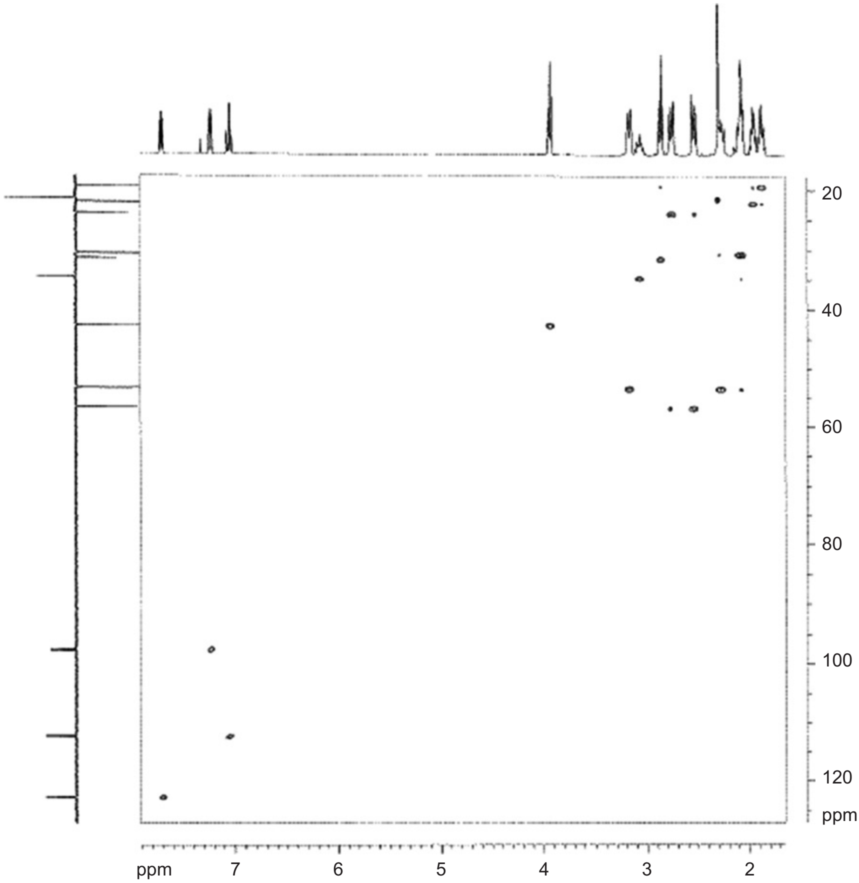

FIGURE 8.10 HSQC NMR spectrum of risperidone.

4.2. Compendial methods of analysis

4.2.1. USP methods of analysis

The USP [1] prescribes the following tests for risperidone drug substance:

- Identification A: infrared absorption ⟨197K⟩.
- Identification B: the retention time of the major peak in the chromatogram of the assay preparation corresponds to that in the chromatogram of the standard preparation as obtained in the Assay.
- Loss on drying ⟨731⟩: in vacuum at 80 °C for 4h; loses not more than 0.5%.
- Residue on ignition ⟨281⟩: not more than 0.1% for a 2.0-g sample.
- Heavy metals, method II⟨231⟩: not more than 0.001%.
- Assay—Gradient HPLC (chromatographic conditions as shown in Table 8.4; ref [1]); 98.0–102.0% calculated on the dried basis.

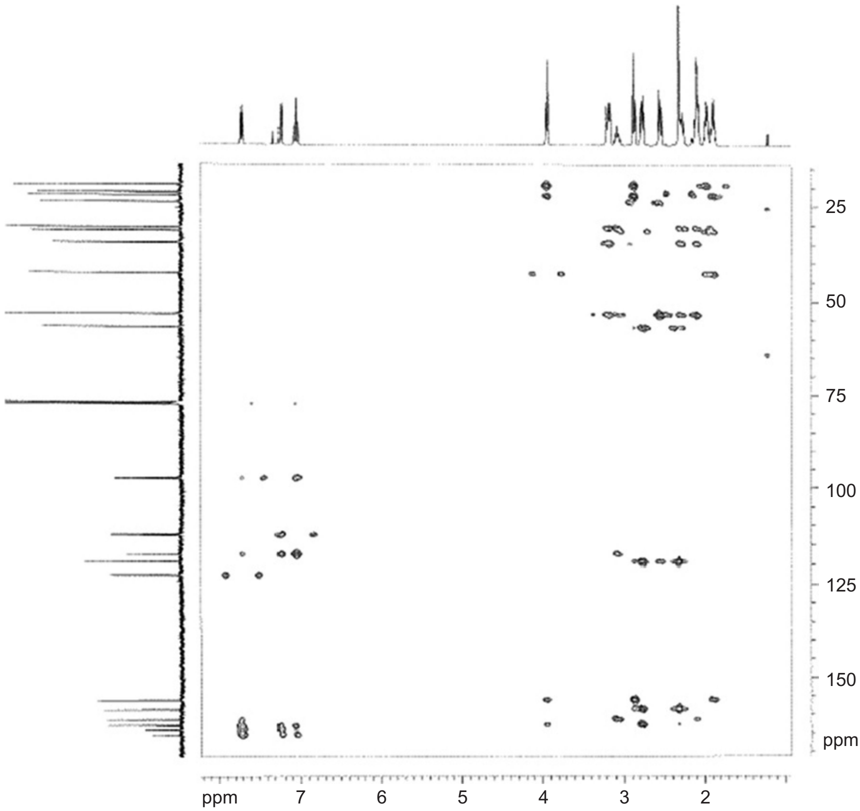

FIGURE 8.11 HMBC NMR spectrum of risperidone.

- Related compounds (HPLC chromatographic conditions as directed in Assay); Impurities A, B, C, D, E (Table 8.3): not more than 0.20% each; not more than 0.10% of any unknown impurity; not more than 0.30% of total impurities found; disregard impurities less than 0.05%.

USP Pharmaceutical preparations include immediate-release oral solid dosage risperidone tablets and risperidone oral solution. The following tests are prescribed for USP risperidone tablets:

- Identification A: infrared absorption ⟨197K⟩—risperidone is extracted as indicated from a suitable number of tablets to prepare a 550±50μg/mL solution in ethyl acetate. Residue from about 5mL of the evaporated and dried extract is mixed with about 150±50mg of KBr and pressed into a transparent pellet. The spectrum of the test material is compared to that obtained from a KBr pellet prepared with 2mg of Risperidone RS and 200mg of KBr powder pressed into a transparent pellet.

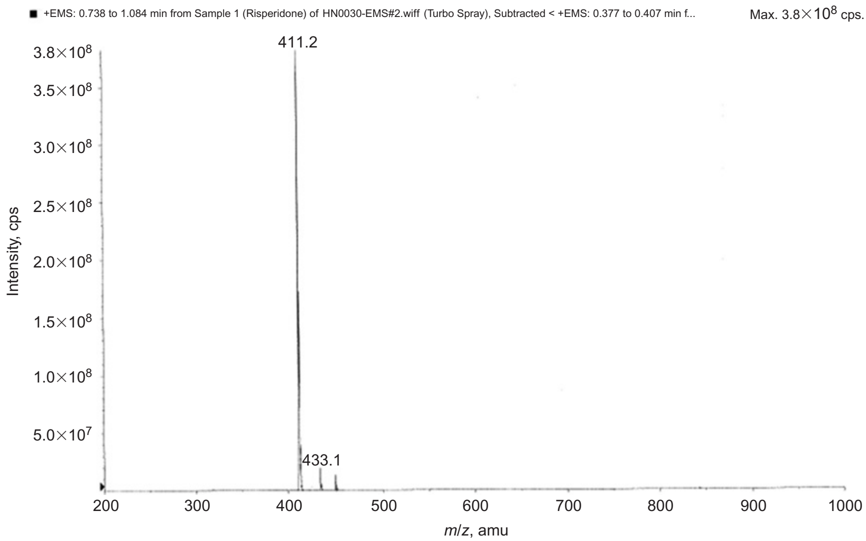

FIGURE 8.12 ESI mass spectrum of risperidone $[M+H]^+$.

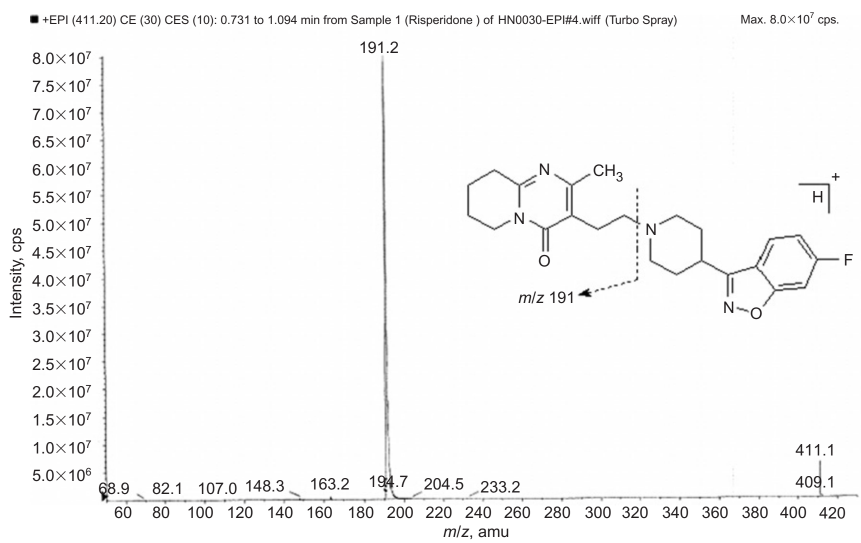

FIGURE 8.13 MS/MS spectrum of risperidone $[M+H]^+$, *m/z* at 411 amu.

- Identification B: the retention time of the major peak in the chromatogram of the assay preparation corresponds to that in the chromatogram of the standard preparation as obtained in the Assay.
- Assay—Gradient HPLC (chromatographic conditions as shown in Table 8.4; ref [1]); 90.0–110.0% of the labeled amount of risperidone.

TABLE 8.3 Impurities of risperidone

Structure	Chemical name	Classification
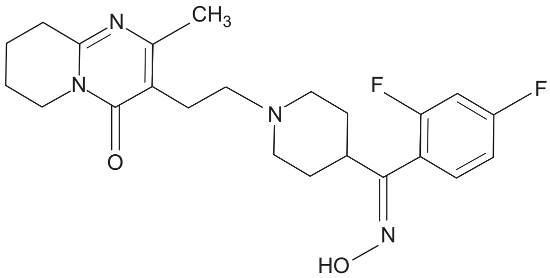 A	3-[2-[4-[(*E*)-(2,4-difluorophenyl)-(hydroxyimino)methyl]-piperidin-1-yl]ethyl]-2-methyl-6,7,8,9-tetrahydro-4*H*-pyrido[1,2-a]pyrimidin-4-one	USP *E*-oxime EP Impurity A Synthetic impurity
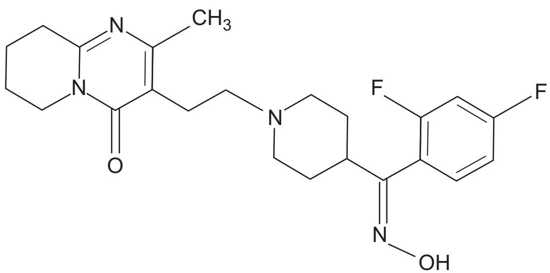 B	3-[2-[4-[(*Z*)-(2,4-difluorophenyl)(hydroxyimino)methyl]-piperidin-1-yl]ethyl]-2-methyl-6,7,8,9-tetrahydro-4*H*-pyrido[1,2-a]pyrimidin-4-one	USP *Z*-oxime EP Impurity B Synthetic impurity

(*continued*)

TABLE 8.3 (*continued*)

Structure	Chemical name	Classification
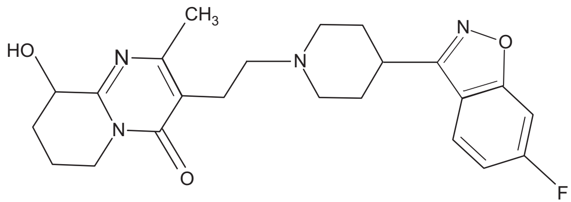 C	(9*RS*)-3-[2-[4-(6-fluoro-1,2-benzisoxazol-3-yl)piperidin-1-yl]ethyl]-9-hydroxy-2-methyl-6,7,8,9-tetrahydro-4*H*-pyrido[1,2-a]pyrimidin-4-one	USP 9-hydroxy-risperidone EP Impurity C Degradation product and active metabolite
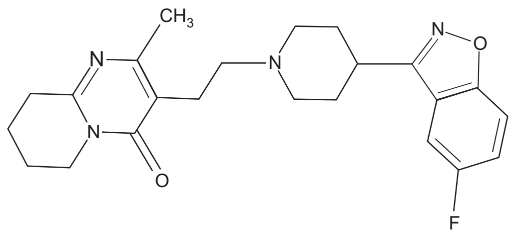 D	3-[2-[4-(5-Fluoro-1,2-benzisoxazol-3-yl)piperidin-1-yl]ethyl]-2-methyl-6,7,8,9-tetrahydro-4*H*-pyrido[1,2-a]pyrimidin-4-one	USP 5-fluororisperidone EP Impurity D Synthetic impurity
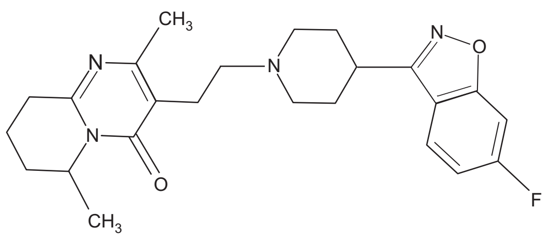 E	(6*RS*)-3-[2-[4-(6-fluoro-1,2-benzisoxazol-3-yl)piperidin-1-yl]ethyl]-2,6-dimethyl-6,7,8,9-tetrahydro-4*H*-pyrido[1,2-a]pyrimidin-4-one	USP 6-methyl-risperidone EP Impurity E Synthetic impurity

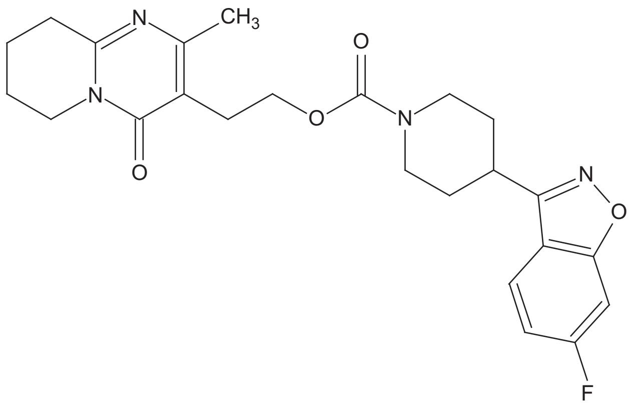

F

2-[2-Methyl-4-oxo-6,7,8,9-tetrahydro-4*H*-pyrido[1,2-a]pyrimidin-3-yl]ethyl 4-(6-fluoro-1,2-benzisoxazol-3-yl)piperidin-1-carboxylate

EP Impurity F
Synthetic impurity

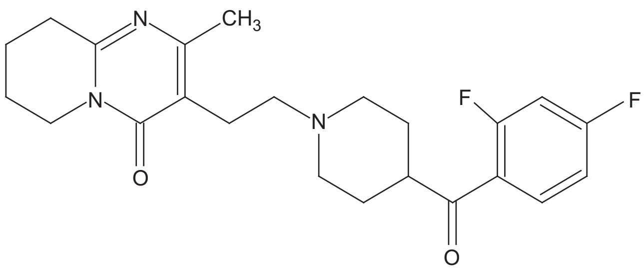

H

3-[2-[4-(2,4-Difluorobenzoyl)piperidin-1-yl]ethyl]-2-methyl-6,7,8,9-tetrahydro-4*H*-pyrido[1,2-a]pyrimidin-4-one

EP Impurity H
Synthetic impurity

(*continued*)

TABLE 8.3 (*continued*)

Structure	Chemical name	Classification
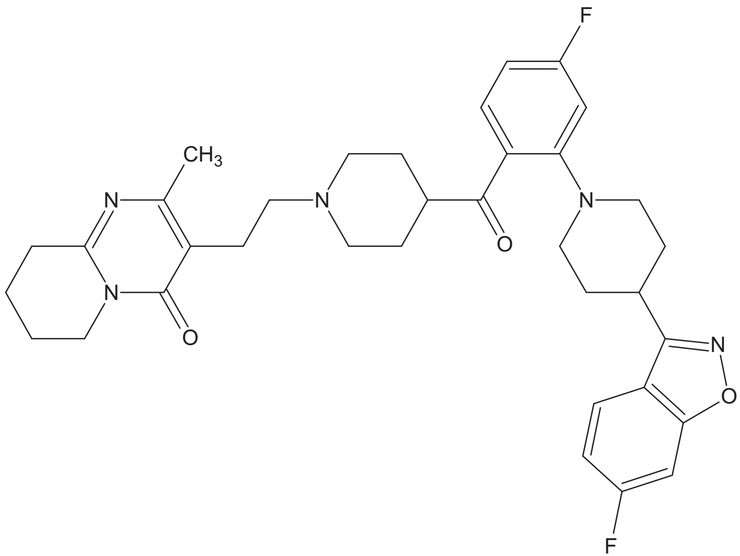 I	3-[2-[4-[4-Fluoro-2-[4-(6-fluoro-1,2-benzisoxazol-3-yl) piperidin-1-yl]benzoyl] piperidin-1-yl]ethyl]-2-methyl-6,7,8,9-tetrahydro-4*H*-pyrido[1,2-a]pyrimidin-4-one	EP Impurity I Synthetic impurity

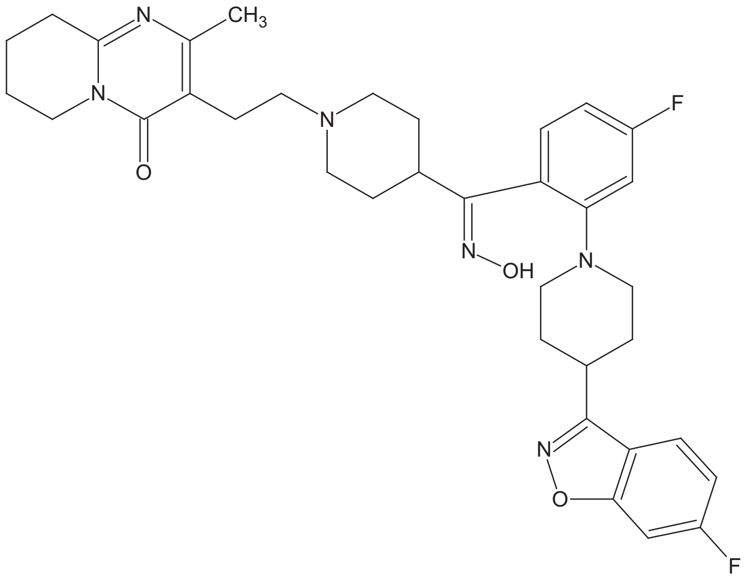 J	3-[2-[4-[(*Z*)-[4-fluoro-2-[4-(6-fluoro-1,2-benzisoxazol-3-yl) piperidin-1-yl]phenyl] (hydroxyimino)methyl]-piperidin-1-yl]ethyl]-2-methyl-6,7,8,9-tetrahydro-4*H*-pyrido[1,2-a]pyrimidin-4-one	EP Impurity J Synthetic impurity

(*continued*)

TABLE 8.3 (*continued*)

Structure	Chemical name	Classification
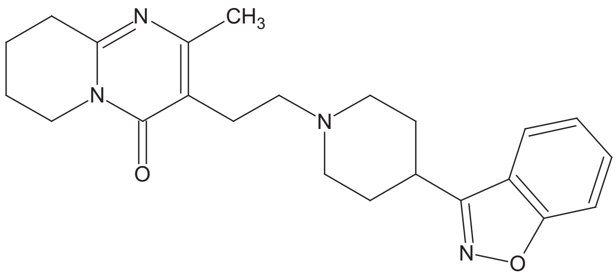 K	3-[2-[4-(1,2-Benzisoxazol-3-yl) piperidin-1-yl]ethyl]-2-methyl-6,7,8,9-tetrahydro-4*H*-pyrido[1,2-a]pyrimidin-4-one	EP Impurity K Synthetic impurity
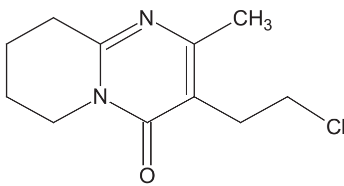 L	3-(2-Chloroethyl)-2-methyl-6,7,8,9-tetrahydro-4*H*-pyrido [1,2-a]pyrimidin-4-one	EP Impurity L Synthetic impurity
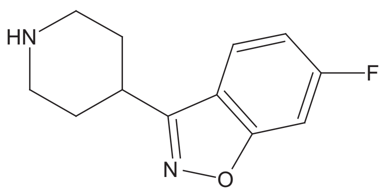 M	6-Fluoro-3-(piperidinyl-4-yl)-1,2-benzisoxazole	EP Impurity M Synthetic impurity

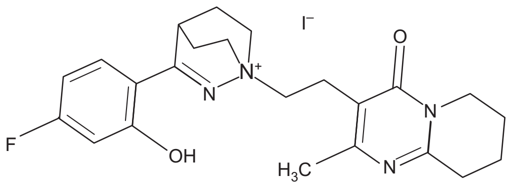 P	3-(4-Fluoro-2-hydroxyphenyl)-1-[2-(6,7,8,9-tetrahydro-2-methyl-4-oxo-4*H*-pyrido-[1,2-a]pyrimidin-3-yl)ethyl]-2-aza-1-azoniabicyclo[2.2.2] oct-2-ene (iodide)	USP bicyclorisperidone Specified impurity
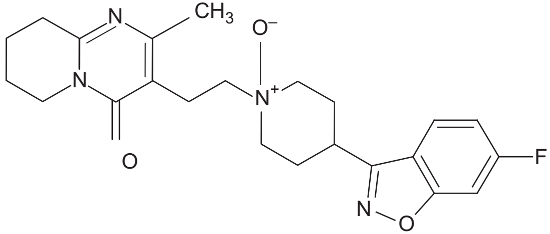 Q	3-[2-[4-(6-Fluoro-1,2-benzisoxazol-3-yl)-1-oxidopiperidin-1-yl]ethyl]-2-methyl-6,7,8,9-tetrahydro-4*H*-pyrido[1,2-a]pyrimidin-4-one (*cis*/*trans*)	USP specified impurity (as *cis*-N-oxide) Degradation product
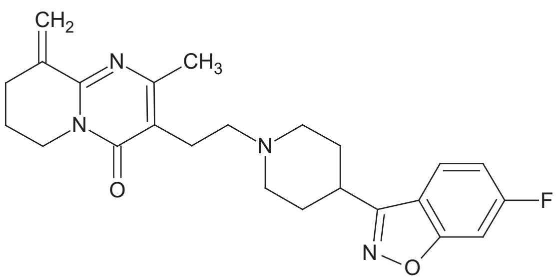 R	3-{2-[4-(6-Fluoro-1,2-benzisoxazol-3-yl)piperidin-1-yl]ethyl}-2-methyl-9-methylidene-6,7,8,9-tetrahydro-4*H*-pyrido[1,2-a] pyrimidin-4-one	Synthetic impurity

(*continued*)

TABLE 8.3 *(continued)*

Structure	Chemical name	Classification
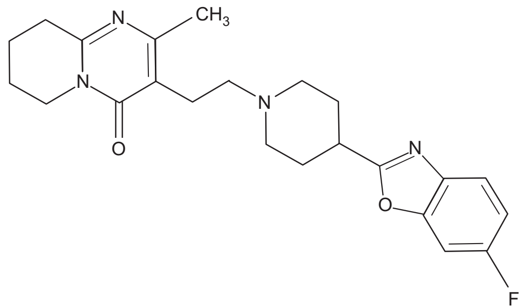 S	3-{2-[4-(6-Fluoro-1,3-benzoxazol-2-yl)piperidin-1-yl]ethyl}-2-methyl-6,7,8,9-tetrahydro-4*H*-pyrido[1,2-a]pyrimidin-4-one	Risperidone isomer Degradation product
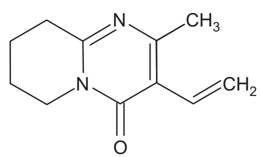 T	3-Ethenyl-2-methyl-6,7,8,9-tetrahydro-4*H*-pyrido[1,2-a]pyrimidin-4-one	Degradation product

TABLE 8.4 Summary of HPLC methods used to analyze risperidone and its impurities/degradation products in bulk drug substance and pharmaceutical dosage forms

Column	Mobile phase/gradient program	Column temperature (°C)	Detection (λ, nm)	Solvent	Sample/test	References
C18 column (3 µm) (10 cm × 4.6 mm)	Mobile phase A: 5 g/L solution of ammonium acetate R Mobile phase B: Methanol R Time (min) / Solution A (%) / Solution B (%) 0–2 / 70 / 30 2–17 / 70→30 / 30→70 17–22 / 30 / 70	Not specified	260	Methanol	Drug substance/impurities	[4]
C18 column (3 µm) (10 cm × 4.6 mm)	Buffer solution: Dissolve 15.4 g of ammonium acetate in 1 L of water. Adjust with 10% acetic acid to a pH of 6.5 and mix Solution A: Mix 100 mL of buffer solution with 150 mL of methanol in a 1000-mL volumetric flask and dilute with water to volume Solution B: Mix 100 mL of buffer solution with 850 mL of methanol in a 1000-mL volumetric flask and dilute with water to volume Time (min) / Solution A (%) / Solution B (%) 0–1 / 70 / 30 1–20 / 70→5 / 30→95 20–25 / 5 / 95 25–27 / 5→70 / 95→30 27–35 / 70 / 30	35	275	Buffer, water, and methanol (1:9:10)	Drug substance/assay and impurities	[1]

(*continued*)

TABLE 8.4 (*continued*)

Column	Mobile phase/gradient program	Column temperature (°C)	Detection (λ, nm)	Solvent	Sample/test	References
C18 column (5 μm) (15 cm × 4.6 mm)	Solution A: Mixture of water, acetonitrile, and trifluoroacetic acid (80:19.5:0.1). Adjust with ammonium hydroxide to a pH of 3.0 Solution B: Mixture of water, methanol, and trifluoroacetic acid (61:39:0.1). Adjust with ammonium hydroxide to a pH of 3.0 Time (min) / Solution A (%) / Solution B (%) 0–8 / 100 / 0 8–16 / 100→0 / 0→100 16–20 / 0 / 100 20–21 / 0→100 / 100→0 21–30 / 100 / 0	RT	275	Methanol: water (80:20)	Tablets/assay and impurities	[1]
C18 column (5 μm) (15 cm × 4.6 mm)	Mixture of water and acetonitrile (65:35). Add 1 mL of trifluoroacetic acid to each 1 L of the mixture. Adjust with ammonium hydroxide to a pH of 3.0	Not specified	237	0.1 N hydrochloric acid	Tablets/dissolution and content uniformity	[1]
C18 column (3 μm) (10 cm × 4.6 mm)	Buffer: 5.0 g/L of ammonium acetate in water Mobile phase: Acetonitrile and buffer (11:39)	Not specified	275	Buffer/methanol	Oral solution/assay and impurities	[1]

Lichrosorb RP C18 (10 µm) (25 cm × 4 mm)	Methanol:0.05 M potassium dihydrogen phosphate, pH 7 (65:35)	Ambient	280	Methanol	Drug substance and tablets/ assay	[32]
Symmetry C18 (5 µm) (25 cm × 4.6 mm)	10 mM of ammonium acetate:acetonitrile (75:25)	Not specified	260	Methanol	Drug substance and tablets/ impurities	[33]
Hypersil BDS C18 (3 µm) (10 cm × 4.6 mm)	Mobile phase A: 5.0 g/L of ammonium acetate in water Mobile phase B: Methanol:acetonitrile (80:20) Time (min) / Solution A (%) / Solution B (%) 0.01 / 80 / 20 15.0 / 70 / 30 25.0 / 60 / 40 35.0 / 50 / 50 45.0 / 30 / 70 50.0 / 30 / 70 51.0 / 80 / 20	45	260	Not specified	Tablets/ impurities	[31]
XTerra RP8 (5 µm) (25 cm × 4.6 mm)	Buffer:methanol:acetonitrile (65:15:20) Buffer: 10 mM potassium dihydrogen phosphate and 0.1% triethylamine, adjust the pH to 3.5 with dilute orthophosphoric acid	25 (ambient)	276	Water: acetonitrile (50:50)	Tablets/assay	[34]
Lichrosorb RP-18 (5 µm) (25 cm × 4 mm)	Acetonitrile:0.05 M potassium dihydrogen phosphate (45:55)	Not specified	278	Not specified	Tablets/assay and dissolution	[35]

- Related compounds—Gradient HPLC (chromatographic conditions as directed in the Assay);
  Bicyclorisperidone and risperidone *cis*-N-oxide (impurities P and Q in Table 8.3): not more than 0.5% each; not more than 0.3% of any unspecified degradation product, and not more than 1.0% of total impurities found.
- Dissolution⟨711⟩
  Medium: 0.1 N HCl; 500 mL
  Apparatus 2: 50 rpm
  Time: 45 min
  Quantitative method by isocratic HPLC method (chromatographic conditions as shown in Table 8.4; ref [1]); not less than 75% (Q) of the labeled amount of risperidone is dissolved in 45 min.
- Uniformity of dosage units⟨905⟩ Quantitative method by isocratic HPLC method (chromatographic conditions as directed for Dissolution); meets the requirements of ⟨905⟩.

The following tests are prescribed for USP risperidone oral solution:

- Identification: the retention time of the major peak in the chromatogram of the sample solution corresponds to that in the chromatogram of the standard solution as obtained in the Assay.
- Deliverable volume⟨698⟩: meets the requirements.
- pH⟨791⟩: 2.0–4.0.
- Assay—Isocratic HPLC (chromatographic conditions as shown in Table 8.4; ref [1]); 90.0–110.0% of the labeled amount of risperidone.
- Organic impurities—Isocratic HPLC (chromatographic conditions as directed in the Assay); Bicyclorisperidone and risperidone *cis*-N-oxide (impurities P and Q in Table 8.3): not more than 0.50% each; not more than 0.20% of any unspecified degradation product, and not more than 1.0% of total impurities found.

4.2.2. EP/BP methods of analysis

The EP/BP harmonized Ph Eur monograph 1559 [4] prescribes the following tests for risperidone drug substance:

- Identification: infrared absorption (*2.2.24*): comparison with risperidone CRS. If spectra show differences, the test and reference substances may be dissolved in *acetone R*, evaporated to dryness, and new spectra recorded using the residues.
- Appearance of solution: the solution (0.1 g in 7.5 g/L of *tartaric acid R*) is clear (*2.2.1*) and colorless (*2.2.2*, *method II*).
- Loss on drying (*2.2.32*): in vacuum at 105 °C for 4 h determined on 1.000 g; loses not more than 0.5%.

- Sulfated ash (*2.4.14*): not more than 0.1% for a 1.0 g sample in a platinum crucible.
- Assay—potentiometric titration using 0.1 M perchloric acid. 0.160 g of sample is dissolved in anhydrous acetic acid:methyl ethyl ketone (1:7 v/v). Titration end point is determined potentiometrically according to (*2.2.20*); 99.0–101.0% (dried substance).
- Related substances—HPLC gradient (chromatographic conditions as shown in Table 8.4; ref [4]); Impurities A, B, C, D, E (Table 8.3): not more than 0.2% each; Impurity K (Table 8.3) not more than 0.15%, not more than 0.10% of any unspecified impurity; not more than 0.3% of total impurities found; disregard limit 0.05%.

5. CHROMATOGRAPHIC METHODS OF ANALYSIS

5.1. Liquid chromatography

A summary of HPLC methods used to analyze risperidone and its impurities and degradation products in bulk drug substance and pharmaceutical dosage forms is set forth in Table 8.4.

5.2. Thin-layer chromatography

El-Sherif *et al.* report a TLC densitometric technique for the analysis of risperidone in the presence of degradation products [32]. The mobile phase used was ACN:methanol:propanol:triethanolamine (8.5:1.2:0.6:0.2 v/v/v/v) and stationary phase consisting of silica gel (0.2 mm layer) on 20×20 cm aluminum cards with fluorescent indicator, 254 nm. A complete separation was obtained with R_f values for risperidone (0.33), and its degradation products (0.1, 1.28, 0.24, 0) for impurities P, T, C, and Q, respectively (Table 8.3). A detection wavelength of 280 nm on a Shimadzu dual wavelength lamp flying spot scanning densitometer (CS 9301) was used for quantifying the drug. Linear range was 2–10 μg per spot, limit of detection 249.69 ng per spot, and limit of quantification was 629.85 ng per spot.

Maślanka report a chromatographic–densitometric assay method for identifying and quantifying risperidone in pharmaceutical preparations [36]. TLC-F_{254} chromatographic plates (10×10 cm) were used as a stationary phase with mobile phase consisting of *n*-butanol:acetic acid:water (12:3:5 v/v/v). A TLC densitometer Scanner 3 equipped with Cats 4.0x software (Linomat IV Camag) was used to make the densitometric recording at 280 nm. Separation of risperidone from its degradation products was satisfactory under the conditions studied which included acidic (0.5 M HCl, 100 °C for 1, 2, 3, and 5 h), basic (0.5 M NaOH:MeOH (3:1),

100°C for 1, 2, 3, and 5h), oxidative (0.9M H_2O_2–methanol, ambient for 0.5, 1, 2, and 5h), and reductive (0.1M Na_2SO_3 for 1, 2, 7h and 14 days). One degradation product was observed in the acidic condition ($R_f \sim 0.79$); three degradation products were observed for the basic condition ($R_f \sim 0.40$, $R_f \sim 0.48$, $R_f \sim 0.72$); one degradation product was detected in the oxidative condition ($R_f \sim 0.50$); and no degradation occurred in the reductive stressed sample. Risperidone was reported to have an $R_f \sim 0.49$. The limit of detection was reported as 0.222 mg/spot and limit of quantitation was 0.672mg/spot. No meaningful differences were reported when TLC plates were replaced by HPTLC plates.

6. DETERMINATION IN BIOLOGICAL SAMPLES

The demands of drug research and development require efficient, accurate, selective, and highly sensitive analytical methods for determining the presence of the drug in biological fluids and tissues of humans and animals. In addition to this, there also exists a need for on-going monitoring of patients under psychotropic drug therapy as this is considered a basic element of their treatment, due to the onset of negative side effects associated with high plasma concentrations of the medication. Advocates for therapeutic drug monitoring of such patients report that on-going monitoring also provides value for detecting poor patient compliance, individual metabolic variability, and optimization of patient treatment dosages [20,37–39]. Since the therapeutic effect of risperidone is manifested through the combined action of risperidone (RISP) and its major active metabolite 9-hydroxy-risperidone (RISP9-OH), nearly all of the analytical methods developed for the determination of the drug in biological fluids, or tissues, simultaneously analyze for both of these active species. The steady-state levels of the active moiety are reported to be typically in the 10–60-ng/mL range [20]. A basic summary of the many bio-analytical methods available is given in Table 8.5. All of the methods utilize HPLC separation with detection either by UV, diode-array, electrochemical detection, or by mass spectrometry (MS) using turbo ion spray, electrospray ionization (ESI), or atmospheric pressure chemical ionization ion source. Sample pretreatment was accomplished by liquid–liquid extraction with organic solvents, deproteinization techniques typically with ACN, solid-phase extraction, or microextraction by packed sorbent. Since the hydroxylated metabolites of risperidone (Fig. 8.14) introduce a chiral carbon into the molecule, some methods employ enantiomer-selective stationary phases. Frequently, the compound designated ''R068808'' (i.e., methyl-risperidone, obtained from Janssen Research) is used as an internal standard, while some methods employ ^2H and ^{13}C isotope-labeled

TABLE 8.5 Summary of HPLC methods used to analyze risperidone and its metabolite in biological samples

Method	Detection	Sample	Method of purification	Analyte(s)	References
HPLC-RP	UV 238nm	Human plasma, urine, saliva	MEPS	RISP, RISP9-OH, I.S. diphenhydramine	[40]
HPLC-RP	ECD, two flow-through electrodes (1) +0.500V (2) +0.700V	Human plasma, saliva	MEPS	RISP, RISP9-OH, I.S. pipamperone	[41]
Chiral-HPLC	ECD 4 sensor analytical cell, (1) +500mV (2) +650mV (3) +950mV (4) +950mV	Human blood plasma	SPE	RISP, (+)-RISP9-OH, (−)-RISP9-OH, I.S. fenoterol	[42]
LC-MS/MS	Duo ion trap with ESI interface in positive ion mode, selected reaction monitoring (SRM) mode	Human hair	LLE	RISP, RISP9-OH, I.S. methaqualone	[43]
HPLC-RP	UV 285nm	Human serum	SPE with on-line column switching	RISP, RISP9-OH, I.S. clozapine	[44]
Chiral LC-MS/MS	Turbo ion spray positive ion mode, multiple reaction monitoring (MRM) mode	Human plasma	SPE	RISP, (+)-RISP9-OH, (-)-RISP9-OH, I.S. $^{2}H_2$-$^{13}C_2$-RISP and $^{2}H_2$-$^{13}C_2$-RISP9-OH	[45]

(continued)

TABLE 8.5 (*continued*)

Method	Detection	Sample	Method of purification	Analyte(s)	References
Chiral LC-MS/MS	ESI, positive ion mode, MRM	Human plasma	LLE	RISP, (+)-RISP9-OH, (-)-RISP9-OH, I.S. R068808 (for RISP only), (±)-RISP9-OH-d_4	[46]
LC-MS/MS	Turbo ion spray positive ion mode, MRM mode	Human plasma	Robotic protein precipitation (ACN) and sub-zero temperature extraction with turbulent flow, dual on-line extraction column switching process	RISP, RISP9-OH, I.S. R068808	[47]
HPLC-RP	UV 280nm	Human plasma	Protein precipitation (ACN)	RISP, I.S. diltiazem	[48]
LC-MS/MS	ESI in positive ion mode, SRM	Human plasma	Protein precipitation (ACN)	RISP, RISP9-OH, I.S. methyl-risperidone	[49]
LC-MS	ESI positive ion mode, selected ion monitoring	Human plasma	LLE	RISP, RISP9-OH, I.S. di-dehydro-risperidone	[50]
HPLC-RP	DAD-UV 240nm	Human plasma	SPE	RISP, RISP9-OH, I.S. clozapine or loxapine	[51]

LC-MS/MS	PE Sciex API-III+triple quadropole MS with TurboIonSpray source	Human plasma, saliva	Protein precipitation, column switching	RISP, RISP9-OH, I.S. R068808	[52]
LC-APCI-MS-MS	APCI, SRM	Human plasma	LLE	RISP, RISP9-OH, I.S. R068808	[53]
LC-MS/MS	TurboIonSpray, positive ion mode, MRM; Method A employs one internal standard, Method B employs 2 internal standards	Human plasma	SPE	RISP, RISP9-OH, internal standards: Method A: R068809 (desfluoro-RISP); Method B: R215640 ($^{2}H_{3}$-$^{13}C_{2}$-RISP), R215639 ($^{2}H_{3}$-$^{13}C_{2}$-RISP9-OH)	[54]
HPLC-RP	UV 278 nm	Human plasma	LLE	RISP, RISP9-OH, I.S. methyl-risperidone	[55]
HPLC-RP	UV 280 nm	Human plasma	LLE	RISP, RISP9-OH, I.S. R068808	[56]
LC-MS/MS	Atmospheric pressure ESI positive ion mode, MRM	Human and rat plasma	LLE	RISP, RISP9-OH, I.S. R68808 (methyl-risperidone)	[57]
HPLC-RP	UV 278 nm	Human plasma	LLE	RISP, RISP9-OH, I.S. clozapine	[58]
HPLC-RP	ECD, two flow-through electrodes	Human plasma	LLE	RISP, RISP9-OH, I.S. R68808	[59]

(*continued*)

TABLE 8.5 (*continued*)

Method	Detection	Sample	Method of purification	Analyte(s)	References
	(1) +0.55 V (2) +0.80 V				
HPLC-RP	UV 280 nm	Human plasma	SPE	RISP, RISP9-OH, I.S. trazodone	[60]
HPLC-RP	UV 280 nm	Human serum	LLE	RISP, RISP9-OH, I.S. haloperidol	[61]
HPLC-RP	ECD, two flow-through electrodes (1) +0.5 V (2) +0.96 V	Human plasma	LLE	RISP, RISP9-OH, I.S. remoxipride	[62]
HPLC-RP	ECD, two flow-through electrodes (1) +0.6 V (2) +0.92 V	Human plasma	LLE	RISP, I.S. remoxipride	[63]
HPLC-RP	ECD, two flow-through electrodes (1) +0.55 V (2) +0.80 V	Human plasma	LLE	RISP, RISP9-OH, I.S. R68808	[64]

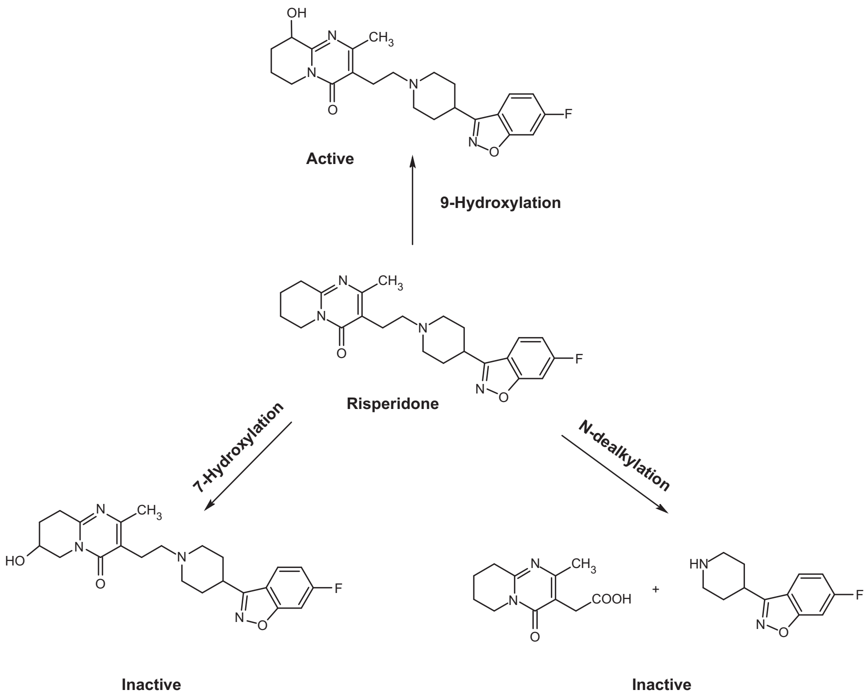

FIGURE 8.14 Metabolic pathway of risperidone in humans.

species as internal standards and other methods utilize existing drugs found to be suitable.

7. PHARMACOKINETICS AND METABOLISM

7.1. Absorption

After oral administration, risperidone is nearly completely absorbed from the gastrointestinal tract. Only 1% of an oral dose was recovered in the feces as unchanged drug [65,66]. The absolute bioavailability of risperidone is 70%. The relative oral bioavailability of risperidone from a tablet is 94% when compared with a solution [67]. Following oral administration of solution or tablet, mean peak plasma concentrations of risperidone occurred at about 1–2h. Peak concentration of its active metabolite, 9-hydroxy-risperidone, occurred at about 3h in extensive metabolizers and 13h in poor metabolizers [68]. Steady-state concentrations of risperidone are reached in 1day in extensive metabolizers and expected to reach in 5 days in poor metabolizers. Food does not affect the rate and extent of absorption of risperidone.

7.2. Distribution

Risperidone has a moderate volume of distribution. The volume of distribution at steady state was 1.1 (±0.2) L/kg for extensive metabolizers [69]. Risperidone was 90% bound in human plasma. The binding of 9-hydroxy-risperidone was lower and averaged 77.4% in human plasma. The protein binding is not affected by age or hepatic and renal impairment. Risperidone and its metabolite are bound to both albumin and α_1-acid glycoprotein [70].

7.3. Metabolism

Risperidone undergoes 9-hydroxylation in the liver, predominantly catalyzed by the cytochrome P450 (CYP) enzyme, CYP2D6, to produce 9-hydroxy-risperidone, a pharmacologically active metabolite considered equipotent to the parent drug (marketed as paliperidone) [67,71]. CYP3A4 also appears to be involved, to a lesser extent, in metabolism of risperidone and 9-hydroxy-risperidone [72]. The minor metabolic routes for risperidone include oxidative N-dealkylation and hydroxylation to 7-hydroxy-risperidone (Fig. 8.14).

These metabolites do not exhibit pharmacologic effects [65,67,69]. The sum of risperidone and 9-hydroxy-risperidone represents the ''active moiety'' or the antipsychotic fraction of risperidone. After oral administration of 1 mg ^{14}C risperidone, 70% of the radioactivity was excreted in the urine and 14% in the feces within 1 week. Unchanged risperidone was excreted mainly in urine (4–30% depending on the subject's metabolism activities) [7]. Trace (~1%) of unchanged drug recovered in feces. 9-Hydroxy-risperidone accounts for 32% of total radioactivity excreted in the urine for extensive metabolizers and only 8% in poor metabolizers [7].

7.4. Elimination

Risperidone is cleared largely through metabolic biotransformation, with 80% of total clearance occurring via a nonrenal route in extensive metabolizers. 9-Hydroxy-risperidone is removed mainly by renal excretion. The mean total body clearance of active moiety is estimated at 100 mL/min/kg [66].

8. PHARMACOLOGICAL EFFECTS

8.1. Mechanism of action

The antipsychotic effects of neuroleptic drugs are believed to be due to the action of these compounds on several neurotransmitter receptors in the brain. The therapeutic efficacy of risperidone in schizophrenia is mediated through a combination of dopamine Type 2 (D2) and serotonin

Type 2 (5HT2) receptor antagonism. Therefore, risperidone belongs to the serotonin–dopamine antagonist class. *In vitro* receptor binding studies showed that risperidone has high affinity for 5HT2, D2, α_1 and α_2 adrenergic, and H1 histaminergic receptors. It also acts as an antagonist at other receptors, but with lower potency [73].

8.2. Adverse reactions

In general, risperidone is well tolerated. It is less likely to provoke extrapyramidal side effects than other conventional neuroleptics [74].

Only about 7% of the patients had been withdrawn from clinical trials due to adverse events. The most common adverse reactions that were associated with discontinuation from clinical trials were somnolence, nausea, abdominal pain, dizziness, vomiting, agitation, and akathisia [75].

8.3. Drug interactions

Risperidone may potentiate the effects of other centrally acting agents, alcohol, and antihypertensive agents. It may antagonize the effects of levodopa and other dopamine agonists. Plasma concentrations of risperidone, but not of the active moiety, may be increased by phenothiazine, tricyclic antidepressants, and some β-blockers [76].

9. STABILITY

Tomar *et al.* [33] identified two major degradation products of risperidone in bulk drug substance and tablets. Acidic (0.5N HCl with reflux), basic (0.1N NaOH:methanol, 1:1, with reflux), and oxidative (3% hydrogen peroxide in methanol) solutions were employed to degrade the drug substance. The tablets were exposed to 60 °C for 1 month. Using LC-MS/MS to analyze enriched fractions of the isolated degradation products, the authors were able to identify the degradants as 9-hydroxy-risperidone (Table 8.3 - Impurity C) and risperidone N-oxide (Table 8.3 - Impurity Q).

Barathi *et al.* [31] placed risperidone tablets powder in an autoclave at 121 °C/15lb pressure/30min for three cycles. An unknown degradation product was detected in the autoclaved sample and was isolated for identification. The ESI mass spectrum of the unknown impurity exhibited a molecular ion peak at *m/z* 411 amu $[M+H]^+$ in positive ion mode which is the same as risperidone. The authors elucidated the structure of the impurity using ^1H and ^{13}C NMR techniques and determined that the degradation product was formed by a thermolytic or light-induced rearrangement of the isoxazole ring of risperidone to the corresponding

oxazole (Table 8.3—Impurity S). The pathway proposed by the authors for this interesting discovery is shown in Scheme 8.6.

El-Sherif *et al.* report five degradation products of risperidone tablets and bulk powder [32]. Among the potential degradation products identified are bicyclorisperidone (impurity P), *cis* and *trans* isomers of risperidone N-oxide (impurity Q), 3-ethenylpyrimidinone derivative (impurity T), and 9-hydroxy-risperidone (impurity C). The authors report the impurities may be formed under inappropriate storage conditions of risperidone tablets but did not elaborate further on the type of conditions required to generate these specific degradation products.

An aqueous solution of risperidone exposed to 1.9 million lux-h of light (310–800nm) suffered a significant potency loss (>5%) and yielded about 0.2% of risperidone N-oxide impurity, 0.1% of 9-hydroxy-risperidone, and approximately 2.9% of unidentified degradation products when analyzed under the chromatographic conditions set forth in the Ph. Eur. Monograph (ref. [4]; Table 8.4). A sample of risperidone drug substance powder exposed under the same light condition was found to be unaffected by

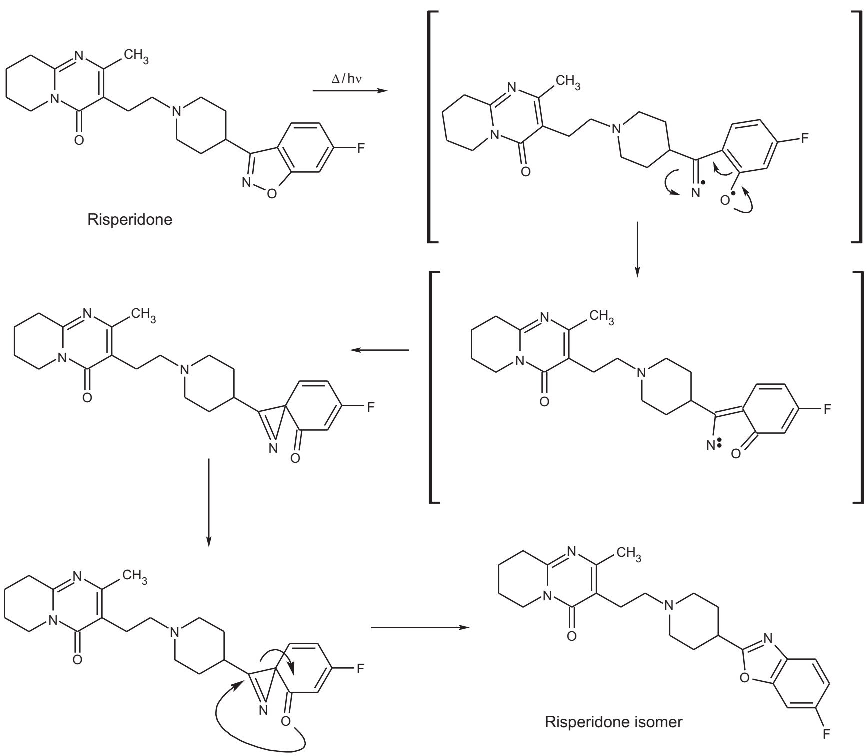

SCHEME 8.6 Risperidone thermal degradation reaction.

the exposure and showed comparable potency and impurity content as an unexposed control sample.

Aki *et al.* reported incompatibility of risperidone with oolong, green, and black teas [77]. Risperidone oral solution may be diluted with liquids such as water, orange juice, or black coffee in order to reduce or mask the bitter taste; however, the monomeric tannins found in tea (-)-epigallocatechin (EGC), (-)-epigallocatechin gallate (EGCg), (-)-epicatechin (EC), (-)-epicatechin gallate (ECg), and theaflavin 3′-O-gallate (TFg) tend to form 1:1 molar ratio complexes with risperidone. The authors used isothermal titration microcalorimetry to rapidly determine the extent of complexation of risperidone with the tea tannins. It was found that the binding affinity of risperidone with monomeric tea tannin increased in the order of TFg>EGCg>ECg>EGC>EC and that tea solutions titrated with risperidone became cloudy, and produced white precipitates when allowed to stand overnight. The amount of risperidone remaining (mass/v%) immediately after diluting risperidone liquid in a 3:97 (v/v) ratio was 77.7% (green tea), 38.3% (black tea), and 22.8% (oolong tea). The authors concluded that the formation of insoluble tea tannin complexes in risperidone oral solution diluted in tea beverages may reduce the risperidone content and cause a reduction in the absorption of the drug.

ACKNOWLEDGMENTS

The authors are indebted to Dr. Pradeep Sanghvi for encouragement and management support. We also wish to express our appreciation to Dr. Yuri Goldberg for his guidance and to Ms. Janet Mensah for her assistance in retrieving the cited literature and finally many thanks go to our colleagues in the laboratories who contributed material needed for the preparation of this manuscript.

REFERENCES

[1] The United States Pharmacopeia 34. National Formulary 29, May 1, 2011.
[2] L. Kennis, J. Vandenberk, US Patent No. 4,804,663, 1989.
[3] *Merck Index*, 14th ed., Merck & Co. Inc., 2006, entry 8316, 1478.
[4] European Pharmacopoeia 7.4, April 2012.
[5] L.A. Trissel, Trissel's™ Stability of Compounded Formulations, 4th ed., American Pharmacists Association (APhA), Washington, D.C., 2009.
[6] P.A.J. Janssen, et al., Pharmacology of risperidone (R64766), a new antipsychotic with serotonin-S2 and dopamine-D2 antagonistic properties, J. Pharmacol. Exp. Ther. 244 (1988) 685–693.
[7] J.E. Leysen, et al., Biochemical profile of risperidone, a new antipsychotic, J. Pharmacol. Exp. Ther. 247 (1988) 661–670.
[8] C. Repchinsky, Editor-in-Chief. (Risperdal®). *Compendium of Pharmaceutical Specialties*, 2011.
[9] (Risperdal® Consta®). *Physician's Desk Reference*, 63rd ed., 2009.
[10] S.R. Marder, R.C. Meibach, Risperidone in the treatment of schizophrenia, Am. J. Psychiatry 151 (1994) 825–835.

[11] H. Jones, Risperidone: a review of its pharmacology and use in the treatment of schizophrenia, J. Serotonin Res. 4 (1997) 17–28.
[12] A. Vermeulen, et al., Population pharmacokinetics of risperidone and 9-hydroxyisperidone in patients with acute episodes associated with bipolar I disorder, J. Pharmacokinet. Pharmacodyn. 34 (2007) 183–206.
[13] R. Bruggeman, et al., Risperidone versus pimozide in Tourette's disorder: a comparative double-blind parallel-group study, J. Clin. Psychiatry 62 (2001) 50–56.
[14] United States Food and Drug Administration. www.fda.gov, New Drug Application # 020272.
[15] G. Galizia, The treatment of schizophrenia: an overview, Pharmacologyonline 2 (2009) 971–1020.
[16] H. He, J.S. Richardson, A pharmacological, pharmacokinetic and clinical overview of risperidone, a new antipsychotic that blocks 5-HT_2 and dopamine D_2 receptors, Int. Clin. Psychopharmacol. 10 (1995) 19–30.
[17] C.R. Craig, R.E. Stitzel, Modern Pharmacology, 4th ed., Little, Brown & Co, Boston, MA, 1994.
[18] R.H. Foster, K.L. Goa, Risperidone: a pharmacoeconomic review of its use in schizophrenia, Pharmacoeconomics (1998) 97–133.
[19] D.H. Wang, Y.J. Pan, Risperidone chloride 2.5 hydrate: a new crystalline form, Acta Crystallogr. E62 (2006) 768–770.
[20] A. Musenga, et al., Antipyschotic and antiepileptic drugs in bipolar disorder: the importance of therapeutic drug monitoring, Curr. Med. Chem. 16 (2009) 1463–1481.
[21] F.M. Olondriz *et al.*, Spanish Patent No. 2,050,069, 1994.
[22] P.D. Barjoan *et al.*, Spanish Patent No. 2,074,966, 1996.
[23] S.S. Nadkarni, R.G. Shah, International Patent WO 2004/020439.
[24] D.-M. Kim, et al., An efficient synthesis of risperidone via Stille reaction: antipsychotic, 5-HT_2 and dopamine-D_2-antagonist, Arch. Pharm. Res. 28 (2005) 1019–1022.
[25] Product monograph, Risperdal® Tablets, Oral solution and Orally disintegrating tablets, Janssen Inc. date of revision March 11, 2011.
[26] A.C. Moffat, M.D. Osselton, B. Widdop, Clarke's Analysis of Drugs and Poisons, 3rd ed., Pharmaceutical Press, London, 2004.
[27] B. Krochma *et al.*, US Patent No. 6,750,341, 2004.
[28] I. Karrabas, et al., Analysis and stability of polymorphs in tablets: the case of risperidone, Talanta 71 (2007) 1382–1386.
[29] Source: Drugs@FDA, Paliperidone, tradename Invega®, NDA#02199, Janssen Pharms, December 19, 2006.
[30] P. Sattanathan, et al., Structural studies of impurities of risperidone by hyphenated techniques, J. Pharm. Biomed. Anal. 40 (2006) 598–604.
[31] C. Barathi, et al., Identification, isolation and characterization of potential degradation product in risperidone tablets, J. Pharm. Biomed. Anal. 46 (2008) 165–169.
[32] Z.A. El-Sherif, et al., High performance liquid chromatographic and thin layer densitometric methods for the determination of risperidone in the presence of its degradation products in bulk powder and in tablets, J. Pharm. Biomed. Anal. 36 (2005) 975–981.
[33] R.S. Tomar, et al., Identification and characterization of major degradation products of risperidone in bulk drug and pharmaceutical forms, J. Pharm. Biomed. Anal. 36 (2004) 231–235.
[34] A.P. Suthar, et al., Determination of risperidone and forced degradation behavior by HPLC in tablet dosage form, Int. J. PharmTech. Res. 1 (2009) 568–574.
[35] C.M.G. Peña, et al., Analytical method for quantification and dissolution assay of 3 mg tablets of risperidone, Revista Cubana de Farmacia 43 (4) (2009) 31–44.
[36] A. Maślanka, Determination of risperidone in tablets in the presence of its degradation products and placebo-derived constituents, Acta Pol. Pharm. 66 (2009) 460–470.

[37] M.A. Raggi, et al., Therapeutic drug monitoring: chemical-clinical correlations of atypical antipsychotic drugs, Curr. Med. Chem. 9 (2002) 1397–1409.
[38] M.A. Raggi, et al., Atypicial antipsychotics: pharmacokinetics, therapeutic drug monitoring and pharmacological interactions, Curr. Med. Chem. 11 (2004) 279–296.
[39] M.A. Raggi, et al., Advances in therapeutic drug monitoring of atypicial antipsychotic drugs, Med. Chem. Rev. 1 (2004) 299–316.
[40] R. Mandrioli, et al., Analysis of risperidone and 9-hydroxyrisperidone in human plasma, urine and saliva by MEPS-LC-UV, J. Chromatogr. B 879 (2011) 167–173.
[41] M.A. Saracinco, et al., Analysis of risperidone and its metabolite in plasma and saliva by LC with coulometric detection and a novel MEPS procedure, Talanta 81 (2010) 1547–1553.
[42] I. Locatelli, et al., Simultaneous determination of risperidone and 9-hydroxyrisperidone enantiomers in human blood plasma by liquid chromatography with electrochemical detection, J. Pharm. Biomed. Anal. 50 (2009) 905–910.
[43] S. Schneider, et al., Time resolved analysis of risperidone and 9-hydroxyrisperidone in hair using LC/MS-MS, J. Chromatogr. B 877 (2009) 2589–2592.
[44] K.M. Kirschbaum, et al., LC with column-switching and spectrophotometric detection for determination of risperidone and 9-hydroxyrisperidone in human serum, Chromatographia 67 (2008) 321–324.
[45] M. De Meulder, et al., Validated LC-MS/MS methods for the determination of risperidone and the enantiomers of 9-hydroxyrisperidone in human plasma and urine, J. Chromatogr. B 870 (2008) 8–16.
[46] B. Čabovska, et al., Determination of risperidone and enantiomers of 9-hydroxyrisperidone in plasma by LC-MS/MS, J. Chromatogr. B 852 (2007) 497–504.
[47] C. Kousoulos, et al., Turbulent flow and ternary column-switching on-line clean-up system for high-throughput quantification of risperidone and its main metabolite in plasma by LC-MS/MS: application to a bioequivalence study, Talanta 72 (2007) 360–367.
[48] S.M. Foroutan, et al., Rapid high performance liquid chromatographic determination of risperidone in human plasma, Iran. J. Pharm. Res. 1 (2006) 37–40.
[49] J. Bhatt, Liquid chromatography/tandem mass spectrometry method for simultaneous determination of risperidone and its active metabolite 9-hydroxyrisperidone in human plasma, Rapid Commun. Mass Spectrom. 20 (2006) 2109–2114.
[50] L. Zhang, et al., The validation of an LC-MS method for the determination of risperidone and its active metabolite 9-hydroxyrisperidone in human plasma, Chromatographia 61 (2005) 245–251.
[51] M.A. Raggi, et al., HPLC-DAD determination of plasma levels of the antipsychotic risperidone and its main metabolite for toxicological purposes, J. Sep. Sci. 28 (2005) 245–250.
[52] J. Flarakos, et al., Quantification of risperidone and 9-hydroxyrisperidone in plasma and saliva from adult and pediatric patients by liquid chromatography-mass spectrometry, J. Chromatogr. A 1026 (2004) 175–183.
[53] D.E. Moody, et al., Technical note: a high-performance liquid chromatographic-atmospheric pressure chemical ionization tandem mass spectrometric method for determination of risperidone and 9-hydroxyrisperidone in human plasma, J. Anal. Toxicol. 28 (2004) 494–497.
[54] B.M.M. Remmerie, et al., Validated method for the determination of risperidone and 9-hydroxyrisperidone in human plasma by liquid chromatography-tandem mass spectrometry, J. Chromatogr. B 783 (2003) 461–472.
[55] A. LLerena, et al., Determination of risperidone and 9-hydroxyrisperidone in human plasma by liquid chromatography: application to the evaluation of CYP2D6 drug interactions, J. Chromatogr. B 783 (2003) 213–219.

[56] K. Titier, et al., Simplified high-performance liquid chromatographic method for determination of risperidone and 9-hydroxyrisperidone in plasma after overdose, J. Chromatogr. B 772 (2002) 373–378.
[57] M. Aravagiri, S.R. Marder, Simultaneous determination of risperidone and 9-hydroxyrisperidone in plasma by liquid chromatography/electrospray tandem mass spectrometry, J. Mass Spectrom. 35 (2000) 718–724.
[58] A. Avenoso, et al., Determination of risperidone and its major metabolite 9-hydroxyrisperidone in human plasma by reversed-phase liquid chromatography with ultra-violet detection, J. Chromatogr. B 746 (2000) 173–181.
[59] A.E. Balant-Gorgia, et al., Therapeutic drug monitoring of risperidone using a new, rapid HPLC method: reappraisal of interindividual variability factors, Ther. Drug Monit. 21 (1999) 105–115.
[60] T. Nagasaki, et al., Determination of risperidone and 9-hydroxyrisperidone in human plasma by high-performance liquid chromatography: application to therapeutic drug monitoring in Japanese patients with schizophrenia, J. Pharm. Biomed. Anal. 19 (1999) 595–601.
[61] O. Olesen, K. Linnet, Simplified high-performance liquid chromatographic method for determination of risperidone and 9-hydroxyrisperidone in serum from patients comedicated with other psychotropic drugs, J. Chromatogr. B 698 (1997) 209–216.
[62] M. Aravagiri, et al., Plasma concentrations of risperidone and its 9-hydroxy metabolite and their relationship to dose in schizophrenic patients: simultaneous determination by a high performance liquid chromatography with electrochemical detection, Pharmacopyschiatry 31 (1998) 102–109.
[63] M. Aravagiri, et al., Determination of risperidone in plasma by high-performance liquid chromatography with electrochemical detection: application to therapeutic drug monitoring in schizophrenic patients, J. Pharm. Sci. 82 (1993) 447–449.
[64] J.P. Le Moing, et al., Determination of risperidone and 9-hydroxyrisperidone in human plasma by high-performance liquid chromatography with electrochemical detection, J. Chromatogr. 614 (1993) 333–339.
[65] G. Mannens, et al., Absorption, metabolism and excretion of risperidone in humans, Am. Soc. Pharmacol. Exp. Ther. 21 (1993) 1134–1141.
[66] J. Heykants, et al., The pharmacokinetics of risperidone in humans: a summary, J. Clin. Psychiatry 55 (1994) 13–17.
[67] FDA Label. Risperdal (risperidone) tablet. Risperdal (risperidone) solution.
[68] J. Novalbos, et al., Effects of CYP2d6 genotype on the pharmacokinetics, pharmacodynamics, and safety of risperidone in healthy volunteers, J. Clin. Psychopharmacol. 30 (2010) 504–511.
[69] M.L. Huang, et al., Pharmacokinetics of the novel antipsychotic agent risperidone and the prolactin response in healthy subjects, Clin. Pharmacol. Ther. 54 (1993) 257–268.
[70] G. Mannens, et al., Plasma protein binding of risperidone and its distribution in blood, Psychopharmacology 114 (1994) 566–572.
[71] L. Va Beijsterveldt, et al., The regional brain distribution of risperidone and its active metabolite 9-hydroxy-risperidone in the rat, Psychopharmacology 114 (1993) 53–62.
[72] J. Fang, et al., Metabolism of risperidone to 9-hydroxy-risperidone by human cytochromes P450 2D6 and 3A4, Naunyn Schmiedebergs Arch. Pharmacol. 359 (1999) 147–151.
[73] J.E. Leysen, et al., *In vitro* and *in vivo* receptor binding and effects on monamine turnover in rat brain regions of the novel antipsychotics risperidone and ocaperidone, Mol. Pharmacol. 41 (1992) 494–508.
[74] C. Correia, A.M. Vicente, Pharmacogenetics of risperidone response and induced side effects, Person. Med. 4 (2007) 271–293.

[75] J. Peusken, et al., Risperidone in the treatment of patients with chronic schizophrenia: a multi-national, multi-centre, double-blind, parallel-group study versus haloperidol, Br. J. Psychiatry 166 (1995) 712–726.
[76] X. Rabasseda, et al., Risperidone: a novel antipsychotic for schizophrenia with broad efficacy and reduced potential for extrapyramidal symptoms, Drugs Today 29 (1993) 535–553.
[77] H. Aki, et al., Compatibility and stability tests of risperidone with soft-drinks by isothermal titration microcalorimetry, J. Therm. Anal. Calorim. 85 (2006) 681–684.

CHAPTER 9

Sunitinib Malate

Mohammed Gabr Kassem,* **A.F.M. Motiur Rahman,*** and **Hesham M. Korashy**†

Contents

* Department of Pharmaceutical Chemistry, College of Pharmacy, King Saud University, Riyadh, Kingdom of Saudi Arabia
† Department of Pharmacology and Toxicology, College of Pharmacy, King Saud University, Riyadh, Kingdom of Saudi Arabia

Profiles of Drug Substances, Excipients, and Related Methodology, Volume 37
ISSN 1871-5125, DOI: 10.1016/B978-0-12-397220-0.00009-X
© 2012 Elsevier Inc.
All rights reserved.

1. INTRODUCTION

Sunitinib maleate is a multitargeted tyrosine kinase inhibitor that inhibits tumor cell proliferation and angiogenesis. It is approved for the treatment of renal cell carcinoma (RCC) and imatinib-resistant gastrointestinal stromal tumor (GIST) [1–4]. Its activity in other tumor types (such as hepatocellular carcinoma or non-small cell lung cancer) is currently being investigated in numerous clinical trials (see www.clinicaltrials.gov). Sunitinib is given orally, once daily as a 50-mg capsule over 4 weeks, followed by a 2-week rest period, in repeated 6-week treatment cycles. At this dose, the most frequently observed adverse effects are fatigue, hypertension, diarrhea, stomatitis, and hand–foot syndrome [4].

Following oral administration, sunitinib is slowly absorbed from the gastrointestinal tract, reaching maximum plasma concentrations after about 6–12h. It is primarily metabolized by CYP 3A4 to its active *N*-desethyl metabolite (SU12662) and is subject to presystemic metabolism by this enzyme [5]. In a mass balance study in humans with ^{14}C-labeled sunitinib, 61% of the radioactive dose was recovered in feces and 16% in urine. In plasma samples, sunitinib and SU12662 accounted for 71% and 20.5% of the total radioactivity, respectively [6].

Approximately 95% (90%) of sunitinib (SU12662) is bound to plasma proteins. Because of the long terminal half-lives of sunitinib and SU12662

(40–60h, and 80–110h, respectively), steady-state concentrations are not achieved until 2 weeks of continuously daily dosing [2].

1.1. Nomenclature

1.1.1. Systematical chemical names

- *N*-[2-(Diethylamino)ethyl]-5-[(*Z*)-(5-fluoro-2-oxo-1,2-dihydro-3H-indol-3-ylidene)methyl]-2,4-dimethyl-1H-pyrrole-3-carboxamide hydrogen (2*S*)-2-hydroxybutanedioate [7]
- *N*-[2-(Diethylamino)ethyl]-5-[(*Z*)-(5-fluoro-2-oxo-1,2-dihydro-3H-indol-3-ylidene)methyl]-2,4-dimethyl-1H-pyrrole-3-carboxamide [7,8]
- 5-[5-Fluoro-2-oxo-1,2-dihydroindol-(3Z)-ylidenemethyl] -1H-pyrrole-3-carboxilic acid (2-diethylaminoethyl)amide [8]
- (2*S*)-2-Hydroxybutanedioic acid-*N*-[2-(diethylamino)ethyl]-5-[(*Z*)-(5-fluoro-2-oxo-1,2-dihydro-3H-indol-3-ylidene)methyl]-2,4-dimethyl-1H-pyrrole-3-carboxamide (1:1) [9]

1.1.2. Nonproprietary names

Sunitinib maleate

1.1.3. Proprietary names

Sutent®, Pfizer Inc., **SU11248**® [7–11]

1.2. Formulae

1.2.1. Empirical formula, molecular weight, and CAS number

Sunitinib maleate	$C_{26}H_{33}FN_4O_7$	532.56	(341031-54-7) [7–9]
Sunitinib base	$C_{22}H_{27}FN_4O_2$	398.47	(557795-19-4) [7–9]

1.2.2. Structural formula [7-9]

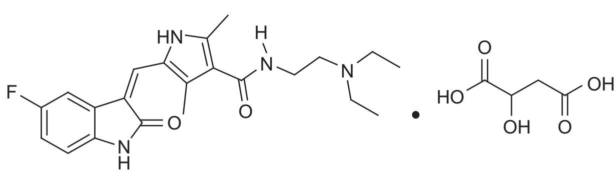

Sunitinib malate

1.2.3. Smiles

CCN(CC)CCNC(=O)C1=C(C)NC(\C=C2/C(=O)NC3=C2C=C(F)C=C3)=C1C.O=C(O)CC(O)C(=O)O

1.3. Elemental analysis

Base: C 66.31%, H 6.83%, F 4.77%, N 14.89% [7]

Malate salt: C 58.62%, H 6.22%, F 3.54%, N 10.47%

1.4. Physical properties

1.4.1. Appearance

Malate salt: yellow powder

Base: orange solid [8]

1.4.2. Solubility

Malate salt: Soluble in dimethyl sulfoxide at 40 mg/mL and very poorly soluble in ethanol and water

1.4.3. Melting point

Malate salt: 194–200 °C

Base: 189–191 °C

1.4.4. Stability

Sunitinib malate is a photosensitive substance [12].

1.4.5. Dissociation constant

pK_a of base: 9.30 [13,14].

1.4.6. Partition coefficient (*P*)

For the water–octanol system: log P=2.5 [15]

1.5. Uses and applications

Sunitinib is an oral multitargeted tyrosine kinase inhibitor with antiangiogenic and antitumor activities attributable to the inhibition of several related tyrosine kinase receptors, including vascular endothelial growth factor receptors (VEGFRs) types 1 and 2 (FLT1 and FLK1/KDR), platelet-derived growth factor receptors (PDGFR-and PDGFR-β), stem cell factor receptor (c-KIT), and Fms-related tyrosine-3 receptor (FLT3), which are implicated in tumor proliferation, angiogenesis, and metastasis [1,4,5,16,17].

2. METHODS OF PREPARATION

2.1. Synthesis of sunitinib 1 [18–21]

The discovery route to sunitinib **1**, as described by Sun and coworkers, commenced with a two-step synthesis of 5-fluorooxindole **10** starting from the corresponding 5-fluoroisatin [22,23]. Heating a neat mixture of 5-fluoroisatin and hydrazine hydrated to 110°C effected a Wolff–Kishner reduction and ring opening to give acyl hydrazine. The crude material was subjected to an intramolecular acylation reaction by exposure to aqueous HCl at room temperature to afford the oxindole **10** in 73% yield over two steps (Scheme 9.1).

The requisite pyrrole subunit was prepared using the Knorr pyrrole synthesis (Scheme 9.2) [23,24]. *tert*-Butyl acetoacetate **2** was reacted with sodium nitrite in acetic acid to furnish oxime **3**. Exposure of this intermediate to ethyl acetoacetate **4** under reductive cyclization conditions using zinc and acetic acid afforded the tetra-substituted pyrrole **5** in 65% yield over two steps. Selective hydrolysis of the *tert*-butyl ester, followed by decarboxylation, was accomplished by stirring **5** in HCl and ethanol to provide intermediate **6** in 87% yield. The unsubstituted position of pyrrole **6** was then formulated in quantitative yield by treatment with Vilsmeier reagent generated from DMF and $POCI_3$ in dichloromethane. Hydrolysis of the ethyl ester using aqueous potassium hydroxide in methanol provided the key intermediate **17** in 94% yield, thus setting the stage for the introduction of the amide side chain and the final coupling reaction with oxindole **10**. The CDI-mediated amidation of carboxylic acid **7** with diamine **8** afforded the desired amide **9**. With sufficient quantities of **9** in hand, the synthesis could be completed via condensation of **9** with 5-fluorooxindole (**10**) to furnish the sunitinib free base **1** in 88% yield.

Sunitinib was also synthesized using the route described below (Scheme 9.3). Treatment of diketene with *N*,*N*-diethylethylenediamine in *tert*-butyl methyl ether furnished â-ketoamide **12** in excellent yield [25]. Oxime **3**, derived from *tert*-butyl acetoacetate, was treated with amide **12** in the presence of zinc and acetic acid according to the classic Knorr pyrrole formation conditions, which led to pyrrole **14**. The α-free pyrrole thus obtained **14** was treated with chloromethylene dimethylammonium

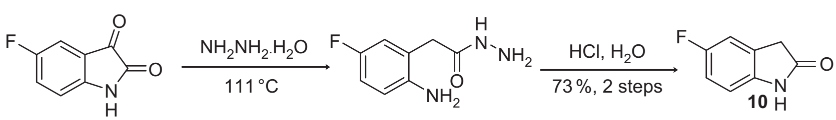

SCHEME 9.1 Synthesis of 5-fluorooxindole **10**.

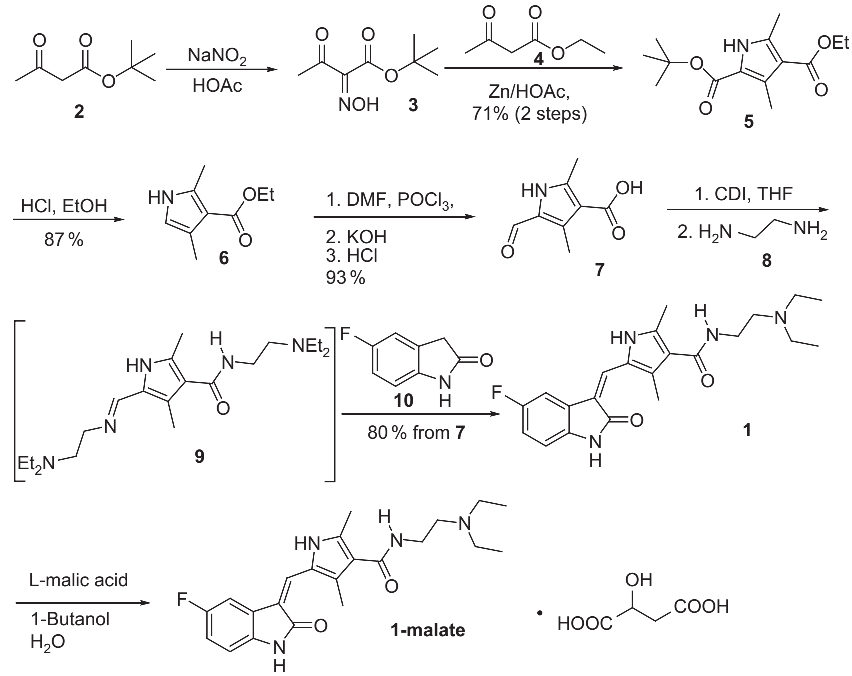

SCHEME 9.2 Synthesis of sunitinib malate **1-malate** via condensation of amide **9** and 5-fluorooxindole **10**.

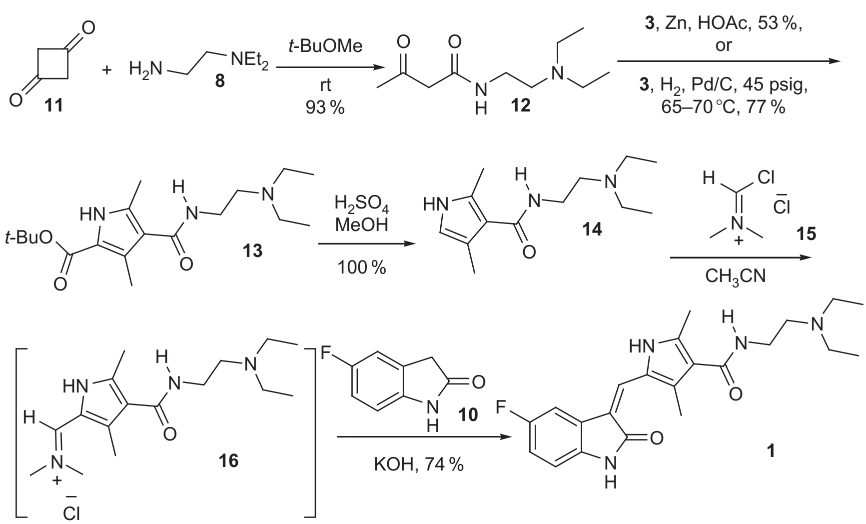

SCHEME 9.3 Synthesis of sunitinib free base **1** from Vilsmeier adduct **16** and **5**-fluorooxindole **10**.

chloride **15** in acetonitrile to form the Vilsmeier adduct **16** *in situ* [26]. Addition of 5-fluorooxindole (**10**) and KOH to the reaction mixture at this stage afforded the desired product **1.**

3. PHYSICAL PROPERTIES

3.1. Spectroscopy

3.1.1. Ultraviolet spectroscopy

The ultraviolet/visible (UV/VIS)-absorption spectrum of sunitinib was recorded, and the wavelength of the maximum absorption peak (λ_{max}) was noted. The absorption spectrum of sunitinib in ethanol was scanned from 200 to 600 nm, using a UV/VIS spectrometer (Varian Cary 50 spectrophotometer). As shown in Fig. 9.1, the λ_{max} of sunitinib is located at 430 nm.

3.1.2. Vibrational spectroscopy

3.1.2.1. Infrared absorption spectroscopy of sunitinib base The principal peaks in the IR spectrum (NaBr pellet sampling) of sunitinib base were reported at 3298, 3230, 2968, 1676, 1627, 1590, 1544, 1498, and 1334 cm^{-1} [18].

3.1.2.2. Infrared absorption spectroscopy of sunitinib malate The infrared absorption spectrum of sunitinib is shown in Fig. 9.2 and was obtained on a Shimadzu infrared spectrophotometer using a NaCl plate. The principal peaks were observed at 3350, 2943, 2831, 1650, and 1031 cm^{-1}.

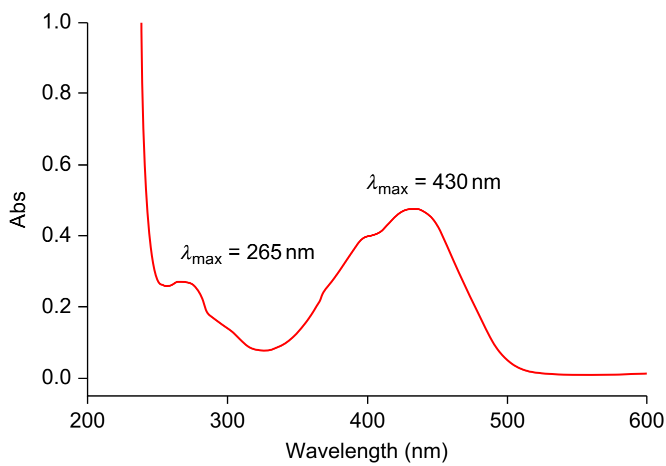

FIGURE 9.1 UV spectra of sunitinib malate (4.0 μM solution in ethanol).

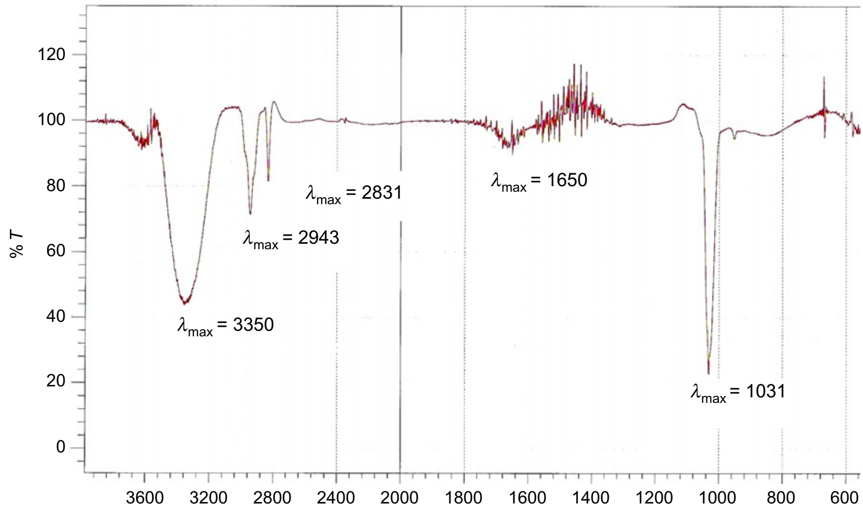

FIGURE 9.2 Infrared spectroscopy of sunitinib malate.

TABLE 9.1 Infrared spectroscopic data for sunitinib malate in NaCl plate

Entry	Bond	Absorption peaks (λ_{max} cm^{-1})	Appearance
1	C—F	1031	Strong
2	—NH—C═O	1650	Normal
3	C—H (alkyl)	2831	Strong
4	HC═CH (aryl)	2943	Strong
5	O—H (acid), N—H	3350	Broad

Assignments for the major absorption bands are provided in Table 9.1. Reported principal peaks were at 3298, 3230, 2968, 1676, 1627, 1590, 1544, 1498, 1334 cm^{-1} [18].

3.1.3. Nuclear magnetic resonance spectrometry

^{1}H and ^{13}C nuclear magnetic resonance (NMR) spectra of sunitinib were obtained with a Bruker 500 MHz NMR spectrometer. Chemical shifts were expressed in parts per million (ppm) (Table 9.2) with respect to the tetramethylsilane reference signal for ^{1}H and ^{13}C NMR (Figs. 9.3 and 9.4, respectively).

3.1.3.1. ^{1}H NMR spectrum ^{1}H NMR (500 MHz, DMSO-d_6): δ 13.73 (s, 1H, NH), 10.93 (s, 1H, NH), 10.80–10.70 (br, 1H, —OH, maleate), 7.77 (d, 1H, J=8.0 Hz), 7.73 (s, 1H, olefinic H), 7.72 (d, 1H, J=8.0 Hz), 6.93 (d, 1H, J=8.0

TABLE 9.2 Comparative study of ^{1}H NMR spectra for sunitinib malate with literature

Entry	Chemical shift[a] (sunitinib malate) (500 MHz, DMSO-d_6)	Chemical shift[b] (400 MHz, $CDCl_3$)	Chemical shift[c] (300 MHz, $CDCl_3$)
1	13.73 (s, 1H, NH)	–	13.31 (s, 1H, NH)
2	10.93 (s, 1H, NH)	–	8.90 (s, 1H, NH)
3	10.80–10.70 (br, 1H, —OH, malate)		–
4	7.77 (d, 1H, J=8.0 Hz)	7.75 (dd, J=9.4, 2.5 Hz, 1H),	7.14 (dd, 1H, J=8.8, 2.2 Hz)
5	7.73 (s, 1H, olefinic H)	7.71 (s, 1H)	7.22 (s, 1H, olefinic H)
6	7.72 (d, 1H, J=8.0 Hz)	7.43 (t, J=5.6 Hz, 1H)	6.85 (td, 1H, J=8.8 2.2 Hz)
7	6.93 (d, 1H, J=8.0 Hz)	6.92 (td, J=9.1, 2.5 Hz, 1H)	6.78 (dd, 1H, J=8.1, 4.4 Hz)
8	6.87 (d, 1H, J=8.0 Hz)	6.84 (dd, J=8.5, 4.6 Hz, 1H)	6.72 (t, 1H, J=4.4 Hz)
9	4.01 (s, 1H, malate)	–	–
10	3.48 (br, 2H)	3.41–3.36 (m, 2H)	3.54 (q, 2H, J=5.2 Hz)
11	2.96 (s, 6H)	2.65–2.58 (m, 6H)	2.71 (t, 2H, J=5.9 Hz), 2.64 (q, 4H, J=6.6 Hz)
12	2.56 (q, 1H, malate)		
13	2.34 (q, 1H, malate)		
14	2.51 (s, 3H)	2.47 (s, 3H)	2.55 (s, 3H)
15	2.44 (s, 3H)	2.43 (s, 3H)	2.31 (s, 3H)
14	1.14 (t, J=7.3 Hz, 6H)	1.07 (t, J=7.1 Hz, 6H)	1.05 (t, 6H, J=7.4 Hz)

[a] ^{1}H NMR was taken in DMSO-d_6.
[b] Reference [18].
[c] Reference [20].

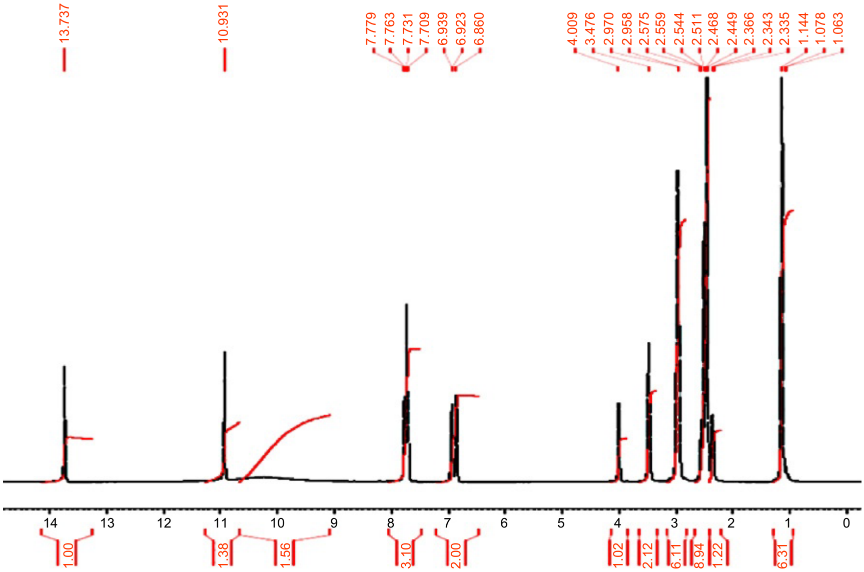

FIGURE 9.3 ^{1}H NMR spectra of sunitinib malate in DMSO-d_6.

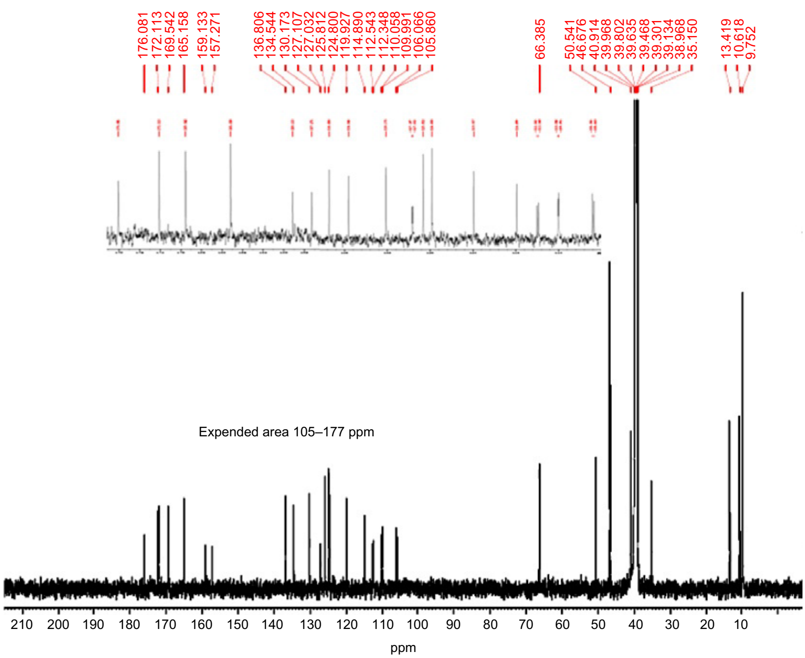

FIGURE 9.4 ^{13}C NMR spectra of sunitinib malate in DMSO-d_6.

Hz), 6.87 (d, 1H, J=8.0Hz), 4.01 (s, 1H, malate), 3.48 (br, 2H), 2.96 (s, 6H), 2.56 (q, 1H, malate), 2.34 (4, 1H, malate), 2.51 (br, 2H), 1.14 (s, 6H)ppm.

3.1.3.2. ^{13}C NMR spectrum Unreported ^{13}C NMR data of sunitinib malate are as follows: ^{13}C NMR (125MHz, DMSO-d_6): δ 176.08 (malate), 172.11 (malate), 169.54, 165.16, 159.13, 157.27, 136.80, 134.54, 130.17, 127.10, 127.03, 125.81, 124.80, 119.93, 114.89, 112.54, 112.35, 110.06, 109.99, 106.07, 105.86, 66.38 (malate), 50.54, 46.68, 40.91 (malate), 35.16, 13.42, 10.62, and 9.75ppm.

3.2. Mass spectrometry

The mass spectral analysis of sunitinib was carried out with an Agilent 6320 Ion Trap LC/MS system by infusion of 2μg of sunitinib solution in 1:1 acetonitrile/water without a column. Smart fragmentor and automatic optimization were performed to obtain the spectra and cause fragmentation. Source parameters were as follows: temperature was 350°C, gas flow was 12L/min, and the nebulizer was set at 60psi. Figure 9.5 shows the mass spectrum for the parent compound (m/z 398); Scheme 9.4 and Figs. 9.6–9.8 show the detailed mass fragmentation pattern interpretation of the drug substance. The reported m/z was 399.2204 (M+H$^+$), $C_{22}H_{27}FN_4O_2$+H (theoretical 399.2196) [27].

Sunitinib malate shows 398.7 (m/z) as a metastable ion peak (Fig. 9.5).

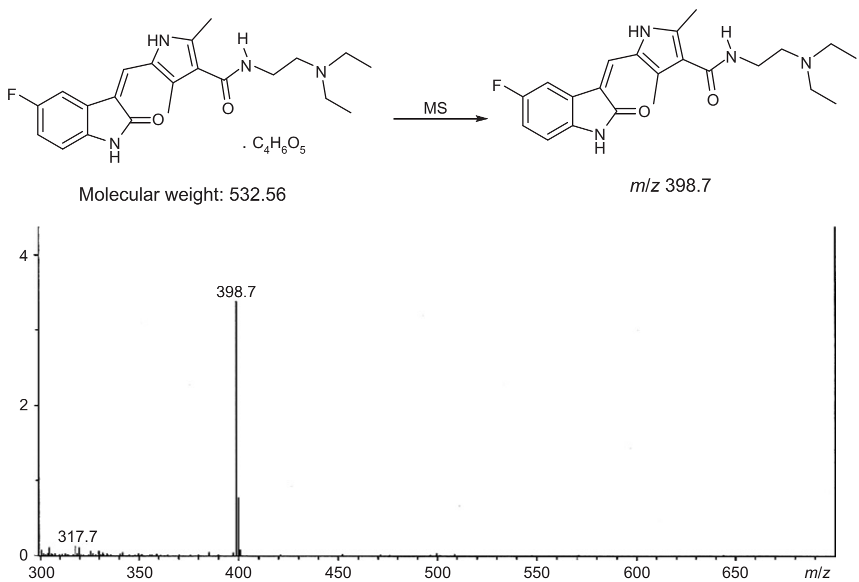

FIGURE 9.5 MS spectra for fragment sunitinib malate molecular weight 532.56 in positive mode gave m/z 398.47 [M-malate]$^+$.

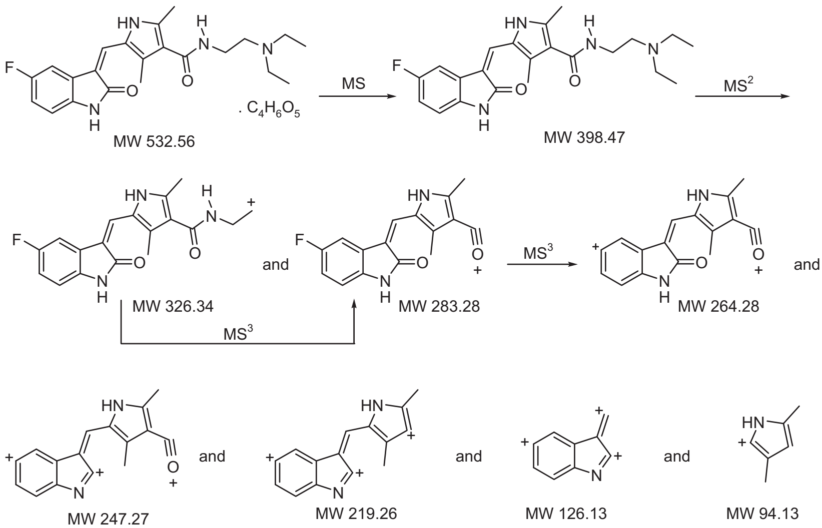

SCHEME 9.4 Fragmentation of sunitinib malate.

3.2.1. Fragmentation pattern of sunitinib

MS^2 scan of the metastable ion peak gives two fragments at 398.7 (m/z, by loss of diethylamine) and 282.7 (m/z, by loss of *N*,*N*-diethyethylene diamine), respectively (see Fig. 9.6).

MS^3 scan of the fragment at 398.7 (m/z) also gave 282.7 (m/z, by loss of ethylamine) (see Fig. 9.7).

MS^3 scan of the 284.7 (m/z) gave the number of fragments majoring 264.7 (m/z), 247.8 (m/z), 217.8 (m/z), 128.4 (m/z), and 94.6 (m/z), respectively (Fig. 9.8).

4. METHODS OF ANALYSIS

4.1. Chromatographic methods

4.1.1. High-performance liquid chromatography (ultraviolet detection)

There are a few high-performance liquid chromatography (ultraviolet detection) (HPLC/UV) methods published to determine sunitinib, either as a single component or simultaneously with its metabolite. In the method developed by Blanchet *et al*. [28], after a liquid–liquid extraction with ethyl acetate, sunitinib and ranitidine (the internal standard (IS)) are separated on cyanopropyl column using a simple binary mobile phase of ammonium acetate buffer (20 mM, pH 6.8):acetonitrile (55:45, v/v). Samples were eluted isocratically at a flow rate of 1 mL/min throughout the 10-min run. A dual wavelength mode was used, with ranitidine

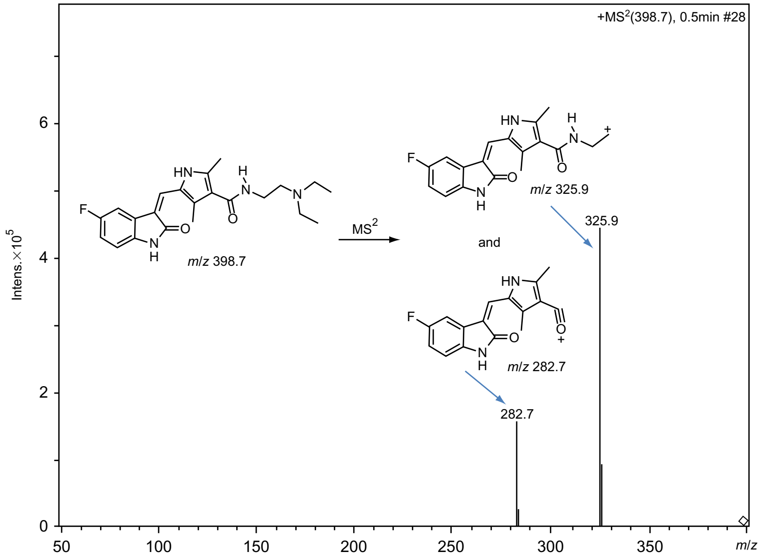

FIGURE 9.6 MS^2 spectra for fragment 398.7 (*m/z*) in positive mode gave 325.9 (*m/z*) and 282.7 (*m/z*).

monitored at 255nm and sunitinib at 431nm. The calibration was linear over the range of 20–200ng/mL. Inter- and intraday coefficients of variation were less than 7%. This method is sensitive, accurate, and selective. It has been successfully implemented to monitor trough sunitinib concentrations in plasma samples (n=39) from 14 unselected cancer patients treated with the recommended once-daily dose of 50mg or less. It has been concluded that this method can be used in routine clinical practice to monitor plasma sunitinib concentrations in cancer patients treated with once-daily administration.

Etienne-Grimaldi *et al*. [12] developed an original, simple, HPLC assay with UV detection, allowing the simultaneous measurement of sunitinib and SU12662 to be performed in plasma after a single organic extraction. This simple and robust analytical assay could be helpful in the setting of pharmacokinetically based dose adaptation for sunitinib. In addition, a stability study of sunitinib and SU12662 in different light exposure conditions was presented. HPLC analysis was performed on an ODS column, and UV detection was monitored at 369nm (run time: 15min). The IS was vandetanib. The mobile phase was composed of 60% ammonium formate 20mM (pH 3.25, adjusted with formic acid) and 40% acetonitrile. The flow rate was 0.8mL/min. This assay was selective and sensitive enough (limit of detection: ~1ng/mL) to quantify minimal concentrations at steady state (Css min) of sunitinib and SU12662 in treated patients.

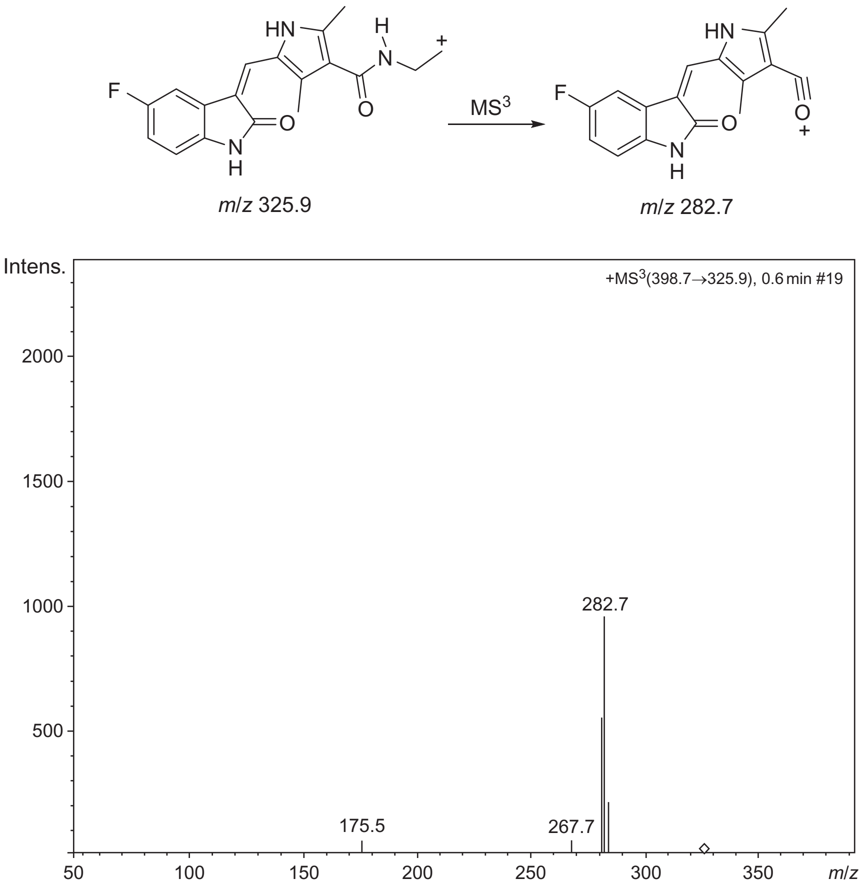

FIGURE 9.7 MS^3 spectra for fragment 398.7 (*m/z*) in positive mode gave 282.7 (*m/z*).

4.1.2. High-performance liquid chromatography/mass spectrometry

Several coupled high-performance liquid chromatography/mass spectrometry (LC-MS/MS) methods have been reported to determine sunitinib, either as a single drug or in combination with other tyrosine kinase inhibitors and/or its metabolite SU12662 in plasma [29–34].

Minkin *et al.* [29] developed and validated an assay using LC-MS/MS for the determination of sunitinib in human plasma. The assay's lower limit of quantitation (LLOQ) is 0.2ng/mL, with a simple sample preparation procedure and a rapid chromatographic run time of 3min. Sample preparation involved a liquid–liquid extraction by the addition of 0.2mL of plasma with 4.0mL *tert*-butyl-methyl ether extraction solution containing 25ng/mL of the IS clozapine. Separation of compounds was achieved on a C18 (50×2.1mm i.d., 3.5μm) analytical column using a mobile phase

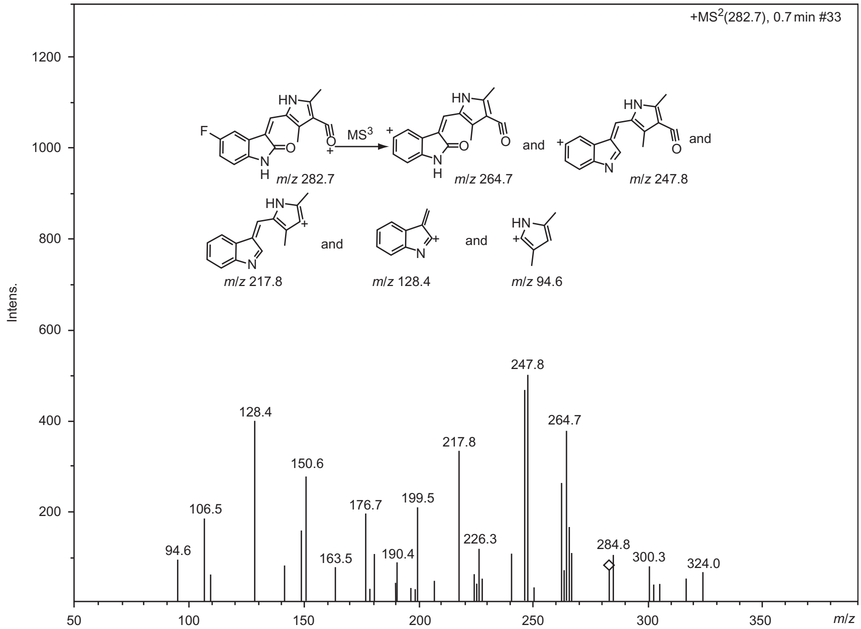

FIGURE 9.8 MS^3 spectra for fragment 282.7 *m/z* in positive mode.

consisting of acetonitrile/water (65:35, v/v) containing 0.1% formic acid and isocratic flow at 0.15 mL/min for 3 min. The analytes were monitored by tandem-mass spectrometry with electrospray positive ionization. The mass spectrum of sunitinib showed a protonated molecular ion [MH^+] at *m/z* 399.0. The major fragment observed was at *m/z* 283.0, which was selected for subsequent monitoring in the third quadrupole. The mass spectrum of the IS, clozapine, showed a [MH^+] at *m/z* 327.0, and the high collision energy gave a major product ion at *m/z* 270.0. Linear calibration curves in human plasma were generated over the range of 0.2–500 ng/mL with values for the coefficient of determination of exceeding 0.9950. Within- and between-day precision and accuracy were less than or equal to 10%. The method was applied to the quantitation of sunitinib in plasma samples from a patient receiving daily oral therapy with sunitinib.

A fast, sensitive, universal, and accurate LC-MS/MS method for the determination of four different tyrosine kinase inhibitors (TKIs) from biological materials was developed by Honeywell *et al.* [30]. Utilizing a simple protein precipitation with acetonitrile, a 20-μL sample volume of biological matrixes can be extracted at 4 °C with minimal effort. After centrifugation, the sample extract is introduced directly onto the LC-MS/MS system without further cleanup and assayed across a linear

range of 1–4000 ng/mL. Chromatography was performed using a Dionex Ultimate 3000 with a Phenomenex prodigy ODS3 (2.0×100 mm, 3 μm) column and eluted at 200 μL/min with a tertiary mobile phase consisting of 20 mM ammonium acetate/acetonitrile/methanol (2.5:6.7:8.3%). Injection volumes varied from 0.1 to 1 μL depending on the concentration of the drug observed. Samples were observed to be stable for a maximum of 48 h after extraction when kept at 4 °C. Detection was performed using a turbo-spray ionization source and mass spectrometric positive multiple reaction monitoring (+MRM) mode for gefitinib (447.1 and 127.9 m/z), erlotinib (393.9 and 278.2 m/z), sunitinib (399.1 and 283.1 m/z), and sorafenib (465.0 and 251.9 m/z) at an ion voltage of +3500 V. The accuracy, precision, and limit of quantification (LOQ) from cell culture medium were as follows: gefitinib: 100.2±3.8%, 11.2 nM; erlotinib: 101.6±3.7%, 12.7 nM; sunitinib: 100.8±4.3%, 12.6 nM; sorafenib: 93.9±3.0%, 10.8 nM, respectively. This was reproducible for plasma, whole blood, and serum. The method was observed to be linear between the LOQ and 4000 ng/mL for each analyte. Effectiveness of the method was illustrated with the analysis of samples from a cellular accumulation investigation and determination of steady-state concentrations in clinically treated patients.

Haouala *et al*. [31] developed a liquid chromatography-tandem-mass spectrometry method (LC-MS/MS), requiring 100 μL of plasma for the simultaneous determination of the six major inhibitors of TKI kinases imatinib, nilotinib, dasatinib, sunitinib, sorafenib, and lapatinib. Plasma is purified by protein precipitation, and the supernatant is diluted in ammonium formate 20 mM (pH 4.0). Reverse-phase chromatographic separation of TKIs is obtained using a gradient elution of 20 mM ammonium formate, pH 2.2 and acetonitrile containing 1% formic acid, followed by rinsing and re-equilibration to the initial solvent composition up to 20 min. Imatinib-d_8 was used as the IS.

Analyte quantification, using matrix-matched calibration samples, is performed by electrospray ionization (ESI)-triple quadrupole mass spectrometry by selected reaction monitoring detection using the positive mode. The method was validated according to FDA recommendations, including assessment of extraction yield, matrix effects variability (<9.6%), overall process efficiency (87.1–104.2%), as well as TKIs short- and long-term stability in plasma. The method is precise (interday CV%: 1.3–9.4%), accurate (−9.2 to +9.9%), and sensitive (lower limits of quantification comprised between 1 and 10 ng/mL). This is the first broad-range LC-MS/MS assay covering the major currently in-use TKIs. It is an improvement over previous methods in terms of convenience (a single extraction procedure for six major TKIs, reducing significantly the analytical time), sensitivity, selectivity, and throughput. It may contribute to filling the current knowledge gaps in the pharmacokinetics/pharmacodynamics

relationships of the latest TKIs developed after imatinib and better define their therapeutic ranges in different patient populations in order to evaluate whether a systematic TDM-guided dose adjustment of these anticancer drugs could contribute to minimize the risk of major adverse reactions and to increase the probability of efficient, long-lasting, therapeutic response.

A high-performance LC-MS/MS method was developed and validated by Haznedar [32] for measurement of sunitinib and SU12662 concentrations in rat plasma samples. The samples were prepared for analysis either by an ethyl acetate extraction (used in only a few initial studies) or after protein precipitation (in test tubes or 96-well plates). The assay used either propranolol or [2H10]-sunitinib as an IS. The concentration range of either 1–2000 or 0.1–200 ng/mL was validated using a Keystone BetaBasic-18 column (4.6×9×100 mm, 5 L) for LC-MS/MS analysis (Shimadzu Series 10 ADVP HPLC system and Perkin-Elmer Sciex API-3000 triple quadrupole mass spectrometer). The gradient mobile phases were 10 mM ammonium acetate in methanol/water (10:90) with 0.1% formic acid (A) and 10 mM ammonium acetate in methanol/water (90:10) with 0.1% formic acid (B). The flow rate was 0.8 mL/min, which was reduced to 0.3 mL/min before introduction into the mass spectrometer. The mass spectrometer was operated using ionization and scan modes of positive ion electrospray and MRM, respectively. Each analyte was detected by tandem MS by monitoring specific molecular ion fragment ion transitions: m/z 399.1 and 325.9 for sunitinib, 371.1 and 283.1 for SU12662, and 360.1 and 116.0 for propranolol. Calibration curves were constructed by plotting the analyte/IS peak area ratios against the analyte concentrations. A weighted linear regression ($1/C2$) was used to calculate the concentrations of sunitinib and SU12662 in the study and QC samples. This assay method demonstrated acceptable selectivity/specificity, linearity, and intra- and interassay precision and accuracy. The blank matrix also showed no significant interference or carryover on the LC-MS/MS system. The LLOQ was 0.1 ng/mL for both sunitinib and SU12662.

Alternatively, a Symmetry Shield C8 column (2.1 9 50 mm, 3.5 l) was used to perform the chromatographic separation. The mobile phase was 15 mM ammonium formate buffer solution (pH 3.25)/acetonitrile (75:25, v/v), with a flow rate of 0.35 mL/min. The mass spectrometer was operated using MRM (m/z for sunitinib and SU12662 were as described above; m/z 409.1, 325.9 for IS) and in a positive ion mode. The lower and upper limits of quantitation were 0.07 and 241 ng/mL for sunitinib and 0.07 and 220 ng/mL for SU12662. This method also showed acceptable assay specificity/selectivity, linearity, sensitivity, precision, accuracy, and stability. Radioactivity in rat and monkey blood, plasma, urine, and fecal samples was measured by liquid scintillation counting (Packard 1900 or 2100 TR Liquid Scintillation Counter). The counting efficiencies were calculated by the external standard method, using a series of quenched standards

(supplied by Packard), generating a calibration curve. The purpose of these extensive nonclinical studies was to assess pharmacokinetics and dispositional properties of sunitinib and its primary active metabolite (SU12662). Sunitinib was administered in single and repeat oral doses in mice, rats, and monkeys. Assessments were made using LC-MS/MS methods, radioactive assays, and quantitative whole body autoradiography. Sunitinib was readily absorbed with good oral bioavailability and linear kinetics at clinically-relevant doses. SU12662 plasma levels were less than those of sunitinib in mice and monkeys, but greater in rats. Sunitinib was extensively distributed with moderate-to-high systemic clearance and eliminated primarily into feces. Single- and repeat-dosing kinetics were similar. A prolonged half-life allowed once-daily dosing, enabling adequate systemic exposure with limited-to-moderate accumulation. In multiple-dose studies with cyclic dosing, drug plasma concentrations cleared from one cycle to the next. Sunitinib exhibited advantageous pharmacokinetic and dispositional properties in nonclinical species, translating into favorable properties in humans.

A LC-MS/MS-based method combined with protein precipitation, liquid–liquid extraction, and solid-phase extraction techniques was developed by Zhou *et al*. [33] for the determination of sunitinib in mouse plasma, brain tumor, and normal brain tissue, respectively. The instrument was operated under the MRM mode using ESI in the positive ion mode. Separation was achieved on a 50×2.0mm Luna 3μm C8 column (Phenomenex Inc., Torrance, CA, USA) with a pre-column of the same material. The sample solutions (10μL) were injected, and the analytes were eluted using acetonitrile/1mM ammonium acetate containing 0.1% acetic acid (28:72, v/v) at a flow rate fixed at 0.3mL/min. The isocratic separation run was completed within 3.2min at 30°C. Camptothecin was used as the IS. A good linear relationship with correlation coefficients greater than 0.99 was achieved over concentration ranges of 1.37–1000ng/mL for plasma and 4.12–1000ng/g for the normal brain and brain tumor. The LOQs for sunitinib in mouse plasma, brain tumor, and normal brain tissue are 1.37ng/mL, 4.12ng/g, and 4.12ng/g, respectively. The reproducibility of the LC-MS/MS method is reliable, with the intra- and interday precision being less than 15% and accuracy within ±15%. The established method was successfully applied to the characterization of sunitinib disposition in the brain and brain tumor as well as its systemic pharmacokinetics in a murine orthotopic glioma model.

In a thesis having the title ''Pharmacokinetic/Pharmacodynamic Modeling and Simulation of Biomarker Response to Venlafaxine and Sunitinib Administration'' [33], Sunitinib and SU12662 concentrations in human plasma were determined by HPLC coupled with mass spectrometry (LC-MS/MS, Applied Biosystems/MDS Sciex API5000 LC-MS/MS). This work was performed by Dr. Martina Kinzig at the Institute for Biomedical

and Pharmaceutical Research (IMBP) under the supervision of Prof. Dr. Fritz Sörgel. The method used d_5-sunitinib as an IS which was synthesized by Elsinghorst [21]. The response from calibration standards of sunitinib and SU12662 was linear from 0.06 to 100ng/mL. The LLOQ for plasma samples was 0.06ng/mL for both analytes. Coefficients of variation (CV) expressing precision and relative errors (RE) expressing analytical accuracy ranged from 1.0% to 5.3% and +0.9% to +5.6% for sunitinib and from 2.9% to 3.9% and −2.2% to +3.9% for SU12662, respectively.

4.1.3. Ultra-performance liquid chromatography/mass spectrometry

Simultaneous determination of nine TKIs in plasma samples by 96-well solid-phase extraction and ultra-performance LC-MS/MS published by Bouchet *et al*. [35]. The described chromatography was performed on a Waters Acquity-UPLC® system with BEH C18-50×2.1mm column, under a gradient of ammonium formate–acetonitrile. An Acquity–TQD® system with ESI was used for detection. Samples were prepared by solid-phase extraction (Oasis® MCX μElution), and eluate was injected in the system. Calibration curves ranged from 10 to 5000ng/mL for imatinib, its metabolite, nilotinib, lapatinib, erlotinib and sorafenib, and from 0.1 to 200ng/mL for dasatinib, axitinib, gefitinib, and sunitinib. Peaks of each compound (retention time from 0.76 to 2.51min) were adequately separated. The mean relative extraction recovery was in the range of 90.3–106.5% thanks to the use of stable isotopes (imatinib-d_8, nilotinib-M+4, dasatinib-M+6, and sorafenib-M+4) as ISs. There was no significant ion suppression observed at the respective TKI retention times. This rapid, sensitive, and specific UPLC-MS/MS method is able to perform simultaneous quantification of nine TKIs in human plasma and usable for routine TDM.

4.2. Immunoassay methods

Establishment of a homogeneous time-resolved fluorescence immunoassay method for high-throughput screening of protein TKIs was reported by Li and coworkers [36]. Specific fluorescence signals at 670 and 612nm were measured by multifunctional microplate reader when the fluorescence was emitted through a resonance energy transfer between fluorescent materials (XL-665 and Eu^{3+}). The inhibitory activity of sunitinib, a standard PTK inhibitor, on vascular endothelia growth factor receptor 2 (VEGFR-2) kinase activity was investigated. A homogeneous time-resolved fluorescence immunoassay was established for high-throughput screening of PTK inhibitor. In this system, the concentrations of VEGFR-2, adenosine triphosphate (ATP), and polypeptide substrate were 5ng/μL, 100μm/L, and 50μm/L, respectively. Sunitinib inhibited VEGFR-2 kinase activity with an IC_{50} value of 86.7nmol/L, which was close to the values

tested using the other method. The homogeneous time-resolved fluorescence immunoassay can be easily used for high-throughput screening of PTK inhibitors.

4.3. Spectrofluorimetry

Arıcı *et al.* [37] described a validated spectrofluorimetric method for the determination of sunitinib malate, using a dye complexation approach. The method was developed for the indirect determination of sunitinib malate in bulk substance and in pharmaceutical preparations. The complex formed in this reaction system was regarded as the ion-association complex between the drug cation and Eosin Y. This method has the advantages of simplicity, sensitivity, and reproducibility and is useful and convenient for quality control and routine determination of drugs in pharmaceutical dosage forms where precision, time, and cost effectiveness of analytical methods are important. The dye complexation spectrofluorimetric quantification of sunitinib malate was performed by monitoring the emission of the free dye at 800 nm, following its excitation at 350 nm. The described method was fully validated as to the analytical parameters of accuracy, linearity, specificity, limit of detection, limit of quantification, precision, reproducibility, and robustness. The described method displayed linearity over the concentration range of 0.08–5.00 μg/mL. The limit of detection was found to be 0.041 μg/mL (7.69×10^{-8}M), and the limit of quantitation was 0.850 μg/mL (1.59×10^{-6}M). Defined parameters of the method (such as medium pH, dissolved oxygen concentration, temperature, dye concentration., incubation time, etc.) were varied systematically to check robustness. Reproducibility was tested by applying the proposed method to the assay of sunitinib malate using the same operational conditions, namely in two different laboratories at different elapsed time and using different instruments. Results obtained from lab-to-lab variations were found to be reproducible, as RSD values did not exceed 2%.

5. PHARMACOLOGY

Sunitinib malate (Sutent®, SU11248) is an oral, multitargeted TKI that specifically inhibits vascular endothelial growth factor receptors 1, 2 and 3 (VEGFR1, -2 and -3, respectively), platelet-derived growth factor receptor alpha and beta (PDGFR-α and -β), FLT3 colony-stimulating factor receptor type 1 (CSF-1R) and the receptor encoded by the ret proto-oncogene (RET) [38,39]. Sunitinib is approved for first line treatment of metastatic renal cell carcinoma (mRCC) and imatinib-resistant metastatic GIST [5,40,41]. Sunitinib is metabolized by cytochrome P450 (CYP) 3A4 to in active metabolites [42].

Clinical pharmacokinetics of sunitinib show a high inter-patient variability (approximately 40%), which is largely unexplained [5]. This could result in supra- or sub-therapeutic sunitinib levels leading to toxicity or inefficacy, respectively. Since sunitinib is predominantly metabolized by CYP3A4, variability in the activity of this enzyme may explain a considerable proportion of the observed inter-patient variability in sunitinib pharmacokinetics.

It is thought that sunitinib is neither an inhibitor nor an inducer of CYP-enzymes and therefore the drug is considered not prone to drug-drug and drug-food interactions, while other TKIs (e.g. imatinib, erlotinib, gefitinib) appear to be substrates and/or inhibitors of several CYP-enzymes *in vivo* and *in vitro* [1,33,43–47]. For sunitinib, *in vivo* confirmatory studies to define an effect of sunitinib on CYP-enzymes are lacking. Moreover, recently it was shown in an *in vitro* study that sunitinib is a substrate for and an inhibitor of the transporter proteins ATP-binding cassette (ABC) ABCG2 and to some extent ABCB1, which may also lead to drug–drug interactions [48].

Mechanism of Action. Sunitinib malate is a small molecule that inhibits multiple receptor tyrosine kinases (RTKs), some of which are implicated in tumor growth, pathologic angiogenesis, and metastatic progression of cancer. Sunitinib was evaluated for its inhibitory activity against a variety of kinases (>80 kinases) and was identified as an inhibitor of platelet-derived growth factor receptors (PDGFRα and PDGFRβ), vascular endothelial growth factor receptors (VEGFR1, -2, and -3), stem cell factor receptor (KIT), Fms-related tyrosine-3 receptor (FLT3), CSF-1R, and the glial cell line-derived neurotrophic factor receptor [48]. Sunitinib inhibition of the activity of these RTKs has been demonstrated in biochemical and cellular assays, and inhibition of function has been demonstrated in cell proliferation assays. The primary metabolite exhibits similar potency compared to sunitinib in biochemical and cellular assays.

Sunitinib inhibited the phosphorylation of multiple RTKs (PDGFRβ, VEGFR2, KIT) in tumor xenografts expressing RTK targets *in vivo* and demonstrated inhibition of tumor growth or tumor regression and/or inhibited metastases in some experimental models of cancer. Sunitinib demonstrated the ability to inhibit growth of tumor cells expressing dysregulated target RTKs (PDGFR, RET, or KIT) *in vitro* and to inhibit PDGFRβ- and VEGFR2-dependent tumor angiogenesis *in vivo* [49].

5.1. Pharmacokinetics

Pharmacokinetic investigations in both healthy volunteers and cancer patients have shown that following a single oral dose, peak plasma sunitinib concentrations occur between 6 and 12h post dose [49]. In addition, sunitinib and SU12662 have previously been shown to display

linear pharmacokinetics and have prolonged half-lives of approximately 40 and 80h, respectively [50,51]. Sunitinib is well absorbed [51], its bioavailability is not affected by food intake [49,50,52], and no significant changes in pharmacokinetics are observed with repeat versus single dosing [49].

No differences in pharmacokinetics have been observed between healthy volunteers and cancer patients in individual studies [49,53]. However, when analyzed across multiple studies, factors such as patient status, age, gender, race, body weight, and clinical performance status may affect the pharmacokinetics of sunitinib in individuals, resulting in increased or decreased exposure to sunitinib, SU12662, or total drug.

5.1.1. Absorption

The maximum plasma concentration of sunitinib is achieved within 6–12 h, and the absolute bioavailability is unknown. The drug may be taken with or without food, since food only has a marginal effect on the exposure [52]. The inter-patient variability is large [5]. A recent case report describes a significant decrease in sunitinib exposure area-under-the-curve (AUC) in an obese patient, which might indicate that body mass index has a pronounced effect on drug exposure and might thereby explain partly the large inter-patient variability [54].

5.1.2. Distribution

The apparent volume of distribution (Vd/F) for sunitinib was 2230L. In the dosing range of 25–100mg, the area under the plasma concentration–time curve and $C_{\max}$ increases proportionately with dose. The terminal half-lives of sunitinib and its primary active metabolite are approximately 40–60 and 80–110h, respectively [5]. Binding of sunitinib and its primary active metabolite to human plasma protein *in vitro* was 95% and 90%, respectively, with no concentration dependence in the range of 100–4000 ng/mL. With repeated daily administration, sunitinib accumulates 3- to 4-fold, while the primary metabolite accumulates 7- to 10-fold. Steady-state concentrations of sunitinib and its primary active metabolite are achieved within 10–14 days.

5.1.3. Metabolism and excretion

Sunitinib is primarily metabolized by CYP3A4 to produce its primary active metabolite, SU12662, which is further metabolized by CYP3A4 into inactive metabolites [52]. The primary active metabolite comprises 23–37% of the total exposure. Data on additional enzymes involved in the metabolism are still unknown.

Sunitinib is primarily eliminated with the feces (61%), with renal elimination accounting for only 16% of the administered dose. However, there are no studies on the pharmacokinetics in patients with serious

hepatic or renal insufficiency [42]. Additionally in a case report describing two hemodialyzed patients on sunitinib therapy, the plasma concentration of the drug and its major metabolite at steady-state were comparable to patients with normal renal function [55].

ACKNOWLEDGEMENT

This work was supported by the College of Pharmacy Research Center, King Saud University.

REFERENCES

[1] M. Atkins, C.A. Jones, P. Kirkpatrick, Sunitinib malate, Nat. Rev. Drug Discov. 5 (2006) 279–280.
[2] S. Faivre, G. Demetri, W. Sargent, E. Raymond, Molecular basis for sunitinib efficacy and future clinical development, Nat. Rev. Drug Discov. 6 (2007) 734–745.
[3] FDA Labeling information (www.fda.gov), 2009.
[4] B.I. Rini, Sunitinib, Expert Opin. Pharmacother. 8 (2007) 2359–2369.
[5] V.L. Goodman, E.P. Rock, R. Dagher, R.P. Ramchandani, S. Abraham, J.V. Gobburu, B. P. Booth, S.L. Verbois, D.E. Morse, C.Y. Liang, N. Chidambaram, J.X. Jiang, S. Tang, K. Mahjoob, R. Justice, R. Pazdur, Approval summary: sunitinib for the treatment of imatinib refractory or intolerant gastrointestinal stromal tumors and advanced renal cell carcinoma, Clin. Cancer Res. 13 (2007) 1367–1373.
[6] L. Sherman, G. Peng, S. Patyna, Open-label, single-dose, phase I study evaluating the mass balance and pharmacokinetics (PKs) of sunitinib (SU) in healthy male subjects, in: 14th European Cancer Conference, 2007.
[7] S. Sweetman, Sunitinib, Martindale: The Complete Drug Reference, Pharmaceutical Press, London, 2007.
[8] The Merck Index—An Encyclopedia of Chemicals, Drugs, and Biologicals, Merck & Co., Inc., Whitehouse Station, NJ, 2006.
[9] http://www.drugbank.ca/drugs/DB01268 (for sunitinib), http://en.wikipedia.org/wiki/Malic_acid (for malate).
[10] P. Tang, T. Miller, X. Miller, L. Sun, C. Wei, S. Shirazian, C. Liang, T. Vojkovsky, A. Nematalla, M. Hawley, Chem. Abstr. 135 (2001) 195497 Patent WO/192001/060814.
[11] M. Moon, W. Morozowich, P. Gao, P.C. Tang, Chem. Abstr 136 (2001) 697 Patent WO/2001/090068.
[12] M.C. Etienne-Grimaldi, N. Renee, H. Izzedine, G. Milano, A routine feasible HPLC analysis for the anti-angiogenic tyrosine kinase inhibitor, sunitinib, and its main metabolite, SU12662, in plasma, J. Chromatogr. B Anal. Technol. Biomed. Life Sci. 877 (2009) 3757–3761.
[13] M. Remko, A. Boháč, L. Kováčiková, Molecular structure, pKa, lipophilicity, solubility, absorption, polar surface area, and blood brain barrier penetration of some antiangiogenic agents, Struct. Chem. 22 (2011) 635–648.
[14] <http://www.acdlabs.com/products/phys_chem_lab/>, 2010 (accessed April 2010).
[15] D.S. Wishart, C. Knox, A.C. Guo, S. Shrivastava, M. Hassanali, P. Stothard, Z. Chang, J. Woolsey, DrugBank: a comprehensive resource for in silico drug discovery and exploration, Nucleic Acids Res. 34 (2006) D668–D672.

[16] T.J. Abrams, L.B. Lee, L.J. Murray, N.K. Pryer, J.M. Cherrington, SU11248 inhibits KIT and platelet-derived growth factor receptor beta in preclinical models of human small cell lung cancer, Mol. Cancer Ther. 2 (2003) 471–478.
[17] L.Q. Chow, S.G. Eckhardt, Sunitinib: from rational design to clinical efficacy, J. Clin. Oncol. 25 (2007) 884–896.
[18] J.M. Manley, M.J. Kalman, B.G. Conway, C.C. Ball, J.L. Havens, R. Vaidyanathan, Early amidation approach to 3-[(4-amido)pyrrol-2-yl]-2-indolinones, J. Org. Chem. 68 (2003) 6447–6450.
[19] M. Pettersson, Sunitinib (Sutent): an angiogenesis inhibitor, in: Jie Jack Li, Douglas S. Johnson (Eds.), Modern Drug Synthesis, John Wiley & Sons Inc., Malden, USA, 2010, pp. 87–98.
[20] J.Q. Wang, K.D. Miller, G.W. Sledge, Q.H. Zheng, Synthesis of [18F]SU11248, a new potential PET tracer for imaging cancer tyrosine kinase, Bioorg. Med. Chem. Lett. 15 (2005) 4380–4384.
[21] P.W. Elsinghorst, M. Gutschow, Synthesis of H-2- and C-13-labelled sunitinib and its primary metabolite, J. Labelled Comp. Rad. 52 (2009) 360–365.
[22] L. Sun, C. Liang, S. Shirazian, Y. Zhou, T. Miller, J. Cui, J.Y. Fukuda, J.Y. Chu, A. Nematalla, X. Wang, H. Chen, A. Sistla, T.C. Luu, F. Tang, J. Wei, C. Tang, Discovery of 5-[5-fluoro-2-oxo-1,2-dihydroindol-(3Z)-ylidenemethyl]-2,4-dimethyl-1H-pyrrole-3-carboxylic acid (2-diethylaminoethyl)amide, a novel tyrosine kinase inhibitor targeting vascular endothelial and platelet-derived growth factor receptor tyrosine kinase, J. Med. Chem. 46 (2003) 1116–1119.
[23] A. Treibs, K. Hintermeier, Chem. Ber. 86 (1954) 1167.
[24] H. Fisher, Organic Synthesis, 2 Wiley, New York, 1943 p. 202.
[25] L.G. Beholz, P. Benovsky, D.L. Ward, N.S. Barta, J.R. Stille, Formation of Dihydropyridone- and Pyridone-Based Peptide Analogs through Aza-Annulation of β-Enamino Ester and Amide Substrates with α-Amido Acrylate Derivatives, J. Org. Chem. 62 (4) (1997) 1033–1042.
[26] K. Hafner, C. Bernhard, Angew. Chem. 69 (1957) 533.
[27] J.M. Manley, M.J. Kalman, B.G. Conway, C.C. Ball, J.L. Havens, R. Vaidyanathan, Early amidation approach to 3-[(4-amido)pyrrol-2-yl]-2-indolinones, J. Org. Chem. 68 (2003) 6447–6450.
[28] B. Blanchet, C. Saboureau, A.S. Benichou, B. Billemont, F. Taieb, S. Ropert, A. Dauphin, F. Goldwasser, M. Tod, Development and validation of an HPLC-UV-visible method for sunitinib quantification in human plasma, Clin. Chim. Acta 404 (2009) 134–139.
[29] P. Minkin, M. Zhao, Z. Chen, J. Ouwerkerk, H. Gelderblom, S.D. Baker, Quantification of sunitinib in human plasma by high-performance liquid chromatography-tandem mass spectrometry, J. Chromatogr. B Anal. Technol. Biomed. Life Sci. 874 (2008) 84–88.
[30] R. Honeywell, K. Yarzadah, E. Giovannetti, N. Losekoot, E.F. Smit, M. Walraven, J.S. Lind, C. Tibaldi, H.M. Verheul, G.J. Peters, Simple and selective method for the determination of various tyrosine kinase inhibitors used in the clinical setting by liquid chromatography tandem mass spectrometry, J. Chromatogr. B Anal. Technol. Biomed. Life Sci. 878 (2010) 1059–1068.
[31] A. Haouala, B. Zanolari, B. Rochat, M. Montemurro, K. Zaman, M.A. Duchosal, H.B. Ris, S. Leyvraz, N. Widmer, L.A. Decosterd, Therapeutic Drug Monitoring of the new targeted anticancer agents imatinib, nilotinib, dasatinib, sunitinib, sorafenib and lapatinib by LC tandem mass spectrometry, J. Chromatogr. B Anal. Technol. Biomed. Life Sci. 877 (2009) 1982–1996.
[32] J.O. Haznedar, S. Patyna, C.L. Bello, G.W. Peng, W. Speed, X. Yu, Q. Zhang, J. Sukbuntherng, D.J. Sweeny, L. Antonian, E.Y. Wu, Single- and multiple-dose disposition kinetics of sunitinib malate, a multitargeted receptor tyrosine kinase inhibitor: comparative plasma kinetics in non-clinical species, Cancer Chemother. Pharmacol. 64 (2009) 691–706.

[33] Q. Zhou, J.M. Gallo, Quantification of sunitinib in mouse plasma, brain tumor and normal brain using liquid chromatography-electrospray ionization-tandem mass spectrometry and pharmacokinetic application, J. Pharm. Biomed. Anal. 51 (2010) 958.
[34] A. Lindauer, Pharmacokinetic/Pharmacodynamic Modeling and Simulation of Biomarker Response to Venlafaxine and Sunitinib Administration, (2010).
[35] S. Bouchet, E. Chauzit, D. Ducint, N. Castaing, M. Canal-Raffin, Hesham M. Korashy, N. Moore, K. Titier, M. Molimard, Simultaneous determination of nine tyrosine kinase inhibitors by 96-well solid-phase extraction and ultra performance LC/MS-MS, Clin. Chim. Acta 412 (2011) 1060–1067.
[36] X.G. Li, G.F. Wang, J.Y. Zhang, S.Y. Wu, W. Xu, S.G. Wu, J.J. Zhang, Establishment of homogeneous time-resolved fluorescence immunoassay for high throughput screening of protein tyrosine kinase inhibitors, Nan Fang Yi Ke Da Xue Xue Bao 29 (2009) 1612–1614.
[37] M. Arıcı, M. Kılınç, Validated spectrofluorimetric method for the determination of sunitinib malate, dye complexation approach for a novel anticancer drug, Acta Pharm. Sci. 52 (2010) 469–485.
[38] D.B. Mendel, A.D. Laird, X. Xin, S.G. Louie, J.G. Christensen, G. Li, R.E. Schreck, T.J. Abrams, T.J. Ngai, L.B. Lee, L.J. Murray, J. Carver, E. Chan, K.G. Moss, J.O. Haznedar, J. Sukbuntherng, R.A. Blake, L. Sun, C. Tang, T. Miller, S. Shirazian, G. McMahon, J.M. Cherrington, In vivo antitumor activity of SU11248, a novel tyrosine kinase inhibitor targeting vascular endothelial growth factor and platelet-derived growth factor receptors: determination of a pharmacokinetic/pharmacodynamic relationship, Clin. Cancer Res. 9 (2003) 327–337.
[39] R.J. Motzer, B.I. Rini, R.M. Bukowski, B.D. Curti, D.J. George, G.R. Hudes, B.G. Redman, K.A. Margolin, J.R. Merchan, G. Wilding, M.S. Ginsberg, J. Bacik, S.T. Kim, C.M. Baum, M.D. Michaelson, Sunitinib in patients with metastatic renal cell carcinoma, JAMA 295 (2006) 2516–2524.
[40] R.J. Motzer, T.E. Hutson, P. Tomczak, M.D. Michaelson, R.M. Bukowski, O. Rixe, S. Oudard, S. Negrier, C. Szczylik, S.T. Kim, I. Chen, P.W. Bycott, C.M. Baum, R.A. Figlin, Sunitinib versus interferon alfa in metastatic renal-cell carcinoma, N. Engl. J. Med. 356 (2007) 115–124.
[41] G.D. Demetri, A.T. van Oosterom, C.R. Garrett, M.E. Blackstein, M.H. Shah, J. Verweij, G. McArthur, I.R. Judson, M.C. Heinrich, J.A. Morgan, J. Desai, C.D. Fletcher, S. George, C.L. Bello, X. Huang, C.M. Baum, P.G. Casali, Efficacy and safety of sunitinib in patients with advanced gastrointestinal stromal tumour after failure of imatinib: a randomised controlled trial, Lancet 368 (2006) 1329–1338.
[42] V.R. Adams, M. Leggas, Sunitinib malate for the treatment of metastatic renal cell carcinoma and gastrointestinal stromal tumors, Clin. Ther. 29 (2007) 1338–1353.
[43] S.G. O'Brien, P. Meinhardt, E. Bond, J. Beck, B. Peng, C. Dutreix, G. Mehring, S. Milosavljev, C. Huber, R. Capdeville, T. Fischer, Effects of imatinib mesylate (STI571, Glivec) on the pharmacokinetics of simvastatin, a cytochrome p450 3A4 substrate, in patients with chronic myeloid leukaemia, Br. J. Cancer 89 (2003) 1855–1859.
[44] C. Tanaka, T. Smith, H. Kantarjian, Clinical pharmacokinetics (PK) of AMN107, a novel inhibitor of Bcr-Abl, in healthy subjects and patients with imatinib resistant or intolerant chronic myelogenous leukemia (CML) or relapsed/refractory Ph+ acute lymphocytic leukemia (Ph+ALL), J. Clin. Oncol. 24 (2006) 3095.
[45] J. Li, M. Zhao, P. He, M. Hidalgo, S.D. Baker, Differential metabolism of gefitinib and erlotinib by human cytochrome P450 enzymes, Clin. Cancer Res. 13 (2007) 3731–3737.
[46] H.C. Swaisland, M. Ranson, R.P. Smith, J. Leadbetter, A. Laight, D. McKillop, M.J. Wild, Pharmacokinetic drug interactions of gefitinib with rifampicin, itraconazole and metoprolol, Clin. Pharmacokinet. 44 (2005) 1067–1081.
[47] M. Hazarika, X. Jiang, Q. Liu, S.L. Lee, R. Ramchandani, C. Garnett, M.S. Orr, R. Sridhara, B. Booth, J.K. Leighton, W. Timmer, R. Harapanhalli, R. Dagher,

R. Justice, R. Pazdur, Tasigna for chronic and accelerated phase Philadelphia chromosome–positive chronic myelogenous leukemia resistant to or intolerant of imatinib, Clin. Cancer Res. 14 (2008) 5325–5331.
[48] S. Shukla, R.W. Robey, S.E. Bates, S.V. Ambudkar, Sunitinib (Sutent, SU11248), a small-molecule receptor tyrosine kinase inhibitor, blocks function of the ATP-binding cassette (ABC) transporters P-glycoprotein (ABCB1) and ABCG2, Drug Metab. Dispos. 37 (2009) 359–365.
[49] SUTENT (Sunitinib Malate) Prescribing Information, Pfizer, Inc., New York (NY), 2009.
[50] S.T. Mahmood, S. Agresta, C. Vigil, X. Zhao, G. Han, G. D'Amato, C.E. Calitri, M. Dean, C. Garrett, M.J. Schell, S. Antonia, A. Chiappori, Phase II study of sunitinib malate, a multi-targeted tyrosine kinase inhibitor in patients with relapsed or refractory soft tissue sarcomas. Focus on 3 prevalent histologies: leiomyosarcoma, liposarcoma, and malignant fibrous histiocytoma, Int. J. Cancer (2010).
[51] K.M. Sakamoto, Su-11248 Sugen, Curr. Opin. Investig. Drugs 5 (2004) 1329–1339.
[52] C.L. Bello, L. Sherman, J. Zhou, L. Verkh, J. Smeraglia, J. Mount, K.J. Klamerus, Effect of food on the pharmacokinetics of sunitinib malate (SU11248), a multi-targeted receptor tyrosine kinase inhibitor: results from a phase I study in healthy subjects, Anticancer Drugs 17 (2006) 353–358.
[53] C.L. Bello, M. Garrett, L. Sherman, J. Smeraglia, B. Ryan, M. Toh, Pharmacokinetics of sunitinib malate in subjects with hepatic impairment, Cancer Chemother. Pharmacol. 66 (2010) 699–707.
[54] I.M. Desar, D.M. Burger, Q.G. Van Hoesel, J.H. Beijnen, C.M. Van Herpen, W.T. Van der Graaf, Pharmacokinetics of sunitinib in an obese patient with a GIST, Ann. Oncol. 20 (2009) 599–600.
[55] H. Izzedine, M.C. Etienne-Grimaldi, N. Renee, S. Vignot, G. Milano, Pharmacokinetics of sunitinib in hemodialysis, Ann. Oncol. 20 (2009) 190–192.

CHAPTER 10

Varenicline

Mohammed Gabr Kassem and
Abdullah M. Al Hossaini

Contents

Department of Pharmaceutical Chemistry, College of Pharmacy, King Saud University, Riyadh, Kingdom of Saudi Arabia

Profiles of Drug Substances, Excipients, and Related Methodology, Volume 37
ISSN 1871-5125, DOI: 10.1016/B978-0-12-397220-0.00010-6
© 2012 Elsevier Inc.
All rights reserved.

1. DESCRIPTION

1.1. Nomenclature

1.1.1. Systematical chemical names

7,8,9,10-Tetrahydro-6,10-methano-6*H*-pyrazino(2,3-*h*)(3) benzazepine [1]
5,8,14-Triazatetracyclo[10.3.1.0^{2,11}.0^{4,9}]hexadeca-2(11)-3,5,7,9-pentaene [1]
7,8,9,10-Tetrahydro-6*H*-6,10-methanoazepino[4,5-*g*]quinoxaline [2]

1.1.2. Nonproprietary names

Varenicline, varenicline tartrate

1.1.3. Proprietary names

Chantix®, Champix®

1.2. Formulae

1.2.1. Empirical formula, molecular weight, and CAS number

Varenicline	$C_{13}H_{13}N_3$	211.26	[249296-44-4]
Varenicline tartrate	$C_{13}H_{13}N_3 \cdot C_4H_6O_6$	361.35	[375815-87-5]

1.2.2. Structural formula

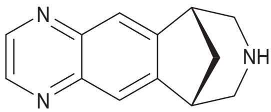

Varenicline

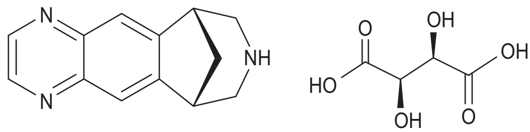

Varenicline tartrate

1.3. Elemental analysis

Base: C 73.91%, H 6.20%, N 19.89% [1]

Tartrate salt: C 56.51%, H 5.30%, N 11.63%, O 26.57%

1.4. Physical properties

1.4.1. Appearance

A cream-colored solid [3].

1.4.2. Solubility

Varenicline tartrate is highly soluble in water [4] and is moderately soluble in dimethylacetamide, acetonitrile, methanol, hexane, and ethyl acetate [5].

1.5. Uses and applications

Varenicline works as a selective nicotinic acetylcholine receptor partial agonist that binds to the $\alpha_4\beta_2$ receptor subtype [6]. Varenicline was approved by the U.S. Food and Drug Administration as an aid for smoking cessation treatment [4,7].

2. METHODS OF PREPARATION

Varenicline was discovered through the synthesis of a series of compounds inspired by the natural product (−)-cytisine [8,9], which was previously known to have partial agonist activity at the $\alpha_4\beta_2$ nicotinic acetylcholine receptors ($\alpha_4\beta_2$ nAChRs) [10–12].

The synthesis of varenicline can be summarized in a total of six steps. The first step begins with the conversion of 2,3-dimethylpyrazine **2** to its analog 2,3-bis(dibromomethyl) pyrazine **3** [13], followed by a sodium iodide mediated Diels–Alder reaction [13,14] between 2,3-bis (dibromomethyl)pyrazine **3** and norbornadiene **4**. The newly obtained olefin **5** was

then converted [15] to its corresponding diol **6** with osmium tetroxide (OsO_4) in the presence of *N*-methylmorpholine-*N*-oxide (NMO). Oxidative cleavage [16] of the diol with $NaIO_4$ provided an intermediate dialdehyde which upon reductive amination with *p*-methoxybenzyl amine (PMB-amine) and sodium cyanoborohydride ($Na(CN)BH_3$) yielded a PMB-protected varenicline compound **7**. Finally, the PMB group was removed by hydrogenation (Pd/C in the presence of ammonium formate in methanol) to yield varenicline. It has been reported that the overall yield of varenicline by this method was approximately 10% [3] (see Scheme 10.1 and experimental procedures a, b, and c) [3].

2.1. Experimental procedure for compound 5

Sodium iodide was added in small portions over a period of 2 min to a solution of the 2,3-bis(dibromomethyl)pyrazine **3** (2.0 g, 4.71 mmol) and norbornadiene **4** (2.16 g, 23.58 mmol) in dry DMF (23 mL) at 60 °C. The mixture was stirred for further 30 min. The reaction mixture was cooled to room temperature, then diluted with ethyl acetate (46 mL), and passed through a small pad of Celite. The filtrate was washed with 10% sodium thiosulfate (3×20 mL), water (2×20 mL), and brine (1×20 mL). The organic layer was dried over anhydrous $MgSO_4$ and concentrated in vacuum. The residue was purified by flash column chromatography (silica gel, EtOAc–hexane, 10:90) to give 420 mg (46%) of **5** as a white solid. Mp: 120–123 °C [3].

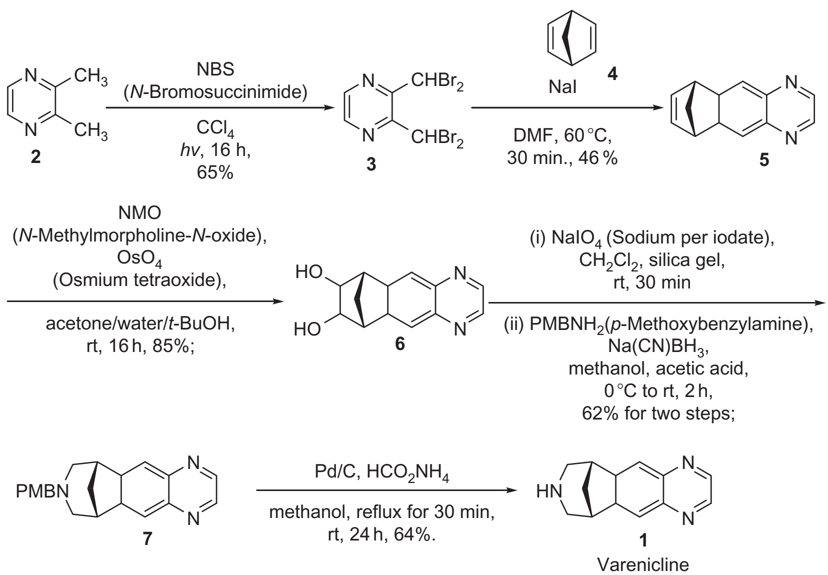

SCHEME 10.1 Total synthesis of varenicline.

2.2. Experimental procedure for compound **7**

A 0.65M aqueous solution of $NaIO_4$ (3.5mL, 2.14mmol) was added dropwise to a vigorously stirred suspension of chromatography-grade silica gel (3.5g) in methylene chloride (59mL). After addition of **6** (350mg, 1.53 mmol) in methylene chloride (78mL) to the resulting flaky solution, stirring was continued for another 30min and then the mixture was passed through a filter pad onto a small amount of Na_2SO_4. The retained silica gel was washed with methylene chloride (20mL), and the washings were pooled with filtrate. Removal of the solvent left the dialdehyde as a solid reddish residue, which was dissolved in methanol (8mL). *p*-Methoxybenzyl amine (210mg, 1.53mmol) in methanol (3mL) followed by AcOH (9µL, 0.15 mmol) was added to the abovementioned solution at 0°C, and after stirring at room temperature for 10min, $Na(CN)BH_3$ (145mg, 2.3mmol) was added at 0°C and stirred at temperature for 2h. Methanol was evaporated, and the residue was dissolved in water (15mL) and extracted with ethyl acetate (3×15mL). The combined organic layers were washed with water (2×15 mL) and brine (1×15mL), dried over anhydrous MgSO4, and concentrated under reduced pressure. The crude product was purified by flash chromatography (silica gel, ethyl acetate–hexane, 15:85) to give 315mg (62%) of **7** as a brown-colored thick liquid [3].

2.3. Experimental procedure for compound **1**

To a solution of **7** (50mg, 0.15mmol) in methanol (2mL) was added 10% Pd/C (125mg, 2.5equiv., w/w), followed by HCO_2NH_4 (100mg, 2equiv., w/w), and heated to reflux for 30min. The reaction mixture was cooled to room temperature and allowed to stand for 24h. This suspension was filtered through a small pad of Celite and was washed with methanol (10 mL). The filtrate was evaporated under reduced pressure and purified by flash chromatography (silica gel, MeOH–$CHCl_3$, 2:98) to give 20mg (64%) of **1** as a cream-colored solid. Mp: 137–139°C [3].

Varenicline base and its pharmaceutically acceptable acid addition salts are described in U.S. Patent No. 6,410,550 [17]. In particular, the preparation of varenicline provided in this reference makes use of 10-aza-tricyclo [6.3.1.0^{2,7}]-dodeca-2(7),3,5-triene (compound **12**), as a key intermediate compound (see Scheme 10.2).

A process for preparing 1,2,3,4-tetrahydro-1,4-methano-naphthalene-*cis*-2,3-diol **9** began with *cis*-dihydroxylating the alkene group of 1,4-dihydro-1,4-methano-naphthalene **8**, by means of treatment with a polymer supported osmium tetroxide as an oxidizing agent (optionally in the presence of a suitable co-oxidizing agent), and in the presence of a suitable solvent comprising water, thereby obtaining a mixture comprising compounds **9** and **8** optionally, isolating compound **9** from the mixture, which

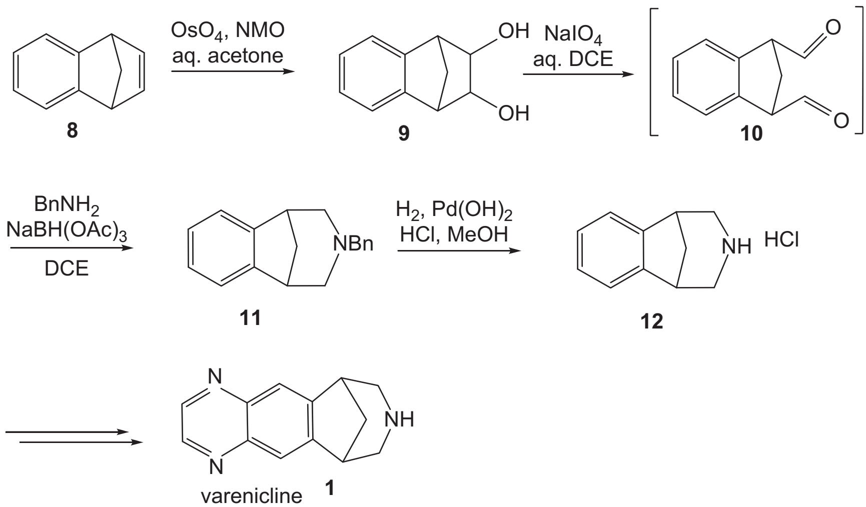

SCHEME 10.2 Synthesis of 10-aza-tricyclo[6.3.1.0^{2,7}]-dodeca-2(7),3,5-triene (compound **12**) as a key intermediate compound in the preparation of varenicline [7].

is followed by oxidative cleaving the *cis*-2,3-diol group of compound **9**, to obtain indane-1,3-dicarbaldehyde **10**. Compound **10** is then undergoes reductive amination reaction, to obtain 3-benzyl-2,3,4,5-tetrahydro-1,5-methano-1*H*-3-benzazepine **11**, debenzylating compound **11**, to obtain 10-aza-tricyclo[6.3.1.0^{2,7}]-dodeca-2(7),3,5-triene **12**, and transforming compound **12** into varenicline, or pharmaceutically acceptable salts or solvates thereof.

2.4. Preparation of varenicline L-tartrate forms

Varenicline (L)-tartrate crystalline Forms A, B, and C were prepared in a manner consistent with that described in the literature (see Section 3.3) [17].

3. PHYSICAL PROPERTIES

3.1. Spectroscopy

3.1.1. Ultraviolet spectroscopy

Varenicline ultraviolet (UV)-absorption spectrum was recorded for selecting the proper maximum absorption peak (λ_{max}) in other analyses. The UV absorption spectrum of varenicline in water was scanned from 200 to 400nm, using UV/VIS spectrometer (Varian Cary 50 Conc. ultraviolet–visible spectrophotometer). As shown in Fig. 10.1, the λ_{max} of varenicline is located at 235nm.

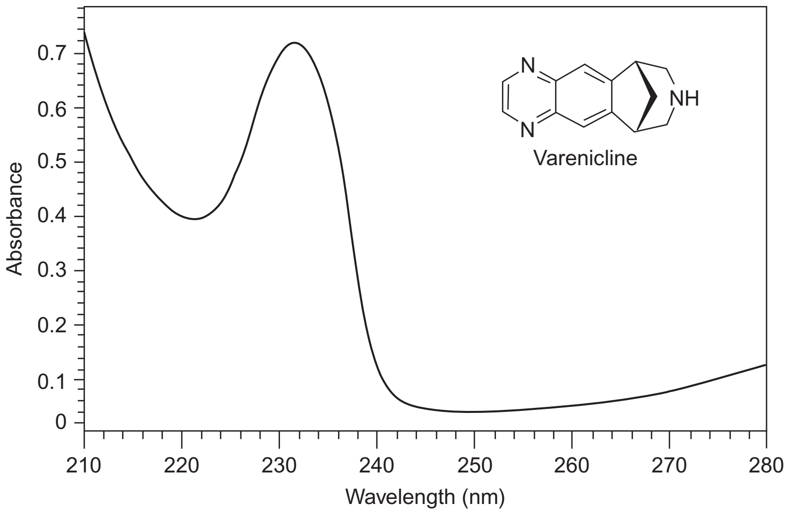

FIGURE 10.1 Ultraviolet absorption spectrum of varenicline in water.

3.1.2. Vibrational spectroscopy

3.1.2.1. Infrared absorption spectroscopy of varenicline base FTIR spectra (Fig. 10.2) were acquired on an Illuminat IR TM Fourier transform infrared microspectrometer with a diamond attenuated total reflectance objective. Each spectrum represents 100 co-added scans using a 100-mm masking aperture collected at a spectral resolution of 4cm^{-1}. Sample preparation consisted of placing the sample on a standard glass microscope slide under ambient conditions. A background spectrum was first acquired using the diamond attenuated total reflectance objective [18]. IR (KBr, cm^{-1}): 3342, 2949, 2924, 2852, 1473, 1354 [3].

3.1.2.2. Infrared absorption spectroscopy of varenicline tartrate The FTIR spectrum of varenicline tartrate was obtained in a KBr pellet using a Perkin-Elmer infrared spectrophotometer (Fig. 10.3). Assignments for the major infrared absorption band are provided in Table 10.1.

3.1.3. Nuclear magnetic resonance spectrometry

^{1}H and ^{13}C nuclear magnetic resonance (NMR) spectra of varenicline tartrate were obtained using a JEOL spectrometer. Chemical shifts were expressed in parts per million (ppm) with respect to the tetramethylsilane signal for ^{1}H and ^{13}C NMR (Figs. 10.4 and 10.5, respectively).

3.1.3.1. ^{1}H NMR spectrum The ^{1}H NMR spectrum of varenicline tartrate dissolved in DMSO-d_6 is shown in Fig. 10.4A and B. The data from the spectrum are as follows: ^{1}H NMR (DMSO-d_6, 400MHz): 2.16 (d, J=11Hz,

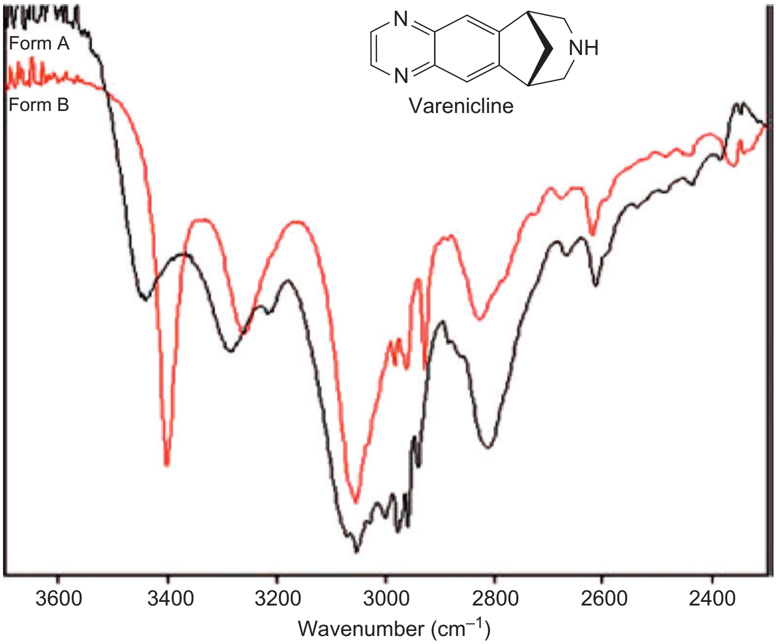

FIGURE 10.2 FTIR spectra of varenicline Form A and Form B [16].

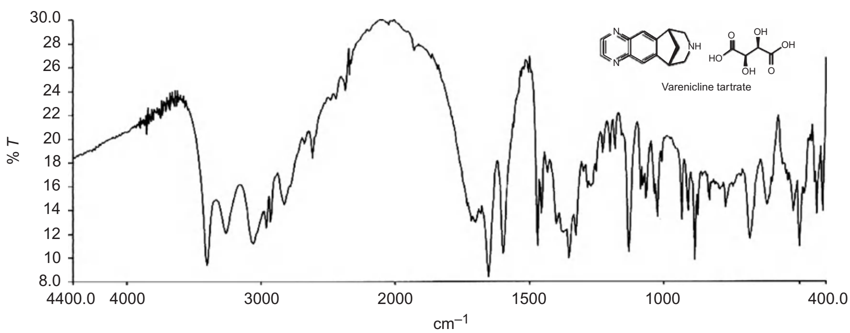

FIGURE 10.3 FTIR spectrum of varenicline tartrate.

1H), 2.32 (m, 1H), 3.12 (d, J=11.7Hz, 2H), 3.32 (d, J=12.5Hz, 2H), 3.52 (s, 2H), 3.89 (s, 2H, —CH of tartaric acid), 4.8 (br, —COOH of tartaric acid), 7.99 (s, 2H), 8.90 (s, 2H)ppm.

3.1.3.2. ^{13}C NMR spectrum The ^{13}C NMR spectrum of varenicline tartrate, dissolved in DMSO-d_6, is shown in Fig. 10.5. The data from the spectrum are as follows: ^{13}C NMR (DMSO-d_6, 100MHz): δ 174.68 (—COOH carbon

TABLE 10.1 Vibrational assignments of varenicline tartrate infrared absorption bands

Frequency (cm^{-1})	Assignment
1600, 1507, 1457	C=C aromatic
1654	C=N
1700	C=O carboxylic acid
2960	C—H aliphatic
3055	C—H aromatic
3403	N—H (secondary amine)
2375–3263 (multiple broad peaks)	N—H ammonium ion

A

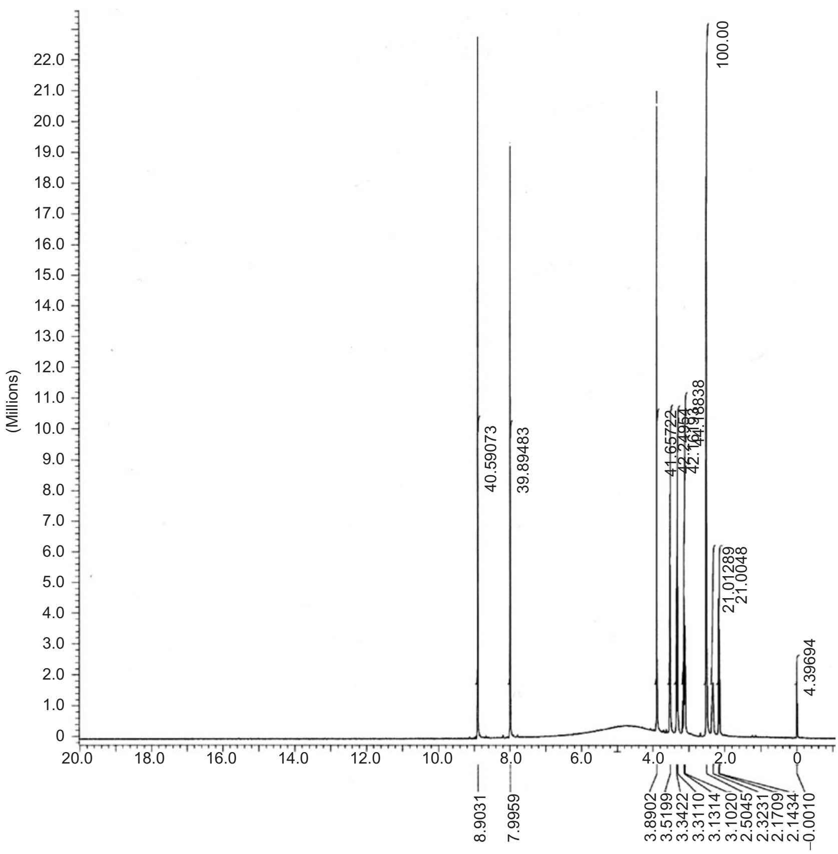

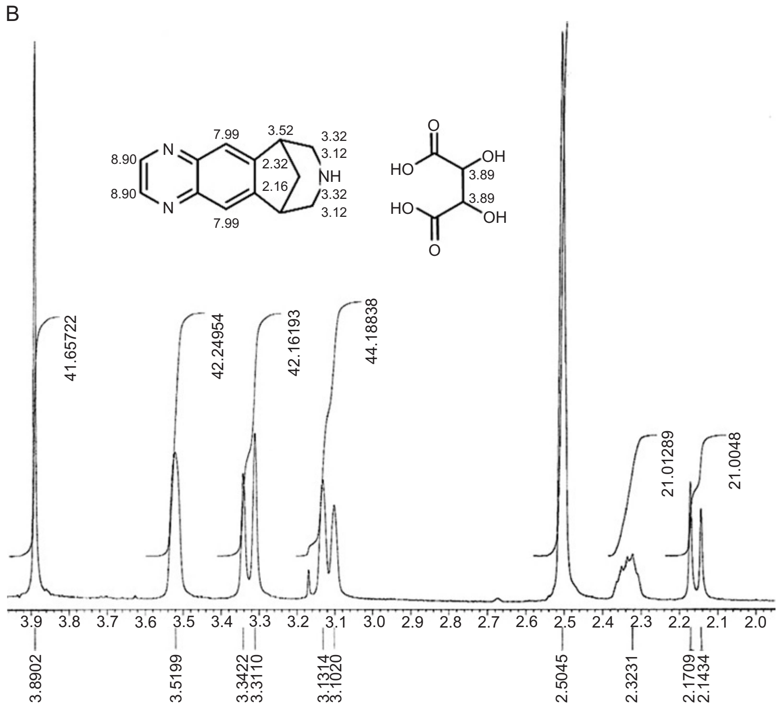

FIGURE 10.4 (A) ^{1}H NMR spectra of varenicline tartrate; (B) ^{1}H NMR spectra of varenicline tartrate in the aliphatic region.

of tartaric acid), 147.38, 145.15, 143.50, 123.75, 71.92 (—CH carbon of tartaric acid), 48.9, 40.8 ppm.

^{1}H and ^{13}C NMR were reported in the literature [3] as follows:

^{1}H NMR (400 MHz; CDC_{13}): d=8.75 (s, 2H), 7.83 (s, 2H), 3.25 (br s, 2H), 3.15 (d, J=13.0 Hz, 2H), 2.92 (d, J=13.0 Hz, 2H), 2.48 (m, 1H), 2.09 (d, J=8.8 Hz, 1H), 1.82 (br s, 1H); ^{13}C NMR (50 MHz; $CDCl_3$): d=149.6, 143.5, 143.6, 121.7, 50.5, 43.1, 42.2.

3.2. Mass spectrometry

Mass spectra of varenicline were carried out with an Agilent 6320 Ion Trap LC/MS system by infusion of 2 μg of solution in H_2O without a column. Source parameters were as follows: temperature was 350 °C, gas flow was 12 L/min, and the nebulizer was 60 psi. Figure 10.6 shows the mass spectrum for the parent compound (m/z=212), Figs. 10.7 and 10.9

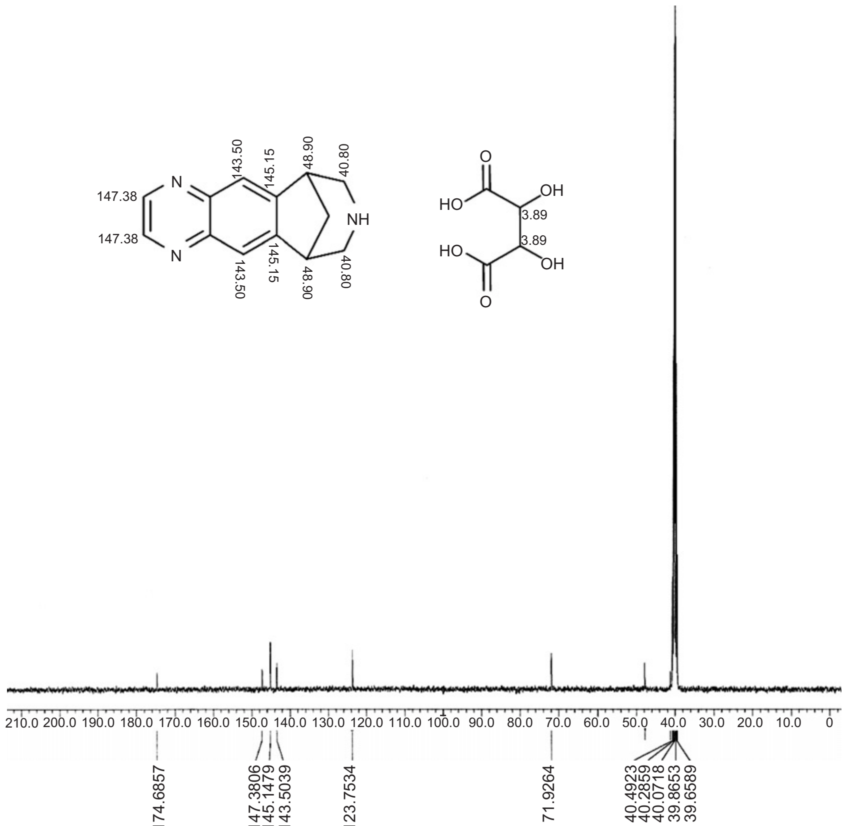

FIGURE 10.5 ^{13}C NMR spectra for varenicline tartrate. ^{13}C NMR (DMSO-d_6, 100 MHz).

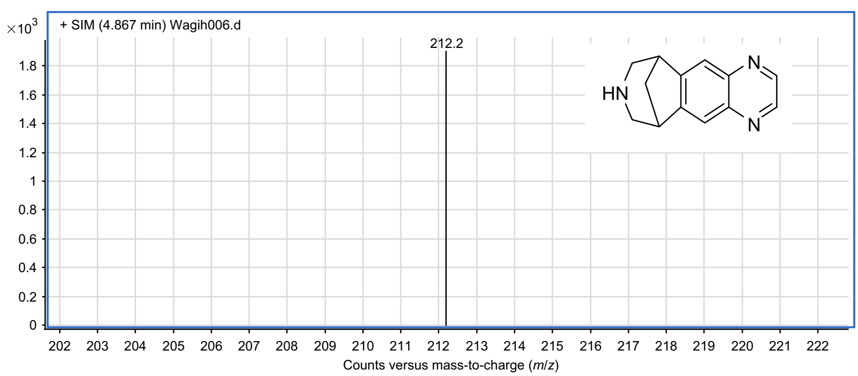

FIGURE 10.6 Mass spectrum for the parent varenicline compound (m/z=212).

show the detailed mass fragmentation pattern, and Fig. 10.8 shows the mass fragmentation pattern interpretation of the drug substance.

3.2.1. Fragmentation pattern of varenicline

Figure 10.6 shows the mass spectrum of varenicline. The collision-induced dissociation mass spectrum for the parent compound (m/z=212) yielded fragments associated with loss of the secondary amine nitrogen. Fragments at m/z of 195, 183, and 169 are proposed to arise via loss of ammonia, methylimine, and dimethylimine as neutral species, respectively (Fig. 10.7). The fragment ion at m/z=141 (Fig. 10.9) represents fragmentation of the quinoxaline ring [19].

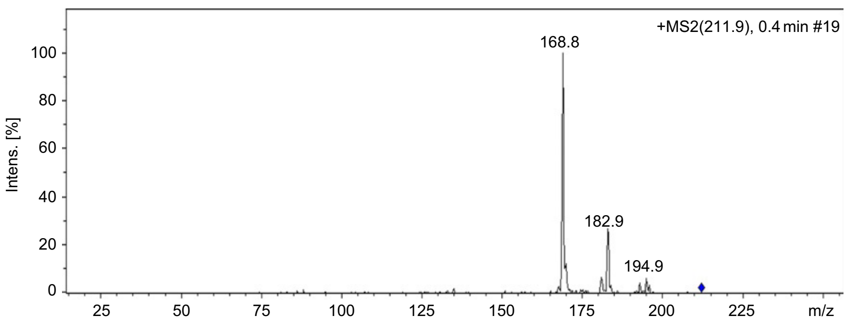

FIGURE 10.7 Mass spectrum of varenicline.

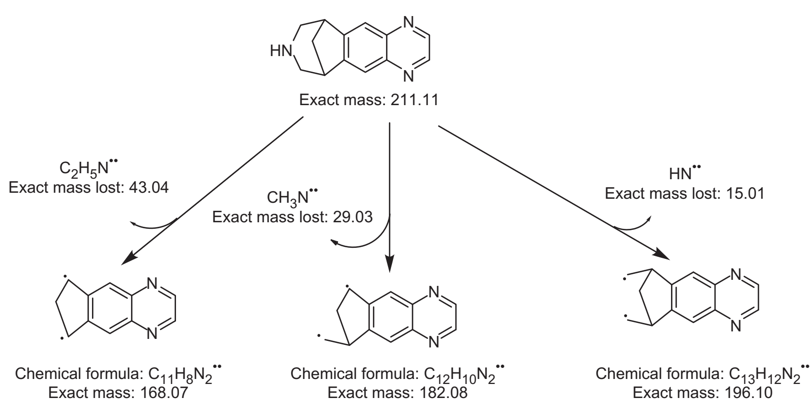

FIGURE 10.8 Fragmentation pattern of varenicline.

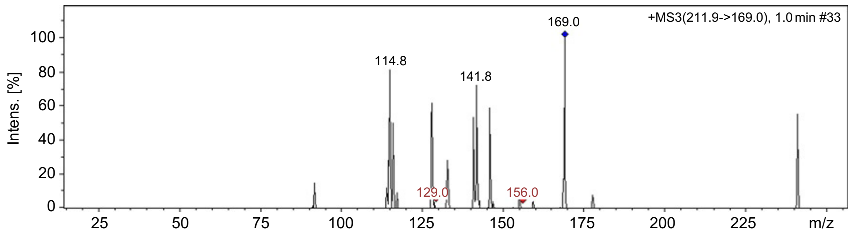

FIGURE 10.9 Mass spectrum of varenicline (additional fragmentation).

3.3. X-ray powder diffraction pattern

Three crystalline forms of varenicline (L)-tartrate are known: two anhydrous forms (Forms A and B), and a monohydrate (Form C) [17]. It was stated within the patent that Form A is the metastable polymorph, which will convert under appropriate conditions to the thermodynamically stable Form B. The monohydrate (L)-tartrate salt is relatively stable under ambient conditions. Single crystals of Form A were grown by antisolvent addition at an elevated temperature using vapor diffusion methods, where an 87 mg/mL varenicline (L)-tartrate solution in dimethyl sulfoxide and an acetonitrile antisolvent were stored in a sealed chamber at 78 °C for 1 week [20]. The X-ray powder diffraction patterns disclosed in the patent for the three crystal forms of varenicline (L)-tartrate are shown in Figs. 10.10–10.12, along with the scattering angles and *d*-spacings of the peaks used by the patent authors to define these forms.

A summary of the crystal structure data and refinement parameters for the three varenicline (L)-tartrate crystal forms is given in Table 10.2. As all crystal structures are available, differentiation of Forms A, B, and C based upon their crystallographic properties and hydrogen-bonding patterns is possible [18].

Although each form demonstrates a unique crystal structure, the unit cell parameters and crystal densities are similar. These similarities likely result from the existence of a common molecular packing arrangement within the varenicline (L)-tartrate crystal forms, as illustrated in Fig. 10.13.

3.4. Thermal method of analysis

3.4.1. Melting point

The melting point range of varenicline (L)-tartrate has been reported as 137–139 °C [3].

3.4.2. Thermal analysis

The heat of fusion rule states that two polymorphs are enantiotropically related if the higher melting form has the lower heat of fusion [21]. Although the heat of fusion rule would suggest the existence of enantiotropy when applied to the DSC data, the presence of congruent decomposition along

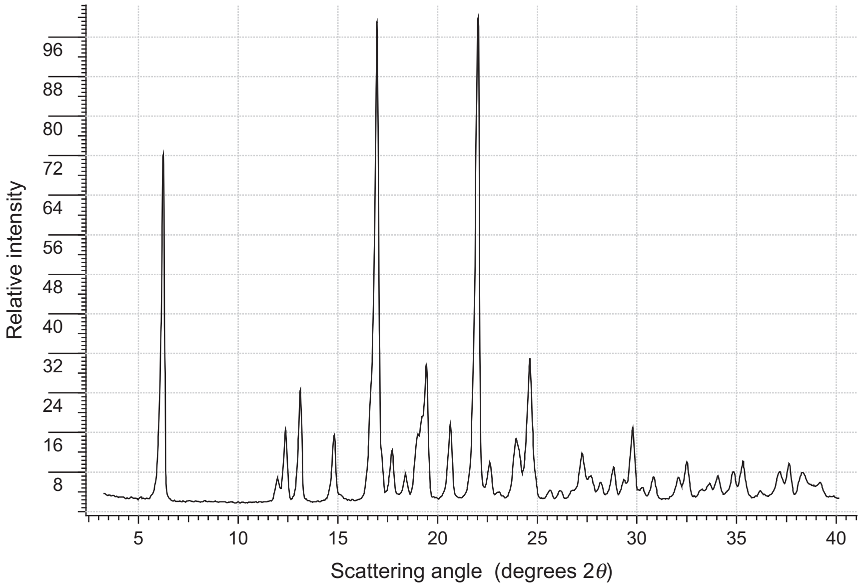

Scattering angle (degrees 2θ)	*d*-Spacing (Å)
6.1	14.5
12.2	7.2
13.0	6.8
14.7	6.0
16.8	5.3
19.4	4.6
21.9	4.1
24.6	3.6

FIGURE 10.10 X-ray powder diffraction pattern of varenicline (L)-tartrate, Form A [17]. Also shown are the scattering angles and *d*-spacings of the peaks used by the patent authors to define this polymorph.

with the melting of Form B prevents accurate application of this rule. However, thermal evaluation of Forms A and B does suggest that Form A is the thermodynamically stable form above the melting onset of Form B (215.98 °C). Thermal analysis data indicate that Form A is thermodynamically stable at high temperatures, namely, above 215.98 °C. These results indicate that an enantiotropic relationship exists between the anhydrous forms of Varenicline (L)-tartrate, with a transition temperature existing between approximately 20 and 215.98 °C. The transition temperature must be accurately determined to identify the stable anhydrous form under normal manufacturing and storage conditions.

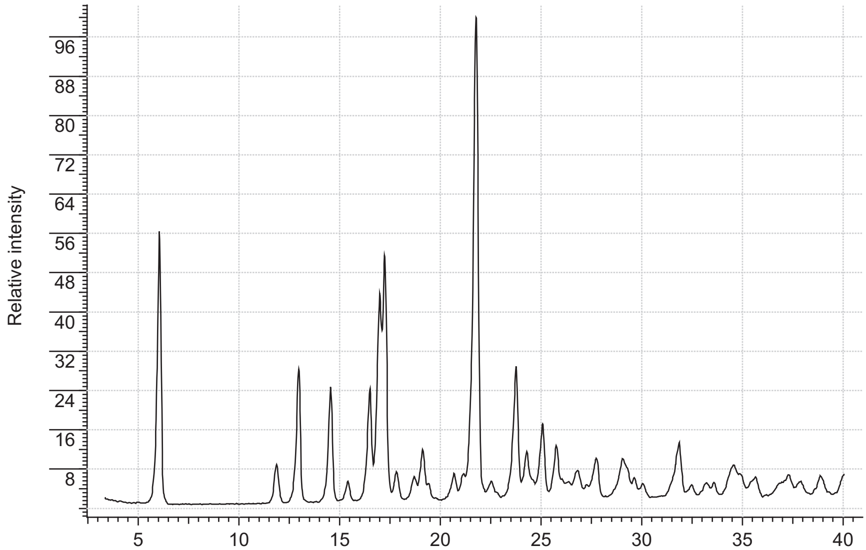

Scattering angle (degrees 2θ)	*d*-Spacing (Å)
5.9	15.0
12.8	6.9
14.4	6.1
15.3	5.8
16.9	5.2
17.2	5.2
21.8	4.1
23.8	3.7
25.1	3.5

FIGURE 10.11 X-ray powder diffraction pattern of varenicline (L)-tartrate, Form B [17]. Also shown are the scattering angles and *d*-spacings of the peaks used by the patent authors to define this polymorph.

4. METHODS OF ANALYSIS

4.1. Chromatographic methods

4.1.1. High-performance liquid chromatography methods

4.1.1.1. UPLC separation and quantification of related substances of varenicline tartrate tablet A new ultra-performance liquid chromatographic (UPLC) method has been developed and validated for quantification of substances related to varenicline tartrate, process-related impurities, and degradation products in pharmaceutical formulations. Chromatographic

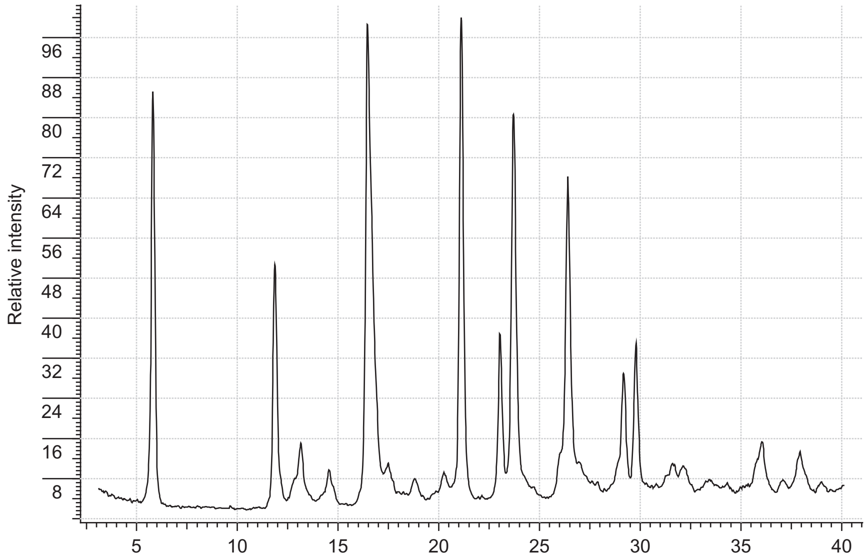

Scattering angle (degrees 2θ)	d-Spacing (Å)
5.9	15.1
11.8	7.5
16.5	5.4
21.2	4.2
23.1	3.8
23.8	3.7
26.5	3.4

FIGURE 10.12 X-ray powder diffraction pattern of varenicline (L)-tartrate, Form C [17]. Also shown are the scattering angles and *d*-spacings of the peaks used by the patent authors to define this solvatomorph.

separation of six impurities was achieved on a reversed phase column. The method was validated for linearity, limits of detection and quantification, accuracy, precision, and selectivity. The calibration plots obtained for the six impurities were linear over the range 0.005–0.30%. The relative standard deviations (RSD) of intra- and interday experiments were less than 1.0%. The detection limits ranged between 0.002% and 0.004%, depending on the impurity. The proposed UPLC method was successfully applied to quantification of varenicline impurities in its pharmaceutical formulation [22].

TABLE 10.2 Crystal structure data and refinement parameters for Forms A, B, and C

	Form A	Form B	Form C
Empirical formula	$C_{13}H_{14}N_3C_4H_5O^{-6}$	$C_{13}H_{14}N_3C_4H_5O^{-6}$	$C_{13}H_{14}N_3C_4H_5O^{-6}\cdot H_2O$
Formula weight ($g mol^{-1}$)	361.35	361.35	379.37
Crystal system	Orthorhombic	Orthorhombic	Monoclinic
Space group	$P2_12_12_1$	$P2_12_12_1$	$P2_1$
Crystal size (mm^3)	$0.10\times0.24\times0.38$	$0.10\times0.08\times0.10$	$0.04\times0.38\times0.30$
A (Å)	7.420	7.075	7.512
B (Å)	7.692	7.785	7.671
C (Å)	28.879	29.870	29.864
Angles (8) $B^{(0)}$	90.0°	90.0°	90.4°
Volume (Å^3)	1648.3	1645.2	1720.3
Z	4	4	4
Calculated density ($g cm^{-3}$)	1.456	1.459	1.465
Absorption coefficient (mm^{-1})	0.942	0.944	0.974
F (000)	760	760	800
Reflections collected	5603	3490	1983
Independent reflections	2311	1318	1817
R_{int} (%)	10.31	5.42	2.24
Parameters	251	251	528
Final R indices [I>2s (I)]	R1¼0.0432	R1¼0.0352	R1¼0.0347
	wR2¼0.0897	wR2¼0.0638	wR2¼0.0834
Goodness of fit on F2	0.973	0.865	1.028
Largest diff. peak and hole (eÅ^{-3})	0.212 and 0.193	0.115 and 0.150	0.168 and 0.230

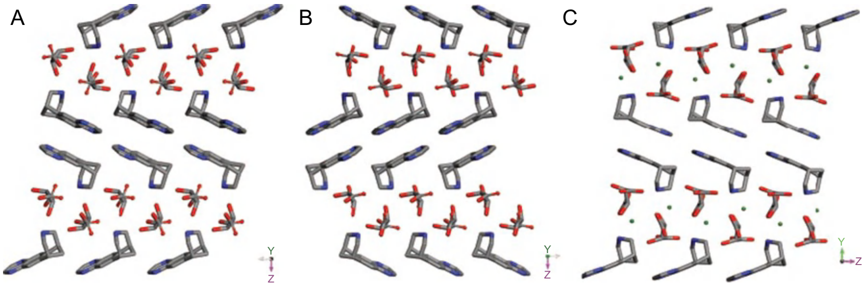

FIGURE 10.13 (A) Crystal packing in Form A, (B) in Form B, and (C) in Form C [18].

4.1.2. High-performance liquid chromatography/mass spectrometry

Circulating varenicline concentrations were measured using a method involving liquid extraction and HPLC-MS/MS analysis. 0.1 mL of CP-533,633 (a structural analog of varenicline) was added to plasma or serum samples (50 μL of a 0.25-μg/mL methanolic solution) as an internal standard and 1 N sodium hydroxide (0.5 mL). The alkalinized samples were subjected to liquid extraction with methyl *tert*-butyl ether (3 mL). The aqueous layer was frozen in a dry ice-acetone bath, and the organic fraction was decanted and evaporated under nitrogen. The residue was reconstituted in 100 μL of HPLC mobile phase.

Reconstituted extracts were injected (50 μL; CTC Analytics LEAP Auto-injector; LEAP Technologies, Carrboro, NC) onto a Monitor C18 column (4.6×150 mm, 5 μm; Column Engineering) equilibrated in 10 mM ammonium acetate (pH unadjusted)/methanol (25:75) at a flow rate of 0.8 mL/min (Shimadzu LC10AD Pumps; Shimadzu, Columbia, MD). The effluent was split 1:1 and was introduced into a Turbo Ionspray source of a Sciex API 3000 mass spectrometer (Applied Biosystems/MDS Sciex) operated in the positive ion mode. The temperature of the probe was 400° C, the orifice voltage was 55 V, the collision energy was 30 V, and the collision gas setting was 10. Varenicline and internal standard (a structural analog of varenicline) were monitored by multiple reaction monitoring of 212.2→169.1 for the parent, 216.2→173.1 for the radiolabeled parent, and 240.2→197.1 for the internal standard. Varenicline and internal standard eluted at 2.5–3.0 min, respectively. The dynamic range of the assay was from 0.5 to 100 ng/mL [19].

5. PHARMACOLOGY

In vitro varenicline displayed high affinity for the rat cortex $\alpha_4\beta_2$ nicotine receptor in radio-ligand displacement binding assays with a K_i value of 0.17 nM. It is believed that the nicotinic $\alpha_4\beta_2$ receptor mediates dopamine

release in the nucleus accumbens and thus is involved in the motivational effects of smoking. Both nicotine and varenicline reversibly bind to the same receptor binding site. Considering the 15-fold higher affinity of varenicline for the $\alpha_4\beta_2$ nicotinic acetylcholine receptor as compared with nicotine, very high nicotine brain concentrations would be required to fully displace varenicline and produce nicotine rewarding in the subject.

In vivo varenicline only partially activates the mesolimbic dopamine system, in comparison to the activation induced by nicotine. Varenicline released ^{3}H-dopamine from rat striatal slices with a maximal response of 51% (relative to the release evoked by nicotine) at 1 μM, indicating that varenicline acts as a partial agonist at the nicotinic acetylcholine receptor. Additionally, 10 μM varenicline reduced the response induced by nicotine by 53%, down to levels induced by varenicline [5].

5.1. Pharmacokinetics

5.1.1. Absorption

The absorption of varenicline was virtually complete after oral administration and systemic availability was high. Maximal plasma concentrations of varenicline are reached within 3–4 h and steady-state concentrations occurs within 4 days. Varenicline has a half-life of 24 h, and its bioavailability is not affected by food or time of administration. Varenicline exhibits a linear pharmacokinetics and low plasma protein binding (20%) [4,23].

5.1.2. Distribution

The tissue distribution of varenicline was in the majority of tissues, varenicline distributed into all tissues except the lens and vitreous humor. Still, varenicline displayed a high affinity for ocular tissues, and there were no apparent gender differences with respect to tissue distribution. Varenicline displays affinity for melanin containing tissues [5].

5.1.3. Metabolism and excretion

Most of orally ingested varenicline is excreted unchanged in urine. However, there are two inactive metabolites that are observed in human urine, namely 2-hydroxyvarenicline and varenicline *N*-carbamoylglucuronide (Table 10.3) [19].

5.2. Drug metabolism

Varenicline was largely excreted as unchanged drug substance, and represented the vast majority of drug-related material in circulation, although some metabolites were observed (see Fig. 10.14). However, in several instances, the amounts of metabolite were limited, precluding

TABLE 10.3 Quantitation of varenicline and major metabolites in excreta of mice, rats, monkeys, and humans after oral administration of [^{14}C] varenicline

	Percentage of dose			
Metabolite (M+H$^+$ ion)	Mouse	Rat	Monkey	Human
M1 (amino acid metabolite; m/z 244)	0.53	0.86	1.1	N.D.
M2 (amino acid metabolite; m/z 244)	0.97	0.72	4.3	N.D.
M3 (unknown m/z 338)	N.D.	0.95	N.D.	N.D.
M3a unknown	0.12	N.D.	1.1	N.D.
M3b (2-hydroxyvarenicline; m/z 228)	N.D	N.D	N.D	2.9
Varenicline (m/z 212)	90	84	75	81
M4 (varenicline *N*-carbamoylglucuronide; m/z 432)	N.D.	1.9	3.6	3.6

N.D., not detected.

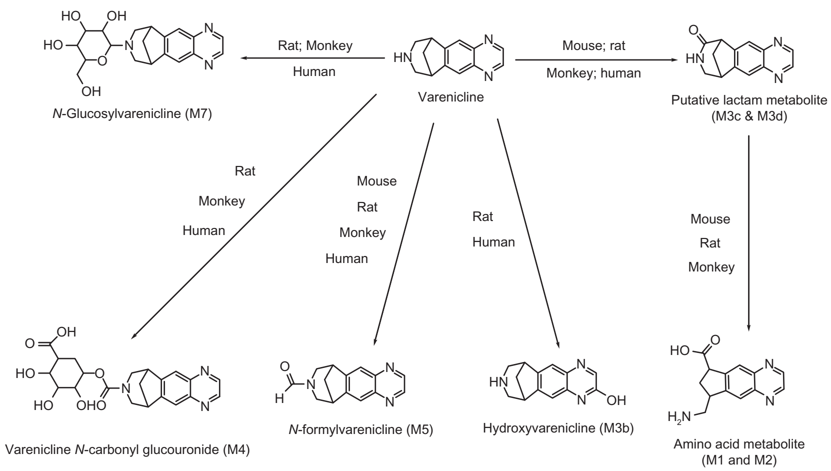

FIGURE 10.14 Metabolism of varenicline in animals and humans [19].

definitive structural assignment, owing to the small amount of metabolism occurring for varenicline and the low doses administered.

5.2.1. Metabolite profiles in circulation of animals and humans

A total of nine metabolites were observed in the circulation of the four species examined (see Table 10.4). Of the nine observed, four were observed in humans, including an *N*-formyl conjugate, an *N*-carbamoylglucuronide, and *N*-hexose conjugate, as well as an unidentified metabolite

TABLE 10.4 Quantitation of varenicline and major metabolites in circulation of mice, rats, monkeys, and humans after oral administration of [^{14}C] varenicline

Metabolite ($M+H^{+}$ ion)	Percentage circulating radioactivity			
	Mouse	Rat	Monkey	Human
M1 (amino acid metabolite; *m/z* 244)	1.4	N.D.	N.D.	N.D.
M2 (amino acid metabolite; *m/z* 244)	3.8	0.7	1.7	N.D.
M3a unknown	1.1	N.D.	0.53	N.D.
M3c (putative lactam; *m/z* 226)	N.D	N.D	0.93	1.1
Varenicline (*m/z* 212)	85	81	80	91
M3d (putative lactam; *m/z* 226)	6.8	N.D	2.1	N.D.
M4 (varenicline *N*-carbamoylglucuronide; *m/z* 432)	N.D.	11	8.7	3.8
M5 (*N*-formylvarenicline; *m/z* 240)	2.5	5.3	2.6	0.9
M6 unknown	N.D.	1.7	N.D	N.D.
M7 (*N*-glucosylvarenicline; *m/z* 374)	N.D.	1.2	2.9	3.5

N.D., not detected.

with a protonated parent ion *m/z* value of 226. The parent drug comprised the great majority of drug-related material [19].

Metabolites observed were primarily derived from reactions at the alicyclic nitrogen. Three conjugates (an *N*-carbamoylglucuronide, an *N*-glucose adduct, and an *N*-formyl conjugate) were observed. Such metabolites are likely due to the nucleophilic nature of the alicyclic nitrogen. Formation of the *N*-glucose conjugate could be observed in a solution of varenicline and concentrated glucose without any catalyst. Whether this metabolite is generated by an enzyme-catalyzed process *in vivo*, or whether it forms spontaneously and reversibly with glucose is not known. Formation of this metabolite was not observed when incubated with liver microsomes supplemented with uridine diphosphoglucose, despite the fact that UGT enzymes can sometimes catalyze glucosation reactions [24,25]. Attempts to observe the *N*-formyl conjugate *in vitro* were unsuccessful; thus, information about the enzyme responsible for generation of this metabolite remains unknown. However, both of these conjugates are very low in abundance and are not observed as excretory pathways.

In humans, only two metabolites were observed in excreta: 2-hydroxyvarenicline and varenicline *N*-carbamoylglucuronide, each at about 3–4% of the total. The *N*-carbamoyl-glucuronide was observed *in vitro*, under conditions required to observe this reaction (e.g., CO_2 atmosphere). UGT2B7 was shown to catalyze this reaction, which is similar to recently reported data for sertraline [26]. Whether the UGT

enzyme catalyzes the association of the carbamic acid followed by conjugation with glucuronic acid, or whether the carbamic acid forms spontaneously and is then conjugated is not known. However, there is precedent for the spontaneous association/dissociation of carbamic acids in aqueous solutions [27,28] and protophilic solvents [29], and since UGT2B7 is also known to catalyze the glucuronidation of carboxylic acids, it is not unreasonable to propose that it is the transiently formed varenicline carbamic acid that serves as the substrate.

The other human excretory metabolite, 2-hydroxyvarenicline, was not observed in human *in vitro* systems active with cytochrome P450 or molybdenum cofactor oxidases, two families of enzymes that are known to catalyze such a reaction. With the metabolic clearance of varenicline being so low, it is not unexpected that this metabolic pathway would be challenging to study *in vitro*.

ACKNOWLEDGMENTS

The authors would deeply like to thank both pharmacists Mohamed W. Attwa and Dr. A.F. M Motior Rahman from the Department of Pharmaceutical Chemistry, College of Pharmacy, King Saud University for their instrumental and practical support.

REFERENCES

[1] M.J. O'Neil, P.E. Heckelman, C.B. Koch, K.J. Roman, C.M. Kenny, M. R. D' Arecca (Eds.), The Merck Index—An Encyclopedia of Chemicals, Drugs, and Biologicals, 14th ed., Merck & Co., Inc., Whitehouse Station, NJ, 2006 p. 1707.
[2] S.C. Sweetman (Editor), Martindale: The Complete Drug Reference, 36th ed., 1 Pharmaceutical Press, 2009, p. 2411.
[3] S. Pasikanti, D.S. Reddy, B. Venkatesham, P.K. Dubey, J. Iqbal, P. Das, An efficient synthesis of varenicline, Tetrahedron Lett. 51 (2010) 151–152.
[4] U.M. Mohanasundram, R. Chitkara, G. Krishna, Smoking cessation therapy with varenicline, Int. J. Chron. Obstruct. Pulmon. Dis. 3 (2008) 239–251.
[5] Scientific Discussion© Emea 2006 (European Medicines Agency), Retrieved from www.ema.eu/humandocs/pdfs/epar/champix/h-699-en6.pdf.
[6] H. Faessel, P. Ravva, K. Williams, Pharmacokinetics, safety, and tolerability of varenicline in healthy adolescent smokers: a multicenter, randomized, double-blind, placebo-controlled, parallel-group study, Clin. Ther. 1 (2009) 177–189.
[7] European Patent Application, Process for Preparing Varenicline and Intermediates for Use Therein, EP 2 204 369 A1, 2009.
[8] D. Stead, P. O'Brien, A. Sanderson, Concise synthesis of (+/−)-cytisine via lithiation of N-Boc-bispidine, Org. Lett. 7 (2005) 4459–4462.
[9] S. Demers, H. Stevenson, J. Candler, C.G. Bashore, E.P. Arnold, B.T. O'Neill, J.W. Coe, Pyridine analogs of (−)-cytisine and varenicline: cholinergic receptor probes, Tetrahedron Lett. 49 (2008) 3368–3371.
[10] L.A. Pabreza, S. Dhawan, K.J. Kellar, [3H]Cytisine binding to nicotinic cholinergic receptors in brain, Mol. Pharmacol. 39 (1991) 9–12 Via Pharmacology, Biochemistry and Behavior Book, Volume 58, Issue 3 Ankho International Inc., 1997.

[11] S.F. Heinemann, R.L. Papke, Partial agonist properties of cytisine on neuronal nicotinic receptors containing the beta 2 subunit, Mol. Pharmacol. 45 (1994) 142–149.
[12] D.J. Anderson, S.P. Arneric, Nicotinic receptor binding of [^{3}H]-cytisine [^{3}H]-nicotine and [^{3}H]-methylcarbamylocholine in rat brain, Eur. J. Pharmacol. 253 (1994) 261–267.
[13] M.K. Shepherd, Cyclobutarenes. Part 2. Azaquinomethanes as reactive intermediates: synthesis of cyclobuta [b]pyridine and cyclobuta[b]pyrazine derivatives, J. Chem. Soc. Perkin Trans. 1 (1986) 1495–1498.
[14] A. Diaz-Ortiz, A. de la Hoz, A. Moreno, P. Prieto, R. Leon, M.A. Herrero, Microwave-enhanced reactivity of non-activated dienophiles towards pyrazine o-quinodimethanes, Syn. Lett. 12 (2002) 2037–2038.
[15] T. Kobayashi, S. Kobayashi, Swern oxidation of bicyclo[2.2.1]hept-5-ene-2,3-diol and its pyrazine-fused derivatives: an improved synthesis of bicyclo[2.2.1]hept-5-ene-2,3-dione and an unexpected ring-opening reaction, Molecules 5 (2000) 1062–1067.
[16] I. Perez-Castro, O. Caamano, M.D. Gracia, F. Fernadez, C. Lopez, Cyclocondensation of ($\pm$)-exo, exo-5,6-(isopropylidenedioxy)-3-(pyrrolidinomethylene)-bicyclo[2.2.1]heptan-2-one with N–C–N dinucleophiles, Synthesis 9 (2007) 1385–1391.
[17] D.E. Bogle, P.R. Rose, G.R. Williams, Tartrate salts of 5,8,14-triazatetracyclo {10.3.1.02,11.04,9}-hexadeca-2(11),3,5,7,9-pentaene and pharmaceutical compositions thereof, (2007) US Patent 7265119.
[18] B.J. Murphy, J. Huang, M.J. Casteel, A. Cobani, J.F. Krzyzaniak, Varenicline L-tartrate crystal forms: characterization through crystallography, spectroscopy, and thermodynamic, J. Pharm. Sci. 99 (2010) 2766–2776.
[19] R. Obach, A. Reed-Hagen, S. Krueger, B. Obach, T. Connell, K. Zandi, S. Miller, J. Coe, Metabolism and disposition of varenicline, a selective $\alpha_4\beta_2$ acetylcholine receptor partial agonist, in vivo and in vitro, Am. Soc. Pharmacol. Exp. Ther. 34 (2006) 121–130.
[20] J.F. Krzyzaniak, G.R. Williams, N. Ni, Identification of phase boundaries in anhydrate/hydrate systems, J. Pharm. Sci. 96 (2007) 1270–1281.
[21] A. Burger, R. Ramberger, On the polymorphism of pharmaceuticals and other molecular crystals. I. Theory of thermodynamic rules. II. Applicability of thermodynamic rules, Mikrochim. Acta 72 (1979) 259–271 273–316.
[22] B. Satheesh, S. Kumarpulluru, V. Raghavan, D. Saravanan, UPLC separation and quantification of related substances of varenicline tartrate tablet, Acta Chromatogr. 22 (2010) 207–218.
[23] H.M. Fassel, B.J. Smith, M.A. Gibbs, Single-dose pharmacokinetics of varenicline, a selective nicotinic receptor partial agonist, in healthy smokers and nonsmokers, J. Clin. Pharmacol. 46 (2006) 991–998.
[24] K. Toide, Y. Terauchi, T. Fujii, H. Yamazaki, T. Kamataki, Uridine diphosphate sugar-selective conjugation of an aldose reductase inhibitor (as-3201) by UDP-glucuronosyltransferase 2B subfamily in human liver microsomes, Biochem. Pharmacol. 67 (2004) 1269–1278.
[25] S.B. Senafi, D.J. Clarke, B. Burchell, Investigation of the substrate specificity of a cloned expressed human bilirubin UDP-glucuronosyltransferase: UDP-sugar specificity and involvement in steroid and xenobiotic glucuronidation, Biochem. J. 303 (1994) 233–240.
[26] R.S. Obach, L.M. Cox, L.M. Tremaine, Sertraline is metabolized by multiple cytochrome P450 enzymes, monoamine oxidases and glucuronyl transferases in human: an in vitro study, Drug Metab. Dispos. 33 (2005) 262–270.
[27] M. Caplow, Kinetics of carbamate formation and breakdown, J. Am. Chem. Soc. 90 (1968) 6795–6803.
[28] J.S. Morrow, P. Keim, F.R.N. Gurd, CO2 Adducts of certain amino acids, peptides and sperm whale myoglobin studied by carbon-13 and proton nuclear magnetic resonance, J. Biol. Chem. 249 (1974) 7484–7494.
[29] K. Masuda, Y. Ito, M. Horiguchi, H. Fujita, Studies on the solvent dependence of the carbamic acid formation from ω-(1-naphthyl)alkylamines and carbon dioxide, Tetrahedron 61 (2005) 213–229.

CHAPTER 11

Zolpidem Tartrate

Nagwa H. Foda and **Shaimaa M. Ali**

Contents

Pharmaceutics Department, Faculty of Pharmacy, King Abdulaziz University, Jeddah, Saudi Arabia

Profiles of Drug Substances, Excipients, and Related Methodology, Volume 37
ISSN 1871-5125, DOI: 10.1016/B978-0-12-397220-0.00011-8

© 2012 Elsevier Inc.
All rights reserved.

1. PHYSICAL PROFILES OF DRUG SUBSTANCES AND EXCIPIENTS

1.1. General information

1.1.1. Nomenclature

1.1.1.1. Systematic chemical name

N,*N*,6-Trimethyl-2-(4-methylphenyl)-imidazo[1,2-*a*]pyridine-3-acetamide.

Bis[*N*,*N*-dimethyl-2-[6-methyl-2-(4-methylphenyl)imidazo[1,2-*a*]pyridin-3-yl]acetamide](2*R*,3*R*)-2,3 dihydroxybutanedioate [1].

1.1.1.2. Nonproprietary name Zolpidem tartrate.

1.1.1.3. Proprietary names Adormix, Ambien, Ambien CR, Edluar, Damixan, Hypnogen, Ivedal, Lioran, Myslee, Nytamel, Sanval, Somidem, Stilnoct, Stilnox, Stilnox CR, Sucedal, Zoldem, Zolnod, and Zolpihexal [2].

1.1.2. Formulae

1.1.2.1. Empirical formula, molecular weight, CAS number [3] $C_{42}H_{48}N_6O_8$; 764.88; *CAS—82626-48-0 (zolpidem), 99294-93-6 (zolpidem tartrate).*

1.1.2.2. Structural formula

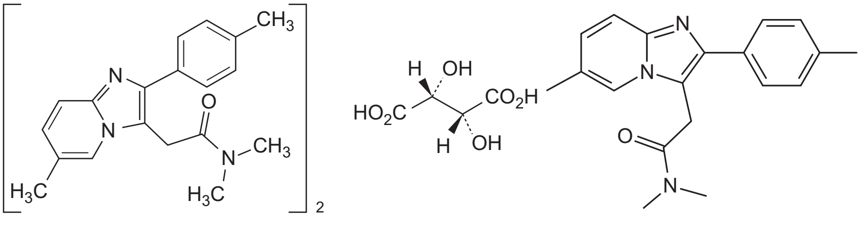

Zolpidem tartrate

Zolpidem base

1.1.3. Elemental analysis

The calculated elemental content of zolpidem and zolpidem tartrate is given in Table 11.1 [3].

1.1.4. Appearance

White or almost white, hygroscopic, crystalline powder [3,4].

1.2. Physical characteristics

1.2.1. Solubility characteristics

The free base of zolpidem is insoluble in water; zolpidem tartrate is slightly soluble in water (23 g/l at 20 °C), practically insoluble in dichloromethane, sparingly soluble in methanol [3].

1.2.2. Partition coefficient

Its partition coefficient (PC) in octanol–water is constant (log PC=3.85) [3].

TABLE 11.1 Elemental analysis

Element	Zolpidem (%w/w)	Zolpidem tartrate (%w/w)
C	74.24	65.89
H	6.89	6.275
N	13.6	10.98
O	5.20	16.73

1.2.3. Ionization constants

Zolpidem is characterized by a single ionization constant, for which the pK_a=6.2 [3].

1.2.4. Hygroscopicity

A white or almost white hygroscopic crystalline powder [3].

1.2.5. Thermal methods of analysis

1.2.5.1. Melting behavior The melting point of zolpidem is 196 °C.

The melting point of zolpidem tartrate is 193–197 °C [3].

1.2.6. Spectroscopy

1.2.6.1. UV–VIS spectroscopy Aqueous acid (pH 2.6)—207 nm; methanol—243, 314 nm; 0.1 M hydrochloric acid—236, 294 nm; 0.2 M H_2SO_4—207, 237, 295 nm; 0.025 M sulfuric acid—238, 294.5 nm; 0.1 M $HCOONH_4$ (pH 3)—238, 296 nm; aqueous alkali (0.1 M sodium hydroxide)—242, 311 nm (Fig. 11.1).

1.2.6.2. Vibrational spectroscopy The infrared absorption spectrum of zolpidem obtained in KBr disk is shown in Fig. 11.2. The spectrum was recorded on Jasco FT/IR 460 plus Fourier transform infrared spectrometer (Table 11.2).

1.2.7. Mass spectrometry

The mass spectrum of zolpidem tartrate is shown in Fig. 11.3 and was recorded on Shimadzu GCMS-QP1000EX mass spectrometer. The fragmentation assignments of the mass spectrum of zaleplon are shown in Table 11.3. Principal ions were detected at m/z 235, 307, 219, 92, 65, 72.

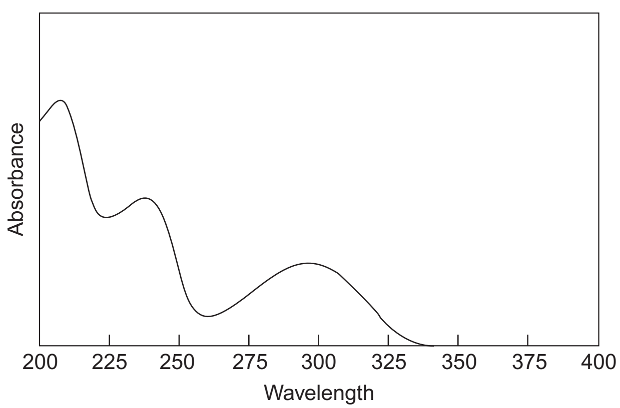

FIGURE 11.1 Ultraviolet spectrum of zolpidem tartrate [3].

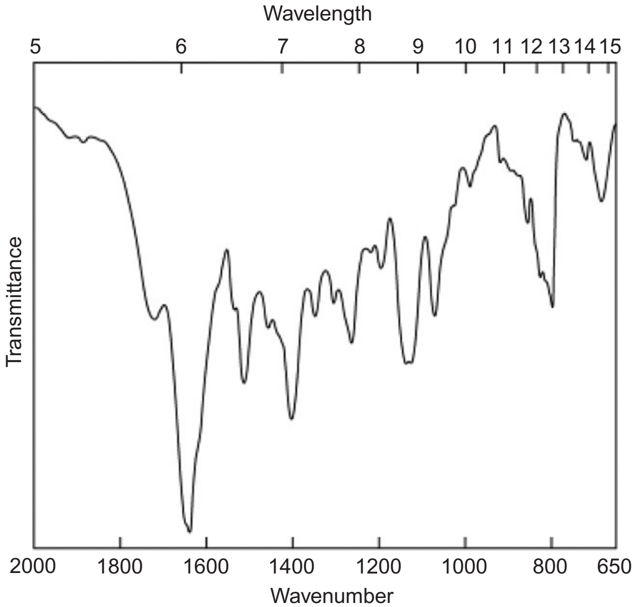

FIGURE 11.2 FTIR spectrum of zolpidem tartrate.

TABLE 11.2 Vibrational spectral assignment of zolpidem tartrate

Frequency (cm^{-1})	Assignment
2690	C—H
1720	C=N
1640	C=O
1580, 1510, 1400	C=C
1260	CH_3
1140	C—N

1.3. Stability

1.3.1. Solid-state stability

Stable under ordinary condition, store in an airtight container, protected from light [4].

Lawecka *et al*. [5] studied the influence of storage conditions on the polymorphic stability of zolpidem tartrate hydrate. Differential scanning calorimetry, thermogravimetric analysis with the support of X-ray powder diffraction, and infrared spectroscopy were used as screening techniques for testing structural changes of zolpidem tartrate hydrate stored

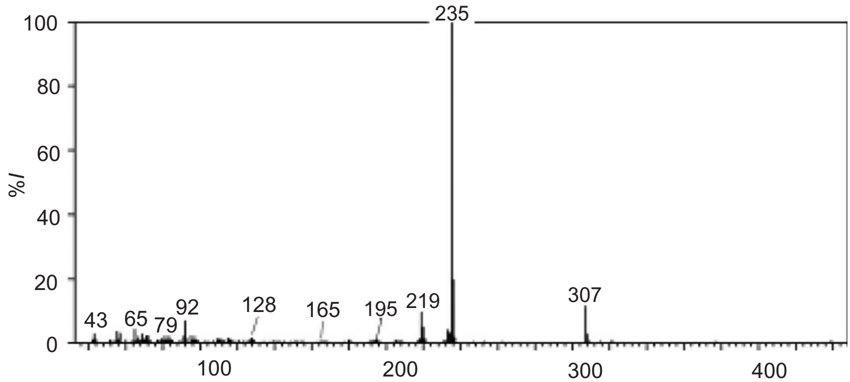

FIGURE 11.3 Mass spectrum of zolpidem.

TABLE 11.3 Mass spectrum of zolpidem tartrate

m/z	Intensity relative to base peak	Structure
307	11.8	Molecular ion
235	100	$[M\text{-}[CH_3]_2 2NCO]$
219	8.2	$M\text{-}[CH_3]_2NCO]{-}CH_4^+$
92	14.3	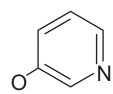
72	13.6	$(CH_3)2N{-}C{=}O^+$
65	12.9	$C_4H_3N^+$

under different conditions. Obtained data suggested that first structural changes occurred at the temperature of 25 °C after 2 months of storage. DSC analysis showed that there was a two-step process of water elimination and lack of a phase transition in the temperature range from 130 °C to 170 °C in comparison with an initial sample. The studies clarified that the water molecule has been incorporated into the zolpidem tartrate crystal lattice. It has been shown that storage conditions have substantial influence on the zolpidem tartrate stability. First structural changes occurred at the temperature of 25 °C after 2 months of storage but the most rapid transformation appeared to be at the temperature of 40 °C. The results demonstrated that DSC technique is a very useful tool for a quick screening of structural changes occurring during long-term stability tests. TG provides solutions for potential problems with solvates. Thermal

analysis results supported by XRPD and IR measurements ensure reliable interpretation of pharmaceuticals studies.

1.3.2. Solution-phase stability

The effect of some chemically modified cyclodextrins [namely, 2-hydroxypropyl-β-, methyl-β-, and 2-hydroxypropyl-γ-cyclodextrin (HP-β-CD, Me-β-CD, and HP-γ-CD, respectively)] on the aqueous solubility and dissolution rate of the hypnotic agent zolpidem (ZP) was investigated. Solid complexes were prepared by freeze drying and characterized by infrared spectroscopy, X-ray powder diffraction, and differential scanning calorimetry. The solubility and dissolution rate of the drug were significantly improved by complexation with HP-β-CD or Me-β-CD. The structure of the inclusion complex ZP-HP-β-CD in CH_3COOD/D_2O was investigated by ^1H and ^{13}C NMR spectroscopy, including NOE measurements. These measurements revealing a weak interaction between the tolyl moiety of the guest molecule and the HP-β-CD cavity. The ataxic activity in rat was also investigated and it was found that ZP-HP-β-CD and ZP-Me-β-CD complexes showed almost twofold longer ataxic induction times than controls [6].

1.3.3. Stability in biological fluids

Bhatt *et al*. [7] studied analysis of stock solution at 300 ng/ml. After storage for 17 days at 2–8 °C and at room temperature for 6 h, more than 98.0% of zolpidem remained unchanged, based on their peak areas in comparison with freshly prepared solution of zolpidem (300 ng/ml). This suggests that the zolpidem in standard solution was stable for at least 17 days when stored at 2–8 °C and 6 h at room temperature. The results revealed that zolpidem in plasma was stable for at least 6 h at room temperature and 24 h in the autosampler.

2. ANALYTICAL PROFILES OF DRUG SUBSTANCES AND EXCIPIENTS

2.1. Compendial methods of analysis

2.1.1. Identification

2.1.1.1. Infrared absorption spectrophotometry, Appendix IIA (2.2.24) B.P. States that 0.1-g sample was dissolved in 10 ml of 0.1 M hydrochloric acid, 10 ml of water was added, 1 ml of dilute ammonia R2 was added dropwise with stirring, and the resulting precipitate was filtered, collected, and washed with water and then dried at 100–105 °C for 2 h. The precipitate were examined as a disc comparison. Repeat the operations using 0.10 g of zolpidem tartrate CRS.

2.1.1.2. Thin-layer chromatography, Appendix IIIA (2.2.27)

Plate TLC silica gel F254 plate R.
Mobile phase diethylamine R, cyclohexane R, ethyl acetate R (10:45:45 *v/v/v*).
Application 5.
Development Over a path of 12 cm.
Drying In air.
Detection Examine in ultraviolet light at 254 nm.
System suitability Reference solution (b): the chromatogram shows two clearly separated spots.
Results The principal spot in the chromatogram obtained with the test solution is similar in position and size to the principal spot in the chromatogram obtained with reference solution.

2.1.2. Assay methods, Appendix VIIIB, B.P. (2.2.20)

0.300 g was dissolved in a mixture of 20 ml of anhydrous acetic acid R and 20 ml of acetic anhydride R and titrated with 0.1 M perchloric acid, determining the end point potentiometrically. 1 ml of 0.1 M perchloric acid is equivalent to 38.24 mg of $C_{42}H_{48}N_6O_8$.

2.2. Tests

2.2.1. Appearance of solution

Appendix IVB

The solution is clear *(2.2.1)* and not more intensely colored than reference solution Y6 or BY6 *(2.2.2, Method II). Prepare the solutions protected from light and carry out the test as rapidly as possible.*

Triturate 0.25 g with 0.125 g of *tartaric acid R*. Dissolve the mixture in 20 ml of *water R* and dilute to 25 ml with the same solvent.

2.3. Related substances

Liquid chromatography Appendix IIID *(2.2.29)*.

Test solution Dissolve 25.0 mg of the substance to be examined in the mobile phase and dilute to 50.0 ml with the mobile phase.

Reference solution (a) Dissolve 5 mg of *zolpidem impurity A CRS* in the mobile phase and dilute to 50 ml with the mobile phase.

Reference solution (b) Dissolve 5 mg of the substance to be examined in the mobile phase and dilute to 50 ml with the mobile phase. To 10 ml of this solution, add 10 ml of reference solution (a).

Reference solution (c) Dilute 2.0 ml of the test solution to 100.0 ml with the mobile phase.

Dilute 1.0 ml of this solution to 10.0 ml with the mobile phase.

Column:

- *size*: l=0.15 m, Ø=3.9 mm;
- *stationary phase: octadecylsilyl silica gel for chromatography R* (4 μm).

Mobile phase Mix 18 volumes of *acetonitrile R*, 23 volumes of *methanol R*, and 59 volumes of a 5.6 g/l solution of *phosphoric acid R* adjusted to pH 5.5 with *triethylamine R*.

Flow rate 1.5 ml/min.

Detection Spectrophotometer at 254 nm.

Injection 20 μl.

System suitability Reference solution (b):

— *resolution*: minimum 2.0 between the peaks due to impurity A and zolpidem.

Limits:

- *total*: not more than the area of the principal peak in the chromatogram obtained with reference solution (c) (0.2%);
- *disregard limit*: 0.1 times the area of the principal peak in the chromatogram obtained with reference solution (c) (0.02%); disregard any peak due to tartaric acid (with a relative retention with reference to zolpidem of 0.16).

Water Appendix IIID *(2.5.12) method 1*

Maximum 3.0%, determined on 0.50 g.

Sulfated ash *(2.4.14)* Appendix IXA, Method II

Maximum 0.1%, determined on 1.0 g.

Storage

In an airtight container, protected from light.

Impurities

N,*N*-dimethyl-2-[7-methyl-2-(4-methylphenyl)imidazo[1,2-*a*]pyridin-3-yl]acetamide.

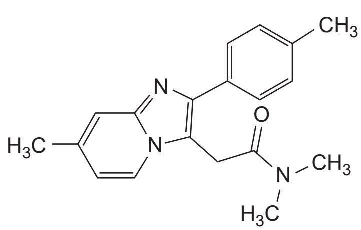

2.4. Titrimetric methods of analysis

2.4.1. Potentiometric titration

Four polymeric membrane sensors were investigated for potentiometric determination of zolpidem hemitartrate in pure form, tablets, and biological fluids [8]. Two of the sensors were constructed by using ammonium reineckate or ammonium tungstate as the fixed ionic site in a polymeric matrix of polyvinyl chloride (PVC). The third sensor was fabricated by using PVC carboxylate (PVC-COOH). The dissociated COOH groups in the PVC-COOH act as a mediator and/or ionic site. Sensor 4 was fabricated by using 2,6-didodecyl-β-cyclodextrin as the ionophore, polyurethane (Tecoflex) as a polymeric matrix, and potassium tetraphenyl borate as the ionic site; associated COOH groups act as a mediator and/or ionic site. The construction of the four sensors was based on the formation of ion-pair complexes between the drug cation and ionic sites in the ratio of 1:2, respectively. The methods were also used to determine the drug in the presence of its degradates and could be used as a stability-indicating assay.

3. ELECTROCHEMICAL METHODS OF ANALYSIS

3.1. Voltammetry

The oxidative behavior of, a hypnotic drug, zolpidem was studied by Radi *et al*. [9] at glassy carbon electrode in Britton–Robinson buffer over the pH range 2.0–11.0 using cyclic, linear sweep, and differential pulse voltammetry. Oxidation of the drug was effected in a single irreversible, diffusion-controlled step. Using differential pulse voltammetry, the drug yielded a well-defined voltammetric response in Britton–Robinson buffer, pH 8.0 at +0.889V (vs. Ag/Ag Cl) on glassy carbon electrode. This process could be used to determine zolpidem concentrations in the range 5.0×10^{-7}M to 1.0×10^{-5}M with a detection limit of 2.0×10^{-7}M. The method was applied, without any interference from the excipients, to the determination of the drug in a tablet dosage form.

4. SPECTROSCOPIC METHODS OF ANALYSIS

4.1. Spectrophotometry

A simple, sensitive, rapid, accurate, and precise spectrophotometric method has been developed for the estimation of zolpidem tartrate in bulk and pharmaceutical dosage forms by Patil *et al*. [10]. Zolpidem tartrate shows maximum absorbance at 238.5nm with molar absorptivity of 4.4648×104 l/mol/cm. Beer's law was obeyed in the concentration

range of 2–16 μg/ml. The limit of detection and limit of quantification were found to be 0.038152 and 0.114577 μg/ml, respectively. Results of analysis were validated statistically and by recovery studies.

5. CHROMATOGRAPHIC METHODS OF ANALYSIS

5.1. Thin-layer chromatography

El Zeany *et al*. [11] described two methods for the determination of zolpidem hemitartrate in presence of its degradation product. The first method was a TLC-UV densitometric one in which the mobile phase methanol:water (20:80) was used for developing the TLC plates. The R_f of zolpidem hemitartrate was found to be 0.29 ± 0.01 and that of its degradation product was 0.59 ± 0.01. Linearity range was 0.5–4 μg/spot with mean recovery percentage ($99.98 \pm 0.988\%$).

5.2. Gas chromatography [12–15]

A gas chromatographic (GC) method using a short, high-resolution capillary column connected to a specific thermo-ionic detector and requiring a simple and short extraction step without evaporation was developed by Debruyne *et al*. [12] for the rapid and precise determination of two new hypnotics, zolpidem and zopiclone, in serum at concentrations >5 ng/ml. The assay was linear between 5 and 200 ng/ml, with coefficients of intra- and interassay variation <5% for both. The method was validated and then used to analyze zolpidem serum concentrations in nine rabbits after oral administration of 0.5 mg/kg and zopiclone serum concentrations in six patients treated orally with a 7.5-mg dose.

Gaillard *et al*. [13] developed a rapid twin-column GC method for simultaneous screening and determination of commonly prescribed benzodiazepines and other new anxiolytics from plasma. Identical fused-silica Ultra 2 (5% phenyl methyl silicone) columns were connected to nitrogen-phosphorus and electron-capture detectors. The drugs were isolated from 1 ml of plasma by solid-phase extraction (SPE) onto a C_8 reversed-phase sorbent and recovered with 0.5% acetic acid in methanol. The eluate was reconstituted with isopropanol which was found suitable for on-column injection. Prazepam was used as internal standard. The method was found appropriate for the quantification in a single run of alpidem, alprazolam, buspirone, chlordiazepoxide, clobazam, clotiazepam, diazepam, estazolam, flunitrazepam, lorazepam, midazolam, oxazepam, tofisopam, triazolam, and zolpidem within 30 min. Limits of quantification allow toxicological or pharmacological determinations, except for buspirone: only toxic blood levels can be quantified by this method. This first SPE of imidazopyridines (alpidem and zolpidem)

provides faster, more efficient, and cheaper sample preparation than the traditional liquid–liquid procedure. This GC analysis of alpidem and zolpidem is also the first described procedure for simultaneous quantification of all different classes of anxiolytics.

A simple, specific, and selective method for the simultaneous determination of zolpidem and zopiclone in human plasma is described by Stanke *et al*. [14]. After a liquid–liquid extraction, the extract is injected into a capillary gas chromatograph with an OV-1 fused-silica column coupled to a nitrogen-phosphorus detector. The detection limits are 1 and 2ng/ml for zolpidem and zopiclone, respectively. The method described is reproducible and linear over a range of concentrations, rendering it suitable for use for pharmacokinetic studies or toxicological evaluations. Absolute identification of the chromatographed compounds is accomplished by gas chromatography–mass spectrometry in both electron-impact and positive-ion chemical ionization modes.

An ingestion of an unknown quantity of Ivadal® (zolpidem) tablets in a case of drug abuse is described by Keller *et al*. [15]. The authors report a new and fast method of analyzing and determining the zolpidem concentration in postmortem specimens. Quantitation of zolpidem was performed by ethyl acetate extraction from alkalinized body fluids before GC/MS analysis. The analyses were performed without any complex sample clean-up steps and with little sample material. Postmortem concentrations of zolpidem in body fluids are given. The proposed method is a rapid procedure of analysis in cases of deliberate poisoning with the sedative–hypnotic drug, zolpidem.

5.3. High-performance liquid chromatography

Laviana *et al*. [16] developed a high-performance liquid chromatographic (HPLC) assay with diode-array detection for the in-process control of zolpidem synthesis and for the analysis of the drug and its synthetic intermediates. The separation uses a 4.6mm i.d. reversed-phase Kromasil C_{18} (150mm) column, 5μm particle size with a gradient elution mode of acetonitrile, and 0.02M NH_4OAc (adjusted to pH 8.0) as the mobile phase (flow rate 1.0mlmin^{-1}). The analysis is performed in 12min. The method is simple, rapid, and highly specific.

Another HPLC method was developed by El Zeany *et al*. [11]. HPLC was performed on a Bondapak C_{18} column. The mobile phase was composed of a mixture of acetonitrile 0.01M KH_2PO_4 (40:60). The pH was adjusted to 3.5$\pm$0.1. Flow rate was 1.2ml/min. Calibration graphs were linear in the range of 0.5–5μg/ml with UV detection at 245nm. Both methods have been successfully applied to pharmaceutical formulations. The results obtained were statistically compared with those obtained by applying the reported methods.

5.4. Capillary electrophoresis

A method for the determination of zolpidem and its main metabolites in urine without extraction using capillary electrophoresis with UV laser-induced fluorescence detection with a He-Cd laser was reported by Hempel and Blaschke [17]. A 10-nl sample of urine can be directly applied to the capillary. The separation is carried out within 10min, and the limit of detection is 2ng/ml. This procedure is very simple and fast. No organic solvents are necessary.

6. DETERMINATION IN BODY FLUIDS AND TISSUES

6.1. Radioimmunoassay methods

The development of a specific and sensitive radioimmunoassay for the detection of zolpidem and its metabolites in urine and serum samples is described [18]. The assay can be used to prescreen forensic and emergency samples. 6-Methyl-2-(4-methylphenyl)imidazo[1,2-a]-pyridine-3-acetic acid was prepared as a hapten and was coupled directly and indirectly to bovine serum albumin. The immunization of rabbits with the hapten–bovine serum albumin conjugates resulted in the production of highly specific antibodies, showing no significant cross-reactivities toward existing drugs. The four-parameter logistic model was used to process the calibration data into a fitting curve (r^2=0.9764). Intra- and interassay relative standard deviations (RSDs) were <6.30 and <12.28%, respectively. The limit of quantification was 0.1 ng ml^{-1}. Using this assay, zolpidem levels were determined in urine and serum and could be easily detected up to 48h after oral intake of 10mg of zolpidem.

6.2. Chromatographic methods

A simple, reliable HPLC method with fluorescence detection (excitation 320 and emission 388nm) was developed and validated by Nirogi *et al.* [19] for quantitation of zolpidem in human plasma. Following a single-step liquid–liquid extraction, the analyte and internal standard (quinine) were separated using an isocratic mobile phase on a reversed-phase C_{18} column. The lower limit of quantitation was 1.8ng/ml, with a RSD of less than 5%. A linear dynamic range of 1.8–288ng/ml was established. This HPLC method was validated with between-batch and within-batch precision of 1.7–4.8% and 1.2–2.3%, respectively. The between-batch and within-batch accuracy was 95.3–100.4% and 95.5–102.7%, respectively. Frequently coadministered drugs did not interfere with the described methodology. Stability of zolpidem in plasma was excellent, with no

evidence of degradation during sample processing (autosampler) and 30 days storage in a freezer. This validated method is simple and repeatable enough to be used in pharmacokinetic studies.

Bhatt *et al*. [7] established a simple and robust method for quantification of zolpidem in human plasma using liquid chromatography–electrospray ionization tandem mass spectrometry (LC-ESI MS/MS). Escitalopram was used as an internal standard. Zolpidem and internal standard in plasma sample were extracted using SPE cartridges (Oasis HLB, $1\,cm^3/30\,mg$). The samples were injected into a C_8 reversed-phase column and the mobile phase used was acetonitrile–ammonium acetate (pH 4.6; 10 mm) (80:20, v/v) at a flow rate of 0.7 ml/min. Using MS/MS in the selected reaction monitoring (SRM) mode, zolpidem and escitalopram were detected without any interference from human plasma matrix. Zolpidem produced a protonated precursor ion ($[M+H]^+$) at *m/z* 308.1 and a corresponding product ion at *m/z* 235.1. The internal standard produced a protonated precursor ion ($[M+H]^+$) at *m/z* 325.1 and a corresponding product ion at *m/z* 262.1. Detection of zolpidem in human plasma by the LC-ESI MS/MS method was accurate and precise with a quantification limit of 2.5 ng/ml. The proposed method was validated in the linear range 2.5–300 ng/ml. Reproducibility, recovery, and stability of the method were evaluated. The method has been successfully applied to bioequivalence studies of zolpidem.

For the determination of zolpidem, a new sleep inducer, and its metabolites in human plasma and urine, three methods were developed by Ascalone *et al*. [20] that are suitable for pharmacokinetics, drug metabolism, and overdosing investigations. The methods used for pharmacokinetic and drug metabolism studies are based on column-switching HPLC; they do not require any sample manipulation because the plasma or diluted urine is injected into a precolumn where clean-up and preconcentration take place. The analytes are transferred by valve-switching to the C_{18} analytical column for chromatography. To investigate overdose cases, urine samples only are used: the method is simple, because the diluted urine can be injected directly into the analytical column (phenyl type). This allows the identification and quantification of the principal urinary metabolite of zolpidem, the unchanged drug being practically undetectable. All the methods use fluorescence detection, which affords high sensitivity and selectivity. It is necessary to use a method capable of determining metabolites even if these are apparently pharmacologically inactive, because in different physiopathological populations, the qualitative and quantitative metabolic profiles of zolpidem could be different. The method designed for the investigation of (accidental or deliberate) overdose cases is, as required on such occasions, simple and rapid, with good selectivity with respect to commonly prescribed psychotropic drugs.

Wanga *et al.* [21] described a single-solvent extraction step HPLC method for quantitating zolpidem in rat serum microsamples (50 μl). The separation used a 2.1 mm i.d. reversed-phase OD-5-100 C_{18} column, 5 μm particle size with an isocratic mobile phase consisting of methanol–acetonitrile–26 m*M* sodium acetate buffer (adjusted to pH 2.0 with 40% phosphoric acid) containing 0.26 m*M* tetrabutylammonium phosphate (13:10:77, v/v/v). The detection limit was 3 ng/ml for zolpidem using an ultraviolet detector operated at 240 nm. The recovery was greater than 87% with analysis performed in 12 min. The method is simple, rapid, and applicable to pharmacokinetic studies of zolpidem after administering two intravenous bolus doses (1 and 4 mg/kg) in rats.

A sensitive and selective HPLC method was developed by Ring and Bostick [22] for the determination of zolpidem in human plasma. Zolpidem and the internal standard (trazodone) were extracted from human plasma that had been made basic. The basic sample was loaded onto a conditioned Bond Elut C_{18} cartridge, rinsed with water and eluted with methanol. Forty microliters was then injected onto the LC system. Separation was achieved on a C_{18} column (150 × 4.6 mm, 5 μm) with a mobile phase composed of acetonitrile:50 mM potassium phosphate monobasic at pH 6.0 (4:6, v/v). Detection was by fluorescence, with excitation at 254 nm and emission at 400 nm. The retention times of zolpidem and internal standard were approximately 4.7 and 5.3 min, respectively. The LC run time was 8 min. The assay was linear in concentration range 1–400 ng/ml for zolpidem in human plasma. The analysis of quality control samples for zolpidem (3, 30, and 300 ng/ml) demonstrated excellent precision with RSDs of 3.7%, 4.6%, and 3.0%, respectively ($n = 18$). The method was accurate with all intraday ($n = 6$) and overall ($n = 18$) mean concentrations within 5.8% from nominal at all quality control sample concentrations. This method was also performed using a Gilson Aspec XL automated sample processor and autoinjector. The samples were manually fortified with internal standard and made basic. The Aspec then performed the SPE and made injections of the samples onto the LC system. Using the automated procedure for analysis, quality control samples for zolpidem (3, 30, and 300 ng/ml) demonstrated acceptable precision with RSD values of 9.0%, 4.9%, and 5.1%, respectively ($n = 12$). The method was accurate with all intracurve ($n = 4$) and overall ($n = 12$) mean values being less than 10.8% from nominal at all quality control sample concentrations.

Ptácek *et al.* [23] developed a simple and reproducible method for the determination of zolpidem in human plasma. This method involves protein precipitation with methanol (2 ml of methanol is added to 0.5 ml of plasma) and reversed-phase chromatography with fluorescence detection (excitation wavelength 244 nm, emission wavelength 388 nm). The mobile phase consists of methanol–30 m*M* dihydrogen potassium

phosphate–triethylamine (30:69:1). The pH of the aqueous part of the mobile phase is 6.8. No internal standard is required. Limit of quantitation is 1.5 ng/ml and the calibration curve is linear up to 400 ng/ml. Within-day and between-day precision expressed by RSD is less than 5% and inaccuracy also does not exceed 9%. The assay is useful for pharmacokinetic studies.

A liquid chromatography–tandem mass spectrometry method was developed by Laloup *et al.* [24] for the simultaneous quantification of 26 benzodiazepines and metabolites, zolpidem and zopiclone, in blood, urine, and hair. Drugs were extracted from all matrices by liquid–liquid extraction with 1-chlorobutane. Chromatography was achieved using an XTerra MS C_{18} column eluted with a mixture of methanol and formate buffer. Data were acquired using positive electrospray ionization and multiple reaction monitoring using one precursor ion/product ion transition per compound. Quantification was performed using 13 deuterated analogues. Further confirmation of the identity of the compounds was achieved through a second injection of positive samples, monitoring two transitions per compound. The limits of quantification for all benzodiazepines ranged from 1 to 2 ng/ml in blood, 10 to 25 ng/ml in urine, and 0.5 to 10 pg/mg in hair. Linearity was observed from the limit of quantification of each compound to 200 ng/ml, 1000 ng/ml, and 1000 pg/mg for blood, urine, and hair, respectively ($r^2 > 0.99$). Precision for quality control samples, spiked at three concentrations, was calculated (CV <20% in most cases). Extraction recoveries for the three matrices ranged from 25.1% to 103.8%, except for one compound (cloxazolam in urine). Ion suppression was studied for all matrices. The validated assay was applied to authentic blood, urine, and hair samples from forensic cases.

7. ADME PROFILES OF DRUG SUBSTANCES AND EXCIPIENTS

7.1. Uses, applications, and pertinent history

Zolpidem is a nonbenzodiazepine sedative–hypnotic drug that became available in the United States in 1993 after 5 years of use in Europe [25]. It is classified as an imidazopyridine.

Although the actions of zolpidem are due to agonist effects on $GABA_A$ receptors and generally resemble those of benzodiazepines, it produces only weak anticonvulsant effects in experimental animals, and its relatively strong sedative actions appear to mask anxiolytic effects in various animal models of anxiety [26]. Although chronic administration of zolpidem to rodents produces neither tolerance to its sedative effects nor signs of withdrawal when the drug is discontinued and flumazenil is injected [27], tolerance and physical dependence have been observed with chronic administration of zolpidem to baboons [28]. Unlike the benzodiazepines, zolpidem has little effect on the stages of sleep in normal human subjects.

The drug is as effective as benzodiazepines in shortening sleep latency and prolonging total sleep time in patients with insomnia. After discontinuation of zolpidem, the beneficial effects on sleep reportedly persist for up to 1 week [29], but mild rebound insomnia on the first night also has occurred [30]. Tolerance and physical dependence develop only rarely and under unusual circumstances [31,32]. Indeed, zolpidem-induced improvement in sleep time of chronic insomniacs was sustained during as much as 6 months of treatment without signs of withdrawal or rebound after stopping the drug [33]. Nevertheless, zolpidem is approved only for the short-term treatment of insomnia. At therapeutic doses (5–10 mg), zolpidem infrequently produces residual daytime sedation or amnesia, and the incidence of other adverse effects (e.g., gastrointestinal complaints or dizziness) also is low. As with the benzodiazepines, large overdoses of zolpidem do not produce severe respiratory depression unless other agents (e.g., ethanol) also are ingested [34]. Hypnotic doses increase the hypoxia and hypercarbia of patients with obstructive sleep apnea.

7.2. Absorption

Zolpidem is absorbed readily from the gastrointestinal tract; first-pass hepatic metabolism results in an oral bioavailability of about 70%, but this value is lower when the drug is ingested with food because of slowed absorption and increased hepatic blood flow.

7.3. Distribution

Protein binding is about 92.5%. Volume of distribution (l/kg)=0.54=0.68.

7.4. Metabolism

Zolpidem produces sedative and hypnotic effects via interaction with the GABA–benzodiazepine receptor complex, with relative selectivity for the Type 1 (omega-1) benzodiazepine receptor subtype [35,36]. Zolpidem is extensively metabolized in humans, with parallel hydroxylation reactions at three distinct sites on the molecule (Figs. 11.4 and 11.5) [37,38]. Further oxidation of the M-3 metabolite yields an acid derivative which is of major quantitative importance [17,20]. Zolpidem metabolism is mediated by human cytochromes P450 (CYPs), with CYP3A reported as having a dominant role based on *in vitro* studies of cDNA-expressed human cytochromes, as well as susceptibility to inhibition by ketoconazole and anti-3A antibodies in liver microsomes [39]. Expressed cytochrome studies also indicated a contributory role of CYP1A2 and 2D6, but not of 2A6, 2E1, and 2C8. However, the possible participation of 2C9 or 2C19 has not been assessed.

HPLC assay for the analysis of zolpidem

Stationary phase	Mobile phase	Detector	Remarks	References
Reversed-phase Kromasil C_{18} (150nm) column, 5-µm particle size	Acetonitrile, 0.02M NH_4OAc (adjusted to pH 8.0)	Diode-array detection	In-process control of zolpidem synthesis and analysis of the drug and its synthetic	[16]
Bondapak C_{18} column	Acetonitrile–0.01M KH_2PO_4 (40:60), pH 3.5±0.1	UV detection at 245nm	Determination of zolpidem hemitartrate in pharmaceutical preparations	[11]
Reversed-phase C_{18} column		Fluorescence detection (excitation 320nm and emission 388nm)	Quantification in human plasma	[19]
C_8 reversed-phase column	Acetonitrile–ammonium acetate (pH 4.6; 10mm) (80:20, v/v)	Electrospray ionization tandem mass spectrometry (LC-ESI MS/MS)	Quantification in human plasma	[7]
C_{18} analytical column		Fluorescence detection	Determination of the drug and its metabolites in biological fluids (plasma and urine)	[20]

(*continued*)

Stationary phase	Mobile phase	Detector	Remarks	References
Reversed-phase OD-5-100 C_{18} column, 2.1 mm i.d., 5-μm particle size	Methanol–acetonitrile–26 mM sodium acetate buffer (adjusted to pH 2.0 with 40% phosphoric acid) containing 0.26 mM tetrabutylammonium phosphate (13:10:77, v/v/v)	UV detection at 240 nm	Determination of the drug in serum microsamples	[21]
C_{18} column (150 × 4.6 mm, 5-μm particle size)	Acetonitrile:50 mM potassium phosphate monobasic at pH 6.0 (4:6, v/v)	Fluorescence detection with excitation at 254 nm and emission at 400 nm	Determination in human plasma	[22]
Reversed phase	Methanol–30 mM dihydrogen potassium phosphate–triethylamine (30:69:1). pH of the aqueous part of the mobile phase is 6.8	Fluorescence detection (excitation wavelength 244 nm, emission wavelength 388 nm)	Determination in human plasma	[23]
XTerra MS C_{18} column	Methanol and formate buffer	Tandem mass spectrometry	Simultaneous quantification of 26 benzodiazepines and metabolites, zolpidem and zopiclone, is blood and urine	[24]
Inertsil ODS-3 column	Ammonium formate buffer/acetonitrile	ESI/MS	Determination of the drug and its metabolites in biological fluids	[20]

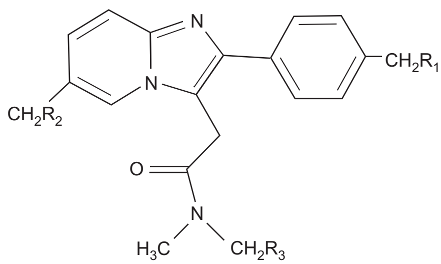

Compound	R_1	R_2	R_3
Zolpidem	H	H	H
M-3 metabolite	OH	H	H
M-4 metabolite	H	OH	H
M-11 metabolite	H	H	OH

FIGURE 11.4 Structure of zolpidem and its principal metabolites.

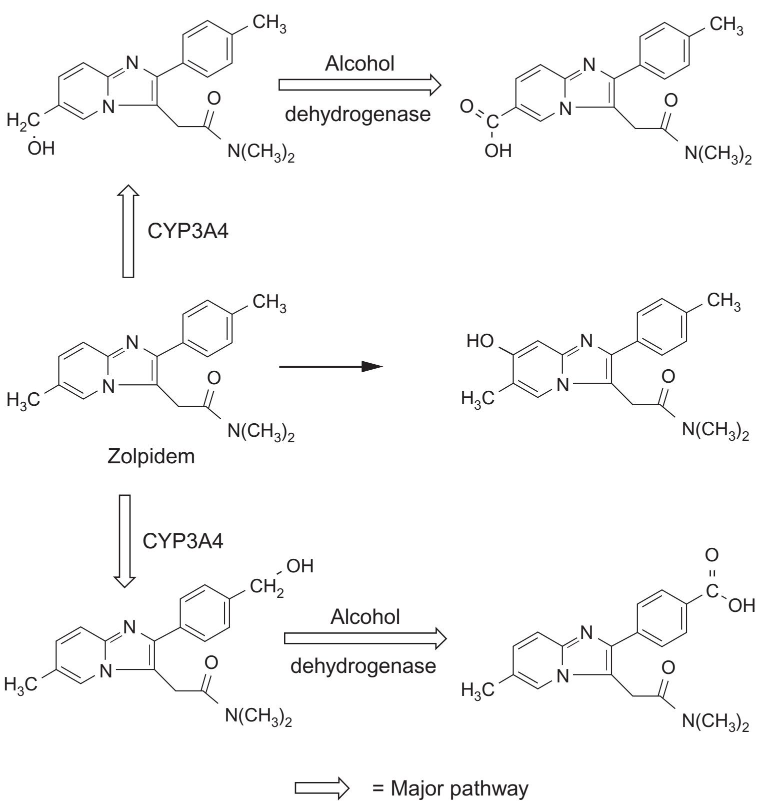

FIGURE 11.5 Metabolic pathway of zolpidem.

7.5. Elimination

Zolpidem is eliminated almost entirely by conversion to inactive products in the liver, largely through oxidation of the methyl groups on the phenyl and imidazopyridine rings to the corresponding carboxylic acids.

Its plasma half-life is approximately 2h in individuals with normal hepatic blood flow or function. This value may be increased twofold or more in those with cirrhosis and also tends to be greater in older patients; adjustment of dosage often is necessary in both categories of patients. Although little or no unchanged zolpidem is found in the urine, elimination of the drug is slower in patients with chronic renal insufficiency largely owing to an increase in its apparent volume of distribution.

7.6. Mechanism of action

Due to its selective binding, zolpidem has very weak anxiolytic, myorelaxant, and anticonvulsant properties but very strong hypnotic properties [40]. Zolpidem binds with high affinity and acts as a full agonist at the α_1-containing $GABA_A$ receptors, about 10-fold lower affinity for those containing the α_2- and α_3-$GABA_A$ receptor subunits, and with no appreciable affinity for α_5 subunit-containing receptors [41,42]. ω_1 Type $GABA_A$ receptors are the α_1-containing $GABA_A$ receptors and ω_2 $GABA_A$ receptors are the α_2-, α_3-, α_4-, α_5-, and α_6-containing $GABA_A$ receptors. ω_1 $GABA_A$ receptors are primarily found in the brain whereas ω_2 receptors are primarily found in the spine. Thus, zolpidem has a preferential binding for the $GABA_A$–benzodiazepine receptor complex in the brain but a low affinity for the $GABA_A$–benzodiazepine receptor complex in the spine [43].

Like the vast majority of benzodiazepine-like molecules, zolpidem has no affinity for α_4 and α_6 subunit-containing receptors [44]. Zolpidem positively modulates $GABA_A$ receptors, probably by increasing the $GABA_A$ receptor complexes' apparent affinity for GABA, without affecting desensitization or peak current [45]. Zolpidem increases slow-wave sleep and caused no effect on stage 2 sleep in laboratory tests [46].

A meta-analysis of the randomized controlled clinical trials that compared benzodiazepines against *Z-drugs* such as zolpidem has shown that there are few consistent differences between zolpidem and benzodiazepines in terms of sleep onset latency, total sleep duration, number of awakenings, quality of sleep, adverse events, tolerance, rebound insomnia, and daytime alertness [47].

7.7. Pharmacological effects

Zolpidem is not a benzodiazepine; it acts on a subunit of the benzodiazepine receptor family BZ1. Zolpidem has no anticonvulsant or muscle-relaxant properties. It shows no withdrawal effects and exhibits minimal

rebound insomnis and little or no tolerance with prolonged use. Zolpidem is rapidly absorbed from the gastrointestinal tract, and it has a rapid onset of action and short elimination half-life (about 2–3h). Zolpidem undergoes hepatic oxidation by the CYP system to inactive products. Drugs such as rifampin, which induce this enzyme system, shorten the half-life of zolpidem. Adverse effects of zolpidem include nightmares, agitation, headache, gastrointestinal upset, dizziness, and daytime drowsiness.

8. METHODS OF CHEMICAL SYNTHESIS

8.1. Preparative chemical methods

The reported synthesis (Scheme 11.1) of zolpidem involved the bromination of 4-methyl acetophenone (2) followed by condensation of resultant bromo derivative (3) with 2-amino 5-methyl pyridine 3 to give an imidazo pyridine intermediate compound 4, which upon Mannich reaction 4 gave *N*,*N*-dimethyl amino imidazopyridine derivative 5. Compound 5 was further converted into its cyano methyl imidazo pyridine derivative 7 through a methyl iodide quaternary salt 6. The cyano compound 7 on alkaline hydrolysis yielded a pyridine acetic acid compound 8[5]. Finally, the key intermediate 8 reacted with carbonyldiimidazole 6 and followed by amidation with anhydrous dimethyl amine yielded zolpidem [48].

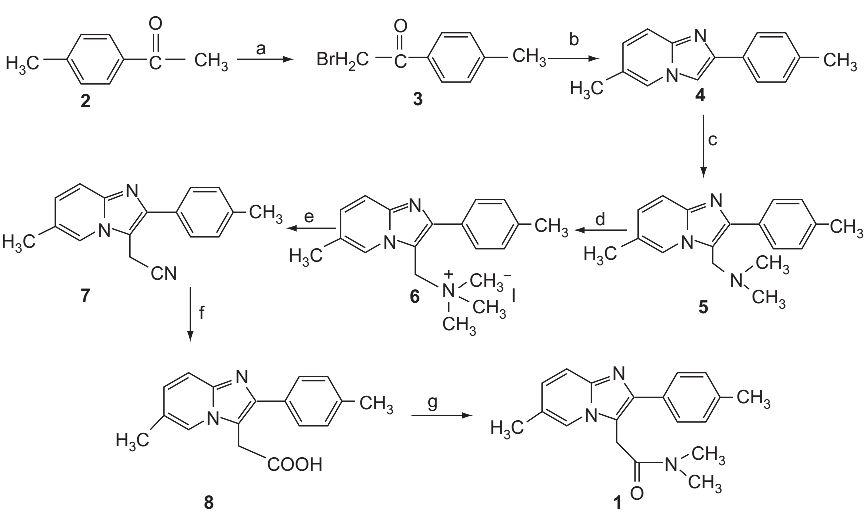

SCHEME 11.1 Reported synthetic scheme for zolpidem [48].

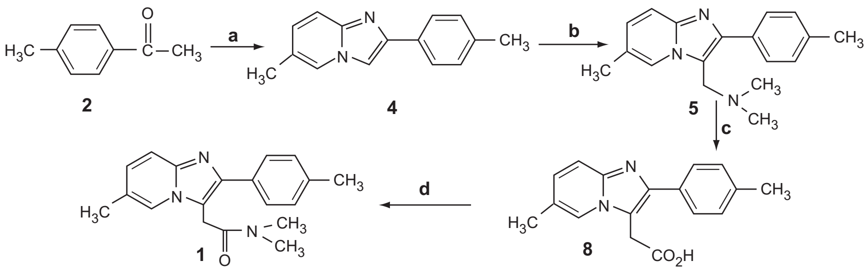

SCHEME 11.2 Improved synthetic scheme for zolpidem [48].

Reagents and conditions: (a) Bromine/acetic acid/-5-0°C. (b) 2-Amino-5-methyl pyridine, ethanol/$NaHCO_3$/reflux. (c) Acetic acid/aq. dimethylamine/formalin/RT. (d) Acetone, CH_3I/reflux. (e) NaCN, ethanol/reflux. (f) KOH/ethanol/reflux. (g) Carbonyldiimidazole, THF/dimethyl amine/RT.

The reported seven-stage process suffers from several disadvantages such as (a) it is very difficult to handle the lachrymatory bromo compound **3** at multi-scale-up level and requires more attention to avoid the exposure to the material, especially at the time of product filtration and drying. (b) Multistep synthesis for compound **8** (3 steps from compound **5**). (c) Isolation (drying operations) of intermediates such as compounds **3**, **6**, and **7** and their individual work-up procedures led to increased life cycle time which in turn led to increase in the manufacturing cost. (d) Fifth stage work-up procedure is hazardous and hence a lot of safety measures need to be taken with respect to handling of stage **5** solid material as it may contain residual cyanide. (e) Usage of carbonyldiimidazole (CDI) in the final stage may pose a big problem as it is a highly moisture-sensitive reagent and some times, reactions are not proceeding for completion if the compound **8** contains even 0.5% of w/w moisture content, in addition to that larger amounts of imidazole is formed as a by-product. (f) The overall yield of 40% from this process is also discouraging, which makes the process less viable for commercial production (Scheme 11.2).

REFERENCES

[1] The Merck Index, 13th ed., Merck Research Laboratories, Division of Merck and Co., Inc, Whitehouse Station, NJ, 2001 p. 10162.
[2] http://www.drugs.com/ppa/zolpidem-tartarate.html.
[3] Clarke's Analysis of Drugs and Poisons, 3rd ed., The Pharmaceutical Press, UK, 2005.
[4] The British Pharmacopeia, Her majesty's Stationary Office, London, 2009.

[5] M. Lawecka, B. Kosmacinska, M. Glice, K. Korczak, The influence of storage conditions on the polymorphic stability of zolpidem tartrate hydrates, J. Therm. Anal. Calorim. 83 (2006) 583–585.
[6] G. Trapani, A. Latrofa, M. Franco, M.R. Pantaleo, E. Sanna, F. Massa, F. Tuveri, G. Liso, Complexation of zolpidem with 2-hydroxypropyl-beta-, methyl-beta-, and 2-hydroxypropyl-gamma-cyclodextrin: effect on aqueous solubility, dissolution rate, and ataxic activity in rat, J. Pharm. Sci. 89 (2000) 1443–1451.
[7] J. Bhatt, A. Jangid, R. Shetty, B. Shah, S. Kambli, G. Subbaiah, S. Singh, Quantification of zolpidem in human plasma by liquid chromatography–electrospray ionization tandem mass spectrometry, Biomed. Chromatogr. 20 (2006) 736–742.
[8] K.M. Kelani, Selective potentiometric determination of zolpidem hemitartrate in tablets and biological fluids by using polymeric membrane electrodes, J. AOAC Int. 87 (6) (2004) 1309–1318.
[9] A. Radi, G. Bekheit, T. Wahdan, Electrochemical study of zolpidem at glassy carbon electrode and its determination in a tablet dosage form by differential pulse voltammetry, Chem. Pharm. Bull. 52 (2004) 1063.
[10] K.S. Patil, et al., Spectrophotometric estimation of zolpidem in tablets, J. Pharm. Sci. Res. 2 (2010) 1–4.
[11] B.A. El Zeany, A.A. Moustafa, N.F. Farid, Determination of zolpidem hemitartrate by quantitative HPTLC and LC, J. Pharm. Biomed. Anal. 33 (2003) 393–401.
[12] D. Debruyne, J. Lacotte, B. De Hurault Ligny, M. Moulin, Determination of zolpidem and zopiclone in serum by capillary column gas chromatography, J. Pharm. Sci. 80 (1991) 71–74.
[13] Y. Gaillard, J.-P. Gay-Montchamp, M. Ollagnier, Simultaneous screening and quantitation of alpidem, zolpidem, buspirone and benzodiazepines by dual-channel gas chromatography using electron-capture and nitrogen-phosphorus detection after solid-phase extraction, J. Chromatogr. 622 (1993) 197–208.
[14] F. Stanke, N. Jourdil, J. Bessard, G. Bessard, Simultaneous determination of zolpidem and zopiclone in human plasma by gas chromatography-nitrogen-phosphorus detection, J. Chromatogr. B Biomed. Sci. Appl. 675 (1996) 43–51.
[15] T. Keller, A. Schneider, E. Tutsch-Bauer, GC/MS determination of zolpidem in postmortem specimens in a voluntary intoxication, Forensic Sci. Int. 106 (1999) 103–108.
[16] L. Lavianaa, C. Mangasa, F. Fernández-Maríb, M. Bayodb, D. Blancoa, Determination and in-process control of zolpidem synthesis by high-performance liquid chromatography, J. Pharm. Biomed. Anal. 36 (2004) 925–928.
[17] G. Hempel, G. Blaschke, Direct determination of zolpidem and its main metabolites in urine using capillary electrophoresis with laser-induced fluorescence detection, J. Chromatogr. B Biomed. Sci. Appl. 675 (1996) 131–137.
[18] I. De Clerck, P. Daenens, Development of a radioimmunoassay for the determination of zolpidem in biological samples, Analyst 122 (1997) 1119–1124.
[19] R.V.S. Nirogi, V.N. Kandikere, W. Shrivasthava, K. Mudigonda, Quantification of zolpidem in human plasma by high-performance liquid chromatography with fluorescence detection, Biomed. Chromatogr. 20 (2006) 1103–1108.
[20] V. Ascalone, L. Flaminio, P. Guinebault, J.P. Thénot, P.L. Morselli, Determination of zolpidem, a new sleep-inducing agent, and its metabolites in biological fluids: pharmacokinetics, drug metabolism and overdosing investigations in humans, J. Chromatogr. 581 (1992) 237–250.
[21] Q. Wanga, L. Sunb, C.E. Lau, Determination of zolpidem in serum microsamples by high-performance liquid chromatography and its application to pharmacokinetics in rats, J. Chromatogr. B Biomed. Sci. Appl. 734 (1999) 299–305.
[22] P.R. Ring, J.M. Bostick, Validation of a method for the determination of zolpidem in human plasma using LC with fluorescence detection, J. Pharm. Biomed. Anal. 22 (2000) 495–504.

[23] P. Ptácek, J. Macek, J. Klíma, Rapid and simple method for the determination of zolpidem in human plasma by high-performance liquid chromatography, J. Chromatogr. B Biomed. Sci. Appl. 694 (1997) 409–413.
[24] M. Laloup, M. Ramirez Fernandez Mdel, G. De Boeck, M. Wood, V. Maes, N. Samyn, Validation of a liquid chromatography-tandem mass spectrometry method for the simultaneous determination of 26 benzodiazepines and metabolites, zolpidem and zopiclone, in blood, urine, and hair, J. Anal. Toxicol. 29 (2005) 616–626.
[25] H.D. Langtry, P. Benfield, Zolpidem: a review of its pharmacodynamic and pharmacokinetic properties and therapeutic potential, Drugs 40 (1990) 291–313.
[26] K.J. Holm, K.L. Goa, Zolpidem: an update of its pharmacology, therapeutic efficacy and tolerability in the treatment of insomnia, Drugs 59 (2000) 865–889.
[27] G. Perrault, E. Morel, D.J. Sanger, B. Zivkovic, Lack of tolerance and physical dependence upon repeated treatment with the novel hypnotic zolpidem, J. Pharmacol. Exp. Ther. 263 (1992) 298–303.
[28] R.R. Griffiths, C.A. Sannerud, N.A. Ator, J.V. Brady, Zolpidem behavioral pharmacology in baboons: self-injection, discrimination, tolerance and withdrawal, J. Pharmacol. Exp. Ther. 260 (1992) 1199–1208.
[29] W.M. Herrmann, S.T. Kubicki, S. Boden, et al., Pilot controlled, double-blind study of the hypnotic effects of zolpidem in patients with chronic ''learned'' insomnia: psychometric and polysomnographic evaluation, J. Int. Med. Res. 21 (1993) 306–322.
[30] Anonymous, Zolpidem for insomnia., Med. Lett. Drugs Ther. 35 (1993) 35–36.
[31] R. Cavallaro, M.G. Regazzetti, G. Covelli, E. Smeraldi, Tolerance and withdrawal with zolpidem, Lancet 342 (1993) 374–375.
[32] P.L. Morselli, Zolpidem side effects, Lancet 342 (1993) 868–869.
[33] J. Kummer, L. Guendel, J. Linden, et al., Long-term polysomnographic study of the efficacy and safety of zolpidem in elderly psychiatric in-patients with insomnia, J. Int. Med. Res. 21 (1993) 171–184.
[34] R. Garnier, E. Guerault, D. Muzard, et al., Acute zolpidem poisoning—analysis of 344 cases, J. Toxicol. Clin. Toxicol. 32 (1994) 391–404.
[35] D.J. Sanger, J. Benavides, G. Perrault, et al., Recent developments in the behavioral pharmacology of benzodiazepine receptors: evidence for the functional significance of receptor subtypes, Neurosci. Biobehav. Rev. 18 (1994) 355–372.
[36] J.J. Byrnes, D.J. Greenblatt, L.G. Miller, Benzodiazepine receptor binding of nonbenzodiazepines *in vivo*: alpidem, zolpidem, and zopiclone, Brain Res. Bull. 29 (1992) 905–908.
[37] P. Salvà, J. Costa, Clinical pharmacokinetics and pharmacodynamics of zolpidem: therapeutic implications, Clin. Pharmacokinet. 29 (1995) 142–153.
[38] A. Durand, J.P. Thénot, G. Bianchetti, et al., Comparative pharmacokinetic profile of two imidazopyridine drugs: zolpidem and alpidem, Drug Metab. Rev. 24 (1992) 239–266.
[39] L. Pichard, G. Gillet, C. Bonfils, et al., Oxidative metabolism of zolpidem by human liver cytochrome P450s, Drug Metab. Dispos. 23 (1995) 1253–1262.
[40] D.B. Pritchett, P.H. Seeburg, Gamma-aminobutyric acidA receptor alpha 5-subunit creates novel type II benzodiazepine receptor pharmacology, J. Neurochem. 54 (1990) 1802–1804.
[41] A.J. Smith, L. Alder, J. Silk, C. Adkins, A.E. Fletcher, T. Scales, J. Kerby, G. Marshall, et al., Effect of alpha subunit on allosteric modulation of ion channel function in stably expressed human recombinant gamma-aminobutyric acid(A) receptors determined using (36)Cl ion flux, Mol. Pharmacol. 59 (2001) 1108–1118.
[42] J.K. Rowlett, W.L. Woolverton, Assessment of benzodiazepine receptor heterogeneity in vivo: apparent pA2 and pKB analyses from behavioral studies, Psychopharmacology (Berl) 128 (1996) 1–16.

[43] K.A. Wafford, S.A. Thompson, D. Thomas, J. Sikela, A.S. Wilcox, P.J. Whiting, Functional characterization of human gamma-aminobutyric acidA receptors containing the alpha 4 subunit, Mol. Pharmacol. 50 (1996) 670–678.
[44] D. Perrais, N. Ropert, Effect of zolpidem on miniature IPSCs and occupancy of postsynaptic GABAA receptors in central synapses, J. Neurosci. 19 (1999) 578–588.
[45] H. Noguchi, K. Kitazumi, M. Mori, T. Shiba, Electroencephalographic properties of zaleplon, a non-benzodiazepine sedative/hypnotic, in rats, J. Pharmacol. Sci. 94 (2004) 246–251.
[46] Y. Dündar, S. Dodd, J. Strobl, A. Boland, R. Dickson, T. Walley, Comparative efficacy of newer hypnotic drugs for the short-term management of insomnia: a systematic review and meta-analysis, Hum. Psychopharmacol. 19 (2004) 305–322.
[47] J.S. Wang, C.L. DeVane, Pharmacokinetics and drug interactions of the sedative hypnotics, Psychopharmacol. Bull. 37 (2003) 10–29.
[48] Y. Sumalatha, T.R. Reddy, P.P. Reddy, B. Satyanarayana, A simple, efficient and scalable synthesis of hypnotic agent, zolpidem, Arkivoc ii (2009) 315–320.

CHAPTER 12

Validation of Analytical Methods—Update 2011

Gunawan Indrayanto

Contents

1. INTRODUCTION

According to the United States Pharmacopoeia, validation of an analytical method is the process by which laboratory studies establish that the performance characteristics of the method meet the requirements for the intended analytical applications. Therefore, the objective of the validation procedure is to ensure that every result of the routine analysis should be close enough to its unknown, but true, value in the samples. The difference

Faculty of Pharmacy, Airlangga University, Surabaya, Indonesia

Profiles of Drug Substances, Excipients, and Related Methodology, Volume 37
ISSN 1871-5125, DOI: 10.1016/B978-0-12-397220-0.00012-X

© 2012 Elsevier Inc.
All rights reserved.

between the measured value and the true value in the samples should be as low as possible, or at least must be within the acceptance limit.

The importance of validation of chromatographic methods of analysis for drug development in the pharmaceutical industry, as well for its quality control (QC) laboratory, has been described in our previous chapter [1]. Due to the increasing applications of high-performance thin-layer chromatography (HP-TLC) in pharmaceutical industry, a brief discussion regarding the validation method of analysis using HP-TLC methodology has been published recently [2]. The aim of this present chapter is to summarize and discuss new aspects and developments of validation procedures which have been recently published over the past 5–10 years.

2. PREVALIDATION REQUIREMENTS

The fundamental requirement for operating under good laboratory practices is to validate and calibrate the analytical instruments, the glassware, and the software. Validation of analytical instruments can be divided into installation qualification (IQ), operation qualification (OQ), and performance qualification (PQ). IQ and OQ are ordinarily performed by the manufacturer of the instrument, while PQ is performed by the user in conjunction with the manufacturer [3].

The availability of chemicals, reagents, and authentic reference standard materials of good quality is also very essential [4,5]. The analyte, as in the standard solutions, in samples, and in the solution of the sample extracts, must be stable over the entire time of analysis (i.e., sample preparation, sample extraction, and chromatographic analyses). The variation of the peak area of the analyte over time should be within ±1–2% when compared to the peak area of the freshly prepared solution with same concentration, and no new peaks can be observed.

In addition, the identity and purity of the analyte peak should be established using an alternate method (e.g., DAD, MS/MS for LC; densitometry for TLC). For LC methods (liquid chromatography) that use an automatic sampling system, it is recommended to do the evaluation at certain time intervals (1–4h) between the initial time point and the final time point (3–72h). For these purposes, solutions of the standard and sample are prepared and analyzed immediately, and these solutions are stored at normal laboratory conditions for the full elapsed time. At the end, the stored solutions are then re-analyzed against freshly prepared standard and sample having the same concentrations [6].

The stability of the analyte on HP-TLC plates should be evaluated every 1h for at least 3h [3]. In the instance of fingerprint evaluation of herbal drugs, Reich *et al.* [7] recommended to test the stability of herbal drugs and their Botanical Reference Materials (BRMs) in solution and on

the plate over at least 3h. Stability during chromatography by TLC should be tested using two-dimensional development. If the standards and samples are stable, all components can be detected on the diagonal line connecting the start position and the intersection of the two solvent fronts. The presence of spots off this line indicates the possibility of degradation. The purity evaluation of the spots can be performed also by using a densitometry method (comparing the spectra at the peak-start, apex, and peak-end) and calculating their r values (which must be greater than 0.999). If visualization requires a derivatization step, the color stability must also be evaluated. It was recommended to obtain images immediately and after 5, 10, 20, 30 min and 1 h after derivatization, and then to compare the images visually or using video-densitometry.

For bioanalytical studies, samples must remain stable during sample collection, processing, storage, extraction, and (LC-MS) analysis [8]. If the prestability testing does not show acceptable results in the desired time, the researcher should try to find more appropriate operating conditions (i.e., solvents, column/plate, working temperature, mobile phase, etc.) before continuing to perform any validation of the method of analysis. Some strategies for analyzing unstable molecules in biological matrices by LC-MS have been described in detail in a recent publication by Li *et al*. [8].

3. SPECIFICITY AND SELECTIVITY

Unfortunately, some authors still used the terms specificity and selectivity without distinction. In validation, selectivity can be graded as low, high, bad, good. etc., but specificity means 100% selectivity or 0% interference [9]. Selectivity or specificity is the most important validation parameter for (chromatographic) analysis. If the identity and the purity or homogeneity of the target peak are not confirmed first, then the results of analysis might be erroneous due to the contamination and misidentification of the desired target peak. Elution peaks are to be pure and do not co-elute with any other compounds that might have identical R_t/R_f value under the same conditions. One single target peak chromatogram which has identical R_t and R_f with the reference standard does not mean the peak is identical with the standard, and that it is pure [10]. For proving the identity and purity of target peak, a multiwave UV-VIS/DAD detector (for LC) and a densitometry method (HP-TLC/TLC) are required. These have been discussed in detail in our previous chapter [1].

At present, applications of GC-MS/MS and LC-MS/MS are significantly increasing in QC laboratories. According to the Commission Decision 2002/657/EC, analysis using a GC/LC-MS system required a minimum of 4 (four) identification points (IPs) for confirmation of the identity of substance(s) listed in Group A, and a minimum 3 (three) IPs for

substances listed in Group B (Substances Annex 1 96/23/EC) [11,12]. For other drugs which were not in the lists, it is recommended to have four IPs for confirmation of their identities.

Table 12.1 describes the number of IPs for which each MS technique can earn, and Table 12.2 shows the number of IPs associated with each chromatography–MS combination system. As example, to obtain four IPs, a GC-MS/MS or LC-MS/MS system requires the use of one precursor and two daughter ions, or two precursor ions each with one daughter ion. If the analysis was performed by using multiple monitoring reactions, a qualifier and quantifier daughter ion should be monitored for each analyte and its internal standard (IS) [13]. The ratio of the detected ions (quantifier and qualifier ions) of the analytes in samples must correspond to those of the calibration standards (CSs) measured under same conditions within the tolerances described in Table 12.3.

The guidelines published by the United States Food and Drug Administration (FDA) [14] describe that the difference of the retention time (R_t) of an analyte in a sample should be not more than 2% (GC-MS) or 5% (LC-MS) relative to its standard. For a full MS scan, at least three structurally specific ions must be identified, and in addition, there should be general correspondence between the relative abundance obtained for sample and

TABLE 12.1 Relationship between a range of classes of mass fragment and identification point earned [modified from ref. 11]

MS technique	Identification point earned per ion
Low-resolution mass spectrometry (LR-MS)	1.0
LR-MS precursor ion	1.0
LR-MS transition products	1.5
High-resolution mass spectrometry (HR-MS)	2.0
HR-MS precursor ion	2.0
HR-MS transition products	2.5

Notes:

1. Each ion is counted only once.
2. GC-MS using EI (electron impact) is regarded as being different technique to GC-MS using CI (chemical ionization).
3. Different analytes can be used to increase the number of IP only if the derivatives employ different reaction chemistries.
4. For substances which included in Group A of Annex to Directive 96/23/EC, if one of the following techniques are used in the analytical procedures: HPLC coupled with full-scan DAD, HPLC coupled with fluorescence detection, HPLC coupled to immunogram, two dimensional TLC coupled with spectrometric detection; a maximum of one IP may be contributed, providing that the relevant criteria for these techniques are fulfilled.
5. Transition products include both daughter and granddaughter products.

TABLE 12.2 The earned number of identification point (IP), *n* is an integer [modified from ref. 11]

Method	Number of ion	IP
GC-MS (EI/CI)	*N*	*n*
GC-MS (EI/CI)	2 (EI)+2 (CI)	4
GC-MS (EI/CI), 2 derivatives	2 (Derivative A) + 2 (Derivative B)	4
GC-MS-MS	1 Precursor and 2 daughter ions	4
LC-MS-MS	1 Precursor and 2 daughter ions	4
GC-MS-MS	2 Precursor ions each with 1 daughter	5
LC-MS-MS	2 Precursor ions each with 1 daughter	5
LC-MS-MS-MS-MS	1 Precursor, 1 daughter, and 2 granddaughter	5.5
HR-MS	*N*	2*n*
GC-MS+LC-MS	2+2	4
GC-MS + HR-MS	2+2	4

GC, gas chromatography; LC, liquid chromatography; EI, electron impact; CI, chemical ionization.

TABLE 12.3 Maximum permitted tolerance for relative ion intensities using a range of mass spectrometric techniques [modified from ref. 11]

Relative intensity (% of the base peak)	GC-EI-MS (relative)	GC-EI-MS, GC-MS^n, LC-MS, LC-MS^n (relative)
>50%	±10%	±20%
>20–50%	±5%	±25%
>10–20%	±20%	±30%
≤10%	±50%	±50%

standard. In addition, the prominent ions other than targets must be explained. If using selected ion monitoring, the relative abundance of three specific ions should match within ±10% compared to standard, while of four or more unique structurally specific ions should match within ±15% compared to the standard. The relative abundance for more than three ions includes ion due to loss of water and isotopes, and should match within ±10% compared to the standard.

If quantification was performed using NMR spectroscopy, the specificity of the target signal (identity and purity) should be evaluated by two-dimensional NMR experiments [15]. When working under quantitative conditions, the NMR signal of the IS (e.g., anthracene) should not overlap with that of the target signal [16].

If the chromatography systems have nonspecific detectors (such as a flame ionization detector, a refractive index detector, an evaporative light scattering detector (ELSD), a corona-charged aerosol detector, or a conductivity detector), the methods that have been described above using DAD, MS, or NMR cannot be applied. In this case, peak purity evaluation can be determined by using peak shape analysis and re-chromatography [17]. A single pure peak results in a symmetrical first-derivative curve, while a co-eluting peak will decrease the height of the maximum and minimum depending on whether the R_t of the co-eluting peak is smaller or larger than that of the analyte peak. A pure tailing peak will also produce an asymmetrical first-derivative curve, but a co-eluting peak will yield irregularities or a shoulder. From the plot of the asymmetry factor against percent peak height, the tailing peak yields a continuously decreasing curve, while a co-eluting peak results a sigmoid decreasing curve. More detailed discussions have been provided by Ermer [17].

Peak purity can be also determined by changing the chromatography conditions, such as mobile phase composition, pH of the mobile phase, column type, and oven temperature. If the target peak is relatively pure, then the relative standard deviation (RSD) associated with the results of the analysis will be not more than 1–2%. Our experience has shown that at least three or more different chromatography conditions should be varied to prove the purity of the target peak. The identity and purity of the peak can also be confirmed by spiking the samples with standard solution. In this case, only one peak needs to be obtained. The enhanced peak height/area should be equivalent to the amount of added analyte, the wide of the peak at half-height must be within 90–110% range of the original width, and the retention time must be identical with a margin of ±5% [11,18].

Another approach for checking peak purity is by determining the intercept of the calibration curve, as the intercept of the pure peak should be not different significantly from zero [19]. Analogously, the peak purity of the target analyte in sample can be evaluated by developing its linear regression plot. If the target peak is pure, its intercept will be not different significantly from zero.

Although the formal requirement by the FDA and the European Medicine Agency is the use of at least six types of blank samples for proving the selectivity of bioanalytical methods, it is recommended to analyze up to 10–20 different sample matrices spiked with potentially interfering compounds (metabolites, isomers, degradation products, endogenous substances, matrix constituents, etc.) as well as the analyte at its lower limit of quantification (LLOQ). There should be no detector response in the chromatogram of the blank matrix at the retention time of the desired analyte. However, some researchers have held that the signal could be less than 20% of the signal of the analyte at its LLOQ for acceptable use. When using MS as a detector, the matrix effects (MEs) must be investigated,

which can be evaluated by using post-column infusion and post-extraction addition [11,20–22]. For eliminating MEs, it is recommended to use a stable isotope-labeled compound at the beginning of sample extraction [12]. A nice discussion regarding the MEs associated with bioanalytical LC-MS assays has been provided by Eeckhaut *et al.* [23].

It is known that if no degradation products and impurities are available, stress-induced degradation should be used [1], but it is strongly recommended that the sum total of degradation products does not exceed more than 5–10% as this condition serves to achieve actual operating conditions [10]. Various conditions for performing degradation studies on drug substances and drug preparations have been proposed by Diana [24]. Our experiences have shown that by adding a few drops of acid, base, or peroxide into powdered standard and samples (approximately 100–500 mg), and then incubating for defined times and temperatures, one can obtain an approximate level of degradation products in the range of 5–25% [25,26].

For demonstrating selectivity in a method for the analysis of botanical drugs (herbal drugs or extract preparations), the availability of BRMs is essential. It is appropriate to have at least three authenticated BRMs from different origins of each species, as this can be used to illustrate natural variability. A method is specific if during validation, a sample representing a target species showed identical chromatography fingerprinting to that of BRM, and samples representing other species give different fingerprinting. Evaluation of HP-TLC fingerprinting can be performed visually or by using a densitometer (manual or video) [7].

The requirements for validation of the selectivity for bulk substances and drug preparations are not the same. For bulk substances, the recommended concentrations are around 100–200 μg/spot or injection, while for drug preparations, the recommended concentrations are around 0.5–2 μg/spot or injection [10].

4. RESPONSE FUNCTION AND CALIBRATION

4.1. Univariate calibration

The response function (detector responses/signals, peak area, absorbance versus concentrations of the analyte, etc.) is usually documented using linear regression analysis. A univariate calibration means that detector response is a linear function of the analyte concentration [27]. It is common practice to check the linearity of a calibration curve by calculating the correlation coefficient (r), which will be close to unity for a linear response. One should not totally rely on the correlation coefficient, as a slightly nonlinear curve can still yield an r-value that is close to 1. It is

advisable to calculate other parameters of linearity, such as the relative process standard deviation (Vxo), the Xp-value, Mandel's test, analysis of variance (ANOVA) linear testing, or the sdv-value (WinCats, Camag). These quantities have been described in the previous chapter [1].

Araujo [9] reported that although r might be close to 1 (e.g., 0.9995) for a slightly nonlinear calibration curve; one should calculate the ''Fischer variance ratio'' (or simply the Fischer-ratio value) to prove the linearity of a calibration curve. The calibration curve is considered to be linear if the calculated Fisher-ratio value is less than the critical F-value from the table with a degree of freedom (df) equal to $(J-2)\times(Jn-n)$, where J is the number of concentration levels (e.g., 5 levels of concentrations) and n is the replication of each level. Detailed equations for calculating Fischer-ratio values have been described [9]. For making a good calibration curve, Ferenzci-Fodor *et al.* [10] recommended using at least six concentrations of Calibration Standard (CS), each in duplicate ($J=6$, $n=2$), and each level of concentration of CS should be weighed independently, and spotted/injected in the same volume. If the ratio of the highest concentration of CS and the lowest concentration of CS is defined as the working range (WR), it is recommended to have a WR less than 10. If WR is more than 10, it is advised to have a weighting regression line [28].

The calibration curve is not always linear and could take the form of a quadratic equation ($Y=aX^2+bX+c$), a Michaelis–Menten function, or some other mathematical relation. A calibration curve consisting of the logarithm of the detector response (Y-axis) against the logarithm of the injected mass (X-axis) is required if ELSD is used as the detector [10,22,29].

Although there are many possible mathematical functions that describe the relationship between detector response (or signal) and concentration, it was recommended to use the simplest mathematical model, that is, regression linear model, whenever possible [30]. Selecting the best relationship between detector response and concentration can also be performed by using an accuracy index (I_A), and this will be discussed latter in Section 7.

For bioanalytical studies, the calibration samples should be prepared in the same biological matrix as in the sample in the intended study, namely by spiking the matrix with known concentrations of the analyte. In this case, a blank sample, a zero sample (blank + IS), and six to eight concentrations covering the expected range (including LLOQ) should be used in an evaluation of the linearity of the calibration curve [21]. For example, owing to the occurrence of endogenous melatonin in the pooled plasma, instead of using a plasma matrix, Wang *et al.* [31] prepared the calibration curve by dissolving standard melatonin in acetonitrile, which was then spiked into water. This approach can only be used if no ME is observed.

For analysis of banned compounds in food, the calibration curve should also be prepared in the same matrix and should consist of samples prepared at the LLOQ, 0.5 maximum residue limit (MRL), and at 1–6 MRL (n=4–7 in duplicate) [20,32].

In natural product chemical research, sometimes the authentic standard is not available or is very expensive. In such cases, it is not recommended to use a single compound for constructing the calibration curve to determine the levels of related compounds by the normalization method. A detailed discussion on this topic has been published by Betz *et al*. [33].

4.2. Multivariate calibration

In general, multivariate regression methods are widely used for numerous purposes, such as the determination of certain chemicals by using some measured physical data, determination of physical data (octane index, viscosity, etc.) by using other physical data, and studies of the correlation between some factors with bioactivity or molecular structures [34].

Typically, the data matrix consists of one row for each observation or sample, and each variable defines a column on the table, so each cell in the table contains the value of a variable measured on one sample. Therefore, the data matrix X will consist of N rows (samples, observation) and K columns (e.g., chromatography data, glucose concentrations). Before performing a multivariate regression (e.g., multilinear regression), principal component regression (or partial least square regression (PLS1 and PLS2)), it is recommended to perform pretreatment (including scaling or normalization) for all the data in K column. At first, the calibration model should be constructed using training or calibration samples, and then the model should be validated. Validation for multivariate calibration modeling can be performed in three ways: a separate test set, cross-validation, or leverage correction. Leverage correction should be used at an intermediate stage of the modeling, and another validation method should be applied before building the final model [35].

Al-Degs *et al.* [36] reported the determination of trace levels of pesticides in water using solid phase extraction and multivariate calibration. The total antioxidant capacity of green tea was predicted using multivariate calibration [37]. The sensory score of Italian traditional balsamic vinegar has been predicted by using mid-infrared spectroscopy with PLS regression [38]. Comprehensive review articles, which described the multivariate calibration including the mathematical equations and their applications, have been published [27,39].

5. ACCURACY, TRUENESS, AND PRECISION

Accuracy can be defined as the degree of agreement between a measured quantity and its true value, while trueness is the degree of agreement between the average of a large numbers/series of measurements and a reference value. This simple definition of accuracy will cause an accuracy result to vary across a sequence of several measurements, due to both random and systematic errors. A high degree of trueness implies a lack of bias in the measurements [40,41]. The term ''accuracy'' cannot be *strictly* applied to the result of a method, because the outcome of such an analysis also includes an estimate of measurement uncertainty [40]. In broader terms, ''accuracy is a combination of trueness and precision components,'' and thus trueness is correlated with systematic errors, while precision measures random errors [22]. This broader term of accuracy will be in the rest of this chapter.

The total error of an analysis is a measure of (in)accuracy [41], and so accuracy can be improved by improving the trueness and precision of the method [40]. Total error is simultaneously the combination of systemic error and random errors [9,42]. If $\overline{Z}$is the average value of the measurements, and the true sample value is T, then total error can be described by Eq. (1). Thus, total error estimates the error distribution around the true or reference value. Total error is directly related to the measurement uncertainty [30,43].

$$\overline{Z} = T \pm f(\text{total error})$$

$$\overline{Z} - T = \text{total error (measurement error)}$$

$$\overline{Z} - T = \text{accuracy} = \text{bias} \tag{1}$$

Precision has three levels, namely, within-run precision/intra-batch precision/intra-day precision/repeatability, between-run/inter-batch precision/intermediate precision, and inter-laboratory precision/reproducible. Precision is usually expressed as the standard deviation (SD), variance (S^2), RSD, or coefficient of variance (CV). Precision studies must be performed using the entire analysis on the real samples, including weighing, pretreatment, extraction, and (chromatographic) analysis [10]. A relatively better way for determining the repeatability and intermediate precision is by using the one-way ANOVA method. In this case, the variance in repeatability can be calculated by using the within-condition variance (S_r^2). If the between-condition variance is expressed as S_B^2, then the intermediate precision variance (S_R^2) can be determined by using Eq. (2) as described by Gonzáles *et al.* [44]:

$$S_R^2 = S_r^2 + S_B^2 \tag{2}$$

From the values of S_r^2 and S_R^2, the corresponding RSD$\left(\frac{\sqrt{S^2}}{\bar{Z}} \times 100\right)$ of the repeatability and intermediate precision can be calculated. Interlaboratory reproducibility can be predicted using the Horwitz equation [44,45]:

$$\mathrm{RSD_H} = 2^{\left(1-0.5\log C\right)} \tag{3}$$

where C is the analyte concentration in decimal fraction units. The RSD's value of intermediate precision is approximately one-half to two-third the value of RSD$_{\mathrm{H}}$ [45] (see Table 12.4). If $R_j{=}S_B^2/S_r^2$ is more than 4, there should be an indication that the results may be vary from one series/run to the other, so the method must be re-developed [30].

According to Eq. (1), the total error is the bias of the method (δ). The bias uncertainty (u) can be calculated according to the Eq. (4) [44]:

$$\frac{u^2(\delta) = S_R^2\left(1 - \gamma + \frac{\gamma}{n}\right)}{p}, \tag{4}$$

with

$$\gamma = \frac{S_r^2}{S_R^2},$$

where "p" is series of the measurements in different conditions (e.g., days) and "n" is the repetitions of each measurements.

Equation (4) can be rewritten as [45]

$$u^2(\delta) = \frac{S_R^2 - \{(n-1)/n\}.S_r^2}{p} \tag{5}$$

TABLE 12.4 Acceptance criteria of accuracy (expressed as % recovery) and precision (expressed as RSD$_{\mathrm{H}}$ and from AOAC per verified method program RSD$_{\mathrm{AOAC}}$) [modified from ref. 44]

Analyte (%)	Analyte fraction	Concentration unit	% Recovery	RSD$_{\mathrm{H}}$	RSD$_{\mathrm{AOAC}}$
100	1	100%	98–102	2	1.3
10	10^{-1}	10%	98–102	2.8	1.8
1	10^{-2}	1%	97–103	4	2.7
0.1	10^{-3}	0.1%	95–105	5.7	3.7
0.01	10^{-4}	100 ppm	90–107	8	5.3
0.001	10^{-5}	10 ppm	80–110	11.3	7.3
0.0001	10^{-6}	1 ppm	80–110	16	11
0.00001	10^{-7}	100 ppb	80–110	22.6	15
0.000001	10^{-8}	10 ppb	60–115	32	21
0.0000001	10^{-9}	1 ppb	40–120	45.3	30

and the Student's t-value can be calculated as:

$$t_\sigma = \frac{\overline{Z} - T}{u^2(\delta)} \tag{6}$$

If the calculated t_σ value is less than critical tabulated value for df=$pn-1$, then there is no significant difference between the overall mean value and the true value.

If R is the recovery (defined as the ratio between the observed concentration of QC samples $\overline{Z}$ and its true value T), then R can be determined as [45]:

$$R = \frac{\overline{Z}}{T} \quad \text{or} \quad \%R = \frac{\overline{Z}}{T} \times 100 \tag{7}$$

From Eqs. (1) and (7), one obtains:

$$R = 1 + \frac{\delta}{T} \tag{8}$$

If the bias is negative (or positive), then the recovery R will be lesser (or higher) than 100% [45].

Generally, accuracy can be expressed as percent recovery by the assay of known added amount of analyte(s) in samples, matrices, or placebos (laboratory-made preparations or QC samples). In addition, for proving the absence of systematic error, a recovery curve must be constructed. Detailed discussion on this topic has been described previously [1]. Although the spiking of standards into placebos could well mimic the behaviors of authentic or real samples, it was recommended whenever possible to use authentic samples in the validation design. This could increase the accuracy and reliability of the analysis results in future routine applications [46].

The determination of percent recovery for the analysis of natural products is performed by spiking the reference standard(s) into the same matrix. The spiking can be performed also in a similar matrix which does not contain the target compounds [47]. It is recommended to spike three different concentrations of standards, and analysis should be performed on three different days. It is known that most of the standards for natural products can be very expensive, and usually only a very limited amount is available, and in some cases, the standards must be self-isolated. In this case, the exhausted extraction method can be used to help the verification of the accuracy of the method [48]. Purity of the reference natural product materials which are used as standard can affect the accuracy results [33].

For bioanalytical studies, accuracy (trueness and precision) can be estimated using validation standards or QC samples; QC samples must be prepared in same biological matrix. The smallest and largest QC

samples should be in the range of the CSs. It is recommended to have at least four levels of QC samples; one at the expected LLOQ, one at three times the LLOQ, a middle one, and a maximum one. For each level of QC sample, at least five replicates should be analyzed. The mean values must be within 15% of the actual value, except at the LLOQ level, where it should be not more than 20% [22,30].

For analyzing banned compounds in food, accuracy was performed by analyzing six replicates of certified reference material (CRM). If no CRM is available, accuracy can performed by the fortifying of six blank-matrixes each at 1, 1.5, and 2 times the minimum required performance limit, or 0.5, 1, and 1.5 the permitted limit (PL), so there will be a total of 18 samples to be analyzed. The recovery should be within ±10% of the target value [11]. The general acceptance criteria of accuracy and precision are presented in Table 12.4.

MEs can be evaluated by measuring and comparing the signals of four types of samples, as described by Rozet *et al.* [22]:

(1) Matrix-free standards
(2) Blank matrices of different sources extracted, and spiked with standards after extraction
(3) Same as (2), but spiked before extraction
(4) Matrix-free standards submitted to extraction.

According to Cronly *et al.* [49], MEs can be defined as the ratio of response type-2 to type-1, while recovery can be estimated from the ratio of response type-3 to type-2. Process efficiency is defined as the ratio of type-3 to type-1, and extraction yield is the ratio of response type-4 to type-1. ME can be evaluated by comparing the slope (b) of the calibration line of sample type-1 (s) and sample type-2 (a) using the Student's t-test as follows [50]:

$$t_{\mathrm{cal}} = \frac{|b_s - b_a|}{\sqrt[Sp]{\left(1/\sum x_{i,s} - \overline{x_s}\right)^2 + \left(1/\sum x_{i,a} - x_a\right)^2}} \tag{9}$$

where

$$\mathrm{Sp} = \sqrt{\frac{(n_a - 2)s_s^2 + (n_a - 2)s_a^2}{n_s + n_a - 4}}$$

In Eq. (9), x is the concentration and n is the number of replicates. If $t_{\mathrm{cal}} < t_{\mathrm{table}}$ (df$=n_s+n_a+4$), there is no significant difference between the slopes, meaning that no ME occurred.

Reich *et al.* [7] reported a detailed method to evaluate precision for qualitative HP-TLC finger print of herbal drugs. They recommended to use at least three portions of the BRM, spotted onto three different

plates. The fingerprint must be identical, meaning that the variability in R_f values of three markers should not exceed 0.01 across each plate, 0.02 for repeatability, 0.05 for intermediate precision (1–3 days), and 0.07 for reproducibility.

6. ROBUSTNESS

A strategy for performing a robustness study has been described by Gonzáles *et al.* [44] and consists of the following steps:

(1) Identify the influencing factors: type of column, oven temperature, mobile phase composition, pH of the mobile phase, etc.
(2) In each factor, define the nominal and extreme values expected in routine situations and code them as nominal value=0, high value=+1, and low value=−1
(3) Arrange the experimental design using a two-level $2^{7\text{-}4}$ fractional Plackett–Burman matrix
(4) Perform the evaluations in random order on a control sample with analyte concentration halfway in the concentration range of the method scope.

A $2^{7\text{-}4}$ Plackett–Burman design (8 experiments) can be applied for 3–7 factors in a robustness evaluation. An example of the design is presented in Table 12.5, so for each *k*-factor, it will consist of 4 high (+) and 4 low (−) levels, respectively. Other Plackett–Burman designs are freely available and can be easily downloaded for free from websites. The effect of each *k*-factor (3–7 factors) for 8 experiments can be estimated by the difference (D) between the mean of the results of level +1 and level −1 [44,51]:

TABLE 12.5 Example of a $2^{7\text{-}4}$ Plackett–Burman design for robustness evaluation [modified from ref. 44]

	Factors (k=3–7)					
Experiment	k_1	k_2	k_3	k_4	........k_7	Response, or result of analysis
1	+1	+1	+1	+1		Z_1
2	+1	+1	−1	+1		Z_2
3	+1	−1	+1	−1		Z_3
4	+1	−1	−1	−1		Z_4
5	−1	+1	+1	−1		Z_5
6	−1	+1	−1	−1		Z_6
7	−1	−1	+1	+1		Z_7
8	−1	−1	−1	+1		Z_8

$$D(x_k) = \frac{1}{4}\left\{\left(\sum_{i=1}^{n} Z_i\right)_{xk=+1} - \left(\sum_{i=1}^{n} Z_i\right)_{xk=-1}\right\} \tag{10}$$

To know whether there is a significant effect of k on the results, the t-test can be used:

$$t(x_k) = \frac{\sqrt{2}|D(x_k)|}{S_R} \tag{11}$$

if the value of $t(x_k) \leq t_{tab}$ (df$=pn-1$, two tailed), then the method is robust against the k-factor. The uncertainty of the robustness study (u_{rob} (Z)) can be calculated [44,51] using:

$$u_{rob}(Z) = \overline{Z}.\mathrm{RSD}_{rob} \tag{12a}$$

$$\mathrm{RSD}_{rob} = \sqrt{\frac{u^2(Z(x_k)}{\overline{Z}^2}} \tag{12b}$$

with:

$$u(Z(x_k) = \frac{t_{crit}S_R}{1.96\sqrt{2}} \frac{\delta_{real}(x_k)}{\delta_{test}(x_k)} \tag{12c}$$

Here, δ_{real} is the change in factor level (pH of mobile phase, temperature, percent concentrations, etc.) that would be expected when the method is operating routinely, while δ_{test} is the change in factor level specified in the robustness study.

Dejaegher and Heyden [52] described in detail the selected factors which were applied on robustness studies for high-performance liquid chromatography, gas chromatography, capillary electrophoresis, ultra-performance chromatography, and supercritical fluid chromatography. For quantification using NMR spectroscopy, some additional factors (such as change of pulse power, pre-acquisition delay, receiver gain, length of acquisition time, and relaxation delay) could be varied in order to evaluate the robustness of the method [15].

7. ACCURACY PROFILE

The concept of ''accuracy profile'' was first introduced by Hubert *et al.* (1999) and Boulanger *et al*. (2000) [cited by references 51, 53, 54]. The basic idea behind this is to translate the ''fitness-for-purpose'' objective into the acceptance limit criterion (λ). This new approach seemed better when compared to the ''traditional or classical'' approach, which evaluated specific indicator performance of validation parameters such as linearity,

accuracy, precision, and recovery. The classical approach has disadvantages due to the separate evaluation of those validation parameters, and so can lead to an ambiguous conclusion [53,54]. Bouabidi *et al.* [55] showed that the concept of the accuracy profile approach has advantages compared to the classical approach (which includes descriptive-, difference-, and equivalent-approaches). The Commission on the validation of analytical procedures of SFSTP (Societé Française des Sciences et Techniques Pharmaceutics) has used the accuracy profile for improving the assessment of the accuracy in validation methods [51].

A "good" method of analysis should "guarantee" that the difference of every results of analysis Z of a sample and its true value T is within the predefined acceptance limit, λ. Thus, the mean of analytical results ($\overline{Z}$) must differ from its true value T in an extent less than the acceptability limit [51,53,54,56]:

$$\left|\overline{Z} - T\right| < \lambda \tag{13}$$

Usually the acceptance limit is dependent on the objective of the analytical procedures, generally 1–2% for bulk substances, 5% for drug preparations, 15% for biological samples, and 30% for immunoassay methods. A valid analytical method should result in a value of $\overline{\mathrm{Z}}$ [45] that meets the requirements:

$$P\left|\overline{Z} - T\right| < \lambda \geq \beta \tag{14}$$

In Eq. (14), β is the probability that the determination will be inside this acceptance limit and, it is therefore termed the *β-expectation tolerance interval* (β-ETI). According to Gonzáles *et al*. [44,45], values for β-ETI can be calculated using:

$$\beta\text{-ETI} = |\delta \pm ku(\mathrm{Z})| < \lambda \tag{15}$$

$$u(Z)^2 = S_{\mathrm{R}}^2 + u^2(\delta) + u_{\mathrm{rob}}^2 \tag{16}$$

With bias (δ) being equal to $\overline{\mathrm{Z}} - T$; $\mathrm{S}_{\mathrm{R}}^2$, then u^2 (δ) and u_{rob}^2 can be determined by Eqs. (2), (4), and (12a). Then, "k" is the called the coverage factor, calculated at the Student's t-value for p=0.05, with a df equal to $pn-1$ [51]. If u_{rob}^2 is not included, then Eq. (16) modifies to [45]:

$$u(\mathrm{Z})^2 = S_{\mathrm{R}}^2 + u^2(\delta) \tag{17}$$

For each of a set of QC samples, the upper and lower tolerance interval limits can be calculated as percentages using [45]:

$$\left[\frac{100[\delta + ku(\mathrm{Z})]}{T}; \quad \frac{100[\delta - ku(\mathrm{Z})]}{T}\right] \tag{18}$$

Rozet *et al.* [57] and Hubert *et al.* [58] described another equation for calculating β-ETI (upper and lower tolerance interval limits) as follows:

$$\left[\overline{Z}_J + Q_t\left[v, \frac{1+\beta}{2}\right]\sqrt{1+\frac{1}{pnB_J^2}}S_R\right],\quad \overline{Z}_J - Q_t\left[v, \frac{1+\beta}{2}\right]\sqrt{1+\frac{1}{pnB_J^2}}S_R\right] \tag{19a}$$

where J is the level of concentration, $\overline{Z_J}$ is the estimated mean of the J^{th} concentration level. Then:

$$B_J = \sqrt{\frac{R_J+1}{nR_J+1}} \tag{19a1}$$

$$R_J = \frac{S_B^2}{S_r^2} \tag{19a2}$$

Where:

Q_t (v; $(1+\beta)/2$) is the β quantile of the Student t distribution with v degree of freedom:

$$v = \frac{(R_J+1)^2}{[R_J+(1/n)]^2/(p-1)+[1-(1/n)]/(pn)} \tag{19a3}$$

If β-ETI is expressed in terms of percentage in relative error scale, Eq. (19a) can be rewritten as Eq. (19b) [57,58]:

$$\begin{gathered}\left[\delta_J(\%) + Q_t\left[v; \frac{1+\beta}{2}\right)\sqrt{1+\frac{1}{pnB_J^2}}\mathrm{RSD_{IP}},\right.\\ \left.\delta_J(\%) - Q_t\left[v; \frac{1+\beta}{2}\right)\sqrt{1+\frac{1}{pnB_J^2}}\mathrm{RSD_{IP}}\right]\end{gathered} \tag{19b}$$

where δ_J (%) is the bias in concentration level $J\left(\frac{\delta}{T}\times 100\right)$, and $\mathrm{RSD_{IP}}$ is the RSD of the intermediate precision, which can be calculated by Eq. (2).

A graphical representation of the accuracy profile can be constructed by connecting each of the upper and each of the lower limit intervals of the QC samples using Eqs. (18) and (19b), yielding two segmented lines. The intersection of these two lines with the acceptance lines ($+\lambda$ and $-\lambda$) leads to the upper and lower quantification limits (QLs) (Fig. 12.1).

When using Eqs. (18) and (19b), Boemer *et al.* [42] reported slight differences in the calculated uncertainty regions for the analysis of a thyroid-stimulating hormone (immunoassay method). Equation (18) yielded smaller values both for the lower and upper limits when compared to the results calculated using Eq. (19b).

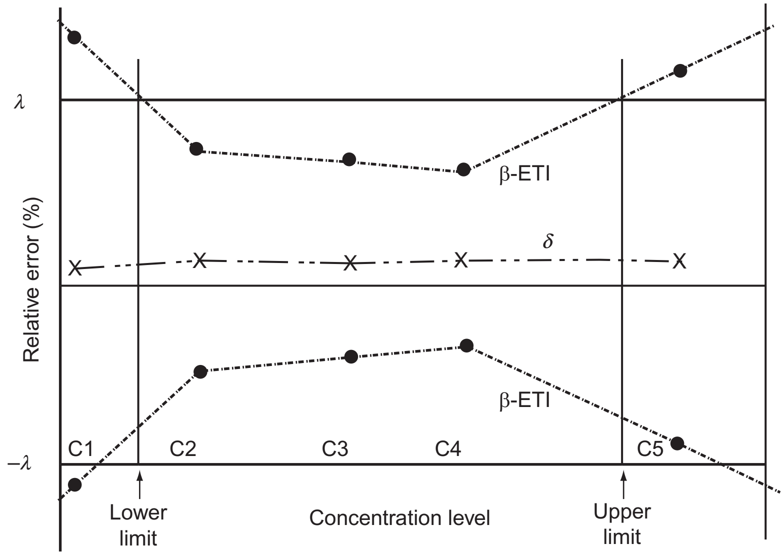

FIG. 12.1 Schematic presentation of an accuracy profile using five levels of QC samples [modified from ref. 57].

Accuracy profiles can be used as decision tools to verify the validity of an analytical procedure, but interpretation of a graphical representation might be susceptible to subjectivity. Therefore, Rozet *et al.* [57] recommended to use an accuracy index (I_A). The I_A value can be calculated by combining the dose range index (I_R), the trueness index (I_T), and the precision index (I_P):

$$I_A = \sqrt[3]{(I_T I_R I_P)} \in [0;1] \tag{20}$$

Using these indices, the best response function can be also selected. Application of the accuracy profile has advantages in that it can be applied to any type of analytical method in any type of industry, and is independent of matrix type [57].

8. DECISION LIMIT AND DETECTION CAPABILITY

In our previous chapter [1], the detection limit (DL) and the QL have been described and discussed. A Commission decision has described related parameters, which have been named as the decision limit (CC_α) and the detection capability (CC_β). According to CD/657/2002/EC, CC_α can be defined as the limit at and above which one can conclude with an error probability of α (1% for substance with non-PL and 5% for substance with

a PL as the MRL) that a sample is non-compliant. CC_β is defined as the smallest content of the substance that may be detected, identified, and/or quantified in a sample with an error probability of β (5% of all substances with permitted or no PLs) [11,32].

Both CC_α and CC_β can be calculated by means of two methods [32,59]. The first method is based on the estimation of the detector response in terms of signal-to-noise ratio at the concentration of interest for at least 20 blank materials. For non-permitted substances:

$$CC_\alpha = 3 \times \left\{ \frac{S}{N_{20\,\text{representative blank sample}}} \right\} \tag{21}$$

$$CC_\beta = CC_\alpha + 1.64\,SD_{20\,\text{represntative samples spiked at}\,CC_\alpha\,\text{level}} \tag{22}$$

For MRL substances:

$$CC_\alpha = C_{MRL} + 1.64\,SD_{20\,\text{representative MRL-spiked samples}} \tag{23}$$

$$CC_\beta = CC_\alpha + 1.64\,SD_{20\,\text{representative samples spiked at}\,CC_\alpha\,\text{level}} \tag{24}$$

The second approach is based on a linear day-to-day calibration curve ($Y = a + bX$, with S_y being the residual SD of the regression curve) of the method. In this case, a set of matrix-spiked calibration samples consisting of at least three levels of equidistant concentrations (J) must be used. If the number of replicates is n, and K is the number of measurements of the unknown samples to be evaluated, then CC_α and CC_β can be calculated using the following equations. For non-permitted substances:

$$CC_\alpha = t_{(\alpha,Jn-2)} \times \frac{S_y}{b} \times \sqrt{\frac{1}{K} + \frac{1}{Jn} + \frac{\bar{x}^2}{\sum\left(x_{ij} - \bar{x}\right)^2}} \tag{25}$$

$$CC_\beta = 2t_{(\alpha,Jn-2)} \times \frac{S_y}{b} \times \sqrt{\frac{1}{K} + \frac{1}{Jn} + \frac{\bar{x}^2}{\sum\left(x_{ij} - \bar{x}\right)^2}} \tag{26}$$

For MRL substances:

$$CC_\alpha = C_{MRL} + t_{(\alpha,Jn-2)} \times \frac{S_y}{b} \times \sqrt{\frac{1}{K} + \frac{1}{Jn} + \frac{x_{MRL} - \bar{x}^2}{\sum\left(x_{ij} - \bar{x}\right)^2}} \tag{27}$$

$$CC_\beta = C_{MRL} + 2\left(t_{(\alpha,Jn-2)}\right) \times \frac{S_y}{b} \times \sqrt{\frac{1}{K} + \frac{1}{Jn} + \frac{x_{MRL} - \bar{x}^2}{\sum\left(x_{ij} - \bar{x}\right)^2}} \tag{28}$$

From the calculated values of CC_α and CC_β, the following deductions may be made [60]:

1. If the result of the analysis is less than CC_α, the sample can be declared as being compliant ($p=\alpha$).
2. If the result of the analysis is greater than CC_β, the sample can be declared as being non-compliant ($p=\beta$).
3. If the result of the analysis is greater than CC_α, but less than CC_β, the sample is probably non-compliant but remains statistically unclassified.

Janiga *et al.* [61] reported that the value of CC_α was almost identical with the value of DL, and the value of CC_β was also almost identical with the value of QL. In this study, DL and QL were calculated using a linear regression curve. Therefore, one may calculate either DL and QL or CC_α and CC_β, but there is no need to calculate all four parameters.

9. UNCERTAINTY

According to the Guide to the expression of Uncertainty Measurement, uncertainty can be defined as "a parameter associated with the result of a measurement that characterizes the dispersion of the values that could reasonably be attributed to the measurand" [cited by reference 43]. Uncertainty defines the region around the measured analytical results where the conventional true or reference value can be found with a defined probability that is the distribution of reference analytical results linked to an observed analytical result [43]. In our previous chapter [1], some simple methods for the determination of uncertainty and confidence interval of results of analysis have been described.

The confidence interval or uncertainty of the analytical result can be expressed as [43,44]:

$$\overline{Z} \pm ku(Z) = Z \pm U(Z) \tag{29}$$

where $ku(Z)$ can be calculated using Eqs. (16) and (17) [44], and k can be set as 2 when $p=0.05$ [43].

Rozet *et al.* [62] described approaches for modeling the overall measurement of uncertainty; namely the sum model, the linear Model, the mean square error model, the SFSTP 97 model, the β-ETI, and the β-content γ-confidence tolerance interval. In this review, it was shown that the β-ETI and the β-content γ-confidence tolerance interval represented the most suitable approaches.

When the mean and SD are known, the general formula describing β-ETI is [62]:

$$E(P)[L \leq Z_i \leq U] = \beta \tag{30}$$

In Eq. (30), E is the estimator of mathematical expectation and P stands for probability. If β=0.95, then in the future, the result of an analysis has a 95% probability that the value will be within the calculated the lower and upper interval [L, U]. If the mean and SD are unknown, then Eq. (30) can be modified as [62]:

$$[L, U] = \left[\overline{Z} - kS_{\mathrm{R}}, \quad \overline{Z} + kS_{\mathrm{R}}\right] \tag{31}$$

S_{R} can be determined using Eq. (2), while k can be calculated according to Eq. (19a) as follows:

$$k = Q_t\left[v; \frac{1+\beta}{2}\right]\sqrt{1 + \frac{1}{pnB_J^2}} \tag{32}$$

By replacing the value of $\overline{Z}$ in Eq. (31) with the estimated bias (δ), the interval will provide the estimation of the overall measurement of uncertainty [62].

The second approach is β-content γ-confidence tolerance interval. If the mean and SD are known, one can calculate [62]:

$$P(P[L \le Z_i \le U] \ge \beta) = \gamma \tag{33}$$

For example, if β=0.95 and γ=0.90, this means that 90 out of 100 and 95% of individual results in the population are included in the interval [L, U]. Usually, however, the mean and SD are not known, so by using one-way ANOVA the following equation is obtained [62]:

$$\overline{Z} \pm Q\left(1 + \frac{\beta}{2}\right)\sqrt{1 + N_{\mathrm{e}}^{-1}}\sqrt{S_{\mathrm{R}}^2 + \left[H_1^2\left(\frac{1}{n}\right)\left(nS_{\mathrm{B}}^2 + S_{\mathrm{r}}^2\right)^2 + H_2^2\left(\frac{n-1}{n}\right)^2\left(S_{\mathrm{r}}^2\right)^2\right]^{1/2}} \tag{34}$$

with

$$N_{\mathrm{e}} = \frac{p\left[\left(nS_{\mathrm{B}}^2 + S_{\mathrm{r}}^2\right) + (n-1)\left(S_{\mathrm{r}}^2\right)^2\right]}{nS_{\mathrm{B}}^2 + S_{\mathrm{r}}^2}$$

and

$$H_1 = \frac{\mathrm{df_B}}{F_{1-\gamma}, \mathrm{df_B}, \infty} - 1, \quad H_2 = \frac{\mathrm{df_W}}{F_{1-\gamma}, \mathrm{df_r}, \infty} - 1$$

Here, $\mathrm{df_B}=p-1$; $\mathrm{df_r}=p(n-1)$; $F_{1-\gamma,\ v1,v2}=1-\gamma$ quantile of an F distribution with $v1$ and $v2$ df. By replacing the value of $\overline{Z}$ in Eq. (34) with the estimated bias (δ), the interval will provide an estimation of the overall measurement of uncertainty [62].

10. TRANSFER OF ANALYTICAL METHODS

In general, analytical methods are developed and validated in the Research & Development (R&D) division, and subsequently, the method is to be used routinely in a QC section. For this purpose, it is necessary to transfer the completed R&D procedures (the sender laboratory) to a QC laboratory (the receiver laboratory). This activity can take place within a company, or within a network of companies, and is termed ''method transfer.'' Analytical method transfer is an important step in the life cycle of analytical method development in the pharmaceutical industry [63–65]. The objective of method transfer is to give assurance that the analysis results obtained by the receiving laboratories will be close enough to the unknown true quantity of the analyte present in the samples in future routine applications. In other words, the results of the receiving laboratory should reliable and comparable with the results of the sending laboratory [63].

Rozet *et al*. [63] have described an analytical method transfer protocol, which entails the following features:

(1). The transfer of scientific documents
(2). The reference samples to be used
(3). The detailed description of analytical procedures
(4). The statistical design, sample size, data analysis, and decision procedures
(5). The training of personnel at the receiving laboratory
(6). The execution of the method transfer
(7). Analysis of the results obtained by the receiving laboratory, and a decision about the acceptability of the method transfer which is included in a transfer report.

Evaluation of method transfer can be performed by using various methodologies, such as descriptive-, difference-, equivalence-, and total error-approaches [63,66,67]. Descriptive statistical evaluation using the Student's *t*-test was not recommended due to its incapability to deal with controlled type-I (α) and type-II (β) errors [64,67]. According to Rozet *et al*. [63] and Dewe *et al.* [68], the best method for the statistical evaluation of the method transfer is by using total error approaches. Use of these methods can control the producer risk (i.e., the transfer is erroneously rejected), the consumer risk (i.e., transfer is erroneously accepted), and the risk of obtaining out-of-acceptance limit (OOAC) results. Total error approach consists of two methods, namely Method-I (β-ETI) and Method-II (risk assessment) [68].

The principle of Method-I is to calculate the β-ETI value for the receiving laboratory. The lower and upper level of β-expectation tolerance limits for the receiving laboratory can be calculated as follows [63,68]:

$$[L_{\mathrm{R}},\ U_{\mathrm{R}}] = [Z_{\mathrm{R}} - kS_{\mathrm{R}},\quad Z_{\mathrm{R}} + kS_{\mathrm{R}}] \tag{35}$$

Where Z_{R} is the mean value of the analysis results of the receiving laboratory, S_{R} is the variance of the intermediate precision obtained using Eq. (2), and k is calculated using to Eqs. (32) or (19a).

The analytical method transfer will be accepted if the interval $[L_{\mathrm{R}}, U_{\mathrm{R}}]$ is included in the interval $[T(1-\lambda), T(1+\lambda)]$. Usually, the value of T is unknown since the transfer method evaluation is performed on a batch or lot of a pharmaceutical product. In this case, the acceptance limit can be estimated by using the Z values of the sender laboratory (S) [68]:

$$\left[Z_S^U(1-\lambda),\quad Z_S^L(1+\lambda)\right] \tag{36}$$

Method-II estimates the probability (P) as to whether the results of the receiving laboratory (Z_{R}) are outside of the acceptance limit [68]:

$$P[Z_{\mathrm{R}} < T(1-\lambda)] + [Z_{\mathrm{R}} > T(1+\lambda)] \tag{37}$$

Using the same principles as for Method-I, Eq. (37) can be written as:

$$P[Z_R < (1-\lambda)] + [Z_R > (1+\lambda)] \tag{38}$$

The probability, P can be estimated [68] using:

$$P\left[t(v) < \frac{(1-\lambda)Z_S^U - \overline{Z_{\mathrm{R}}}}{S_{\mathrm{R}}\sqrt{1+\frac{nR+1}{pn(R+1)}}}\right] + \left[t(v) > \frac{(1+\lambda)Z_S^L - \overline{Z_{\mathrm{R}}}}{S_{\mathrm{R}}\sqrt{1+\frac{nR+1}{pn(R+1)}}}\right] \tag{39}$$

where S_{R}, R, and the df v can be calculated according to Eqs. (2), ($19a_2$), and ($19a_3$), respectively. If the calculated probability from Eq. (39) is smaller than $1-\beta$, then the method transfer can be accepted.

Other acceptance criteria of method transfer for various assay methods, including degradation products, impurities, and dissolution, have been proposed by Diana [24]. In the pharmaceutical industry, an analytical transfer from R&D to QC is usually performed with samples from the same batch to ensure that those laboratories work on the same materials. If the evaluations are performed on different batches, the statistical calculations should be performed separately for each batch. Pooling all the data was not recommended [63] due to the possible variation between batches.

11. CONCLUDING REMARKS

According to our experience, the most important parameter of the validation method for univariate calibration is the "selectivity/specificity" quantity. Without performing this at the outset of the process, the identity

and purity of the target peak of the compound cannot be confirmed, and so reliable accuracy profiles and reliable analysis results may not be achieved. Thus, the selectivity/specificity of the proposed method must be checked first [69]. This means that the total selectivity is needed, so a complete separation of the target analyte with other compounds must be obtained [27]. The best method for evaluating the selectivity of a proposed method is by using a chromatography system equipped with an MS/MS detector, or by using two-dimensional NMR methodology.

If multivariate calibration is used, then the target HPLC peaks do not need to be pure, and overlapping peaks can be determined without any prior separation [70]. Direct determination (without any extraction) of ibuprofen in tablets can be performed by using combined methods of NIR-spectroscopy and PLS regression [71]. At the present time, most of the applications of multivariate statistical analysis are for metabolomic studies and metabolite profiling of herbal drugs [72,73].

Due to possible inadequate or ambiguous conclusions associated with use of the ''classical approach'' for validation of analytical methods, the concept of ''accuracy profile'' has been proposed. This concept is based on total measurement errors, namely simultaneous combination of systemic errors and random errors [53,55]. Intra-laboratory testing for the ''accuracy of analytical methods'' using an accuracy profile can be easily performed using QC samples [45]. An acceptable accuracy profile of a proposed method can strongly reduce the risk of a validated method becoming unfit for its routine application in the future.

Another relatively new method, which is very similar to the accuracy profile, is the concept of an ''uncertainty profile'' that was proposed recently by Saffaj and Ihssane [74]. The uncertainty profile can be constructed using:

$$\left|\overline{Z} \pm ku(Z)\right| < \lambda, \tag{40}$$

where k=2, for p=0.05, and $u(Z) = \frac{U-L}{2t(v)}$. Detailed mathematical equations for calculating and then building uncertainty profiles have been described [74].

The determination of CC_α (or DL) and CC_β (or QL) is very essential for controlling banned compounds in food. If the result of an analysis is negative for a certain banned compound in food preparations, it must mean that the concentration of the banned compound is lower than the CC_α (or DL) of the method used [59].

A relative good transfer method from the sender laboratory (typically, R&D) to the receiver laboratory (typically, QC) is very important in the life cycle of analytical method development in the pharmaceutical industry. The main purpose of method transfer is to guarantee that the receiving laboratory can perform the analytical method with controlled risk in decision making, so the results of analyses in future application will be close enough to true quantities in samples [62,75].

Due to the complexity of the mathematical equations for evaluation of the validation method parameters as described in this chapter, a software VMA solution has been developed by the author [76].

REFERENCES

[1] M. Yuwono, G. Indrayanto, Validation of Chromatographic Method of Analysis, in: H.G. Brittain (Ed.), Profile of Drug Substances, Excipients and Related Methodology, vol. 32, Elsevier, Amsterdam, 2005.
[2] G. Indrayanto, Analytical Aspects of High Performance Thin Layer Chromatography, in: M.M. Srivastava (Ed.), High Performance Thin Layer Chromatography, Springer, Heidelberg, 2011.
[3] E. Reich, A. Schibli, High-Performance Thin Layer Chromatography for the Analysis of Medicinal Plants, Thieme, New York, Stuttgart, 2006.
[4] M. Stuart, A. Squirrell, L. Besley, Accred. Qual. Assur. 9 (2004) 209–215.
[5] L.G. Mackay, R. Kazlauskas, Anal. Bioanal. Chem. 401 (2011) 483–492.
[6] R. LoBrutto, T. Patel, Method Validation, in: Y. Kazakevich, R. LoBrutto (Eds.), HPLC for Pharmaceutical Scientist, Wiley Interscience, Hoboken, NJ, 2007.
[7] E. Reich, A. Schibli, A. DeBatt, J. AOAC Int. 91 (2008) 13–20.
[8] W. Li, J. Zhang, F.L.S. Tse, Biomed. Chromatogr. 25 (2011) 258–277.
[9] P. Araujo, J. Chromatogr. B 877 (2009) 2224–2234.
[10] K. Ferenzci-Fodor, B. Renger, Z. Végh, J. Planar Chromatogr. 23 (2010) 173–179.
[11] Commission of the European Communities, Commission Decision 2002/657/EC 14 August 2002, Implementing Council Directive 96/23/EC (http://www.bsmi.gov.tw/wSite/public/Attachment/ff224039659469.pdf).
[12] M. Careri, A. Mangia, Anal. Biochem. Chem. 386 (2006) 38–45.
[13] T.A. Sasaki, *Chromatography Techniques* July/August (2008) 18–21.
[14] FDA Guidance for Industry, Mass Spectrometry for Confirmation of the Identity of Animal Drug Residues., (2003) US Department of Health and Human Service. Food and Drug Administration, Center for veterinary Medicine.
[15] U. Holzgrabe, Prog. Nucl. Magn. Reson. Spectrosc. 57 (2010) 229–240.
[16] A. Hazekamp, Y.H. Choi, R. Verpoorte, Chem. Pharm. Bull. 52 (2004) 718–721.
[17] J. Ermer, Specificity, in: J. Ermer, J.H. McB. Miller (Eds.), Method Validation in Pharmaceutical Analysis, Wiley-VCH, Weinheim, 2005, 52–62.
[18] P. Kaur, A. Chaudhary, B. Singh, Gopichand, J. Pharm. Biomed. Anal. 50 (2009) 1060–1064.
[19] I.N. Papadoyannis, F. Samanidou, J. Cazes (Ed.), Encyclopedia of Chromatography, 3rd ed., Taylor & Francis, New York, NY, 2009 vol. 1.
[20] M.P. Hermo, E. Nemutlu, S. Kir, D. Barrón, J. Barbosa, Anal. Chim. Acta 613 (2008) 98–107.
[21] S.A.R. Wille, F.T. Peters, V.D. Fazio, N. Samyn. Accred. Qual. Assur. 16 (2011) 279–292.
[22] E. Rozet, R.D. Marini, E. Ziemons, E. Boulanger, P. Hubert, J. Pharm. Biomed. Anal. 55 (2011) 848–858.
[23] A.V. Eeckhaut, K. Lanckmans, S. Sarre, I. Smolders, Y. Michhotte, J. Chromatgr. B 877 (2009) 2198–2207.
[24] F.J. Diana, Method Validation and Transfer, in: K. Hyunh-Ba (Ed.), Handbook of Stability Testing in pharmaceutical Development, Springer Sciences Business Media LLC, New York, 2009.
[25] D. Widiretnani, S.I. Wahyuni, F. Kartinasari, G. Indrayanto, J. Liquid Chromatogr. Relat. Technol. 32 (2009) 154–165.
[26] S. Cholifah, W.F. Kartinasari, G. Indrayanto, J. Liquid Chromatogr. Relat. Technol. 31 (2008) 281–291.

[27] M.C. Ortiz, L. Sarabia, J. Chromatogr. A 1158 (2007) 94–110.
[28] H.J. Kuss, Optimization of the Evaluation in Chromatography, in: S. Kromidas (Ed.), HPLC Made to Measure, Wiley-VCH, Weinheim, 2006.
[29] W. Kong, C. Jin, W. Liu, X. Xiao, Y. Zhao, Z. Li, P. Zhang, X. Li, Food Chem. 120 (2010) 1193–1200.
[30] E. Rozet, A. Ceccato, C. Hubert, E. Ziemons, R. Oprean, S. Rudaz, B. Boulanger, P. Hubert, J. Chromatogr. A 1158 (2007) 111–125.
[31] A.Q. Wang, B.P. Wei, Y. Zhang, Y.J. Wang, L. Xu, K. Lan, J. Chromatogr. B 879 (2011) 2259–2264.
[32] E. Verdon, D. Hurtaud-Pessel, P. Sanders, Accred. Qual. Assur. 11 (2006) 58–62.
[33] J.M. Betz, P.N. Brown, M.C. Roman, Fitoterapia 82 (2011) 44–52.
[34] M. Florina, S. Lanteri, M.C.C. Oliveros, C.P. Millan, Anal. Bioanal. Chem. 380 (2004) 397–418.
[35] CAMO Courses in Multivariate Analysis, CAMO Process AS, Malaysia August 2005.
[36] Y.S. Al-Degs, M.A. Al-Ghouti, A.H. El-Sheikh, J. Hazard. Mater. 169 (2009) 128–135.
[37] M. Dumarey, A.M. van Nederkassel, E. Deconinck, Y. Vander Heyden, J. Chromatogr. A 1192 (2008) 81–88.
[38] A. Fersari, G.P. Parpinello, F. Chinnici, G. Meglioli, Food Chem. 125 (2011) 1345–1350.
[39] J. Gabrielsson, J. Trygg, Crit. Rev. Anal. Chem. 36 (2006) 243–255.
[40] C. Burgess, Aberrant or Atypical Results, in: J. Ermer, J.H.McB. Miller (Eds.), Method Validation in Pharmaceutical Analysis, Wiley-VCH, Weinheim, 2005, 335–386.
[41] D. Stöckl, H. D'Hondt, L.M. Thiepont, J. Chromatogr. B 877 (2009) 2180–2190.
[42] F. Boemer, V. Bours, R. Schoos, P. Hubert, E. Rozet, J. Chromatogr. B 877 (2009) 2412–2417.
[43] E. Rozet, R.D. Marini, E. Ziemons, W. Dewé, S. Rudaz, B. Boulanger, P. Hubert, Trends Anal. Chem. 30 (2011) 797–806.
[44] A.G. Gonzáles, M.A. Herrador, Trends Anal. Chem. 26 (2007) 227–237.
[45] A.G. Gonzáles, M.A. Herrador, A.G. Asuero, Talanta 82 (2010) 1995–1998.
[46] A. Bouabidi, M. Talbi, A. Bouklouze, M.E. Karbane, H. Bourichi, M.E. Goezzar, E. Ziemons, P. Hubert, E. Rozet, J. Pharm. Biomed. Anal. 55 (2011) 583–590.
[47] B.D. Backer, B. Debrus, P. Lebrun, L. Theunis, N. Dubois, L. Decock, A. Verstraete, P. Hubert, C. Charlier, J. Chromatogr. B 877 (2009) 4115–4124.
[48] F. Melianita, S. Cholifah, E. Sumarlik, W.F. Kartinasari, G. Indrayanto, J. Liquid Chromatogr. Relat. Technol. 30 (2007) 2941–2951.
[49] M. Cronly, P. Behan, B. Foley, E. Malone, L. Regan, J. Chromatogr. B. 877 (2009) 1494–1500.
[50] S. Fraselle, V. Derop, J.M. Degroodt, J.V. Loco, Anal. Chim. Acta 586 (2007) 383–393.
[51] A. Gonzáles, M.A. Herrador, Talanta 70 (2006) 896–901.
[52] B. Dejaegher, Y.V. Heyden, J. Chromatogr. A 1158 (2007) 138–157.
[53] M. Feinberg, J. Chromatogr. A. 1158 (2007) 174–183.
[54] M. Feinberg, B. Boulanger, W. Dewė, P. Hubert, Anal. Biochem. Chem. 380 (2004) 502–514.
[55] A. Bouabidi, E. Rozet, M. Fillet, E. Ziemons, E. Chapuzet, B. Mertens, R. Klinkenberg, A. Ceccato, M. Talbi, B. Streel, A. Bouklouze, B. Boulanger, P. Hubert, J. Chromatogr. A 1217 (2010) 3180–3192.
[56] P. Hubert, J.J. Nguyen-Huu, B. Boulanger, E. Chapuzet, P. Chiap, N. Cohen, P.A. Compagnon, W. Dewe, M. Feinberg, M. Lallier, M. Laurentie, N. Mercier, G. Muzard, C. Nivet, L. Valat, J. Pharm. Biomed. Anal. 36 (2004) 579–586.
[57] E. Rozet, V. Wascotte, N. Lecouturier, D. Préat, W. Dewé, B. Boulanger, P. Hubert, Anal. Chim. Acta 591 (2007) 239–247.
[58] P. Hubert, J.J. Nguyen-Huu, B. Boulanger, E. Chapuzet, N. Cohen, P.A. Compagnon, W. Dewe, M. Feinberg, M. Laurantie, N. Mercier, G. Muzard, L. Valat, E. Rozet, J. Pharm. Biomed. Anal. 45 (2007) 82–96.

[59] J.V. Loco, A. Jánosi, S. Impens, S. Fraselle, V. Cornet, J.M. Degroodt, Anal. Chim. Acta 586 (2007) 8–12.
[60] E. Desimoni, Accred. Qual. Assur. 9 (2004) 724–725.
[61] I. Janiga, J. Mocak, I. Garaj, Meas. Sci. Rev. 8 (2008) 108–110.
[62] E. Rozet, S. Rudaz, R.D. Marini, E. Ziémons, B. Boulanger, P. Hubert, Anal. Chim. Acta 702 (2011) 160–171.
[63] E. Rozet, W. Dewe, E. Ziemons, A. Bouklouze, B. Boulanger, P. Hubert, J. Chromatogr. B 877 (2009) 2214–2223.
[64] G. de Fontenay, J. Pharm. Biomed. Anal. 46 (2008) 104–112.
[65] U. Schepers, H. Wätzig, J. Pharm. Biomed. Anal. 41 (2006) 290–292.
[66] E. Rozet, W. Dewe, R. Morello, P. Chiap, F. Lecomte, E. Ziemons, K.S. Bosos, B. Boulanger, J. Cromen, P. Hubert, J. Chromatogr. A 1189 (2008) 32–41.
[67] L. Kaminski, U. Schepers, H. Wätzig, J. Pharm. Biomed. Anal. 53 (2010) 1124–1129.
[68] W. Dewe, B. Govaerts, B. Boulanger, E. Rozet, P. Chiap, P. Hubert, Chemometr. Intell. Lab. Syst. 85 (2007) 262–268.
[69] P. Hubert, J.-J. Nguyen-Hu, B. Boulanger, E. Chapuzet, P. Chiap, N. Cohen, P.A. Compagnon, W. Dewe, M. Feinberg, M. Lallier, M. Lauraentie, N. Mercier, G. Muzard, C. Nivet, L. Valat, E. Rozet, J. Pharm. Biomed. Anal. 45 (2007) 70–81.
[70] P.P. Váquez, M.M. Galera, A.G. Frenich, J.L.M. Vidal, Anal. Sci. 16 (2000) 49–55.
[71] M. Alcala, J. Leon, J. Ropero, M. Blanco, R.J. Romanach, J. Pharm. Sci. (2008). www.interscience.wiley.com. doi:10.1002/jps.21373.
[72] K. Saito, R.A. Dixon, L. Willmitzer (Eds.), Plant Metabolomic, in: (eds. T. Nagata, H. Lörz, J.M. Widholm) (Series Eds), Biotechnology in Agriculture and Forestry, vol. 57, Springer, Berlin, 2006.
[73] J. Nielsen, M.C. Jewett (Eds.), Metabolomics: A Powerful Tool in System Biology, Springer, Berlin, 2007.
[74] T. Saffaj, B. Ihssane, Talanta 85 (2011) 1535–1542.
[75] C. Agut, A. Caron, C. Giordano, D. Hoffman, A. Ségalini, J. Pharm. Biomed. Anal. 56 (2011) 293–303.
[76] A. Indrayanto, G. Indrayanto, VMA, Solutions (http://AnimoneSoft.com).

Cumulative Index

Bold numerals refer to volume numbers.